EMERGING INFECTIOUS DISEASES®

U.S. CENTERS FOR DISEASE CONTROL AND PREVENTION

Vaccine-Preventable Diseases

February 2025

Franz (Ferenc) Paczka (1856–1925), *Un Cas Grave ou La Leçon de Médecine* (*A Serious Case or The Medical Lesson*), (ca. 1875–1880).
Oil on canvas, 39.5 in × 53.3 in/100.3 cm × 135.5 cm. Image courtesy of Musée de Fécamp, Fécamp, France.

EMERGING INFECTIOUS DISEASES®

EDITOR-IN-CHIEF
D. Peter Drotman

ASSOCIATE EDITORS

Charles Ben Beard, Fort Collins, Colorado, USA
Ermias Belay, Atlanta, Georgia, USA
Sharon Bloom, Atlanta, Georgia, USA
Richard S. Bradbury, Townsville, Queensland, Australia
Corrie Brown, Athens, Georgia, USA
Benjamin J. Cowling, Hong Kong, China
Michel Drancourt, Marseille, France
Paul V. Effler, Perth, Western Australia, Australia
Anthony Fiore, Atlanta, Georgia, USA
David O. Freedman, Birmingham, Alabama, USA
Isaac Chun-Hai Fung, Statesboro, Georgia, USA
Peter Gerner-Smidt, Atlanta, Georgia, USA
Stephen Hadler, Atlanta, Georgia, USA
Shawn Lockhart, Atlanta, Georgia, USA
Nina Marano, Atlanta, Georgia, USA
Martin I. Meltzer, Atlanta, Georgia, USA
Nkuchia M. M'ikanatha, Harrisburg, Pennsylvania, USA
David Morens, Bethesda, Maryland, USA
J. Glenn Morris, Jr., Gainesville, Florida, USA
Patrice Nordmann, Fribourg, Switzerland
Johann D.D. Pitout, Calgary, Alberta, Canada
Ann Powers, Fort Collins, Colorado, USA
Didier Raoult, Marseille, France
Pierre E. Rollin, Atlanta, Georgia, USA
Frederic E. Shaw, Atlanta, Georgia, USA
Neil M. Vora, New York, New York, USA
David H. Walker, Galveston, Texas, USA
J. Scott Weese, Guelph, Ontario, Canada

Deputy Editor-in-Chief
Matthew J. Kuehnert, Westfield, New Jersey, USA

Managing Editor
Byron Breedlove, Atlanta, Georgia, USA

Technical Writer-Editors Shannon O'Connor, Team Lead; Dana Dolan, Amy J. Guinn, Tony Pearson-Clarke, Jill Russell, Jude Rutledge, Cheryl Salerno, Bryce Simons, P. Lynne Stockton, Denise Welk, Susan Zunino

Production, Graphics, and Information Technology Staff
Reginald Tucker, Team Lead; William Hale, Tae Kim, Barbara Segal

Journal Administrator J. McLean Boggess

Editorial Assistants Claudia Johnson, Nell Stultz, Jeffrey Terrell

Communications/Social Media Candice Hoffmann, Team Lead; Patricia A. Carrington-Adkins, Heidi Floyd

Associate Editor Emeritus
Charles H. Calisher, Fort Collins, Colorado, USA

Founding Editor
Joseph E. McDade, Rome, Georgia, USA

EDITORIAL BOARD

Barry J. Beaty, Fort Collins, Colorado, USA
David M. Bell, Atlanta, Georgia, USA
Martin J. Blaser, New York, New York, USA
Andrea Boggild, Toronto, Ontario, Canada
Christopher Braden, Atlanta, Georgia, USA
Arturo Casadevall, New York, New York, USA
Kenneth G. Castro, Atlanta, Georgia, USA
Gerardo Chowell, Atlanta, Georgia, USA
Adam Cohen, Atlanta, Georgia USA
Christian Drosten, Berlin, Germany
Clare A. Dykewicz, Atlanta, Georgia, USA
Kathleen Gensheimer, Phippsburg, Maine, USA
Rachel Gorwitz, Atlanta, Georgia, USA
Patricia M. Griffin, Decatur, Georgia, USA
Duane J. Gubler, Singapore
Scott Halstead, Westwood, Massachusetts, USA
David L. Heymann, London, UK
Keith Klugman, Seattle, Washington, USA
S.K. Lam, Kuala Lumpur, Malaysia
Ajit P. Limaye, Seattle, Washington, USA
Alexandre Macedo de Oliveira, Atlanta, Georgia, USA
John S. Mackenzie, Perth, Western Australia, Australia
Jennifer H. McQuiston, Atlanta, Georgia, USA
Joel Montgomery, Lilburn, GA, USA
Frederick A. Murphy, Bethesda, Maryland, USA
Kristy O. Murray, Atlanta, Georgia, USA
Stephen M. Ostroff, Silver Spring, Maryland, USA
Christopher D. Paddock, Atlanta, Georgia, USA
W. Clyde Partin, Jr., Atlanta, Georgia, USA
David A. Pegues, Philadelphia, Pennsylvania, USA
Mario Raviglione, Milan, Italy, and Geneva, Switzerland
David Relman, Palo Alto, California, USA
Connie Schmaljohn, Frederick, Maryland, USA
Tom Schwan, Hamilton, Montana, USA
Wun-Ju Shieh, Taipei, Taiwan
Rosemary Soave, New York, New York, USA
Robert Swanepoel, Pretoria, South Africa
David E. Swayne, Athens, Georgia, USA
Kathrine R. Tan, Atlanta, Georgia, USA
Phillip Tarr, St. Louis, Missouri, USA
Kenneth L. Tyler, Aurora, Colorado, USA
Duc Vugia, Richmond, California, USA
Mary Edythe Wilson, Iowa City, Iowa, USA

Emerging Infectious Diseases is published monthly by the Centers for Disease Control and Prevention, 1600 Clifton Rd NE, Mailstop H16-2, Atlanta, GA 30329-4018, USA. Telephone 404-639-1960; email, eideditor@cdc.gov

The conclusions, findings, and opinions expressed by authors contributing to this journal do not necessarily reflect the official position of the U.S. Department of Health and Human Services, the Public Health Service, the Centers for Disease Control and Prevention, or the authors' affiliated institutions. Use of trade names is for identification only and does not imply endorsement by any of the groups named above.

All material published in *Emerging Infectious Diseases* is in the public domain and may be used and reprinted without special permission; proper citation, however, is required.

Use of trade names is for identification only and does not imply endorsement by the Public Health Service or by the U.S. Department of Health and Human Services.

EMERGING INFECTIOUS DISEASES is a registered service mark of the U.S. Department of Health & Human Services (HHS).

EMERGING INFECTIOUS DISEASES®

Vaccine-Preventable Diseases **February 2025**

On the Cover

Franz (Ferenc) Paczka (1856–1925), *Un Cas Grave ou La Leçon de Médecine* (*A Serious Case or The Medical Lesson*), (ca. 1875–1880). Oil on canvas, 39.5 in × 53.3 in/100.3 cm × 135.5 cm. Image courtesy of Musée de Fécamp, Fécamp, France.

About the Cover p. 410

Synopses

Medscape EDUCATION ACTIVITY

Research

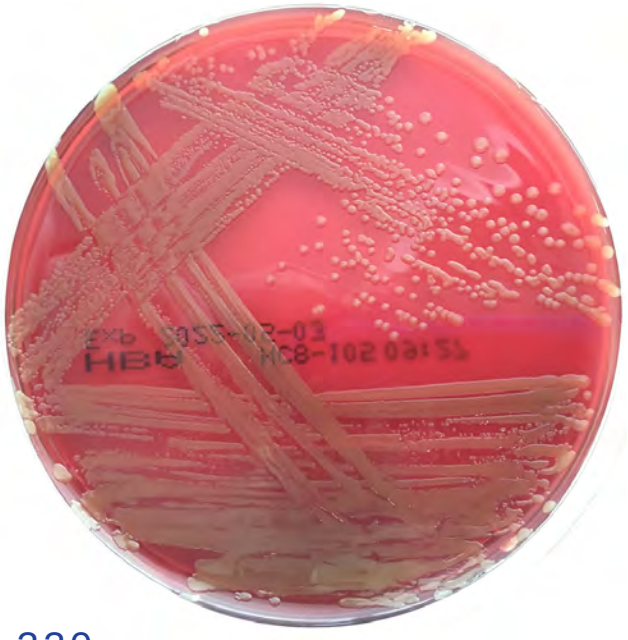

330

EMERGING INFECTIOUS DISEASES®

February 2025

Dispatches

350

EMERGING INFECTIOUS DISEASES®
February 2025

Research Letters

Books and Media

About the Cover

Online Reports

Etymologia

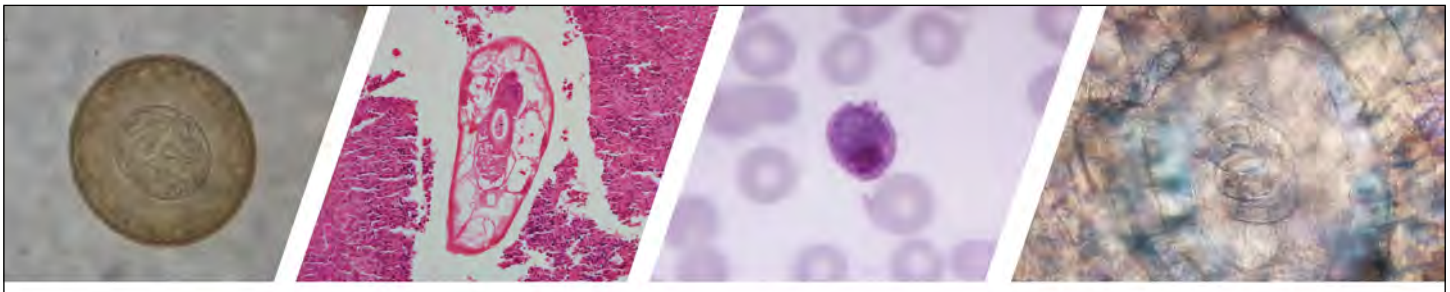

DPDx

Diagnostic Assistance and Training in Laboratory Identification of Parasites

A free service of CDC available to laboratorians, pathologists, and other health professionals in the United States and abroad

- Diagnosis from photographs of worms, histological sections, fecal, blood, and other specimen types
- Expert diagnostic review
- Formal diagnostic laboratory report
- Submission of samples via secure file share

Visit the DPDx website for information on laboratory diagnosis, geographic distribution, clinical features, parasite life cycles, and training via Monthly Case Studies of parasitic diseases.

www.cdc.gov/dpdx
dpdx@cdc.gov

U.S. Department of Health and Human Services
Centers for Disease Control and Prevention

CS272346-DE

Two Human Cases of Fatal Meningoencephalitis Associated with Potosi and Lone Star Virus Infections, United States, 2020–2023

Charles Y. Chiu, Raja Rama Godasi, Holly R. Hughes, Venice Servellita, Kafaya Foresythe, Asritha Tubati, Kelsey Zorn, Sukhman Sidhu, Michael R. Wilson, Sai Varun Bethina, Daniel Abenroth, Yee Cheng, Raymond Grams, Camilla Reese, Carlos Isada, Neeharika Thottempudi

We used clinical metagenomic next-generation sequencing of cerebrospinal fluid to investigate bunyavirus infections in 2 immunocompromised patients in the United States who had fatal meningoencephalitis. Potosi virus has been isolated from mosquito vectors and Lone Star virus from tick vectors. These findings highlight the power of metagenomic next-generation sequencing in broad-based, agnostic detection of emerging viral infections that test negative using conventional targeted diagnostic methods.

Viruses in the class *Bunyaviricetes* comprise a diverse group of infectious RNA viruses transmitted by arthropods, including mosquitoes and ticks (*1*). Most bunyavirus infections are asymptomatic or manifest as a mild, self-limited febrile illness; however, severe complications, including severe hemorrhagic or neurologic disease, can occur (*2*). We describe fatal bunyavirus infections in 2 immunocompromised patients whose cases we investigated by using clinical metagenomic next-generation sequencing (mNGS) of cerebrospinal fluid (CSF) (*3*,*4*). We also discuss the clinical and public health implications of these findings and the potential utility of mNGS for discovery and surveillance of newly emerging viral pathogens.

Case 1

In 2020, a 60-year-old man from Ohio, USA, with a history of stage IV non-Hodgkin follicular lymphoma was admitted to the hospital after 4 weeks of progressive cognitive decline, weight loss, headache, and fatigue. He had become bedbound and mute and could not perform activities of daily living. On admission, the patient was noted to be intermittently confused and ataxic with an unsteady gait. Results of a contrast magnetic resonance imaging (MRI) scan of the brain were unremarkable (Figure, panels A, B), showing only moderate diffuse cerebral atrophy with moderately enlarged ventricles consistent with advanced age. Cerebrospinal fluid (CSF) by lumbar puncture on hospital day 2 showed an unremarkable leukocyte count of 1 cell/mm^3 (reference range 0–5 cells/mm^3), an elevated erythrocyte count of 67 cells/mm^3 (reference range 0–5 cells/mm^3), elevated protein of 75 mg/dL (reference range 15–45 mg/dL), and an unremarkable glucose level of 67 mg/dL (reference range 40–70 mg/dL). Results of a positron emission tomography scan were negative, as were electroencephalogram results, which showed diffuse slowing consistent with encephalopathy and no seizure activity.

The patient resided in rural Ohio and worked at a manufacturing facility. He had completed chemotherapy with rituximab followed by 2 years of maintenance rituximab (completed 4 months before this admission, around the time of symptom onset) and was deemed to be in remission by his oncologist. He was married and monogamous with his wife and

Author affiliations: Chan–Zuckerberg Biohub, San Francisco, California, USA (C.Y. Chiu); Abbott Pandemic Defense Coalition, Abbott Park, Illinois, USA (C.Y. Chiu, V. Servellita, K. Foresythe); University of California, San Francisco (C.Y. Chiu, V. Servellita, K. Foresythe, A. Tubati, K. Zorn, S. Sidhu, M.R. Wilson); St. Luke's Boise Medical Center, Boise, Idaho, USA (R. Rama Godasi, D. Abenroth, Y. Cheng, R. Grams, C. Reese); Centers for Disease Control and Prevention, Fort Collins, Colorado, USA (H.R. Hughes); Wake Forest Baptist Medical Center, Winston-Salem, North Carolina, USA (S. Varun Bethina); Cleveland Clinic, Cleveland, Ohio, USA (C. Isada); University of Nevada, Reno, Nevada USA (N. Thottempudi)

DOI: https://doi.org/10.3201/eid3102.240831

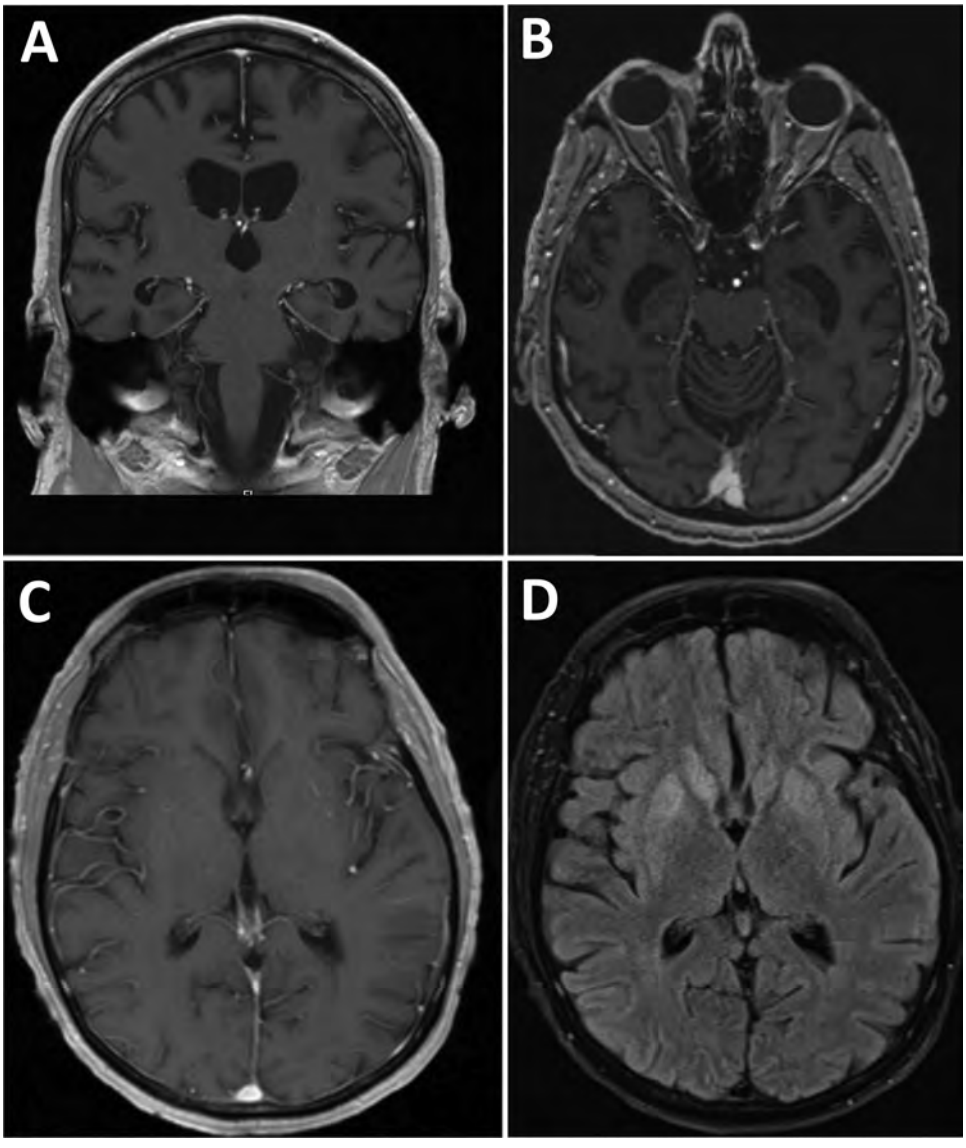

Figure. Brain magnetic resonance imaging scans from 2 patients with bunyavirus-associated meningoencephalitis, United States, 2020–2023. A, B) Case-patient 1 brain T1 postcontrast images of coronal (A) and axial (B) sections showing moderately enlarged ventricles and cerebral atrophy. C, D) Case-patient 2 brain T1 postcontrast (C) and T2 postcontrast fluid attenuated inversion recovery (D) images demonstrating bilateral basal ganglia hyperintensities with no contrast enhancement.

had no history of sexually transmitted infection. He reported no international travel in the previous 20 years, as well as no sick contacts, pets, farm animal exposures, or risk factors for tuberculosis.

We administered treatment for possible autoimmune encephalitis with high-dose intravenous methylprednisolone and plasma exchange, which led to minimal improvement. The patient clinically worsened; he had fever, declining mental status, paratonia (increased passive muscle tone), and conjunctivitis with subconjunctival hemorrhages, and we treated him empirically with broad-spectrum antibiotics. CSF examination on hospital day 14 showed unremarkable results for leukocyte count (2 cell/mm^3), erythrocyte count (0 cells/mm^3), protein (75 mg/dL), and glucose (57 mg/dL). After transfer to a tertiary care hospital for higher-level care, the patient remained febrile; he had poor mental status and had a new transaminitis of unclear etiology (liver enzyme levels at baseline were within reference ranges). Immunologic evaluation showed severe hypogammaglobulinemia, with total serum IgG levels of 89 mg/dL and CD4 cell counts of 114 cells/mL (reference range 533–1,674 cells/mL). Results of repeat MRI scans of the brain remained negative. We repeated CSF examinations on hospital days 17 and 31, and findings were similar to those previously observed. Extensive autoimmune and microbiologic test results were negative (Table), except for mNGS testing at the University of California San Francisco (UCSF; San Francisco, CA, USA) Clinical Microbiology Laboratory of 2 CSF samples collected on hospital

days 4 and 14. We detected Potosi virus (POTV) from both samples. Additional mNGS testing of residual RNA from CSF at the Centers for Disease Control and Prevention (CDC; Fort Collins, CO, USA) detected 87 reads aligning to the small and large segments of POTV. The patient's neurologic status progressively declined despite supportive therapy, and he died 37 days after admission.

Case 2

A 60-year-old man from Idaho, USA, with a history of common variable immunodeficiency that was being treated with weekly subcutaneous intravenous IgG was admitted to a tertiary care hospital in 2023 with a 1-week history of headache and myalgias. He had mental status changes, including difficulty with memory, performance of complex motor movements, strange behaviors, and nonsensical conversations, 1 day before hospitalization. He was very active, often hiking and biking outdoors. The patient was retired, owned no pets, and reported no risk factors for tuberculosis or animal or rural exposures.

At admission, the patient was afebrile and alert but confused. Physical examination was unremarkable except for altered sensorium, including the inability to recall his location and various life events. We administered empiric broad-spectrum antibiotics

Table. Laboratory test results for 2 patients with bunyavirus-associated meningoencephalitis, United States, 2020–2023*

Case-patient and test performed	Sample type	Test site	No. tests	Result
Case-patient 1				
Bacterial, fungal, or AFB culture	CSF, blood	C, T	4	Negative
Mayo autoimmune or neoplastic panel	CSF, serum	Mayo	6	Negative
Cryptococcal antigen	CSF, serum	C	3	Negative
Neurosyphilis test	CSF, serum	C	3	Negative
FilmArray M/E panel	CSF	C	3	Negative
HIV-1 serologic test	Serum	C	1	Negative
Lyme disease serologic test	Serum	C	1	Negative
Hepatitis A–C serologic test	Serum	C	1	Negative
WNV PCR	CSF	T	1	Negative
HSV-1/2 PCR	CSF	T	1	Negative
VZV PCR	CSF	T	1	Negative
HHV-6 PCR	CSF	T	1	Negative
Parvovirus B19 PCR	CSF	T	1	Negative
Toxoplasma gondii PCR	CSF	T	1	Negative
Histoplasma capsulatum PCR	CSF	T	1	Negative
H. capsulatum IgG or IgM	CSF, serum	T	2	Negative
Coccidioides IgG or IgM	CSF, serum	T	2	Negative
Adenovirus PCR	CSF	T	1	Negative
(1,3)-β-D glucan assay	CSF, serum	T	2	Negative
Cytologic test	CSF	T	1	Negative
mNGS pathogen diagnosis	CSF	UCSF	2	POTV detected; reads from all 3 segments (S, M, and L)
mNGS	CSF	CDC	1	POTV detected; reads from 2 segments (S and L)
Case-patient 2				
Bacterial, fungal, or AFB culture	CSF, blood	T	3	Negative
Mayo autoimmune/neoplastic panel	CSF, serum	Mayo	1	Elevated GAD65 antibody in serum†
Cryptococcal antigen	CSF, serum	C	3	Negative
Histoplasma urinary antigen	Urine	T	1	Negative
Lyme disease serologic test	Serum	T	1	Negative
Babesia spp. PCR	CSF	T	1	Negative
Toxoplasma gondii PCR	CSF	T	1	Negative
Histoplasma capsulatum PCR	CSF	T	1	Negative
H. capsulatum IgG or IgM	CSF, serum	T	2	Negative
WNV PCR	CSF	T	1	Negative
HSV-1/2 PCR	CSF	T	1	Negative
FilmArray M/E panel	CSF	T	1	Negative
VZV PCR	CSF	T	1	Negative
HHV-6 PCR	CSF	T	1	Negative
mNGS pathogen diagnosis	CSF	UCSF	2	LSV detected; reads from all 3 segments (S, M, and L)
Virus isolation	CSF	CDC	1	Negative
mNGS	CSF	CDC	1	Negative (no reads to LSV)
PRNT	CSF, serum	CDC	1	Negative

*AFB, acid-fast bacilli; C, community hospital; CDC, Centers for Disease Control and Prevention; HHV-6, human herpesvirus 6; HSV, herpes simplex virus; GAD65, glutamic acid decarboxylase 65; L, large; LSV, Lone star virus; M, medium; M/E, meningitis/encephalitis; Mayo, Mayo Clinic; mNGS, metagenomic next-generation sequencing; POTV, Potosi virus; PRNT, plaque reduction neutralizing testing; S, small; T, tertiary care hospital; UCSF, University of California San Francisco; VZV, varicella zoster virus; WNV, West Nile virus.
†0.37 nmol/L (reference range $\leq$0.02 nmol/L).

and acyclovir because of a high suspicion of meningoencephalitis. Initial laboratory testing was unremarkable except for mild thrombocytopenia (platelet count of 144,000 [reference range 150,000–450,000]) that reached a nadir of 111,000 on hospital day 4.

CSF obtained on admission showed a lymphocytic pleocytosis with leukocyte count of 6 cells/mm^3 and 79% lymphocytes, 16% monocytes, and 5% neutrophils; elevated protein of 80 mg/dL, and unremarkable glucose of 66 mg/dL. On hospital day 2, the patient became febrile (temperature up to 38.7°C), so we administered broad-spectrum antibiotics empirically; the patient had unrelenting fevers throughout the rest of the hospital course. On hospital day 3, we performed a repeat lumbar puncture, which continued to show an elevated leukocyte count of 40 cells/mm^3, elevated protein of 92 mg/dL, and unremarkable glucose of 53 mg/dL. Results of a CSF cytologic test result were negative, as were CSF, serum autoimmune, and serum paraneoplastic panel test results, except for mildly elevated serum glutamic acid decarboxylase 65 antibody of 0.37 nmol/L (reference range ≤0.02 nmol/L) with corresponding negative CSF glutamic acid decarboxylase 65 antibody.

We performed brain MRI 3 times; the first 2 results were unremarkable, but the third result, obtained on hospital day 14, showed mild interval hyperintensity of the basal ganglia and posterior hippocampi without contrast enhancement (Figure, panels C, D). Continuous electroencephalogram monitoring for 72 hours revealed mild to moderate background slowing with no seizure activity. All microbiologic test results except for CSF mNGS were negative (Table). CSF mNGS testing, which we performed twice on a hospital day 3 sample, was positive for Lone star virus (LSV). Additional testing of residual CSF by CDC did not detect reads from LSV on mNGS, and confirmatory testing with viral isolation and plaque reduction neutralization testing was negative. We attributed the discrepant sequencing results between UCSF and CDC to potential sample degradation caused by multiple freeze–thaw cycles and longer storage times. In addition, differences in sample preparation methods, such as treatment of extracts with DNase (which was performed by UCSF but not by CDC) and kits, could contribute to differences in sensitivity.

The patient remained confused and uncommunicative, and his neurologic status deteriorated such that he could no longer eat or walk. In discussions with his family, we decided to place the patient on comfort measures, and he died 26 days after admission.

CSF mNGS Analyses

We obtained informed consent from the patients or a surrogate for review of the medical charts under a protocol approved by the UCSF Institutional Review Board (protocol no. 13-12,236). For case 1, the initial sequencing run identified 15 of 4,677,264 reads aligning to Bunyamwera virus in the genus *Orthobunyavirus*, family *Peribunyaviridae* (Appendix Figure, panel A, https://wwwnc.cdc.gov/EID/article/31/2/24-0831-App1.pdf). Of note, the SURPI+ bioinformatics pipeline that was run at the time used a 2016 GenBank reference database (*3*), and the genome of POTV (GenBank accession no. IL94–1899) was deposited in 2017. Thus, POTV was not specifically identified by the SURPI+ pipeline because its genome was not part of the database. By using BLAST (https://blast.ncbi.nlm.nih.gov) to manually align to a 2020 GenBank database and incorporating additional data from a repeat run, we could identify and map 72 POTV reads with coverage of 636 bp (5.1%) of the 12,548-bp trisegmented genome (Appendix Figure, panel A). We identified 50 single-nucleotide polymorphisms (SNPs) within covered regions corresponding to a pairwise identity of 92.1%, and analysis of representative stretches of sequence consisting of ≤100-bp segments showed that most SNPs were located in the medium segment (Appendix Figure, panel A). We performed multiple sequence alignment of the concatenated genome (with Ns filling the missing regions) and 10 related representative *Orthobunyavirus* genomes by using MAFFT 7.388 (*5*). We conducted maximum-likelihood analysis by using PHYML 3.0 (*6*) to construct a nucleotide phylogenetic tree, which confirmed that the case 1 virus was most closely related to POTV (Appendix Figure, panel A).

For case 2, we identified 50 of 14,386,666 reads aligning to the LSV genome (genus *Bandavirus,* family *Phenuiviridae*) with 84%–95% identity by using the SURPI+ pipeline (Appendix Figure, panel B). Subsequent mNGS runs at high sequencing depth yielded 2,460 reads mapping to all 3 genome segments and covering 1,601 bp (13.6%) of the 11,730-bp trisegmented genome (Appendix Figure, panel B); 183 SNPs corresponded to a pairwise identity of 88.6% within covered regions. Analysis of representative stretches of sequence consisting of ≤100-bp segments showed that the distribution of SNPs was random but spanned across all 3 segments (Appendix Figure, panel B). We performed multiple sequence alignment of the concatenated genome and 13 related representative genomes in the genus *Bandavirus*. We conducted maximum-likelihood nucleotide phylogenetic analysis by using Gouleako virus as an outgroup, revealing that

the case 2 virus was most closely related to LSV (Appendix Figure, panel B). We have submitted partial POTV (n = 5) and LSV sequences (n = 14) to GenBank (accession nos. PQ347819–32).

For both patients, the high nucleotide identity (≈90%) to reference POTV and LSV genomes in GenBank within covered regions and identification of reads from all 3 segments provided confidence in bona fide identification of bunyaviral infections of the central nervous system. Of note, we did not detect bunyavirus reads in the no-template negative control consisting of synthetic CSF matrix in any of the other unrelated patient CSF samples on the sequencing run.

Conclusions

The class *Bunyaviricetes* comprises a diverse group of >500 arthropodborne or rodentborne viruses characterized by an enveloped trisegmented negative-sense RNA genome (*1*,*7*). Several bunyaviruses, including Rift Valley fever virus, La Crosse virus, Cache Valley virus (CVV), and Jamestown Canyon virus, can cause encephalitis (*2*). We identified 2 bunyaviruses, POTV and LSV, associated with fatal cases of meningoencephalitis in immunocompromised patients. POTV, which is closely related to CVV, was originally isolated from *Aedes albopictus* mosquito pools (*8*); that mosquito species is also an efficient vector for CVV transmission (*9*). LSV, in the genus *Bandavirus*, was isolated from the *Amblyomma americanum* tick (*10*), >10 years after our group reported the genome sequence of LSV (*11*). The key findings of our study include detection of emerging bunyaviruses that had been previously characterized by screening of mosquito and tick populations, underscoring the importance of continued arbovirus surveillance efforts; detection in transplant recipients, who may exhibit atypical or more severe clinical manifestations of infection (*12*); and use of agnostic mNGS for identification of viral infections that are challenging to diagnose (*13*).

Bhanja virus is a bandavirus that was isolated from a *Haemaphysalis intermedia* tick in Bhanjanagar, India, in 1954 and since then has been associated with sporadic cases of febrile illness in encephalitis in humans (*14*). More recently, Heartland virus, another bandavirus, was reported by CDC in 2009 in severely ill patients from the midwestern and southeastern United States with fever, leukopenia, and transaminitis (*15*). Both Heartland virus and LSV use *A. americanum* ticks as a putative tick vector.

The recent emergence of novel bunyaviruses in the United States might be related in part to the increased number of vulnerable persons undergoing transplantation, being treated with immunosuppressive drugs, or both, as well as to changes in the geographic expansion of mosquito and tick vectors that can transmit arboviruses northward and westward (*16*), probably because of climate and environmental factors. An example is a 2023 report of a fatal case of Heartland virus disease acquired in the mid-Atlantic region of the United States (*17*).

This study highlights the importance of broad-spectrum testing such as mNGS for the discovery of emerging viral infections (*13*). Currently, many viral infections are diagnosed by PCR (*18*), which requires the development of targeted primers and probes a priori. In contrast, mNGS is an agnostic approach, by which both known and novel emerging viruses can be identified by their distinct sequence signature (*19*). The minimal CSF pleocytosis in case 1 (1–2 cells/mm^3) and low to moderate pleocytosis in case 2 (peak leukocyte count of 40 cells/mm^3) are not necessarily unexpected, given that both patients were severely immunocompromised. In our 7-year longitudinal study of the performance and diagnostic yield of CSF mNGS testing (*20*), we found that the absence of CSF inflammation is observed in more than half of bona fide CNS infections in immunocompromised patients; 39 (53.4%) of 73 UCSF patients exhibited leukocyte counts of ≤5 cells/mm^3. A study by Benoit et al. (*21*) also identified several additional CNS bunyavirus infections by metagenomic sequencing, including those caused by CVV (*19*) and Jamestown Canyon virus. Diagnosis of bunyavirus infections typically relies on serologic tests, given that immunocompetent patients rapidly clear the virus and thus results from direct detection testing such as mNGS and reverse transcription PCR are negative. However, serologic testing is problematic for highly immunocompromised patients, for whom results can be false-negative (*22*). In addition, both serologic and molecular testing for several bunyaviruses might only be available in specialized reference laboratories such as at CDC, underscoring the potential utility of mNGS in expanding access to diagnostic testing for patients with bunyaviral encephalitis.

Because mNGS is a molecular detection technique and positive testing alone is insufficient to fulfill Koch's postulates (*23*), caution is warranted with clinical interpretation of mNGS results, especially with detection of a novel agent of unclear pathogenicity in highly susceptible immunocompromised hosts. Further clinical and epidemiologic studies are needed to characterize the spectrum of clinical disease and pathogenicity associated with POTV and LSV infections in humans. In addition, mNGS is not considered a first-line diagnostic test, given its cost,

complexity, and availability only in specialized reference laboratories. The costs of clinical mNGS testing might be reduced once regulatory approval for the test is obtained, prompting more expanded coverage from health insurance providers. Costs might also go down when running the test becomes more efficient, such as by transferring the assay to a commercial partner, thus scaling up access for patients with neurologic infections (*24*). A ≈1-month window occurred for both of our patients during which expedited mNGS testing, with a current laboratory turnaround time of 3–4 days (*19*), might have resulted in an earlier diagnosis. Although no approved treatment for bunyavirus infection is available, the experimental drug favipravir (T-705) is effective against orthobunyaviruses in vitro and in rodent models (*25*–*28*) and efficiently crosses the blood–brain barrier (*29*). Ribavirin also has some activity against bunyaviruses, but its potential efficacy might be limited by poor penetration into the CNS (*30*). Furthermore, we note that in the cases described here, and in many other cases of chronic neurologic bunyavirus infections (*31*), patients specifically have deficiencies in the humoral arm of the immune system. This finding suggests convalescent serum or, in the future, targeted antiviral monoclonal antibodies, could play a role in treatment.

Acknowledgments

We thank the dedicated staff at the UCSF Clinical Microbiology Laboratory for their efforts in maintaining and performing the UCSF mNGS test (>600 sequencing runs as of April 2024).

This work was financially supported in part by grants from CDC (grant nos. 75D30122C15360 and 75D30121C12641, awarded to C.Y.C.), Abbott Laboratories (awarded to C.Y.C.), and the Chan–Zuckerberg Biohub (awarded to C.Y.C.). The funders had no role in the design and conduct of the study; collection, management, analysis, and interpretation of the data; preparation, review, or approval of the manuscript; and decision to submit the manuscript for publication.

Competing interests: C.Y.C. and M.R.W. are co-founders of Delve Bio. C.Y.C. is on the scientific advisory board and M.R.W. is on the board of directors for Delve Bio. C.Y.C. also is on the scientific advisory boards for Flightpath Biosciences, Biomeme, Mammoth Biosciences, BiomeSense, and Poppy Health. C.Y.C. is an inventor on US patent no. 11380421 (pathogen detection using next-generation sequencing), under which algorithms for taxonomic classification, filtering, and pathogen detection are used by SURPI+ software. C.Y.C. receives research support from Delve Bio and Abbott Laboratories. The other authors declare no competing interests.

Author contributions: C.Y.C conceived and designed the study. R.R.G., S.V.B., D.A., Y.C., R.G., C.R., C.I., and N.T cared for the patient, performed medical chart review, or both. A.T., K.Z., and S.S. assisted with patient recruitment. H.H., V.S., and K.F. biobanked, generated, and analyzed mNGS data from patient CSF samples. H.H., C.G., E.S., and L.T. collected clinical and epidemiologic data and samples and performed confirmatory laboratory testing. C.Y.C. analyzed the data and prepared the figures. C.Y.C., R.R.G., C.R., C.I., M.W., and N.T. wrote the manuscript. C.Y.C., M.W., and N.T. provided laboratory oversight. All authors read the manuscript and agree to its contents.

About the Author

Dr. Chiu is a professor at UCSF in laboratory medicine and infectious diseases and director of the UCSF Clinical Microbiology Laboratory. He leads a translational research laboratory focused on clinical metagenomic assay development for infectious diseases and characterization of emerging outbreak viruses.

References

1. Boshra H. An overview of the infectious cycle of bunyaviruses. Viruses. 2022;14:2139. https://doi.org/10.3390/v14102139
2. Soldan SS, González-Scarano F. Emerging infectious diseases: the *Bunyaviridae*. J Neurovirol. 2005;11:412–23. https://doi.org/10.1080/13550280591002496
3. Miller S, Naccache SN, Samayoa E, Messacar K, Arevalo S, Federman S, et al. Laboratory validation of a clinical metagenomic sequencing assay for pathogen detection in cerebrospinal fluid. Genome Res. 2019;29:831–42. https://doi.org/10.1101/gr.238170.118
4. Wilson MR, Sample HA, Zorn KC, Arevalo S, Yu G, Neuhaus J, et al. Clinical metagenomic sequencing for diagnosis of meningitis and encephalitis. N Engl J Med. 2019;380:2327–40. https://doi.org/10.1056/NEJMoa1803396
5. Katoh K, Standley DM. MAFFT multiple sequence alignment software version 7: improvements in performance and usability. Mol Biol Evol. 2013;30:772–80. https://doi.org/10.1093/molbev/mst010
6. Guindon S, Dufayard JF, Lefort V, Anisimova M, Hordijk W, Gascuel O. New algorithms and methods to estimate maximum-likelihood phylogenies: assessing the performance of PhyML 3.0. Syst Biol. 2010;59:307–21. https://doi.org/10.1093/sysbio/syq010
7. Elliott RM. Orthobunyaviruses: recent genetic and structural insights. Nat Rev Microbiol. 2014;12:673–85. https://doi.org/10.1038/nrmicro3332
8. Armstrong PM, Andreadis TG, Anderson JF, Main AJ. Isolations of Potosi virus from mosquitoes (Diptera: Culicidae) collected in Connecticut. J Med Entomol. 2005;42:875–81. https://doi.org/10.1093/jmedent/42.5.875
9. Dieme C, Maffei JG, Diarra M, Koetzner CA, Kuo L, Ngo KA, et al. *Aedes Albopictus* and Cache Valley virus: a new threat for virus transmission in New York State. Emerg Microbes

Infect. 2022;11:741–8. https://doi.org/10.1080/22221751.2022.2044733
10. Kokernot RH, Calisher CH, Stannard LJ, Hayes J. Arbovirus studies in the Ohio-Mississippi Basin, 1964-1967. VII. Lone Star virus, a hitherto unknown agent isolated from the tick *Amblyomma americanum* (Linn). Am J Trop Med Hyg. 1969;18:789–95. https://doi.org/10.4269/ajtmh.1969.18.789
11. Swei A, Russell BJ, Naccache SN, Kabre B, Veeraraghavan N, Pilgard MA, et al. The genome sequence of Lone Star virus, a highly divergent bunyavirus found in the *Amblyomma americanum* tick. PLoS One. 2013;8:e62083. https://doi.org/10.1371/journal.pone.0062083
12. Waggoner JJ, Soda EA, Deresinski S. Rare and emerging viral infections in transplant recipients. Clin Infect Dis. 2013;57:1182–8. https://doi.org/10.1093/cid/cit456
13. Chiu CY, Miller SA. Clinical metagenomics. Nat Rev Genet. 2019;20:341–55. https://doi.org/10.1038/s41576-019-0113-7
14. Matsuno K, Weisend C, Travassos da Rosa AP, Anzick SL, Dahlstrom E, Porcella SF, et al. Characterization of the Bhanja serogroup viruses (*Bunyaviridae*): a novel species of the genus *Phlebovirus* and its relationship with other emerging tick-borne phleboviruses. J Virol. 2013;87:3719–28. https://doi.org/10.1128/JVI.02845-12
15. McMullan LK, Folk SM, Kelly AJ, MacNeil A, Goldsmith CS, Metcalfe MG, et al. A new phlebovirus associated with severe febrile illness in Missouri. N Engl J Med. 2012;367:834–41. https://doi.org/10.1056/NEJMoa1203378
16. Levy BS, Patz JA. Climate change and public health. Second edition. New York: Oxford University Press; 2024.
17. Liu S, Kannan S, Meeks M, Sanchez S, Girone KW, Broyhill JC, et al. Fatal case of heartland virus disease acquired in the mid-Atlantic region, United States. Emerg Infect Dis. 2023;29:992–6. https://doi.org/10.3201/eid2905.221488
18. DeBiasi RL, Tyler KL. Polymerase chain reaction in the diagnosis and management of central nervous system infections. Arch Neurol. 1999;56:1215–9. https://doi.org/10.1001/archneur.56.10.1215
19. Bohl JA, Lay S, Chea S, Ahyong V, Parker DM, Gallagher S, et al. Discovering disease-causing pathogens in resource-scarce Southeast Asia using a global metagenomic pathogen monitoring system. Proc Natl Acad Sci U S A. 2022;119:e2115285119. https://doi.org/10.1073/pnas.2115285119
20. Benoit P, Brazer N, de Lorenzi-Tognon M, Kelly E, Servellita V, Oseguera M, et al. Seven-year performance of a clinical metagenomic next-generation sequencing test for diagnosis of central nervous system infections. Nat Med. 2024;30:3522–33. https://doi.org/10.1038/s41591-024-03275-1
21. Solomon IH, Ganesh VS, Yu G, Deng XD, Wilson MR, Miller S, et al. Fatal case of chronic Jamestown Canyon virus encephalitis diagnosed by metagenomic sequencing in patient receiving rituximab. Emerg Infect Dis. 2021;27:238–42. https://doi.org/10.3201/eid2701.203448
22. Varghese J, De Silva I, Millar DS. Latest advances in arbovirus diagnostics. Microorganisms. 2023;11:1159. https://doi.org/10.3390/microorganisms11051159
23. Chiu CY. Viral pathogen discovery. Curr Opin Microbiol. 2013;16:468–78. https://doi.org/10.1016/j.mib.2013.05.001
24. Business Wire. Delve Biol announces launch of its groundbreaking genomic infectious disease test, Delve Detect. 2024 [cited 2024 Dec 17]. https://www.businesswire.com/news/home/20241204755302/en/delve-bio-announces-launch-of-its-groundbreaking-genomic-infectious-disease-test-delve-detect
25. Gowen BB, Wong MH, Jung KH, Sanders AB, Mendenhall M, Bailey KW, et al. In vitro and in vivo activities of T-705 against arenavirus and bunyavirus infections. Antimicrob Agents Chemother. 2007;51:3168–76. https://doi.org/10.1128/AAC.00356-07
26. Gowen BB, Wong MH, Jung KH, Smee DF, Morrey JD, Furuta Y. Efficacy of favipiravir (T-705) and T-1106 pyrazine derivatives in phlebovirus disease models. Antiviral Res. 2010;86:121–7. https://doi.org/10.1016/j.antiviral.2009.10.015
27. Oestereich L, Rieger T, Neumann M, Bernreuther C, Lehmann M, Krasemann S, et al. Evaluation of antiviral efficacy of ribavirin, arbidol, and T-705 (favipiravir) in a mouse model for Crimean-Congo hemorrhagic fever. PLoS Negl Trop Dis. 2014;8:e2804. https://doi.org/10.1371/journal.pntd.0002804
28. Tani H, Fukuma A, Fukushi S, Taniguchi S, Yoshikawa T, Iwata-Yoshikawa N, et al. Efficacy of T-705 (favipiravir) in the treatment of infections with lethal severe fever with thrombocytopenia syndrome virus. MSphere. 2016;1:e00061–15. https://doi.org/10.1128/mSphere.00061-15
29. Morrey JD, Taro BS, Siddharthan V, Wang H, Smee DF, Christensen AJ, et al. Efficacy of orally administered T-705 pyrazine analog on lethal West Nile virus infection in rodents. Antiviral Res. 2008;80:377–9. https://doi.org/10.1016/j.antiviral.2008.07.009
30. Livonesi MC, De Sousa RL, Badra SJ, Figueiredo LT. In vitro and in vivo studies of ribavirin action on Brazilian orthobunyavirus. Am J Trop Med Hyg. 2006;75:1011–6. https://doi.org/10.4269/ajtmh.2006.75.1011
31. Kapadia RK, Staples JE, Gill CM, Fischer M, Khan E, Laven JJ, et al. Severe arboviral neuroinvasive disease in patients on rituximab therapy: a review. Clin Infect Dis. 2023;76:1142–8. https://doi.org/10.1093/cid/ciac766

Address for correspondence: Charles Y. Chiu, Department of Laboratory Medicine, University of California–San Francisco, 185 Berry St, Box 0134, San Francisco, CA 94158, USA; email: charles.chiu@ucsf.edu

National Surveillance of Human Ehrlichiosis Caused by *Ehrlichia ewingii*, United States, 2013–2021

Sydney N. Adams, Nicolette C. Bestul, Kimberly N. Calloway, Gilbert J. Kersh, Johanna S. Salzer

Medscape CME Activity

In support of improving patient care, this activity has been planned and implemented by Medscape, LLC and Emerging Infectious Diseases. Medscape, LLC is jointly accredited with commendation by the Accreditation Council for Continuing Medical Education (ACCME), the Accreditation Council for Pharmacy Education (ACPE), and the American Nurses Credentialing Center (ANCC), to provide continuing education for the healthcare team.

Medscape, LLC designates this Journal-based CME activity for a maximum of 1.00 ***AMA PRA Category 1 Credit(s)™***. Physicians should claim only the credit commensurate with the extent of their participation in the activity.

Successful completion of this CME activity, which includes participation in the evaluation component, enables the participant to earn up to 1.0 MOC points in the American Board of Internal Medicine's (ABIM) Maintenance of Certification (MOC) program. Participants will earn MOC points equivalent to the amount of CME credits claimed for the activity. It is the CME activity provider's responsibility to submit participant completion information to ACCME for the purpose of granting ABIM MOC credit.

All other clinicians completing this activity will be issued a certificate of participation. To participate in this journal CME activity: (1) review the learning objectives and author disclosures; (2) study the education content; (3) take the post-test with a 75% minimum passing score and complete the evaluation at https://www.medscape.org/qna/processor/73487?showStandAlone=true&src=prt_jcme_eid_mscpedu; and (4) view/print certificate. For CME questions, see page 414.

NOTE: It is Medscape's policy to avoid the use of Brand names in accredited activities. However, in an effort to be as clear as possible, trade names are used in this activity to distinguish between the mixtures and different tests. It is not meant to promote any particular product.

Release date: January 23, 2025; Expiration date: January 23, 2026

Learning Objectives

Upon completion of this activity, participants will be able to:

- Compare rates of ehrlichiosis in the United States based on *Ehrlichia* species
- Analyze clinical features and outcomes of ehrlichiosis
- Evaluate the epidemiology of ehrlichiosis due to *E. ewingii* infection in the United States
- Assess variables associated with *E. ewingii* ehrlichiosis.

CME Editor

Susan Zunino, PhD, Technical Writer/Editor, Emerging Infectious Diseases. *Disclosure: Susan Zunino, PhD, has no relevant financial relationships.*

CME Author

Charles P. Vega, MD, Health Sciences Clinical Professor of Family Medicine, University of California, Irvine School of Medicine, Irvine, California. *Disclosure: Charles P. Vega, MD, has the following relevant financial relationships: served as consultant or advisor for Boehringer Ingelheim; GlaxoSmithKline.*

Authors

Sydney N. Adams, MPH; Nicolette C. Bestul, MPH; Kimberly N. Calloway, DVM; Gilbert J. Kersh, PhD; Johanna S. Salzer, DVM, PhD.

Human ehrlichiosis is a potentially fatal tickborne disease caused by 3 species: *Ehrlichia chaffeensis*, *E. ewingii*, and *E. muris eauclairensis*. In the United States, 234 confirmed cases of *E. ewingii* ehrlichiosis were reported to the Centers for Disease Control and Prevention through the National Notifiable Diseases Surveillance System during 2013–2021; average annual incidence was 0.08 cases/1 million population. *E. ewingii* ehrlichiosis was reported more commonly among older, White, non-Hispanic, and male patients. Incidence and case counts generally increased yearly, except for 2020 and 2021. The highest number of cases were reported from Missouri and Arkansas. We report the geographic expansion of *E. ewingii* ehrlichiosis and the continued public health challenge of clarifying clinical manifestations of this infection. Clinician education will be essential to implement molecular assays to properly diagnose *E. ewingii* infection in patients and gain a better understanding of the epidemiology of this emerging disease.

In the United States, human ehrlichioses are potentially fatal tickborne rickettsial diseases caused by the intracellular bacterium belonging to the genus *Ehrlichia* (*1*). Three species of *Ehrlichia* are primarily associated with human disease: *E. chaffeensis*, *E. ewingii*, and *E. muris eauclairensis*. Most ehrlichiosis cases reported to the Centers for Disease Control and Prevention (CDC) have been caused by *E. chaffeensis*. Although *E. ewingii* ehrlichiosis cases are reported less frequently to CDC, the numbers of reported cases have increased overall since 2008 (*2*).

The clinical severity of ehrlichiosis depends upon the *Ehrlichia* species causing infection and underlying risk factors. In general, *E. ewingii* infections have been considered milder than infections caused by *E. chaffeensis* (*3*). Persons with ehrlichiosis who are immunocompromised, especially those who have HIV, are receiving cancer treatments, or had organ transplants, are at the highest risk for severe outcomes (*3*–*9*). Only 1 fatal case of *E. ewingii* ehrlichiosis was reported to CDC in 2018.

Various methods can be used to diagnose ehrlichiosis in patients. However, to differentiate between *E. ewingii* and other *Ehrlichia* spp., PCR or other molecular methods are necessary. Serologic testing cannot differentiate among *Ehrlichia* spp. responsible for human infections (*10*,*11*).

Author affiliations: Oak Ridge Institute for Science and Education, Oak Ridge, Tennessee, USA (S.N. Adams); Centers for Disease Control and Prevention, Atlanta, Georgia, USA (S.N. Adams, N.C. Bestul, K.N. Calloway, G.J. Kersh, J.S. Salzer)

DOI: https://doi.org/10.3201/eid3102.240279

Ehrlichiosis was first made nationally notifiable in the United States in 1999 by the Council of State and Territorial Epidemiologists (CSTE) (*12*). However, the case definition at that time did not differentiate between infections caused by *Ehrlichia* spp. or *Anaplasma* spp. and did not permit species-specific reporting. In 2008, the CSTE case definition was revised to distinguish between ehrlichiosis and anaplasmosis and to include the following categories for ehrlichiosis: *E. chaffeensis* infection (formerly human monocytic ehrlichiosis); *E. ewingii* infection (formerly ehrlichiosis [unspecified or other agent]); and ehrlichiosis/anaplasmosis, human, undetermined. Because *E. muris eauclairensis* was discovered after the adoption of the 2008 case definition, it was not included in the categories of ehrlichiosis until a revised case definition was established in 2024.

Although *E. ewingii* ehrlichiosis is a nationally notifiable condition, each jurisdiction in the United States determines what conditions are reportable in their respective area through the local legislative process. Therefore, *E. ewingii* ehrlichiosis is not a reportable infection in some jurisdictions. Here, we describe the passive surveillance of *E. ewingii* ehrlichiosis reported to the National Notifiable Diseases Surveillance System (NNDSS) in the United States during 2013–2021.

Methods

State and territorial health departments voluntarily submit confirmed and probable cases of ehrlichiosis to CDC through NNDSS. During 2013–2021, *E. ewingii* infection was reportable in 44 US states and the District of Columbia. Variables transmitted to the NNDSS are sex, age, race, ethnicity, event date, county and state of residence, import status (outside county, state, or country), case status, and whether the case is associated with an outbreak. Cases were defined by using the 2008 CSTE case definition (*12*). The event date is the earliest date associated with the case, which can be the symptom onset date, diagnosis date, laboratory test date, or the date the case was reported to the county or state health department. We included in the analysis all confirmed *E. ewingii* ehrlichiosis cases reported to CDC through NNDSS until November 1, 2023, that had event dates during January 1, 2013–December 31, 2021.

We used NNDSS data and population estimates from the US Census Bureau to calculate national-, state-, county-, and age-specific ehrlichiosis incidence. We calculated each year's cumulative incidence and then averaged those data over the study period to produce the average annual incidence; we did not include states where *E. ewingii* ehrlichiosis was not a notifiable condition. *E. ewingii* infection was not considered a notifiable disease during some years in

Table 1. Demographic characteristics of patients in study of national surveillance of human ehrlichiosis caused by *Ehrlichia ewingii*, United States, 2013–2021*

Characteristics	No. patients (%)	Incidence†
Total no. patients	234	NA
Sex		
M	149 (63.7)	0.14
F	84 (35.9)	0.06
Unknown	1 (0.4)	NA
Race‡		
White	163 (69.7)	NA
Black	2 (0.9)	NA
American Indian/Alaska Native	0	NA
Asian/Pacific Islander	3 (1.3)	NA
Other	7 (3.0)	NA
Missing	2 (0.9)	NA
Unknown	57 (24.4)	NA
Ethnicity‡		
Hispanic	3 (1.3)	NA
Non-Hispanic	193 (82.5)	NA
Unknown	38 (16.2)	NA
Age, y		
<10	0	NA
10–19	6 (2.6)	0.08
20–29	8 (3.4)	0.08
30–39	18 (7.7)	0.12
40–49	25 (10.7)	0.09
50–59	62 (26.5)	0.17
60–69	54 (23.1)	0.13
≥70	61 (26.1)	0.13
Unknown	0	NA
Median age, y (IQR)	59 (50–70)	NA

*Values are no. (%) except as indicated. Confirmed cases of ehrlichiosis caused by *Ehrlichia ewingii* were reported to the US National Notifiable Disease Surveillance System. IQR, interquartile range, NA, not applicable.
†Average incidence over the reporting period.
‡Because of large proportions of missing data, incidence was not calculated for race or ethnicity.

Alaska (2013–2021), Colorado (2013–2021), Connecticut (2015–2021), District of Columbia (2013), Hawaii (2013–2021), Idaho (2013–2021), Iowa (2013–2015), and New Mexico (2013–2021). We included cases reported as infections acquired outside of the state of residence or outside of the United States in the overall case counts but did not include those cases in state or county level counts or incidence. We did not include infections acquired outside of the United States in the national incidence calculations. We did not include missing values in the denominator for frequencies and rates, unless otherwise noted. We analyzed data by using SAS version 9.4 (SAS Institute Inc.).

Results

A total of 245 ehrlichiosis cases caused by *E. ewingii* with an event date during 2013–2021 were reported to NNDSS. Of those cases, 234 (96%) were reported as confirmed (Table 1). Eleven cases were reported as probable; we did not include those cases in the analysis because we were unable to apply CSTE case definitions post hoc. Case counts generally increased over the study period, peaking in 2019 (Figure 1). The average annual incidence for the study period was 0.08 cases/1 million population. The annual incidence during the study period varied but peaked at 0.13 cases/1 million population in 2017 and in 2019. States that reported the most cases were Missouri (n = 112), Arkansas (n = 22), Kansas (n = 11), New Jersey (n = 11), Tennessee (n = 10), Virginia (n = 10), Maryland (n = 7), Oklahoma (n = 6), Delaware (n = 5), and Kentucky (n = 5) (Table 2). Those 10 states accounted for 86% (n = 199) of all reported *E. ewingii* infection cases in the United States; Missouri alone

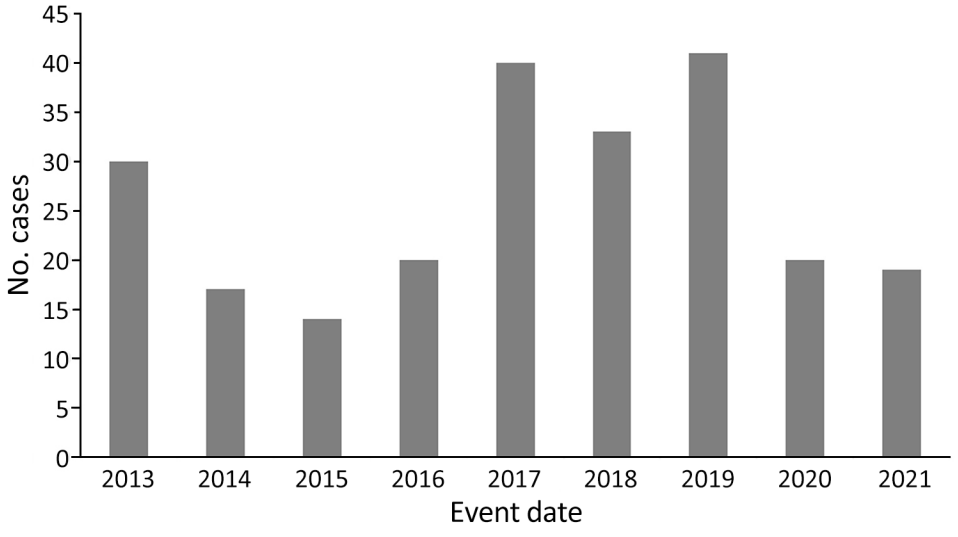

Figure 1. Annual number of human ehrlichiosis cases caused by *Ehrlichia ewingii* according to event date, United States, 2013–2021. Confirmed cases of *E. ewingii* ehrlichiosis were reported to the Centers of Disease Control and Prevention through the National Notifiable Disease Surveillance System. Event dates were the earliest date associated with the case, which could be the symptom onset date, diagnosis date, laboratory test date, or the date the case was reported to the county or state health department.

accounted for 48% of all cases reported and had the highest incidence (Figure 2). Overall, 24 jurisdictions reported ≥1 case of *E. ewingii* ehrlichiosis, and 15 (63%) states reported cases for the first time during 2013–2021 (Table 2). Kansas and Virginia both had low case counts but had the largest increases in cases during the study period; Kansas had a 3.2-fold (n = 11) increase, and Virginia had a 2-fold (n = 11) increase in reported incidence.

More cases of *E. ewingii* ehrlichiosis were reported in male (n = 149 [64%]) than female (n = 84 [36%]) persons (Table 1). The highest numbers of cases by race were among White persons (n = 163 [70%]) and by ethnicity were among all non-Hispanic persons (n = 193 [82%]). We did not calculate incidence for race or ethnicity because it was a small dataset, and 25% of data for race and 16% for ethnicity were missing or unknown. The median age of patients was 59 (interquartile range 50–70) years. Most cases occurred among those 50–59 years of age (Table 1). Incidence generally increased with age; the lowest incidence was reported in persons 10–19 and 20–29 years of age (both 0.08 cases/1 million population).

Discussion

Ehrlichiosis caused by *E. ewingii* is a growing concern in the United States because of increasing geographic distribution and incidence, although cases are likely underreported. When comparing the 2013–2021 and 2008–2012 reporting periods, we observed an ≈2-fold increase in the average number of reported cases during the 2013–2021 period. In addition, during 2013–2021, *E. ewingii* ehrlichiosis was reported from 15 jurisdictions that had not previously reported cases. Although cases increased overall during the reporting period, the number of cases decreased in 2020 and 2021 compared with previous years, likely attributable to the COVID-19 pandemic. Similar trends have been observed for other ehrlichioses and tickborne diseases (*13*). It is unclear if the increase in reported cases is because of improved healthcare provider awareness, availability of molecular testing, increased reporting capabilities, a genuine increase in the number of infected persons, or a combination of those factors.

Reliance on serologic testing to diagnose ehrlichiosis in disease-endemic areas likely contributes to underreporting. During the 2013–2021 period, 56% of *E. chaffeensis* cases reported through NNDSS were classified as probable. Specific laboratory methods for diagnosis are not provided in NNDSS. However, historically, most probable *E. chaffeensis* ehrlichiosis cases have relied on a single serologic result for case classification (*2*). Therefore, it is highly likely that some cases reported as probable *E. chaffeensis* ehrlichiosis were, in fact, *E. ewingii* ehrlichiosis cases, although the proportion is unknown. Reliance on serologic testing could also

Table 2. Ehrlichiosis cases caused by *Ehrlichia ewingii* reported to the National Notifiable Disease Surveillance System, United States, during 2013–2021 and 2008–2012*

State or region	No. cases, 2013–2021	No. cases, 2008–2012
Alabama	1	0
Alaska	NN	NN
Arizona	0	0
Arkansas	22	0
California	0	0
Colorado	NN	NN
Connecticut†	0	0
Delaware	5	5
District of Columbia†	0	NN
Florida	3	0
Georgia	0	1
Hawaii	NN	NN
Idaho	NN	NN
Illinois	4	1
Indiana	4	0
Iowa†	1	NN
Kansas	11	1
Kentucky	5	0
Louisiana	0	1
Maine	1	0
Maryland	7	2
Massachusetts	0	0
Michigan	0	0
Minnesota	2	2
Mississippi	2	0
Missouri	112	33
Montana	1	NN
Nebraska	0	0
Nevada	0	0
New Hampshire	2	0
New Jersey	11	0
New Mexico	NN	NN
New York City	2	0
New York	5	0
North Carolina	0	0
North Dakota	1	0
Ohio	0	1
Oklahoma	6	0
Oregon	0	0
Pennsylvania	0	0
Rhode Island	0	0
South Carolina	0	1
South Dakota	0	0
Tennessee	10	5
Texas	0	0
Utah	0	0
Vermont	0	0
Virginia	10	2
Washington	0	0
West Virginia	0	0
Wisconsin	3	0
Wyoming	0	0

*Ehrlichiosis caused by *E. ewingii* is not a notifiable disease in some states. NN, not notifiable (during the entire study period).
†Ehrlichiosis caused by *E. ewingii* was not notifiable in the jurisdiction for part of the reporting period (Connecticut 2015–2021, District of Colombia 2013, Iowa 2013–2015). Data represent the years when the condition was notifiable in the jurisdiction.

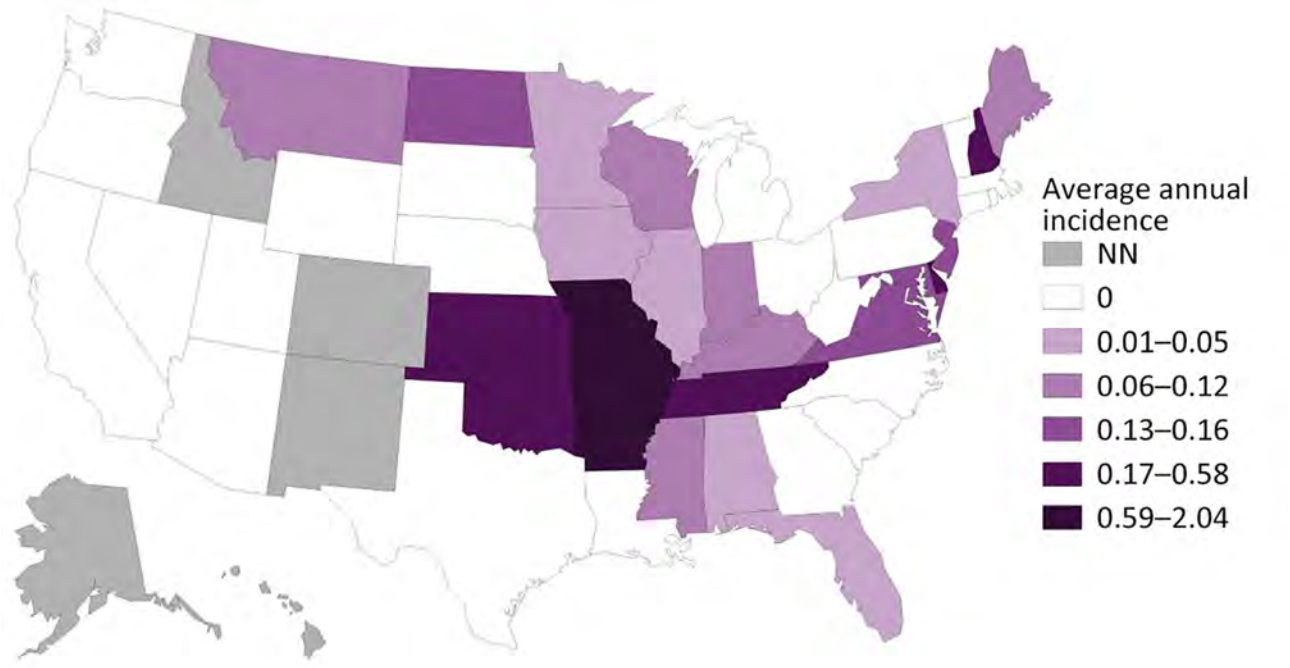

Figure 2. Average annual incidence (cases/1 million persons) of human ehrlichiosis caused by *Ehrlichia ewingii*, United States, 2013–2021. Confirmed cases of *E. ewingii* ehrlichiosis were reported to the Centers of Disease Control and Prevention through the National Notifiable Disease Surveillance System. *E. ewingii* ehrlichiosis was not a notifiable disease in some states. NN, not notifiable (during the entire study period).

explain why some states, such as North Carolina, a region with a high incidence of *E. chaffeensis* ehrlichiosis, reported no cases of *E. ewingii* ehrlichiosis. It is possible that healthcare providers in North Carolina were not regularly ordering species-specific PCR testing to identify *E. ewingii* compared with other states.

Molecular testing for *E. ewingii* is available at several commercial laboratories in the United States and at CDC. Although healthcare providers should not wait for diagnostic test results before treating patients with suspected ehrlichiosis, PCR can confirm a patient's illness during the acute phase of infection. PCR provides a rapid confirmation for the healthcare provider and patient and does not require the patient to return for additional serologic testing, saving the patient time and money. In addition to reducing patient costs, improved provider awareness and uptake of PCR-based testing will help define the true burden associated with different *Ehrlichia* spp. In 2024, the ehrlichiosis case definition was revised. The case definition now requires the use of molecular methods to identify and classify specific *Ehrlichia* spp. The 2024 case definition might affect provider testing choices and will likely permit more certainty when describing species-specific cases.

The first limitation of our study is that all case information relied on passive surveillance through NNDSS and not active case finding. A positive *E. ewingii* test result must be reported to public health authorities for investigation and then submitted to NNDSS to be captured in national statistics. If local health departments are unable to investigate cases, those cases would not be reported to NNDSS. Second, cases might be underrepresented because patients had asymptomatic or mild infections. If a person is mildly ill, they might not seek care from their healthcare provider. Thus, cases reported through passive surveillance are more likely to represent patients who are more severely ill and are from disease-endemic areas where healthcare providers have increased awareness of the condition. Finally, results from passive surveillance are not generalizable to the whole population and likely underestimate the true disease burden.

E. ewingii infection is an emerging public health concern in the United States. Serologic testing for ehrlichiosis is not species-specific; therefore, molecular testing is essential for diagnosing this disease. Healthcare providers should be aware that PCR testing for ehrlichiosis is highly sensitive and specific during the acute phase of illness. CDC and other partners should also explore novel methods to increase healthcare provider awareness, such as using electronic medical record alerts or working with clinical solutions platforms, such as UpToDate. Novel approaches, along with targeted provider education on *E. ewingii* ehrlichiosis in disease-endemic and emerging regions,

could address existing knowledge gaps, improve patient outcomes, and provide a better picture of the epidemiology of this emerging disease.

Acknowledgments

We thank the healthcare providers, laboratory workers, and public health partners for their dedication and work, which are indispensable to rickettsial disease surveillance, and Naomi Drexler and Kristen Nichols Heitman for their guidance and work on the study data.

This work was partly supported by a Research Participation Program fellowship (to S.N.A.) at CDC, administered by the Oak Ridge Institute for Science and Education through an interagency agreement between the US Department of Energy and CDC.

About the Author

Ms. Adams is an Oak Ridge Institute for Science and Education Research Participation Program fellow in the Rickettsial Zoonoses Branch, Division of Vector-Borne Diseases, National Center for Emerging and Zoonotic Infectious Diseases, Centers for Disease Control and Prevention, Atlanta, Georgia, USA. Her research interests focus on ehrlichiosis, murine typhus, and other zoonotic and vectorborne diseases.

References

1. Ismail N, McBride JW. Tick-borne emerging infections: ehrlichiosis and anaplasmosis. Clin Lab Med. 2017;37:317–40. https://doi.org/10.1016/j.cll.2017.01.006
2. Nichols Heitman K, Dahlgren FS, Drexler NA, Massung RF, Behravesh CB. Increasing incidence of ehrlichiosis in the United States: a summary of national surveillance of *Ehrlichia chaffeensis* and *Ehrlichia ewingii* infections in the United States, 2008–2012. Am J Trop Med Hyg. 2016;94:52–60. https://doi.org/10.4269/ajtmh.15-0540
3. Paddock CD, Folk SM, Shore GM, Machado LJ, Huycke MM, Slater LN, et al. Infections with *Ehrlichia chaffeensis* and *Ehrlichia ewingii* in persons coinfected with human immunodeficiency virus. Clin Infect Dis. 2001;33:1586–94. https://doi.org/10.1086/323981
4. Thomas LD, Hongo I, Bloch KC, Tang YW, Dummer S. Human ehrlichiosis in transplant recipients. Am J Transplant. 2007;7:1641–7. https://doi.org/10.1111/j.1600-6143.2007.01821.x
5. Barenfanger J, Patel PG, Dumler JS, Walker DH. Identifying human ehrlichiosis. Lab Med. 1996;27:372–4. https://doi.org/10.1093/labmed/27.6.372
6. Regan J, Matthias J, Green-Murphy A, Stanek D, Bertholf M, Pritt BS, et al. A confirmed *Ehrlichia ewingii* infection likely acquired through platelet transfusion. Clin Infect Dis. 2013;56:e105–7. https://doi.org/10.1093/cid/cit177
7. Antony SJ, Dummer JS, Hunter E. Human ehrlichiosis in a liver transplant recipient. Transplantation. 1995;60:879–81. https://doi.org/10.1097/00007890-199510270-00021
8. Sadikot R, Shaver MJ, Reeves WB. *Ehrlichia chaffeensis* in a renal transplant recipient. Am J Nephrol. 1999;19:674–6. https://doi.org/10.1159/000013540
9. Lawrence KL, Morrell MR, Storch GA, Hachem RR, Trulock EP. Clinical outcomes of solid organ transplant recipients with ehrlichiosis. Transpl Infect Dis. 2009;11:203–10. https://doi.org/10.1111/j.1399-3062.2009.00373.x
10. Paddock CD, Childs JE. *Ehrlichia chaffeensis*: a prototypical emerging pathogen. Clin Microbiol Rev. 2003;16:37–64. https://doi.org/10.1128/CMR.16.1.37-64.2003
11. Chapman AS, Bakken JS, Folk SM, Paddock CD, Bloch KC, Krusell A, et al.; Tickborne Rickettsial Diseases Working Group; CDC. Diagnosis and management of tickborne rickettsial diseases: Rocky Mountain spotted fever, ehrlichioses, and anaplasmosis—United States: a practical guide for physicians and other health-care and public health professionals. MMWR Recomm Rep. 2006;55:1–27.
12. Council of State and Territorial Epidemiologists. Position statement 07-ID-03: revision of the national surveillance case definition for ehrlichiosis (ehrlichiosis/anaplasmosis). 2007 [cited 2024 Jan 7]. https://cdn.ymaws.com/www.cste.org/resource/resmgr/PS/07-ID-03.pdf
13. McCormick DW, Kugeler KJ, Marx GE, Jayanthi P, Dietz S, Mead P, et al. Effects of COVID-19 pandemic on reported Lyme disease, United States, 2020. Emerg Infect Dis. 2021;27:2715–7. https://doi.org/10.3201/eid2710.210903

Address for correspondence: Johanna Salzer, Centers for Disease Control and Prevention, 1600 Clifton Rd NE, Mailstop H24-12, Atlanta, GA 30329-4018, USA; email: hio7@cdc.gov

Streptococcus pyogenes emm Type 3.93 Emergence, the Netherlands and England

Matthew A. Davies,[1] Brechje de Gier,[1] Rebecca L. Guy, Juliana Coelho, Alje P. van Dam, Robin van Houdt, Sébastien Matamoros, Marit van den Berg, Patrick E. Habermehl, Kartyk Moganeradj, Yan Ryan, Steve Platt, Henry Hearn, Eleanor Blakey, Darren Chooneea, Bart J.M. Vlaminckx, Theresa Lamagni, Nina M. van Sorge

Medscape CME Activity

In support of improving patient care, this activity has been planned and implemented by Medscape, LLC and Emerging Infectious Diseases. Medscape, LLC is jointly accredited with commendation by the Accreditation Council for Continuing Medical Education (ACCME), the Accreditation Council for Pharmacy Education (ACPE), and the American Nurses Credentialing Center (ANCC), to provide continuing education for the healthcare team.

Medscape, LLC designates this Journal-based CME activity for a maximum of 1.00 ***AMA PRA Category 1 Credit(s)™***. Physicians should claim only the credit commensurate with the extent of their participation in the activity.

Successful completion of this CME activity, which includes participation in the evaluation component, enables the participant to earn up to 1.0 MOC points in the American Board of Internal Medicine's (ABIM) Maintenance of Certification (MOC) program. Participants will earn MOC points equivalent to the amount of CME credits claimed for the activity. It is the CME activity provider's responsibility to submit participant completion information to ACCME for the purpose of granting ABIM MOC credit.

All other clinicians completing this activity will be issued a certificate of participation. To participate in this journal CME activity: (1) review the learning objectives and author disclosures; (2) study the education content; (3) take the post-test with a 75% minimum passing score and complete the evaluation at https://www.medscape.org/qna/processor/73460?showStandAlone=true&src=prt_jcme_eid_mscpedu; and (4) view/print certificate. For CME questions, see page 415.

NOTE: It is Medscape's policy to avoid the use of Brand names in accredited activities. However, in an effort to be as clear as possible, trade names are used in this activity to distinguish between the mixtures and different tests. It is not meant to promote any particular product.

Release date: January 22, 2025; Expiration date: January 22, 2026

Learning Objectives

Upon completion of this activity, participants will be able to:

- Evaluate the epidemiology of invasive group A *Streptococcus* (iGAS) infections caused by *emm* type 3.93 (*emm*.393)
- Analyze age groups at high risk for iGAS caused by *emm*.393
- Distinguish anatomic sites with a higher propensity for iGAS caused by *emm*.393
- Assess the genomics of *emm*.393 in the current study

CME Editor

Bryce Simons, MPH, Technical Writer/Editor, Emerging Infectious Diseases. *Disclosure: Bryce Simons, MPH, has no relevant financial relationships.*

CME Author

Charles P. Vega, MD, Health Sciences Clinical Professor of Family Medicine, University of California, Irvine School of Medicine, Irvine, California. *Disclosure: Charles P. Vega, MD, has the following relevant financial relationships: served as consultant or advisor for Boehringer Ingelheim; GlaxoSmithKline.*

Authors

Matthew Davies, MSc, PhD; Brechje De Gier, MSc, PhD; Rebecca L. Guy, MSc; Juliana Coelho, PhD; Alje P. van Dam, MSc, MD, PhD; Robin van Houdt, MSc, PhD; Sébastien Matamoros, MSc, PhD; Marit van den Berg, BSc; Patrick H. Habermehl, BSc; Kartyk Moganeradj, BVSc, MSc, PhD; Yan Ryan, MSc, MRes, PhD; Steve Platt, MSc, PhD; Henry Hearn, MSc; Eleanor Blakey, MBio; Darren Chooneea, PhD; Bart J.M. Vlamincks, MSc, MD, PhD; Theresa Lamagni, MSc, PhD; Nina M. van Sorge, MSc, PharmD, PhD.

Author affiliations: Amsterdam University Medical Center, Amsterdam, the Netherlands (M.A. Davies, A.P. van Dam, R. van Houdt, S. Matamoros, M. van den Berg, P.E. Habermehl, N.M. van Sorge); National Institute for Public Health and the Environment, Bilthoven, the Netherlands (B. de Gier); UK Health Security Agency, London, UK (R.L. Guy, J. Coelho, K. Moganeradj, Y. Ryan, S. Platt, H. Hearn, E. Blakey, D. Chooneea, T. Lamagni); University Medical Center Utrecht, Utrecht, the Netherlands (B.J.M. Vlaminckx)

DOI: https://doi.org/10.3201/eid3102.240880

[1]These authors contributed equally.

A global increase in the incidence of invasive group A *Streptococcus* (iGAS) infections was observed after lifting of COVID-19 related restrictions in 2022, and type $M1_{UK}$ dominated in many countries. After seasonal declines in iGAS incidence during the summer of 2023, simultaneous, rapid expansion of a previously rare *emm* type 3.93 was seen beginning in November, increasing to 20% of all cases in England and 60% of all cases in the Netherlands within 4 months. *emm*3.93 was associated with iGAS in children 6–17 years of age and with increased risk for pneumonia or pleural empyema and meningitis in both countries. No excess risk of death was identified for *emm*3.93 compared with other types. Genomic analysis of historic and contemporary *emm*3.93 isolates revealed the emergence of 3 new clades with a potentially advantageous genomic configuration. Our findings demonstrate the value of molecular surveillance, including long-read sequencing, in identifying clinical and public health threats.

In several countries, including the Netherlands and England, an increase in invasive group A *Streptococcus* (iGAS) infections was observed after lifting of COVID-19 restrictions during 2022 and 2023 (*1*,*2*). The reason for this sudden upsurge has yet to be completely explained but likely resulted from a perfect storm scenario: an increased population susceptibility to *Streptococcus pyogenes* infections after 2 years of reduced circulation that coincided with an increased incidence of predisposing viral infections and further expansion of the *emm*1.0 sublineage $M1_{UK}$ (*3*), which produces increased amounts of the virulence factor and streptococcal pyrogenic exotoxin A compared with its progenitor, $M1_{global}$ (*3*). Similar to the case in other countries, *emm*1.0 was the dominant *emm* type in the Netherlands and England (*1*,*4*,*5*). However, beginning in June 2023, the proportion of *emm*1.0 among clinical *S. pyogenes* isolates diminished in the Netherlands and England, coinciding with a seasonal decrease in iGAS incidence. An increase in a previously rare type, *emm*3.93, was identified among iGAS patients in the Netherlands and England beginning in November 2023. We report a cross-border increase in iGAS with increased infections in particular age groups and specific clinical manifestations related to an *emm*3.93 variant that displays a previously unreported genome configuration.

Methods

S. pyogenes Isolate Collection, *emm* Typing, and Genome Sequencing

Beginning in April 2022, all medical microbiology laboratories in the Netherlands were asked to submit *S. pyogenes* isolates from patients with iGAS disease (defined as either the detection of *S. pyogenes* from a normally sterile site or from a nonsterile site in combination with a clinical manifestation of iGAS) to the Netherlands Reference Laboratory for Bacterial Meningitis (NRLBM; Amsterdam, the Netherlands) for *emm* typing as part of national bacterial surveillance. Isolates are submitted with limited patient information (patient birth year, sex, and postal code). In addition to recent isolates from prospective bacterial surveillance, we screened an existing bacterial isolate collection (*4*) consisting of *S. pyogenes* carriage isolates (2009–2023, n = 349) and iGAS disease (2009–2019, n = 272) for the presence of *emm*3.93. In England, medical microbiology laboratories were asked to submit *S. pyogenes* isolates to the UK Health Security Agency (London, UK) reference laboratory for *emm* typing as part of active surveillance.

We conducted *emm* genotyping according to US Centers for Disease Control and Prevention protocol (*6*) by using conventional PCR amplification and Sanger sequencing of a 180-bp domain encoding the 50 hypervariable codons that determine *emm* subtype. The *emm*3.93 sequence and information were provided by the National Health Service (NHS) of Greater Glasgow and Clyde, Scotland, UK. We found or generated short-read sequence (Illumina) data for 104 *emm*3.93 isolates, including 11 strains from the Netherlands, 9 from New Zealand, and 84 from England. In addition, we conducted long-read (Oxford Nanopore) sequencing on 14 of the *emm*3.93 isolates, 5 from the Netherlands and 9 from England, for hybrid assembly of the complete genome.

Raw sequencing data and complete genomes are available from the National Center for Biotechnology Information BioProject database (accession nos. PRJNA1125189, PRJEB43915, PRJEB13551, and PRJNA1100230). Sample accession numbers are provided (Appendix Table 1, https://wwwnc.cdc.gov/EID/article/31/2/24-0880-App1.pdf).

Genome Assembly

We processed raw Illumina reads by using Trimmomatic v0.39 (*7*) to remove adaptor sequences and bases of insufficient quality with the parameters ILLUMINACLIP:TruSeq3-SE:2:30:10 LEADING:3 TRAILING:3 SLIDINGWINDOW:4:15 MINLEN:36. We de novo assembled trimmed reads into scaffolds by using SPAdes v3.15.5 (*8*) and assessed assembly quality by using QUAST v5.0.2 (*9*). We processed raw Nanopore reads by using Porechop v0.2.4 (*10*) with default parameters and assembled the reads by using Flye v2.9.2 (*11*) with parameters -g 5.6m and -i 2. We

created closed genomes by using hybrid assembly via Unicycler v0.4.8 (*12*) with default parameters.

Detection of Genomic Rearrangements

To determine the presence of the genomic inversion, we annotated complete genomes by using bakta (*13*) then aligned and visualized the genomes by using EasyFig (*14*) and its default use of blastn (*15*). We determined the location of prophage sequences MGAS315.1 (RefSeq accession no. NC_004584.1) and MGAS315.2 (RefSeq accession no. NC_004585.1) by using blastN with default parameters. We produced whole genome alignment dotplots by using the web interface version of D-GENIES (*16*) via the built-in aligner, Mashmap v2.0.

Core Single-Nucleotide Polymorphism Phylogenetic Analysis

We created a core single-nucleotide polymorphism (SNP) alignment by calling SNPs by using snippy v4.6.0 against the reference genome MGAS315 (RefSeq accession no. NC_004070.1) with default parameters. We used Gubbins v2.3.4 (*17*) to detect and mask sites of recombination and performed a phylogenetic inference by maximum likelihood on the subsequent alignment by IQ-TREE (*18*) using the general time-reversible plus gamma plus invariate sites substitution model and visualizing in iTOL v6.9 (*19*). We determined the lineage-defining SNPs to be synonymous, nonsynonymous, or insertion or deletion by using snippy. We created the SNP distance matrix by using SNP-dists v0.8.2 and performed the hierarchical clustering and visualization by using the R package pheatmap (The R Project for Statistical Computing).

Clinical Information of iGAS Patients

In the Netherlands, clinical manifestations of iGAS with *S. pyogenes* cultured from any site are notifiable by law since January 2023. Pseudonymized notifications, which contain information on the clinical manifestations, onset, and *emm* type (when available), are analyzed by the National Institute for Public Health and the Environment (Bilthoven, the Netherlands). Unknown *emm* types are supplemented by probabilistic linkage of notifications to the NRLBM data on the basis of birth year, gender, postal code, and date of diagnosis.

In England, iGAS has been a notifiable disease since April 2010 (*20*). Notifications include date of birth, sex, postal code, and date of specimen collection. Clinical manifestation information is not collected, but the focus of infection is inferred from the specimen type, in particular, cerebrospinal fluid, pleural fluid, and synovial fluid specimens. All iGAS notifications were submitted to the NHS Demographic Batch Tracing Service to identify the date of death (*21*). We calculated all-cause death by using all deaths within 7 days of a positive iGAS specimen, including all postmortem diagnoses. We used multivariable logistic regression to assess all-cause death and to compare *emm*3.93 with other contemporaneous *emm* types. We retrieved antimicrobial susceptibility testing results from routine laboratory surveillance data.

Ethics Statement

This study was conducted in accordance with the European Statements for Good Clinical Practice and the Declaration of Helsinki of the World Medical Association. In the Netherlands, invasive *S. pyogenes* isolates were collected as part of routine care. This study was not reviewed by an ethics review board because it is based on anonymized surveillance data. UK Health Security Agency have legal permission under Regulation 3 of the Health Service (Control of Patient Information) Regulations 2002 to process patient identifiable information without consent. This process considers the ethics and purpose of collecting and analyzing the data; therefore, ethics approval was not separately sought for this work.

Results

*emm*3.93 Epidemiology among iGAS Patients

We extracted iGAS notifications with disease onset during November 1, 2023–March 31, 2024, from the notification databases of the Netherlands on April 11, 2024 (798 cases) and England on April 12, 2024 (1,510 cases). Of reported cases, 665 (83.3%) isolates from the Netherlands and 1,351 (89.5%) isolates from England had a known *emm* type. In both countries, the monthly number of submitted *S. pyogenes* isolates from iGAS patients showed a seasonal decrease during June–October 2023, coinciding with a decrease in the proportion of *emm*1.0 isolates (Figure 1). Beginning in November 2023, iGAS cases increased in line with usual seasonal patterns (Figure 1). Of note, the proportion of *emm*3.93 among typed iGAS isolates in the Netherlands increased from 8% (6/73) in November 2023 to 61% (126/207) in February 2024 and in England from 4% (8/219) in November 2023 to 24% (66/274) in March 2024 (Figure 1, 2). From available *S. pyogenes* isolates from the Netherlands in iGAS patients and asymptomatic carriers (2009–2019), *emm*3.93 was rare, with only 6/577 (1%) typed strains. Similarly, *emm*3.93 only constituted 3% (400/11,194) of *S. pyogenes* isolates in England during 2016–2019. A short

upsurge in prevalence to 9% (224/2,597) was seen in 2018, but afterward, *emm*3.93 strains decreased to <1% of typed isolates per year (*22*). Phenotypic antimicrobial susceptibility testing demonstrated low resistance to clindamycin (1.4%, 95% CI 0.0%–7.4%), erythromycin (1.4%, 95% CI 0.0%–7.5%), or tetracycline (0%, 95% CI 0%–4.4%) in *emm*3.93 specimens in England during November 2023–March 2024.

Clinical Manifestations and Case-Fatality Rate of *emm*3.93 Compared with Other *emm* Types

A multivariable logistic regression model with covariates age group, sex, and month of disease onset revealed that children 6–17 years of age had higher risk for iGAS caused by *emm*3.93 than for other *emm* types in both countries (Table 1). In addition, in England, *emm*3.93 also affected children 0–5 years of age more often (adjusted odds ratio [aOR] 1.7, 95% CI 1.1–2.8) (Table 1). Type *emm*3.93 was recovered less often from patients 18–44 years of age in both countries (Table 1). There was a slight association of *emm*3.93 with female sex compared with other types (aOR 1.4, 95% CI 1.0–1.8) in England, which was not observed in the Netherlands (Table 1).

Regarding clinical manifestations, *emm*3.93 was associated with pneumonia or pleural empyema in both countries and with streptococcal toxic shock syndrome (aOR 2.2, 95% CI 1.1–4.3) in the Netherlands (Table 1). Furthermore, *emm*3.93 was associated with an increased risk for meningitis (Table 1), which was significant in England (aOR 28.6, 95% CI 2.6–320.1) but not in the Netherlands (aOR 2.7, 95% CI 0.9–8.8). In the Netherlands, *emm*3.93 was less often recovered from patients with skin or soft tissue infections or puerperal iGAS infection (aOR 0.5, 95% CI 0.3–0.8) (Table 1).

All-cause 7-day case-fatality rate data were available for England only. Case-fatality rate for *emm*3.93 was 13.8% (95% CI 9.6%–18.9%, 32/232) compared with 12.0% (95% CI 10.2%–14.1%, 127/1,059) for other types during November 2023–March 2024. A multivariable logistic regression adjusting for age, sex, specimen month, and *emm* type (*emm*3.93 or other) did not identify a significant difference for 7-day deaths between types (aOR 1.2, 95% CI 0.8–1.8); however, significant differences were noted by age, group, and sex (Table 2).

Genomic Analysis of *emm*3.93 Isolates in 3 Emergent Clades

Phylogenetic analysis of the core SNP genomes of 104 *emm*3.93 of ST315 from the Netherlands, England, and New Zealand showed that recently expanded

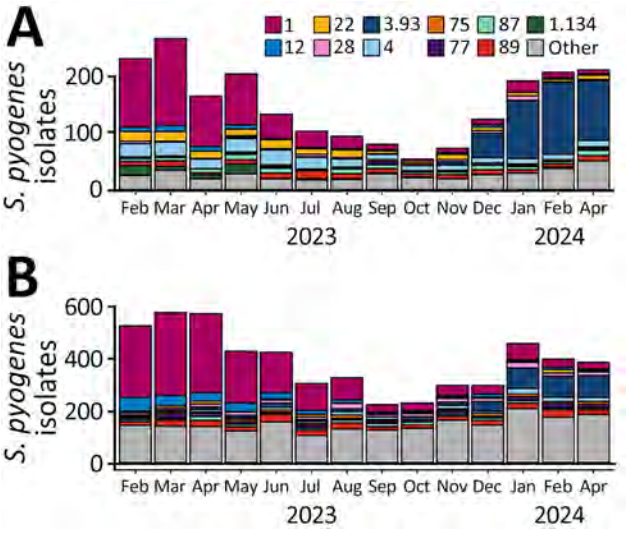

Figure 1. Absolute number of *Streptococcus pyogenes* isolates recovered from patients with invasive group A *Streptococcus*, by *emm* type and month, February 1, 2023–March 31, 2024. A) The Netherlands; B) England.

*emm*3.93 isolates clustered into 3 distinct clades (Figure 3, panel A). Clades were determined as clusters containing <10 core SNPs difference whereas between-clade SNP distance was typically 20–50 SNPs (Appendix Figure 1). Lineage-defining SNPs were determined by clade-specific SNP annotations against reference strain MGAS315 (Appendix Table 2). Clades 1 and 2 only contained isolates from England, whereas clade 3 consisted of a mix of isolates from the Netherlands and England (Figure 3, panel A).

We explored possible genomic rearrangements because previous studies have described distinct genome configurations among *emm*3 consensus reference genomes MGAS315 and SSI-1, where SSI-1 contained large-scale genomic rearrangements

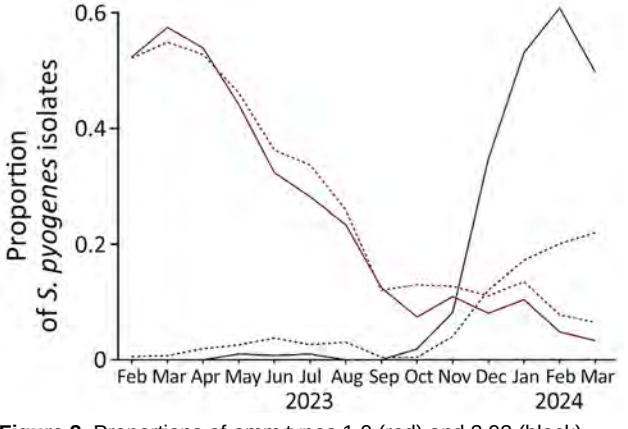

Figure 2. Proportions of *emm* types 1.0 (red) and 3.93 (black) among all typed invasive *Streptococcus pyogenes* isolates in the Netherlands (solid lines) and England (dashed lines), February 1, 2023–March 31, 2024.

compared with MGAS315 (*23*). Hybrid genome assembly for 14 *S. pyogenes emm*3.93 isolates (5 from the Netherlands and 9 from England) revealed that 12 isolates shared a genomic configuration that differed from MGAS315 by a ≈200-kb inversion around the terminus (*ter*) and from SSI-1 by a ≈521-kb inversion around the origin of replication (*ori*) (Figure 3, panel B; Appendix Figure 2). Of the 12 isolates, 11 belonged to *emm*3.93 surge isolates in each of the 3 clades and 1 was obtained from a patient with invasive disease from 2017 in England (Figure 3, panel A). The 200-kb genomic inversion around the *ter* is prophage-mediated and results in the movement of phage-encoded superantigen gene *ssa* and *holin* genes between prophages MGAS315.1 and MGAS315.2 (*24*) (Figure 3, panel B). The ≈521-kb inversion around the *ori* is spanned by 2 repeat regions of 6,200 bp (Figure 3, panel B). The inversions around the *ori* and the *ter* can occur independently, as indicated by strain ABC020055675, which lacks prophages MGAS315.1

Table 1. Characteristics of patients with invasive group A *Streptococcus* infection in the Netherlands and England caused by *emm*3.93 or other *emm* types during November 1, 2023–March 31, 2024*

	The Netherlands				England			
Characteristic	*emm*3.93, no. (%)	Other *emm* type, no. (%)	aOR (95% CI)	p value	*emm*3.93, no. (%)	Other *emm* type, no. (%)	aOR (95% CI)	p value
No. patients	319	346			240	1,158		
Age group, y								
0–5	23 (7.2)	17 (4.9)	1.5 (0.7–3.2)	0.2675	30 (12.5)	93 (8.0)	1.7 (1.1–2.8)	0.030
6–17	33 (10.3)	16 (4.6)	2.4 (1.2–5.0)	0.0139	30 (12.5)	60 (5.2)	2.4 (1.4–3.9)	0.001
18–44	65 (20.4)	112 (32.4)	0.6 (0.4–0.9)	0.0204	31 (12.9)	284 (24.5)	0.6 (0.4–0.9)	0.022
45–64	76 (23.8)	84 (24.3)	0.9 (0.6–1.3)	0.5046	63 (26.3)	258 (22.3)	1.4 (0.9–2.0)	0.103
≥65	122 (38.2)	117 (33.8)	Referent		86 (35.8)	463 (40.0)	Referent	
Sex								
M	151 (47.3)	159 (46.0)	Referent		123 (51.3)	667 (57.6)	Referent	
F	168 (52.7)	187 (54.0)	1.1 (0.8–1.5)	0.5416	115 (47.9)	477 (41.2)	1.4 (1.0–1.8)	0.033
STSS								
No	265 (88.9)	318 (95.2)	Referent					
Yes	33 (11.1)	16 (4.8)	2.2 (1.1–4.3)	0.0225				
Necrotizing fasciitis								
No	279 (93.6)	302 (90.4)	Referent					
Yes	19 (6.4)	32 (9.6)	0.7 (0.4–1.4)	0.3468				
Puerperal fever or sepsis								
No	270 (90.6)	273 (81.7)	Referent					
Yes	28 (9.4)	61 (18.3)	0.5 (0.3–0.8)	0.004				
Meningitis†								
No	286 (96.0)	328 (98.2)	Referent		228 (98.3)	1,058 (99.9)	Referent	
Yes	12 (4.0)	6 (1.8)	2.7 (0.9–8.8)	0.0818	4 (1.7)	1 (0.1)	28.6 (2.6–320.1)	0.006
Bone or joint infection‡								
No	271 (90.9)	312 (93.4)	Referent		221 (95.3)	1,006 (95.0)	Referent	
Yes	27 (9.1)	22 (6.6)	1.2 (0.6–2.4)	0.586	11 (4.7)	53 (5.0)	1.1 (0.6–2.3)	0.858
Pneumonia/pleural empyema§								
No	217 (72.8)	298 (89.2)	Referent		218 (94.3)	1,039 (98.1)	Referent	
Yes	81 (27.2)	36 (10.8)	2.9 (1.9–4.6)	<0.001	14 (6.0)	20 (1.9)	3.4 (1.6–73)	0.001
Cardiovascular infection								
No	297 (99.7)	329 (98.5)	Referent					
Yes	1 (0.3)	5 (1.5)	0.2 (0.0–1.8)	0.2252				
Skin and soft tissue infection								
No	260 (87.2)	264 (79.0)	Referent					
Yes	38 (12.8)	70 (21.0)	0.5 (0.3–0.8)	0.0032				
Sepsis								
No	231 (77.5)	240 (71.9)	Referent					
Yes	67 (22.5)	94 (28.1)	0.7 (0.5–1.0)	0.055				
Month								
2023 Nov	4 (1.3)	63 (18.2)	Referent		9 (3.8)	218 (18.8)	Referent	
2023 Dec	60 (18.8)	74 (21.4)	12.5 (4.8–43.2)	<0.0001	44 (18.3)	223 (19.3)	4.7 (2.2–9.9)	<0.0001
2024 Jan	86 (27.0)	73 (21.1)	19.1 (7.3–65.6)	<0.0001	61 (25.4)	258 (22.3)	5.7 (2.8–11.8)	<0.0001
2024 Feb	102 (32.0)	69 (19.9)	24.1 (9.3–82.6)	<0.0001	62 (25.8)	227 (19.6)	6.3 (3.1–13.2)	<0.0001
2024 Mar	67 (21.0)	67 (19.4)	14.8 (5.7–51.2)	<0.0001	64 (26.7)	232 (20.0)	6.7 (3.2–13.8)	<0.0001

*Odds ratios for age group, sex, and month are derived from a multivariable model containing those 3 variables. Odds ratios for clinical manifestations are adjusted for age group, sex, and month, but the puerperal fever or sepsis aOR is adjusted for month only. aOR, adjusted odds ratio; STSS, streptococcal toxic shock syndrome.
†Cerebral spinal fluid specimens used as proxy in data from England.
‡Joint or synovial fluid specimens used for data from England.
§Pleural specimens used as proxy for data from England.

Table 2. Characteristics of patients with invasive group A *Streptococcus* infection caused by *emm*3.93 or other *emm* types according to whether all-cause death was recorded within 7 days of diagnosis, November 1, 2023–March 31, 2024, England*

Characteristics	Died within 7 days, no. (%)	Alive at 7 days, no. (%)	aOR (95% CI)	p value
No. patients	159	1,132		
emm type				
Other	127 (12.0)	932 (88.0)	Referent	
*emm*3.93	32 (13.8)	200 (86.2)	1.2 (0.8–1.8)	0.501
Age group, y				
0–17	11 (5.7)	182 (94.3)	0.3 (0.1–0.5)	<0.0001
18–44	10 (3.5)	276 (96.5)	0.2 (0.1–0.3)	<0.0001
45–64	42 (14.4)	250 (85.6)	0.7 (0.5–1.1)	0.146
≥65+	96 (18.5)	424 (82.5)	Referent	
Sex				
M	77 (10.6)	651 (89.4)	Referent	
F	82 (14.6)	481 (85.4)	1.4 (1.0–2.0)	0.045
Month				
2023 Nov	24 (11.4)	187 (88.6)	Referent	
2023 Dec	32 (12.8)	218 (87.2)	1.1 (0.6–2.0)	0.663
2024 Jan	44 (14.9)	251 (85.1)	1.3 (0.8–2.3)	0.339
2024 Feb	34 (12.6)	237 (87.4)	1.2 (0.7–2.1)	0.583
2024 Mar	25 (9.5)	239 (90.5)	0.8 (0.4–1.5)	0.503

*Odds ratios for *emm* type, age group, sex, and month are derived from a multivariable model containing these 4 variables. aOR, adjusted odds ratio.

and MGAS315.2 (Figure 3, panel B; Appendix Figure 2). Of interest, the genomic configuration of the remaining 2 isolates was identical to the consensus MGAS315 genome (Appendix Figure 2). One isolate was obtained from a patient with invasive disease in 2017 in the Netherlands with a common ancestor to clade 3 and the other from a patient with noninvasive infection from clade 1 (Figure 3, panel A). Although we analyzed a limited number of strains, our observations suggest the described genome configuration in the 11 recent *emm*3.93 isolates confers a survival advantage to *S. pyogenes*.

Discussion

We report the rapid synchronous upsurge of *S. pyogenes emm* type 3.93 in the Netherlands and England during November 2023–March 2024. Epidemiologic analysis showed that *emm*3.93 was isolated more often from children 6–17 years of age with iGAS in both countries. The data from the Netherlands revealed a significant association between *emm*3.93 and pneumonia or pleural empyema, which was corroborated by an increase of *emm*3.93 among pleural isolates in England. Although the numbers were low, *emm*3.93 showed an increased risk for causing meningitis, which was significant in the data from England. Furthermore, *emm*3.93 was associated with streptococcal toxic shock syndrome in the Netherlands. Despite those concerning associations, the data from England showed no significant elevation in 7-day mortality for *emm*3.93 compared with mortality associated with other contemporaneous *emm* types.

Genomic analysis revealed 3 distinct clades among recent *emm*3.93 surge isolates. Clades 1 and 2 consisted only of isolates from England, whereas *emm*3.93 clade 3 contained a mix of isolates from the Netherlands and England. This analysis contrasts with previous analysis of the post–COVID-19 *emm*1 iGAS isolates, which showed predominantly country-specific surges of *emm*1 and little evidence of transmission of UK isolates to the Netherlands (*4*,*5*). This finding suggests that *emm*3.93 has had cross-border transmission events.

Analysis of complete genomes revealed a shared genomic configuration in all but 1 recent isolate from the 3 observed clades. When compared with other publicly available *emm*3 consensus reference genomes, the genomic configuration differed by either a ≈200-kb inversion around the *ter* or a ≈521-kb inversion around the *ori*. An identical genomic configuration was also identified in an invasive *emm*3.93 isolate from England from 2017, suggesting that this genome configuration was already circulating in the population before the surge. Of interest, *emm*3.93 caused a small surge of iGAS in England in 2018 (*22*) but did not expand to the levels observed in 2023–2024, nor did other countries report an increase in iGAS caused by *emm*3.93. We speculate that this 2017 isolate from England could have been a precursor to the 2023–2024 surge isolates but did not have a major advantage in the pre–COVID-19 climate because of sufficient population immunity.

Inverted repeats between prophages MGAS315.1 and MGAS315.2 have likely permitted the observed prophage-mediated homologous recombination. This phenomenon has been observed before in *emm*3.1 strains, which contained an alternative large-scale genomic rearrangement of 1 Mb because of chromosomal inverted repeats and was associated with invasive disease (*23*). However, because the inversion

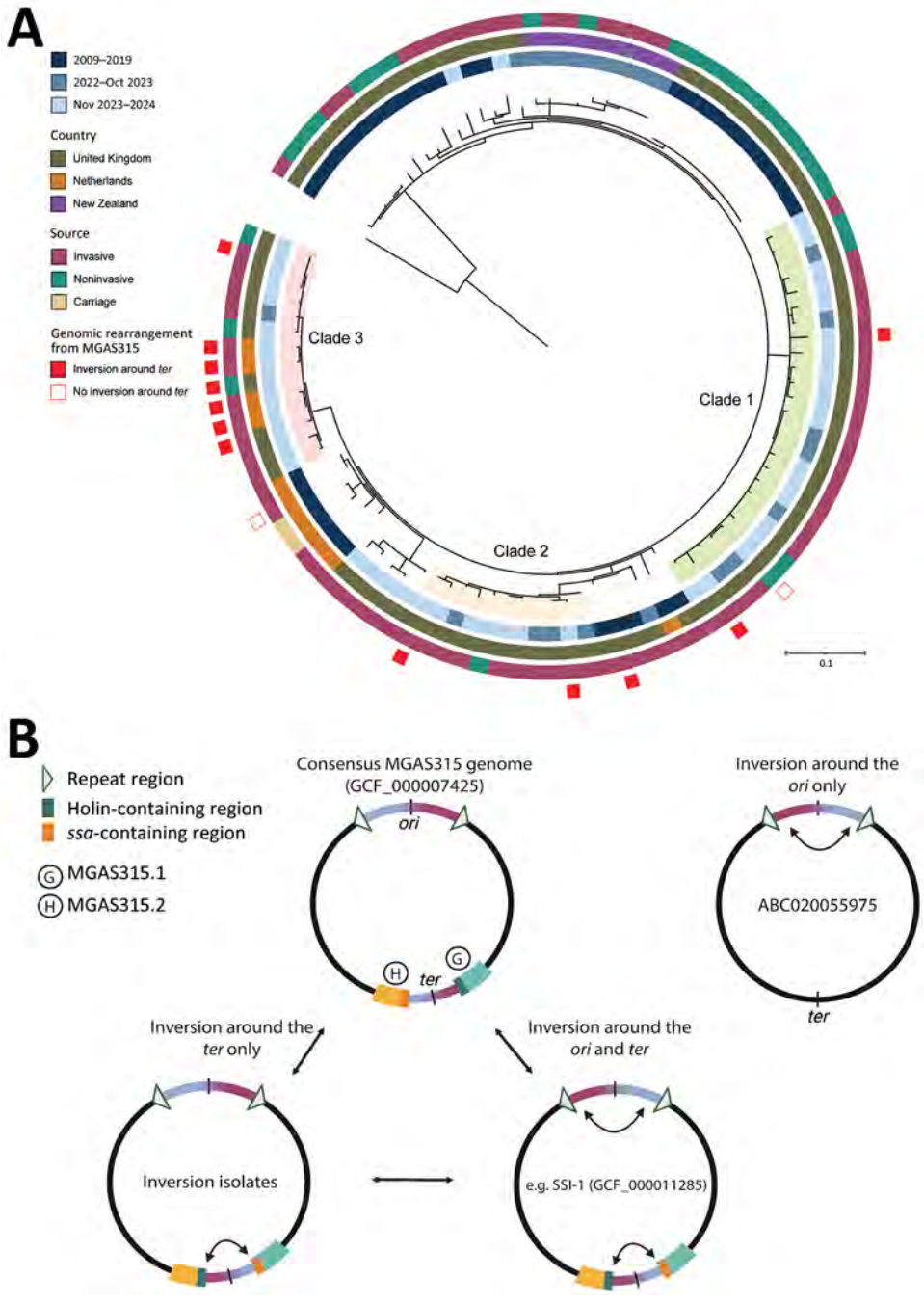

Figure 3. Genetic information about *emm*3.93 *Streptococcus pyogenes* isolates collected in the Netherlands and England, February 1, 2023–March 31, 2024, and reference isolates. A) Maximum-likelihood phylogenetic tree of 114 parsimony informative sites and 255 distinct site patterns from the core genome single-nucleotide polymorphism alignment of 104 *emm*3.93 isolates from the Netherlands, England, and New Zealand (2009–2024), compared with MGAS315 reference genome (RefSeq accession no. GCF_000007425). The tree was rooted on MGAS315, and colored rings outside the tree represent year of isolation, country, source, and presence of genomic inversion around the *ter*. Scale bar represents substitutions per site. B) Schematic of the 4 genomic conformations detected in the *emm*3 lineage. When compared with the consensus reference genome of strain MGAS315, an inversion around both the *ori* and *ter*, or around the *ter* alone (as detected in 11/12 surge isolates) is observed. Genome ABC020055975 indicates a strain lacking prophages MGAS315.1 and MGAS315.2 but with a detected inversion around the *ori*. G, MGAS315.1; H, MGAS315.2.

around the *ori* is also detected in an isolate without prophages MGAS315.1 and MGAS315.2 and without the inversion around the *ter*, we propose an updated view of the relationship between genomic configurations within *emm*3 *S. pyogenes*.

Because only single complete genomes are available of each of the reference strains, only a snapshot of the genomic configuration is being represented and then determined as consensus. Although our analysis of the individual isolates did not indicate a mixed population of inverted and noninverted genomes, care should be taken when interpreting the stability of an inversion that may occur in recombination hot spots with inverted homologous regions (*25*), because the switch back to its previous configuration may occur stochastically. For example, a recent emergent *emm*82 strain was detected to display an array of genome configurations among closely related isolates (*26*). Regardless, further information on the frequencies and selective pressures that cause

inversions needs to be determined to make strong associations with epidemiologic data. Our dataset provided 2 observations that may suggest the observed genome configuration in the surge isolates conferred a survival benefit or affected virulence (*27*). First, an isolate from 2017 sharing a close common ancestor with the strains in clade 3 lacked the ≈200-kb inversion around the terminus and did not expand among iGAS patients. Second, we identified a single recent isolate in clade 1 without the surge-associated genomic configuration. Because the isolate was collected from a noninvasive wound swab, we speculate that specific genomic inversions are preferentially selected for during an infection pathway. The orientation in the recent surge isolates may affect virulence potential by shifting the location of the phage-encoded superantigen gene *ssa*, which was previously shown to be pyrogenic and toxic in rabbits (*28*). Additional research is needed to demonstrate if the observed genomic inversion affects *ssa* expression. Regardless, this clade 1 isolate demonstrates the dynamic nature and stochasticity of genome rearrangements within the *emm*3 population.

The first limitation of our study is the difference between the clinical data collected in the Netherlands and England with the lack of formal registration for death after infection in the Netherlands. The second limitation is the low number of genomes sequenced from isolates from the Netherlands collected during the recent outbreak. Although all 4 recent *emm*3.93 isolates from the Netherlands are in a single clade, other nonsequenced isolates might fall into the other outbreak-associated clades.

In conclusion, combined epidemiologic and molecular surveillance is key to detect emergence of new or more virulent *S. pyogenes* variants and to rapidly assess their clinical and epidemiologic relevance. *emm* typing revealed a replacement of *emm*1.0 by *emm*3.93 as the dominant type from November 2023 onwards, continuing over a few months. It is possible that population immunity to *emm*1.0 developed during 2023, leaving increased susceptibility to potentially new virulence traits of the new clades of *emm*3.93. Alternatively, the genomic inversion may have resulted in a competitive advantage of *emm*3.93 over *emm*1.0. In the context of the current upsurge of *S. pyogenes emm*3.93, international collaboration proved invaluable to assess the spread of the new clades and provide a more comprehensive picture of the associations of *emm*3.93 with both clinical manifestations and case fatality. In addition, a combination of long- and short-read sequencing was necessary to reveal the extent of genetic diversity for the emerged *emm*3.93 clades.

Acknowledgments

We thank Roisin Ure for providing the *emm*3.93 sequence and information. We thank Una Ren and our colleagues of the Institute of Environmental Science and Research in New Zealand for sharing genome sequences of recent *emm*3.93 strains. We thank all microbiology laboratories for submitting isolates to the UK Health Security Agency national reference laboratory and the Netherlands Reference Laboratory for Bacterial Meningitis. This report would not have been possible without the contribution of clinical and laboratory colleagues across the healthcare systems in England and the Netherlands. We thank the Centers for Disease Control for maintaining and updating the *emm* database.

This study was funded in part by the Dutch Research Council through the research program Infectieziektebestrijding 3 (BEATGAS project grant no. 10150022310004, awarded to N.M.v.S., M.A.D., B.d.G., and B.J.M.V.). This study was funded in part by the Dutch Ministry of Health, Welfare, and Sport. All work was performed as part of service delivery of the contributing authors for UK Health Security Agency.

About the Author

Dr. Davies is a postdoctoral fellow with the Amsterdam University Medical Center. His current work focuses on streptococcal genomics in the context of public health and disease pathogenesis.

References

1. de Gier B, Marchal N, de Beer-Schuurman I, Te Wierik M, Hooiveld M, de Melker HE, et al.; ISIS-AR Study Group; GAS Study group; Members of the GAS study group; Members of the ISIS-AR study group. Increase in invasive group A streptococcal (*Streptococcus pyogenes*) infections (iGAS) in young children in the Netherlands, 2022. Euro Surveill. 2023;28:28. https://doi.org/10.2807/1560-7917.ES.2023.28.1.2200941
2. Guy R, Henderson KL, Coelho J, Hughes H, Mason EL, Gerver SM, et al. Increase in invasive group A streptococcal infection notifications, England, 2022. Euro Surveill. 2023;28:28.https://doi.org/10.2807/1560-7917.ES.2023.28.1.2200942
3. Lynskey NN, Jauneikaite E, Li HK, Zhi X, Turner CE, Mosavie M, et al. Emergence of dominant toxigenic M1T1 *Streptococcus pyogenes* clone during increased scarlet fever activity in England: a population-based molecular epidemiological study. Lancet Infect Dis. 2019;19:1209–18. https://doi.org/10.1016/S1473-3099(19)30446-3
4. Rümke LW, Davies MA, Vestjens SMT, van der Putten BCL, Bril-Keijzers WCM, van Houten MA, et al. Nationwide upsurge in invasive disease in the context of longitudinal surveillance of carriage and invasive *Streptococcus pyogenes* 2009–2023, the Netherlands: a molecular epidemiological study. J Clin Microbiol. 2024;62:e0076624. https://doi.org/10.1128/jcm.00766-24
5. Vieira A, Wan Y, Ryan Y, Li HK, Guy RL, Papangeli M, et al. Rapid expansion and international spread of $M1_{UK}$ in

the post-pandemic UK upsurge of *Streptococcus pyogenes*. Nat Commun. 2024;15:3916. https://doi.org/10.1038/s41467-024-47929-7
6. Centers for Disease Control and Prevention. Streptococcus laboratory. April 8, 2024 [cited 2024 Apr 22] https://www.cdc.gov/strep-lab/php/group-a-strep
7. Bolger AM, Lohse M, Usadel B. Trimmomatic: a flexible trimmer for Illumina sequence data. Bioinformatics. 2014;30:2114–20. https://doi.org/10.1093/bioinformatics/btu170
8. Bankevich A, Nurk S, Antipov D, Gurevich AA, Dvorkin M, Kulikov AS, et al. SPAdes: a new genome assembly algorithm and its applications to single-cell sequencing. J Comput Biol. 2012;19:455–77. https://doi.org/10.1089/cmb.2012.0021
9. Gurevich A, Saveliev V, Vyahhi N, Tesler G. QUAST: quality assessment tool for genome assemblies. Bioinformatics. 2013;29:1072–5. https://doi.org/10.1093/bioinformatics/btt086
10. Wick RR, Judd LM, Gorrie CL, Holt KE. Completing bacterial genome assemblies with multiplex MinION sequencing. Microb Genom. 2017;3:e000132. https://doi.org/10.1099/mgen.0.000132
11. Kolmogorov M, Yuan J, Lin Y, Pevzner PA. Assembly of long, error-prone reads using repeat graphs. Nat Biotechnol. 2019;37:540–6. https://doi.org/10.1038/s41587-019-0072-8
12. Wick RR, Judd LM, Gorrie CL, Holt KE. Unicycler: resolving bacterial genome assemblies from short and long sequencing reads. PLOS Comput Biol. 2017;13:e1005595. https://doi.org/10.1371/journal.pcbi.1005595
13. Schwengers O, Jelonek L, Dieckmann MA, Beyvers S, Blom J, Goesmann A. Bakta: rapid and standardized annotation of bacterial genomes via alignment-free sequence identification. Microb Genom. 2021;7:7. https://doi.org/10.1099/mgen.0.000685
14. Sullivan MJ, Petty NK, Beatson SA. Easyfig: a genome comparison visualizer. Bioinformatics. 2011;27:1009–10. https://doi.org/10.1093/bioinformatics/btr039
15. Altschul SF, Gish W, Miller W, Myers EW, Lipman DJ. Basic local alignment search tool. J Mol Biol. 1990;215:403–10. https://doi.org/10.1016/S0022-2836(05)80360-2
16. Cabanettes F, Klopp C. D-GENIES: dot plot large genomes in an interactive, efficient and simple way. PeerJ. 2018;6:e4958. https://doi.org/10.7717/peerj.4958
17. Croucher NJ, Page AJ, Connor TR, Delaney AJ, Keane JA, Bentley SD, et al. Rapid phylogenetic analysis of large samples of recombinant bacterial whole genome sequences using Gubbins. Nucleic Acids Res. 2015;43:e15. https://doi.org/10.1093/nar/gku1196
18. Nguyen LT, Schmidt HA, von Haeseler A, Minh BQ. IQ-TREE: a fast and effective stochastic algorithm for estimating maximum-likelihood phylogenies. Mol Biol Evol. 2015;32:268–74. https://doi.org/10.1093/molbev/msu300
19. Letunic I, Bork P. Interactive tree of life (iTOL) v5: an online tool for phylogenetic tree display and annotation. Nucleic Acids Res. 2021;49:W293–6. https://doi.org/10.1093/nar/gkab301
20. Department of Health and Social Care. Health protection legislation (England) guidance 2010. 2010 [cited 2024 Apr 22] https://www.legislation.gov.uk/uksi/2010/659
21. National Health Service England. The NHS Spine. 2023 [cited 2024 Apr 22] https://digital.nhs.uk/services/spine
22. UK Health Security Agency. Group A streptococcal infections: fourth update on seasonal activity in England, 2023 to 2024. 2024 [cited 2024 Apr 22] https://www.gov.uk/government/publications/group-a-streptococcal-infections-report-on-seasonal-activity-in-england-2023-to-2024
23. Nakagawa I, Kurokawa K, Yamashita A, Nakata M, Tomiyasu Y, Okahashi N, et al. Genome sequence of an M3 strain of *Streptococcus pyogenes* reveals a large-scale genomic rearrangement in invasive strains and new insights into phage evolution. Genome Res. 2003;13:1042–55. https://doi.org/10.1101/gr.1096703
24. McShan WM, Nguyen SV. The bacteriophages of *Streptococcus pyogenes*. 2016 edition. Oklahoma City (OK): University of Oklahoma Health Sciences Center; 2016.
25. Mackiewicz P, Mackiewicz D, Kowalczuk M, Cebrat S. Flip-flop around the origin and terminus of replication in prokaryotic genomes. Genome Biol. 2001;2:INTERACTIONS1004. https://doi.org/10.1186/gb-2001-2-12-interactions1004
26. Unoarumhi Y, Davis ML, Rowe LA, Mathis S, Li Z, Chochua S, et al. A novel invasive *Streptococcus pyogenes* variant sublineage derived through recombinational replacement of the emm12 genomic region. Sci Rep. 2023;13:21510. https://doi.org/10.1038/s41598-023-48035-2
27. Jespersen MG, Hayes AJ, Tong SYC, Davies MR. Insertion sequence elements and unique symmetrical genomic regions mediate chromosomal inversions in *Streptococcus pyogenes*. Nucleic Acids Res. 2024;52:13128–37. https://doi.org/10.1093/nar/gkae948
28. Beres SB, Sylva GL, Barbian KD, Lei B, Hoff JS, Mammarella ND, et al. Genome sequence of a serotype M3 strain of group A streptococcus: phage-encoded toxins, the high-virulence phenotype, and clone emergence. Proc Natl Acad Sci USA. 2002;99:10078–83. https://doi.org/10.1073/pnas.152298499

Address for correspondence: Nina M. van Sorge, Amsterdam UMC, Department of Medical Microbiology and Infection Prevention, Meibergdreef 9 IWO building, 1105 AZ Amsterdam, the Netherlands; email: n.m.vansorge@amsterdamumc.nl

Short-Lived Neutralizing Antibody Responses to Monkeypox Virus in Smallpox Vaccine–Naive Persons after JYNNEOS Vaccination

Kara Phipps, Jennifer Yates, Jessica Pettit, Sean Bialosuknia, Danielle Hunt, Alan P. DuPuis II, Anne Payne, William Lee, Kathleen A. McDonough

JYNNEOS, a third-generation smallpox vaccine, is integral to monkeypox virus (MPXV) control efforts, but the durability of this modified vaccinia Ankara–Bavarian Nordic (MVA-BN) vaccine's effectiveness is undefined. We optimized and used a plaque reduction neutralization test (PRNT) with authentic clade IIa MPXV and vaccinia virus to assess antibody responses over 12 months in 8 donors vaccinated with 2 doses of JYNNEOS. One donor previously received the ACAM2000 vaccine; 7 donors were smallpox vaccine–naive. IgG responses of the donors to vaccinia virus (L1, B5, and A33) or MPXV (E8, H3, A35) antigens and PRNT titers to both viruses peaked at 8 weeks postvaccination and waned rapidly thereafter in naive donors. MPXV PRNT titers were especially low; no naive donors demonstrated 90% plaque reduction. These data indicate a need for improved correlates of MPXV immunity to enable MVA-BN durability studies, given that recent clinical data support MVA-BN vaccine efficacy against MPXV despite low antibody responses.

Monkeypox virus (MPXV), the causative agent of mpox disease, is an ongoing public health concern in the United States and internationally. In 2022, a large global outbreak of mpox spread primarily among men who have sex with men. The 2022 outbreak heightened awareness of the need for preventive measures against transmission and severe mpox disease, triggering a public health campaign that included recommending behavioral changes and vaccination with the modified vaccinia Ankara–Bavarian Nordic (MVA-BN) vaccine JYNNEOS (Bavarian Nordic, https://www.bavarian-nordic) for populations most at risk. MPXV infection is considered endemic in areas of central and western Africa, where it causes thousands of cases annually and where a current multicountry outbreak of clade Ib MPXV infection has escalated to what the World Health Organization has declared a Public Health Emergency of International Concern (*1*,*2*).

MPXV is a member of the *Orthopoxvirus* genus and is related to variola virus, the causative agent of smallpox, and to less virulent genus members, including cowpox virus and vaccinia virus (VACV). Vaccination with VACV provided protection from smallpox and led to its eradication. VACV-based smallpox vaccines are expected to protect against mpox because of cross-reactivity between VACV and MPXV antigens (*3*,*4*). First- and second-generation smallpox vaccines, which consist of replication competent strains of vaccinia, are not recommended for the general population because of potentially severe or fatal side effects for some persons, including those with HIV (*5*). MVA-BN is considered a safer, third-generation smallpox vaccine because it is a highly passaged vaccinia strain; however, unlike prior smallpox vaccines, MVA-BN does not replicate in humans.

Understanding of the protection MVA-BN provides against MPXV is incomplete and emerging. The US Food and Drug Administration approved use of MVA-BN for mpox prevention under the brand name JYNNEOS (Bavarian Nordic) in 2019 (*6*), whereas the European Medicines Agency approved it under the brand name IMVANEX in 2022 (*7*). Epidemiologic studies from the United States support vaccine efficacy for MVA-BN and have estimated its effectiveness against mpox to range from 66% to 88.5% in

Author affiliations: Wadsworth Center, New York State Department of Health, Albany, New York, USA (K. Phipps, J. Yates, J. Pettit, S. Bialosuknia, D. Hunt, A.P. DuPuis II, A. Payne, W. Lee, K.A. McDonough); University at Albany, Albany (J. Yates, K.A. McDonough)

DOI: https://doi.org/10.3201/eid3102.241300

fully vaccinated persons (*8*–*11*). However, duration for many of those studies was <1 year after the peak of MVA-BN vaccine administration in the United States, so the potential for waning efficacy was not fully captured. Determining the role of MVA-BN in quelling the mpox outbreak in the United States has been challenging because the effects of behavioral changes on mpox transmission are difficult to quantify. Paredes et al. (*12*) modeled infection rates during the 2022 epidemic and concluded that mpox transmission dropped dramatically before vaccination-induced immunity could play a role. Virus-specific neutralizing antibody (nAb) titers are considered an indicator of the smallpox vaccination response and have served as a metric for evaluating noninferiority in clinical studies of MVA-BN (*13*,*14*). We characterized the durability of nAb response generated by the JYNNEOS vaccine to MPXV in a small cohort of naive donors by using a native MPXV plaque reduction neutralization test (PRNT).

Materials and Methods

Samples and Ethics

We conducted this assay development study by using deidentified serum and plasma samples for a public health function in a declared Public Health Emergency. This activity has been deemed non–human subjects research by the New York State Institutional Review Board. The vaccinee cohort consists of serum samples from 8 New York State Department of Health employee donors who were vaccinated with JYNNEOS because of potential occupational exposure.

Recombinant Orthopoxvirus Antigens

We obtained recombinant proteins from several sources. We obtained recombinant A33 (VAC-WR-A33R), B5 (VAC-WR-B5R), and L1 (VAC-WR-L2R) from BEI Resources. We purchased mpox A35, E8, and H3 from Ray Biotech (https://www.raybiotech.com).

Orthopoxvirus-Specific Multiplex Microsphere Immunoassay

We assessed specimens for the presence of antibodies reactive to orthopoxvirus antigens by using a multiplex microsphere immunoassay, as previously described (*15*). We linked recombinant proteins covalently to the surface of fluorescent, magnetic microspheres (Luminex MagPlex Microspheres; Diasorin, https://us.diasorin.com). We mixed serum or plasma samples (25 μL at 1:100 dilution) and antigen-coupled microspheres (25 μL at 5×10^4 microspheres/mL, per manufacturer instructions) and incubated them for 30 minutes at 37°C. We washed serum-bound microspheres and incubated them with phycoerythrin-conjugated secondary antibody specific for human IgG (Southern Biotech, https://www.southernbiotech.com). After washing and final resuspension of samples in buffer, we analyzed them on a FlexMap 3D analyzer (Diasorin) by using xPONENT version 4.3 (Diasorin).

Calculation of Cutoffs and Index Values

We generated receiving operator characteristic (ROC) curves in GraphPad Prism 9.1.0 (https://www.graphpad.com) for each antigen on the basis of the mean fluorescence intensity (MFI) values of 120 MPXV-negative donors born after 1970 and 40 MPXV-positive confirmed donors, as previously described (*15*). We used sensitivity and specificity values generated by the ROC curve to calculate cutoffs with a Youden J index (J = sensitivity + specificity – 1) for the range of MFI values in the ROC analysis. We set the cutoff value as the MFI equaling the highest Youden J index, which represents the best balance of specificity and sensitivity over the range of the assay. We normalized MFI signals for antigen comparisons for background fluorescence by using an index value (MFI/clinical cutoff).

Viruses and Cells

We obtained the following reagents through the Biodefense and Emerging Infections Research Resources Repository (BEI Resources, https://www.beiresources.org) at the National Institutes of Health's National Institute of Allergy and Infectious Diseases: VACV, Western Reserve (National Institute of Allergy and Infectious Diseases, tissue-culture adapted) NR-55; MPXV, USA-2003, NR-2500; and MPXV, Walter Reed Army Institute of Research 7-61, NR-27. We passaged virus stocks once in Vero E6 cells (African green monkey kidney, American Type Culture Collection CRL-1587) maintained in Eagle minimum essential medium (EMEM) with 2% heat-inactivated fetal bovine serum, penicillin (100 unit/mL), and streptomycin (100 μg/mL).

Sonication

We performed sonication in sealed tubes with the Virtis Virsonic 100-cup horn sonicator continuously cooled to 4°C with a circulating water bath. We diluted virus in EMEM with 2% heat-inactivated fetal bovine serum, and we sonicated separate aliquots with increasing intensity at settings 2, 3, 4, and 5 for four 5-second bursts separated by 5-second rest intervals to determine optimal sonication conditions (Appendix Table 1, Appendix Figures 1, 2, https://wwwnc.cdc.gov/EID/article/31/2/24-1300-App1.pdf). Thereafter, we used intensity setting 3 as part of a standardized protocol.

PRNT

Virus strains used in PRNT were VACV Western Reserve and MPXV USA-2003. We did not heat-inactivate test serum unless otherwise noted. We serially diluted each serum sample 2-fold in EMEM with 2% heat-inactivated fetal bovine serum. We sonicated an equal volume of media containing either VACV or MPXV at setting 3 and added it to each sample at a concentration expected to yield ≈100 PFU. We incubated virus–serum mixtures at 37°C for 1 hour, with the exception of experiments that lasted 24 hours (Appendix Figure 3). We then inoculated the mixture onto Vero E6 cell monolayers and adsorbed them for 1 hour at 37°C. We added EMEM media containing 0.6% oxoid agarose to wells, allowed them to solidify, and incubated them at 37°C with 5% CO_2. We added a secondary overlay containing 0.2% neutral red (Sigma-Aldrich, https://www.sigmaaldrich.com) for plaque visualization at 48 hours postinfection. We determined the timing of the secondary overlay after finding that overlays performed at 48 hours and 72 hours produced similar results (Appendix Table 2). We counted plaques 24 hours after the second overlay. We determined neutralization titers to be the serum dilution resulting in a 50% ($PRNT_{50}$) or 90% ($PRNT_{90}$) plaque reduction compared with the virus working dilution (≈100–250 PFU). We incubated virus inoculum and used it to enumerate the working dilution in media alone alongside samples containing virus–serum before infection and then titrated it by using a plaque assay in parallel to PRNT. We included positive- and negative-control antibodies in each assay, and we rejected assay results with a 4-fold difference in the range of control antibodies. PRNT titers measuring the efficacy of JYNNEOS in vaccinated donors over time are the result of 2 independent experiments, except for the experiments using only a single assay (Appendix Figure 3). We gave samples that did not neutralize at the 1:20 limit of detection an arbitrary neutralization value of 1:10 for geometric mean titer (GMT) calculations.

Statistical Analyses

We used 1-way analysis of variance to assess statistical significance. For multiple comparisons of the differences in means of ≥3 groups to a control group, we used 1-way analysis of variance followed by Dunnett multiple comparison test.

Results

We performed studies with donated serum samples from persons (n = 8) vaccinated with a 2-dose regimen of the JYNNEOS vaccine against potential occupational exposure. Vaccine doses were administered ≈28 days apart, and serum samples were collected from all participants shortly before JYNNEOS vaccination and at sequential time points until 12 months postvaccination. Seven donors were administered the vaccine subcutaneously, and 1 donor received the vaccine intradermally. One donor had received ACAM2000 (Sanofi, https://www.sanofi.com), a second-generation smallpox vaccine, ≈5 years before JYNNEOS vaccination. The remaining donors were determined to be previously smallpox vaccine–naive on the basis of their personal account, a lack of a vaccine take scar, their age, or a combination of those factors. Because of differences in timing of vaccination, the 12-month sampling point included serum samples for only 7 of the 8 participants.

We examined donor serum samples for IgG reactivity to MPXV- and VACV-derived antigens by using a previously described microsphere immunoassay (*15*) to assess overall antibody levels and cross-reactivity to MPXV in response to JYNNEOS vaccination. Orthopoxvirus virions have 2 forms, which differ in their surface proteins, intracellular mature virions (IMVs) and extracellular enveloped virions, so we tested antigens from each form. VACV L1 and MPXV E8 and H3 antigens are found on IMVs, whereas the remaining antigens are found on extracellular enveloped virions. We selected VACV recombinant proteins L1, A33, and B5 for quantification because immunization by those antigens and VACV A27 demonstrated protection from lethal mpox in nonhuman primates (*16*). We selected MPXV recombinant protein antigens on the basis of commercial availability.

Serum samples from the donor with prior smallpox vaccination (Figure 1, panels A, B) displayed much higher IgG reactivity than did the samples from the naive donors, so we excluded those samples from the mean values (Figure 1, panels C, D). The previously vaccinated donor produced detectable IgG response for all MPXV and VACV antigens. In naive donors, the mean serum IgG reactivity became positive for all VACV antigens assayed; VACV L1 showed the highest mean IgG reactivity of all antigens tested (Figure 1, panel D). E8 was the sole MPXV antigen with positive mean IgG reactivity in naive donors, despite MPXV A35 being homologous to VACV A33 (Figure 1, panel C). We also noted that serum samples from all donors reacted most strongly to IMV antigens from both viruses (L1 and E8). For all antigens, IgG reactivity peaked at ≈8 weeks after the initial dose and waned thereafter, indicating the antibody response generated by JYNNEOS is short-

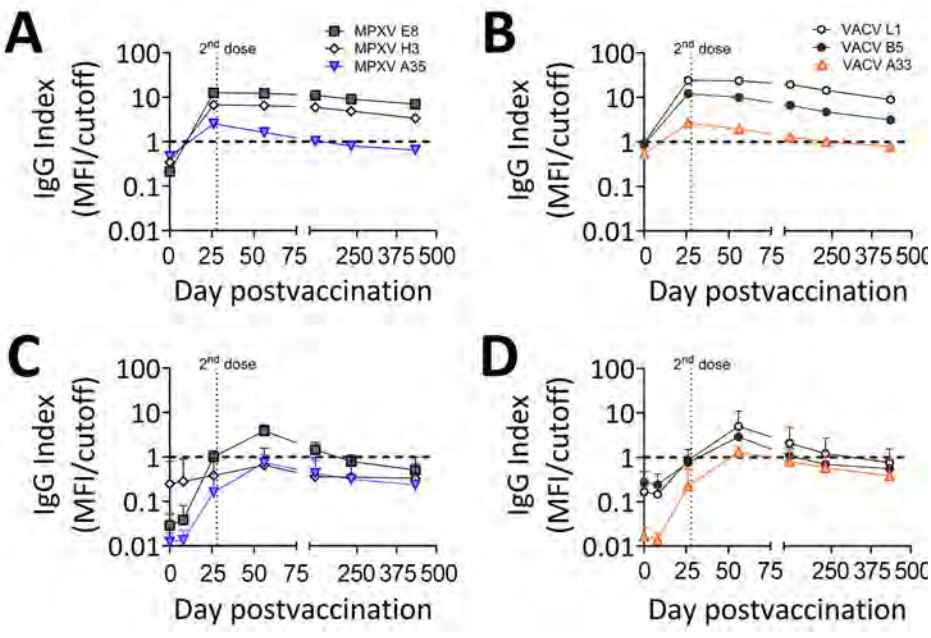

Figure 1. IgG reactivity to orthopoxvirus antigens in JYNNEOS vaccinees with and without prior smallpox vaccination in a study to assess neutralizing antibody responses to MPXV in smallpox vaccine–naive persons after JYNNEOS vaccination. We analyzed serum specimens from 8 JYNNEOS vaccine recipients for IgG reactivity to recombinant protein antigens derived from MPXV or VACV by using multiplex microsphere immunoassay. One donor who received ACAM2000 vaccine before JYNNEOS vaccine is shown separately in panels A and B. Means of 7 persons who had no prior smallpox vaccination are shown in panels C and D. We plotted mean index values (MFI/cutoff) of MPXV E8 (gray squares), MPXV A35 (blue triangles), and MPXV H3 (white diamonds) for days 0, 8, 26, 56, 118, 231, and 434 postvaccination (panels A, C). We plotted mean index values (MFI/cutoff) of VACV L1 (white circles), VACV A33 (orange triangles), and VACV B5 (gray circles) for days 0, 8, 26, 56, 118, 231, and 434 postvaccination (panels B, D). The horizontal black dashed line at y = 1.0 indicates the cutoff value. The vertical dotted line indicates the second dose of vaccine at day 28 postvaccination. MFI, mean fluorescence intensity; MPXV, monkeypox virus; VACV, vaccinia virus.

lived in naive persons (*17*). Serum samples from the previously vaccinated person remained stably positive beyond 250 days postvaccination for all antigens except MPXV A35 (Figure 1, panels A, B).

PRNT is considered the standard for measuring nAb levels because it directly measures inhibition of native virus infection. We developed our PRNT by making minor modifications to a standard assay (*18*,*19*). Orthopoxviruses such as VACV are known to form multivirion aggregates (*20*,*21*), and such structures can affect antibody-binding interactions and neutralizing properties (*22*,*23*). Sonication has been used with VACV infections, but more recent MPXV studies have omitted this step either in practice or in reporting (*24*–*29*). Because preliminary MPXV assays showed variability and nonuniform plaque clusters (Appendix Figures 1, 2), we introduced a sonication step. We empirically determined the sonication conditions of VACV and MPXV stocks used in our study by sonicating at increasing levels of intensity with a cup horn sonicator. Although plaque titrations of MPXV without sonication produced visible clusters of plaques that prevented accurate titer estimation, low levels of sonication treatment resulted in well-separated MPXV plaques and significantly increased titers (p = 0.0166) (Appendix Figure 2). We selected intensity setting 3 for subsequent use because it was the lowest setting that provided significantly increased plaque numbers for both viruses (p = 0.0185) (Appendix Figure 2). We sonicated virus by using this procedure at the start of each PRNT.

We also considered the duration of virus incubation with serum samples before infection, given that some PRNT studies of MPXV and VACV neutralization extend the virus–serum incubation to overnight rather than 1 hour at 37°C (*24*,*30*). We found that the extended incubation time was suboptimal despite producing increased $PRNT_{50}$ titers because infectivity of the viruses also decreased independently of nAb with the extended adsorption time. MPXV demonstrated a 43.2% reduction in mean working dilution (p<0.00001), whereas VACV demonstrated a 20.9% reduction (p = 0.00121) (Appendix Figure 3, panel B). This decreased infectivity suggested virus instability during the extended incubation time, which was greater for MPXV than VACV (Appendix Figure 3, panel B).

We used PRNT to measure nAb responses for MPXV and VACV (Figure 2). Samples from the donor with prior smallpox vaccination had higher levels of neutralization than did the samples from naive donors (Figures 2, 3). The previously vaccinated donor was also the only person whose sample produced a positive $PRNT_{90}$ result (Figure 2). Because of the difference in vaccination history, datapoints from that person are shown in plots (Figures 2, 3)

but were excluded from the overall mean PRNT titer calculations.

In all previously naive persons tested, nAb responses toward MPXV peaked at an average geometric mean $PRNT_{50}$ titer (GMT) of 1:35 ≈1 month after the second dose of JYNNEOS and quickly waned to below the 1:20 limit of detection (LOD) (Figure 2). Neutralization of VACV was better than MPXV after only 1 dose of vaccine and was more robust, having a peak GMT $PRNT_{50}$ of 1:61 at 8 weeks after the initial dose (Figures 2, 3). Neutralization of either virus waned similarly over time after vaccination (Figure 2). One person mounted no detectable neutralization response to MPXV (Figure 2, panel A). For most persons, $PRNT_{50}$ titers to MPXV and VACV were below the LOD for both viruses by 12 weeks after the initial vaccine dose (Figure 2, panels A, B). At 12 months, postvaccination serum samples from previously naive persons retained some reactivity to VACV ($PRNT_{50}$ GMT 1:23), but neutralization of MPXV was at or below the $PRNT_{50}$ LOD (GMT 1:12) (Figure 3). No naive donors produced a detectable $PRNT_{90}$ titer of ≥1:20 to either MPXV or VACV at any timepoint.

Discussion

The low levels of MPXV-neutralizing activity induced by JYNNEOS vaccination observed in this study are consistent with results of other recent studies, some of which have raised concerns over the efficacy and durability of MVA-BN vaccines in preventing mpox disease and spread (*26*–*29*,*31*). We also found that neutralization titers can be affected by assay conditions, which should be considered when comparing neutralizing activity levels from different studies. Empirical testing of MPXV PRNT assay conditions showed that sonication improves MPXV plaque quality and assay reliability, supporting its inclusion as part of a standardized protocol, as it is for VACV (*32*). In addition, significantly reduced MPXV infectivity with an overnight preincubation period (Appendix Figure 3, panel B) leads us to propose that shorter preincubation times are preferable for MPXV neutralization assays, despite some increased sensitivity with extended preincubation.

One limitation of this study is the small number of donors that were assessed. Nonetheless, our results align well with those of studies that had greater

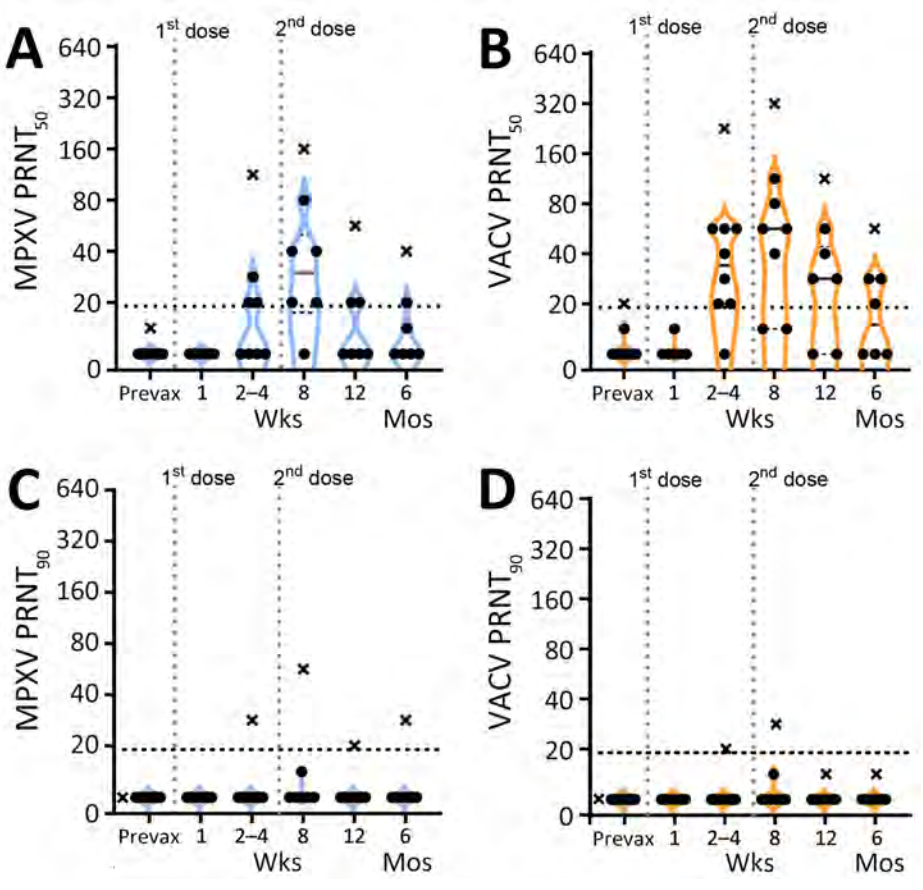

Figure 2. PRNT titers for participants vaccinated with JYNNEOS vaccine up to 6 months prior in a study to assess neutralizing antibody responses to MPXV in smallpox vaccine–naive persons after JYNNEOS vaccination. We used PRNT to test serum samples from donors vaccinated with 2 doses of JYNNEOS vaccine ≈28 days apart. We performed assays with sonicated virus and a 1-hour virus–serum incubation. A) MPXV $PRNT_{50}$ results; B) VACV $PRNT_{50}$ results; C) MPXV $PRNT_{90}$ results; D) VACV $PRNT_{90}$ results. Participants with no known vaccinia exposure (black circles) are used for mean calculations. Data from a single donor with prior smallpox vaccination (black Xs) are plotted separately and excluded from mean calculations. Each datapoint represents the geometric mean titer of 2 independent experiments. The vertical dotted lines represent the timing of the vaccine doses, and the horizontal dotted lines indicate limits of detection. MPXV, monkeypox virus; prevax, prevaccination; PRNT, plaque reduction neutralization test; $PRNT_{50}$, 50% plaque reduction as measured by PRNT; $PRNT_{90}$, 90% plaque reduction as measured by PRNT; VACV, vaccinia virus.

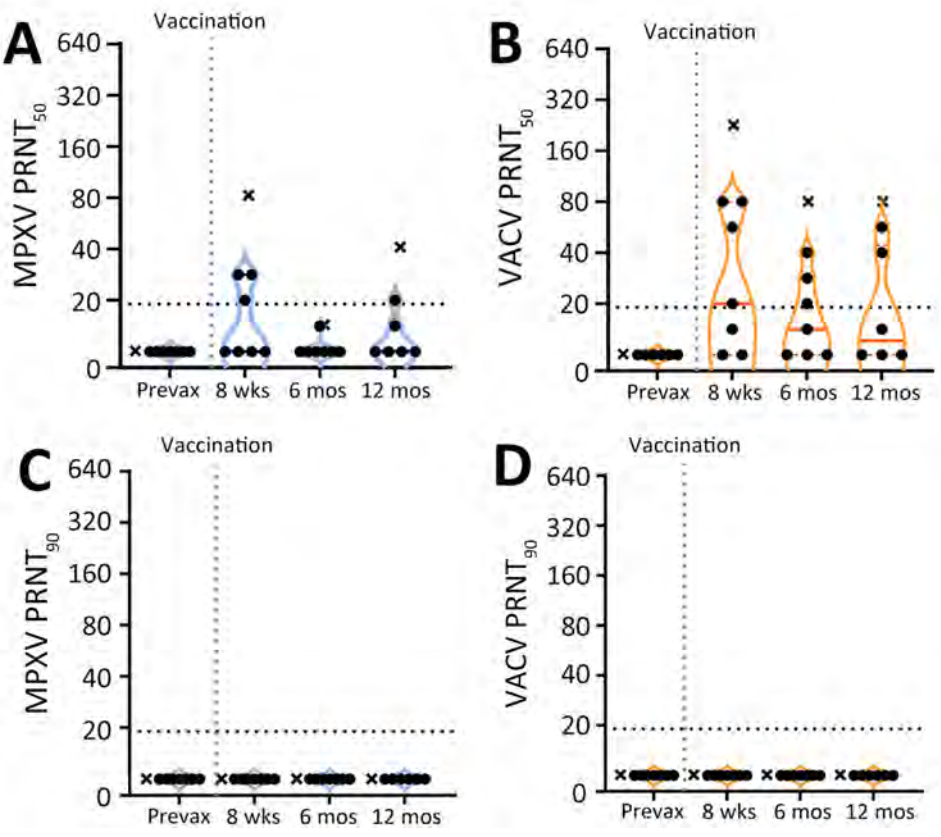

Figure 3. Longitudinal neutralizing antibody response by JYNNEOS vaccination extending to 12 months in a study to assess neutralizing antibody responses to MPXV in smallpox vaccine–naive persons after JYNNEOS vaccination. We used PRNT to test serum samples from donors vaccinated with 2 doses of JYNNEOS ≈28 days apart. We performed assays with sonicated virus and a 1-hour virus–serum incubation. A) MPXV $PRNT_{50}$ results; B) VACV $PRNT_{50}$ results; C) MPXV $PRNT_{90}$ results; D) VACV $PRNT_{90}$ results. Data from a single donor with prior smallpox vaccination are plotted separately (black Xs). We used data from participants with no known vaccinia exposure for mean calculations (black circles). Each datapoint represents the geometric mean titer of 2 independent experiments, and the limits of detection are expressed by horizontal dotted lines. MPXV, monkeypox virus; prevax, prevaccination; PRNT, plaque reduction neutralization test; $PRNT_{50}$, 50% plaque reduction as measured by PRNT; $PRNT_{90}$, 90% plaque reduction as measured by PRNT; VACV, vaccinia virus.

numbers of participants (*27*,*28*,*31*). In addition, our antigen-binding data are limited by the subset of MPXV and VACV antigens that were measured. Protective epitopes from MPXV have not been well defined and might not have been present among the tested antigens.

The low nAb levels that we and others (*27*–*29*,*31*) observed after MVA-BN vaccination of smallpox vaccine–naive persons differ from those of prior studies that showed first-generation smallpox vaccines can produce a long-lasting humoral response to MPXV (*25*,*29*,*33*). This durable antibody response is consistent with the finding that nAb levels remain elevated for decades in those who recover from smallpox infection, a condition that is assumed to produce lifelong immunity (*34*). In addition, a previous study comparing the effect of depleting either B cell or CD8 T-cell responses in a nonhuman primate challenge model led to the conclusion that nAb responses are a primary means of protection against mpox (*35*). Animals immunized with a first-generation smallpox vaccine demonstrated that an intact humoral response alone or passive antibody transfer was sufficient to protect the animals from lethal MPXV infection (*35*). Despite our observation of a limited antibody response after JYNNEOS vaccination, recent reports indicate that MVA-BN vaccine efficacy against mpox is strong (*36*,*37*) and breakthrough infections that occur in a minority of vaccinated persons (*10*) generally result in mild disease (*38*–*40*). In contrast to studies with earlier-generation smallpox vaccines, these results suggest that sustained nAb levels are not the most reliable correlate of immunity to mpox after MVA-BN vaccination, which is a critical issue for further investigation.

ACAM2000 is a closely related derivative of first-generation smallpox vaccines that are known to produce durable antibody responses (*33*). However, long-term studies on the durability of the antibody response generated by ACAM2000 against either VACV or MPXV in humans were not available when the US Food and Drug Administration established noninferiority of JYNNEOS to ACAM2000 (*13*,*14*,*41*). Because of the difference in its replicative ability postvaccination, the durability and the specificity of immune response elicited by MVA-BN to MPXV might bear less similarity to historical smallpox vaccination than expected and should continue to be evaluated.

The donor who received prior ACAM2000 vaccination produced a greater IgG response and higher neutralization titers than naive donors. However, the extent to which that person's nAb response to MPXV was affected by intrinsic differences between ACAM2000 and JYNNEOS (e.g., replication competence) versus the boosting of a memory response by additional vaccine doses is unclear and warrants further investigation. Other studies suggest that nAb responses to MPXV can be enhanced by either a third MVA-BN dose after the initial MVA-BN 2-dose series or MVA-BN vaccination after a first-generation smallpox vaccination (*25*,*29*). Both immunization strategies produced elevated nAb levels to VACV that were stable when measured out to 6 months (*42*). MPXV nAb levels can likewise be enhanced by either strategy, albeit to a lesser degree (*25*,*28*,*29*). Two doses of MVA-BN after historical smallpox vaccination can boost MPXV nAb levels out to 1 year (*28*). A study that measured MPXV nAb levels after a third dose of a recombinant modified vaccina Ankara engineered to express influenza H5 protein did so only up to 4 weeks after dose 3 (*29*), and further study is needed to address the durability of this boosted response to MPXV in naive persons.

It is possible that protection against mpox after MVA-BN vaccination is more dependent on memory B cells, production of a robust cellular immune response, or both, compared with the earlier-generation smallpox vaccines. Rhesus macaques vaccinated with recombinant MVA containing HIV or simian human immunodeficiency virus genes survived a lethal dose of MPXV up to 3 years post-vaccination, despite most animals displaying low nAb levels before MPXV challenge (*43*,*44*). Cohn et al. (*17*) found that JYNNEOS vaccination led to an increase in CD4 and CD8 T cells that could recognize and respond to orthopoxvirus-specific antigens. Those CD4 and CD8 T-cell responses from the JYNNEOS 2-dose recipients were similar to those of MPXV-convalescent donors. Cytokine responses were also comparable in the vaccinated versus convalescent groups. A comparative challenge study of rhesus macaques immunized with MVA-BN or ACAM2000 also found that both vaccines produced similar T-cell responses to VACV lysate (*45*). Furthermore, T-cell responses to MVA-BN antigens were found to persist in a group of MVA-BN vaccinees when tested out to 1 year (*28*).

Further examination of immune durability and correlates of protection in MVA-BN vaccinees is urgently needed to address public health concerns associated with the ongoing spread of mpox. Topics of particular importance include the roles of memory B-cell and T-cell responses in mpox immunity and the immune mechanisms engendered by earlier-generation replication-competent smallpox vaccines versus MVA-BN. Understanding the mechanisms by which the third-generation MVA-BN vaccine generates immunity against MPXV infection will be central to informing public health responses to mpox disease.

Acknowledgments

We gratefully acknowledge BEI Resources as a source for virus and the donors who generously contributed material. H. Dillenbeck, S. Griesemer, and the Wadsworth Center Tissue Culture and Media Core provided outstanding technical assistance that greatly facilitated the work.

This work was supported in part by New York State Department of Health and funding from the Centers for Disease Control and Prevention (grant no. NU50CK000516).

Author contributions: K.P. contributed to the experimental design, data acquisition and analysis, interpretation of data, and writing of the manuscript; J.Y. contributed to conception of the work, experimental design, interpretation of data, and writing of manuscript; J.P., S.B., and D.H. contributed to data acquisition and analysis; A.D., A.P., and W.L. contributed to conception of the work, experimental design, and interpretation of data. K.M. contributed to conception of the work, experimental design, interpretation of data, and writing of the manuscript.

About the Author

Dr. Phipps is a scientist in the Severe Respiratory Pathogen Laboratory of the Wadsworth Center, New York State Department of Health, Albany. Her research focuses on antibody responses to emerging viral pathogens and relevant vaccines.

References

1. Thornhill JP, Gandhi M, Orkin C. Mpox: the reemergence of an old disease and inequities. Annu Rev Med. 2023.
2. Adepoju P. Mpox declared a public health emergency. Lancet. 2024;404:e1–2. https://doi.org/10.1016/S0140-6736(24)01751-3
3. Gilchuk I, Gilchuk P, Sapparapu G, Lampley R, Singh V, Kose N, et al. Cross-neutralizing and protective human antibody specificities to poxvirus infections. Cell. 2016;167:684–694.e9. https://doi.org/10.1016/j.cell.2016.09.049
4. Hammarlund E, Lewis MW, Carter SV, Amanna I, Hansen SG, Strelow LI, et al. Multiple diagnostic techniques identify previously vaccinated individuals with protective immunity against monkeypox. Nat Med. 2005;11:1005–11. https://doi.org/10.1038/nm1273

5. Kennedy RB, Ovsyannikova I, Poland GA. Smallpox vaccines for biodefense. Vaccine. 2009;27(Suppl 4):D73–9. https://doi.org/10.1016/j.vaccine.2009.07.103
6. US Food and Drug Administration. FDA approves first live, non-replicating vaccine to prevent smallpox and monkeypox. 2019 [cited 2024 Aug 28]. https://www.fda.gov/news-events/press-announcements/fda-approves-first-live-non-replicating-vaccine-prevent-smallpox-and-monkeypox
7. European Medicines Agency. EMA recommends approval of Imvanex for the prevention of monkeypox disease. 2022 [cited 2024 Aug 28]. https://www.ema.europa.eu/en/news/ema-recommends-approval-imvanex-prevention-monkeypox-disease
8. Dalton AF, Diallo AO, Chard AN, Moulia DL, Deputy NP, Fothergill A, et al.; CDC Multijurisdictional Mpox Case Control Study Group. Estimated effectiveness of JYNNEOS vaccine in preventing mpox: a multijurisdictional case-control study—United States, August 19, 2022–March 31, 2023. MMWR Morb Mortal Wkly Rep. 2023;72:553–8. https://doi.org/10.15585/mmwr.mm7220a3
9. Deputy NP, Deckert J, Chard AN, Sandberg N, Moulia DL, Barkley E, et al. Vaccine effectiveness of JYNNEOS against mpox disease in the United States. N Engl J Med. 2023;388:2434–43. https://doi.org/10.1056/NEJMoa2215201
10. Guagliardo SAJ, Kracalik I, Carter RJ, Braden C, Free R, Hamal M, et al. Monkeypox virus infections after 2 preexposure doses of JYNNEOS vaccine—United States, May 2022–May 2024. MMWR Morb Mortal Wkly Rep. 2024;73:460–6. https://doi.org/10.15585/mmwr.mm7320a3
11. Rosenberg ES, Dorabawila V, Hart-Malloy R, Anderson BJ, Miranda W, O'Donnell T, et al. Effectiveness of JYNNEOS vaccine against diagnosed mpox infection—New York, 2022. MMWR Morb Mortal Wkly Rep. 2023;72:559–63. https://doi.org/10.15585/mmwr.mm7220a4
12. Paredes MI, Ahmed N, Figgins M, Colizza V, Lemey P, McCrone JT, et al. Underdetected dispersal and extensive local transmission drove the 2022 mpox epidemic. Cell. 2024;187:1374–1386.e13. https://doi.org/10.1016/j.cell.2024.02.003
13. Pittman PR, Hahn M, Lee HS, Koca C, Samy N, Schmidt D, et al. Phase 3 efficacy trial of modified vaccinia Ankara as a vaccine against smallpox. N Engl J Med. 2019;381:1897–908. https://doi.org/10.1056/NEJMoa1817307
14. US Food and Drug Administration. JYNNEOS (smallpox and monkeypox vaccine, live, nonreplicating) [package insert]. 2023 [cited 2024 Aug 28]. https://www.fda.gov/media/131078/download
15. Yates JL, Hunt DT, Kulas KE, Chave KJ, Styer L, Chakravarthi ST, et al.; PVI Study Group. Development of a novel serological assay for the detection of mpox infection in vaccinated populations. J Med Virol. 2023;95:e29134. https://doi.org/10.1002/jmv.29134
16. Hooper JW, Thompson E, Wilhelmsen C, Zimmerman M, Ichou MA, Steffen SE, et al. Smallpox DNA vaccine protects nonhuman primates against lethal monkeypox. J Virol. 2004;78:4433–43. https://doi.org/10.1128/JVI.78.9.4433-4443.2004
17. Cohn H, Bloom N, Cai GY, Clark JJ, Tarke A, Bermúdez-González MC, et al.; PVI study group. Mpox vaccine and infection-driven human immune signatures: an immunological analysis of an observational study. Lancet Infect Dis. 2023;23:1302–12. https://doi.org/10.1016/S1473-3099(23)00352-3
18. Lee WT, Girardin RC, Dupuis AP II, Kulas KE, Payne AF, Wong SJ, et al. Neutralizing antibody responses in COVID-19 convalescent sera. J Infect Dis. 2021;223:47–55. https://doi.org/10.1093/infdis/jiaa673
19. Beaty BJ, Calisher CH, Shope RE. Arboviruses. In: Lennette EH, Lennette D, Lennette E, editors. Diagnostic procedures for viral, rickettsial, and chlamydial infections. Washington: American Public Health Association; 1995. p. 189–212.
20. Galasso GJ, Sharp DG. Virus particle aggregation and the plaque-forming unit. J Immunol. 1962;88:339–47. https://doi.org/10.4049/jimmunol.88.3.339
21. Kotwal GJ, Abrahams MR. Growing poxviruses and determining virus titer. Methods Mol Biol. 2004;269:101–12.
22. Burton DR. Antiviral neutralizing antibodies: from in vitro to in vivo activity. Nat Rev Immunol. 2023;23:720–34. https://doi.org/10.1038/s41577-023-00858-w
23. Pradhan S, Varsani A, Leff C, Swanson CJ, Hariadi RF. Viral aggregation: the knowns and unknowns. Viruses. 2022;14:438. https://doi.org/10.3390/v14020438
24. Priyamvada L, Carson WC, Ortega E, Navarra T, Tran S, Smith TG, et al. Serological responses to the MVA-based JYNNEOS monkeypox vaccine in a cohort of participants from the Democratic Republic of Congo. Vaccine. 2022;40:7321–7. https://doi.org/10.1016/j.vaccine.2022.10.078
25. Hubert M, Guivel-Benhassine F, Bruel T, Porrot F, Planas D, Vanhomwegen J, et al. Complement-dependent mpox-virus-neutralizing antibodies in infected and vaccinated individuals. Cell Host Microbe. 2023;31:937–948.e4. https://doi.org/10.1016/j.chom.2023.05.001
26. Moschetta N, Raccagni AR, Bianchi M, Diotallevi S, Lolatto R, Candela C, et al. Mpox neutralising antibodies at 6 months from mpox infection or MVA-BN vaccination: a comparative analysis. Lancet Infect Dis. 2023;23:e455–6. https://doi.org/10.1016/S1473-3099(23)00571-6
27. Collier AY, McMahan K, Jacob-Dolan C, Liu J, Borducchi EN, Moss B, et al. Decline of mpox antibody responses after modified vaccinia Ankara–Bavarian Nordic Vaccination. JAMA. 2024;332:1669–72. https://doi.org/10.1001/jama.2024.20951
28. Matusali G, Cimini E, Mazzotta V, Colavita F, Maggi F, Antinori A. Mpox immune response elicited by MVA-BN vaccine over 12 months of follow-up. J Infect. 2024;89:106309. https://doi.org/10.1016/j.jinf.2024.106309
29. Zaeck LM, Lamers MM, Verstrepen BE, Bestebroer TM, van Royen ME, Götz H, et al. Low levels of monkeypox virus-neutralizing antibodies after MVA-BN vaccination in healthy individuals. Nat Med. 2023;29:270–8. https://doi.org/10.1038/s41591-022-02090-w
30. Newman FK, Frey SE, Blevins TP, Mandava M, Bonifacio A Jr, Yan L, et al. Improved assay to detect neutralizing antibody following vaccination with diluted or undiluted vaccinia (Dryvax) vaccine. J Clin Microbiol. 2003;41:3154–7. https://doi.org/10.1128/JCM.41.7.3154-3157.2003
31. van Leeuwen LP, Shamier MC, Verstrepen BE, Götz HM, Schmitz KS, Akhiyate N, et al. Orthopoxvirus-specific antibodies wane to undetectable levels 1 year after MVA-BN vaccination of at-risk individuals, the Netherlands, 2022 to 2023. Euro Surveill. 2024;29:2400575. https://doi.org/10.2807/1560-7917.ES.2024.29.38.2400575
32. Cotter CA, Earl PL, Wyatt LS, Moss B. Preparation of cell cultures and vaccinia virus stocks. Curr Protoc Protein Sci. 2017;89:5.12.1–5.12.18. PMID 28762495.
33. Asquith W, Hueston L, Dwyer D, Kok J, Ko D, Fennel M, et al. Characterizing the acute antibody response of monkeypox and MVA-BN vaccine following an Australian outbreak. J Med Virol. 2024;96:e29407. https://doi.org/10.1002/jmv.29407
34. Taub DD, Ershler WB, Janowski M, Artz A, Key ML, McKelvey J, et al. Immunity from smallpox vaccine persists

for decades: a longitudinal study. Am J Med. 2008;121:1058–64. https://doi.org/10.1016/j.amjmed.2008.08.019
35. Edghill-Smith Y, Golding H, Manischewitz J, King LR, Scott D, Bray M, et al. Smallpox vaccine-induced antibodies are necessary and sufficient for protection against monkeypox virus. Nat Med. 2005;11:740–7. https://doi.org/10.1038/nm1261
36. Mason LMK, Betancur E, Riera-Montes M, Lienert F, Scheele S. MVA-BN vaccine effectiveness: a systematic review of real-world evidence in outbreak settings. Vaccine. 2024;42:126409. https://doi.org/10.1016/j.vaccine.2024.126409
37. Charles H, Thorley K, Turner C, Bennet KF, Andrews N, Bertran M, et al. Mpox epidemiology and vaccine effectiveness, England, 2023. Emerg Infect Dis. 2024;30:2145–8. https://doi.org/10.3201/eid3010.240292
38. Eustaquio PC, Salmon-Trejo LAT, McGuire LC, Ellington SR. Epidemiologic and clinical features of mpox in adults aged >50 years—United States, May 2022–May 2023. MMWR Morb Mortal Wkly Rep. 2023;72:893–6. https://doi.org/10.15585/mmwr.mm7233a3
39. Aparício Martins I, João AL, Neves JM, Fernandes C. Mpox after vaccination: a case series. Sex Transm Infect. 2024;100:120–120. https://doi.org/10.1136/sextrans-2023-056055
40. Hazra A, Zucker J, Bell E, Flores J, Gordon L, Mitjà O, et al.; SHARE-NET writing group. Mpox in people with past infection or a complete vaccination course: a global case series. Lancet Infect Dis. 2024;24:57–64. https://doi.org/10.1016/S1473-3099(23)00492-9
41. United States Food and Drug Administration. ACAM2000: smallpox vaccine. Vaccines and Related Biological Products Advisory Committee (VRBPAC) briefing document. 2007 Apr 18 [cited 2024 Aug 28]. https://wayback.archive-it.org/7993/20170405044400/https:/www.fda.gov/ohrms/dockets/ac/07/briefing/2007-4292B2-02.pdf
42. Ilchmann H, Samy N, Reichhardt D, Schmidt D, Powell JD, Meyer TPH, et al. One- and two-dose vaccinations with modified vaccinia Ankara–Bavarian Nordic induce durable B-cell memory responses comparable to replicating smallpox vaccines. J Infect Dis. 2023;227:1203–13. https://doi.org/10.1093/infdis/jiac455
43. Nigam P, Earl PL, Americo JL, Sharma S, Wyatt LS, Edghill-Spano Y, et al. DNA/MVA HIV-1/AIDS vaccine elicits long-lived vaccinia virus–specific immunity and confers protection against a lethal monkeypox challenge. Virology. 2007;366:73–83. https://doi.org/10.1016/j.virol.2007.04.010
44. Earl PL, Americo JL, Wyatt LS, Eller LA, Montefiori DC, Byrum R, et al. Recombinant modified vaccinia virus Ankara provides durable protection against disease caused by an immunodeficiency virus as well as long-term immunity to an orthopoxvirus in a non-human primate. Virology. 2007;366:84–97. https://doi.org/10.1016/j.virol.2007.02.041
45. Jacob-Dolan C, Ty D, Hope D, McMahan K, Liu J, Powers OC, et al. Comparison of the immunogenicity and protective efficacy of ACAM2000, MVA, and vectored subunit vaccines for mpox in rhesus macaques. Sci Transl Med. 2024;16:eadl4317. https://doi.org/10.1126/scitranslmed.adl4317

Address for correspondence: Kathleen A. McDonough, Wadsworth Center, NYSDOH, 120 New Scotland Ave, Albany, NY 12208, USA; email: kathleen.mcdonough@health.ny.gov

EID Podcast

***Thelazia callipaeda* Eyeworms in American Black Bear, Pennsylvania, USA, 2023**

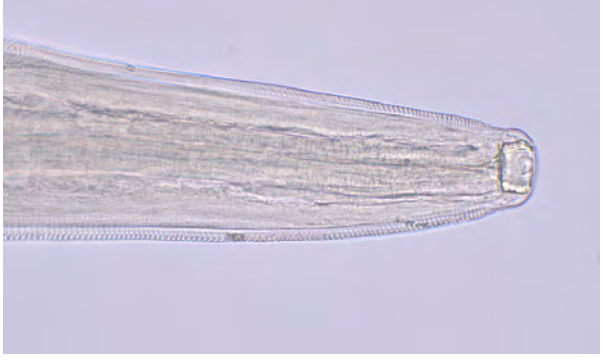

In November 2023, an American black bear was legally harvested in Coolbaugh Township, Monroe County, Pennsylvania. Multiple linear nematodes observed behind the third eyelid were later identified as *Thelazia callipaeda*. The presence of adult *T. callipaeda* eyeworms in an American black bear suggests the establishment of a sylvatic transmission cycle in the United States and expansion of the number of definitive host species used by the zoonotic nematode.

In this EID podcast, Dr. Carol Sobotyk, an assistant professor of clinical parasitology and director of the Clinical Parasitology Laboratory at the University of Pennsylvania, discusses *T. callipaeda* eyeworms in an American black bear.

Visit our website to listen: https://bit.ly/3P5bj94

EMERGING INFECTIOUS DISEASES®

Prions in Muscles of Cervids with Chronic Wasting Disease, Norway

Tram T. Vuong,[1] Federico A. Cazzaniga,[1] Linh Tran, Jørn Våge, Michele Di Bari, Laura Pirisinu, Claudia D'Agostino, Romolo Nonno, Fabio Moda,[2] Sylvie L. Benestad[2]

Chronic wasting disease (CWD) is an emerging prion disease in Nordic countries and has been detected in reindeer, moose, and red deer since 2016. CWD sporadically detected in moose and red deer in 3 Nordic countries demonstrated pathologic and strain characteristics different from CWD in reindeer, including an unexpected lack of prions outside the central nervous system as measured by standard diagnostic tests. Using protein misfolding cyclic amplification, we detected prions in the lymphoreticular system of moose and red deer with CWD in Norway and, remarkably, in muscles of both of those species and in CWD-infected reindeer. One moose lymph node and 1 moose muscle sample showed infectivity when experimentally transmitted to bank voles. Our findings highlight the systemic nature of CWD strains in Europe and raise questions regarding the risk of human exposure through edible tissues.

Chronic wasting disease (CWD) is a fatal disease affecting several species of cervids (*1*,*2*). It belongs to the group of transmissible spongiform encephalopathies, including scrapie in sheep and goats, bovine spongiform encephalopathy (BSE) in cattle, and Creutzfeldt-Jakob disease in humans (*3*). Transmissible spongiform encephalopathies are caused by misfolded forms of the prion protein (PrP^{C}), known as PrP^{Sc} (prions), which are thought to replicate in an autocatalytic process that converts PrP^{C} into PrP^{Sc} (*4*). The diseases are characterized by spongiform changes and the accumulation of PrP^{Sc} in the central nervous system (CNS).

Researchers first described CWD in North America in 1967, and evidence of the disease has since then inexorably expanded across 34 states in the United States and 4 provinces in Canada (*5*). CWD emerged for the first time in Europe in a wild reindeer (*Rangifer tarandus*) in Norway and, shortly thereafter, in 2 moose (*Alces alces*). As part of an extensive surveillance program in Norway, investigators have identified 21 reindeer, 13 moose, and 3 red deer (*Cervus elaphus*) as being infected with CWD. A 3-year surveillance program in countries in Europe that have wild reindeer or moose revealed CWD in 3 moose in Finland and in 4 moose in Sweden.

The origin of the CWD disease identified in Europe is not known. Increasing data showed that the prion strains found in cases from northern Europe were multiple and different from those in North America (*6*–*8*). The strain found in reindeer closely resembled the North America strains in terms of distribution of PrP^{Sc}, first in the lymphoreticular system and later in the brain, and the contagious characteristics in the natural host. Nevertheless, the strain of CWD found in reindeer in Europe was not identical to the CWD characterized from North America (*9*,*10*). Furthermore, CWD strains from moose in Nordic countries demonstrated substantial differences when compared with North America strains. Those moose, primarily old animals with a sporadic geographic distribution in Norway, Finland, and Sweden, exhibited unique characteristics not previously documented, and their infections were proposed as sporadic CWD (*11*). Transmission studies in bank voles and in transgenic mice expressing cervid PrP revealed that CWD prions in moose clearly differ from CWD prions from both reindeer in Norway and from the North America isolates studied. Furthermore, researchers have observed PrP^{Sc} and strain variation among individual moose isolates (*9*,*10*,*12*,*13*). Researchers studying CWD-affected moose and using traditional immunodetection tests (ELISA, Western

Author affiliations: Norwegian Veterinary Institute, Ås, Norway (T.T. Vuong, L. Tran, J. Våge, S.L. Benestad); Fondazione IRCCS Istituto Neurologico Carlo Besta, Milano, Italy (F.A. Cazzaniga, F. Moda); Istituto Superiore di Sanità, Rome, Italy (M.D. Bari, L. Pirisinu, C. D'Agostino, R. Nonno); Università degli Studi di Milano (F. Moda)

DOI: http://doi.org/10.3201/eid3102.240903

[1]These first authors contributed equally to this article.

[2]These authors are co–senior authors.

blot [WB], and immunohistochemistry) detected PrP^{Sc} in the CNS and not in the lymphoreticular system (*13*,*14*). As in moose, PrP^{Sc} is not lymphotropic in red deer, but analysis on the first CWD-affected red deer in Norway revealed numerous characteristics that point to a unique CWD strain (*6*,*15*–*18*).

CWD has an incubation period of several years, during which time infected animals can shed prions in excreta, even before showing clinical signs (*19*–*22*). On the basis of investigations of sheep scrapie and cattle BSE, researchers have commonly hypothesized that CWD cases demonstrating a disease phenotype with general lymphoreticular involvement have higher potential to transmit the disease in field conditions (*23*). The anatomic distribution in the CNS and the lymphotropic properties of PrP^{Sc} distinguish the different prion strains (*24*,*25*). Those insights have inspired conjecture regarding a possible (albeit undetectable with conventional assays) accumulation of infectious prions in the peripheral tissues of the newly emerged strains in cervids in Norway, especially in the strains identified in moose and red deer. We used protein misfolding cyclic amplification (PMCA) and animal bioassay to assess the presence of CWD prions and their potential infectivity in lymph nodes, nerves, and muscles from CWD field cases in Norway.

Materials and Methods

Animal Tissues

We detected CWD-affected animals (Table 1) through Norway's surveillance program for CWD by using TeSeE (Bio-Rad Laboratories, https://www.bio-rad.com) or HerdChek (IDEXX, https://www.idexx.com) ELISA tests and confirmed results by TeSeE Western blot (Bio-Rad). We collected tissue samples from different parts of 2 reindeer, 4 moose, and 1 red deer by using disposable instruments to avoid cross contamination (Table 2). We used 3 reindeer, 3 moose and 1 red deer, all healthy and confirmed PrP^{Sc}-negative, as negative controls.

Tissues Preparation

We homogenized all biologic tissues in phosphate-buffered saline at 10% wt/vol and used grinding tubes with silica beads and TeSeE PRECESS 48 homogenizer (Bio-Rad). For the muscle and lymph node tissues, we applied 2 ribolysing cycles of 60 seconds ribolysis and 30 seconds rest to improve the homogenization quality. Except for the brain samples that were tested at 10^{-4} to 10^{-8} dilutions to assess PMCA sensitivity, we tested all samples undiluted.

PMCA

Scientists performed PMCA in parallel in laboratories in Ås (Lab-Å) and in Milan (Lab-M). We prepared PMCA substrate by homogenizing bank vole brains (PRNP 109M; obtained from the Italian National Institute of Health, Rome) at 10% wt/vol in conversion buffer consisting of phosphate-buffered saline supplemented with a cocktail of 150 mM NaCl, 1% Triton X-100, and protease inhibitors (Roche, https://www.roche.com). We removed debris by centrifugation at 800 × *g* for 1 minute before aliquoting and storing the supernatant at −80°C. Before PMCA, we supplemented the substrate with 0.1 mg/mL heparin and 0.05% digitonin to increase the amplification efficiency.

To run PMCA analyses, we added 10 μL of each sample to 90 μL of PMCA reaction substrate in a PCR tube with 3 poly(tetrafluoroethylene) beads (Marteau & Lemarié, https://www.marteau-lemarie.fr). We then subjected the mixtures to cycles of sonication (30 seconds at 230–250 watts) and incubation (29 minutes 30 seconds at 36°C–40°C) using a Q700 sonicator (QSonica, https://www.sonicator.com), in 96 cycles for 1 PMCA round. We employed a slightly different experimental setting in Lab-M: 20 seconds sonication at 150–170 watts and 29 minutes 40 seconds incubation at 37°C. When available, we analyzed equivalent tissues from CWD-negative animals in parallel as negative controls for the amplification. We performed a maximum of 6 PMCA rounds and evaluated the resulting PMCA products by WB.

Table 1. Information for animals included in a study of prions in muscles of cervids with CWD, Norway*

Species	ID number	Code	CWD genotype	Animal sex	Area detected	Diagnostic status†	
						Brain	Lymph node
Rangifer tarandus	17-CD20830	Reindeer A	A/A‡	M	Nordfjella	Positive	Positive
	18-CD3207	Reindeer B	A/B‡	F	Nordfjella	Negative	Positive
Alces alces	17-CD11399	Moose A	KK_{109}	F	Lierne	Positive	Negative
	21-CD41	Moose B	KK_{109}	M	Telemark	Positive	Negative
	19-CD24854	Moose C	QQ_{109}	F	Sigdal	Positive	Negative
	22-CD29	Moose D	QQ_{109}	F	Tynset	Positive	Negative
Cervus elaphus	17-CD14051	Red deer	QQ_{226}	F	Gjemnes	Positive	Negative

*Animals detected through Norway's CWD surveillance program. CWD, chronic wasting disease; ID, identification.
†PrP^{Sc} detected by traditional diagnostic methods: ELISA, Western blot, and immunohistochemistry.
‡Nomenclature according to Güere et al. (*26*).

Table 2. Summary of PMCA amplification of prions in selected peripheral tissues from CWD-affected reindeer, moose, and a red deer with different strains in a study of prions in muscles of cervids with CWD, Norway*

	Reindeer		Moose				
Tissues or organs	A	B	A	B	C	D	Red deer
Lymph nodes							
Retropharyngeal	NA	NA	NA	Amp	NA	NA	Amp
Parotid	Amp	Amp	Amp, inf	NA	Amp	NA	NA
Mandibular	NA	NA	NA	NA	NA	No Amp	NA
Prescapular	Amp	Amp	NA	NA	No amp, no inf	Inc	No amp, no inf
Axillary	NA	NA	Amp	NA	NA	NA	NA
Popliteal	Amp	Amp	No amp, no inf	NA	No amp	No amp	NA
Peripheral nerves							
Brachial plexus	Amp	NA	Amp	NA	Amp	NA	Amp
Ischiadic nerve	Amp	Amp	Amp	NA	Amp	Amp	Amp
Optic nerve	Amp	NA	Amp	NA	Amp	NA	Amp
Muscles							
Masseter	Amp	Amp	Amp	Amp	Amp	Amp	Amp
Triceps brachii	Inc	No amp	Amp	Amp	Amp	Inc	Amp
Psoas	Amp	Amp	Amp	Amp	Amp	No amp	No amp
Longissimus dorsi	Amp	NA	Amp, no inf	Amp	Amp, no Inf	No amp	Inc
Semitendinosus	No amp	NA	No amp	Amp	Amp	No amp	No amp
Ocular	Amp	NA	Amp, inf	NA	Amp	NA	Amp
Lingual	Amp	Amp	Amp	NA	Amp	NA	Amp
Cardiac	Amp	Amp	NA	Amp	No amp	No amp	NA

*Amp, positive amplification; CWD, chronic wasting disease; inc, inconclusive results due to inconsistencies in the 2 laboratories; inf, positive infectivity in Bv109I voles; NA, not available/not tested; no amp, no amplification; no inf, no infectivity in Bv109I voles; PMCA, protein misfolding cyclic amplification.

WB Analysis

Brain Isolates

We prepared and analyzed brain homogenates according to the instructions of the TeSeE Western blot kit (Bio-Rad), with a slight modification: we performed the electrophoresis using NuPAGE 12% Bis-Tris protein gels (Thermo Scientific, https://www.thermofisher.com). To distinguish the PrP^{res} (protease-resistant prion) types according to the differential proteinase K cleavage at the N terminus, we used 2 different antibodies: Sha31 antibody (TeSeE Western blot kit), which recognizes the epitope (aa 145–152) in the core protein; and monoclonal antibody (mAb) 12B2 (1:1000; Wageningen Bioveterinary Research, https://www.wur.nl), which binds the epitope (aa 89–93) situated at N-terminal of the prion protein.

PMCA Products

We performed WB analysis of the PMCA products by using a standard protocol, with slight differences between Lab-Å and Lab-M. We treated the amplified products with proteinase K (Sigma-Aldrich Solutions, https://www.sigmaaldrich.com) at a final concentration of 100 μg/mL (or 50 μg/mL) for 1 hour at 37°C. We halted digestion by adding Laemmli buffer and boiling the samples at 100°C for 5 minutes (or 10 minutes) before conducting sodium dodecyl sulfate–polyacrylamide gel electrophoresis by using NuPAGE 12% Bis-Tris protein gels (Thermo Scientific). We transferred proteins onto a polyvinylidene difluoride membrane and subjected them to immunodetection using the mAb Sha31clone, at a dilution of 1:10 (TeSeE Western blot kit [Bio-Rad]), or the mAb 6D11 clone (Biolegend, https://www.biolegend.com), at a dilution of 1:5000. We developed results by using SuperSignal West Pico plus chemiluminescent substrate (Thermo Scientific) or ECL Prime (GE Healthcare, https://www.gehealthcare.com) and visualized using Azure c280 (Azure Biosystems, https://azurebiosystems.com). We considered a sample positive upon detection of a pattern of 3 protease-resistant bands at expected electrophoretic mobility within 6 rounds of PMCA. We considered samples inconclusive when results differed in 2 different laboratories.

Bioassay

Bank voles carrying isoleucine at the polymorphic PRNP codon 109 (Bv109I) were bred and inoculated at the Istituto Superiore di Sanità after approval of the experimental protocol from the Italian Ministry of Health (decree number 1122/2020-PR). We carried out all procedures in accordance with European Council directive 2010/63 and in compliance with the Italian Legislative Decree 26/2014. We inoculated 8-week-old Bv109I voles intracerebrally with 20 μL of 10% wt/vol tissue homogenates. We performed inoculations, clinical examinations, sampling, neuropathologic diagnosis, and WB analysis of PrP^{Sc} as previously described (*10*).

Results

Amplification of CWD Strains by PMCA Using Bank Vole Substrate

WBs of brain homogenates of the animals used in this study confirmed the presence or absence of PrP^{Sc} in the materials. This analysis highlighted the presence of various types of PrP^{res} in relation to the known differences among species and within moose samples, using Sha31 antibodies, targeting the protein core, and 12B2 antibodies, targeting the N-terminal part of PrP protein (Figure 1, panel A). As expected, we detected PrP^{res} in the brain of all CWD-affected animals, with the exception of reindeer B, where we detected it only in the lymph node by ELISA. The WB analysis showed the typical molecular profile of PrP^{res} of the different strains, with banding patterns distinct across species, and among the moose with different genotypes. We observed a noticeable lower migration of the PrP^{res} bands and a substantial reduction of signal with the N-terminal antibody in moose A and B, as described in Pirisinu et al. (*13*), and in red deer, indicative of a truncation of the N terminus of PrP^{res} in these animals (Figure 1, panel A). In contrast to results for moose A and B, PrP^{res} in moose C and D were not N-terminal truncated (*17*). Those results confirmed the known PrP^{Sc} variability in CWD isolates from different cervid species in Norway and showed that the moose samples included in this study have 2 different PrP^{Sc} types.

We assessed the efficiency of the bank vole substrate in amplifying the Norway CWD prions by subjecting 2 dilutions (10^{-4} and 10^{-8}, vol/vol) of infected brains to PMCA amplifications. We also included brain homogenates from healthy animals as negative controls. After 4 rounds of amplification, WB analysis

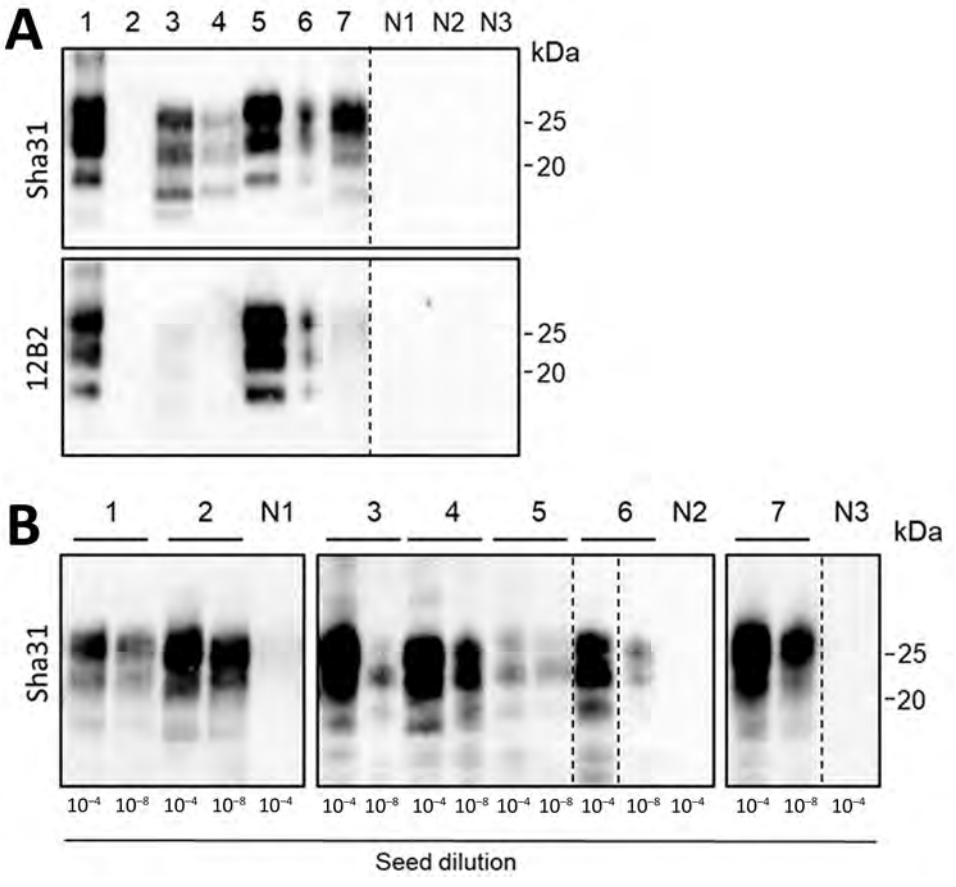

Figure 1. Western blots and protein misfolding cyclic amplification (PMCA; using bank vole substrate) of brain isolates of animals analyzed in a study of prions in muscles of cervids with chronic wasting disease, Norway. A) Western blot analyses of proteinase K–digested brain samples demonstrate the different PrP^{Sc} (misfolded forms of the prion protein) molecular profiles of the chronic wasting disease strains present in reindeer, moose (affected by different strains: N-terminally truncated PrP^{Sc} in moose A and B, and not N terminally truncated PrP^{Sc} in moose C and D), and a red deer. The PrP^{res} (protease-resistant prion) signal visualized by Sha31 antibody demonstrates the typical electrophoretic migration of PrP^{Sc} protein bands, and the 12B2 antibody demonstrates the different cleavages at the N- terminal of the PrP (major prion) protein, which are characteristic for the different strains. B) PMCA amplification of the same brain samples (10^{-4} and 10^{-8} dilutions as indicated) using bank vole brain substrate. After 4 rounds of PMCA, amplicons were treated with proteinase K, and PrP^{res} was visualized by Western blot using Sha31 antibody. Our PMCA protocol efficiently amplified prions from all chronic wasting disease–affected samples, regardless of the different strains. No PrP^{Sc} amplification was observed in the brain of healthy negative control reindeer (N1), moose (N2), and red deer (N3). Lane designations: 1, reindeer A; 2, reindeer B; 3, moose A; 4, moose B; 5, moose C; 6, moose D; 7, red deer. In panel A, tissue equivalents of 10 mg were loaded for each lane, except lanes 3 (tissue equivalents: 2 mg) and 5 (tissue equivalents: 1 mg). The same quantities of PrP^{res} were loaded for both antibody visualizations. In panel B, equivalent sample volumes were loaded for all lanes. Numbers at the right indicate the molecular weight marker. Dashed lines between images depict membrane splicing.

of the products revealed PrP^{res} from all infected brain dilutions, indicating that the PMCA protocol used was successfully amplifying prions in reindeer, moose, and red deer, regardless of the CWD prion strains (Figure 1, panel B). We were unable to amplify PrP^{Sc} from the negative controls. Of interest, we also amplified PrP^{Sc} from the brain of reindeer B, an animal that had tested positive only in lymphoid tissue with traditional diagnostic tests.

PrP^{Sc} Detected in Lymph Nodes and Peripheral Nerves of CWD-Affected Cervids

Our primary objective was to investigate the lymphatic dissemination of CWD prions in moose and red deer by PMCA. To assess the presence of potential tissue inhibitors in the amplification process, we spiked brain-derived CWD reindeer prions in tissue homogenates from healthy reindeer and then subjected them to PMCA. Results showed that spiked CWD prions in muscle and lymph node homogenates induced a similar amplification efficiency as those in brain homogenate (Appendix Figure 1, https://wwwnc.cdc.gov/EID/article/31/2/24-0903-App1.pdf), suggesting the lack of tissue-specific inhibitors in the samples.

WB analysis of available lymph nodes collected from the head (parotid, retropharyngeal) or body (prescapular, axillary, and popliteal) before PMCA showed detection of PrP^{res} only in reindeer, and in none of the other samples (Appendix Figure 2, panel A). Strikingly, we also detected seeding activity in the red deer and moose after amplification. In those cases, we were able to detect PrP^{res} more readily in lymph nodes from the head than those located in the body (Table 2; Figure 2).

To examine the neural distribution of PrP^{Sc} in sites peripheral to the CNS, which was not detectable in moose and the red deer (Appendix Figure 2, panel B), we performed PMCA on the brachialis plexus, ischiadic nerve, and the optic nerve. The results showed prion amplification in all tested nerves (Figure 2).

Detection of PrP^{Sc} Seeding Activity in Muscle Tissues of CWD-Affected Cervids

Because of the popularity of venison in the human food chain, it is important to assess the presence of prions in the musculature of CWD-affected cervids. We examined 8 different muscles (Table 2), all of which were negative for PrP^{res} by direct WB (Appendix Figure 2, panel C). By PMCA, we amplified PrP^{Sc} from all muscle types tested, although with some individual variation (Table 2; Figure 3). Most muscles tested positive in reindeer and in 3 of 4 moose. We observed less positive PrP^{Sc} results in muscles from

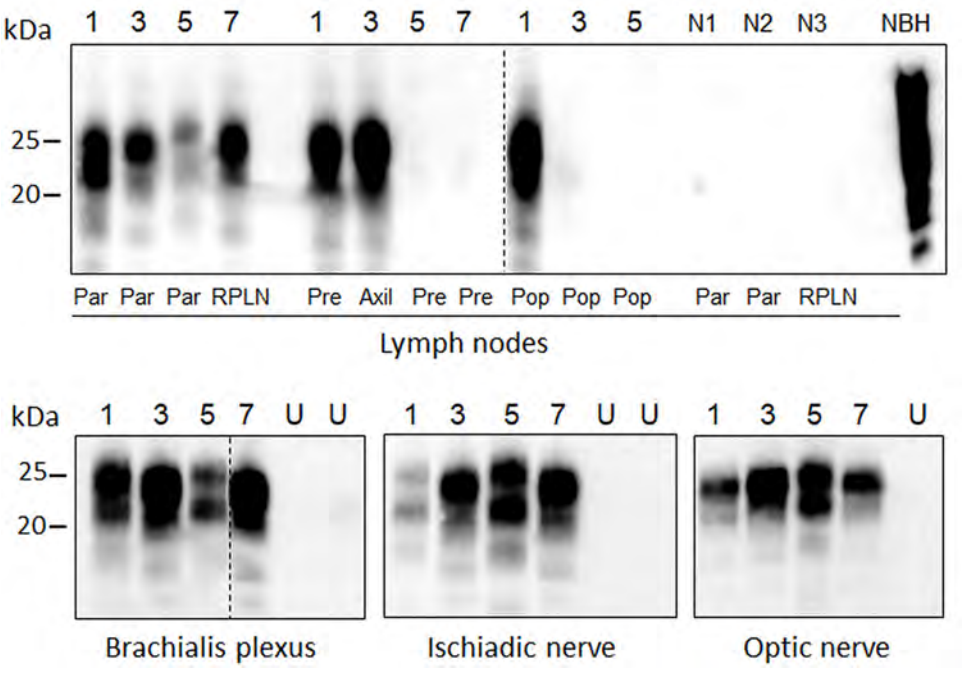

Figure 2. Protein misfolding cyclic amplification (PMCA) amplification of PrP^{Sc} (misfolded forms of the prion protein) in the lymphoreticular system and peripheral nerves of chronic wasting disease–affected animals from a study of prions in muscles of cervids with chronic wasting disease, Norway. We subjected lymph nodes and nerves collected from chronic wasting disease–affected cervids in Norway to serial PMCA before proteinase K digestion and Western blot analysis using Sha31 antibody. Example Western blots of samples from 1 representative animal of the different species and strains are shown; a more comprehensive result of all analyzed samples is summarized in Table 2. Lane designations: 1, reindeer A; 3, moose A; 5, moose C; 7, red deer. N lanes show lymph node from healthy, negative reindeer (N1), moose (N2), and red deer (N3). Dashed lines between images depict membrane splicing. Axil, axillary node; NBH, proteinase K–undigested bank vole brain homogenate used as electrophoretic migration marker of normal prion protein; par, parotid node; pre, prescapular node; pop, popliteal node; RPLN, retropharyngeal node; U, unseeded reaction included as a specificity control of PMCA reaction.

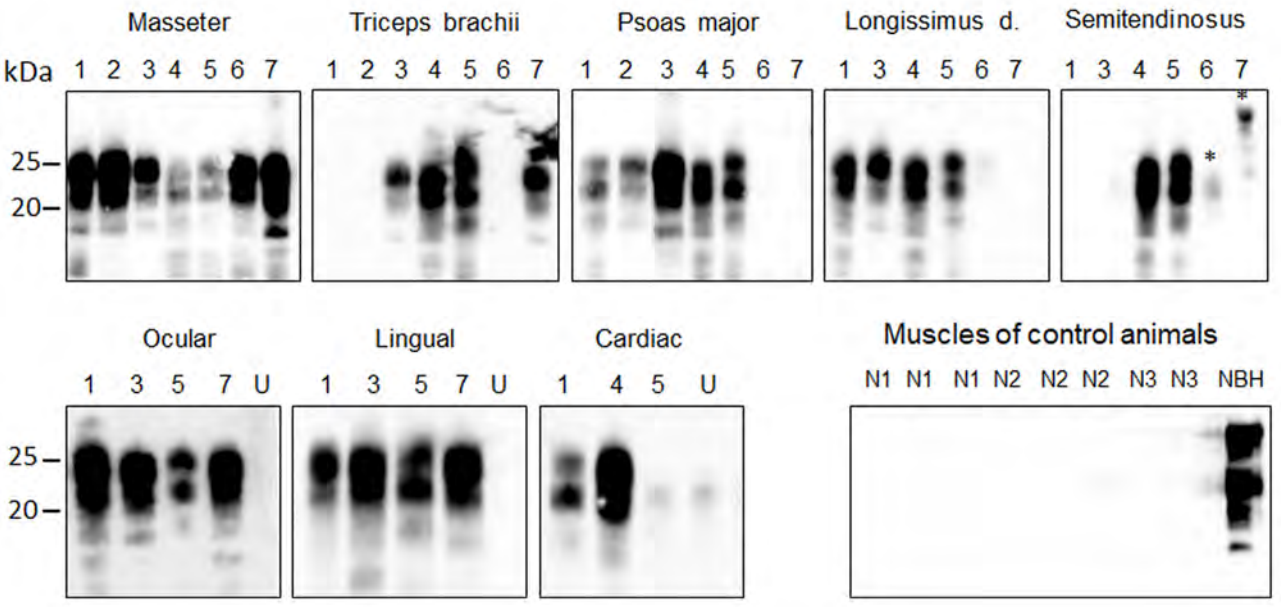

Figure 3. Detection of PrP^{Sc} (misfolded forms of the prion protein) amplification in muscle tissues of chronic wasting disease–affected cervids by protein misfolding cyclic amplification (PMCA) from a study of prions in muscles of cervids with chronic wasting disease, Norway. Muscle samples (10% homogenates) were subjected to 6 rounds of PMCA using bank vole brain homogenate substrate. PMCA products were treated with proteinase K before being analyzed by Western blot using Sha31 antibody to identify presence of PrP^{Sc}. Results demonstrate efficient amplification of PrP^{Sc} in skeletal and cardiac muscles of chronic wasting disease–affected reindeer, moose, and a red deer. No PrP^{Sc} was amplified in negative control samples. Lane designations: 1, reindeer A; 2, reindeer B; 3, moose A; 4, moose B; 5, moose C; 6, moose D; 7, red deer. Numbers at left indicate the molecular weight marker. Asterisks indicate unspecific signals. NBH, proteinase K–undigested bank vole brain homogenate used as electrophoretic migration marker of normal prion protein (PrP^{C}); U, unseeded reaction included as a specificity control of PMCA reaction.

moose D and the red deer. Of the different muscles tested, masseter, ocular and lingual muscles from the head were always positive. In contrast, muscles located more peripherally from the head were negative in some animals. The semitendinosus muscle was the least frequently positive; only 2 of 6 samples tested positive. The efficiency of prion detection in skeletal muscles in moose, the red deer, and reindeer were similar in both laboratories, Ås and Milan, showing 92% agreement in the PMCA results (Appendix Table).

Bioassay of Peripheral Tissues from Moose in Bank Voles

To determine whether prions amplified in peripheral tissues by PMCA are also infectious, we intracerebrally inoculated Bv109I animals with selected tissues (Table 3). We chose moose and red deer tissues because of the high susceptibility of Bv109I voles to CWD strains in those species (*10*,*18*), which we confirmed by the efficient transmission of the moose C brain homogenate (Table 3), compared with the very low susceptibility observed for reindeer CWD (*10*). Of the 7 peripheral tissues tested, the ocular muscle and parotideal lymph node from moose A transmitted the disease in Bv109I voles, but with a lower attack rate and longer survival time compared with the brain of the same moose (Table 3). We observed no evidence of infectivity in the popliteal lymph node and longissimus dorsi muscle of moose A, the prescapular lymph nodes of moose C and the red deer, and the longissimus dorsi muscle of moose C.

Discussion

Animals affected by CWD can remain asymptomatic for months, during which time prions can spread to various tissues and be shed into the environment, contributing to horizontal transmission (*1*). Depending on the prion strains, the PrP^{Sc} distribution pattern and tissue accumulation might differ in the host (*24*). Reports have identified 2 distinct patterns of prion spread in animal prion diseases (*6*,*27*–*30*). The first pattern involves the initial replication of prions in tissues from the lymphoreticular system, followed by spread to the peripheral nervous system before entering the brain. This pattern is observed in contagious strains, such as classical scrapie and North American CWD. The second pattern involves prion replication primarily in the CNS, as observed in less contagious

Table 3. Transmission in Bv109I voles of peripheral tissue from moose and red deer with CWD in a study of prions in muscles of cervids with CWD, Norway*

Animal	Inocula	Infectivity	
		Survival time†	Attack rate
Moose A	Brain‡	312 ± 46‡	13/13‡
	Parotid lymph node	561 ± 114	8/13
	Popliteal lymph node	>817	0/13
	Longissimus dorsi muscle	>944§	0/12
	Ocular muscle	494 ± 135¶	5/14
Moose C	Brain	150 ± 28	13/13
	Prescapular lymph node	>959	0/14
	Longissimus dorsi muscle	>936§	0/14
Red deer	Brain#	221 ± 36#	13/13#
	Prescapular lymph node	>1017	0/13

*Bv109I, bank voles carrying isoleucine at the polymorphic PRNP codon 109; CWD, chronic wasting disease.
†Expressed as days postinoculation ± SD.
‡Transmission reported in Nono et al. (*10*)
§Ongoing experiments; 3 inoculated Bv109I voles were healthy at the indicated days postinoculation. All other Bv109I voles were negative at postmortem.
¶Ongoing experiment; 4 inoculated Bv109I voles remained healthy at 932 days postinoculation.
#Transmission reported in Marín-Moreno et al. (*18*).

or noncontagious prion diseases, such as BSE and Nor98/atypical scrapie.

There is limited research on the tissue distribution of the infectious agent in the newly emerging CWD strains in cervids in Norway. Through conventional diagnostic methods, investigators detected PrP^{Sc} in the lymph nodes of all reindeer with CWD but detected the prion in the CNS of only 50% of them. Conversely, researchers detected PrP^{Sc} in only the CNS in moose and the red deer (*13*,*15*). Using conventional WB in this study, we confirmed the presence of PrP^{res} in brain, lymph nodes, and nerves in reindeer, but only moose and the red deer demonstrated evidence of PrP^{res} in the brain (Figure 1, panel A; Appendix Figure 1). However, by using PMCA, we were able to demonstrate PrP^{Sc} seeding activity in all 3 species in various peripheral tissues, including the peripheral nerves, lymph nodes, and a variety of muscles. This finding illustrates the shortcomings of the conventional diagnostic methods in detecting minute quantities of prions, which impedes the accurate assessment of peripheral CWD distribution (*31*,*32*). Previous studies have demonstrated the presence of prions in multiple peripheral tissues and body fluids, including lymphoid tissues, peripheral nerves, muscles, blood, and excreta, in animals infected with North America CWD strains (*20*,*22*,*33*–*38*). The tissue distribution of PrP^{Sc} in reindeer, with a CWD strain similar to cases found in North America, was therefore not surprising. However, the findings of PrP^{Sc} in peripheral tissues in moose and red deer by PMCA were less expected, especially in muscles, given the sporadic occurrence and lack of evidence, to date, for contagiousness of these new CWD strains (*11*).

We confirmed the presence of prion infectivity in PMCA-positive lymphoid and muscle tissues by transmission in bank voles. Despite the limited number of samples examined, infectivity and seeding activity showed a good correlation: 2 of 4 positive transmissions from PMCA-positive samples and 0 of 3 from PMCA-negative samples. This correlation suggested PMCA to be a good proxy for CWD infectivity in bank voles, as observed in sheep scrapie (*39*). The negative transmission observed with 2 PMCA-positive tissues could be the result of the presence of very low levels of infectivity, below the detection limit of the vole bioassay. This finding is consistent with the partial transmission rate observed in the positive transmissions.

Identifying prions outside of CNS in cases of CWD in moose and the red deer mirrors the pattern observed in Nor98/atypical scrapie in sheep and atypical BSE forms in cattle, which represent additional sporadic animal prion diseases. Initially, researchers believed the accumulation of PrP^{Sc} to be confined to the CNS in these diseases (*27*). Nevertheless, subsequent studies using bioassay experiments demonstrated that infectivity could be detected in peripheral tissues that had been considered negative by traditional PrP^{Sc} detection techniques, including lymphoid tissues, nerves, and muscles (*40*,*41*).

Transmission studies have reported the presence of PrP^{Sc} in muscles in hamsters and sheep orally challenged with classical scrapie and, subsequently, in CWD-infected deer (*27*). Other studies reported detection of PrP^{Sc} in muscles of intracerebrally inoculated hamsters and mice, as well as in patients with Creutzfeldt-Jakob disease (*42*,*43*). In those instances, PrP^{Sc} may have reached the muscles via centrifugal spread, through peripheral nerves and the innervation of efferent and sensory nerve fibers to the tissues (*27*). Our investigation indicated that a similar phenomenon might occur in Norway strains, regardless of the cervid species involved. Of note, we observed

a more efficient amplification of PrP^{Sc} in muscle and lymph node samples that were closer to the head and CNS compared with those further apart. Similarly, we detected infectivity in tissues from the head, the parotid lymph node, and the ocular muscle from moose A; however, the PMCA-positive popliteal lymph node and longissimus muscle from the same moose did not transmit in bank voles. Considering the incomplete transmission rate we observed in analyzing positive transmissions from peripheral tissues compared with the brain, we theorize that CWD prions accumulate at low titers in peripheral tissues and that prion titers might be higher in tissues closer to the CNS.

Unfortunately, in examining only field cases in our study, we concede that the lack of clinical status of the animals precludes establishing a correlation between the peripheral distribution of PrP^{Sc} and the disease stage. For instance, we were unable to determine whether the absence of seeding activity in some specific muscles and lymph nodes was a result of these animals being culled during early stages of the disease. We also could not rule out that the observed variation could be the result of very low prion titers in peripheral tissues or of individual strain characteristics.

In summary, the results of our study indicate that prions are widely distributed in peripheral and edible tissues of cervids in Norway, including muscles. This finding highlights the risk of human exposure to small amounts of prions through handling and consuming infected cervids. Nevertheless, we note that this study did not investigate the zoonotic potential of the Norway CWD prions. In North America, humans have historically consumed meat from CWD-infected animals, which has been documented to harbor prions (*35*,*44*–*47*). Despite the potential exposure to prions, no epidemiologic evidence indicates a correlation between the occurrence of CWD cases in animals and the prevalence of human prion diseases (*48*). A recent bioassay study reported no transmissions from 3 Nordic isolates into transgenic mice expressing human PrP (*49*). Therefore, our findings should be interpreted with caution in terms of human health implications, and further research is required to determine the zoonotic potential of these CWD strains.

The presence of prions in peripheral tissues indicates that CWD may have a systemic nature in all Norwegian cervid species, challenging the view that prions are exclusively localized in the CNS in sporadic CWD of moose and red deer. Our findings expand the notion of just how widely distributed prions can be in cervids affected with CWD and call into question the capability of emerging CWD strains in terms of infectivity to other species, including humans.

This study was funded by the internal CWD project 12081 at the Norwegian Veterinary institute, Research Council of Norway project no. 334585, and Italian Ministry of Health (to F.M.).

About the Author

Dr. Vuong is a research scientist at Norwegian Veterinary Institute in Ås, Norway. Her research interests are the pathogenesis of chronic wasting disease and the development of biochemical techniques to detect prions.

References

1. Otero A, Velásquez CD, Aiken J, McKenzie D. Chronic wasting disease: a cervid prion infection looming to spillover. Vet Res. 2021;52:115. https://doi.org/10.1186/s13567-021-00986-y
2. Williams ES. Chronic wasting disease. Vet Pathol. 2005;42:530–49. https://doi.org/10.1354/vp.42-5-530
3. Sejvar JJ, Schonberger LB, Belay ED. Transmissible spongiform encephalopathies. J Am Vet Med Assoc. 2008; 233:1705–12. https://doi.org/10.2460/javma.233.11.1705
4. Prusiner SB. Novel proteinaceous infectious particles cause scrapie. Science. 1982;216:136–44. https://doi.org/10.1126/science.6801762
5. US Geological Survey National Wildlife Health Center. Distribution of chronic wasting disease in North America [cited 2024 Jun 20] https://www.usgs.gov/centers/nwhc/science/expanding-distribution-chronic-wasting-disease
6. Tranulis MA, Gavier-Widén D, Våge J, Nöremark M, Korpenfelt S-L, Hautaniemi M, et al. Chronic wasting disease in Europe: new strains on the horizon. Acta Vet Scand. 2021;63:48. https://doi.org/10.1186/s13028-021-00606-x
7. Sun JL, Kim S, Crowell J, Webster BK, Raisley EK, Lowe DC, et al. Novel prion strain as cause of chronic wasting disease in a moose, Finland. Emerg Infect Dis. 2023;29:323–32. https://doi.org/10.3201/eid2902.220882
8. Sola D, Tran L, Våge J, Madslien K, Vuong TT, Korpenfelt SL, et al. Heterogeneity of pathological prion protein accumulation in the brain of moose (*Alces alces*) from Norway, Sweden and Finland with chronic wasting disease. Vet Res. 2023;54:74. https://doi.org/10.1186/s13567-023-01208-3
9. Bian J, Kim S, Kane SJ, Crowell J, Sun JL, Christiansen J, et al. Adaptive selection of a prion strain conformer corresponding to established North American CWD during propagation of novel emergent Norwegian strains in mice expressing elk or deer prion protein. PLoS Pathog. 2021;17:e1009748. https://doi.org/10.1371/journal.ppat.1009748
10. Nonno R, Di Bari MA, Pirisinu L, D'Agostino C, Vanni I, Chiappini B, et al. Studies in bank voles reveal strain differences between chronic wasting disease prions from Norway and North America. Proc Natl Acad Sci U S A. 2020; 117:31417–26. https://doi.org/10.1073/pnas.2013237117
11. Hopp P, Rolandsen CM, Korpenfelt SL, Våge J, Sörén K, Solberg EJ, et al. Sporadic cases of chronic wasting disease in old moose—an epidemiological study. J Gen Virol. 2024;105. https://doi.org/10.1099/jgv.0.001952
12. Di Bari MA, Nonno R, Castilla J, D'Agostino C, Pirisinu L, Riccardi G, et al. Chronic wasting disease in bank voles:

characterisation of the shortest incubation time model for prion diseases. PLoS Pathog. 2013;9:e1003219. https://doi.org/10.1371/journal.ppat.1003219
13. Pirisinu L, Tran L, Chiappini B, Vanni I, Di Bari MA, Vaccari G, et al. Novel type of chronic wasting disease detected in moose (*Alces alces*), Norway. Emerg Infect Dis. 2018;24:2210–8. https://doi.org/10.3201/eid2412.180702
14. Koutsoumanis K, Allende A, Alvarez-Ordoňez A, Bolton D, Bover-Cid S, Chemaly M, et al.; EFSA Panel on Biological Hazards (BIOHAZ). Update on chronic wasting disease (CWD) III. EFSA J. 2019;17:e05863.
15. Vikøren T, Våge J, Madslien KI, Røed KH, Rolandsen CM, Tran L, et al. First detection of chronic wasting disease in a wild red deer (*Cervus elaphus*) in Europe. J Wildl Dis. 2019;55:970–2. https://doi.org/10.7589/2018-10-262
16. Pritzkow S, Gorski D, Ramirez F, Telling GC, Benestad SL, Soto C. North American and Norwegian chronic wasting disease prions exhibit different potential for interspecies transmission and zoonotic risk. J Infect Dis. 2022;225:542–51. https://doi.org/10.1093/infdis/jiab385
17. Harpaz E, Vuong TT, Tran L, Tranulis MA, Benestad SL, Ersdal C. Inter- and intra-species conversion efficacies of Norwegian prion isolates estimated by serial protein misfolding cyclic amplification. Vet Res. 2023;54:84. https://doi.org/10.1186/s13567-023-01220-7
18. Marín-Moreno A, Benestad SL, Barrio T, Pirisinu L, Espinosa JC, Tran L, et al. Classical BSE dismissed as the cause of CWD in Norwegian red deer despite strain similarities between both prion agents. Vet Res. 2024;55:62. https://doi.org/10.1186/s13567-024-01320-y
19. Race BL, Meade-White KD, Ward A, Jewell J, Miller MW, Williams ES, et al. Levels of abnormal prion protein in deer and elk with chronic wasting disease. Emerg Infect Dis. 2007;13:824–29. https://doi.org/10.3201/eid1306.070186
20. Mathiason CK, Hays SA, Powers J, Hayes-Klug J, Langenberg J, Dahmes SJ, et al. Infectious prions in pre-clinical deer and transmission of chronic wasting disease solely by environmental exposure. PLoS One. 2009;4:e5916. https://doi.org/10.1371/journal.pone.0005916
21. John TR, Schätzl HM, Gilch S. Early detection of chronic wasting disease prions in urine of pre-symptomatic deer by real-time quaking-induced conversion assay. Prion. 2013;7:253–8. https://doi.org/10.4161/pri.24430
22. Henderson DM, Manca M, Haley NJ, Denkers ND, Nalls AV, Mathiason CK, et al. Rapid antemortem detection of CWD prions in deer saliva. PLoS One. 2013; 8:e74377. https://doi.org/10.1371/journal.pone.0074377
23. Koutsoumanis K, Allende A, Alvarez-Ordoñez A, Bolton D, Bover-Cid S, Chemaly M, et al.; EFSA Panel on Biological Hazards (BIOHAZ). Monitoring of chronic wasting disease (CWD) (IV). EFSA J. 2023;21:e07936.
24. Lambert ZJ, Greenlee JJ, Cassmann ED, West Greenlee MH. Differential accumulation of misfolded prion strains in natural hosts of prion diseases. Viruses. 2021;13:2453. https://doi.org/10.3390/v13122453
25. Simmons SM, Bartz JC. Strain-specific targeting and destruction of cells by prions. Biology (Basel). 2024;13:57. https://doi.org/10.3390/biology13010057
26. Güere ME, Våge J, Tharaldsen H, Benestad SL, Vikøren T, Madslien K, et al. Chronic wasting disease associated with prion protein gene (*PRNP*) variation in Norwegian wild reindeer (*Rangifer tarandus*). Prion. 2020;14:1–10. https://doi.org/10.1080/19336896.2019.1702446
27. Beekes M, McBride PA. The spread of prions through the body in naturally acquired transmissible spongiform encephalopathies. FEBS J. 2007;274:588–605. https://doi.org/10.1111/j.1742-4658.2007.05631.x
28. Fox KA, Jewell JE, Williams ES, Miller MW. Patterns of PrP^{CWD} accumulation during the course of chronic wasting disease infection in orally inoculated mule deer (*Odocoileus hemionus*). J Gen Virol. 2006;87:3451–61. https://doi.org/10.1099/vir.0.81999-0
29. Hoover CE, Davenport KA, Henderson DM, Denkers ND, Mathiason CK, Soto C, et al. Pathways of prion spread during early chronic wasting disease in deer. J Virol. 2017;91:e00077-17. https://doi.org/10.1128/JVI.00077-17
30. Sigurdson CJ, Williams ES, Miller MW, Spraker TR, O'Rourke KI, Hoover EA. Oral transmission and early lymphoid tropism of chronic wasting disease PrP^{res} in mule deer fawns (*Odocoileus hemionus*). J Gen Virol. 1999;80:2757–64. https://doi.org/10.1099/0022-1317-80-10-2757
31. Benavente R, Reed JH, Lockwood M, Morales R. PMCA screening of retropharyngeal lymph nodes in white-tailed deer and comparisons with ELISA and IHC. Sci Rep. 2023;13:20171. https://doi.org/10.1038/s41598-023-47105-9
32. Haley NJ, Mathiason CK, Carver S, Zabel M, Telling GC, Hoover EA. Detection of chronic wasting disease prions in salivary, urinary, and intestinal tissues of deer: potential mechanisms of prion shedding and transmission. J Virol. 2011;85:6309–18. https://doi.org/10.1128/JVI.00425-11
33. Ferreira NC, Charco JM, Plagenz J, Orru CD, Denkers ND, Metrick MA II, et al. Detection of chronic wasting disease in mule and white-tailed deer by RT-QuIC analysis of outer ear. Sci Rep. 2021;11:7702. https://doi.org/10.1038/s41598-021-87295-8
34. Cooper SK, Hoover CE, Henderson DM, Haley NJ, Mathiason CK, Hoover EA. Detection of CWD in cervids by RT-QuIC assay of third eyelids. PLoS One. 2019;14:e0221654. https://doi.org/10.1371/journal.pone.0221654
35. Angers RC, Browning SR, Seward TS, Sigurdson CJ, Miller MW, Hoover EA, et al. Prions in skeletal muscles of deer with chronic wasting disease. Science. 2006;311:1117. https://doi.org/10.1126/science.1122864
36. Henderson DM, Denkers ND, Hoover CE, McNulty EE, Cooper SK, Bracchi LA, et al. Progression of chronic wasting disease in white-tailed deer analyzed by serial biopsy RT-QuIC and immunohistochemistry. PLoS One. 2020; 15:e0228327. https://doi.org/10.1371/journal.pone.0228327
37. Kramm C, Soto P, Nichols TA, Morales R. Chronic wasting disease (CWD) prion detection in blood from pre-symptomatic white-tailed deer harboring PRNP polymorphic variants. Sci Rep. 2020;10:19763. https://doi.org/10.1038/s41598-020-75681-7
38. Henderson DM, Tennant JM, Haley NJ, Denkers ND, Mathiason CK, Hoover EA. Detection of chronic wasting disease prion seeding activity in deer and elk feces by real-time quaking-induced conversion. J Gen Virol. 2017;98:1953–62. https://doi.org/10.1099/jgv.0.000844
39. Chianini F, Cosseddu GM, Steele P, Hamilton S, Hawthorn J, Síso S, et al. Correlation between infectivity and disease associated prion protein in the nervous system and selected edible tissues of naturally affected scrapie sheep. PLoS One. 2015;10:e0122785. https://doi.org/10.1371/journal.pone.0122785
40. Andréoletti O, Orge L, Benestad SL, Beringue V, Litaise C, Simon S, et al. Atypical/Nor98 scrapie infectivity in sheep peripheral tissues. PLoS Pathog. 2011;7:e1001285. https://doi.org/10.1371/journal.ppat.1001285
41. Kumagai S, Daikai T, Onodera T. Bovine spongiform encephalopathy—a review from the perspective of food

safety. Food Saf (Tokyo). 2019;7:21–47. https://doi.org/10.14252/foodsafetyfscj.2018009
42. Peden AH, Ritchie DL, Head MW, Ironside JW. Detection and localization of PrP^{Sc} in the skeletal muscle of patients with variant, iatrogenic, and sporadic forms of Creutzfeldt-Jakob disease. Am J Pathol. 2006;168:927–35. https://doi.org/10.2353/ajpath.2006.050788
43. Thomzig A, Cardone F, Krüger D, Pocchiari M, Brown P, Beekes M. Pathological prion protein in muscles of hamsters and mice infected with rodent-adapted BSE or vCJD. J Gen Virol. 2006;87:251–4. https://doi.org/10.1099/vir.0.81277-0
44. Bosque PJ, Ryou C, Telling G, Peretz D, Legname G, DeArmond SJ, et al. Prions in skeletal muscle. Proc Natl Acad Sci U S A. 2002;99:3812–7. https://doi.org/10.1073/pnas.052707499
45. Daus ML, Breyer J, Wagenfuehr K, Wemheuer WM, Thomzig A, Schulz-Schaeffer WJ, et al. Presence and seeding activity of pathological prion protein (PrP^{TSE}) in skeletal muscles of white-tailed deer infected with chronic wasting disease. PLoS One. 2011;6:e18345. https://doi.org/10.1371/journal.pone.0018345
46. Jewell JE, Brown J, Kreeger T, Williams ES. Prion protein in cardiac muscle of elk (*Cervus elaphus nelsoni*) and white-tailed deer (Odocoileus virginianus) infected with chronic wasting disease. J Gen Virol. 2006;87:3443–50. https://doi.org/10.1099/vir.0.81777-0
47. Li M, Schwabenlander MD, Rowden GR, Schefers JM, Jennelle CS, Carstensen M, et al. RT-QuIC detection of CWD prion seeding activity in white-tailed deer muscle tissues. Sci Rep. 2021;11:16759. https://doi.org/10.1038/s41598-021-96127-8
48. Tranulis MA, Tryland M. The zoonotic potential of chronic wasting disease—a review. Foods. 2023;12:824. https://doi.org/10.3390/foods12040824
49. Wadsworth JDF, Joiner S, Linehan JM, Jack K, Al-Doujaily H, Costa H, et al. Humanized transgenic mice are resistant to chronic wasting disease prions from Norwegian reindeer and moose. J Infect Dis. 2022;226:933–7. https://doi.org/10.1093/infdis/jiab033

Address for correspondence: Tram Thu Vuong, Norwegian Veterinary Institute, Arboretveien 57, 1433 Ås, Norway; email: tram.thu.vuong@vetinst.no

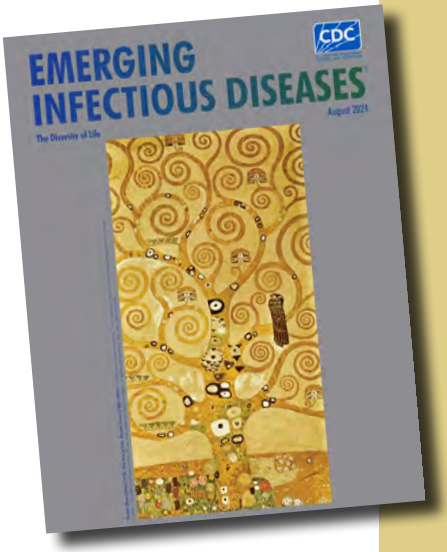

Originally published in August 2024

etymologia revisited

Microbiota microbiome

[mī′′-krō-bī′-ō-′tə], mī′′-krō-bī′-ōm]

From the Greek micro- (small) and -bios (life), microbiota was coined in the late 19th Century to denote the microorganisms residing in a specific environment. During the 20th Century, microbiota became more specifically associated with the microorganisms inhabiting the human body. Today, the term encompasses the collective genetic material of microorganisms, spanning viruses, archaea, bacteria, and fungi, and the intricate ecosystems of microorganisms, including commensal, symbiotic, and pathogenic ones, that exist within or on the human body or other environmental niches. Exploring microbiota and its implications in various aspects has rapidly gained momentum as a dynamic field of research.

Sources:

1. Dorland's illustrated medical dictionary. 32nd ed. Philadelphia: Elsevier Saunders; 2012.
2. Berg G, Rybakova D, Fischer D, Cernava T, Vergès MC, Charles T, et al. Microbiome definition re-visited: old concepts and new challenges. Microbiome. 2020;8:103. https://doi.org/10.1186/s40168-020-00875-0
3. Lederberg J, Mccray AT. 'Ome sweet 'omics—a genealogical treasury of words. Scientist. 2001;15:8–9.
4. Liu X. Microbiome. Yale J Biol Med. 2016;89:275–6.
5. Marchesi JR, Ravel J. The vocabulary of microbiome research: a proposal. Microbiome. 2015;3:31. https://doi.org/10.1186/s40168-015-0094-5

https://wwwnc.cdc.gov/eid/article/30/8/23-0677_article

Cyclospora Genotypic Variations and Associated Epidemiologic Characteristics, United States, 2018–2021

John Shen, Vitaliano A. Cama,[1] David Jacobson, Joel Barratt, Anne Straily[1]

Seasonal cyclosporiasis outbreaks occur in the United States every year. To better understand the disease, the Centers for Disease Control and Prevention developed a novel genotyping system that successfully clusters nonclonal eukaryotes. We examined temporal-geographic distributions of *Cyclospora* cluster consensus genotypes (CCGs) and applied regression analyses to identify correlations between *Cyclospora* spp. parasites and clinical manifestations or epidemiologic risk factors, using data collected during 2018–2021. No CCG was uniquely associated with or consistently detected in a state during the study, suggesting that cyclosporiasis in the United States is likely caused by frequent parasite introductions. We identified positive associations between infection with *C. ashfordi* and *C. cayetanensis* and consumption of specific produce items: cilantro, mango, and onion for *C. ashfordi* and iceberg lettuce, carrot, and cauliflower for *C. cayetanensis*. Our findings can guide future research into public health interventions aimed at reducing the burden of cyclosporiasis in the United States.

Cyclospora spp. are foodborne parasites that cause seasonal outbreaks of cyclosporiasis in the United States (*1*). Cases of this diarrheal disease are often sporadic and geographically dispersed; those characteristics, combined with the lengthy lag period between illness onset and patient interview (typically 4–6 weeks), make it difficult to identify the food vehicles of infection (*2*). Although cyclosporiasis has been reported year-round in the United States, most cases occur during May–August (*3*). Molecular typing, in conjunction with epidemiologic methods, has increased our understanding of disease transmission dynamics for other pathogens (*4*). For cyclosporiasis, the Centers for Disease Control and Prevention (CDC) developed a *Cyclospora* genotyping system, Cybernetic Clustering Of Nonclonal Eukaryotes (CYCLONE) bioinformatic workflow (*5*–*7*), that uses Illumina (https://www.illumina.com) sequence data generated from a set of 8 PCR-amplified *Cyclospora* genetic markers as input and computes a pairwise distance similarity matrix that is hierarchically clustered to yield clusters of genetically similar samples (*8*).

Application of CYCLONE previously revealed 2 distinct species of *Cyclospora*, *C. cayetanensis,* and *C. ashfordi*, as agents of cyclosporiasis in the United States (*7*). Those species are distinguished at the 360i2 nuclear locus and several other loci throughout the *Cyclospora* genome not included in CYCLONE; alleles are exclusive to each species (*7*). That study reported geographic and temporal trends during 2018–2020, when *C. cayetanensis* accounted for an estimated two thirds of documented cyclosporiasis in the United States and was generally a more common cause of illness in northern and midwestern states, whereas Texas and Florida had greater proportions of *C. ashfordi* infections (*7*).

The previous observations required deeper analysis, which is the focus of our study. To more precisely track genetic types over different time periods and determine the possibility for locally established foci of infection, we developed a novel approach for cluster categorization, termed cluster-consensus genotypes (CCGs). First, we analyzed observed temporal and geographic patterns by CCG among specimens submitted for *Cyclospora* genotyping during

Author affiliations: Oak Ridge Institute for Science and Education, Oak Ridge, Tennessee, USA (J. Shen); Centers for Disease Control and Prevention, Atlanta, Georgia, USA. (J. Shen, V.A. Cama, D. Jacobson, J. Barratt, A. Straily)

DOI: https://doi.org/10.3201/eid3102.240399

[1]These senior authors were co–principal investigators.

2018–2021 to better understand annual variation of *Cyclospora* CCGs by year and reporting state. Second, we analyzed clinical, biologic, or epidemiologic features that could be associated with the different species of *Cyclospora*, as has been observed for species of *Cryptosporidium* (*9*). We anticipate that our results will serve to bolster our understanding of cyclosporiasis in the United States.

The human subjects coordinator at CDC's National Center for Emerging and Zoonotic Infectious Diseases reviewed this project and deemed it a nonresearch public health surveillance activity. We conducted the activity consistent with applicable federal law and CDC policy (45 C.F.R. part 46; 21 C.F.R. part 56).

Methods

The study is based on 2,770 *Cyclospora*-positive fecal samples successfully genotyped by CDC during January 2018–December 2021 as available via National Center for Biotechnology Information under BioProject no. PRJNA578931 (*5*,*10*,*11*). We excluded from the analyses 1 fecal sample that was positive for *C. henanensis* and sequenced as part of the genotyping reference set (*7*) and samples for which the state of origin could not be ascertained.

Determination of *Cyclospora* CCGs

We submitted sequencing reads to CYCLONE for genotyping and used specimens with haplotypes detected for ≥5 of the 8 markers to generate genotypes and a pairwise distance matrix in CYCLONE. We clustered the resulting matrix hierarchically to produce a tree, which we dissected into discrete clusters of closely related specimens (*8*,*12*). Within each cluster, the genotype found in >50% of specimens became the representative CCG. Because CCGs are an emergent property of the clustering process, the individual genotypes within a cluster might vary slightly from the representative consensus genotype despite sharing most of their core haplotypes. For this study, we identified each CCG with the letter S and a 3-digit number (e.g., S001) (Figure 1). We analyzed proportional distribution of the 2 *Cyclospora* species on the basis of the submitting state and year of submission. A similar analysis at the CCG level looked at the 5 most frequently detected CCGs within states across the 4 years of the study and presented results as heatmaps. Within our study dataset, some genotyped specimens were previously epidemiologically linked to defined outbreak clusters, but others were not. Therefore, we conducted the CCG analysis first on all available samples (linked and not linked to an outbreak), and then once again only with specimens not linked to epidemiologically identified outbreak clusters, to determine if similar patterns were observed among non–outbreak-related samples.

Associations between Species and Disease Symptoms or Reported Produce Consumption

We filtered the dataset to keep only genotypes with associated epidemiologic data and complete genotype data at the 360i2 locus that was previously described as a species-defining allele for human-infecting

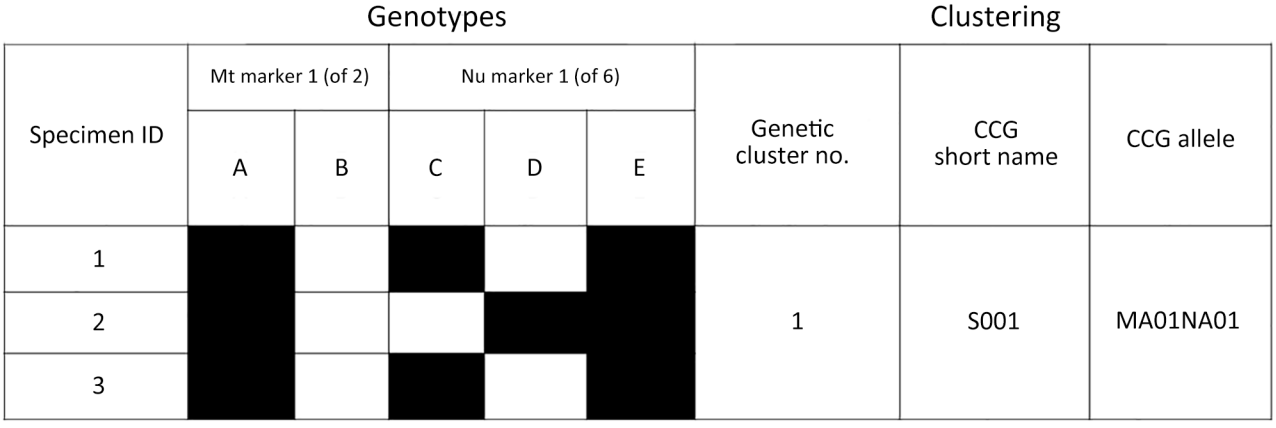

Figure 1. Schematic representation of a cluster consensus genotype in study of *Cyclospora* genotypic variations and associated epidemiologic characteristics United States, 2018–2021. Genotypes are derived from 8 markers, 2 Mt and 6 Nu; this schematic representation is based on 1 Mt and 1 Nu marker, where the haplotypes for this Mt marker are A or B, and the Nu haplotypes are C, D, or E. The Centers for Disease Control and Prevention *Cyclospora* genotyping system, Cybernetic Clustering Of Nonclonal Eukaryotes (CYCLONE) bioinformatic workflow, was used to determine the genetic similarity and clustered specimens 1, 2, and 3 in genetic cluster 1. Specimens 1 and 3 have genotype ACE, and specimen 2 has genotype ADE. Because genotype ACE is present in ≥50% of samples, it is the CCG for cluster 1, and its short name for this example is S001. The corresponding allele for this specific CCG is MA01 (Mt marker A) NA01 (Nu markers C and E). CCG, cluster consensus genotype; ID, identification; Mt, mitochondrial; Nu, nuclear.

Cyclospora (*7*). When a patient had >1 specimen genotyped, we kept the sample with the most complete genotype. However, if a patient's samples had discordant genotypes (e.g., for patients who became infected with different species on separate occasions), we excluded all patient samples from the analyses.

We used epidemiologic data from Cyclosporiasis National Hypothesis Generating Questionnaires (CNHGQs), completed by US cyclosporiasis patients during routine public health surveillance, to determine statistical associations between each species of *Cyclospora* and patient-reported clinical manifestations and produce consumption. The CNHGQ includes questions on patient demographics, state of residence, travel, clinical manifestations, and food consumption in the 2 weeks before symptom onset. We dichotomized responses about symptoms or consumption of food, using yes for yes/maybe responses and no for don't know/no responses. We used a patient's home state of residence as a proxy for the site of infection acquisition. Because domestic or international travel affected the validity of this proxy variable, we included travel variables in a regression model described in the next section. The CNHGQ includes food parent variables (e.g., bell pepper); if those elicit an affirmative response, the next question is for specific subset exposures within that parent variable (e.g., red bell pepper, orange bell pepper). We selected food parent variables for analysis and not the subset questions, which frequently had missing responses. *Cyclospora* outbreak investigations identified whether a person belonged to a specific epidemiologic cluster, in which ≥2 patients were linked to the same source of infection (i.e., food vehicle, store, or restaurant); such clustering was also factored into the final regression model.

Statistical Analysis

We described continuous variables by mean and SD or median and interquartile range and categorical variables by count and percentage. We assessed potential associations between *Cyclospora* species and epidemiologic features using Welch 2- sample *t*-tests for continuous variables and Pearson χ^2 or Fisher exact tests for categorical variables. If we could not assume a normal distribution for a continuous variable, we performed a Kruskal-Wallis rank-sum test instead. We presented missing data as the count of patients without a recorded value for a characteristic. We determined $p<0.05$ as statistically significant.

We used a generalized estimating equation (GEE) with a homogeneous exchangeable/compound symmetric covariance and correlation matrix structure to estimate associations between statistically significant variables from univariate analyses and *Cyclospora* species. This method enables clustering of outcomes as a result of genetically similar pathogens being connected with a common food vehicle in routine epidemiologic surveillance. Because a previous study (*7*) observed statistically significant temporal and geographic differences between *Cyclospora* species, we included both those characteristics in the model. The temporal component comprised 2 variables: year of detection and

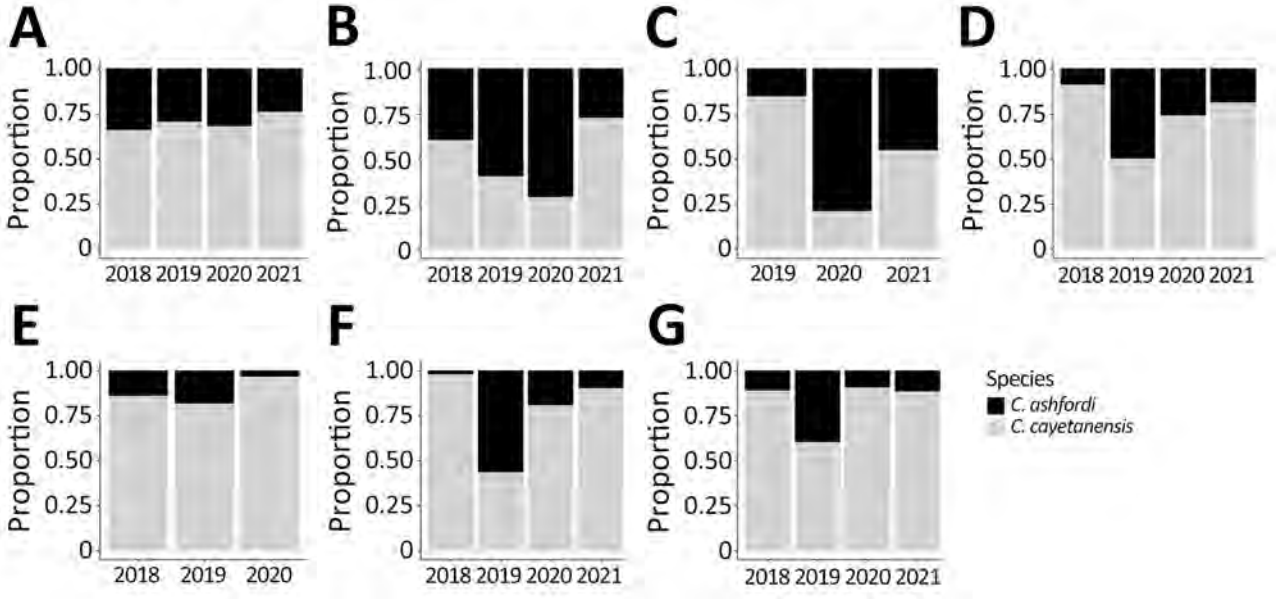

Figure 2. Proportion of *Cyclospora cayetanensis* and *C. ashfordi* in 7 states with highest number of specimens in study of *Cyclospora* genotypic variations and associated epidemiologic characteristics United States, 2018–2021. A) New York; B) Texas; C) Florida; D) Illinois; E) Iowa; F) Wisconsin; G) Minnesota. No specimens were submitted for genotyping from Florida in 2018 or from Iowa in 2021.

Table 1. Classification of CCGs by *Cyclospora* species and distribution by year in study of *Cyclospora* genotypic variations and associated epidemiologic characteristics, United States, 2018–2021*

Species	CCG ID	2018	2019	2020	2021
C. cayetanensis	S001	2.3	17.3†	3.1	10.4
	S002	1.6	2.7	0.3	2.6
	S003	2.0	2.7	0.6	3.4
	S005	1.8	3.5	0.5	2.4
	S006	1.6	0.4	16.9†	4.4
	S007	14.2	7.1	8.3	9.0
	S008	1.3	1.5	0.0	11.4
	S009	2.5	1.8	0.5	1.1
	S012	1.4	3.1	23.0†	19.7
	S013	0.4	0.9	0.3	1.3
	S014	0.4	1.5	0.0	0.8
	S015	0.7	1.1	1.0	0.7
	S018	1.1	1.3	0.1	1.3
	S021	0.7	3.9	0.6	1.5
	S022	20.2†	0.5	0.5	0.8
	S025	0.5	1.2	1.3	1.0
	S027	0.4	1.1	1.0	1.5
	S028	1.1	1.7	0.5	1.5
	S029	27.6†	1.3	0.4	0.0
	S033	0.0	0.2	4.0	0.3
C. ashfordi	S004	7.2	17.5†	21.4†	9.6
	S010	1.8	0.7	0.1	0.7
	S011	2.2	1.5	2.6	0.5
	S016	0.5	5.9	0.0	0.2
	S017	0.5	1.6	0.5	0.8
	S019	0.5	3.5	6.8	0.5
	S020	3.2	2.1	2.1	7.7
	S023	0.5	8.3	0.5	0.7
	S024	0.4	1.6	0.4	2.1
	S026	0.4	0.4	0.0	0.7
	S030	0.4	0.7	0.6	0.5
	S031	0.2	0.6	1.4	0.5
	S032	0.4	0.9	0.4	0.5

*Values are percentages. Species assignments apply to the consensus genotype for the whole cluster. CCG. cluster-consensus genotype.
†CCGs with distribution >15%.

day of the year (i.e., ordinal date) of symptom onset. Geographic variables included indicators for whether patients lived in Texas or Florida (2 states with higher proportions of *C. ashfordi* infection in the previous study [*7*]), whether they traveled out of state, and whether they traveled out of country. We added food and demographic variables to assess if statistically significant differences from bivariate analyses would be maintained after adjusting for covariates. We excluded patients missing any data for selected predictors. We performed all data cleaning, variable transformations, and statistical analyses using R statistical computing and graphics software (The R Project for Statistical Computing, https://www.R-project.org). We used the geepack package (*13*–*15*) to fit the GEE and ggplot2 (*16*) to produce the plots.

Results

Temporal-Geographic Distribution of *Cyclospora* Species and CCGs

Of the 2,770 specimens processed through CYCLONE, we excluded 9 *Cyclospora* specimens (0.3%): 1 reference isolate from China and 8 specimens for which the state of origin could not be ascertained. The evaluable 2,761 specimens originated from 33 states. The 7 states with the most isolates genotyped over the 4-year study period were New York (n = 651), Texas (n = 551), Florida (n = 222), Illinois (n = 212), Wisconsin (n = 224), Minnesota (n = 204), and Iowa (n = 185) (Figure 2; Appendix, https://wwwnc.cdc.gov/EID/article/31/2/24-0399-App1.pdf).

Overall, 67.1% of samples were *C. cayetanensis* and 32.9% were *C. ashfordi*; those percentages varied by state and year (Figure 2). In New York, *C. cayetanensis* accounted for 65.7%–76.3% of all genotyped specimens. In Iowa, the prevalence of *C. cayetanensis* fluctuated from 81.5% in 2018 to 96.6% in 2020; no specimens were genotyped in 2021. In Texas, we identified *C. ashfordi* in 71.4% of specimens submitted in 2020, dropping to 27.3% in 2021. In Florida, the prevalence of *C. ashfordi* ranged from 15.4% in 2019 to 78.9% in 2020. *C. cayetanensis* was more prevalent in Illinois, Wisconsin, and Minnesota except for 2019, when the prevalence of *C. ashfordi* increased to 50.0% in Illinois and 56.7% in Wisconsin.

In this study we identified 33 CCGs; 20 belonged to *C. cayetanensis* and 13 belonged to *C. ashfordi* (Table 1; Appendix Table 2). The annual distribution of CCGs (Table 1) varied considerably year-to-year. The predominant CCG in 2018 was S029 (27.6%, *C. cayetanensis*), in 2019 was S004 (17.5%, *C. ashfordi*), in 2020 was S012 (23.0%, *C. cayetanensis*), and in 2021 was S012 (19.7%). Of note, CCG S012 represented only 1.4% of specimens in 2018, but its proportion increased in 2020 to 23.0%. Furthermore, we noted high heterogeneity in CCG prevalence within each state over the study period. In some instances, CCGs that were abundant one year were nearly absent in subsequent years (e.g., S029 in Illinois) (Figure 3). Such shifts were less extreme in states like New York, Texas, and Florida that had more cyclosporiasis cases. In general, no specific CCG was uniquely associated with a state, and most CCGs were not detected in similar proportions over the study period. Similarly, no CCG was uniquely associated with a state or year in the analysis of the 2,044 specimens (74.0%) not related to outbreak clusters (Appendix Figure).

Associations between Species and Reported Manifestations or Produce Consumption

Of the 2,761 evaluable genotyped specimens, we excluded 1,045 (37.8%) that lacked an associated CNHGQ record. Seventeen patients had repeat collections, providing 2 *Cyclospora* specimens each; of those, we excluded 5 patients who exhibited discordant genotypes (10 samples [0.4%]). For the remaining 12

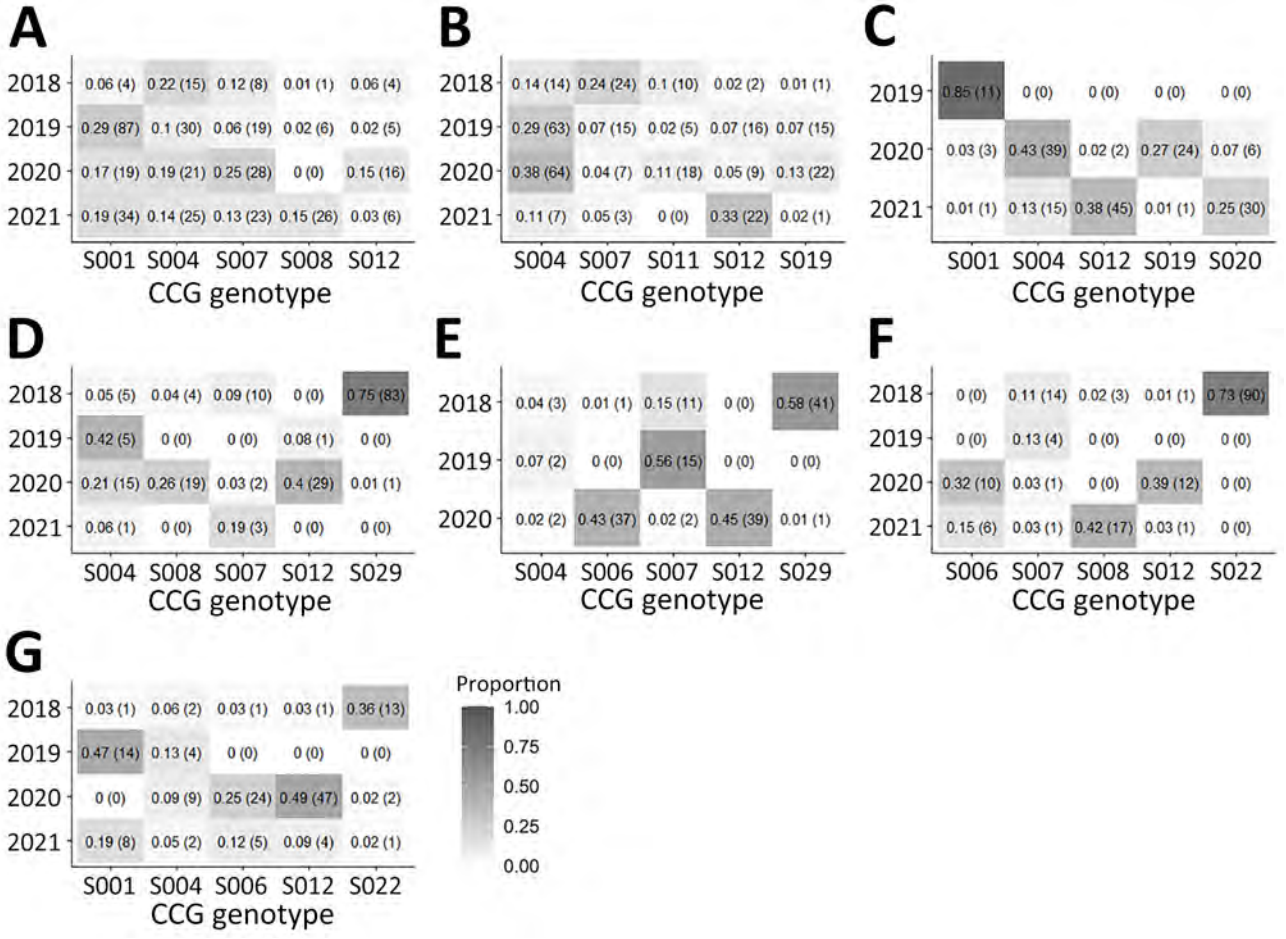

Figure 3. Heatmaps illustrating the proportions of the top 5 most prevalent CCGs in each of the 7 states with highest number of specimens in study of *Cyclospora* genotypic variations and associated epidemiologic characteristics United States, 2018–2021. A) New York; B) Texas; C) Florida; D) Illinois; E) Iowa; F) Wisconsin; G) Minnesota. Values within each box represent the percentage of the total number of specimens within a state for a given year. Numbers in parentheses represent the corresponding number of specimens. Darker shades represent higher proportions. The total number of specimens submitted per year is as follows: New York, 67 (2018), 297 (2019), 110 (2020), 177 (2021); Texas, 98 (2018), 219 (2019), 168 (2020), 66 (2021); Florida 0 (2018), 13 (2019), 90 (2020), 118 (2021); Illinois, 111 (2018), 12 (2019), 73 (2020), 16 (2021); Iowa, 71 (2018), 27 (2019), 87 (2020), 0 (2021); Wisconsin, 123 (2018), 30 (2019), 31 (2020), 40 (2021); Minnesota, 36 (2018), 30 (2019), 95 (2020), 43 (2021). CCG, cluster consensus genotype.

Table 2. Characteristics of patients in study of *Cyclospora* genotypic variations and associated epidemiologic characteristics, United States, 2018–2021*

Characteristic	Overall	Infected with *C. ashfordi*	Infected with *C. cayetanensis*	p value
No. patients	1,538	437	1,101	
Age, y				0.10
Mean (SD)	50.7 (16.6)	49.6 (16.5)	51.1 (16.6)	
Missing, no.	22	8	14	
Race				0.11
White	1,048 (94)	306 (92)	742 (95)	
Black or African American	45 (4.0)	21 (6.3)	24 (3.1)	
Asian	13 (1.2)	3 (0.9)	10 (1.3)	
American Indian or Alaska Native	6 (0.5)	2 (0.6)	4 (0.5)	
Native Hawaiian or Pacific Islander	1 (<0.1)	0 (0)	1 (0.1)	
Missing, no.	425	105	320	
Ethnicity				<0.001
Non-Hispanic	1,080 (86)	310 (80)	770 (88)	
Hispanic	183 (14)	78 (20)	105 (12)	
Missing, no.	275	49	226	
Sex				>0.99
F	862 (57)	244 (57)	618 (57)	
M	640 (43)	181 (43)	459 (43)	
Missing, no.	36	12	24	

*Values are no. (%) except as indicated.

patients, we retained the sample with more complete genotype data (12 exclusions [0.4%]). We also excluded sequences with ambiguous 360i2 data (n = 156 [5.7%]). We used a final sample set of 1,538 patient sequences (55.7% of the evaluable genotyping set) for analyses (n = 214 from 2018, n = 413 from 2019, n = 482 from 2020, n = 429 from 2021). Of the final set, 437 (28.4%) sequences were *C. ashfordi* and 1,101 (71.6%) were *C. cayetanensis*.

Most patients were White (n = 1,048 [94%] of 1,113 with race data), and more were female than male (n = 862 [57%] female, n = 650 male [43%], of 1,502 with sex data). The average age was 50.7 years. We detected no statistically significant difference between species groups (p = 0.10). More patients infected with *C. ashfordi* self-identified as Hispanic (n = 78 [20%]) than those infected with *C. cayetanensis* (n = 105 [12%]; p<0.001) (Table 2). Eight cyclosporiasis clinical manifestations were documented in the CNHGQ (Table 3). Diarrhea was most commonly reported (n = 1,224 [98%]), followed by abdominal cramps (n = 921 [77%]), fatigue (n = 920 [76%]), weight loss (n = 856 [72%]), nausea (n = 829 [69%]), vomiting (n = 823 [68%]), fever (n = 758 [63%]), and anorexia (n = 751 [63%]). More patients infected with *C. cayetanensis* than *C. ashfordi* reported experiencing fatigue (79% vs. 71%; p = 0.003). Among those who responded to all symptom-related questions (n = 1,159), the median number of symptoms in patients with *C. cayetanensis* was 6 and in patients with *C. ashfordi* was 5, although this difference was not statistically significant (p = 0.070). Of the 1,416 patients who responded to questions about hospitalization, 81 (5.7%) were hospitalized a median of 3 nights (interquartile range 2–4 nights); maximum stay was 16 nights. A slightly larger percentage of patients with *C. ashfordi* (n = 30 [7.7%]) were hospitalized than were patients with *C. cayetanensis* (n = 51 [5.0%]), although the difference was not statistically significant (p = 0.053).

We included 64 produce items for bivariate analysis, although 26.5% of patients (n = 408) did not respond to produce-related questions. A greater percentage of patients infected with *C. ashfordi* recalled eating cilantro (44% vs. 28%; p<0.001), squash (14% vs. 8.9%; p = 0.010), guacamole (31% vs. 23%; p = 0.003), pico de gallo (32% vs. 25%; p = 0.022), plum (8.8% vs. 4.9%; p = 0.015), onion (49% vs. 41%; p = 0.018), mango (18% vs. 13%; p = 0.024), and lemon or lime (43% vs. 35%; p = 0.014) (Table 4). More patients infected with *C. cayetanensis* reported consumption of iceberg lettuce (49% vs. 39%; p = 0.001), cauliflower (23% vs. 11%; p<0.001), bagged salad kit (15% vs. 9.4%; p = 0.013), and carrot (30% vs. 23%; p = 0.018).

In addition to covariates for time and geography, we included covariates for ethnicity and produce items with statistically significant results (Table 4) in a GEE model with *Cyclospora* species as the outcome. We dropped patients with missing covariate values, leaving 908 patients (59%) for analysis (*C. ashfordi*, n = 277; *C. cayetanensis*, n = 631). The species proportions remained similar even with such exclusions, suggesting an equitable distribution of missing data across species. The model included year and ordinal date of illness onset to control for temporal variations in species prevalence, but we did not interpret those data for analysis. We detected no multicollinearity among the predictor variables.

Geography and the produce items cilantro, mango, onion, iceberg lettuce, carrot, and cauliflower all had a statistically significant association with *Cyclospora* species, all else being equal (Figure 4). In patients from Texas or Florida, prevalence of infection with *C. ashfordi* was 2.18 (95% CI 1.76–2.70) times greater than for *C. cayetanensis*. Patients reporting international travel were also more frequently infected with *C. ashfordi* (prevalence ratio [PR] 1.56 [95% CI 1.04–2.34]) than were those who remained in-country. Infections with *C. ashfordi* were associated with consumption of cilantro (PR 1.32 [95% CI 1.08–1.61]), mango (PR 1.27 [95% CI 1.01–1.59]), and onion (PR 1.45 [95% CI 1.01–1.21]), whereas consumption of iceberg lettuce (PR 0.77 [95% CI 0.65–0.92]), carrot (PR 0.75 [95% CI 0.61–0.92]), and cauliflower (PR 0.69 [95% CI 0.53–0.91]) were significantly associated with *C. cayetanensis* infections.

Discussion

This study used a novel genotype designation to understand the genetic diversity and molecular epidemiologic trends of cyclosporiasis in the United States over 4 consecutive years. The data we used are likely representative of the US cyclosporiasis trends given our relatively large and diverse sample size, including samples collected over multiple years.

Although there are annual cyclosporiasis outbreaks in the United States, our understanding of the transmission dynamics of *Cyclospora* is limited. One such knowledge gap is where produce originally becomes contaminated. One hypothesis suggests that contamination arises from local prevalence or persistence of *Cyclospora* within the United States (*17*). Other theories posit that sources of contamination originate outside the United States from repeated introductions such as imported produce, migrant or seasonal farmworkers, travelers carrying the parasite, or other yet-to-be-investigated means (*17*,*18*).

This study detected high heterogeneity of CCGs, both over time and by state, findings that may support the hypothesis that cases of cyclosporiasis in the United States are likely caused by frequent new introductions, rather than *Cyclospora* parasites that persist in the local environment. For example, the high heterogeneity of CCGs observed by state and over time could be attributable to imported produce. Given the globalization of food supplies, produce sold in the United States are imported from many areas, some of which may be endemic for *Cyclospora* at different times, which might explain the diversity of CCGs we reported.

Table 3. Patient-reported clinical symptoms and outcomes overall and by *Cyclospora* species exposure in study of *Cyclospora* genotypic variations and associated epidemiologic characteristics, United States, 2018–2021*

Clinical symptom or outcome	Overall	Infected with *C. ashfordi*	Infected with *C. cayetanensis*	p value
No. patients	1,538	437	1,101	
Diarrhea				0.92
Y	1,224 (98)	365 (98)	859 (98)	
N	26 (2.1)	8 (2.1)	18 (2.1)	
Missing, no.	288	64	224	
Weight loss				0.71
Y	856 (72)	255 (71)	601 (72)	
N	340 (28)	105 (29)	235 (28)	
Missing, no.	342	77	265	
Fever				0.71
Y	758 (63)	231 (64)	527 (63)	
N	445 (37)	131 (36)	314 (37)	
Missing, no.	335	75	260	
Fatigue				0.003
Y	920 (76)	257 (71)	663 (79)	
N	283 (24)	105 (29)	178 (21)	
Missing, no.	335	75	260	
Anorexia				0.86
Y	751 (63)	229 (63)	522 (63)	
N	440 (37)	132 (37)	308 (37)	
Missing, no.	347	76	271	
Nausea				0.076
Y	829 (69)	236 (65)	593 (70)	
N	379 (31)	127 (35)	252 (30)	
Missing, no.	330	74	256	
Vomiting				0.14
Y	823 (68)	258 (71)	565 (67)	
N	380 (32)	103 (29)	277 (33)	
Missing, no.	335	76	259	

*Values are no. (%) except as indicated.

Table 4. Patient-reported produce consumption in the 2 weeks before symptom onset, overall and by *Cyclospora* species exposure, in study of *Cyclospora* genotypic variations and associated epidemiologic characteristics United States, 2018–2021*

Produce	Overall	Infected with *C. ashfordi*	Infected with *C. cayetanensis*	p value
No. patients	1,538	437	1,101	
Produce consumed more commonly by patients infected with *C. ashfordi*				
Cilantro				<0.001
Y	356 (33)	145 (44)	211 (28)	
N	725 (67)	183 (56)	542 (72)	
Missing, no.	457	109	348	
Plum				0.015
Y	63 (6.1)	28 (8.8)	35 (4.9)	
N	978 (94)	292 (91)	686 (95)	
Missing, no.	497	117	380	
Lemon or lime				0.014
Y	390 (37)	137 (43)	253 (35)	
N	652 (63)	182 (57)	470 (65)	
Missing, no.	496	118	378	
Mango				0.024
Y	150 (14)	58 (18)	92 (13)	
N	896 (86)	264 (82)	632 (87)	
Missing, no.	492	115	377	
Squash				0.010
Y	110 (11)	46 (14)	64 (8.9)	
N	931 (89)	278 (86)	653 (91)	
Missing, no.	497	113	384	
Onion				0.018
Y	459 (44)	159 (49)	300 (41)	
N	596 (56)	166 (51)	430 (59)	
Missing, no.	483	112	371	
Pico de gallo				0.022
Y	288 (27)	103 (32)	185 (25)	
N	782 (73)	223 (68)	559 (75)	
Missing, no.	468	111	357	
Guacamole				0.003
Y	271 (25)	102 (31)	169 (23)	
N	799 (75)	224 (69)	575 (77)	
Missing, no.	468	111	357	
Produce more commonly consumed among patients infected with *C. cayetanensis*				
Iceberg lettuce				0.001
Y	509 (46)	128 (39)	381 (49)	
N	592 (54)	201 (61)	391 (51)	
Missing, no.	437	108	329	
Bagged salad kit				0.013
Y	142 (13)	30 (9.4)	112 (15)	
N	925 (87)	290 (91)	635 (85)	
Missing, no.	471	117	354	
Carrot				0.018
Y	298 (28)	73 (23)	225 (30)	
N	779 (72)	248 (77)	531 (70)	
Missing, no.	461	116	345	
Cauliflower				<0.001
Y	202 (19)	34 (11)	168 (23)	
N	865 (81)	289 (89)	576 (77)	
Missing, no.	471	114	357	

*Values are no. (%) except as indicated. We included produce items with statistically significant differences by χ^2 test.

We found that New York, Texas, and Florida tended to have higher numbers of reported cyclosporiasis cases than other states. The reasons for this observation are outside the scope of this study but could be attributed to population size or myriad differences related to public health reporting requirements and investigation capacities, access to healthcare, availability of diagnostic testing, or healthcare provider knowledge. For those same reasons, there is an inherent potential for sampling bias to occur in surveillance data. Although those 3 states saw less-pronounced shifts in *Cyclospora* genetic diversity, we observed no clear dominant or persistent pattern either at the species or CCG level, contrary to what we would expect if the parasite were persisting in the local environment.

The separation of *C. cayetanensis* into 3 species is a recent taxonomic change (*7*) and is yet to gain

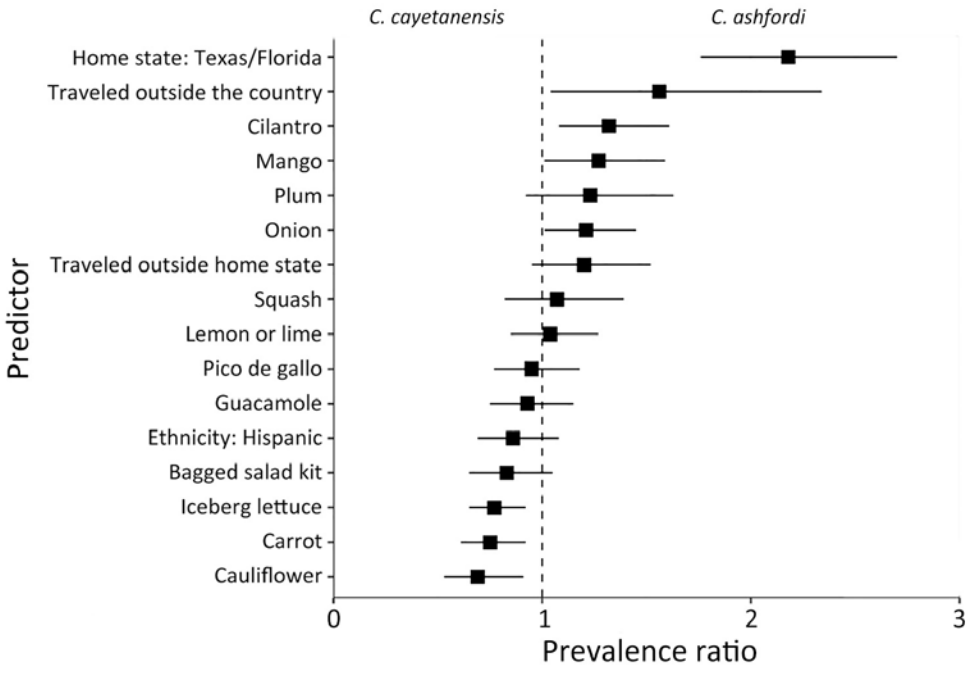

Figure 4. Forest plot presenting prevalence ratio point estimates for all predictors in the generalized estimating equation model in study of *Cyclospora* genotypic variations and associated epidemiologic characteristics United States, 2018–2021. Prevalence ratios are determined with *C. ashfordi* as the numerator and *C. cayetanensis* as the denominator, illustrating the comparative prevalence of these species across the various predictors. Boxes represent prevalence ratio point estimates; whiskers, 95% CI. The dashed line represents a prevalence ratio of 1.

widespread acceptance, as is typical for recent taxonomic revisions, particularly for medically important pathogens. We chose to retain the use of those proposed species' names for the purposes of this article. Another main finding of this analysis is that the 2 *Cyclospora* species described previously (*7*) showed distinct epidemiologic characteristics, potentially underpinning some presently unknown biologic differences between *C. cayetanensis* and *C. ashfordi* and providing further evidence in support of their taxonomic separation. Certain produce items were more commonly associated with *C. cayetanensis* and others with *C. ashfordi*. Because numerous specimens were collected during outbreak investigations, it is likely that related specimens will be found within clusters that are determined through epidemiologic analysis, with one food source serving as a common link. The occurrence of such clustering can create spurious associations; we used a multivariate GEE model to establish the relationship between predictor variables and *Cyclospora* species while considering the correlation between specimens within the same cluster (*19*). To account for spatiotemporal variability in CCG distribution, the model included covariates for geography and year. Our findings demonstrated that associations between some produce items and species remained statistically significant even after adjusting for clustering and spatiotemporal variance. However, certain produce items may be underreported because they do not constitute a major ingredient in a dish and persons may not recall consuming them; herbs are a prime example. In addition, because many fresh produce items are consumed in mixtures such as bagged salad mixes, guacamole, or pico de gallo, it can be difficult to pinpoint the true vehicles or predictors for *Cyclospora*. Despite those drawbacks, our findings identified several produce items of interest, and determining if there are factors in growing, harvesting, handling, or storage conditions of those produce items that may increase the likelihood of *Cyclospora* contamination is an area for further research.

Given that CCGs are an emergent property of probabilistic genetic clustering and the genetic clusters themselves are composed of similar but not always identical genotypes (*5*,*6*), the CCGs reported here may change in future studies. For example, a set of isolates may always genetically cluster together, but their CCG may change if isolates added or removed from the dataset cause the consensus genotype of the genetic cluster to change. Furthermore, the CCGs we described were created using 8 genetic markers; future addition of genotyping markers will increase the discriminatory capacity and long-term stability of CCGs but will also lead to the redefinition of genetic clusters. For those reasons, the CCGs we identified are robust for this study but may evolve when using either additional markers or other datasets, and the produce relationships identified in these analyses may change in future analyses. Overall, this study provides a foundation for improving our understanding of cyclosporiasis epidemiology in the United States.

The CNHGQ surveys were administered to patients after a confirmed laboratory diagnosis of cyclosporiasis, typically many days after infection has occurred. Therefore, the data may be affected by recall or symptom-associated biases (*20*), missing data, discrepancies, or errors. For this study, more than one third of samples from the genotyping dataset lacked corresponding CNHGQ data. Given their contributions to this type of molecular epidemiology study, having more complete CNHGQ information should be a focus for future work.

This study highlights several opportunities for future work. First, the CCGs were determined using at most 8 genetic markers that may not capture differences in other regions of the *Cyclospora* genome. Therefore, including additional genotyping markers could enhance the use of CCGs for molecular epidemiologic studies. Second, there is a need to collect and sequence *Cyclospora* samples from endemic areas because those data will enhance the understanding of the genetic diversity of *Cyclospora* and CCGs over space and time, and their genetic information may improve the stability of CCGs and genotyping methods.

Understanding food distribution networks and their variations can offer valuable insights into why specific species and CCGs appear in certain locations during particular times of year; that knowledge could shed light on whether CCGs are associated with the origin, processing or distribution of produce. Continued genotyping as part of ongoing, routine cyclosporiasis surveillance will bolster knowledge on temporal patterns of *Cyclospora*. Overall, such studies promise to improve cyclosporiasis outbreak investigations, potentially enabling investigators to trace the origins of *Cyclospora*-contaminated produce with heightened precision and fostering the development of prevention and control programs.

Acknowledgments

We thank the state and local health departments who worked diligently to collect epidemiological data and stool specimens from cyclosporiasis cases and provide those data to CDC. We thank Yvonne Qvarnstrom, Katelyn Houghton, Travis Richins, Anna Peterson, Lauren Ahart, Cody Bennett, Shannon Casillas, and Marion Rice, whose labors also contributed to the epidemiological data that made this study possible.

About the Author

Mr. Shen is a researcher, as part of the Oak Ridge Institute for Science and Education (ORISE) fellowship program, in the Division of Parasitic Diseases and Malaria, National Center for Emerging and Zoonotic Infectious Diseases, Centers for Disease Control and Prevention, Atlanta, Georgia, USA. His research interests include the epidemiology and prevention of zoonotic and human infectious diseases.

References

1. Casillas SM, Bennett C, Straily A. Notes from the field: multiple cyclosporiasis outbreaks—United States, 2018. MMWR Morb Mortal Wkly Rep. 2018;67:1101–2. https://doi.org/10.15585/mmwr.mm6739a6
2. Casillas SM, Hall RL, Herwaldt BL. Cyclosporiasis surveillance—United States, 2011–2015. MMWR Surveill Summ. 2019;68:1–16. https://doi.org/10.15585/mmwr.ss6803a1
3. Centers for Disease Control and Prevention. Domestically acquired cases of cyclosporiasis — United States, May–August 2022. 2022 [cited 2023 Mar 27]. https://web.archive.org/web/20230328230137/https://www.cdc.gov/parasites/cyclosporiasis/outbreaks/2022/seasonal/index.html
4. Sulaiman IM, Xiao L, Yang C, Escalante L, Moore A, Beard CB, et al. Differentiating human from animal isolates of *Cryptosporidium parvum*. Emerg Infect Dis. 1998;4:681–5. https://doi.org/10.3201/eid0404.980424
5. Nascimento FS, Barratt J, Houghton K, Plucinski M, Kelley J, Casillas S, et al. Evaluation of an ensemble-based distance statistic for clustering MLST datasets using epidemiologically defined clusters of cyclosporiasis. Epidemiol Infect. 2020;148:e172.
6. Barratt JLN, Park S, Nascimento FS, Hofstetter J, Plucinski M, Casillas S, et al. Genotyping genetically heterogeneous *Cyclospora cayetanensis* infections to complement epidemiological case linkage. Parasitology. 2019;146:1275–83. https://doi.org/10.1017/S0031182019000581
7. Barratt JLN, Shen J, Houghton K, Richins T, Sapp SGH, Cama V, et al. *Cyclospora cayetanensis* comprises at least 3 species that cause human cyclosporiasis. Parasitology. 2023;150:269–85.
8. Jacobson D, Barratt J. Optimizing hierarchical tree dissection parameters using historic epidemiologic data as 'ground truth'. PLoS One. 2023;18:e0282154. https://doi.org/10.1371/journal.pone.0282154
9. Cama VA, Ross JM, Crawford S, Kawai V, Chavez-Valdez R, Vargas D, et al. Differences in clinical manifestations among *Cryptosporidium* species and subtypes in HIV-infected persons. J Infect Dis. 2007;196:684–91. https://doi.org/10.1086/519842
10. Barratt J, Houghton K, Richins T, Straily A, Threlkel R, Bera B, et al. Investigation of US *Cyclospora cayetanensis* outbreaks in 2019 and evaluation of an improved *Cyclospora* genotyping system against 2019 cyclosporiasis outbreak clusters. Epidemiol Infect. 2021;149:e214. https://doi.org/10.1017/S0950268821002090
11. Ahart L, Jacobson D, Rice M, Richins T, Peterson A, Zheng Y, et al. Retrospective evaluation of an integrated molecular-epidemiological approach to cyclosporiasis outbreak investigations—United States, 2021. Epidemiol Infect. 2023;151:e131. https://doi.org/10.1017/S0950268823001176
12. Barratt JLN, Plucinski MM. Epidemiologic utility of a framework for partition number selection when

dissecting hierarchically clustered genetic data evaluated on the intestinal parasite *Cyclospora cayetanensis*. Am J Epidemiol. 2023;192:772–81. https://doi.org/10.1093/aje/kwad006
13. Yan J. geepack: yet another package for generalized estimating equations. R J. 2002;2:12–4
14. Yan J, Fine J. Estimating equations for association structures. Stat Med. 2004;23:859–74, discussion 875–7, 879–80. https://doi.org/10.1002/sim.1650
15. Halekoh U, Højsgaard S, Yan J. The R package geepack for generalized estimating equations. J Stat Softw. 2005;15:1–11.
16. Wickham H. ggplot2: Elegant graphics for data analysis. New York: Springer-Verlag; 2016.
17. Chacin-Bonilla L, Santin M. *Cyclospora cayetanensis* infection in developed countries: potential endemic foci? Microorganisms. 2023;11:540. https://doi.org/10.3390/microorganisms11030540
18. National Advisory Committee on Microbiological Criteria for Foods (NACMCF). Response to questions posed by the Food and Drug Administration (FDA): *Cyclospora cayetanensis* in produce. 2023. [cited 2023 Nov 15] https://www.fsis.usda.gov/sites/default/files/media_file/documents/NACMCF_Cyclospora_Report_2023_Final.pdf
19. Zeger SL, Liang KY, Albert PS. Models for longitudinal data: a generalized estimating equation approach. Biometrics. 1988;44:1049–60. https://doi.org/10.2307/2531734
20. Raphael K. Recall bias: a proposal for assessment and control. Int J Epidemiol. 1987;16:167–70. https://doi.org/10.1093/ije/16.2.167

Address for correspondence: Anne Straily, Centers for Disease Control and Prevention, 1600 Clifton Rd NE, Mailstop H16-4. Atlanta, GA 30329-4018, USA; email: yzv2@cdc.gov

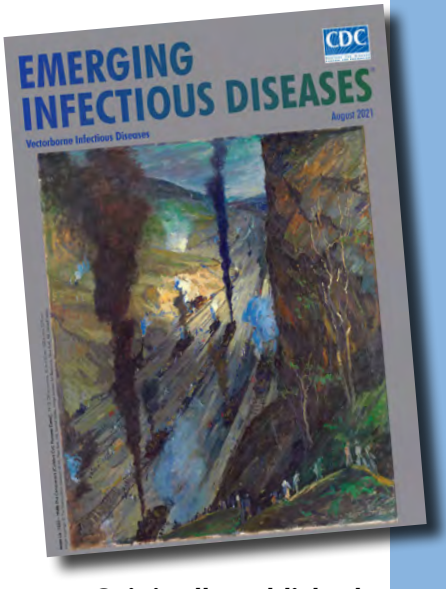

Originally published in August 2021

etymologia revisited

Culex quinquefasciatus
['kyo͞o leks 'kwinkwə fa she 'ah tus]

In 1823, the American entomologist Thomas Say described *Culex* (Latin for "gnat") *quinquefasciatus*, which he collected along the Mississippi River. Originally written as "C. 5-fasciatus," the name refers to 5 ("quinque") black, broad, transverse bands ("fasciatus" or "fasciae") on the mosquito's dorsal abdomen. The name remains despite later revelations of more than 5 fasciae, thanks to improved microscopy. Although quinquefasciatus is the official scientific name, there are at least 5 synonymous names for this species.

Say described this species as "exceedingly numerous and troublesome." "Quinx" are among the world's most abundant peridomestic mosquitoes, earning the nickname "southern house mosquito." *Cx. quinquefasciatus* is found throughout subtropical and tropical areas worldwide, except for exceedingly dry or cold regions. This mosquito is a principal vector of many pathogens, transmitting the phlebovirus Rift Valley fever virus and the 2 flaviviruses St. Louis encephalitis virus and West Nile virus, in addition to filarial worms and avian malarial parasites.

Sources

1. Belkin J. *Quinquefasciatus* or *Fatigans* for the tropical (Southern) house mosquito (Diptera: Culicidae). Proc Entomol Soc Wash. 1977;79:45–52.
2. Farajollahi A, Fonseca DM, Kramer LD, Marm Kilpatrick A. "Bird biting" mosquitoes and human disease: a review of the role of *Culex pipiens* complex mosquitoes in epidemiology. Infect Genet Evol. 2011;11:1577–85. https://doi.org/10.1016/j.meegid.2011.08.013
3. Harrison BA, Byrd BD, Sither CB, Whitt PB. The Mosquitoes of the Mid-Atlantic Region: An Identification Guide. Cullowhee (NC): Western Carolina University; 2016.
4. Say T. Descriptions of dipterous insects of the United States. Journal of the Academy of Natural Sciences. 1823;3:9–54.
5 University of Florida, Department of Entomology and Nematology. Featured creatures. [cited 2021 Mar 3]. http://entnemdept.ufl.edu/creatures/aquatic/southern_house_mosquito.htm

https//wwwnc.cdc.gov/eid/article/27/8/et-2708_article

Respiratory Shedding of Infectious SARS-CoV-2 Omicron XBB.1.41.1 Lineage among Captive White-Tailed Deer, Texas, USA

Francisco C. Ferreira, Tahmina Pervin, Wendy W. Tang, Joseph A. Hediger, Logan F. Thomas, Walter E. Cook, Michael J. Cherry, Benjamin W. Neuman, Gabriel L. Hamer, Sarah A. Hamer

White-tailed deer (*Odocoileus virginianus*) have high value for research, conservation, agriculture, and recreation and might be key SARS-CoV-2 reservoirs. In November 2023, we sampled 15 female deer in a captive facility in Texas, USA. All deer had neutralizing antibodies to SARS-CoV-2; respiratory swab samples from 11 deer were SARS-CoV-2–positive by quantitative reverse transcription PCR, and 1 deer also had a positive rectal swab sample. Six of the 11 respiratory swab samples yielded infectious virus; replication kinetics of most samples displayed lower growth 24–48 hours postinfection in vitro than Omicron lineages isolated from humans in Texas in the same period. Virus growth was similar between groups by 72 hours, suggesting no strong attenuation of deer-derived virus. All deer viruses clustered in XBB Omicron clade and demonstrated more mutations than expected compared with contemporaneous viruses in humans, suggesting that crossing the species barrier was accompanied by a high substitution rate.

The white-tailed deer (*Odocoileus virginianus*) (henceforth referred to as deer), a species native to North America, is highly susceptible to SARS-CoV-2 infection (*1*,*2*) and might serve as a viral reservoir because infected free-ranging deer can initiate onward intraspecies transmission (*3*,*4*). SARS-CoV-2 lineages have been detected in deer sampled up to 4–5 months after the same viral lineages were displaced from human populations by other lineages (*5*,*6*), suggesting sustained transmission within free-ranging animals. Transmission within deer can lead to a gradual accumulation of mutations in animal-adapted SARS-CoV-2 (*7*), which could alter infection kinetics or immune response when transmitted back into human populations (*8*). In addition, detections of deer-adapted virus infecting humans in Canada (*9*) and the United States (*3*) raise concerns about the emergence of sustained human–deer–human SARS-CoV-2 transmission cycles.

Captive animal herds with increased population densities and frequent human intervention might support transmission of zoonotic pathogens (*10*,*11*). Captive deer were also found to be naturally exposed to SARS-CoV-2, demonstrated by high rates of detection of viral RNA (*12*) and by high titers of neutralizing antibodies among deer (*13*). Managing highly susceptible animal species under human care creates opportunities for human-to-deer transmission and subsequent rapid dissemination within herds (*14*).

Data collected in 2012 estimated that ≈5,500 white-tailed deer breeding facilities exist in the United States (*15*). In the state of Texas, >1,000 existing facilities manage an average of 180–242 deer each (*16*,*17*). Having such large numbers of deer under human management might favor human-to-deer and deer-to-deer transmission events, leading to subsequent spread of deer-adapted viruses from farmed animals back into humans, which has been documented with farmed minks (*Neovison vison*) in Europe (*18*,*19*) and as a possibility in the United States (*20*).

Despite continued testing of deer for SARS-CoV-2 since the Omicron variant of concern emerged in the United States in November 2021, the detection rate of recent lineages in deer remains low (*3*,*21*). For example, only 2.5% (16 out of 648 genomes) of deer-derived sequences in GISAID (https://www.gisaid.org) as of August 14, 2024, belonged to the Omicron variant (GRA clade) (*22*). Those findings suggest deer are susceptible to new emerging lineages, yet the cause of a salient reduction in infection is unclear; reduced deer

Author affiliations: Texas A&M University, College Station, Texas, USA (F. Ferreira, T. Pervin, W.W. Tang, L.F. Thomas, W.E. Cook, B.W. Neuman, G.L. Hamer, S.A. Hamer); Texas A&M University—Kingsville, Kingsville, Texas, USA (J.A. Hediger, M.J. Cherry)

DOI: https://doi.org/10.3201/eid3102.241458

exposure to SARS-CoV-2, reduced virus fitness and detectability, protective immunity caused by exposure to pre-Omicron variants, reduced surveillance efforts, a lag between detection and reporting, or a combination of those factors could all play a role. Therefore, continued genomic surveillance of highly susceptible species remains critical to understand the current landscape of SARS-CoV-2 transmission and evolution in wildlife reservoirs.

We established an active surveillance program to determine SARS-CoV-2 circulation in captive deer in Texas to understand and mitigate transmission risk between humans and animals. In this study, we describe a SARS-CoV-2 outbreak in a captive deer-breeding facility in November 2023.

Methods

Cervid Facility

On November 15, 2023, we visited a private cervid facility in Milam County, Texas, as part of a larger project about SARS-CoV-2 surveillance in captive deer in the state. Deer were restricted to 2 pens separated by a fence and were able to have direct contact through the fence line. This facility falls into the category of outdoor ranch (*23*), although human–deer contact rates are high in our case because of veterinary care and animal husbandry.

Deer Sampling

Fifteen apparently healthy female white-tailed deer were chemically immobilized for chronic wasting disease testing and endectocide treatment (unrelated to our research), at which time samples were collected for this SARS-CoV-2 investigation. We collected oral and nasal swab samples from deer using sterile polyester-tipped applicators with polystyrene handles (Puritan Medical Products, https://www.puritanmedproducts.com) and combined samples (henceforth referred to as respiratory swab samples) for each animal into a vial containing 3 mL of viral transport media (VTM) made following Centers for Disease Control and Prevention standard operating procedure number DSR-052-02. We collected rectal swab samples from the same animals into a separate vial with VTM. We collected blood (≈10 mL) from all animals through jugular venipuncture using sterile needles and syringes, transferred samples to tubes without anticoagulants, and aliquoted the obtained serum samples into microtubes. Our study followed relevant guidelines and regulations approved by the Texas A&M University Institutional Animal Care and Use Committee and Clinical Research Review Committee (2022-0001 CA).

Molecular Detection and Whole-Genome Sequencing

We extracted total nucleic acid (TNA) from respiratory and rectal swab samples using the MagMax CORE Nucleic Acid Purification Kits on a 96-well Kingfisher Flex System (Thermo Fisher Scientific, https://www.thermofisher.com) following manufacturer instructions, using 200 µL of VTM from each sample and 90 µL of elution buffer. We added phosphate buffered saline 1× and a plasmid containing a portion of the RNA-dependent RNA polymerase SARS-CoV-2 gene to the TNA extraction plate as negative and positive extraction controls. We tested 5 µL of TNA for SARS-CoV-2 by quantitative reverse transcription PCR (qRT-PCR) targeting the RNA-dependent RNA polymerase (RdRp) gene of the virus following reagent concentrations as described in Corman et al. (*24*). We used molecular grade water as negative control and the same positive control described previously for qRT-PCR and yielded their expected results. We considered samples with cycle threshold (Ct) values <40 as positive.

We submitted all qRT-PCR–positive samples to whole-genome sequencing at the Texas A&M University Institute for Genome Sciences and Society Molecular Genomics Core. For each sample, 20 µL of TNA was submitted to library preparation using the xGen SARS-CoV-2 Amplicon Panel (Integrated DNA Technologies, https://www.idtdna.com). Sequencing was performed in an Illumina NovaSeq SP PE 2 × 150 flowcell version 1.5 (https://www.illumina.com) to generate an average of 3 million reads per sample.

Bioinformatics

We processed raw reads for each sample through a pipeline developed by the Institute for Genome Sciences and Society Bioinformatics Core. Briefly, raw reads from the sequenced libraries were trimmed of low-quality bases and intact adaptor sequences using trim_galore version 0.6.10 (https://zenodo.org/records/5127899). We then mapped trimmed reads against the SARS-CoV-2 wild-type isolate genome assembly (National Center for Biotechnology Information RefSeq accession no. GCF_009858895.2) using the bwa aligner (*25*). Aligned reads for each sample then had variants called and filtered using BCFtools (*26*). Variant call files were then subset to further remove ambiguously called variants (defined as the ratio of an alternative variant called over the reference, <0.8) before International Union of Pure and Applied Chemistry (IUPAC) interrogation using a combination of Python and BCFtools. Finally, consensus sequences were called using BCFtools.

All SARS-CoV-2 genomes we obtained had ≥99.8% coverage. We interrogated positions with missing sequence data or mixed sequence data,

indicated by IUPAC nucleotide uncertainty codes K, S, R, Y, M, W, or N in the assembled genome by BLAST+ 2.15.0 (https://blast.ncbi.nlm.nih.gov), to verify the presence of insertions/deletions and generate a majority-rule consensus sequence for each sample, which we used in subsequent phylogenetic analysis. We analyzed consensus sequences on Nextclade version 3.2.0 (https://clades.nextstrain.org) for clade and lineage assignment (*27*).

We investigated mutations, insertions, and deletions in the consensus sequences using NextClade and the GISAID database (*22*). Sequence differences are reported relative to the strain genetically closest to the deer-derived SARS-CoV-2 isolates (GISAID accession no. hCoV-19/USA/CA-HLX-STM-DTH-MADVDZ/2023), which was collected from a human in California on November 11, 2023. We used UShER (https://genome.ucsc.edu/cgi-bin/hgPhyloPlace) (*28*) (assessed August 14, 2024) to determine the 10 available SARS-CoV-2 genomes most closely related to the sequences obtained in this study.

Virus Isolation

We isolated SARS-CoV-2 in a Biosafety Level 3 laboratory at the Global Health Research Complex at Texas A&M University by passaging a mix of 100 µL of VTM with 900 µL of 1× Dulbecco modified Eagle medium through syringe filtration using an 0.2 micron pore size onto Vero E6-TMPRSS2-T2A-ACE2 (BEI Resources, https://www.beiresources.org) cells expressing both endogenous cercopithecine angiotensin-converting enzyme 2 (ACE2) and transmembrane serine protease 2 (TMPRSS2), as well as transgenic human ACE2 and TMPRSS2. We cultured these cells in Dulbecco modified Eagle medium supplemented with 10% fetal bovine serum, 1× antibiotic/antimycotic and puromycin dihydrochloride (10 µg/mL final concentration). We incubated cell plates at 37°C with 5% CO_2 and collected the supernatants from samples exhibiting cytopathic effects within 24–72 hours for titration of infectivity. Those cytopathic effects are characterized by syncytium formation followed by rounding and detachment.

We performed titration of infectious virus by using the 50% tissue culture infectious dose ($TCID_{50}$) method onto Vero E6-TMPRSS2-T2A-ACE2 cells. In brief, we prepared serial 3-fold dilutions of inocula in culture medium and then used them to inoculate monolayers of cells in tissue culture–treated 96-well plates. After 72 hours, we fixed the cells with phosphate buffered physiologic saline containing 25% final concentration of formalin and stained with crystal violet. We calculated titers of infectious virus using the Reed-Muench method (*29*).

Virus Growth Curves

We used freshly titrated virus stocks with equal infectivity to inoculate onto Vero E6-TMPRSS2-T2A-ACE2 cells for 30 minutes, removed inoculum by 3 rinses with phosphate-buffered saline, and replaced it with culture medium. Through Global Health Research Complex at Texas A&M University, we obtained contemporaneous human clinical samples from nasal swab samples that were collected at various medical centers in southeastern Texas as part of an ongoing Texas Department of State Health Services virus surveillance project. We worked under approval from the Texas A&M University Institutional Review Board. The samples selected for use here included 1 isolate from each Pango lineage (*30*,*31*) obtained from patient clinical samples at our COVID-19 screening facility during October 1–November 30, 2023 (namely Pango lineages HV.1, HY.1, HK.11, HK.3, EG.10, EG.5, and JD.1) and were processed (isolated and titrated) in parallel with deer-isolated viruses. These human-derived isolates include all the distinct Pango lineages that were obtained 1 month before to 1 month after the deer-derived samples. In addition, the selected lineages represent the genotypes of 864 (38%) of 2,253 total sequenced SARS-CoV-2 complete genomes (excluding low-coverage and partial sequences) reported to GISAID from Texas during October 1–November 30, 2023. Performing experiments in parallel using human and deer samples enabled us to compare in vitro growth rates for both sample types. We collected small aliquots (100 µL) of medium at 8, 24, 48, and 72 hours after inoculation and submitted them to RNA extraction and Luna One-Step qRT-PCR (New England Biolabs, https://www.neb.com) targeting the nucleoprotein gene. We conducted a 1-way analysis of variance with Tukey correction for multiple comparisons to compare growth curves of human- and deer-derived isolates. Growth curve plots were generated using GraphPad version 10.0.0 (https://www.graphpad.com).

Plaque Reduction Neutralization Tests

Serum samples from all deer were tested for the presence of neutralizing antibodies against SARS-CoV-2 (BEI Resources; isolate USAIL1/2020) through plaque reduction neutralization tests (PRNT) in Vero-CCL-81 (*13*). Aliquots of the samples were inactivated at 56°C for 30 minutes and screened at an initial dilution of 1:10. Samples that neutralized ≥90% of viral plaques, in comparison with the virus control, were further tested with serial 2-fold dilutions to determine the 90% endpoint titers ($PRNT_{90}$).

Results

SARS-CoV-2 Detection and Serology in White-Tailed Deer

The respiratory swab samples of 11 (73.3%) of the 15 deer tested positive for SARS-CoV-2; of those SARS-CoV-2–positive deer, 1 (animal identification no. 231115-USDA-D89) also had a SARS-CoV-2–positive rectal swab sample, whereas all other rectal swab samples tested negative. The mean for the Ct values for respiratory samples was 27.93 (SD = 3.20, range 22.12–31.92) (Table).

All 15 deer had neutralizing antibodies against SARS-CoV-2 as demonstrated by PRNT. $PRNT_{90}$ endpoint titers varied from 1:10 to 1:320 in qRT-PCR–positive animals (mean 91, SD 93) and ranged from 1:20 to 1:640 in qRT-PCR–negative animals (mean 210, SD 294) (Table).

Virus Isolation

To assess whether deer-derived SARS-CoV-2 was able to efficiently use human ACE2 and TMPRSS2 for cell entry, we inoculated Vero E6-TMPRSS2-T2A-ACE2 cells with all 12 qRT-PCR–positive respiratory and rectal swab samples. Six respiratory samples (D92, D93, D94, D95, D96, D100) (Figure 1) produced cytopathic effects characteristic of SARS-CoV-2 on this cell line (Table). Each of those viral isolates was designated as recovered to differentiate the isolates from the potentially broader SARS-CoV-2 populations present in the original samples from infected animals (Figure 1). We grew and titrated stocks of each isolate by the $TCID_{50}$ method for further study.

To compare growth rates of viruses isolated from deer with strains that were circulating in humans in Texas at the same time, we performed multistep growth curves, starting at low multiplicity of infection (0.002). We observed that 5 of 6 deer-derived viruses showed lower growth rates than did human-derived isolates at 24 hours, and 4 of 6 deer-derived viruses showed lower growth rates than did human-derived isolates at 48 hours ($p<0.05$) (Figure 1, panel B). We noted no differences in growth at 8 hours or 72 hours (Figure 1, panel A). Those data indicated that deer-derived SARS-CoV-2 isolates were able to efficiently grow in cells expressing human ACE2 and TMPRSS2, with a delay in early growth and no difference in burst size compared with contemporaneous SARS-CoV-2 isolated from humans.

SARS-CoV-2 Sequencing

We obtained complete (>99.8%) SARS-CoV-2 genomes from all 12 qRT-PCR–positive samples (11 respiratory samples and 1 rectal swab sample) belonging to 11 animals. Analysis by Nextclade revealed that all viruses fell within the XBB clade (XBB.1.41.1 lineage assigned by Pangolin version 4.3, also known as JC.5). Viruses most closely related to the ones sequenced from deer were collected from humans in California on November 11, 2023 (GISAID accession no. hCoV-19/USA/CA-HLX-STM-DTHMADVDZ/2023); from Texas on December 19, 2023; and from Texas in January 2024 (Figure 2). Those sequences from humans were obtained from different GISAID submitters and had identities ranging from 95.5% (1,352-base difference) to 99.9% (21-nt difference) in relation to the sequences we obtained from deer. No SARS-CoV-2 detected in deer in other regions of North America clustered together with the genomes obtained here.

Our deer-derived sequences had 15 nt substitutions not found in the closest human-derived isolates

Table. Quantitative reverse transcription PCR Ct values, virus isolation results, and $PRNT_{90}$ results in study of respiratory shedding of infectious SARS-CoV_2 Omicron XBB 1.41.1 lineage among captive white-tailed deer (*Odocoileus virginianus*), Texas, USA, November 2023*

Animal identification no.	Ct value for respiratory swab samples	Ct value for rectal swab samples	Virus isolation from respiratory swab samples	$PRNT_{90}$ endpoint titer
231115-USDA-D87	28.04	NA	Negative	1:80
231115-USDA-D88	29.02	33.44	Negative†	1:320
231115-USDA-D89	31.62	NA	Negative	1:80
231115-USDA-D90	28.30	NA	Negative	1:80
231115-USDA-D91	NA	NA	NA	1:640
231115-USDA-D92	28.66	NA	Positive	1:160
231115-USDA-D93	28.11	NA	Positive	1:20
231115-USDA-D94	24.73	NA	Positive	1:40
231115-USDA-D95	22.12	NA	Positive	1:40
231115-USDA-D96	23.78	NA	Positive	1:10
231115-USDA-D97	NA	NA	NA	1:160
231115-USDA-D98	NA	NA	NA	1:20
231115-USDA-D99	NA	NA	NA	1:20
231115-USDA-D100	31.92	NA	Positive	1:10
231115-USDA-D101	31.07	NA	Negative	1:160

*Ct, cycle threshold; NA, not applicable; $PRNT_{90}$, 90% plaque reduction neutralization test.
†Neither respiratory nor rectal swab samples yielded infectious virus.

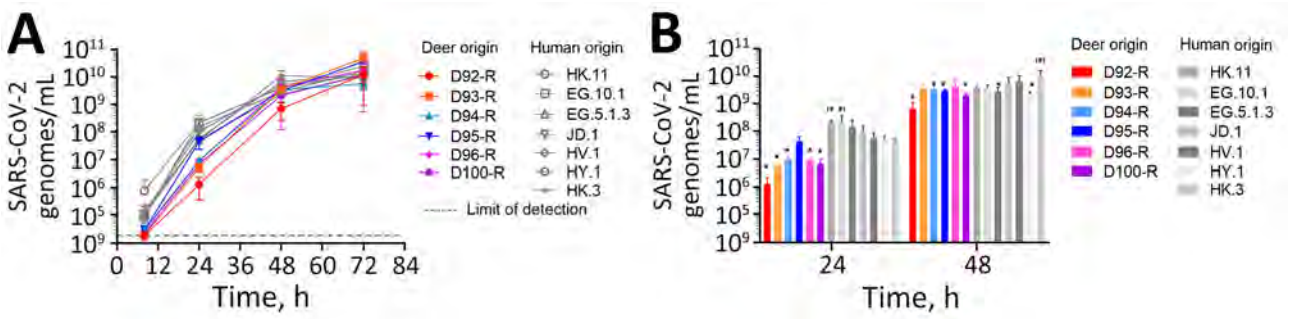

Figure 1. Multistep growth characteristics of contemporaneous strains isolated from captive white-tailed deer and humans in study of respiratory shedding of infectious SARS-CoV-2 Omicron XBB 1.41.1 lineage among captive white-tailed deer, Texas, USA, November 2023. A) Vero E6-TMPRSS2-T2A-ACE2 cells were inoculated with SARS-CoV-2 recovered from deer (D92-R to D100-R) or from human clinical nasopharyngeal samples (EG.10.1, EG.5.1.3, HK.11, JD.1, HV.1, HY.1, HK.3) at a multiplicity of infection of 0.002. Samples of the supernatant were collected and titrated by 1-step quantitative PCR. Lower limit of detection is indicated. B) Averaged data for the 24-hour and 48-hour timepoints. Statistically significant differences after 1-way analysis of variance with Tukey correction are indicated by asterisks for values significantly lower than aggregated human samples and asterisks in parentheses for values significantly higher than aggregated human samples. Error bars indicate SDs calculated from 3 replicates. We added "-R" to the name of each animal identification number to indicate that samples used in these experiments were recovered from the initial virus isolation step.

and up to 11 substitutions shared by some or none of the other deer-derived sequences. Compared with those closely related human samples, the viruses detected in deer did not have unique mutations in the spike protein. However, the viruses detected from humans in Lubbock County, Texas, and in Oklahoma had amino acid changes (N74S [Lubbock County] and Q146H [Oklahoma]) not present in the deer samples when using the lineage XBB as a reference.

Discussion

All 15 deer sampled in a captive facility in Texas had evidence of exposure to SARS-CoV-2, and 11 (73%) deer were shedding viral RNA, showing a widespread virus dissemination among the animals. In addition, whole-genome sequencing that revealed that recent Omicron lineages continue to be detected within deer in North America. Of the qRT-PCR–positive deer assessed, 6 had infectious virus in their upper respiratory tract. Although viruses isolated from most deer showed slower growth at 24 hours and 48 hours after inoculation in vitro than did contemporaneous human-isolated viruses, the number of viral copies at 72 hours was similar between groups, showing no attenuation in deer-adapted viruses. The XBB lineage detected in our study was circulating at low frequency in human populations in the United States; cumulative prevalence was <0.5% during May 2023–January 2024 (*32*), concurrent with the period in which deer were sampled for this study.

Human-derived SARS-CoV-2 have 30–32 substitutions/genome/year (≈2.5/month; https://nextstrain.org/ncov/gisaid/global/6m?l=clock). The human strainhCoV-19/USA/CA-HLX-STM-DTHMADVDZ/2023 and our deer samples were collected 7 days apart and displayed 15–22 nt substitutions among them, suggesting that crossing the species barrier from human to captive deer was accompanied by a high substitution rate. However, determining that pace is difficult without knowing when the initial spillover into this population occurred. Possible explanations for the proposed burst of evolution include bottlenecking and strong activation of mutagenic intracellular factors, such as RNA editing enzymes (ADAR1) and apolipoprotein B mRNA editing enzyme, catalytic polypeptide-like (APOBECs) in deer (*9*). For instance, APOBECs play a key role during natural infections, and the catalytic subunit 3H was shown to display stronger upregulation in infected deer than in humans with natural infections (*33*). Furthermore, the comparable to slightly attenuated growth of deer and human isolates suggests that deer-to-human transmission, and concomitant bursts of evolution within deer, have the potential to produce variants that might not display substantial loss of adaptation for infection and development in humans. This finding suggests that Omicron SARS-CoV-2 lineages circulating in deer might be efficiently transmitted back to humans.

Further, the role of other wild or domestic animals in generating, harboring, or transmitting mutated virus at such deer facilities is unknown. The XBB clade has been detected in multiple wildlife species in areas within a rural-to-urban gradient; ≥5 transmission events from human to animals have occurred (*34*). Because wildlife species susceptible to SARS-CoV-2 share habitat with captive deer (*34*,*35*), our results suggest that infectious deer have the potential to infect and be infected by commingling species. Assessments of wildlife, livestock, and humans that

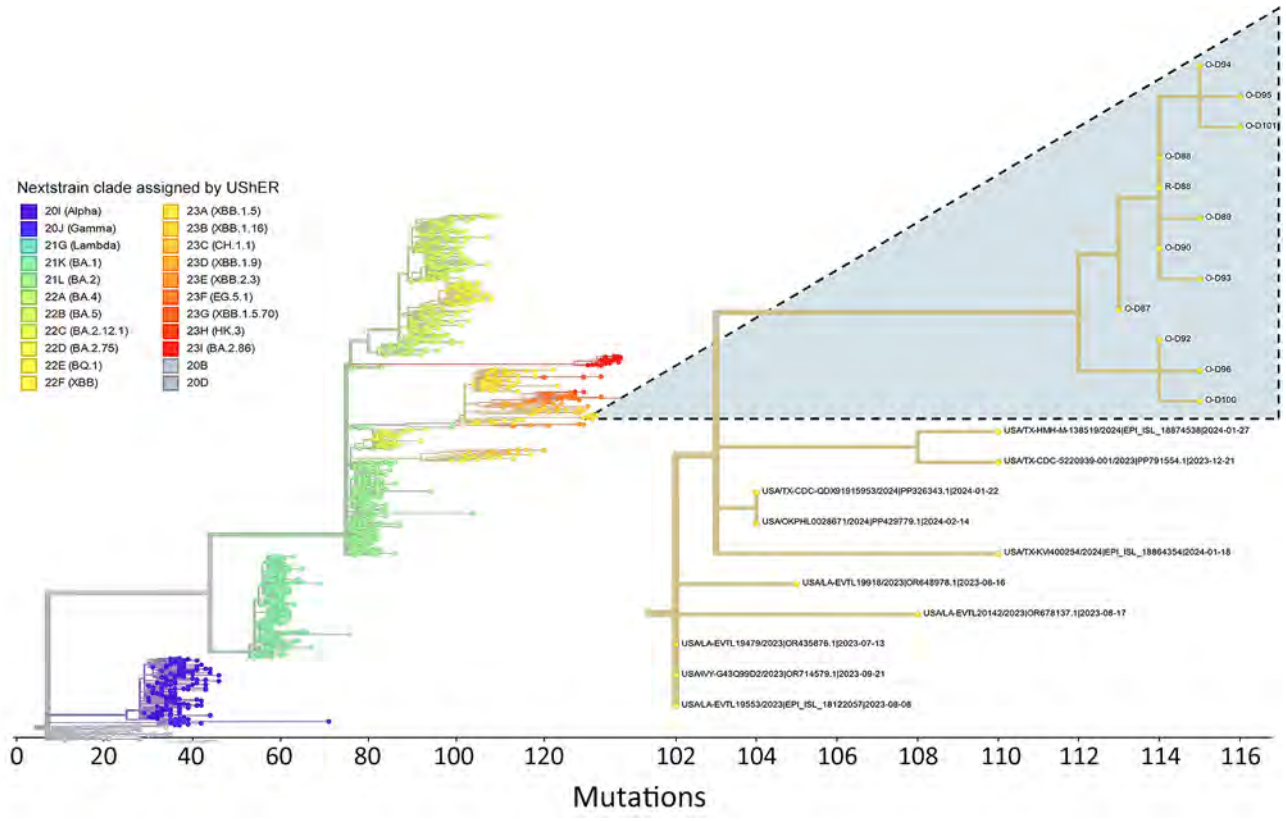

Figure 2. Phylogenetic context of SARS-CoV-2 from captive white-tailed deer in study of respiratory shedding of infectious SARS-CoV-2 Omicron XBB 1.41.1 lineage, Texas, USA, November 2023. Genome sequences from deer were compared in the main phylogenetic tree with genomes representative of the main virus Nextstrain clades as assigned by UShER (https://genome.ucsc.edu/cgi-bin/hgPhyloPlace) (28). The secondary tree at right details the 22F (XBB) clade and displays the placement of genomes obtained in our study (highlighted clade; O indicates oral/nasal swab, R indicates rectal swab) in relation to 10 of the most closely related samples deposited in GISAID (https://www.gisaid.org) as of August 14, 2024.

commingle with infected captive deer are a high priority for testing for cross-species transmission events.

Free-ranging deer are predicted to be at higher risk for exposure to SARS-CoV-2 when sharing fence line with captive populations (*23*), and the high frequency of infectious deer we detected emphasizes that transmission from captive to wild deer should be empirically tested. In addition, fence line transmission could explain, at least partially, the widespread sustained SARS-CoV-2 transmission among wild deer in North America (*36*).

Some wildlife species found to be shedding RNA of XBB lineages under natural conditions (e.g., raccoons [*Procyon lotor*] and cottontail rabbits [*Sylvilagus floridanus*]) (*34*) did not show clinical signs of infection, nor did they shed viral RNA when experimentally infected with early, pre-Omicron lineages (*37*,*38*). Those studies together provide strong evidence that, as new lineages emerge, the breadth of competent hosts for the virus changes, highlighting the importance of continued surveillance to assess risks of establishment of transmission cycles of SARS-CoV-2 among wildlife species.

Infectious virus can be isolated from nasal swab samples up to 6 days after infection in deer, whereas viral RNA can be detected in respiratory swab samples up to 22 days after direct experimental infection and up to 21 days after contact with infected deer (*1*,*2*). Those studies, which used pre-Omicron lineages, revealed efficient horizontal transmission among deer. Of the qRT-PCR–positive deer from our study, 6 of 11 had infectious virus, suggesting they became infected within ≈6 days before our sampling, although that timeframe might vary under natural conditions compared with laboratory-based experiments. Nevertheless, our results show that more recent lineages are also efficiently and quickly transmitted among deer. However, controlled laboratory experiments are needed to confirm the duration of infectious virus shedding during infections with more recent SARS-CoV-2 lineages in deer.

Our study demonstrates the continued and efficient spread of SARS-CoV-2 among deer as new

virus lineages emerge and infect nonhuman species; an XBB lineage concurrently circulating in human populations spread rapidly within deer. These findings corroborate epidemiologic models predicting that deer facilities favor high virus dissemination within captive populations (*23*), and transmission potential might vary across the spectrum of scenarios in which deer and humans interact (e.g., deer ranches, wildlife sanctuaries, safaris, zoos, outdoor recreation with free-ranging animals). Our study cannot determine how SARS-CoV-2 entered the target deer population. This knowledge gap needs to be addressed to mitigate transmission risks among humans, deer, and other commingling species. Given the uncertain public health and animal health implications of viral maintenance within captive deer, agricultural biosecurity practices could be useful in reducing the possibility of establishing long-term animal reservoirs for the virus. The mid- to long-term evolutionary consequences for SARS-CoV-2 circulating in nonhuman populations is unknown, and captive facilities might provide opportunities for sustained transmission at this human–deer–wildlife interface.

This article was originally published as a preprint at https://www.biorxiv.org/content/10.1101/2024.09.24.613938v1.

Acknowledgments

We thank deer producers across Texas. Laboratory support was provided by Sankar Chaki and Lisa Auckland. Tom Gary, Isabel McAllister, and Yuexun Tian assisted in the field.

Virus genome sequences are available in GISAID (accession nos. EPI_ISL_19411338-48 and EPI_ISL_19413822). Raw sequencing data are available in the National Center for Biotechnology Information (BioProject no. PRJNA1149050). The following reagent was obtained through BEI Resources, National Institute of Allergy and Infectious Diseases, National Institutes of Health: *Cercopithecus aethiops* Kidney Epithelial Cells Expressing Transmembrane Protease, Serine 2 and Human Angiotensin-Converting Enzyme 2 (Vero E6-TMPRSS2-T2A-ACE2), NR-54970.

Funding was provided by the American Rescue Plan Act through USDA APHIS A1181 Agricultural Biosecurity 2023-70432-39559 and by Texas A&M AgriLife Research. Use of the Global Health Research Complex, TIGSS Molecular Genomics Core, and TIGSS Bioinformatics Core is acknowledged. Portions of this research were conducted with the advanced computing resources provided by Texas A&M High Performance Research Computing. The findings and conclusions in this publication are those of the authors and should not be construed to represent any official USDA or US government determination or policy.

About the Author

Dr. Ferreira is an assistant research scientist in the Entomology Department at Texas A&M University. He is interested in wildlife and zoonotic pathogens at the human–animal–environment interface.

References

1. Martins M, Boggiatto PM, Buckley A, Cassmann ED, Falkenberg S, Caserta LC, et al. From deer-to-deer: SARS-CoV-2 is efficiently transmitted and presents broad tissue tropism and replication sites in white-tailed deer. PLoS Pathog. 2022;18:e1010197. https://doi.org/10.1371/journal.ppat.1010197
2. Palmer MV, Martins M, Falkenberg S, Buckley A, Caserta LC, Mitchell PK, et al. Susceptibility of white-tailed deer (*Odocoileus virginianus*) to SARS-CoV-2. J Virol. 2021;95:e00083-21. https://doi.org/10.1128/JVI.00083-21
3. Feng A, Bevins S, Chandler J, DeLiberto TJ, Ghai R, Lantz K, et al. Transmission of SARS-CoV-2 in free-ranging white-tailed deer in the United States. Nat Commun. 2023;14:4078. https://doi.org/10.1038/s41467-023-39782-x
4. Hale VL, Dennis PM, McBride DS, Nolting JM, Madden C, Huey D, et al. SARS-CoV-2 infection in free-ranging white-tailed deer. Nature. 2022;602:481–6. https://doi.org/10.1038/s41586-021-04353-x
5. Caserta LC, Martins M, Butt SL, Hollingshead NA, Covaleda LM, Ahmed S, et al. White-tailed deer (*Odocoileus virginianus*) may serve as a wildlife reservoir for nearly extinct SARS-CoV-2 variants of concern. Proc Natl Acad Sci U S A. 2023;120:e2215067120. https://doi.org/10.1073/pnas.2215067120
6. Marques AD, Sherrill-Mix S, Everett JK, Adhikari H, Reddy S, Ellis JC, et al. Multiple introductions of SARS-CoV-2 Alpha and Delta variants into white-tailed deer in Pennsylvania. MBio. 2022;13:e0210122. https://doi.org/10.1128/mbio.02101-22
7. McBride DS, Garushyants SK, Franks J, Magee AF, Overend SH, Huey D, et al. Accelerated evolution of SARS-CoV-2 in free-ranging white-tailed deer. Nat Commun. 2023;14:5105. https://doi.org/10.1038/s41467-023-40706-y
8. Zhao J, Kang M, Wu H, Sun B, Baele G, He W-T, et al. Risk assessment of SARS-CoV-2 replicating and evolving in animals. Trends Microbiol. 2024;32:79–92.
9. Pickering B, Lung O, Maguire F, Kruczkiewicz P, Kotwa JD, Buchanan T, et al. Divergent SARS-CoV-2 variant emerges in white-tailed deer with deer-to-human transmission. Nat Microbiol. 2022;7:2011–24. https://doi.org/10.1038/s41564-022-01268-9
10. Palmer MV, O'Brien DJ, Griffin JF, Nugent G. Lisle Gd, Ward A, et al. Tuberculosis in wild and captive deer. In: Mukundan H, Chambers MA, Waters, WRR, Larsen MH, editors. Tuberculosis, leprosy and mycobacterial diseases of man and animals: the many hosts of mycobacteria. Wallingforth, UK: CABI; 2015. p. 334–64.
11. Tomori O, Oluwayelu DO. Domestic animals as potential reservoirs of zoonotic viral diseases. Annu Rev Anim Biosci. 2023;11:33–55. https://doi.org/10.1146/annurev-animal-062922-060125
12. Kuchipudi SV, Tan C, van Dorp L, Lichtveld M, Pickering B, Bowman J, et al. Coordinated surveillance is essential to monitor and mitigate the evolutionary impacts of SARS-CoV-2 spillover and circulation in animal hosts. Nat Ecol Evol. 2023;7:956–9. https://doi.org/10.1038/s41559-023-02082-0

13. Roundy CM, Nunez CM, Thomas LF, Auckland LD, Tang W, Richison JJ III, et al. High seroprevalence of SARS-CoV-2 in white-tailed deer (*Odocoileus virginianus*) at one of three captive cervid facilities in Texas. Microbiol Spectr. 2022;10:e0057622. https://doi.org/10.1128/spectrum.00576-22
14. Hamer SA, Nunez C, Roundy CM, Tang W, Thomas L, Richison J, et al. Persistence of SARS-CoV-2 neutralizing antibodies longer than 13 months in naturally infected, captive white-tailed deer (*Odocoileus virginianus*), Texas. Emerg Microbes Infect. 2022;11:2112–5.
15. Adams KP, Murphy BP, Ross MD. Captive white-tailed deer industry—current status and growing threat. Wildl Soc Bull. 2016;40:14–9. https://doi.org/10.1002/wsb.627
16. Chiavacci SJ. The economic costs of chronic wasting disease in the United States. PLoS One. 2022;17:e0278366. https://doi.org/10.1371/journal.pone.0278366
17. Outlaw JL, Anderson DP, Earle ML, Richardson JW. Economic impact of the Texas deer breeding and hunting operations. College Station (TX): Agricultural and Food Policy Center, The Texas A&M University System; 2017.
18. Oude Munnink BB, Sikkema RS, Nieuwenhuijse DF, Molenaar RJ, Munger E, Molenkamp R, et al. Transmission of SARS-CoV-2 on mink farms between humans and mink and back to humans. Science. 2021;371:172–7. https://doi.org/10.1126/science.abe5901
19. Rabalski L, Kosinski M, Mazur-Panasiuk N, Szewczyk B, Bienkowska-Szewczyk K, Kant R, et al. Zoonotic spill-over of SARS-CoV-2: mink-adapted virus in humans. Clin Microbiol Infect. 2022;28:451.e1–4.
20. Ghai RR, Straily A, Wineland N, Calogero J, Stobierski MG, Signs K, et al. Epidemiologic and genomic evidence for zoonotic transmission of SARS-CoV-2 among people and animals on a Michigan mink farm, United States, 2020. Viruses. 2023;15:2436. https://doi.org/10.3390/v15122436
21. Barua S, Newbolt CH, Ditchkoff SS, Johnson C, Zohdy S, Smith R, et al. Absence of SARS-CoV-2 in a captive white-tailed deer population in Alabama, USA. Emerg Microbes Infect. 2022;11:1707–10.
22. Shu Y, McCauley J. GISAID: Global initiative on sharing all influenza data—from vision to reality. Euro Surveill. 2017;22:30494. https://doi.org/10.2807/1560-7917.ES.2017.22.13.30494
23. Rosenblatt E, Cook JD, DiRenzo GV, Grant EHC, Arce F, Pepin KM, et al. Epidemiological modeling of SARS-CoV-2 in white-tailed deer (*Odocoileus virginianus*) reveals conditions for introduction and widespread transmission. PLOS Comput Biol. 2024;20:e1012263. https://doi.org/10.1371/journal.pcbi.1012263
24. Corman VM, Landt O, Kaiser M, Molenkamp R, Meijer A, Chu DK, et al. Detection of 2019 novel coronavirus (2019-nCoV) by real-time RT-PCR. Euro Surveill. 2020;25:2000045. https://doi.org/10.2807/1560-7917.ES.2020.25.3.2000045
25. Li H, Durbin R. Fast and accurate short read alignment with Burrows–Wheeler transform. bioinformatics. Bioinformatics. 2009;25:1754–60.
26. Danecek P, Bonfield JK, Liddle J, Marshall J, Ohan V, Pollard MO, et al. Twelve years of SAMtools and BCFtools. Gigascience. 2021;10:giab008. https://doi.org/10.1093/gigascience/giab008
27. Aksamentov I, Roemer C, Hodcroft EB, Neher RA. Nextclade: clade assignment, mutation calling and quality control for viral genomes. J Open Source Softw. 2021;6:3773. https://doi.org/10.21105/joss.03773
28. Turakhia Y, Thornlow B, Hinrichs AS, De Maio N, Gozashti L, Lanfear R, et al. Ultrafast Sample placement on Existing tRees (UShER) enables real-time phylogenetics for the SARS-CoV-2 pandemic. Nat Genet. 2021;53:809–16. https://doi.org/10.1038/s41588-021-00862-7
29. Lei C, Yang J, Hu J, Sun X. On the calculation of $TCID_{50}$ for quantitation of virus infectivity. Virol Sin. 2021;36:141–4. https://doi.org/10.1007/s12250-020-00230-5
30. O'Toole Á, Scher E, Underwood A, Jackson B, Hill V, McCrone JT, et al. Assignment of epidemiological lineages in an emerging pandemic using the pangolin tool. Virus Evol. 2021;7:veab064. https://doi.org/10.1093/ve/veab064
31. Rambaut A, Holmes EC, O'Toole Á, Hill V, McCrone JT, Ruis C, et al. A dynamic nomenclature proposal for SARS-CoV-2 lineages to assist genomic epidemiology. Nat Microbiol. 2020;5:1403–7. https://doi.org/10.1038/s41564-020-0770-5
32. Gangavarapu K, Latif AA, Mullen JL, Alkuzweny M, Hufbauer E, Tsueng G, et al.; GISAID Core and Curation Team. Outbreak.info genomic reports: scalable and dynamic surveillance of SARS-CoV-2 variants and mutations. Nat Methods. 2023;20:512–22. https://doi.org/10.1038/s41592-023-01769-3
33. Kotwa JD, Lobb B, Massé A, Gagnier M, Aftanas P, Banerjee A, et al. Genomic and transcriptomic characterization of delta SARS-CoV-2 infection in free-ranging white-tailed deer (*Odocoileus virginianus*). iScience. 2023;26:108319.
34. Goldberg AR, Langwig KE, Brown KL, Marano JM, Rai P, King KM, et al. Widespread exposure to SARS-CoV-2 in wildlife communities. Nat Commun. 2024;15:6210. https://doi.org/10.1038/s41467-024-49891-w
35. Moseley WA, Cooper SM, Hewitt DG, Fulbright TE, Deyoung CA. Effects of supplemental feeding and density of white-tailed deer on rodents. J Wildl Manage. 2011;75:675–81. https://doi.org/10.1002/jwmg.71
36. Hewitt J, Wilson-Henjum G, Collins DT, Linder TJ, Lenoch JB, Heale JD, et al. Landscape-scale epidemiological dynamics of SARS-CoV-2 in white-tailed deer. Transbound Emerg Dis. 2024:1–11.
37. Bosco-Lauth AM, Root JJ, Porter SM, Walker AE, Guilbert L, Hawvermale D, et al. Peridomestic mammal susceptibility to severe acute respiratory syndrome coronavirus 2 infection. Emerg Infect Dis. 2021;27:2073–80. https://doi.org/10.3201/eid2708.210180
38. Francisco R, Hernandez SM, Mead DG, Adcock KG, Burke SC, Nemeth NM, et al. Experimental susceptibility of North American raccoons (*Procyon lotor*) and striped skunks (*Mephitis mephitis*) to SARS-CoV-2. Front Vet Sci. 2022;8:715307. https://doi.org/10.3389/fvets.2021.715307

Address for correspondence: Francisco C. Ferreira, Department of Entomology, Texas A&M University, TAMU 2475, College Station, TX 77843-2475, USA; email: franciscocarlosfj@gmail.com; Sarah A. Hamer, Department of Veterinary Integrative Biosciences, Texas A&M University, TAMU 4458, College Station, TX 77843, USA; email: shamer@cvm.tamu.edu

Sudan Virus Persistence in Immune-Privileged Organs of Nonhuman Primate Survivors

Brittany B. Beavis, Jun Liu, Elizabeth E. Zumbrun, Ashley V. Bryan, April M. Babka, Nancy A. Twenhafel, Derron A. Alves,[1] Margaret L. Pitt, Aysegul Nalca, Xiankun Zeng

After the 2022–2023 Sudan virus (SUDV) disease outbreak in Uganda, we studied SUDV persistence in nonhuman primates that had survived acute infection without therapeutic intervention. We identified SUDV persistence in the vitreous chamber and immediately adjacent tissue in the eyes as well as in the seminiferous tubules in the testes but not in common target organs typically infected during the acute phase of disease. Specifically, SUDV persists primarily in macrophages in the eyes and Sertoli cells in the testes. Ocular and testicular SUDV persistence in nonhuman primates is accompanied by tissue damage, including inflammatory cell invasion. Our study suggests that long-term follow-up efforts are needed to reduce possible recrudescent disease and reignition of outbreaks caused by virus persistence in human survivors of SUDV infection.

Members of the viral genera *Orthoebolavirus* and *Orthomarburgvirus* in the family *Filoviridae* cause severe viral hemorrhagic fevers in humans; case-fatality rates are high. Ebola disease is caused by infection with Bundibugyo virus, Ebola virus (EBOV), Sudan virus (SUDV), or Taï Forest virus, whereas Marburg disease is caused by infection with Marburg virus (MARV) or Ravn virus (*1*,*2*). Most Ebola disease outbreaks in humans to date have been caused by EBOV and SUDV. Before the 2013–2016 epidemic of Ebola virus disease (EVD, caused by EBOV only) in West Africa and the 2018–2020 EVD outbreak in the Democratic Republic of the Congo, the largest Ebola disease outbreak was in the Gulu District of Uganda, caused by SUDV; 425 persons were infected and 224 deaths were recorded (*3*,*4*). SUDV has been responsible for the second most cases of filovirus disease, after EBOV; 8 sporadic SUDV outbreaks have been reported in equatorial Africa since discovery of the virus in 1976 (*5*). The recent outbreak caused by SUDV in Uganda (September 2022–January 2023) resulted in 142 confirmed cases and 55 deaths (*6*). Although substantial progress has been made in preclinical studies of vaccines and therapeutics against SUDV, no approved vaccines or therapeutics against SUDV are available for patients. Although therapeutics and vaccines licensed for use against EBOV are available, EBOV is antigenically distinct, and current evidence suggests that those products would be ineffective against SUDV (*7*).

Persistent filovirus infection was originally identified in 1967, during the first Marburg disease outbreak in Marburg, Germany (*8*). In that case, MARV persisted in the seminal fluid of a convalescent patient, resulting in sexual transmission of MARV to his wife about 2 months after his recovery. Before the 2013–2016 epidemic of EVD in western Africa, filovirus persistence in the eyes and semen of convalescent survivors was sparsely reported (*9*,*10*). The studies performed among unprecedented numbers of EVD survivors of that epidemic demonstrated a previously underappreciated and unfortunate fact of EBOV infection: the persistence of EBOV in immune-privileged organs, associated body fluids, or both, including brain/cerebrospinal fluid, eyes/ocular fluid, and testes/seminal fluids. Among patients who survive acute EVD, the virus remains in those tissues despite virus clearance from blood, EBOV-specific immune responses, and apparent clinical recovery. Multiple disease flare-ups or re-emergence events associated with virus persistence were reported and attributed

Author affiliations: United States Army Medical Research Institute of Infectious Diseases, Fort Detrick, Frederick, Maryland, USA (B.B. Beavis, J. Liu, E.E. Zumbrun, A.V. Bryan, A.M. Babka, N.A. Twenhafel, D.A. Alves, M.L. Pitt, A. Nalca, X. Zeng); Chenega Corporation, Chesapeake, Virginia, USA (J. Liu)

DOI: https://doi.org/10.3201/eid3102.240983

[1]Current affiliation: National Institute of Allergy and Infectious Diseases, Rockville, Maryland, USA.

to sexual transmission or breastfeeding during the 2013–2016 EVD epidemic (*11*). Persistent infectious virus has been isolated from ocular fluid of an EVD survivor with recrudescent uveitis and from the cerebrospinal fluid of an EVD survivor with meningoencephalitis (*12*,*13*). At the end of the 2018–2020 EVD outbreak in the Democratic Republic of the Congo, a lethal relapse in a survivor 6 months after treatment with monoclonal antibody mAb114 led to multiple subsequent transmission events and extended the outbreak and response efforts another 6 months (*14*,*15*). More recently, genetic epidemiology suggested that 3 separate EVD outbreaks (in the Democratic Republic of the Congo during February 2021 and October 2021 and in Guinea during February 2021) were probably associated with virus persistence in a survivor of a prior local outbreak rather than with spillover from an unknown zoonotic source. In particular, the 2021 Guinea EVD outbreak reemerged from a persistently infected survivor of the major 2013–2016 EVD epidemic (at least 5 years earlier) (*16*). Those events have resulted in a paradigm shift with regard to knowledge of EBOV persistence and outbreak response and prevention.

Studies of EBOV persistence in humans and experimentally infected nonhuman primates (NHPs) have revolutionized our knowledge of EBOV infection and changed the guidelines of clinical operation and the recommendations of the World Health Organization for EVD survivors. MARV persistence in NHP survivors has also been investigated (*17*). However, our knowledge of SUDV persistence has lagged substantially, although SUDV has been responsible for numerous filovirus outbreaks. With this study, we sought to fill the knowledge gap and identify and characterize ocular and testicular SUDV persistence in NHPs that naturally survived experimental SUDV exposure without therapeutic interventions.

Materials and Methods

Study Design

We searched the internal pathology database at United States Army Medical Research Institute of Infectious Diseases (USAMRIID) for NHPs that had survived ≥28 days after exposure to SUDV without therapeutic interference (defined as administration of experimental therapeutics or vaccines). Meeting the inclusion criteria were 8 rhesus monkeys (*Macaca mulatta*, also known as rhesus macaques), 5 crab-eating macaques (*Macaca fascicularis*, also known as cynomologus macaques), and 3 vervets (*Chlorocebus aethiops sabaeus*, also known as African green monkeys). We selected the immune-privileged organs (eye, brain, and testes) and common target organs (liver, spleen, lymph nodes) of those NHPs for analysis. From the USAMRIID Pathology Division tissue archives, we retrieved formalin-fixed paraffin-embedded (FFPE) tissue samples from those animals. We verified detection of SUDV infection by ≥2 different methods (in situ hybridization, immunohistochemistry, immunofluorescence staining).

We conducted our research under an Institutional Animal Care and Use Committee–approved protocol in compliance with the Animal Welfare Act, Public Health Service policy, and other federal statutes and regulations relating to animals and experiments involving animals. The facility where our research was conducted is accredited by the Association for Assessment and Accreditation of Laboratory Animal Care International and adheres to principles stated in the Guide for the Care and Use of Laboratory Animals, National Research Council, 2011.

Animals

We experimentally exposed the 16 NHPs to various doses of the Boniface, Gulu, or Yambio variants of SUDV via aerosol or intramuscular route (Appendix Table, https://wwwnc.cdc.gov/EID/article/31/2/24-0983-App1.pdf). For histologic evaluation, we processed tissue sections in accordance with routine hematoxylin and eosin staining procedures and used sections of tissues from an uninfected rhesus macaque and an uninfected crab-eating macaque as controls.

RNA In Situ Hybridization

To detect SUDV genomic RNA in FFPE tissues, we performed RNA in situ hybridization (ISH) by using an RNAscope 2.5 HD Detection (RED) kit (Advanced Cell Diagnostics, https://acdbio.com), according to the manufacturer's instructions. In brief, Advanced Cell Diagnostics designed and synthesized an ISH probe targeting the genomic fragment of the SUDV nucleoprotein (NP) gene. We used uninfected NHP tissue sections as negative controls and SUDV-infected NHP tissue sections as positive controls. Tissue sections deparaffinized with Xyless II (Val Tech Diagnostics, https://valtechnologies.com) underwent a series of ethanol washes and peroxidase blocking, were heated in kit-provided decrosslinking buffer, and were then digested by kit-provided proteinase. We exposed sections to ISH target probe pairs and incubated them at 40°C in a hybridization oven for 2 hours. After rinsing the sections, we amplified the ISH signal by using kit-provided preamplifier and

amplifier conjugated to alkaline phosphatase and incubated them with a Fast Red substrate solution for 10 minutes at room temperature. We then stained the sections with hematoxylin, air-dried them, and placed coverslips.

Immunohistochemistry

We performed SUDV immunohistochemistry testing on FFPE tissue sections by using the EnVision Detection System (Dako Agilent Pathology Solutions, https://www.agilent.com). We used uninfected NHP tissue sections as negative controls and SUDV-infected NHP tissue sections as positive controls. After we deparaffinized, rehydrated, and blocked the sections with methanol/hydrogen peroxide, we stained the slides by using rabbit polyclonal anti-SUDV VP40 antibody (IBT Bioservices, https://ibtbioservices.com) at a dilution of 1:4,000, followed by a horseradish peroxidase-conjugated secondary anti-mouse polymer (Dako Agilent Pathology Solutions). We exposed all slides to brown chromogenic substrate, 3,3′-diaminobenzidine (Dako Agilent Pathology Solutions), counterstained them with hematoxylin, dehydrated them, and placed coverslips.

Immunofluorescence Staining

We deparaffinized FFPE tissue sections by using Xyless II (Val Tech Diagnostics) and a series of ethanol washes. To reverse formaldehyde crosslinks, we heated the sections in Tris-EDTA buffer (10 mM Tris base, 1 mM EDTA solution, 0.05% Tween 20, pH 9.0) for 20 minutes. After rinses with phosphate-buffered saline (PBS), we blocked pH 7.4 sections with CAS-Block ((Thermo Fisher Scientific, https://www.thermofisher.com) containing 5% normal goat serum (Millipore Sigma, https://www.sigmaaldrich.com) for 1 hour at room temperature or overnight at 4°C. We then incubated sections with the primary antibodies overnight at 4°C or for 2 hours at room temperature as follows: a rabbit polyclonal antibody against SUDV VP40 antibody (IBT Bioservices) at a dilution of 1:500, a mouse monoclonal anti-human CD68 antibody (Dako Agilent Pathology Solutions) at a dilution of 1:200, a rabbit polyclonal anti-CD3 antibody at a dilution of 1:200 (Dako Agilent Pathology Solutions), a rabbit polyclonal anti-CD4 antibody (Abcam, https://www.abcam.com) or a mouse monoclonal anti-CD8α antibody at a dilution of 1:200 (Thermo Fisher Scientific). After rinsing sections in PBS + 0.1% Tween-20, we incubated them with secondary goat Alexa Fluor 488-conjugated anti-rabbit antibody and with goat Alexa Fluor 561 anti-mouse antibody (Thermo Fisher Scientific) for 1 hour at room temperature. We counterstained sections with 4′,6-diamidino-2-phenylindole and placed coverslips by using fluorescent mounting media (Dako Agilent Pathology Solutions). Images were captured on an LSM 880 confocal microscope (Zeiss, https://www.zeiss.com) and processed by using open-source ImageJ software (National Institutes of Health, Bethesda, MD, USA).

Results

SUDV Virus Persistence

Of the 16 survivors, 4 (25%) had detectable SUDV genomic RNA in eye or testis tissues. Specifically, 3 (23.1%) of 13 NHPs (no eye and brain tissues were collected for 3 surviving NHPs; Appendix Table) had SUDV genomic RNA in eye tissues and 1 (9%) of 11 NHPs (the other 5 were female) had SUDV genomic RNA in testis tissues. In contrast, SUDV genomic RNA was undetectable in the brain tissues of all 13 NHPs for which brain tissues were collected, the ovary tissues of all 5 female survivors, and common acute SUDV infection target organ tissues (liver, lymph node, and spleen) of all 16 NHP survivors (Appendix Table).

Ocular Sudan Virus Persistence

We previously reported ocular EBOV persistence in NHPs that survived EBOV exposure with or without therapeutic interventions (*18*,*19*). Similarly, in this study, using ISH we detected SUDV genomic RNA in the vitreous chamber and the interface between the vitreous chamber and its adjacent structures within the eyes of 3 (23.1%) of 13 NHP survivors (Appendix Figure 1, panels A–N). In contrast, we did not detect genomic SUDV RNA in brain, liver, lymph node, spleen, or testicular tissues from the same 3 NHPs (Appendix Table). To identify the cellular targets of persistent SUDV infection, we stained survivor eye tissues by using immunofluorescence and an SUDV NP antibody and antibody against a macrophage marker, CD68. SUDV NPs were detected primarily in CD68+ macrophages (Appendix Figure 1, panels O–P), suggesting that SUDV primarily persists in ocular macrophages.

Uveitis, Retinitis, and Vitritis

A high prevalence of ophthalmic sequelae, including sight-threatening uveitis, in EVD survivors has been reported (*20*,*21*). To examine the ocular complications in SUDV NHP survivors, we performed histopathologic evaluation of all eye tissues. Overall, 7 (53.8%) of 13 NHP survivors, including the 3 survivors with ocular SUDV persistence, displayed unilateral or

bilateral inflammation of mild to moderate severity in multiple locations. Uveitis, characterized by lymphoplasmacytic infiltration in ciliary body, choroid, and iris, was observed in 7 (100%) of 7 survivors with ocular lesions. Unilateral or bilateral retinitis, characterized by multifocal perivascular accumulation of mononuclear cells and stromal infiltrates of plasma cells, was also observed in the same NHPs. Vitritis, unilateral or bilateral, characterized by infiltration of plasma cells, macrophages, and lymphocytes in the vitreous chamber adjacent to ciliary body, lens, and retina was observed in 6 (85.7%) of 7 of NHP survivors with ocular lesions (Appendix Table, Figure 2, panels A–C, E–G). Optic neuritis was observed in 5 (71.4%) of 7 survivors with ocular lesions, and optic perineuritis was observed in 4 (57.1%) of 7 survivors with ocular lesions (Appendix Table, Figure 2, panels D, H). Less commonly, we detected conjunctivitis, keratitis, and scleritis. Immunofluorescence staining further characterized the infiltrating cells as predominantly CD3+ T cells and CD68+ macrophages in the uvea, retina, vitreous chamber, and optic nerve (Appendix Figure 2, panels I–P). Of note, most T cells in those sites are CD8+ cytotoxic cells rather than CD4+ helper T cells (Appendix Figure 2, panels Q–T). Our data suggest that ocular lesions persist in a subset of NHPs that survive acute SUDV infection.

Testicular SUDV Persistence

One (9%) of 11 NHP survivors had detectable SUDV genomic RNA (Appendix Figure 3, panels A–B) in testicular tissue. SUDV antigen was also detected at the same location via immunohistochemistry (Appendix Figure 3, panel C). Of note, both SUDV genomic RNA and SUDV antigen were specifically detected in the seminiferous tubules, sites of immune privilege and sperm production (Appendix Figure 3, panels B–C). Immunofluorescence staining confirmed SUDV antigen presence in the seminiferous tubules, specifically within testicular Sertoli cells. The presence of virus antigen and genomic RNA after resolution of the clinical course of disease suggests a persistent state of infection at that location. We performed histologic analyses of testicular tissues from 11 NHP survivors with available tissues. The NHP with detectable SUDV genomic RNA and antigen demonstrated multifocal interstitial orchitis characterized by expansion of the interstitium by a lymphoplasmacytic infiltrate (Appendix Figure 3, panels F–G). Seminiferous tubules in those areas demonstrated degeneration, characterized by vacuolation, loss of Sertoli cells, and a lack of organized spermatogenesis.

Consistent with histologic analysis, immunofluorescence staining demonstrated that CD68+ macrophages, CD3+ T cells, and CD20+ B cells infiltrated interstitial tissues and seminiferous tubules of testicular sites with SUDV persistence (Appendix Figure 3, panels H–K). We detected abundant IgG in the interstitial tissues and seminiferous tubules but not in uninfected control testicular tissues (Appendix Figure 3, panels J–K). However, whether the IgG responses are SUDV antigen–specific remains to be investigated. Our data suggest that persistent testicular SUDV infection results in orchitis and loss or partial loss of immune privilege.

Discussion

Asymptomatic persistent infection in clinically recovered Ebola patients may cause recrudescent disease and may spark new outbreaks months, or even years, later. The 2022–2023 outbreak of Ebola disease caused by SUDV in Uganda reminded the field of the need for more information about the pathogenesis and transmission of SUDV. Our data demonstrate that SUDV persists beyond the conclusion of acute clinical disease, specifically in the vitreous chamber and its adjacent structures of the eyes and in the seminiferous tubules of the testes in some NHPs that naturally survived experimental exposure of SUDV without therapeutic treatment. Our data suggest that persistence is linked to the presence of ongoing inflammatory infiltrates. The primary targets of SUDV persistence are macrophages in the eyes and Sertoli cells in the testes.

Consistent with our finding of ocular SUDV persistence and inflammation, a previous animal efficacy study briefly mentioned inflammatory ocular lesions, including uveitis, and detectable viral RNA in the eye tissues of NHPs that survived experimental SUDV exposure after combination therapy with remdesivir and monoclonal antibodies or after monotherapy with remdesivir or monoclonal antibodies (*22*). Natural history studies demonstrate that SUDV infection in NHPs, including rhesus monkeys and crab-eating macaques, results in systemic viremia and characteristic clinical signs, recapitulating many manifestations of human SUDV disease (*23*–*27*). Although SUDV persistence and related sequelae have not been reported for human survivors, given our NHP data and similar pathogenesis between SUDV and EBOV, we posit that SUDV can most likely persist in immune-privileged organs in patients. The clinical observations and data of the Survivor Care Program, established by public health authorities during the 2022–2023

SUDV disease outbreak in Uganda but not yet published, may help prove such deduction (*28*).

SUDV persistence was detected only in the eye and testicular tissues but not in the brain tissues we analyzed. We suspect that SUDV could persist in the brain of NHP survivors because we previously reported virus persistence in the brain of NHPs exposed to EBOV (*19*). However, in that study we identified that NHP survivors experiencing EBOV persistence in the brain had higher viral loads in the blood than NHP survivors without EBOV persistence in the brain. The lack of brain persistence in those NHP survivors might result from lower viral load, and NHPs with the high viral load needed to result in brain SUDV persistence might have succumbed during the acute phase of disease.

Among its limitations, the retrospective nature of our study means that no virologic data are available to determine infectious virus in the eye and testicular tissues. Second, our observations of SUDV persistence were based on NHP survivors at ≈30 days after exposure. Analysis of NHPs at different stages of the convalescent disease course could provide information about the dynamics of virus persistence. Last, all NHP survivors that we report are natural survivors without therapeutic interference. SUDV persistence should be further investigated in future NHP studies evaluating efficacy of medical countermeasures candidates, including monoclonal antibodies, small molecules, and vaccines. Of note, a recent study demonstrated that infectious SUDV was undetectable in the immune-privileged tissues of NHPs that survived SUDV exposure after treatment with obeldesivir, an oral alternative to parenterally administered remdesivir (*29*).

Persistent SUDV infection in even a very small subset of individual human survivors has consequences for the individuals and for public health, particularly with respect to the potential for reignition of human-to-human transmission chains leading to a new outbreak. Our study suggests the need for long-term follow-up (clinical and potentially virologic surveillance) of convalescent SUDV patients to prevent disease recrudescence and reignition of outbreaks.

Acknowledgments

We thank Holly Bloomfield and Neil Davis for their histologic support, Jamie Blue for retrieving the information of the animal studies, and Nora Azzi for critically reading the manuscript.

This study was funded by the Defense Threat Reduction Agency (CB11408 to X.Z.).

The opinions, interpretations, conclusions, and recommendations presented are those of the author and are not necessarily endorsed by the US Army, Department of Defense, or the institutions and companies affiliated with the authors. The use of either trade or manufacturers' names in this article does not constitute an official endorsement of any commercial products. This report may not be cited for purposes of advertisement. The authors declare no competing interests. This article does not constitute an endorsement by the US government of this or any other contractor.

About the Author

Dr. Beavis is a veterinary pathologist in the Pathology Division of USAMRIID. Her primary research interests include molecular mechanisms of infectious disease pathogenesis in animal models and development of molecular pathology assays.

References

1. Jacob ST, Crozier I, Fischer WA II, Hewlett A, Kraft CS, Vega MA, et al. Ebola virus disease. Nat Rev Dis Primers. 2020;6:13. https://doi.org/10.1038/s41572-020-0147-3
2. Biedenkopf N, Bukreyev A, Chandran K, Di Paola N, Formenty PBH, Griffiths A, et al. Renaming of genera *Ebolavirus* and *Marburgvirus* to *Orthoebolavirus* and *Orthomarburgvirus*, respectively, and introduction of binomial species names within family *Filoviridae*. Arch Virol. 2023;168:220. https://doi.org/10.1007/s00705-023-05834-2
3. Centers for Disease Control and Prevention. Ebola virus disease outbreak history [cited 2024 May 28]. https://wwwcdcgov/ebola/outbreaks/index.html
4. Towner JS, Rollin PE, Bausch DG, Sanchez A, Crary SM, Vincent M, et al. Rapid diagnosis of Ebola hemorrhagic fever by reverse transcription-PCR in an outbreak setting and assessment of patient viral load as a predictor of outcome. J Virol. 2004;78:4330–41. https://doi.org/10.1128/JVI.78.8.4330-4341.2004
5. Languon S, Quaye O. Filovirus disease outbreaks: a chronological overview. Virology (Auckl). 2019; 10:1178122X19849927.
6. Balinandi S, Whitmer S, Mulei S, Nassuna C, Pimundu G, Muyigi T, et al. Molecular characterization of the 2022 Sudan virus disease outbreak in Uganda. J Virol. 2023;97:e0059023. https://doi.org/10.1128/jvi.00590-23
7. Ibrahim SK, Ndwandwe DE, Thomas K, Sigfrid L, Norton A. Sudan virus disease outbreak in Uganda: urgent research gaps. BMJ Glob Health. 2022;7:e010982. https://doi.org/10.1136/bmjgh-2022-010982
8. Martini GA, Schmidt HA. Spermatogene Ubertragung des "Virus Marburg." Klin Wochenschr. 1968;46:398–400. https://doi.org/10.1007/BF01734141
9. Schindell BG, Webb AL, Kindrachuk J. Persistence and sexual transmission of filoviruses. Viruses. 2018;10:683. https://doi.org/10.3390/v10120683
10. Di Paola N, Sanchez-Lockhart M, Zeng X, Kuhn JH, Palacios G. Viral genomics in Ebola virus research. Nat Rev Microbiol. 2020;18:365–78. https://doi.org/10.1038/s41579-020-0354-7
11. Subissi L, Keita M, Mesfin S, Rezza G, Diallo B, Van Gucht S, et al. Ebola virus transmission caused by persistently infected

survivors of the 2014–2016 outbreak in West Africa. J Infect Dis. 2018;218(suppl_5):S287–91. https://doi.org/10.1093/infdis/jiy280
12. Varkey JB, Shantha JG, Crozier I, Kraft CS, Lyon GM, Mehta AK, et al. Persistence of Ebola virus in ocular fluid during convalescence. N Engl J Med. 2015;372:2423–7. https://doi.org/10.1056/NEJMoa1500306
13. Jacobs M, Rodger A, Bell DJ, Bhagani S, Cropley I, Filipe A, et al. Late Ebola virus relapse causing meningoencephalitis: a case report. Lancet. 2016;388:498–503. https://doi.org/10.1016/S0140-6736(16)30386-5
14. Mbala-Kingebeni P, Pratt C, Mutafali-Ruffin M, Pauthner MG, Bile F, Nkuba-Ndaye A, et al. Ebola virus transmission initiated by relapse of systemic Ebola virus disease. N Engl J Med. 2021;384:1240–7. https://doi.org/10.1056/NEJMoa2024670
15. Crozier I, Britson KA, Wolfe DN, Klena JD, Hensley LE, Lee JS, et al. The evolution of medical countermeasures for Ebola virus disease: lessons learned and next steps. Vaccines (Basel). 2022;10:1213. https://doi.org/10.3390/vaccines10081213
16. Keita AK, Koundouno FR, Faye M, Düx A, Hinzmann J, Diallo H, et al. Resurgence of Ebola virus in 2021 in Guinea suggests a new paradigm for outbreaks. Nature. 2021;597:539–43. https://doi.org/10.1038/s41586-021-03901-9
17. Coffin KM, Liu J, Warren TK, Blancett CD, Kuehl KA, Nichols DK, et al. Persistent Marburg virus infection in the testes of nonhuman primate survivors. Cell Host Microbe. 2018;24:405–416.e3. https://doi.org/10.1016/j.chom.2018.08.003
18. Zeng X, Blancett CD, Koistinen KA, Schellhase CW, Bearss JJ, Radoshitzky SR, et al. Identification and pathological characterization of persistent asymptomatic Ebola virus infection in rhesus monkeys. Nat Microbiol. 2017;2:17113. https://doi.org/10.1038/nmicrobiol.2017.113
19. Liu J, Trefry JC, Babka AM, Schellhase CW, Coffin KM, Williams JA, et al. Ebola virus persistence and disease recrudescence in the brains of antibody-treated nonhuman primate survivors. Sci Transl Med. 2022;14:eabi5229. https://doi.org/10.1126/scitranslmed.abi5229
20. Sneller MC, Reilly C, Badio M, Bishop RJ, Eghrari AO, Moses SJ, et al.; PREVAIL III Study Group. A longitudinal study of Ebola sequelae in Liberia. N Engl J Med. 2019;380:924–34. https://doi.org/10.1056/NEJMoa1805435
21. Shantha JG, Mattia JG, Goba A, Barnes KG, Ebrahim FK, Kraft CS, et al. Ebola Virus Persistence in Ocular Tissues and Fluids (EVICT) Study: reverse transcription-polymerase chain reaction and cataract surgery outcomes of Ebola survivors in Sierra Leone. EBioMedicine. 2018;30:217–24. https://doi.org/10.1016/j.ebiom.2018.03.020
22. Cross RW, Bornholdt ZA, Prasad AN, Woolsey C, Borisevich V, Agans KN, et al. Combination therapy with remdesivir and monoclonal antibodies protects nonhuman primates against advanced Sudan virus disease. JCI Insight. 2022;7:e159090. https://doi.org/10.1172/jci.insight.159090
23. Zumbrun EE, Bloomfield HA, Dye JM, Hunter TC, Dabisch PA, Garza NL, et al. A characterization of aerosolized Sudan virus infection in African green monkeys, cynomolgus macaques, and rhesus macaques. Viruses. 2012;4:2115–36. https://doi.org/10.3390/v4102115
24. Carbonnelle C, Moroso M, Pannetier D, Godard S, Mély S, Thomas D, et al. Natural history of *Sudan ebolavirus* to support medical countermeasure development. Vaccines (Basel). 2022;10:963. https://doi.org/10.3390/vaccines10060963
25. Woolsey C, Fears AC, Borisevich V, Agans KN, Dobias NS, Prasad AN, et al. Natural history of *Sudan ebolavirus* infection in rhesus and cynomolgus macaques. Emerg Microbes Infect. 2022;11:1635–46. https://doi.org/10.1080/22221751.2022.2086072
26. Marzi A, Fletcher P, Feldmann F, Saturday G, Hanley PW, Feldmann H. Species-specific immunogenicity and protective efficacy of a vesicular stomatitis virus-based Sudan virus vaccine: a challenge study in macaques. Lancet Microbe. 2023;4:e171–8. https://doi.org/10.1016/S2666-5247(23)00001-0
27. Alfson KJ, Goez-Gazi Y, Gazi M, Chou YL, Niemuth NA, Mattix ME, et al. Development of a well-characterized cynomolgus macaque model of Sudan virus disease for support of product development. Vaccines (Basel). 2022;10:1723. https://doi.org/10.3390/vaccines10101723
28. World Health Organization. Ebola disease caused by Sudan ebolavirus—Uganda [cited 2024 May 28]. https://wwwwhoint/emergencies/disease-outbreak-news/item/2023-DON433
29. Cross RW, Woolsey C, Chu VC, Babusis D, Bannister R, Vermillion MS, et al. Oral administration of obeldesivir protects nonhuman primates against *Sudan ebolavirus*. Science. 2024;383:eadk6176. https://doi.org/10.1126/science.adk6176

Address for correspondence: Xiankun (Kevin) Zeng, United States Army Medical Research Institute of Infectious Diseases, 1425 Porter St, Fort Detrick, Frederick, MD 21702, USA; email: xiankun.zeng.civ@health.mil

Contribution of Limited Molecular Testing to Low Ehrlichiosis Diagnosis in High Incidence Area, North Carolina, USA

Alexis Siegler, Lauryn Ursery, Dana A. Giandomenico, Melissa B. Miller, Johanna S. Salzer, Alexis M. Barbarin, Carl Williams, Ross M. Boyce

Indirect immunofluorescence antibody assays have been the primary method for laboratory diagnosis of ehrlichiosis. Detection of *Ehrlichia* spp. DNA by using PCR is now widely available through commercial laboratories. To prepare for *Ehrlichia* spp. PCR introduction, we assessed ehrlichiosis testing practices, quantified the proportion of samples eligible for PCR testing, and estimated the potential effect of implementing PCR at the University of North Carolina health system in North Carolina, USA, which is in an area with a high-incidence of ehrlichiosis. We found <1% of patient samples underwent PCR testing, even though rates of serodiagnostic algorithm completion (testing of acute and convalescent samples) were low (18.4%). Our findings show a need to educate providers on diagnostic and treatment guidelines for ehrlichiosis and raise awareness of the availability and advantage of PCR testing.

Since 2000, the number of ehrlichiosis cases in the United States reported to the Centers for Disease Control and Prevention (CDC) has increased >10-fold (*1*). Yet, ehrlichiosis is frequently misdiagnosed and underreported because of its relatively nonspecific clinical manifestations (e.g., fever, malaise, headache, myalgia) (*2*). Whereas associated laboratory abnormalities such as thrombocytopenia, hepatic transaminase elevation, and leukopenia may provide further diagnostic clues, similar abnormalities can be seen in other infections. The potential consequences of misdiagnosis are substantial because *Ehrlichia* spp. infection can lead to severe disease. For example, 57% of ehrlichiosis cases reported to CDC during 2008–2012 (1,584 cases) resulted in hospitalization (*3*). Delayed antimicrobial drug treatment is strongly associated with clinical deterioration, characterized by organ failure and death, particularly in children and older adults (*4*,*5*).

Historically, paired acute and convalescent serum samples tested by using an indirect immunofluorescence antibody (IFA) assay that detects IgG against *E. chaffeensis* antigens have been the primary method of laboratory diagnosis (*6*). However, the serodiagnosis of ehrlichiosis is error-prone. IgG may not be detectable early in the course of infection, when most patients seek care (*7*). In addition, a positive acute serologic result may not indicate current infection but rather a prior infection, which may occur in ≈10% of the population in endemic areas (*8*,*9*). Because of the possibility of prior infection, a single acute serologic result cannot be used to confirm a diagnosis, and clinicians must make treatment decisions on the basis of a thorough clinical evaluation, considering a patient's history, symptoms, and laboratory test results. Providers often wait for the results of the initial IFA assay before beginning antimicrobial drug treatment (*10*), which can lead to disease progression. A second convalescent sample taken 2–10 weeks after the initial acute serologic result is required to confirm the diagnosis of ehrlichiosis and for epidemiologic surveillance data (*11*).

Few patients complete both acute and convalescent testing. For example, in North Carolina, of 105 cases reported in 2020, only 14 (13.3%) were classified as confirmed because of the lack of a paired convalescent result (*12*). Even within a large academic

Author affiliations: University of North Carolina at Chapel Hill, Chapel Hill, North Carolina, USA (A. Siegler, L. Ursery, D.A. Giandomenico, M.B. Miller, R.M. Boyce); Centers for Disease Control and Prevention, Atlanta, Georgia, USA (J.S. Salzer); North Carolina Department of Health and Human Services, Raleigh, North Carolina, USA (A.M. Barbarin, C. Williams)

DOI: https://doi.org/10.3201/eid3102.240281

medical center, only 1 in 4 patients tested for ehrlichiosis completed a convalescent test (*13*). Multiple factors may explain the low obtainment of paired serologic results, including the resolution of clinical symptoms because of treatment or self-limited disease, evidence of another cause of illness, or lack of clinician knowledge of testing algorithms.

Molecular approaches that use PCR can detect *Ehrlichia* spp. DNA with high sensitivity and specificity in acute whole blood samples, thereby eliminating the need for convalescent specimens to confirm the diagnosis (*14*). Although treatment for ehrlichiosis must be initiated presumptively, positive *Ehrlichia* PCR results can provide confirmatory evidence of the diagnosis more quickly than paired acute and convalescent samples. Molecular assays can also differentiate between infecting species such as *E. chaffeensis*, *E. ewingii*, and *E. muris eauclairensis*, which can advance our understanding of distinct syndromes associated with each species. However, PCR does have limitations, including increased cost (≈5× that of paired acute and convalescent IFAs at our institution, the University of North Carolina [UNC; Chapel Hill, NC, USA]), uncertainty in the ability to detect *Ehrlichia* sp. DNA after antimicrobial drugs are administered, and the lack of Food and Drug Administration–approved assays.

In preparation for the implementation of a laboratory-developed *Ehrlichia* PCR, we assessed current diagnostic testing practices, quantified the proportion of serologically tested patients that would be eligible for PCR testing, and estimated the potential effect of PCR on the diagnosis and management of ehrlichiosis within the UNC Health System. To accomplish this goal, we conducted a retrospective chart review of all patients tested for *Ehrlichia* over a 12-month period. We hypothesized that serologic testing was poorly targeted, and obtainment of paired specimens (acute and convalescent) would be infrequent, whereas *Ehrlichia* PCR, previously available only through a commercial reference laboratory, was underused.

Methods

Data Sources

We obtained diagnostic test results from patients tested for ehrlichiosis as ordered through Epic, the electronic medical record (EMR) system for UNC Health. UNC Health is the largest academic health system in North Carolina, comprising 14 hospitals and ≈500 clinics located throughout the state (*15*). In 2018, UNC Health reported 3.5 million clinical visits, which included nearly 500,000 emergency department visits. Patients were tested for ehrlichiosis by using IFA (Biocell Diagnostics, Inc, http://biocelldx.com) through UNC's McLendon Clinical Laboratories or by using PCR as a referral or send out test to Mayo Clinical Laboratories (Rochester, MN, USA), which was the institutional provider for *Ehrlichia* PCR testing during March 24, 2022–April 14, 2023 (*16*). Demographic, laboratory, and clinical data associated with each test order were entered into an electronic database (*17*).

Statistical Analysis

We stratified patients on the basis of 3 criteria: test appropriateness, PCR eligibility, and epidemiologic case classification. We first reviewed symptoms documented in the EMR to identify patients who were appropriately tested, defined as those who met the 2007 Council of State and Territorial Epidemiologists (CSTE) case definition for ehrlichiosis, which was in place at the time the samples were tested (*18*). Although the 2007 CSTE case definition was not intended to determine when to use diagnostics, it offers clear criteria for clinical assessment. Clinical evidence was defined as a subjectively reported or objectively measured fever (temperature ≥38°C) as documented in the EMR and ≥1 of the following symptoms: headache, myalgia, anemia (hemoglobin <13.5 g/dL for men, <12.0 g/dL for women), thrombocytopenia (platelets <150/μL), hepatic transaminase elevation (aspartate aminotransferase ≥33 U/L or alanine aminotransferase >36 U/L), or leukopenia (leukocyte count <4,000 cells/μL) (*18*). We classified patients as eligible for PCR testing if they were prescribed tetracycline antimicrobial drugs the same day as or after initial specimen collection because antimicrobial drugs can remove *Ehrlichia* DNA from patient blood and decrease the sensitivity of PCR testing (*8*). By using the CSTE case classifications, we determined the proportion of cases classified as confirmed, probable, or suspect. A confirmed case demonstrated a 4-fold or greater increase between acute and convalescent IgG titers and consistent clinical evidence of ehrlichiosis. A positive *Ehrlichia* PCR test with consistent clinical evidence was also considered a confirmed case. A probable case did not demonstrate a 4-fold increase but had ≥1 positive serologic specimen along with clinical evidence of ehrlichiosis. The threshold for a positive serologic test was a 1:64 IgG titer, selected to align with the cutoff used by the CDC to meet laboratory supportive evidence for ehrlichiosis (*11*). A case was classified as suspect if the patient had a positive laboratory test but no clinical information was available to determine if they had relevant symptoms. The

number of cases in each category was summarized and shown with relevant proportions.

Ethical Review

The study was approved by the institutional review board of the University of North Carolina at Chapel Hill (institutional review board no. 21-0356). Because this is a limited dataset under Code of Federal Regulations 45, part 164.514(e), written informed consent or waiver of authorization was not required.

Results

A total of 945 patient samples were tested for ehrlichiosis during the ≈12-month period observed, 5 of which underwent *Ehrlichia* PCR testing. Among all patients tested, the most frequently recorded symptoms at the time of testing were myalgia (33.9%, n = 320) and headache (31.3%, n = 296) (Table 1). Of those, only 273 (28.9%) were classified as appropriately tested; the most common reasons for exclusion were the absence of documented fever in the EMR (97.9%, n = 658), patient complaint including only 1 symptom (15.8%, n = 106), a lack of any symptoms, or failure to document any symptoms in the EMR (10.4%, n = 70), or a combination. Of the patients who underwent PCR testing, 4 of 5 were not classified as appropriately tested because of the absence of fever. Of note, among the patients excluded, 30.5% reported a tick bite in the 2 weeks before the visit. Most of the appropriately tested patients (93.8%, n = 256) had not received doxycycline at the time of sample collection and therefore would have been eligible for a PCR test (Figure). However, only 1 patient meeting clinical criteria (0.4%) underwent PCR, whereas the remaining had serologic testing performed.

Among the 256 patients who were eligible for PCR, 69 (27.0%) had an acute titer result of ≥1:64. Only 47 (18.4%) patients completed convalescent testing. Among those who underwent convalescent testing, 6 (12.8%) demonstrated seroconversion and 12 (17.4%) who were positive at acute testing showed a 4-fold or greater titer increase. In addition, 5 (10.6%) reverted from a positive to a negative titer (Table 2). Of note, 106 (38.8%) of 256 patients had a negative acute *Ehrlichia* IgG titer and were started on antimicrobial drugs but did not return for convalescent blood testing. Similarly, 58 (22.7%) of 256 patients had a negative acute titer and neither received antimicrobial drugs nor returned for a convalescent test. Of the 47 patients who completed acute and convalescent *Ehrlichia* IgG testing, the median number of days between tests was 22 (interquartile range 17–32).

Of the 5 patients who had whole blood samples collected and tested by PCR, 1 test was positive. Attending physicians in the emergency department were responsible for ordering 3 of 5 PCR tests. In all 5 cases, serologic testing for *Ehrlichia* was also conducted. Three of the 5 had an acute but not a convalescent *Ehrlichia* IgG test, whereas 4 of 5 were classified as not appropriately tested because no fever was reported in the EMR (all had ≥1 other symptom in the CSTE criteria). However, the single positive PCR sample was from a patient whose clinical manifestations included a fever and several other consistent symptoms. The send-out PCR test took an average of 6.2 days to receive a result from the reference laboratory.

Overall, 12 (4.7%) of 256 patients who were eligible for PCR were classified as confirmed ehrlichiosis cases (11 by serology and 1 by PCR and serology); and 75 (29.3%) were classified as probable cases. However, on further review of cases that we defined as not appropriately tested, 228 (33.9%) of 673 patients also had 1 positive *Ehrlichia* spp. test, including 193 (28.7%) who had a positive acute IgG test and 90 (13.4%) who had a convalescent IgG test. Among those who returned for a convalescent test, 35 patients showed seroconversion. Of probable cases, 7 exhibited a 4-fold IgG increase from acute to convalescent titers, raising the total number of laboratory-confirmed cases to 48.

Discussion

Our study of routine diagnostic testing practices demonstrated that most patients suspected of having ehrlichiosis did not undergo PCR testing when it was

Table 1. Clinical symptoms among patients tested for tickborne disease at a visit within the University of North Carolina health system, March 24, 2022–April 14, 2023

Clinical symptoms	No. (%) patients
Meets clinical criteria	273 (28.9)
Fever and headache	151 (55.3)
Fever and myalgia	152 (55.7)
Fever and anemia	92 (33.7)
Fever and thrombocytopenia*	65 (23.8)
Fever and hepatic transaminase elevation†	78 (28.6)
Fever and leukopenia‡	42 (15.4)
Tick bite noticed in previous 2 weeks	77 (28.3)
Does not meet clinical criteria	672 (71.1)
Fever	14 (2.1)
Headache	145 (21.6)
Myalgia	168 (25)
Anemia	50 (7.3)
Thrombocytopenia	28 (4.2)
Hepatic transaminase elevation	47 (7)
Leukopenia	26 (3.9)
Bite noticed in 2 weeks prior	205 (30.5)
No symptoms or bite noticed	69 (10.3)

*Platelets <150,000/μL.
†Aspartate aminotransferase ≥33 U/L or alanine aminotransferase >36 U/L.
‡Leukocytes <4,000 cells/μL.

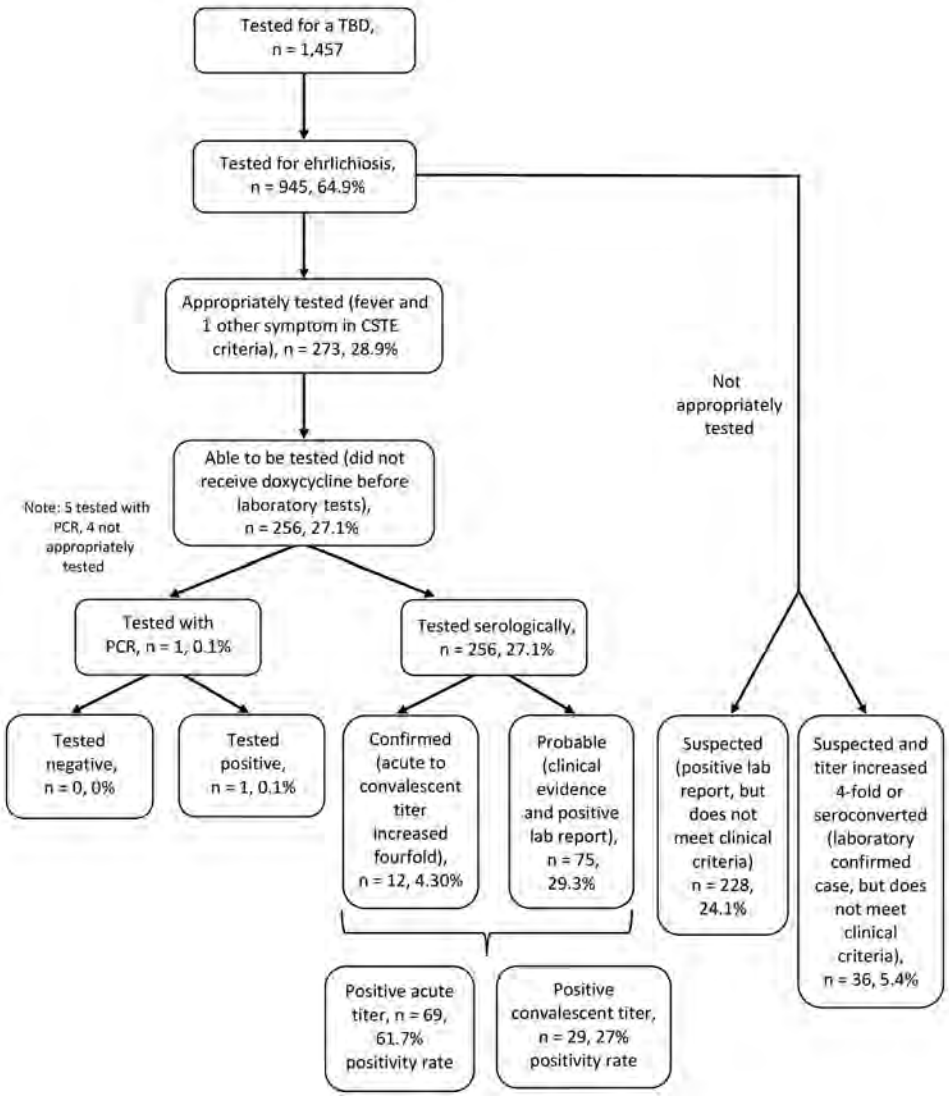

Figure. Flowchart describing use of testing to diagnose ehrlichiosis within the University of North Carolina health system, March 24, 2022–April 14, 2023. CSTE criteria are described in (*18*). CSTE, Council of State and Territorial Epidemiologists; TBD, tickborne disease.

available only as a send-out test, despite the multiple advantages of this testing method. Instead, providers continued to rely on serologic testing, even though rates of diagnostic algorithm completion were low (18.4%). Because the lone star tick (which does not transmit *Rickettsia rickettsii*, the causative bacteria of Rocky Mountain spotted fever) is the primary vector in the state (*19*), it is very likely that ehrlichiosis, along with *R. parkeri*, accounts for most symptomatic, tickborne illness episodes (2). The limited understanding of the diagnosis and management of ehrlichiosis and the underuse of *Ehrlichia* PCR as a confirmatory assay is particularly concerning. Those issues underscore the need to educate providers at all levels of training and across specialties on the diagnosis and management of ehrlichiosis. In addition, improved uptake of PCR can increase knowledge of the true rate of ehrlichiosis cases in the United States, specifically through a higher rate of confirmation and additional information regarding infecting species.

Several factors may explain the underuse of PCR testing. First, few health facilities have the capability or resources to perform an *Ehrlichia* PCR test in their own laboratories. At the time of this study, *Ehrlichia* PCR was only available at UNC Health as a referral test, with samples sent to Mayo Clinical Laboratories. Many providers may not have been aware that an *Ehrlichia* PCR test was available because it did not appear in the standard order menus. Instead, when ordering an *Ehrlichia* PCR, providers were required to order a generic referral test, which then launched a separate screen where the requested test can be entered as a free text. Ordering the test this way requires knowledge of the *Ehrlichia* PCR, the required sample type, and the receiving laboratory. In contrast,

serologic testing, which is performed in-house, can be ordered by a simple search term lookup. This difference in processes might have affected ordering patterns, especially among nonspecialists who are not familiar with the test options. In addition, send-out PCR results still took nearly a week to return to the ordering provider. This timeline might have been insufficient for providers to perceive a benefit to guide treatment decisions, especially when other infections were on the differential diagnosis. Therefore, for optimal implementation, testing likely needs to be performed in-house, and the PCR order should be more prominent and easier to locate within routine test menus.

Whereas empirical antimicrobial drug treatment is recommended when there is a reasonable pretest probability of ehrlichiosis, the relatively fast turnaround of PCR, at least compared with paired serologic testing, offers a timely and objective result to confirm the diagnosis, thereby providing valuable information to both the patient and provider regarding the cause of illness. In our cohort, the number of patients for whom testing was ordered but were not empirically treated with doxycycline is concerning. Because the providers believed there was sufficient evidence to order an ehrlichiosis test, they also should have provided empirical treatment to patients. Without a convalescent blood test, an acute titer result cannot be used to either confirm or rule out ehrlichiosis. Positive PCR results can offer timelier confirmation of ehrlichiosis confirmation and subsequently ensure an appropriate treatment plan. Whereas treatment is ideally prescribed with clinical suspicion, findings show that this is not always the case, and a positive PCR may prompt more immediate action if otherwise not taken. Moreover, because convalescent testing has a much higher positivity rate than acute testing (61.7% vs. 27.0%) but most patients who receive a negative acute IgG titer fail to return for a convalescent titer, there are likely patients with ehrlichiosis who go undetected (*2*). Differing titer values in more than half of paired acute and convalescent samples indicate the convalescent test is clearly needed to interpret serologic results accurately, consistent with current guidelines (*6*). The relatively large proportion of paired titers of the same value implies prior infection and reinforces the importance of paired serologic specimens in areas where baseline seroprevalence is high.

Surprisingly, many patients tested for ehrlichiosis were considered not appropriately tested according to the 2007 CSTE criteria, primarily because of the absence of a subjectively reported fever as documented in the medical record. Yet, the number of laboratory-positive cases and seroconversion rates among patients without clinical evidence was notably higher than that for patients with clinical evidence (36 vs. 12). Those findings suggest that fever is not always a symptom associated with ehrlichiosis. It is also possible that fever is underrecognized because of antipyretic drugs used for headaches and pain control. Largely because of a lack of speciation with serodiagnostic testing, it is possible that infections with non–*E. chaffeensis* species, such as *E. ewingii* and *E. muris eaclairensis*, may exhibit different clinical manifestations than *E. chaffeensis*, which historically is the prototypical pathogen. Previous studies have identified *E. ewingii* in ticks across North Carolina, frequently in higher prevalence than *E. chaffeensis*, which has also been observed in other states (*19*,*20*). Those observations drove changes to the CSTE case definition, which removed fever as a required symptom.

Table 2. Clinical manifestations and titers of patients confirmed with *Ehrlichia* sp. infection within the University of North Carolina health system, March 24, 2022–April 14, 2023*

	Patient identification no.											
Category	548	549	640	765	935	951	1278	1337	1339	1370	1466	1655
Serologic testing results												
Acute *Ehrlichia* IgG titer	≥1:64	1:128	1:128	<1:64	<1:64	≥1:64	1:128	<1:64	<1:64	1:128	<1:64	<1:64
Convalescent *Ehrlichia* IgG titer	1:256	1:1,024	1:1,024	1:128	1:1,024	1:1,024	1:512	1:128	1:128	1:512	1:512	1:128
Days between testing	19	30	18	17	19	22	16	29	29	24	21	8
Clinical manifestations												
Fever	Y	Y	Y	Y	Y	Y	Y	Y	Y	Y	Y	Y
Headache	Y	N	Y	Y	Y	Y	N	N	N	N	N	Y
Myalgia	NA	N	N	N	Y	N	Y	Y	Y	N	N	Y
Anemia	Y	Y	Y	Y	Y	Y	N	N	N	Y	Y	N
Thrombocytopenia	N	Y	N	N	Y	Y	Y	N	N	Y	Y	Y
Hepatic transaminase elevation	N	Y	Y	N	N	Y	Y	Y	Y	N	N	Y
Leukopenia	N	N	N	N	N	Y	N	N	N	Y	N	Y

*N, no; NA, not available; Y, yes.

Our study strengths include conduct in an area with high incidence of ehrlichiosis and the use of a robust electronic database. The first limitation of the study is its retrospective nature and that it relied on routine clinical records to determine clinical symptoms associated with manifestation. Second, unknown data, such as the presence of fever not being entered into a patient's chart, might have resulted in the misclassification of patients. Third, the occurrence of and reliance on single serologic tests has major drawbacks, as described in this article. Fourth, there is potential uncertainty about the true disease state of the patients described in this study. Fifth, the study took place during the COVID-19 pandemic, when care-seeking patterns and diagnostic testing algorithms were disrupted. Finally, we do not have long-term outcomes to assess if participants experienced adverse clinical outcomes because of delayed or lack of antimicrobial drug administration resulting from incomplete testing.

In conclusion, our investigation revealed major underuse of molecular testing for ehrlichiosis in a disease-endemic area, despite the well-established issues associated with serologic testing. Our findings highlight the potential gains that can be made with increased uptake through both provider education and implementation of local testing. Molecular testing could provide information on infecting species, which could help clarify the clinical spectrum, epidemiology, and geographic distribution of different *Ehrlichia* species, and ultimately improve surveillance for this emerging disease and more accurately identify patients at risk of infection.

Acknowledgments

We wish to thank the regulatory team at the University of North Carolina Institute of Global Health and Infectious Diseases, as well as the data management team at the Carolina Data Warehouse for their efforts.

Deidentified individual data from this study will be shared beginning 9–36 months following publication, provided the investigator who proposes to use the data has approval from an Institutional Review Board, Independent Ethics Committee, or Research Ethics Board, as applicable, and executes a data use or sharing agreement with the University of North Carolina.

Funding for this study was provided in part by a Creativity Hub Award from the University of North Carolina Office of the Vice Chancellor for Research (to R.M.B). This study was partially supported by the North Carolina Translational and Clinical Sciences Institute, which is supported by the National Center for Advancing Translational Sciences, National Institutes of Health (grant award no. UL1TR002489).

Author contributions: study conception and design, R.M.B. and A.S.; funding, R.M.B.; implementation, A.S., L.T.U., and E.W.; data analysis, A.S. and R.M.B.; first draft, A.S. and R.M.B.; and manuscript revisions, all authors.

About the Author

Ms. Siegler is an undergraduate student at the University of North Carolina at Chapel Hill studying neuroscience and political science. She is a research assistant at the vectorborne epidemiology, ecology, and response hub investigating the epidemiology of tickborne diseases.

References

1. Centers for Disease Control and Prevention. Ehrlichiosis epidemiology and statistics [cited 2023 May 13]. https://www.cdc.gov/ehrlichiosis/stats
2. Boyce RM, Sanfilippo AM, Boulos JM, Cleinmark M, Schmitz J, Meshnick S. *Ehrlichia* infections, North Carolina, USA, 2016. Emerg Infect Dis. 2018;24:2087–90. https://doi.org/10.3201/eid2411.180496
3. Nichols Heitman K, Dahlgren FS, Drexler NA, Massung RF, Behravesh CB. Increasing incidence of ehrlichiosis in the United States: a summary of national surveillance of *Ehrlichia chaffeensis* and *Ehrlichia ewingii* infections in the United States, 2008–2012. Am J Trop Med Hyg. 2016;94:52–60. https://doi.org/10.4269/ajtmh.15-0540
4. Kuriakose K, Pettit AC, Schmitz J, Moncayo A, Bloch KC. Assessment of risk factors and outcomes of severe ehrlichiosis infection. JAMA Netw Open. 2020;3:e2025577. https://doi.org/10.1001/jamanetworkopen.2020.25577
5. Hamburg BJ, Storch GA, Micek ST, Kollef MH. The importance of early treatment with doxycycline in human ehrlichiosis. Medicine (Baltimore). 2008;87:53–60. https://doi.org/10.1097/MD.0b013e318168da1d
6. Biggs HM, Behravesh CB, Bradley KK, Dahlgren FS, Drexler NA, Dumler JS, et al. Diagnosis and management of tickborne rickettsial diseases: Rocky Mountain spotted fever and other spotted fever group rickettsioses, ehrlichioses, and anaplasmosis—United States. MMWR Recomm Rep. 2016;65:1–44. https://doi.org/10.15585/mmwr.rr6502a1
7. Bakken JS, Haller I, Riddell D, Walls JJ, Dumler JS. The serological response of patients infected with the agent of human granulocytic ehrlichiosis. Clin Infect Dis. 2002;34:22–7. https://doi.org/10.1086/323811
8. Dumler JS, Madigan JE, Pusterla N, Bakken JS. Ehrlichioses in humans: epidemiology, clinical presentation, diagnosis, and treatment. Clin Infect Dis. 2007;45(Suppl 1):S45–51. https://doi.org/10.1086/518146
9. Zychowski DL, Alvarez C, Abernathy H, Giandomenico D, Choudhary SK, Vorobiov JM, et al. Tick-borne disease infections and chronic musculoskeletal pain. JAMA Netw Open. 2024;7:e2351418. https://doi.org/10.1001/jamanetworkopen.2023.51418
10. Mokashi NV, Brown Marusiak A, Giandomenico D, Cleinmark M, Schmitz JL, Boyce RM. Does paging clinicians about tick-borne disease serological results impact clinical care? A retrospective analysis of 70 cases

in North Carolina. Am J Trop Med Hyg. 2024;110:815–8. https://doi.org/10.4269/ajtmh.23-0251
11. Council of State and Territorial Epidemiologists. Update to public health reporting and national notification for ehrlichiosis. Vol. 23-ID-04. 2023 [cited 2024 Feb 2]. https://cdn.ymaws.com/www.cste.org/resource/resmgr/ps/ps_2023/23-ID-04_Ehrlichiosis.pdf
12. North Carolina Division of Public Health. Ehrlichiosis surveillance from 2016–2021 [cited 2023 Jan 10]. https://epi.dph.ncdhhs.gov/cd/ehrlichiosis/EhrlichiosisSurveillanceSummary2021.pdf
13. Brown Marusiak A, Hollingsworth BD, Abernathy H, Alejo A, Arahirwa V, Mansour O, et al. Patterns testing for tick-borne diseases and implications for surveillance in the southeastern US. JAMA Netw Open. 2022;5:e2212334. https://doi.org/10.1001/jamanetworkopen.2022.12334
14. Eshoo MW, Crowder CD, Li H, Matthews HE, Meng S, Sefers SE, et al. Detection and identification of *Ehrlichia* species in blood by use of PCR and electrospray ionization mass spectrometry. J Clin Microbiol. 2010;48:472–8. https://doi.org/10.1128/JCM.01669-09
15. The University of North Carolina Health System. 2021 Annual report [cited 2023 Dec 20]. https://www.unchealthcare.org/app/files/public/9676dff4-3a41-42ce-b177-1a25647a0c62/pdf-UNC_Health_2021_Annual_Report.pdf
16. Mayo Foundation for Medical Education and Research. TEST ID: EPCRB—*Ehrlichia*/*Anaplasma*, molecular detection, PCR, blood [cited 2023 Dec 21]. https://www.mayocliniclabs.com/test-catalog/Overview/618301#Performance
17. Harris PA, Taylor R, Thielke R, Payne J, Gonzalez N, Conde JG. Research electronic data capture (REDCap)—a metadata-driven methodology and workflow process for providing translational research informatics support. J Biomed Inform. 2009;42:377–81. https://doi.org/10.1016/j.jbi.2008.08.010
18. Council of State and Territorial Epidemiologists. Revision of the national surveillance case definition for ehrlichiosis (Ehrlichiosis/Anaplasmosis). Vol. 07-ID-03. 2007 [cited 2024 Feb 21]. https://cdn.ymaws.com/www.cste.org/resource/resmgr/PS/07-ID-03.pdf
19. Lee S, Kakumanu ML, Ponnusamy L, Vaughn M, Funkhouser S, Thornton H, et al. Prevalence of rickettsiales in ticks removed from the skin of outdoor workers in North Carolina. Parasit Vectors. 2014;7:607. https://doi.org/10.1186/s13071-014-0607-2
20. Wolf L, McPherson T, Harrison B, Engber B, Anderson A, Whitt P. Prevalence of *Ehrlichia ewingii* in *Amblyomma americanum* in North Carolina. J Clin Microbiol. 2000; 38:2795. https://doi.org/10.1128/JCM.38.7.2795-2795.2000

Address for correspondence: Ross M. Boyce, University of North Carolina at Chapel Hill, 123 W Franklin St, Ste 2151, Chapel Hill, NC 27516, USA; email: roboyce@med.unc.edu

etymologia revisited

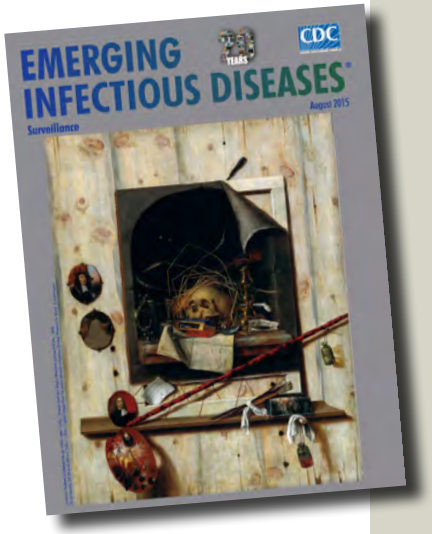

Originally published in August 2015

Escherichia coli

[esh″ə-rik′e-ə co′lī]

A gram-negative, facultatively anaerobic rod, *Escherichia coli* was named for Theodor Escherich, a German-Austrian pediatrician. Escherich isolated a variety of bacteria from infant fecal samples by using his own anaerobic culture methods and Hans Christian Gram's new staining technique. Escherich originally named the common colon bacillus *Bacterium coli commune*. Castellani and Chalmers proposed the name *E. coli* in 1919, but it was not officially recognized until 1958.

References:

1. Oberbauer BA. Theodor Escherich—Leben und Werk. Munich: Futuramed-Verlag; 1992.
2. Shulman ST, Friedmann HC, Sims RH. Theodor Escherich: the first pediatric infectious diseases physician? Clin Infect Dis. 2007;45:1025–9 .

https://wwwnc.cdc.gov/eid/article/21/8/et-2108_article

Epidemiologic and Genomic Surveillance of *Vibrio cholerae* and Effectiveness of Single-Dose Oral Cholera Vaccine, Democratic Republic of the Congo

Christine Marie George,[1] Alves Namunesha,[1] Kelly Endres, Willy Felicien, Presence Sanvura, Jean-Claude Bisimwa, Jamie Perin, Justin Bengehya, Jean Claude Kulondwa, Ghislain Maheshe, Cirhuza Cikomola, Lucien Bisimwa, Alain Mwishingo, David A. Sack, Daryl Domman

We conducted 4 years of epidemiologic and genomic surveillance of single-dose effectiveness of a killed whole-cell oral cholera vaccine (kOCV) and *Vibrio cholerae* transmission in the Democratic Republic of the Congo. We enrolled 1,154 patients with diarrhea; 342 of those had culture-confirmed cholera. We performed whole-genome sequencing on clinical and water *V. cholerae* isolates from 200 patient households, which showed annual bimodal peaks of *V. cholerae* clade AFR10e infections. A large clonal cholera outbreak occurred 14 months after a kOCV campaign of >1 million doses, likely because of low (9%) vaccine coverage in informal settlements. Clinical and water isolates collected in the same household were closely related, suggesting person-to-person and water-to-person transmission. Single-dose kOCV vaccine effectiveness 24 months after vaccination was 59.8% (95% CI 19.7%–79.9%), suggesting modest single-dose kOCV protection. kOCV campaigns combined with water, sanitation, and hygiene programs should be used to reduce cholera in disease-endemic settings worldwide.

An estimated 2.9 million cholera cases and 95,000 deaths occur annually in cholera-endemic countries (*1*). The Democratic Republic of the Congo (DRC) has one of the highest rates of cholera in Africa (*2*). In 2017, the Global Task Force on Cholera Control released the document Ending Cholera: A Global Roadmap to 2030 to reduce cholera deaths by 90% in the DRC and eliminate cholera in 20 other countries by 2030 (*3*). To address cholera in transmission hotspots, the task force recommends oral cholera vaccine (OCV) campaigns and case area–targeted water, sanitation, and hygiene (WASH) interventions should be implemented in a ring around cholera cases. However, a global OCV stockpile shortage has necessitated identifying the duration of protection conferred by OCVs to determine the optimal frequency for OCV campaigns (*4*). Most studies on OCV effectiveness have been from India and Bangladesh and have evaluated the effectiveness of 2-dose OCV protection (H. Xu et al., unpub. data, https://doi.org/10.1101/2024.08.13.24311930). Only 4 studies have evaluated single-dose OCV vaccine effectiveness (2 of those for a duration of ≥24 months), and all except 1 used the Shanchol vaccine, which is no longer produced (H. Xu et al., unpub. data).

Few studies have combined evaluations of OCV effectiveness and genomic surveillance of clinical and environmental *Vibrio cholerae* isolates by using whole-genome sequencing (WGS), which can provide valuable information on how OCV campaigns affect *V. cholerae* transmission dynamics and can identify genetic characteristics of circulating *V. cholerae* strains. WGS is also a valuable tool to link cholera epidemics

Author affiliations: Johns Hopkins Bloomberg School of Public Health, Baltimore, Maryland, USA (C.M. George, K. Endres, J. Perin, D.A. Sack); Université Catholique de Bukavu, Bukavu, Democratic Republic of the Congo (A. Namunesha, W. Felicien, P. Sanvura, J.-C. Bisimwa, G. Maheshe, C. Cikomola, L. Bisimwa, A. Mwishingo); Ministère de la Santé, Bukavu (J. Bengehya, J.C. Kulondwa); University of New Mexico Health Sciences Center, Albuquerque, New Mexico, USA (D. Domman)

DOI: https://doi.org/10.3201/eid3102.241777

[1]These first authors contributed equally to this article.

globally and investigate *V. cholerae* transmission by distinguishing strains on the basis of single-nucleotide polymorphisms (SNPs) (*5*). Genomic data from 45 countries in Africa revealed that the *V. cholerae* seventh pandemic El Tor (7PET) strain was introduced into Africa ≥15 times since 1970 (*6*). Previous genomic studies (2018–2024) in DRC have found *V. cholerae* 7PET strains belong to clades AFR10d, AFR10e, and ARFR10w (*7*,*8*).

We previously used WGS to analyze water and clinical sources of *V. cholerae* collected from patient households to investigate cholera transmission dynamics in Bangladesh (*9*). We found that 80% of cholera patient households had isolates from water that were closely related to clinical isolates; whereas 20% of households had clinical isolates from infected persons that were more closely related to clinical isolates from other households than to source water isolates in their own household. Those results were consistent with person-to-person and water-to-person *V. cholerae* transmission. Genomic studies to elucidate transmission dynamics of *V. cholerae* infection in cholera patient households in sub-Saharan Africa are lacking; previous studies have been exclusively in South Asia.

We conducted 4 years of epidemiologic and genomic surveillance of *V. cholerae* in eastern DRC to achieve the following aims. First, we evaluated the effectiveness of a single-dose of Euvichol-Plus (EuBiologics, http://eubiologics.com), a killed whole-cell OCV (kOCV), during the 24-month period after a preventive kOCV campaign. Second, we investigated *V. cholerae* transmission dynamics among cholera patients, household members, and water sources by using WGS. Third, we determined the spatiotemporal spread of *V. cholerae* in this cholera-hyperendemic region.

Methods

Ethics Approval

We conducted this study in urban Bukavu, South Kivu Province, DRC. We received ethics approval for this study from Johns Hopkins Bloomberg School of Public Health, (Baltimore, Maryland, USA) and Catholic University of Bukavu (Bukavu, DRC). All participants or their guardians provided written informed consent.

Study Design and Protocol

During March 2020–March 2024, we conducted passive cholera surveillance at 115 healthcare facilities in Bukavu. Patients with diarrhea who were admitted during this time had their feces tested for *V. cholerae* by using bacterial culture. We defined cholera patients as patients with diarrhea who had a *V. cholerae*–positive fecal sample by bacterial culture. We conducted a prospective cohort study of household contacts of cholera patients during December 2021–December 2023 to investigate cholera transmission dynamics within cholera patients' households. We defined household contacts of cholera patients as those sharing a cooking pot and residing in the same home with the cholera patient for the previous 3 days. We enrolled household contacts in the study within 24 hours of enrolling the corresponding cholera patient. We determined the sample size for the prospective cohort study by using the number of cholera patients who could be screened and who were willing to participate in the cohort study. We visited cholera patient households on days 1, 3, 5, 7, 9, and 11 (visits 1–6) after the household's index cholera patient was admitted at a health facility to conduct clinical surveillance. For clinical surveillance, we collected a fecal sample from the cholera patient and household contacts during each household visit to test for *V. cholerae* by using bacterial culture. We conducted an unannounced spot check at each timepoint to collect a sample of the household's water source and stored drinking water to test for *V. cholerae* by bacterial culture.

During December 28, 2021–January 2, 2022, and March 31–April 4, 2022, the DRC Ministry of Health delivered 1.04 million doses of Euvichol-Plus kOCV in Bukavu as a preventive OCV campaign. Vaccines were delivered through a combination of door-to-door visits and designated healthcare facilities. We assessed OCV vaccination status for patients with diarrhea and their household members through self or caregiver reporting during the time of patient treatment in the healthcare facility or during a home visit conducted the same or the following day. Study research officers administered a structured questionnaire, which obtained information on OCV administration and the date and number of doses. An OCV vaccine card was shown, along with a photo of the person consuming OCV. We defined informal settlements as areas where no household connections to piped water existed.

Laboratory Analyses

All whole fecal samples were brought to the Preventative Intervention for Cholera for 7 Days program Enteric Disease Microbiology Laboratory in Bukavu within 3 hours of the sample being produced, and water samples were brought to the laboratory within 3 hours of collection for *V. cholerae* analysis by bacterial

culture as previously described (*10*). We preserved isolated bacteria as stabs in nutrient agar or on Whatman filter paper to preserve bacterial DNA.

WGS

We extracted DNA from isolates preserved as agar stabs by using the ZymoBIOMICS DNA Miniprep Kit (Zymo Research, https://www.zymoresearch.com) and extracted genomic bacterial DNA from filter paper by using published Chelex methods (*11*). The SeqCenter (https://www.seqcenter.com) and University of New Mexico Health Sciences Center performed WGS. We processed short reads by using the Bactopia pipeline (*12*) and SPAdes version 3.10.0 (*13*) and annotated by using Prokka version 1.520 (*14*). We performed genome completeness estimates and checks for contamination by using CheckM version 1.0.722 and Kraken version 0.10.6 (*15*,*16*). We deposited all next-generation sequencing data from this study under the National Center for Biotechnology Information BioProject database (https://www.ncbi.nlm.nih.gov/bioproject; no. PRJNA1210607).

Genomic and Phylogenetic Analyses

We mapped paired-end reads for 255 7PET isolates and compared variants with the *V. cholerae* O1 El Tor reference genome N16961 (GenBank accession nos. LT907989 and LT907990) by using snippy version 4.6.0 (https://github.com/tseemann/snippy) via the Bactopia pipeline (*12*) to generate a reference-based alignment containing 329 variable SNP sites. All 255 isolates mapped with >90% of the reference genome; thus, we further analyzed all 255 isolates. We generated a pairwise SNP matrix for the 255 7PET isolates by using pairsnp (https://github.com/gtonkinhill/pairsnp). We used ARIBA version 2.14.7 (https://github.com/sanger-pathogens/ariba) to determine mutations in the *wbeT* gene by comparing sequences with a reference wild-type Ogawa *wbeT* gene from the European Nucleotide Archive database (https://www.ebi.ac.uk/ena; accession no. AEN80191.1)

We compared 7PET isolates from this study with 1,418 globally representative 7PET strains to assess phylogeographic relatedness (*17*). We used the 12,561 variable site (SNPs) alignment to build a maximum-likelihood phylogeny; we used IQ-Tree version 1.6.12 and the general time reversible substitution model with the gamma distribution to model site heterogeneity with 10,000 ultrafast bootstraps and used 10,000 bootstraps for the Shimodaira-Hasegawa–like approximate-likelihood ratio tests (*18*). We visualized phylogenies by using ggtree version 1.6.11 (*19*) and rooted the trees by using the pre-seventh pandemic *V. cholerae* strain M66.

Local Transmission Analyses

We gained insights into local transmission dynamics from a 329 SNP reference-based alignment of the 255 7PET isolates. We built a maximum-likelihood tree by using IQ-Tree and the models and bootstraps as described previously. We visualized phylogenies by using Microreact (*20*). We created minimum spanning trees by using GrapeTree version 1.5.0 (*21*) and visualized geospatial data for cases by using Python geopandas (https://github.com/geopandas/geopandas) and contextily (https://github.com/geopandas/contextily) packages.

Statistical Analysis

We assessed single-dose Euvichol-Plus kOCV effectiveness during the 24-month period after vaccination by using a test-negative design among patients with diarrhea. We used logistic regression models with cholera infection as the outcome (defined as a positive *V. cholerae* bacterial culture) and kOCV vaccination status (whether patients with diarrhea reported receiving 1 dose of kOCV during the kOCV campaign period) as the predictor. In this model, the odds ratio was the odds of single-dose kOCV vaccination effectiveness in the cholera-positive patients with diarrhea compared with controls (non–cholera patients with diarrhea). We calculated vaccine effectiveness by using the equation $(1 - \text{OR}) \times 100\%$, and we excluded persons who reported receiving 2 doses of kOCV from the analysis. We performed analyses by using SAS version 9.4 (SAS Institute Inc., https://www.sas.com). We performed permutation tests by using R (The R Project for Statistical Computing, https://www.r-project.org) and Python to analyze pairwise comparisons of genomic data. For pairwise comparisons, we compared SNP counts for each strain with those from the *V. cholerae* reference strain N16961.

Results

Epidemiology

During March 2020–March 2024, we identified *V. cholerae* in fecal samples from 342 (30%) of 1,154 patients with diarrhea via bacterial culture (Appendix Figure 1, https://wwwnc.cdc.gov/EID/article/31/2/24-1777-App1.pdf). We mapped the 115 healthcare facilities and households of patients with diarrhea surveilled in this study (Figure 1). We observed an annual bimodal peak of cholera during

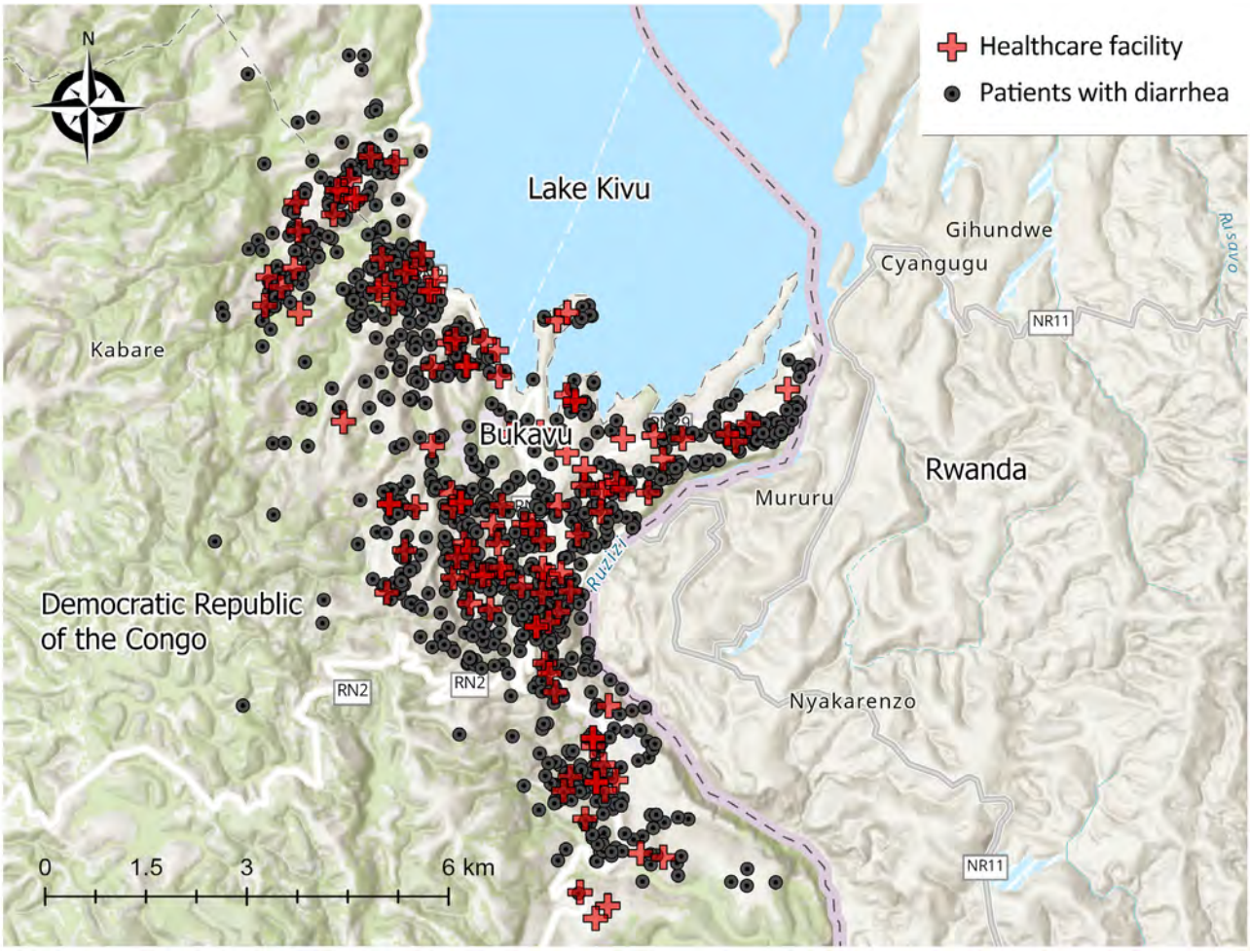

Figure 1. Location of patients with diarrhea and the corresponding healthcare facilities where they sought treatment in a surveillance study of *Vibrio cholerae* and effectiveness of single-dose oral cholera vaccine, Democratic Republic of the Congo, 2020–2024. A total of 115 healthcare facilities and 1,098 households of patients with diarrhea are shown; 56 patient households had missing Global Positioning System coordinates.

the dry (June–August) and rainy (September–January) seasons in 2020 and 2023 (Appendix Figure 2). In December 2021, a kOCV campaign distributed 1.04 million doses of Euvichol-Plus within Bukavu (study surveillance site). After that kOCV campaign, sporadic cholera patients were observed through January 2023. Then, ≈14 months after the kOCV campaign (June–November 2023), a large cholera outbreak occurred in this same area. Nine percent (309/3,395) of persons residing in informal settlements within the study area reported receiving ≥1 kOCV dose during December 2021–April 2022. During the 4-year surveillance period, stored and source water samples were collected from 178 cholera patient households; 9% (16/173) of households had *V. cholerae*–positive stored water samples and 6% (9/157) of households had positive source water samples. A total of 29 water samples were *V. cholerae* positive over the study period (Appendix Figure 3). During October 2021–November 2022 (including the 12-month period after the kOCV campaign was initiated), no *V. cholerae* was detected in drinking water samples, despite the presence of culture-confirmed cholera patients.

OCV Vaccine Effectiveness

Surveillance healthcare facilities admitted 750 patients with diarrhea during the 24-month period after the kOCV campaign (December 2021–December 2023). We recorded demographic characteristics for kOCV vaccinated and unvaccinated persons (Table). During the 3 nights before hospitalization, 94% (708/750) of patients with diarrhea reported residing in their current residences; 12% (93/748) had running water inside their home. Twelve percent (93/750) (15 cholera patients and 78 non–cholera patients with diarrhea) of

patients reported receiving ≥1 dose of kOCV during December 2021–April 2022; only 2% (14/750) of patients reported receiving 2 kOCV doses, and 13% (12/93) of kOCV-vaccinated patients showed a vaccination card. During this period, 208 (193 unvaccinated and 15 kOCV vaccinated) patients had cholera; 531 patients with diarrhea were >1 year of age. The unadjusted single-dose kOCV vaccine effectiveness in the first 24 months after vaccination was 59.8% (95% CI 19.7%–79.9%) for persons >1 year of age and, after adjustment for age (continuous variable), was 58.7% (95% CI 17.3%–79.4%). We also calculated the single-dose kOCV vaccine effectiveness according to time interval (first 12-month and second 12-month period after vaccination) for persons >1 year of age (Appendix Table). We excluded 10 patients with diarrhea from this analysis because they received 2 doses of kOCV.

Genomic Analyses

We sequenced 255 *V. cholerae* 7PET genomes from samples collected within the study area. Of those genomes, 247 were clinical isolates from the fecal samples of 243 persons residing in 200 households (198 patients and 45 household contacts), and 8 were from water samples. The WGS analysis included 75% (255/342) of cholera patient households during the surveillance period, and all available isolates were sequenced. To investigate the genetic relatedness of the *V. cholerae* isolates, we analyzed the pairwise SNP differences across 255 genomes. Of the 200 households in the study, 31 households were represented by >1 sample, 26 households had >1 study participant with samples, and 5 households had both clinical and water *V. cholerae* isolates. Maximum-likelihood phylogenic analyses of the 255 7PET *V. cholerae* genomes indicated the *V. cholerae* isolated from both clinical and water samples were closely related, and limited genetic divergence occurred over the study period (Figure 2, panels A, B). Among all isolates, the minimum number of SNP differences was 0 and the maximum number was 65 (median 13) (Figure 3, panel A). For isolates from the same person, the range was 0–1 SNP and median 0 SNPs. For isolates from the same household (isolated from both clinical and water samples), the pairwise differences range was 0–14 SNPs (median 0) (Figure 3, panel B). We found a significant difference in the median number of SNPs among isolates from different households compared with those from the same household ($p<0.0001$ by Mann-Whitney U test). In the 3 of 5 households with both clinical and water *V. cholerae* isolates, the isolates had 0 SNP differences among them; the other 2 households had 1–3 SNP differences between the clinical and water samples. This result provides evidence that the same strain causing infections in household members was also detected in the household water. However, we cannot determine whether the water was the source of infection or whether the water was contaminated after an infection occurred in a household member. The median difference in the number of SNPs was significantly lower for isolates from cholera patients before the kOCV vaccine campaign (median 6 [range 0–58]) compared with the number of SNPs after the kOCV vaccine campaign (median 12 [range 0–31]) ($p<0.0001$ by Mann-Whitney U test).

To determine how the 255 *V. cholerae* isolates from this study fit within the larger diversity of 7PET strains, we contextualized those genomes within a global collection of 1,422 additional 7PET genomes (Figure 4)

Table. Demographic characteristics of patients with diarrhea in study of effectiveness of single-dose oral cholera vaccine, Democratic Republic of the Congo*

Characteristics	All patients with diarrhea, n = 750	Vaccination status		p value
		Received kOCV, n = 93	No kOCV, n = 657	
Age, y				
Median ±SD (min–max)	5 ±19 (0–82)	2 ±15 (0–63)	7 ±19 (0–82)	
0–1	217/750 (29)	30/93 (32)	187/657 (28)	0.527
1–4	148/750 (20)	28/93 (30)	120/657 (18)	0.011
5–14	96/750 (13)	11/93 (12)	85/657 (13)	0.893
≥14	289/750 (39)	24/93 (26)	265/657 (40)	0.009
Patient sex				
F	368/750 (49)	45/93 (48)	323/657 (49)	0.977
M	382/750 (51)	48/93 (52)	334/657 (51)	
Running water inside home	93/748 (12)	12/93 (13)	81/655 (12)	1.000
Working mobile phone in home	565/663 (85)	78/85 (92)	487/587 (83)	0.097
Resided in home, y, median ±SD (min–max)	7 ±3 (1–23)	7 ±2 (3–16)	7 ±3 (1–23)	0.098
Formal education,† y, median ±SD (min–max)	9 ±5 (0–23)	7 ±5 (0–15)	9 ±5 (0–23)	0.028

*Values are no. patients in each group/total no. patients analyzed (%) except as indicated. p values compare vaccination status. kOCV, killed whole-cell oral cholera vaccine.
†For those patients ≥18 years of age.

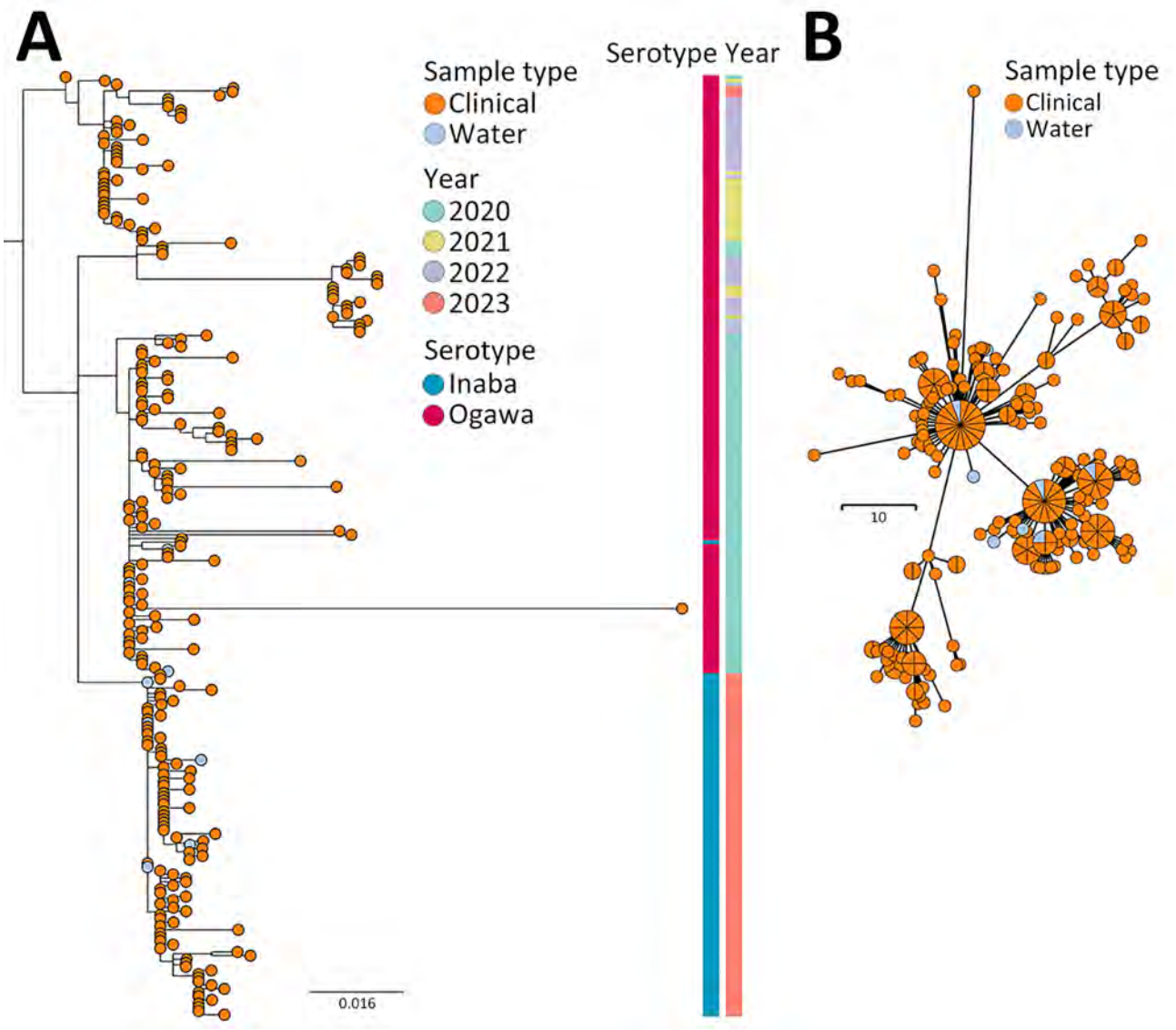

Figure 2. Phylogenetic analysis of *Vibrio cholerae* seventh pandemic El Tor (7PET) isolates collected during study of *V. cholerae* transmission and effectiveness of single-dose oral cholera vaccine, Democratic Republic of the Congo. A) Maximum-likelihood tree of 255 7PET *V. cholerae* genomes sampled in Bukavu during 2020–2023. Node colors indicate sample type. Associated colored metadata indicate sampling year and inferred serotypes according to genome analysis. Scale bar indicates nucleotide substitutions per site. B) Minimum spanning tree of 255 7PET *V. cholerae* genomes sampled in Bukavu during 2020–2023. Node colors indicate sample type. Isolates with 0 single-nucleotide polymorphism differences between each other are collapsed into single node. Node sizes are scaled according to the number of samples. Scale bar indicates single-nucleotide polymorphisms.

(*17*). Phylogenetic analysis placed the 255 isolates within the T10 lineage of the AFR10e clade. Our isolates, sampled during 2020–2023, were similar to other recent samples (2015–2020) from DRC in the same region of South Kivu (*8*). Genomic analysis of the *wbeT* gene indicated that samples from 2020–2022 had intact wild-type *wbeT* genes, which indicates an Ogawa serotype; we observed 1 exception for a sample from 2020 with a frameshift mutation (N165fs), which would likely result in an Inaba serotype. However, all samples from 2023 after the OCV campaign appear to have a fragmented *wbeT* gene marked by insertion of mobile elements, likely conferring an Inaba serotype. In line with other AFR10e strains, our isolates harbored mutations in *gyrA* (S83I) and *parC* (S85L) genes, which have been proposed to reduce susceptibility to fluoroquinolones (*8*).

Discussion

In the urban cholera-endemic setting in DRC where we conducted our study, annual bimodal peaks of

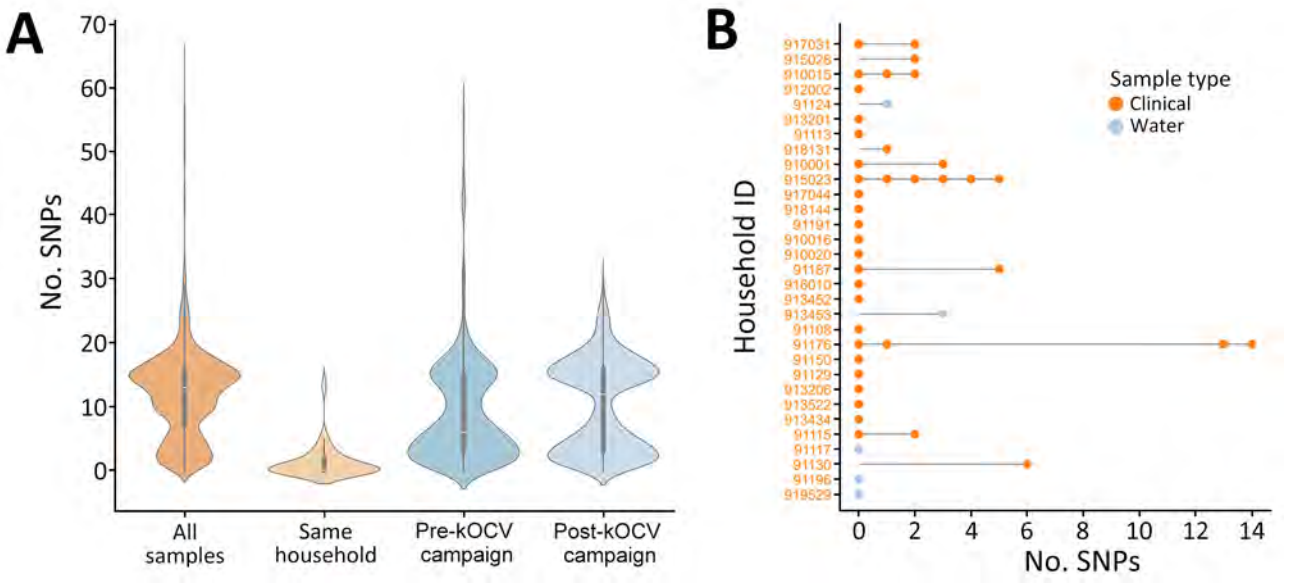

Figure 3. Pairwise comparisons of SNPs in surveillance study of *Vibrio cholerae* and effectiveness of single-dose killed oral cholera vaccine (kOCV), Democratic Republic of the Congo. A) Violin plot showing distribution of pairwise SNP differences from all isolates collected during the study, those from the same household, and those pre-kOCV and post-kOCV campaign. Density curves indicate frequency of data points. Inside each density plot, horizontal white lines within boxes indicate medians; box tops and bottoms indicate upper (third) and lower (first) quartiles; and whiskers indicate minimum and maximum values. Number of pairwise comparisons for each category is as follows: all samples, n = 32,385; same household, n = 99; pre-kOCV campaign, n = 6,205; and post-kOCV campaign, n = 10,296. B) SNP differences per household. Pairwise SNP differences are relative to the first sample in the household. Node colors indicate sample type; stems connect samples to their household. ID, identification; SNP, single-nucleotide polymorphism.

V. cholerae clade AFR10e infections corresponded with the dry and rainy seasons. One third of patients with diarrhea attending 115 surveillance healthcare facilities were confirmed to have cholera by bacterial culture; 9% of stored water and 6% of source water samples from cholera patient households contained *V. cholerae*. This finding suggests that both source water and contamination of stored water might be potential transmission routes for *V. cholerae* infections in cholera patient households. A large clonal cholera outbreak occurred 14 months after >1 million doses of Euvichol-Plus kOCV vaccines were distributed in the same area. This large outbreak occurred despite the vaccine campaign, possibly because of the low (9%) kOCV coverage within informal settlements in Bukavu, which are often hotspots for cholera because of limited access to improved drinking water sources, sanitation options, and poor hygienic conditions (22). No water samples were positive for *V. cholerae* during the 12-month period after the kOCV campaign was initiated, despite the presence of cholera patients. Future studies should investigate the effect of kOCV campaigns on *V. cholerae* persistence in the environment.

Using a test-negative design, we found that a single dose of Euvichol-Plus provided modest protection against medically attended cholera during the 24 months after vaccination, consistent with findings from other studies (H. Xu et al., unpub. data). This test-negative design to evaluate kOCV effectiveness could be incorporated into existing cholera surveillance activities globally and could be integrated as part of kOCV vaccine campaign rollouts. Our findings suggest that, with increased vaccination coverage in informal settlements, single-dose kOCV campaigns are a promising approach to deliver vaccines along with WASH programs to reduce cholera in the DRC.

Our genomic findings highlight several points. First, we did not detect any samples that grouped in the *V. cholerae* clade AFR10d, a finding that seems to further corroborate that clade AFR10e replaced AFR10d around 2018 in this region (23). Second, during the subsequent cholera outbreak after the large kOCV campaign, we observed a change in *V. cholerae* serotype from Ogawa to Inaba, which was likely related to a fragmented *wbeT* gene marked by insertion of mobile elements. This finding is consistent with another study that observed a serotype switch after an OCV vaccination campaign (24). In addition, we observed an increase in the number of SNP differences among *V. cholerae* isolates collected after the kOCV campaign, compared with those collected before the

campaign. However, both our findings and those from the previous study are observational, and causality cannot be inferred. Third, this study provided evidence that household water source contained the same isolates that caused cholera infections among household members. This result combined with the finding that clinical isolates in the same household were more closely related than isolates from different households (even when no *V. cholerae* was found in household drinking water source) suggests a combination of person-to-person and water-to-person cholera transmission. Our findings suggest it is critical for WASH programs to place emphasis on both chlorination of household water and handwashing with soap to prevent cholera transmission.

The first strength of our study is the 4-year duration of epidemiologic and genomic surveillance of cholera patients and their water sources before and after a kOCV campaign. Previous longitudinal studies including both clinical and environmental surveillance have been almost exclusively performed in South Asia. Second, we evaluated the effectiveness of a single-dose of Euvichol-Plus over a 24-month period, building on previous studies that focused mostly on 2-doses of kOCV and evaluated the Shanchol kOCV, which is no longer produced. One study evaluated the single-dose kOCV effectiveness of Euvichol-Plus for a period of ≥24 months in DRC and found 54% effectiveness 12–17 months after vaccination, similar to our study (*25*). In addition, the test-negative design for kOCV effectiveness builds on observational studies using community controls by reducing the likelihood of differences in care-seeking behavior between *V. cholerae*–infected persons and controls, which can introduce substantial bias in observational studies of vaccine effectiveness. Finally, the inclusion of the genomics data enabled us to investigate how water and clinical *V. cholerae* strains evolved over time before and after a kOCV campaign and to investigate *V. cholerae* transmission dynamics in cholera patient households.

The first limitation of our study is that our surveillance focused only on an urban setting; therefore, we cannot generalize our findings to rural settings. Additional data on single-dose kOCV vaccine effectiveness is needed in rural settings globally. Second, as with all observational study designs, misclassification of a patient's vaccination status and cholera infection outcome is possible. Also, the vaccine campaign in this study was a preventive campaign in an area identified as a hotspot; however, because of a global kOCV vaccine shortage, all cholera vaccination campaigns are currentlly reactive and respond to outbreaks. Future studies are needed to evaluate single-dose kOCV effectiveness during reactive kOCV campaigns worldwide.

In conclusion, we observed annual bimodal peaks of *V. cholerae* clade AFR10e in an urban cholera-endemic area in eastern DRC. One third of patients with

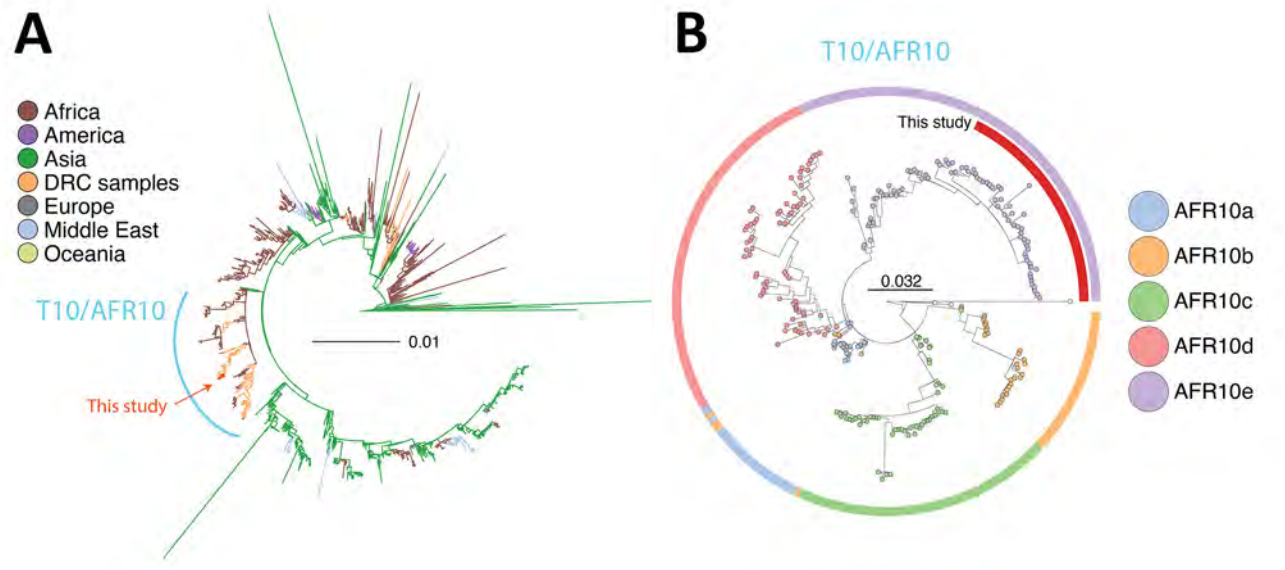

Figure 4. Phylogenetic analysis of *Vibrio cholerae* strains in study of *V. cholerae* transmission and effectiveness of single-dose killed oral cholera vaccine, DRC. Maximum-likelihood phylogenetic trees were prepared to compare *V. cholerae* seventh pandemic El Tor (7PET) isolates. A) Globally representative phylogeny of 1,428 7PET strains; 5 representative isolates from this study (red) were placed within the larger context of those 7PET strains. Tree was rooted on the A6 strain. Branch colors indicate geographic origin of the strain. B) Phylogeny of the T10/AFR10 lineage of *V. cholerae*. Colors indicate different *V. cholerae* lineages. Representative isolates from this study (n = 46; red) were placed within the context of 221 T10/AFR10 lineage strains. Tree was rooted on the reference strain N16961. Scale bars indicate nucleotide substitutions per site. DRC, Democratic Republic of the Congo.

diarrhea admitted to surveillance healthcare facilities were confirmed to have cholera by bacterial culture. A large clonal cholera outbreak occurred 14 months after a single dose kOCV campaign, and the severity of the outbreak might have been related to the low vaccine coverage in informal settlements. Genomic analyses suggest that both person-to-person and water-to-person transmission occurred. A single-dose of Euvichol-Plus kOCV provided modest protection against medically attended cholera during the 24 months after vaccination. Our findings indicate that single-dose kOCV campaigns in combination with WASH programs should be used to reduce cholera disease in cholera-endemic settings worldwide.

Acknowledgments

We thank the study participants for their support in implementing this study, our funders, and our research officers Raissa Boroto, Freddy Mwambusa, Pacifique Kitumaini, Blessing Muderhwa, Jean Claude Lunyelunye, Feza Rugusha, Gisele Kasanziki, Brigitte Munyerenkana, Jessy Tumsifu, Pascal Kitumaini, Emmanuel Buhendwa, and Julienne Rushago, who played a crucial role in the success of this work.

This work was funded by Wellcome and UK aid from the Foreign and Commonwealth Development Office (grant no. 215674Z19Z to C.M.G.) and by the National Institutes of Health (grant nos. 4R01AI148332-01 to C.M.G., UL1TR001449 and KL2TR001448 to D.D., and 2R01AI123422-06A1 to D.A.S.).

The funding agencies were not involved in study design, data collection, data analysis, and data interpretation, or manuscript submission. The views expressed do not necessarily reflect the official policies or views of the Foreign and Commonwealth Development Office.

About the Author

Dr. George is a professor and infectious disease epidemiologist. Her research focuses on developing and evaluating community and healthcare facility–based infectious disease control programs to reduce infections in low- and middle-income countries and low-resource settings globally.

References

1. Ali M, Nelson AR, Lopez AL, Sack DA. Updated global burden of cholera in endemic countries. PLoS Negl Trop Dis. 2015;9:e0003832. https://doi.org/10.1371/journal.pntd.0003832
2. Lessler J, Moore SM, Luquero FJ, McKay HS, Grais R, Henkens M, et al. Mapping the burden of cholera in sub-Saharan Africa and implications for control: an analysis of data across geographical scales. Lancet. 2018;391:1908–15. https://doi.org/10.1016/S0140-6736(17)33050-7
3. Global Task Force on Cholera Control. Ending cholera: a global roadmap to 2030 [cited 2024 Sep 23]. https://www.gtfcc.org/wp-content/uploads/2020/09/ending-cholera-a-global-roadmap-to-2030.pdf
4. World Health Organization. Shortage of cholera vaccines leads to temporary suspension of two-dose strategy, as cases rise worldwide [cited 2024 Oct 13]. https://www.who.int/news/item/19-10-2022-shortage-of-cholera-vaccines-leads-to-temporary-suspension-of-two-dose-strategy--as-cases-rise-worldwide
5. Chaguza C, Chibwe I, Chaima D, Musicha P, Ndeketa L, Kasambara W, et al. Genomic insights into the 2022–2023 *Vibrio cholerae* outbreak in Malawi. Nat Commun. 2024;15:6291. https://doi.org/10.1038/s41467-024-50484-w
6. Weill FX, Domman D, Njamkepo E, Tarr C, Rauzier J, Fawal N, et al. Genomic history of the seventh pandemic of cholera in Africa. Science. 2017;358:785–9. https://doi.org/10.1126/science.aad5901
7. Irenge LM, Ambroise J, Bearzatto B, Durant JF, Bonjean M, Wimba LK, et al. Genomic evolution and rearrangement of CTX–Φ prophage elements in *Vibrio cholerae* during the 2018–2024 cholera outbreaks in eastern Democratic Republic of the Congo. Emerg Microbes Infect. 2024; 13:2399950. https://doi.org/10.1080/22221751.2024.2399950
8. Hounmanou YMG, Njamkepo E, Rauzier J, Gallandat K, Jeandron A, Kamwiziku G, et al. Genomic microevolution of *Vibrio cholerae* O1, Lake Tanganyika Basin, Africa. Emerg Infect Dis. 2023;29:149–53. https://doi.org/10.3201/eid2901.220641
9. George CM, Rashid M, Almeida M, Saif-Ur-Rahman KM, Monira S, Bhuyian MSI, et al. Genetic relatedness of *Vibrio cholerae* isolates within and between households during outbreaks in Dhaka, Bangladesh. BMC Genomics. 2017;18:903. https://doi.org/10.1186/s12864-017-4254-9
10. World Health Organization. Manual for the laboratory identification and antimicrobial susceptibility testing of bacterial pathogens of public health importance in the developing world. 2003 [cited 2024 Sep 20]. https://www.who.int/publications/i/item/WHO-CDS-CSR-RMD-2003.6
11. Debes AK, Ateudjieu J, Guenou E, Ebile W, Sonkoua IT, Njimbia AC, et al. Clinical and environmental surveillance for *Vibrio cholerae* in resource constrained areas: application during a 1-year surveillance in the far north region of Cameroon. Am J Trop Med Hyg. 2016;94:537–43. https://doi.org/10.4269/ajtmh.15-0496
12. Petit RA 3rd, Read TD. Bactopia: a flexible pipeline for complete analysis of bacterial genomes. mSystems. 2020; 5:e00190-20. https://doi.org/10.1128/mSystems.00190-20
13. Bankevich A, Nurk S, Antipov D, Gurevich AA, Dvorkin M, Kulikov AS, et al. SPAdes: a new genome assembly algorithm and its applications to single-cell sequencing. J Comput Biol. 2012;19:455–77. https://doi.org/10.1089/cmb.2012.0021
14. Seemann T. Prokka: rapid prokaryotic genome annotation. Bioinformatics. 2014;30:2068–9. https://doi.org/10.1093/bioinformatics/btu153
15. Parks DH, Imelfort M, Skennerton CT, Hugenholtz P, Tyson GW. CheckM: assessing the quality of microbial genomes recovered from isolates, single cells, and metagenomes. Genome Res. 2015;25:1043–55. https://doi.org/10.1101/gr.186072.114
16. Wood DE, Salzberg SL. Kraken: ultrafast metagenomic sequence classification using exact alignments. Genome Biol. 2014;15:R46. https://doi.org/10.1186/gb-2014-15-3-r46

17. Smith AM, Sekwadi P, Erasmus LK, Lee CC, Stroika SG, Ndzabandzaba S, et al. Imported cholera cases, South Africa, 2023. Emerg Infect Dis. 2023;29:1687–90. https://doi.org/10.3201/eid2908.230750
18. Minh BQ, Schmidt HA, Chernomor O, Schrempf D, Woodhams MD, von Haeseler A, et al. IQ-TREE 2: new models and efficient methods for phylogenetic inference in the genomic era. Mol Biol Evol. 2020;37:1530–4. https://doi.org/10.1093/molbev/msaa015
19. Yu G, Smith DK, Zhu H, Guan Y, Lam TTY. Evolution. GGTREE: an R package for visualization and annotation of phylogenetic trees with their covariates and other associated data. Methods Ecol. Evol. 2017;8: 28–36. https://doi.org/10.1111/2041-210X.12628
20. Argimón S, Abudahab K, Goater RJE, Fedosejev A, Bhai J, Glasner C, et al. Microreact: visualizing and sharing data for genomic epidemiology and phylogeography. Microb Genom. 2016;2:e000093. https://doi.org/10.1099/mgen.0.000093
21. Zhou Z, Alikhan NF, Sergeant MJ, Luhmann N, Vaz C, Francisco AP, et al. GrapeTree: visualization of core genomic relationships among 100,000 bacterial pathogens. Genome Res. 2018;28:1395–404. https://doi.org/10.1101/gr.232397.117
22. Satterthwaite D, Sverdlik A, Brown D. Revealing and responding to multiple health risks in informal settlements in sub-Saharan African cities. J Urban Health. 2019;96:112–22. https://doi.org/10.1007/s11524-018-0264-4
23. Alam MT, Mavian C, Paisie TK, Tagliamonte MS, Cash MN, Angermeyer A, et al. Emergence and evolutionary response of *Vibrio cholerae* to novel bacteriophage, Democratic Republic of the Congo. Emerg Infect Dis. 2022;28:2482–90. https://doi.org/10.3201/eid2812.220572
24. Karlsson SL, Thomson N, Mutreja A, Connor T, Sur D, Ali M, et al. Retrospective analysis of serotype switching of *Vibrio cholerae* O1 in a cholera endemic region shows it is a non-random process. PLoS Negl Trop Dis. 2016;10:e0005044. https://doi.org/10.1371/journal.pntd.0005044
25. Malembaka EB, Bugeme PM, Hutchins C, Xu H, Hulse JD, Demby MN, et al. Effectiveness of one dose of killed oral cholera vaccine in an endemic community in the Democratic Republic of the Congo: a matched case-control study. Lancet Infect Dis. 2024;24:514–22. https://doi.org/10.1016/S1473-3099(23)00742-9

Address for correspondence: Christine Marie George, Professor, Department of International Health, Johns Hopkins Bloomberg School of Public Health, 615 N. Wolfe St, Baltimore, MD 21205, USA; email: cmgeorge@jhu.edu

etymologia revisited

Originally published in March 2019

Streptomycin

strep'to-mi'sin

In the late 1930s, Selman Waksman, a soil microbiologist working at the New Jersey Agricultural Station of Rutgers University, began a large-scale program to screen soil bacteria for antimicrobial activity. By 1943, Albert Schatz, a PhD student working in Waksman's laboratory, had isolated streptomycin from *Streptomyces griseus* (from the Greek *strepto-* ["twisted"] + *mykēs* ["fungus"] and the Latin *griseus*, "gray").

In 1944, Willam H. Feldman and H. Corwin Hinshaw at the Mayo Clinic showed its efficacy against *Mycobacterium tuberculosis*. Waksman was awarded a Nobel Prize in 1952 for his discovery of streptomycin, although much of the credit for the discovery has since been ascribed to Schatz. Schatz later successfully sued to be legally recognized as a co-discoverer of streptomycin.

References:

1. Comroe JH Jr. Pay dirt: the story of streptomycin. Part I. From Waksman to Waksman. Am Rev Respir Dis. 1978;117:773–81.
2. Wainwright M. Streptomycin: discovery and resultant controversy. Hist Philos Life Sci. 1991;13:97–124.

https://wwwnc.cdc.gov/eid/article/25/3/et-2503_article

Global Epidemiology of Outbreaks of Unknown Cause Identified by Open-Source Intelligence, 2020–2022

Damian Honeyman, Deepti Gurdasani, Adriana Notaras, Zubair Akhtar, Jared Edgeworth, Aye Moa, Abrar Ahmad Chughtai, Ashley Quigley, Samsung Lim, Chandini Raina MacIntyre,

Epidemic surveillance using traditional approaches is dependent on case ascertainment and is delayed. Open-source intelligence (OSINT)–based syndromic surveillance can overcome limitations of delayed surveillance and poor case ascertainment, providing early warnings to guide outbreak response. It can identify outbreaks of unknown cause for which no other global surveillance exists. Using the artificial intelligence–based OSINT early warning system EPIWATCH, we describe the global epidemiology of 310 outbreaks of unknown cause that occurred December 31, 2019–January 1, 2023. The outbreaks were associated with 75,968 reported human cases and 4,235 deaths. We identified where OSINT signaled outbreaks earlier than official sources and before diagnoses were made. We identified possible signals of known disease outbreaks with poor case ascertainment. A cause was subsequently reported for only 14% of outbreaks analyzed; the percentage was substantially lower in lower/upper-middle–income economies than high-income economies, highlighting the utility of OSINT-based syndromic surveillance for early warnings, particularly in resource-poor settings.

Emerging and reemerging pathogens causing infectious diseases in human and animal populations are an ongoing and substantial public health threat. The threat is particularly relevant as climate change and land use alter patterns of illness and increase the frequency of high-consequence zoonotic infection spillover into human populations (*1*). Traditional surveillance systems (*2*) often rely on validated data from laboratories or hospitals. Approaches that do not depend on laboratory confirmation, such as clinical syndromic or sentinel surveillance, can provide earlier warnings of outbreaks and detect signals of newly emerged infections for which no diagnostics are yet available. Such approaches can overcome the lack of robust traditional surveillance and limited testing capabilities for many diseases in resource-poor settings.

Open-source epidemic intelligence (OSINT) is the collection, analysis, and use of information from open sources such as news media, websites, or social media (*3*). OSINT provides an alternative method for syndromic surveillance. Such surveillance can enhance early detection of novel emerging infections (e.g., SARS-CoV-2 in 2020), missed outbreaks of known pathogens, or delayed reporting via traditional surveillance.

Novel infections will initially emerge as an illness or syndrome of unknown cause before diagnostic tests are developed. If diagnostic capabilities are limited, even for known illnesses, a cause may not be identified for many outbreaks. According to a study of 109 outbreaks of unknown cause identified during 2016–2019, a cause was later confirmed for only 18% of the outbreaks; the most frequently identified pathogens were measles virus, Nipah virus, norovirus, and influenza virus (*4*). The lack of pathogen identification for >80% of outbreaks is concerning, underlining the value of syndromic surveillance. The outbreaks could be sporadic zoonotic outbreaks with no available diagnostics, emerging infections of pandemic potential, or outbreaks in low-resource countries with weak health systems.

Knowledge of the incidence, burden, and identified causes of outbreaks of unknown etiology is

Author affiliations: The University of New South Wales, Sydney, New South Wales, Australia (D. Honeyman, D. Gurdasani, A. Notaras, Z. Akhtar, J. Edgeworth, A. Moa, A.A. Chughtai, A. Quigley, S. Lim, C.R. MacIntyre); University of Western Australia, Perth, Western Australia, Australia (D. Gurdasani); Queen Mary University of London, London, UK (D. Gurdasani); Arizona State University, Tempe, Arizona, USA (C.R. MacIntyre)

DOI: https://doi.org/10.3201/eid3102.241533

essential. Such data cannot be collected routinely because they are not collected by traditional surveillance methods. Syndromic surveillance could address that gap; however, when conducted as part of routine national surveillance programs, syndromic surveillance is often restricted to clinical rather than community settings and to specific syndromes only (e.g., influenza-like illness) (*5*). OSINT-based syndromic surveillance can provide broader insights into the frequency and outcomes of outbreaks of unknown cause across the globe, providing a useful epidemiologic tool for the timely detection of infectious disease outbreaks, thus providing rapid outbreak alerts, guiding early responses, and minimizing disease spread (*6*,*7*).

EPIWATCH (https://www.epiwatch.org) is an artificial intelligence–based surveillance system that collects and processes vast amounts of multilingual OSINT data from news media and publicly available online sources worldwide to provide early warnings about potential outbreaks (*8*). EPIWATCH has been evaluated extensively and found to be a valid tool for epidemic surveillance and early warnings (*8*–*10*). EPIWATCH provides accurate information regarding trends and case numbers, particularly when case ascertainment has been poor (*11*), making it ideal for broad syndromic surveillance.

We used the EPIWATCH database to analyze reports of unknown and syndromic disease outbreaks to describe the epidemiology of those reported outbreaks globally during 2020–2022. No ethics application was required for this study because publicly available aggregate data were used.

Methods

Search Strategy

We curated a list of search terms and syndromes reflecting outbreaks of unknown cause based on similar work from existing literature (*4*) and discussion within our expert panel (authors D.H., A.Q., A.C., and D.G.) to add relevant terms (Table 1; Figure 1). We retrieved a dataset from the EPIWATCH database by using those search terms to locate articles published during December 31, 2019–January 1, 2023. We defined an outbreak of unknown cause as an outbreak for which the cause was unknown at the time of the outbreak and the suspected cause was an infection with ≥2 linked cases.

Inclusion and Exclusion Criteria

We filtered articles according to the presence of any of the prespecified syndrome-related search terms within the title (Table 1; Figure 1). We excluded articles about routine monthly, quarterly, or yearly syndromic surveillance (e.g., national pneumonia surveillance) because we wanted to capture articles via OSINT rather than official surveillance reports. We also excluded articles reporting on multicountry outbreaks because detections were likely to be later (after spread had occurred) and unlikely to constitute early warnings.

Data Extraction

Four analysts (authors D.H., A.N., Z.A., and J.E.) extracted prespecified data from all eligible full-text articles. We first removed duplicated articles and then removed any inaccessible articles (e.g., broken URLs, subscription required), articles about

Table 1. Search terms used for data retrieval and syndromes identified from EPIWATCH, 2020–2022

Category
Search terms
Acute flaccid paralysis
Acute gastroenteritis
Bronchiolitis
Bronchitis
Death
Die off
Encephalitis
Encephalomyelitis
Fever
Food poisoning
Illness
Influenza-like illness
Meningitis
Mortality
Mysterious
Mystery
Not known
Not specified
Not yet classified
Pneumonia
Rash
Suspicious
Severe acute respiratory illness
Suspicious
Unclassified
Unclear
Undiagnosed
Unexplained
Unidentified
Unknown
Syndromes
Acute flaccid paralysis
Acute gastroenteritis
Encephalitic
Febrile
Fever with rash
Respiratory*
Meningitis
Unknown†

*Includes influenza-like-illness, severe acute respiratory infection, and pneumonia.
†Insufficient information in the article for classification.

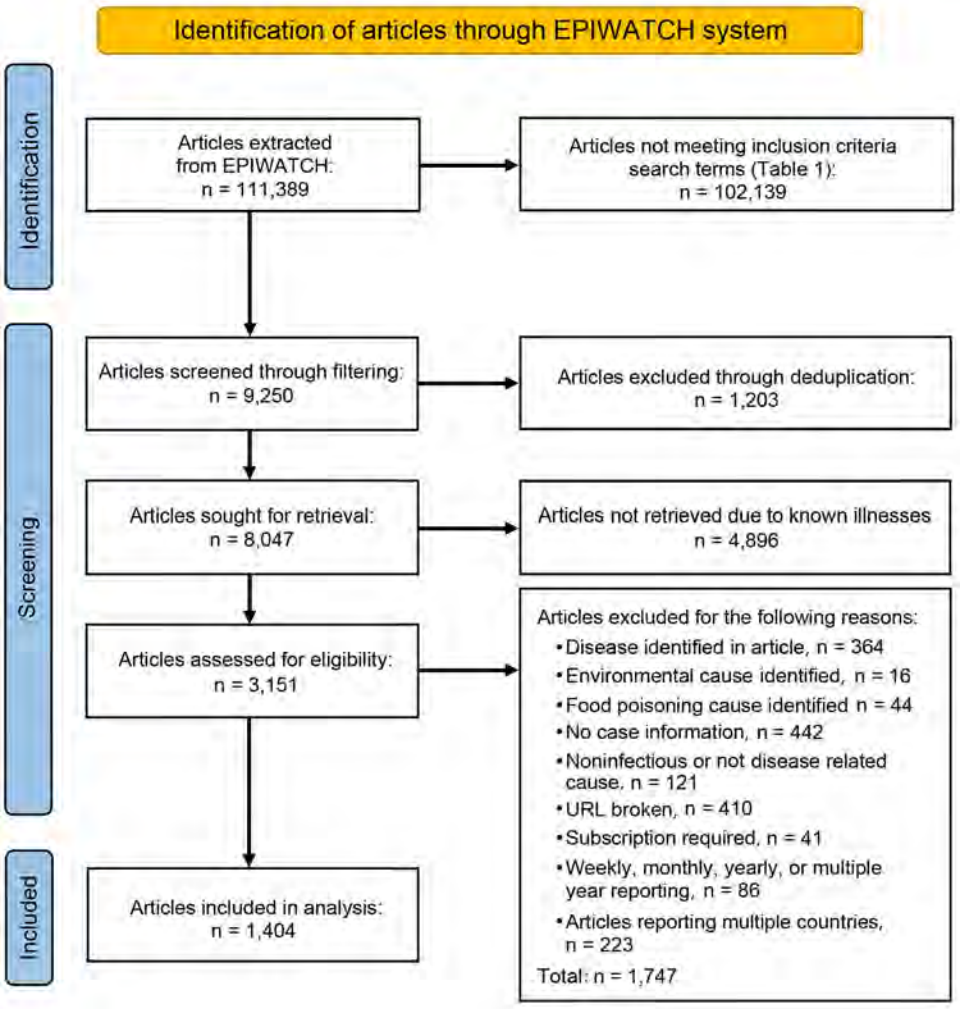

Figure 1. Articles extracted from EPIWATCH system (https://www.epiwatch.org), December 31, 2019–January 1, 2023.

outbreaks with a confirmed cause of illness, or articles that did not mention case numbers or location (Table 2; Figure 1). We extracted data for country, event date, state/province/city (where available), adult symptoms, child symptoms, syndrome, human or animal outbreak, case numbers, sex distribution of patients, and deaths. We classified syndromes into prespecified categories on the basis of the dominant clinical manifestations (Table 1). To ensure consistency and accuracy, we randomly checked 100 articles.

Syndromic Outbreak Cause Identification

To identify whether a cause had been subsequently identified, we followed outbreaks of unknown etiology for 3 months after the initial event date. Doing so involved conducting independent web searches and reviewing data within the EPIWATCH database, mapping the syndromic outbreak to subsequent laboratory-confirmed diseases identified within the same location. We examined selected case studies in more detail, focusing on the timeliness of EPIWATCH data compared with official sources and laboratory confirmation of the outbreak.

Table 2. Inclusion and exclusion criteria used in study of global epidemiology of outbreaks of unknown cause identified by open-source intelligence, 2020–2022

Inclusion criteria: all criteria must be met	Exclusion criteria: any 1 criterion must be met
Article describes a syndromic outbreak in humans or animals.	Article does not describe a syndromic outbreak, and case numbers not mentioned.
Title contains ≥1 search term, and article published Dec 31, 2019–Jan 1, 2023.	Infectious or noninfectious cause of syndrome identified in article.
Article includes case numbers and location.	Article not accessible.
Cause of syndrome is unknown, and article describes an outbreak in <3 countries.	Article outlines routine monthly, quarterly, or annual syndromic surveillance.

Analyses

We conducted data cleaning and performed statistical analyses by using Stata/BE 17.0 (StataCorp LLC, https://www.stata.com). To assess the number of unique outbreaks described by the reports, we considered different articles to be describing the same event if they discussed a similar number of cases of the same syndrome/symptoms in the same location <30 days apart.

To identify the most frequent syndromic outbreaks for humans and animals reported globally and their locations, we calculated the frequency of reported syndromes and locations of outbreaks. We measured the association of outbreak diagnosis by income status, using a χ^2 test for high-income economies (HIEs) or low-middle–income economies/upper-middle–income economies (LMIEs/UMIEs). As defined by the World Bank, an HIE has a gross national income (GNI) per capita of >$14,005 (in US dollars), a UMIE has a GNI per capita of $4,516–$14,005, and an LMIE has a GNI per capita of $1,145–$4,515 (*12*). We used ArcGIS Pro v.3.1 (https://www.esri.com) to map the geographic distribution of global reports for animal and human outbreaks.

Results

For our final analysis, we included 1,404 eligible articles (Figure 1). Of those, 1,257 (89.5%) reported outbreaks among humans and 147 (10.5%) reported outbreaks among and animals. The articles described 310 syndromic outbreaks overall, including 249 (80.3%) affecting humans and 61 (19.7%) affecting animals during the study period. Among outbreaks of unknown etiology, 75,968 human cases of illness and 4,235 deaths were recorded. Of the outbreaks of unknown cause among humans reported from 61 countries and among animals from 21 countries, the largest numbers for both were reported from India, followed by the United States (Table 3).

Among 249 articles for which the clinical syndrome could be classified, the most commonly reported syndromes in humans were respiratory syndrome (15.3%; n = 38), febrile syndromes (15.3%; n = 38), and acute gastroenteritis (14.5%; n = 36) (Table 4). Among reported clinical signs for 417 outbreaks among humans, the most frequent were fever (21.6%; n = 90), diarrhea (14.9%; n = 62), and vomiting (13.4%; n = 56) (Table 5). For 43% of syndromic outbreaks, the sign/symptom information provided in articles reviewed was inadequate for classifying the syndrome.

Reports of syndromic illnesses increased notably over the study period, from 16 reports in 2020 to 69 reports in 2021 and 171 reports in 2022 (Figures 2, 3).

Table 3. Top 5 countries reporting syndromic outbreaks among humans and animals, 2020–2022

Country	No. (%) events
Human	
India	110 (44.2)
United States	13 (5.3)
Bangladesh	13(2.8)
Indonesia	7 (2.4)
Russia	6 (2.4)
Animal	
India	28 (46.7)
United States	5 (8.3)
Kazakhstan	3 (5.0)
Russia	3 (5.0)
United Kingdom	2 (3.3)

Although outbreaks associated with all syndromes seem to have increased during that period, the increases seemed to be driven primarily by increased gastrointestinal syndromes and syndromes that could not be classified. Respiratory syndromes seem to have been suppressed in 2020, consistent with the known suppression of respiratory infections during 2020 resulting from COVID-19 mitigation efforts. We also noted seasonal patterns of syndromes in particular regions (e.g., febrile syndrome reports in India peaked during July–September, and respiratory syndrome reports peaked in December) (Figure 4).

For only 32 (12.9%) of 249 syndromic outbreaks was a cause subsequently reported for humans, and for 14 (23.0%) of 61 syndromic outbreaks was a cause subsequently reported for animals. The 5 most commonly identified causes of syndromic outbreaks among humans were norovirus infection (15.2%; n = 5), bronchiolitis (6.1%; n = 2), carbon monoxide poisoning (6.1%; n = 2), malaria (6.1%; n = 2), and meningococcal infection (6.1%; n = 2) (Table 6). The proportion of diagnoses was higher in HIEs (40%) than in LMIEs/UMIEs (11%; p<0.001) (Table 7).

Outbreaks in India

The 110 outbreaks of unknown cause in India were identified across different states; several outbreaks affected predominantly children, with no cause found for most. On August 16, 2020, an outbreak of fever

Table 4. Frequency of reported syndromes during outbreaks of unknown cause identified by open-source intelligence, 2020–2022*

Disease or syndrome	Frequency, no. (%)
Unknown	107 (43.0)
Respiratory syndrome	38 (15.3)
Febrile syndrome	38 (15.3)
Acute gastroenteritis	36 (14.5)
Meningitis	16 (6.4)
Fever with rash	7 (2.8)
Encephalitis syndrome	6 (2.4)
Acute flaccid paralysis	1 (0.4)

*Total 249 reports with data on syndromes.

Table 5. Ten most frequent signs/symptoms reported during outbreaks of unknown cause identified by open-source intelligence, 2020–2022*

Symptoms	Frequency, no. (%)
Fever	90 (21.6)
Diarrhea	62 (14.9)
Vomiting	56 (13.4)
Breathing difficulties	41 (9.8)
Headache	22 (5.3)
Cough	16 (3.8)
Nausea	16 (3.8)
Stomachache	13 (3.1)
Peripheral swelling	11 (2.6)
Hemorrhagic fever	10 (2.4)

*Total 417 outbreaks with clinical signs/symptoms reported.

and throat swelling was recorded in Bageshwar, Uttarakhand, where 43 children were affected, 6 of whom were admitted to local hospitals (*13*). On April 9, 2021, another outbreak of fever and stomachaches was reported in Uttar Pradesh; 60 children died, and several hundred were hospitalized (*13*). Although dengue fever was suspected in that outbreak, it was not confirmed. On August 24, 2021, in Mathura, Uttar Pradesh, 6 children, 5–15 years of age, died of an unknown illness over a 1-week period (*14*). On June 22, 2022, a large outbreak of fever among 250 persons from Kanakatte, Karnataka, was recorded; signs/symptoms included headaches, blisters, and joint pain (*15*). On July 24, 2022, in Sheopur, Madya Pradesh, 3 persons died and 15 other persons were reportedly ill with gastroenteritis and fever of unknown cause (*16*). On August 31, 2022, in Garhwal village, Uttarakhand, a mysterious disease was reported of which >100 persons fell ill with fever, chest pain, vomiting, and pain in joints of their hands and feet (*17*). The large numbers of cases and fatalities (including among children) and lack of clear causes found for all of those outbreaks highlight the need for syndromic surveillance to guide outbreak investigation and diagnostic testing.

Pneumonia in Argentina

During August 18–22, 2022, EPIWATCH identified reports of bilateral pneumonia in a cluster of 3 hospitalized patients in San Miguel de Tucumán City, Tucuman Province, Argentina. Early cases were among healthcare workers, resulting in their admission to intensive care units. Six days later, on August 29, 2022, the Argentine Ministry of Health of Tucumán Province notified the World Health Organization (WHO) of a cluster of 6 cases of bilateral pneumonia lacking cause; 1 patient died on August 30, 2022 (*18*). On September 3, 2022, the cause was identified as *Legionella pneumophila* and *Legionella* spp. (*19*), although the cause was only officially reported by WHO on September 5, 2022, prompting an investigation of the source, which identified 22 suspected cases and 6 fatalities. Four of the patients tested positive for *L. pneumophila* and *Legionella* spp. and had clinically compatible illnesses (*19*). We note that EPIWATCH identified this syndromic outbreak before it was reported through official sources.

Hepatitis among Children, Worldwide

On March 31, 2022, severe acute hepatitis of unknown origin in children was reported for the first time among children in Scotland for causes other than common hepatitis A–E virus infection; patients experienced jaundice, vomiting, gastrointestinal symptoms, and fever (*20*). On April 6, 2022, EPIWATCH identified reports of 11 children, 1–5 years of age, who were receiving treatment for a hepatitis-like infection with jaundice as the primary syndrome (*21*). On April 15, 2022, WHO released its first related report, stating that 10 cases across the United Kingdom and Europe were detected on April 5, 2022 (*22*). Two retrospective studies that analyzed surveillance data in Japan and Israel showed possible syndrome onset as early as September and October 2021 (*23*,*24*). By August 2022, a total of 35 countries reported 1,115 cases of acute hepatitis of unknown origin that fulfilled the WHO definition (*25*). Among those patients, 47 (4%) of children required liver transplants because of organ failure associated with infection and 22 (2%) deaths were reported (*25*). Only 479 case reports contained

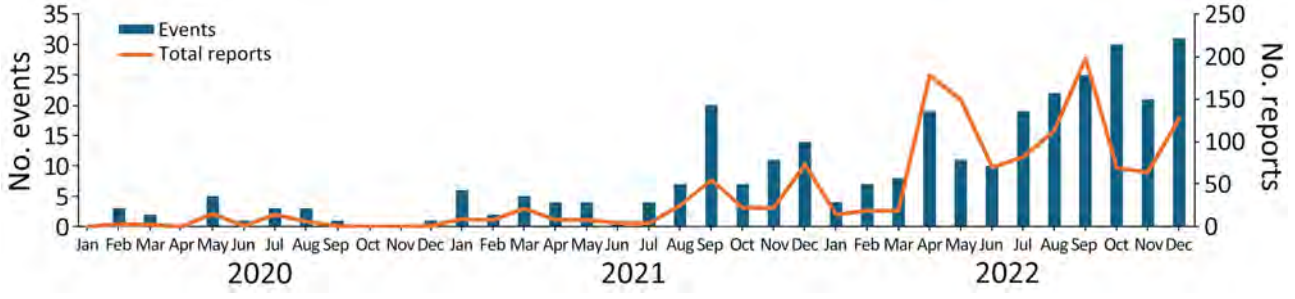

Figure 2. Total reports and events that met study inclusion criteria, by month, for study of global epidemiology of outbreaks of unknown cause identified by open-source intelligence, 2020–2022. Scales for the y-axes differ substantially to underscore patterns but do not permit direct comparisons.

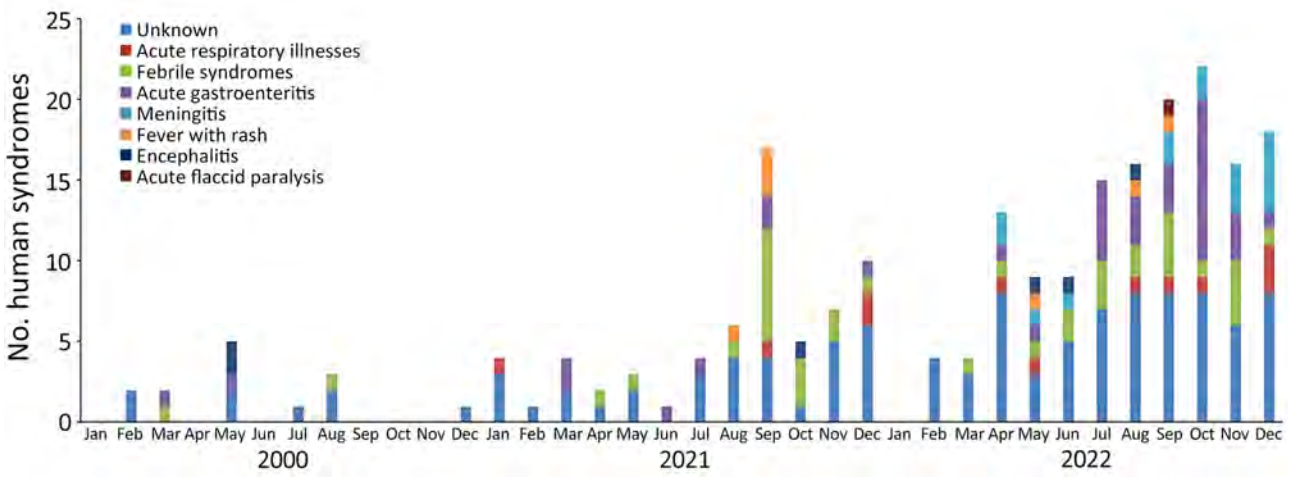

Figure 3. Frequency of human syndromic events, by month, identified in study of global epidemiology of outbreaks of unknown cause identified by open-source intelligence, 2020–2022.

information for age and sex; 78% of patients were <6 years of age, and 48% were boys and 52% girls (*25*). Investigations to determine the potential cause of acute hepatitis of unknown origin around the world are ongoing. However, limited evidence suggested a postinflammatory syndrome with potential links to SARS-CoV-2 infection (*25*), with stronger evidence for SARS-CoV-2 being associated with this syndrome.

Pneumonia in Kazakhstan

On July 9, 2020, an unusual increase in cases of pneumonia of unknown cause in Kazakhstan was reported (*26*). The increase began in January 2020 at the early stages of the COVID-19 pandemic. Although 264 deaths from COVID-19 had been reported in the country until July 2020, Kazakhstan reported 1,772 deaths in the first 6 months of 2020 from pneumonia of unknown cause; 628 were reported in June alone (*27*). Reports stated that 300 persons were being hospitalized daily and up to 600 new cases of pneumonia were reported daily, compared with an average of 80 cases per day before the outbreak of COVID-19 (*27*). In March 2020, Kazakhstan implemented a short, sharp lockdown because of the COVID-19 outbreak, and at the end of May 2020, quarantine measures were lifted (*28*), supporting the hypothesis that the increased pneumonia cases were probably directly associated with a resurgence of COVID-19 cases.

Discussion

During 2020–2022, outbreaks of unknown illnesses affecting human and animal populations occurred regularly; for most outbreaks, a cause was never identified. However, outbreaks with unidentified causes will not be formally reported because national notifiable disease systems are for identified diseases only. Most outbreak patients exhibited sign/symptoms consistent with infectious causes; however, the cause of some outbreaks may be noninfectious (e.g., chemical exposure). Open-source syndromic surveillance

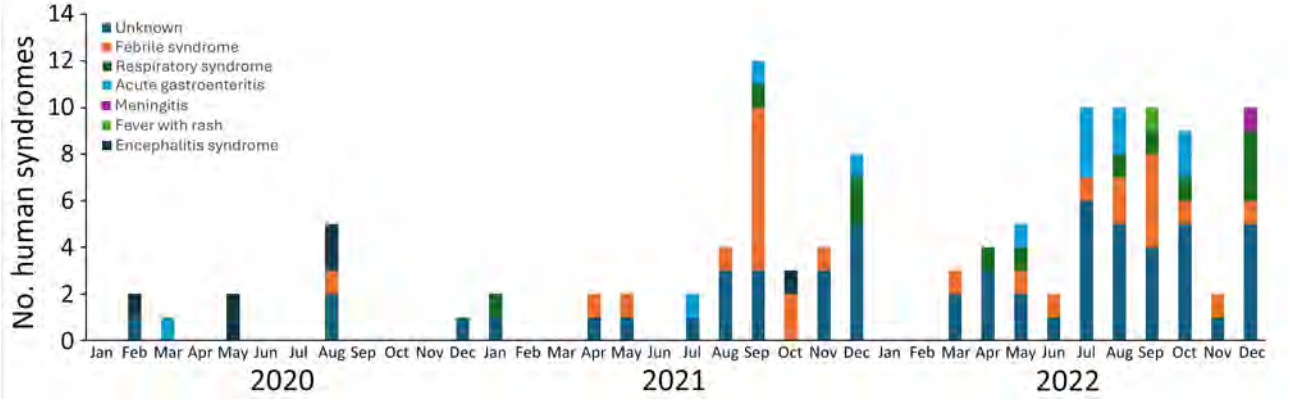

Figure 4. Frequency of human syndromes reported in events in India, by month, identified in study of global epidemiology of outbreaks of unknown cause identified by open-source intelligence, 2020–2022.

Table 6. Five most frequent causes of 32 reports with listed cause found during analysis of global epidemiology of outbreaks of unknown cause identified by open-source intelligence, 2020–2022

Disease found during analysis	Frequency, no. (%)
Norovirus infection	5 (15.1)
Bronchiolitis	2 (6.1)
Carbon monoxide poisoning	2 (6.1)
Malaria	2 (6.1)
Meningococcal infection	2 (6.1)

provides a unique means for understanding the global epidemiology of outbreaks of unknown etiology and probably represents the only available public record of those illnesses.

We describe examples in which EPIWATCH OSINT detected an early signal of an unknown respiratory outbreak with fatalities before an official diagnosis was made (e.g., pneumonia subsequently diagnosed as legionellosis in Argentina). We also describe instances in which syndromic surveillance can provide possible indicators of a surge of known disease with pandemic potential in areas where diagnostic capability is limited (e.g., pneumonia surge, thought to be caused by COVID-19, in Kazakhstan). In India, no cause has been identified for recurrent, large outbreaks of encephalitis in certain states, such as Bihar (*29*). Those findings highlight the vital role of syndromic illness surveillance and OSINT to bridge the gap between formal surveillance and provide early warnings of syndromic outbreaks before diagnosis. Early warnings can enhance rapid response (e.g., quarantine) while laboratory diagnosis is in progress.

Approximately 80% of outbreaks assessed in our final analysis did not have a cause subsequently identified or reported, possibly because of lack of formal diagnosis, media reporting, or censorship (*30*). Outbreaks for which a cause was eventually identified were more frequent in HIEs with well-developed surveillance systems (Table 7). That finding highlights the vital role of syndromic surveillance, particularly in LMIEs, where disease-based surveillance may be less robust. Even in HIEs, the cause of most outbreaks of unknown cause was not identified or reported. OSINT is useful for providing early intelligence to public health officials for targeted outbreak investigations independent of formal surveillance.

Over the 3-year study period, we observed increased reports of unknown syndromic illnesses, which may be attributable to the upscaling of the EPIWATCH system, increased reporting of syndromes after the COVID-19 pandemic, or real increases in illness. COVID-19 mitigation strategies contributed to decreased incidence of respiratory and other illnesses, which our finding may reflect (*31*). However, in recent years, respiratory infections have begun to increase, including respiratory syncytial virus, influenza virus, and SARS-CoV-2 (known as the tripledemic) infection.

The geographic distribution of unknown illnesses affecting humans and animals indicates that outbreaks were reported most frequently from India and the United States (Figures 5, 6). That finding may be attributable to higher coverage by print and electronic media, inclusion of multiple Indian languages in EPIWATCH, and increased reporting of infectious diseases in some locations (*32*), which could be contributing to increased signals in India. However, our results are conservative because of the way events have been inferred from articles and the use of OSINT. Our estimates represent the lower end of reported outbreaks of unknown cause.

The strengths of our study include use of OSINT to detect early epidemic signals, especially in countries with poor surveillance capacity (*33*). Use of OSINT overcomes issues associated with formal surveillance and diagnostic dependence, providing a means for syndromic surveillance. The strength of EPIWATCH lies in its capacity to search in 46 languages, incorporating Natural Language Processing, which seeks to offset, to some extent, the Anglocentric bias inherent in OSINT and search algorithms (e.g., Google). To our knowledge, EPIWATCH is the most comprehensive publicly available OSINT platform to date (*33*). As an example of an early warning, in November 2019 before COVID-19 was identified, we previously showed a signal of unknown pneumonia in Wuhan, China, as well as evidence of redacted news reports with "SARS" in the title (*8*). EPIWATCH is not directly comparable with ProMED Mail, which is qualitative and relies on reports of outbreaks from clinicians in the field, rather than OSINT (*34*). Both are valuable sources of early warning.

Table 7. Proportion of syndromes diagnosed across high and lower-middle and upper-middle–income economies identified during analysis of global epidemiology of outbreaks of unknown cause identified by open-source intelligence, 2020–2022*

	Income, no. (%)		
Cause	High	LMIE/UMIE	Total
Unknown	29 (60)	235 (89)	264 (85)
Known	19 (40)	28 (11)	47 (15
Total	48 (100)	263 (100	311 (100)

*Pearson $\chi^2(1) = 26.49$; p<0.0001. LMIE, low-middle-income economies; UMIE, upper-middle-income economies.

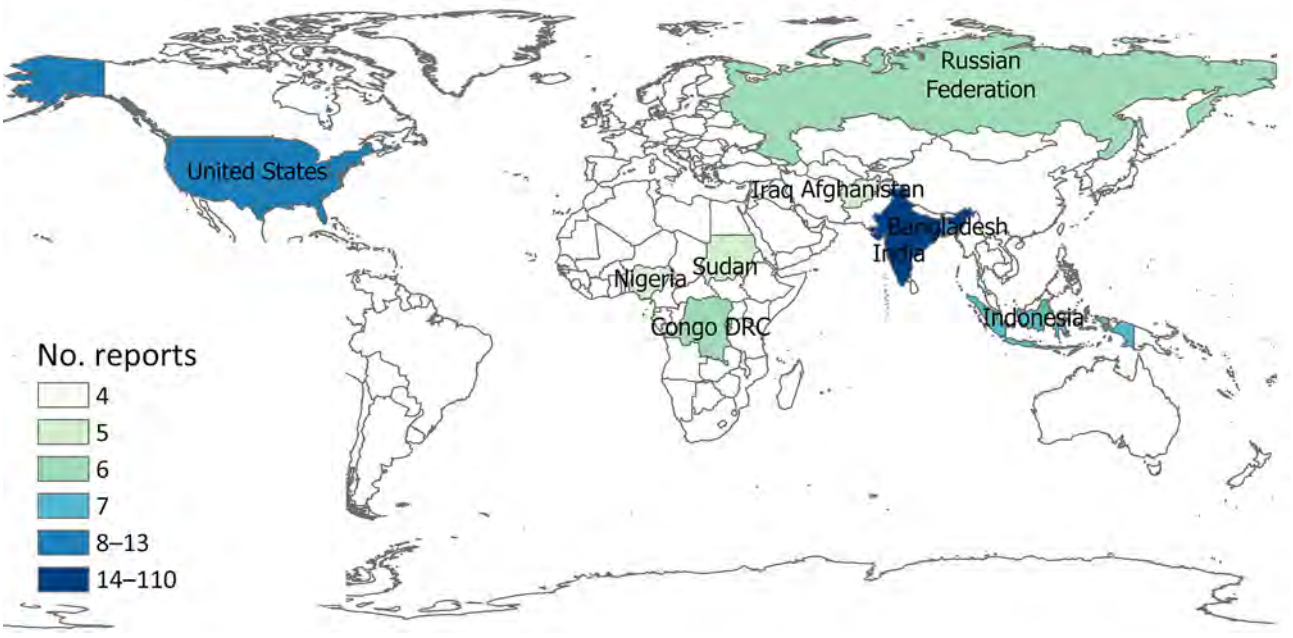

Figure 5. Geographic distribution of top 10 countries reporting unknown illnesses in humans, identified in study of global epidemiology of outbreaks of unknown cause identified by open-source intelligence, 2020–2022.

The limitations of our study include the fact that OSINT, as used in our study, ultimately depends on reporting patterns and search algorithms, which may change over time, may prioritize information in biased ways, and may not capture every early signal. Therefore, changes over time and differences in geographic reporting may reflect differences in media practice and search algorithms rather than actual disease burden. OSINT relies heavily on publication of correct information, which requires further analysis to determine if outbreaks are accurately reported. Another limitation is the short duration of follow-up with no data from the prepandemic period in this study, making the effects of the pandemic and mitigations during the pandemic difficult to assess. Another limitation

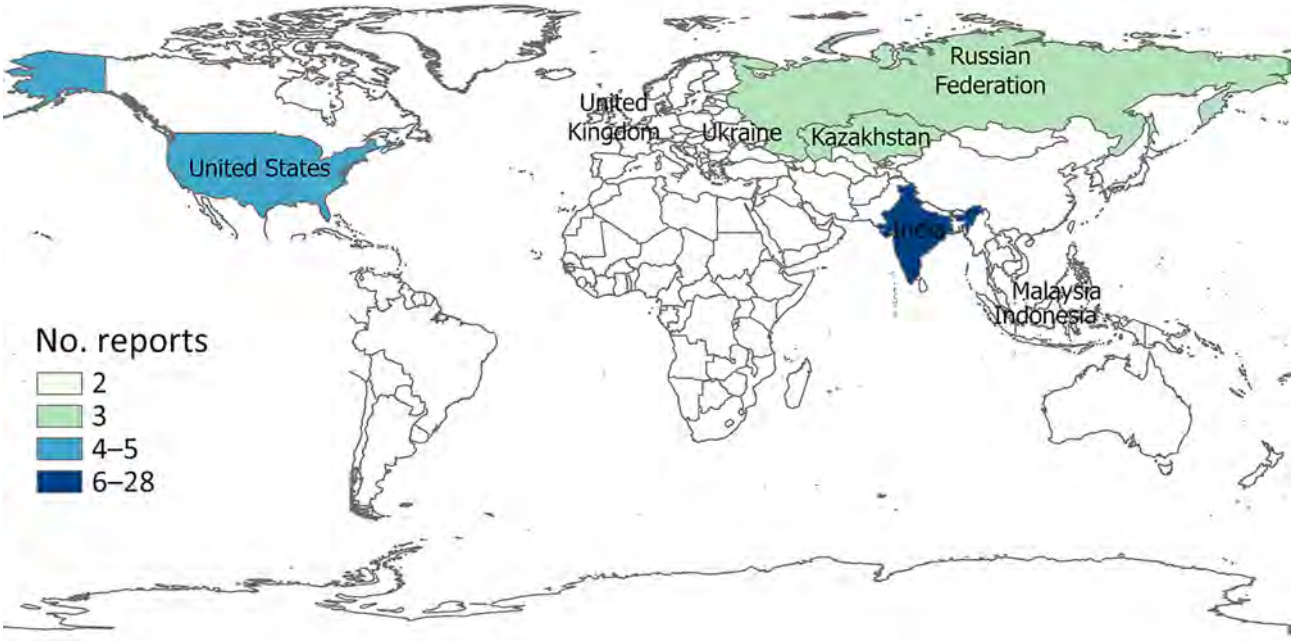

Figure 6. Geographic distribution of top 8 countries reporting unknown illnesses in animals, identified in study of global epidemiology of outbreaks of unknown cause identified by open-source intelligence, 2020–2022.

of our results is that the true number of events within countries has not been corrected for population size.

Although similar work using the EPIWATCH system has been previously conducted (*4*), the search terms and algorithms used were not comparable to those that we used. Syndromic surveillance (focusing on diseases of unknown cause) is likely to capture different diseases in different regions (*35*). Differences observed with syndromic surveillance may reflect resources available for ascertainment rather than disease burden. Data are frequently reported from a country level, meaning granular analysis is difficult because of a lack of confirmed province, state, or city. Geopolitical factors may also influence the number of reports. For example, war or other events may increase surrounding health issues and subsequent regional reporting (*36*). The purpose of OSINT in that context should be seen not as a tool to provide diagnostics but rather as an adjunct to formal surveillance and an early warning system to alert authorities to potential threats and guide outbreak responses.

Our study using EPIWATCH provides a global surveillance data resource enabling public health professionals to assess hot spots of unknown disease outbreaks and the presence of potential new unknown illnesses as early warning signals to be used to enhance surveillance and reporting capacities. EPIWATCH provides a framework for open-source syndromic surveillance for public health agencies, especially in low-income and under-resourced settings where formal surveillance systems are not adequately linked. The EPIWATCH system aims to identify outbreak signals before government authorities are aware of them. As such, it should be an adjunct to formal surveillance rather than a replacement, with the understanding that the data are not validated. Where national health organizations fail to disclose outbreaks of concern internationally, web-based syndromic surveillance can act as the first line of defense for surrounding countries to encourage the initiation of outbreak response and investigation to prevent the next pandemic.

In conclusion, using OSINT for syndromic surveillance from the EPIWATCH system, we found early signals of human and animal unknown illnesses across 310 outbreaks. The cause was not identified for most outbreaks, especially in LMIEs. Our work highlights the value of OSINT-based digital surveillance systems for identifying syndromic outbreaks and guiding rapid outbreak response.

D.H. and A.N. are funded by a Medical Research Future Fund (MRFF) National Health & Medical Research Council/COVID-19 Treatment Access and Public Health Activities grant (MRFF) ID 2017048; Z.A., J.E., A.M., A.G., D.G., and S.L. are supported by the Balvi Filantropic Fund; C.R.M. is funded by National Health and Medical Research Council Investigator grant 2016907.

EPIWATCH was developed at the University of New South Wales Sydney by Professor Raina MacIntyre, and the authors are employed by or affiliated with EPIWATCH.

D.H., A.N., Z.A., J.E., A.A.G., A.G., and S.L. have no declarations of interest. D.G. is a member of OzSAGE. C.R.M. is on the WHO COVID-19 Vaccine Composition Technical Advisory Group and the WHO SAGE Working Group on Smallpox and Monkeypox. She receives funding from Sanofi for influenza and pertussis research and from the National Health and Medical Research Council and MRFF.

D.H. contributed to the formal analysis, investigation, data extraction, methodology, and writing (original draft, review, and editing); A.N. contributed to investigation, data extraction, and writing (original draft, review, and editing); Z.A. contributed to investigation, data extraction, and writing (original draft, review, and editing); J.E. contributed to investigation, data extraction, and writing (original draft, review, and editing); A.M. conceived the study and contributed to writing (original draft, review, and editing); A.C. conceived the study and contributed to writing (original draft, review, and editing); A.Q. contributed to investigation, directed the analysis and methodology, and contributed to writing (original draft, review, and editing); S. L. contributed to formal analysis, investigation, and writing (original draft, review, and editing); C.R.M. conceived the study, funded the study, leads EPIWATCH, contributed to methodology, directed the analysis, and contributed to writing (original draft, review, and editing); D.G. contributed to investigation, directed the analysis and methodology, and contributed to writing (original draft, review, and editing).

About the Author

Mr. Honeyman is a senior research officer and PhD student at the Kirby Institute in Sydney, New South Wales, Australia. His research interests include detecting public health threats by using artificial intelligence.

References

1. Meadows AJ, Stephenson N, Madhav NK, Oppenheim B. Historical trends demonstrate a pattern of increasingly frequent and severe spillover events of high-consequence

zoonotic viruses. BMJ Glob Health. 2023;8:e012026. https://doi.org/10.1136/bmjgh-2023-012026
2. Saied AA, Metwally AA, Dhawan M, Chandran D, Chakraborty C, Dhama K. Wastewater surveillance strategy as an early warning system for detecting cryptic spread of pandemic viruses. QJM. 2023;116:741–4. https://doi.org/10.1093/qjmed/hcad130
3. Evangelista JRG, Sassi RJ, Romero M, Napolitano D. Systematic literature review to investigate the application of open source intelligence (OSINT) with artificial intelligence. Journal of Applied Security Research. 2021; 16:345–69. https://doi.org/10.1080/19361610.2020.1761737
4. Mao RJ, Moa A, Chughtai A. The epidemiology of unknown disease outbreak reports globally. Global Biosecurity. 2020;2. https://doi.org/10.31646/gbio.62
5. Bernardo CO, González-Chica DA, Chilver M, Stocks N. Influenza-like illness in Australia: a comparison of general practice surveillance system with electronic medical records. Influenza Other Respir Viruses. 2020;14:605–9. https://doi.org/10.1111/irv.12774
6. MacIntyre CR, Lim S, Quigley A. Preventing the next pandemic: use of artificial intelligence for epidemic monitoring and alerts. Cell Rep Med. 2022;3:100867. https://doi.org/10.1016/j.xcrm.2022.100867
7. Yan SJ, Chughtai AA, Macintyre CR. Utility and potential of rapid epidemic intelligence from internet-based sources. Int J Infect Dis. 2017;63:77–87. https://doi.org/10.1016/j.ijid.2017.07.020
8. Kpozehouen EB, Chen X, Zhu M, Macintyre CR. Using open-source intelligence to detect early signals of COVID-19 in China: descriptive study. JMIR Public Health Surveill. 2020;6:e18939. https://doi.org/10.2196/18939
9. Thamtono Y, Moa A, MacIntyre CR. Using open-source intelligence to identify early signals of COVID-19 in Indonesia. Western Pac Surveill Response J. 2021;12:40–5. https://doi.org/10.5365/wpsar.2020.11.2.010
10. Puca C, Trent M. Using the surveillance tool EpiWATCH to rapidly detect global mumps outbreaks. Global Biosecurity. 2020;1. https://doi.org/10.31646/gbio.54
11. Nair SP, Moa A, Macintyre CR. Investigation of early epidemiological signals of COVID-19 in India using outbreak surveillance data. Global Biosecurity. 2020;2. https://doi.org/10.31646/gbio.72
12. The World Bank. World Bank country and lending groups [cited 2024 Jul 8]. https://datahelpdesk.worldbank.org/knowledgebase/articles/906519-world-bank-country-and-lending-groups
13. Sundinfo. Mysterious fever kills more than 60 people and spreads rapidly in India [in French] [cited 2024 Jul 8]. https://www.sudinfo.be/id414774/article/2021-09-04/une-mysterieuse-fievre-tue-plus-de-60-personnes-et-se-propage-rapidement-en-inde
14. Saraswat A. Children death: 6 children died due to unknown disease, panic in health department (in Hindi] [cited 2023 Dec 12]. https://www.abplive.com/states/up-uk/mathura-6-children-died-due-to-unknown-disease-there-was-a-stir-in-the-health-department-ann-1958179
15. Saboji G. Davanagere: Village hit by mysterious fever, people suffering in more than 250 houses [in Kannada] [cited 2023 Dec 12]. https://tv9kannada.com/karnataka/davanagere/davangere-a-village-afflicted-with-mysterious-fever-people-suffering-in-over-250-houses-ggs-au52-402524.html
16. Zee Media Bureau. 3 dead, 15 people critical in Sheopur due to unknown disease [in Hindi] [cited 2023 Dec 12]. https://zeenews.india.com/hindi/india/madhya-pradesh-chhattisgarh/mp/there-was-a-stir-in-sheopur-due-to-unknown-disease-3-killed-15-serious-apmp/1272444
17. FluTrackers.com. India—Uttarakhand: more than 100 people fell ill of mysterious disease in Garhwal village—August 31, 2022 [cited 2023 Dec 12]. https://flutrackers.com/forum/forum/india/india-emerging-diseases-and-other-health-threats/957845-india-uttarakhand-more-than-100-people-fell-ill-of-mysterious-disease-in-garhwal-village-august-31-2022
18. Malik S, Al-Tammemi AB, Mohanty A, Satapathy P, Padhi BK, Kabi A, et al. *Legionella* pneumonia as a rising public health threat in Argentina: is it the time to worry? Ann Med Surg (Lond). 2022;83:104801. https://doi.org/10.1016/j.amsu.2022.104801
19. Gardiner ERK, Notaras A, Kunasekaran MP, Quigley A. Legionnaires' disease: a critical report of the pneumonia of unknown origin outbreak in Argentina. Global Biosecurity. 2022;4. https://doi.org/10.31646/gbio.180
20. Marsh K, Tayler R, Pollock L, Roy K, Lakha F, Ho A, et al. Investigation into cases of hepatitis of unknown aetiology among young children, Scotland, 1 January 2022 to 12 April 2022. Euro Surveill. 2022;27:2200318. https://doi.org/10.2807/1560-7917.ES.2022.27.15.2200318
21. Scott K. At least 11 children in hospital after hepatitis outbreak [cited 2022 Dec 12]. https://news.stv.tv/scotland/at-least-11-children-in-hospital-after-hepatitis-outbreak-across-glasgow-lanarkshire-tayside-and-fife
22. World Health Organization. Acute hepatitis of unknown aetiology—the United Kingdom of Great Britain and Northern Ireland [cited 2023 Sep 15]. https://www.who.int/emergencies/disease-outbreak-news/item/2022-DON368
23. Otake S, Ikenoue C, Sudani N, Kobayashi M, Takahashi K, Shimada T, et al. National surveillance of pediatric acute hepatitis of unknown etiology, Japan, October 2021–December 2022. Emerg Infect Dis. 2023;29:1288–91. https://doi.org/10.3201/eid2906.221579
24. Zhang LY, Huang LS, Yue YH, Fawaz R, Lim JK, Fan JG. Acute hepatitis of unknown origin in children: early observations from the 2022 outbreak. J Clin Transl Hepatol. 2022;10:522–30. https://doi.org/10.14218/JCTH.2022.00281
25. Gurdasani D, Trent M, Ziauddeen H, Mnatzaganian E, Turville S, Chen X, et al. Acute hepatitis of unknown aetiology in children: evidence for and against causal relationships with SARS-CoV-2, HAdv, and AAV2. BMJ Paediatr Open. 2024;8:e002410.
26. Wu W. 'Unknown pneumonia' deadlier than coronavirus sweeping Kazakhstan, Chinese embassy warns [cited 2023 Nov 17]. https://www.scmp.com/news/china/diplomacy/article/3092563/chinese-embassy-warns-deadly-unknown-pneumonia-kazakhstan
27. Christmass P. Chinese embassy in Kazakhstan issues alert over new 'unknown' infection 'much deadlier than COVID' [cited 2023 Nov 17]. https://7news.com.au/news/public-health/chinese-embassy-in-kazakhstan-issues-alert-over-new-unknown-infection-much-deadlier-than-covid-c-1158992
28. Nguyen P-Y, Chen XJ, Kunasekaran M. Rise in pneumonia cases of unknown aetiology in Kazakhstan in June 2020: a rapid analysis. Global Biosecurity. 2020;2. https://doi.org/10.31646/gbio.81
29. Narain JP, Dhariwal AC, MacIntyre CR. Acute encephalitis in India: an unfolding tragedy. Indian J Med Res. 2017;145:584–7. https://doi.org/10.4103/ijmr.IJMR_409_17
30. Aljaeera. India's media – captured and censored [cited 2024 Jul 9]. https://www.aljazeera.com/program/the-india-report/2024/3/28/indias-media-captured-and-censored

31. Ullrich A, Schranz M, Rexroth U, Hamouda O, Schaade L, Diercke M, et al.; Robert Koch's Infectious Disease Surveillance Group. Impact of the COVID-19 pandemic and associated non-pharmaceutical interventions on other notifiable infectious diseases in Germany: an analysis of national surveillance data during week 1-2016–week 32-2020. Lancet Reg Health Eur. 2021;6:100103. https://doi.org/10.1016/j.lanepe.2021.100103
32. Statista. Indian newspaper industry—statistics & facts [cited 2023 Sep 19]. https://www.statista.com/topics/4726/newspaper-industry-in-india/#topicOverview
33. MacIntyre CR, Chen X, Kunasekaran M, Quigley A, Lim S, Stone H, et al. Artificial intelligence in public health: the potential of epidemic early warning systems. J Int Med Res. 2023;51:3000605231159335. https://doi.org/10.1177/03000605231159335
34. Rolland C, Lazarus C, Giese C, Monate B, Travert AS, Salomon J. Early detection of public health emergencies of international concern through undiagnosed disease reports in ProMED-Mail. Emerg Infect Dis. 2020;26:336–9. https://doi.org/10.3201/eid2602.191043
35. Yadav H, Shah D, Sayed S, Horton S, Schroeder LF. Availability of essential diagnostics in ten low-income and middle-income countries: results from national health facility surveys. Lancet Glob Health. 2021;9:e1553–60. https://doi.org/10.1016/S2214-109X(21)00442-3
36. Stone H, Heslop D, Lim S, Sarmiento I, Kunasekaran M, MacIntyre CR. Open-source intelligence for detection of radiological events and syndromes following the invasion of Ukraine in 2022: observational study. JMIR Infodemiology. 2023;3:e39895. https://doi.org/10.2196/39895

Address for correspondence: Chandini Raina MacIntyre, The Kirby Institute, Biosecurity Program, University of New South Wales 2052, Sydney, NSW, Australia; email: r.macintyre@unsw.edu.au

etymologia revisited

Salmonella

[sal''mo-nel'ə]

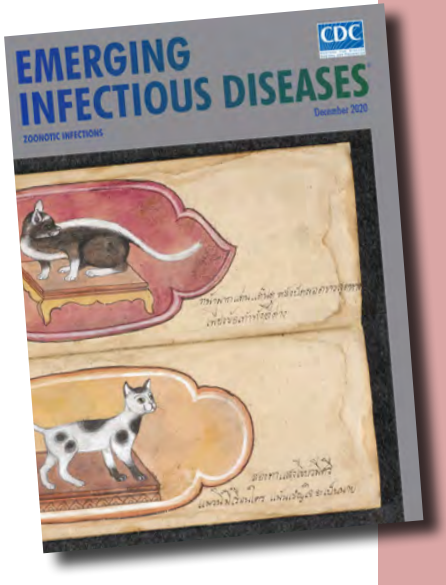

Originally published in December 2020

Named in honor of Daniel Elmer Salmon, an American veterinary pathologist, *Salmonella* is a genus of motile, gram-negative bacillus, nonspore-forming, aerobic to facultatively anaerobic bacteria of the family Enterobacteriaceae. In 1880, Karl Joseph Eberth was the first to observe *Salmonella* from specimens of patients with typhoid fever (from the Greek *typhōdes* [like smoke; delirious]), which was formerly called *Eberthella typhosa* in his tribute. In 1884, Georg Gaffky successfully isolated this bacillus (later described as *Salmonella* Typhi) from patients with typhoid fever, confirming Eberth's findings. Shortly afterward, Salmon and his assistant Theobald Smith, an American bacteriologist, isolated *Salmonella* Choleraesuis from swine, incorrectly assuming that this germ was the causative agent of hog cholera. Later, Joseph Lignières, a French bacteriologist, proposed the genus name *Salmonella* in recognition of Salmon's efforts.

References:

1. Dorland's Illustrated Medical Dictionary. 32nd ed. Philadelphia: Elsevier Saunders; 2012.
2. Gossner CM, Le Hello S, de Jong B, Rolfhamre P, Faensen D, Weill FX, et al. Around the world in 1,475 Salmonella geo-serotypes [Another Dimension]. Emerg Infect Dis. 2016;22:1298–302.
3. Issenhuth-Jeanjean S, Roggentin P, Mikoleit M, Guibourdenche M, de Pinna E, Nair S, et al. Supplement 2008-2010 (no. 48) to the White-Kauffmann-Le Minor scheme. Res Microbiol. 2014;165:526–30.
4. Salmon DE. The discovery of the germ of swine-plague. Science. 1884; 3:155–8.
5. Su LH, Chiu CH. Salmonella: clinical importance and evolution of nomenclature. Chang Gung Med J. 2007;30:210–9.

Seoul Virus Infection and Subsequent Guillain-Barré Syndrome in Traveler Returning to France from Kenya, 2022

Tristan M. Lepage, Charlotte Boullé, Vincent Le Moing, Vincent Foulongne, Virginie Sauvage

Seoul virus (SEOV) is a worldwide ratborne orthohantavirus. We describe an SEOV infection in an adult returning to France from Kenya, followed by Guillain-Barré syndrome. We confirmed SEOV infection by PCR and sequencing. Although transmission might have occurred in Kenya, the epidemiologic information available is not sufficient to confirm that possibility.

Seoul virus (SEOV), an orthohantavirus member of the Hantaviridae family, was first identified in South Korea in 1982 (*1*). Hosted in brown rats (*Rattus norvegicus*), SEOV has been isolated multiple times on 4 continents (Asia, Europe, America, and Africa) because of the worldwide distribution of its host (*2*). SEOV can cause mild to moderate hemorrhagic fever with renal syndrome (HFRS), which has a case-fatality rate of ≈1%–2% (*3*). Transmission to humans occurs through inhalation of aerosolized rodent excreta (saliva, urine, or feces) or through direct contacts and bites (*4*). Virologically confirmed SEOV human infections have been reported in America, Europe, and Asia, but not yet in Africa, despite virus detection in rats in Senegal (*5*) and Benin (*6*) and serologic hints of its circulation in humans (*2*,*7*).

We report an unexpected SEOV infection in an adult returning from Kenya. The infection was complicated by Guillain-Barré syndrome (GBS), a rare condition associated with hantavirus infections (*8*).

Author affiliations: Centre Hospitalier Universitaire de Montpellier, Montpellier, France (T.M. Lepage, C. Boullé, V. Le Moing, V. Foulongne); Institut de Recherche pour le Développement, Montpellier (T.M. Lepage, C. Boullé, V. Le Moing); Institut Pasteur, Paris, France (V. Sauvage); Université Paris Cité, Paris (V. Sauvage)

DOI: https://doi.org/10.3201/eid3102.241387

Case Report

A 54-year-old man with a remote history of mitral and tricuspid valve repair caused by Barlow's disease sought treatment at an emergency department in August 2022 in Montpellier, France. He had a 6-day history of fever up to 40°C and had chills and generalized myalgias. The night before admission, he had a single episode of hematemesis. Two weeks before, he had returned from a 5-day business trip in Nairobi, Kenya. He visited warehouses and stayed in urban areas and reported having no freshwater baths, animal contact, or unprotected sex. He was not taking any medications.

At admission, the patient was afebrile (37.8°C) and hemodynamically stable. Physical examination was unremarkable, indicating no mucocutaneous petechiae or any other signs of bleeding. Laboratory results were notable for elevated hepatic transaminases (aspartate aminotransferase 335 U/L [reference range <40 U/L], alanine aminotransferase 347 U/L [reference range <41 U/L]), unremarkable prothrombin time and bilirubin, elevated serum creatinine (324 μM [reference range 59–104 μM]) with proteinuria (protein-to-creatinine ratio 240 mg/mmol [reference range <23 mg/mmol]), increased C-reactive protein (70.5 mg/L [reference range <5 mg/L]), and thrombocytopenia (54,000 platelets/μL [reference range 150,000–400,000 platelets/μL]). Peripheral leukocyte counts were within reference ranges. Results of a chest radiograph followed by an abdominal computed tomography with contrast were unremarkable. Blood and urine cultures were sterile. A *Plasmodium*-specific PCR result was negative. Serologic tests for hepatitis viruses, HIV, cytomegalovirus, *Coxiella*, *Rickettsia*, and *Bartonella* were negative, whereas *Toxoplasma* and Epstein-Barr virus serologic tests were consistent with past infections. PCR and serologic tests for arboviruses (dengue, chikungunya, Zika, West Nile,

yellow fever, and Rift Valley fever virus) and *Leptospira* were negative.

We hydrated the patient intravenously and administered intravenous ceftriaxone (2 g/d) for presumed leptospirosis, which was stopped 4 days after admission. He remained afebrile during his stay and had no recurrent bleeding. Levels of serum creatinine (218 μM), aspartate aminotransferase (93 UI/L), alanine aminotransferase (187 UI/L) and platelets (327,000/μL) improved, and the patient was discharged on day 5 of hospitalization.

Three days after discharge, the patient's hantavirus-specific IgM and IgG serologic tests returned positive results (Hantavirus Mosaic 1 IgM and IgG

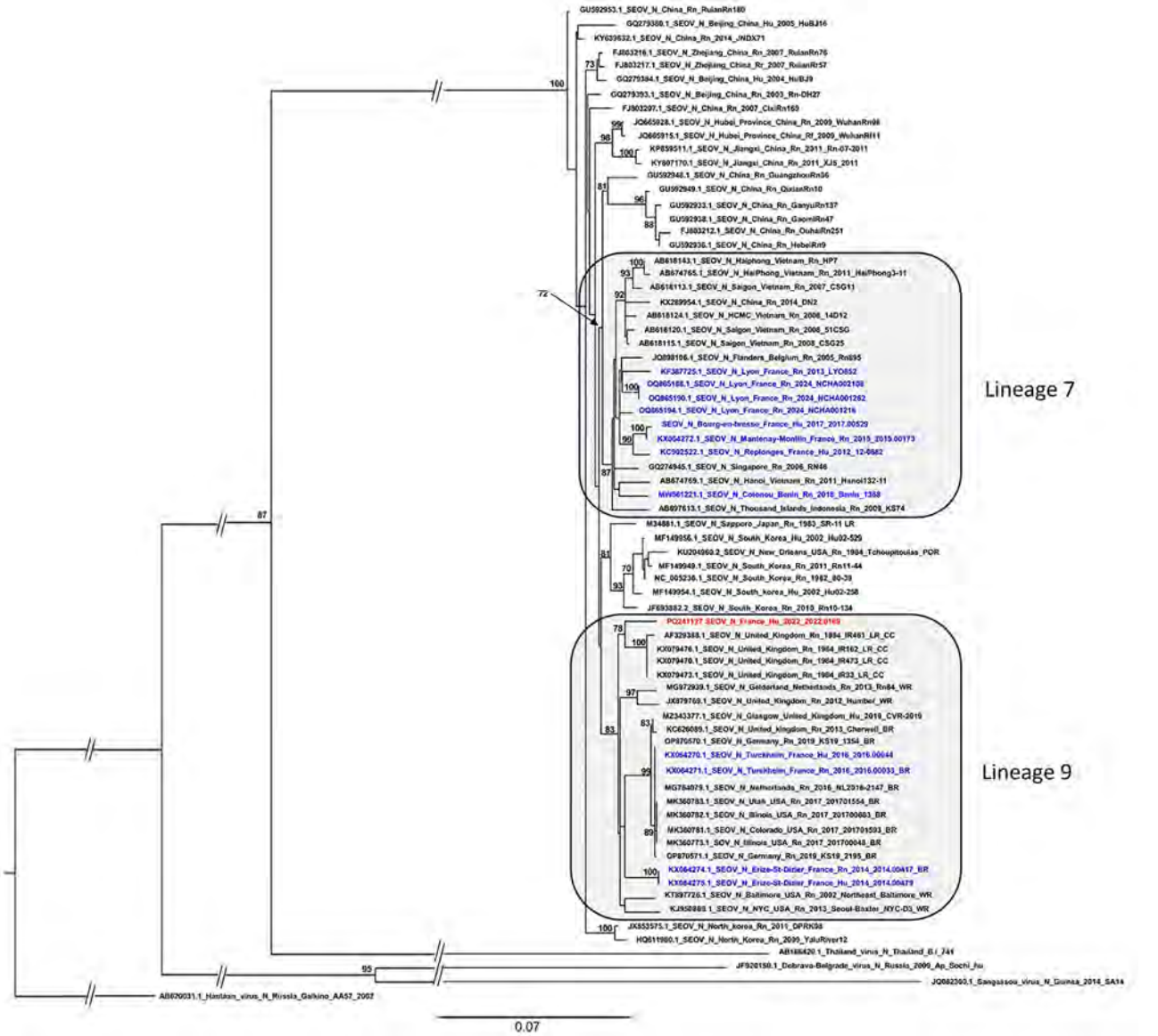

Figure. Phylogenetic tree based on the complete coding region (1,290 bp) of the small segment of SEOV strain detected in an infected patient in France, 2022, and representative strains of SEOV and other hantavirus species. The complete segment Bayesian tree was reconstructed using MAFFT version 7.023b (https://mafft.cbrc.jp/alignment/software) and RAxML 8.2 (https://cme.h-its.org/exelixis/web/software/raxml) with the general time-reversible plus gamma distribution substitution model and a rapid bootstrap (i.e., general time-reversible invariable site plus discrete Gamma model, bootstraps = 1,000). The numbers at each node are bootstrap probabilities (>70%) as determined for 1,000 iterations. The SEOV strain Hu_2022_2022.0169 (GenBank accession no. PQ241127) retrieved in this study is indicated in red, whereas other sequences from France and Benin are represented in blue. GenBank accession numbers are provided for reference viruses. Hantaan virus was used as outgroup. Scale bars indicate nucleotide substitutions per site. BR, breeder rat (includes feeder and pet rats); CC, cell culture; Hu, human; LR, laboratory rat; N, nucleoprotein; Rn, Rattus norvegicus; Rr, R. rattus; SEOV, Seoul virus; WR, wild rat.

indirect immunofluorescence assay; EUROIMMUN, https://www.euroimmun.com). As is usual in France, for surveillance purposes, we transferred the positive sample to the National Reference Centre for Hantavirus, which confirmed the result by ELISA and indirect immunofluorescence. We then identified SEOV in the patient's serum sample (collected on day 6 after symptom onset) by real-time reverse transcription PCR (cycle threshold 34.37) (*9*). We obtained a complete SEOV small segment sequence and partial medium and large segment sequences by using an in-house amplicon-based nanopore sequencing method (GenBank accession nos. PQ241127–9). We performed a phylogenetic analysis of the complete coding sequence of the small segment (Figure).

Five days after his discharge, the patient was admitted to the neurology department because of progressive ascending paresthesia and unsteady gait that manifested 10 days after symptom onset. On physical examination, he had ataxia with a positive Romberg test, diffuse areflexia, apallesthesia, and paresthesia of both lower legs. He had no motor deficit or respiratory failure, and cranial nerve testing was unremarkable. Cerebrospinal fluid analysis was notable for albuminocytologic dissociation (proteinorachia 1.48 g/L [reference range <0.4 g/L]), a negative meningitis multiplex PCR panel, and sterile culture. Electromyoneurographic analysis revealed demyelinating motor neuropathy and non–length dependent sensory neuropathy. Results of a spinal cord magnetic resonance imaging were unremarkable, and antiganglioside antibody test results were negative. We made a diagnosis of GBS and treated the patient with intravenous immunoglobulins (2 g/kg for 5 d). His neurologic impairments gradually improved, and the patient was discharged 5 days after admission. Complete resolution of disease ensued ≈90 days after symptom onset.

Conclusions

We identified SEOV in an adult with moderate HFRS, which is the 10th confirmed SEOV infection in France since SEOV was isolated in a human in 2012 (*10*). Unlike previous cases, this infection occurred in a traveler returning from Kenya, where he had visited warehouses. Although no signs of rodent presence were reported, transmission might have occurred through aerosolized rodent excreta. Symptom onset occurred 13 days after arrival in Kenya, which is consistent with transmission occurring in Kenya, given SEOV's known incubation period of ≈2–3 weeks (*3*).

Until the early 2000s, evidence of hantavirus circulation in Africa relied solely on seroprevalence studies in small mammals and humans (*11*,*12*), which were prone to cross-reactivity and lacked confirmatory assays. In 2006, Sangassou virus was isolated from mice in Guinea, constituting the first virologic evidence of hantaviruses in Africa (*13*). Further investigations then revealed several novel hantaviruses across the entire continent in rodents, shrews, and bats (*14*). SEOV strains were identified in black rats in Senegal (*5*) and in brown rats in Benin (*6*), confirming circulation in West Africa. To date, only a few human hantavirus infections have been described in Africa on the basis of serologic evidence (*15*), although amplification of hantavirus virologic material from human samples would provide more specific proof of infection.

Phylogenetic analysis of the complete small segment coding sequence of this patient's SEOV strain (Figure) showed that it belongs to lineage 9 (as partial segments of medium and large sequences). This result was unexpected, given that lineage 9 strains have mostly been identified in pet, feeder, and laboratory rats (from Europe and the United States), whereas the patient reported no contact with such rats. In comparison, SEOV sequences isolated in Benin belonged to lineage 7, whereas those isolated in Senegal were only partial, belonging to lineages 3 and 4.

We acknowledge that the patient might also have been infected in France, potentially through exposure to rodent excreta while handling boxes in his garage days before traveling to Kenya, although no signs of rodent presence were reported. However, given the absence of lineage 9 circulation data in wild rats both in France and Africa, we cannot confirm either hypothesis.

Ten days after symptom onset, SEOV infection was followed by GBS, which fully resolved after immunoglobulin administration. To date, 6 cases of hantavirus-related GBS have been reported in Europe and China since 1992 (*8*), occurring 1–2 weeks after the onset of HFRS. However, hantavirus diagnoses were made on the basis of serologic evidence alone, limiting further virus characterization. Whether the risk for GBS varies according to the hantavirus species involved remains unclear.

In conclusion, SEOV can cause moderate infections but might also lead to severe complications such as GBS. Greater awareness of SEOV among healthcare providers and policymakers is essential to improve access to testing and enhance data on global circulation.

Acknowledgments

We thank the patient for agreeing to the publication of this report. We also thank all healthcare professionals in

Montpellier University Hospital, Dieyenaba Siby–Diakite and Jean-Marc Reynes, and Aurélia Kwasiborski, Véronique Hourdel, and Valérie Caro for virus sequencing.

About the Author

Dr. Lepage is a clinician specialized in infectious and tropical diseases at Montpellier University Hospital. His research interests include tropical diseases with a focus on filarial infections.

References

1. Lee HW, Baek LJ, Johnson KM. Isolation of Hantaan virus, the etiologic agent of Korean hemorrhagic fever, from wild urban rats. J Infect Dis. 1982;146:638–44. https://doi.org/10.1093/infdis/146.5.638
2. Clement J, LeDuc JW, Lloyd G, Reynes JM, McElhinney L, Van Ranst M, et al. Wild rats, laboratory rats, pet rats: global Seoul hantavirus disease revisited. Viruses. 2019;11:652. https://doi.org/10.3390/v11070652
3. Goeijenbier M, Verner-Carlsson J, van Gorp ECM, Rockx B, Koopmans MPG, Lundkvist Å, et al. Seoul hantavirus in brown rats in the Netherlands: implications for physicians—epidemiology, clinical aspects, treatment and diagnostics. Neth J Med. 2015;73:155–60.
4. Jonsson CB, Figueiredo LTM, Vapalahti O. A global perspective on hantavirus ecology, epidemiology, and disease. Clin Microbiol Rev. 2010;23:412–41. https://doi.org/10.1128/CMR.00062-09
5. Diagne MM, Dieng I, Granjon L, Lucaccioni H, Sow A, Ndiaye O, et al. Seoul orthohantavirus in wild black rats, Senegal, 2012–2013. Emerg Infect Dis. 2020;26:2460–4. https://doi.org/10.3201/eid2610.201306
6. Castel G, Kant R, Badou S, Etougbétché J, Dossou HJ, Gauthier P, et al. Genetic characterization of Seoul virus in the seaport of Cotonou, Benin. Emerg Infect Dis. 2021;27:2704–6. https://doi.org/10.3201/eid2710.210268
7. Coulaud X, Chouaib E, Georges AJ, Rollin P, Gonzalez JP. First human case of haemorrhagic fever with renal syndrome in the Central African Republic. Trans R Soc Trop Med Hyg. 1987;81:686. https://doi.org/10.1016/0035-9203(87)90455-X
8. Zhou Y, Yang J, Hai H, Dong J, Wen Y. Hantavirus infection–related acute inflammatory demyelinative polyradiculoneuropathy: a case report and literature review. Medicine (Baltimore). 2024;103:e37332. https://doi.org/10.1097/MD.0000000000037332
9. Kramski M, Meisel H, Klempa B, Krüger DH, Pauli G, Nitsche A. Detection and typing of human pathogenic hantaviruses by real-time reverse transcription-PCR and pyrosequencing. Clin Chem. 2007;53:1899–905. https://doi.org/10.1373/clinchem.2007.093245
10. Macé G, Feyeux C, Mollard N, Chantegret C, Audia S, Rebibou JM, et al. Severe Seoul hantavirus infection in a pregnant woman, France, October 2012. Euro Surveill. 2013;18:20464. https://doi.org/10.2807/ese.18.17.20464-en
11. Gonzalez JP, McCormick JB, Baudon D, Gautun JP, Meunier DY, Dournon E, et al. Serological evidence for Hantaan-related virus in Africa. Lancet. 1984;2:1036–7. https://doi.org/10.1016/S0140-6736(84)91130-9
12. Lee PW, Gibbs C, Gajdusek DC, Svedmyr A. Antibody to Korean haemorrhagic fever virus in man in parts of the world where haemorrhagic fever with renal syndrome is not known. Lancet. 1981;318:256. https://doi.org/10.1016/S0140-6736(81)90504-3
13. Klempa B, Fichet-Calvet E, Lecompte E, Auste B, Aniskin V, Meisel H, et al. Hantavirus in African wood mouse, Guinea. Emerg Infect Dis. 2006;12:838–40. https://doi.org/10.3201/eid1205.051487
14. Witkowski PT, Klempa B, Ithete NL, Auste B, Mfune JKE, Hoveka J, et al. Hantaviruses in Africa. Virus Res. 2014;187:34–42. https://doi.org/10.1016/j.virusres. 2013.12.039
15. Klempa B, Koivogui L, Sylla O, Koulemou K, Auste B, Krüger DH, et al. Serological evidence of human hantavirus infections in Guinea, West Africa. J Infect Dis. 2010;201:1031–4. https://doi.org/10.1086/651169

Address for correspondence: T.M. Lepage, Service des Maladies Infectieuses et Tropicales, Hôpital La Colombière, CHU de Montpellier, 39 ave Charles Flahaut, 34090, Montpellier, France; email: tristanlepage77@gmail.com

Two Human Infections with Diverse Europe-1 Crimean-Congo Hemorrhagic Fever Virus Strains, North Macedonia, 2024

Dejan Jakimovski, Kostadin Poposki, Marija Dimzova, Marija Cvetanovska, Fadil Cana, Ivana Bogdan, Alejandro Cabezas-Cruz, Brigitta Zana, Zsófia Lanszki, Zsófia Tauber, Tamás Görföl, Krisztián Bányai, Ágota Ábrahám, Pavle Banović,[1] Gábor Kemenesi[1]

Until 2023, North Macedonia had not reported a Crimean-Congo hemorrhagic fever (CCHF) case for >50 years. In 2024, increased clinical vigilance identified and characterized 2 novel CCHF cases. Genetic analysis and the identification of possible reassortment indicate North Macedonia as an interaction zone between CCHF virus isolates from Turkey and Kosovo.

Crimean-Congo hemorrhagic fever (CCHF) is a severe zoonotic disease endemic in various regions of Europe, Asia, and Africa, including the Balkans, central Asia, and sub-Saharan Africa (*1*). The disease is caused by the CCHF virus (CCHFV), which is predominantly maintained and transmitted by *Hyalomma* spp. ticks. However, the virus also can be transmitted to humans through direct contact with the bodily fluids of infected animals and humans (*2*). In 2023, CCHF reemerged in North Macedonia (*3*; D. Jakimovski et al., unpub. data, https://doi.org/10.21203/rs.3.rs-4360716/v1), having been absent for >50 years since a 1970 outbreak. The combined mortality rate for the 1970 and 2023 outbreaks was 18.75% (3/16 cases) (*4*; D. Jakimovski et al., unpub. data). In response to this escalating public health concern in the Balkan Region (D. Jakimovski et al., unpub. data), the Balkan Association for Vector-Borne Diseases implemented a strategic plan emphasizing clinical vigilance and capacity sharing. Those efforts culminated in the detection and characterization of an autochthonous CCHFV strain linked to the 2023 outbreak (D. Jakimovski et al., unpub. data). Our study explored the reemergence of CCHF cases in North Macedonia, emphasizing the co-circulation of multiple autochthonous viral strains.

The Study

On April 26, 2024, a man in his 60s (case-patient 1) with no notable medical history was admitted to the Clinic for Infectious Diseases in Skopje (CIDS), Skopje, North Macedonia. He resided alone in a rural village in the northeastern region of North Macedonia in the municipality of Kriva Palanka (Figure 1). He worked as a self-employed herder and had not traveled outside the region in the preceding month. On April 14, 2024, the patient noticed a tick attached on his left lower leg and removed it with tweezers. The exposure site was ≈17 km south of the border with Serbia and ≈15 km east of the border with Bulgaria (Figure 1). Seven days after tick removal (day 0), the patient had malaise and persistent nosebleeds, which continued despite nasal tamponade. On day 4, he noticed dark stools, prompting a visit to an internal medicine specialist. Laboratory tests revealed leucopenia, thrombocytopenia, and elevated aminotransferase levels (Appendix 1,

Author affiliations: Saints Cyril and Methodius University in Skopje Faculty of Medicine, Skopje, North Macedonia (D. Jakimovski, K. Poposki, M. Dimzova, M. Cvetanovska); University Clinic for Infectious Diseases and Febrile Conditions, Skopje (D. Jakimovski, K. Poposki, M. Dimzova, M. Cvetanovska, F. Cana); Balkan Association for Vector-Borne Diseases, Novi Sad, Serbia (D. Jakimovski, K. Poposki, I. Bogdan, P. Banović, G. Kemenesi); Pasteur Institute Novi Sad, Novi Sad (I. Bogdan, P. Banović); Laboratoire de Santé Animale, Maisons-Alfort, France (A. Cabezas-Cruz); University of Pécs Szentágothai Research Centre, Pécs, Hungary (B. Zana, Z. Lanszki, Z. Tauber, T. Görföl, K. Bányai, A. Ábrahám, G. Kemenesi); University of Veterinary Medicine, Budapest (K. Bányai); University of Novi Sad Faculty of Medicine, Novi Sad (P. Banović)

DOI: https://doi.org/10.3201/eid3102.241249

[1]These senior authors contributed equally to this article.

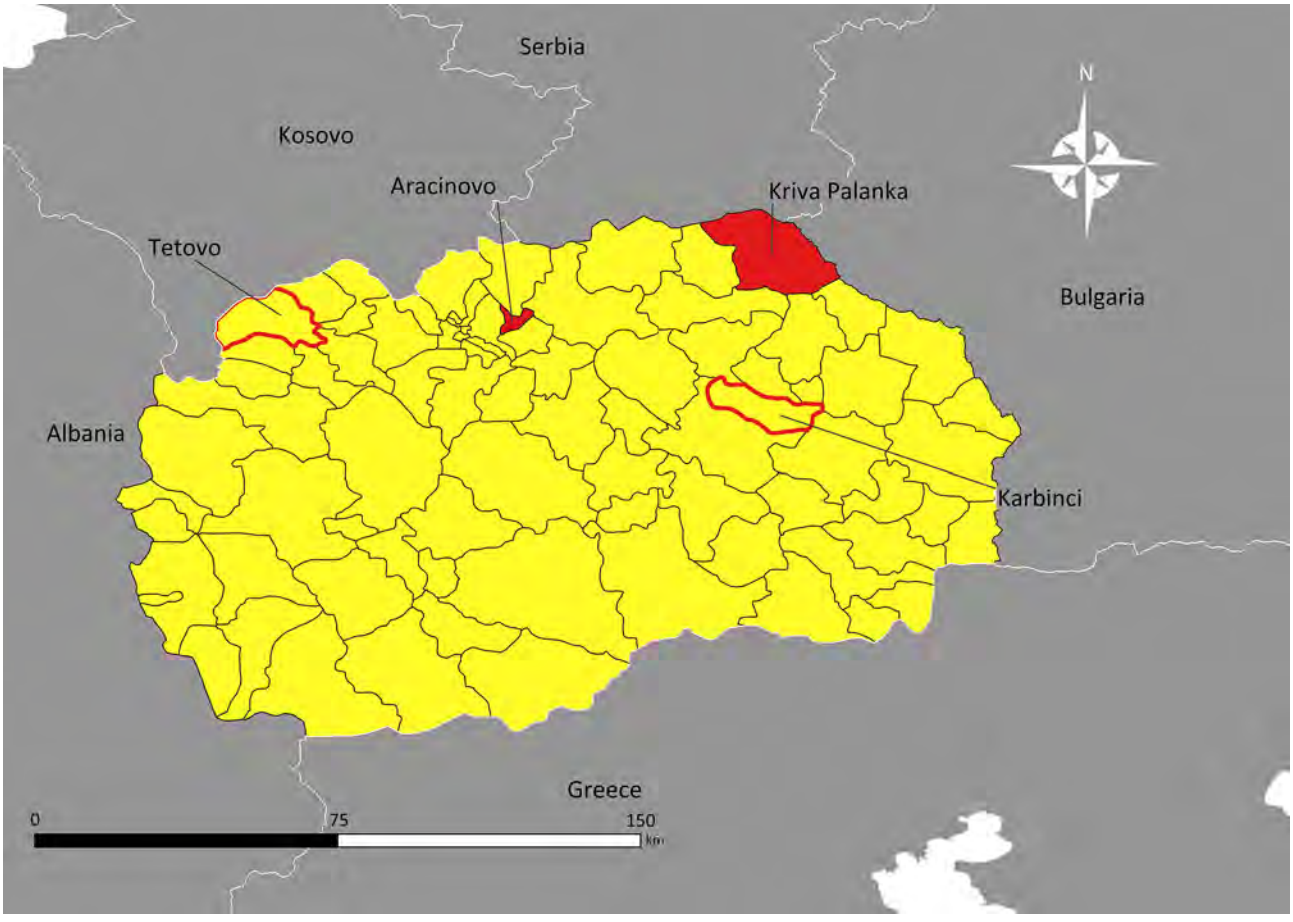

Figure 1. Locations of Crimean-Congo hemorrhagic fever cases in North Macedonia. Red shading indicates municipalities where cases emerged in April–May 2024; red outlines indicate municipalities where previous cases occurred (cases of 1970 and 2023). Shapefile for mapping North Macedonia at district and municipality levels available through GADM Database of Global Administrative Areas version 2.8 (https://gadm.org). Map generated by using QGIS version 3.12 (https://www.qgis.org).

https://wwwnc.cdc.gov/EID/article/31/2/24-1249-App1.xlsx). The patient was evaluated by multiple specialists and admitted to the intensive care unit at 8th September City General Hospital in Skopje. On day 5, we detected CCHFV in blood and urine samples by using Viasure reverse transcription PCR (RT-PCR) (Certest Biotec, https://www.certest.es), which had a sensitivity of ≥10 RNA copies/reaction. Upon confirmation of CCHF, the patient was transferred to CIDS for further treatment (Figure 2). We have detailed his clinical course, diagnostic findings, treatment, and outcome (Figure 2).

On April 30, 2024, a man in his 30s (case-patient 2) with no notable medical history was admitted to CIDS. On April 21, after a local hike, he had noticed a tick attached to his right ankle and removed it with his hands. The patient resided in a rural area of the Skopje Region in the municipality of Arachinovo (Figure 1) and had not traveled outside the area in the preceding month. Three days after tick removal (day 0), he experienced the sudden onset of fever, malaise, and abdominal pain accompanied by nausea (Figure 3). On day 1, he experienced 2 episodes of vomiting and consulted his family physician, who administered parenteral vitamin infusion, H2 blockers, and paracetamol. On day 5, because of persistent symptoms, the patient was referred to CIDS (Figure 3). Upon evaluation at CIDS on day 6, he had a temperature of 39°C and petechial rash distributed on his chest, abdomen, back, and lower extremities. Laboratory findings revealed leucopenia, severe thrombocytopenia, and elevated aminotransferases (Appendix 1). We confirmed CCHFV infection through analysis of blood using Viasure RT-PCR, which had a sensitivity of ≥10 RNA copies/reaction, as previously described. The patient was hospitalized. We have detailed his clinical course, diagnostic findings, treatment, and outcome (Figure 3).

To characterize the CCHFV strains from the 2 patients, we conducted molecular analysis of blood

samples from both patients, followed by phylogenetic analysis of all 3 viral segments. In brief, we collected blood samples on day 5 (case-patient 1) and day 6 (case-patient 2) after symptom onset. After heat inactivation, we extracted nucleic acids and confirmed the presence of CCHFV RNA through RT-PCR as described by Atkinson et al (*5*). Cycle threshold (Ct) values were 35 for case-patient 1 and 37 for case-patient 2, indicating positive results. To further analyze the viral genome, we performed amplicon-based sequencing targeting the Europe-1 genotype on the Oxford Nanopore platform (*6*). We conducted sequence processing and assembly by using Geneious Prime 2024.0.5 (https://www.geneious.com). For case-patient 1, we obtained complete sequences of the small and medium segments and a partial sequence of the large segment. For case-patient 2, we generated only partial sequences of all 3 segments (GenBank accession nos. PQ031235–40). We reconstructed phylogenetic trees by using the IQ-TREE software with the maximum-likelihood method and the general time-reversible plus empirical base frequencies plus invariable site plus discrete gamma 4 substitution model, supported by 1,000 bootstrap replicates for robust statistical inference (*7*). We visualized and edited the trees by using the iTol online tool (*8*).

Phylogenetic analysis revealed the viral isolates from both patients clustered with regional strains within the Europe-1 lineage (genotype V). Of note, the medium segment from case-patient 1 showed high similarity to sequences from Turkey, suggesting a possible reassortment event. To investigate further, we conducted recombination analysis by concatenating genomic segments and aligning them with 5 selected CCHFV genomes using the MUSCLE plugin in Geneious Prime 2024.0.5. We trimmed the alignment to equal lengths and excluded regions containing gaps. We conducted recombination analysis by using RDP4 software (https://rdp4.software.informer.com) with 90% cutoff value for tree permutations, a 500-bp window size, and Bonferroni correction for a p value threshold of 0.05. Bootscan analysis confirmed the reassortment event associated with the medium segment of the virus from case-patient 1

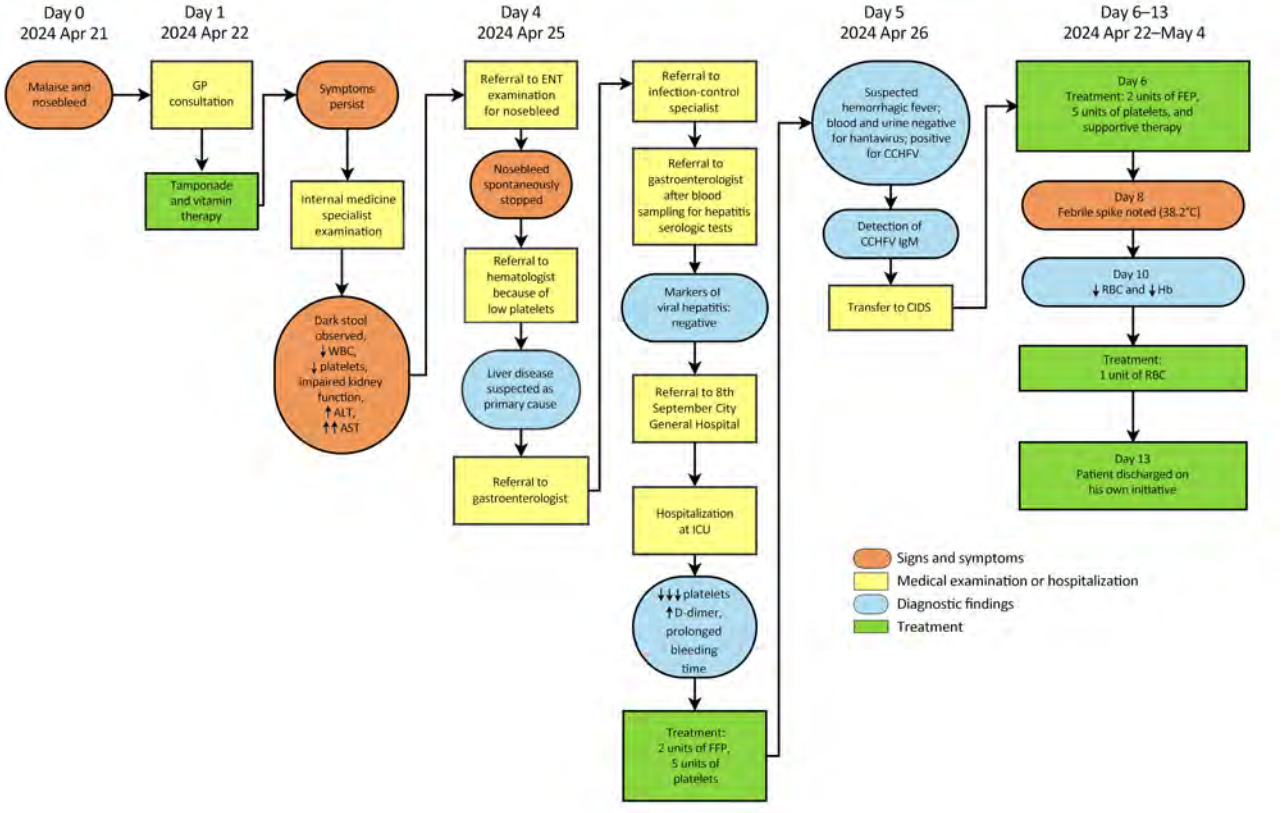

Figure 2. Clinical course, diagnostic findings, treatment, and outcome for CCHF case-patient 1 during CCHF outbreak, North Macedonia, April–May 2024. Up arrows (↑) indicate that a parameter increased and down arrows (↓) that a parameter decreased; multiple up or down arrows indicate degree of increase or decrease. Timeline generated by using open-source software draw.io (https://app.diagrams.net). ALT, alanine transaminase; AST, aspartate aminotransferase; CCHF, Crimean-Congo hemorrhagic fever; CCHFV, CCHF virus; CIDS, Clinic for Infectious Diseases in Skopje; ENT, ear, nose, and throat specialist; FFP, fresh frozen plasma; GP, general practitioner; Hb, hemoglobin; ICU, intensive care unit; RBC, red blood cells (erythrocytes); WBC, white blood cells (leukocytes).

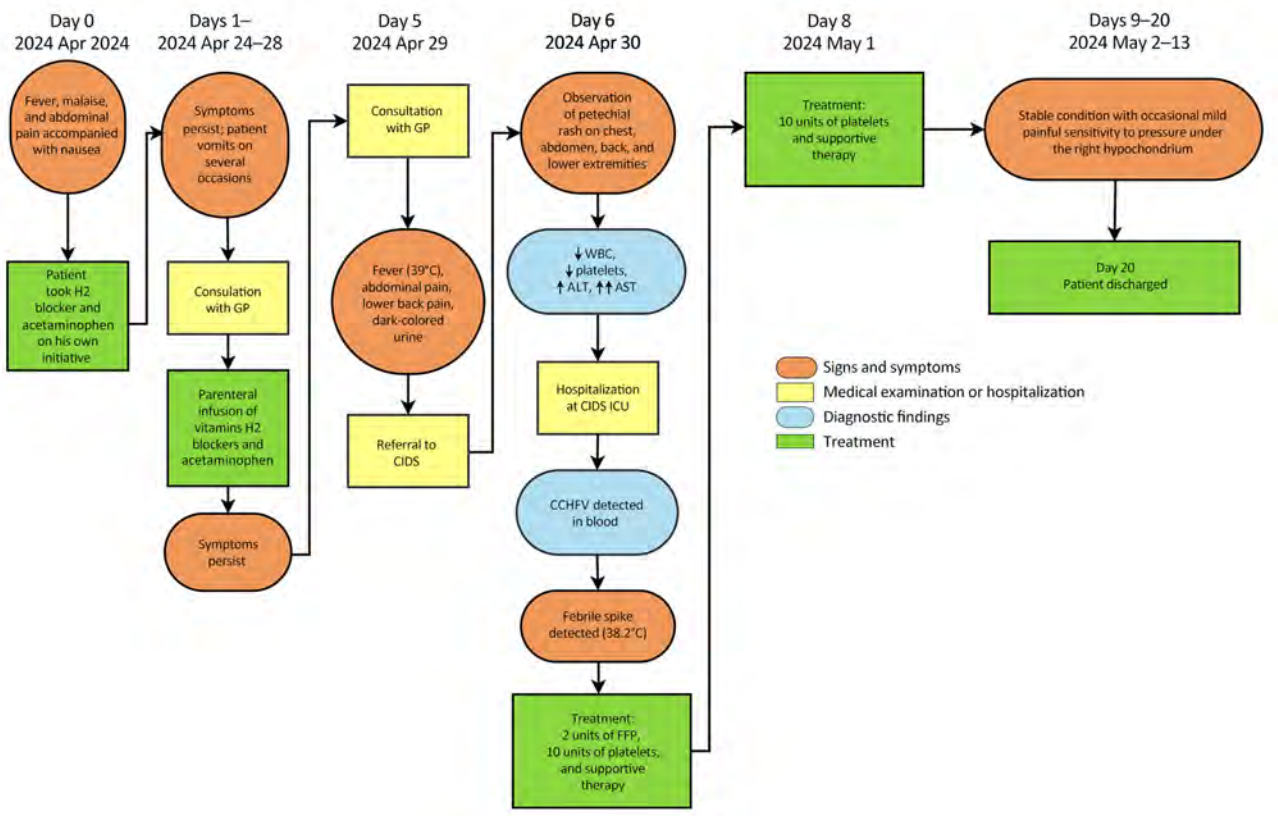

Figure 3. Clinical course, diagnostic findings, treatment, and outcome for CCHF case-patient 2 during CCHF outbreak, North Macedonia, April–May 2024. Up arrows (↑) indicate that a parameter increased and down arrows (↓) that a parameter decreased; multiple up or down arrows indicate degree of increase or decrease. Timeline generated by using opensource software draw.io (https://app.diagrams.net). ALT, alanine transaminase; AST, aspartate aminotransferase; CCHF, Crimean-Congo hemorrhagic fever; CCHFV, CCHF virus; CIDS, Clinic for Infectious Diseases in Skopje; ENT, ear, nose, and throat specialist; FFP, fresh frozen plasma; GP, general practitioner; ICU, intensive care unit; WBC, white blood cells (leukocytes).

(GenBank accession no. PQ031235.1) (Appendix 2, https://wwwnc.cdc.gov/EID/article/31/2/24-1249-App2.pdf). This evidence strongly supports the hypothesis that the virus infecting case-patient 1 underwent reassortment, probably involving gene flow between CCHFV isolates from Turkey and Kosovo within the Europe-1 lineage.

To evaluate the immune response in both cases, we analyzed serum samples for the presence of CCHFV IgM and IgG by using VectoCrimean-CHF-IgM ELISA and VectoCrimean-CHF-IgG ELISA (Vector-BEST, https://en.vector-best.ru), following the manufacturer's protocols. Both patients exhibited strong IgM reactivity against CCHFV, indicating acute infection. In contrast, CCHFV IgG was undetectable in both cases, consistent with a primary immune response during the early stages of infection.

Conclusions

Our detailed case studies illustrate the clinical variability and severity of CCHFV infections. Both patients had hallmark symptoms, such as fever, malaise, and thrombocytopenia, but their clinical courses varied considerably in progression and intensity. This study emphasizes the importance of coordinated efforts by the Balkan Association for Vector-Borne Diseases in managing and mitigating the effect of zoonotic diseases in the region. The reemergence of CCHF in North Macedonia, which had 5 cases reported in 2023 and 2024 from 4 distinct regions, underscores the necessity for sustained surveillance of all components of the infection chain, including ticks, wildlife, domestic animals, and humans. Rapid diagnostic tools and comprehensive public health strategies are critical in preventing and controlling future outbreaks. Of note, the identification of possible reassortment events involving CCHFV isolates from Turkey and Kosovo within the Europe-1 lineage highlights the importance of North Macedonia as a geographic interaction zone for multiple viral lineages. These findings emphasize the need for further research into ecology and evolution of the virus in this region to better assess the risks to human and animal health.

Acknowledgments

The authors extend their gratitude to the staff members of the 8th September City General Hospital, the Institute for Public Health of the Republic of North Macedonia, and the Clinic for Infectious Diseases.

This study was approved by the Ethics Committee of the University of Saints Cyril and Methodius in Skopje's Faculty of Medicine (approval no. 03–1835/2). The research was conducted in compliance with the principles outlined in the Declaration of Helsinki and adhered to the Patient Rights Law of the Republic of North Macedonia. Written informed consent has been obtained from the patients to publish this paper.

This work was supported by Hungary's National Research, Development, and Innovation Office (grant no. TKP2021-NVA-07) and the Strategic Plan of the Balkan Association for Vector-Borne Diseases (https://www.bavbd.org).

About the Author

Dr. Jakimovski is an infectious diseases specialist at the Clinic for Infectious Diseases in Skopje, North Macedonia. His research focuses on vectorborne diseases, particularly tickborne diseases, and emphasizes improving diagnostic and therapeutic capacities within the country through international collaborative efforts and state-of-the-art research.

References

1. Nasirian H. Ticks infected with Crimean-Congo hemorrhagic fever virus (CCHFV): a decision approach systematic review and meta-analysis regarding their role as vectors. Travel Med Infect Dis. 2022;47:102309. https://doi.org/10.1016/j.tmaid.2022.102309
2. Frank MG, Weaver G, Raabe V; State of the Clinical Science Working Group of the National Emerging Pathogens Training and Education Center's Special Pathogens Research Network. Crimean Congo hemorrhagic fever virus for clinicians—virology, pathogenesis, and pathology. Emerg Infect Dis. 2024;30:847–53. https://doi.org/10.3201/eid3005.231646
3. Jakimovski D, Grozdanovski K, Rangelov G, Pavleva V, Banović P, Cabezas-Cruz A, et al. Cases of Crimean-Congo haemorrhagic fever in North Macedonia, July to August 2023. Euro Surveill. 2023;28:2300409. https://doi.org/10.2807/1560-7917.ES.2023.28.34.2300409
4. Gligić A, Stamatović L, Stojanović R, Obradović M, Bosković R. The first isolation of the Crimean hemorraghic fever virus in Yugoslavia [in Serbian]. Vojnosanit Pregl. 1977;34:318–21.
5. Atkinson B, Chamberlain J, Logue CH, Cook N, Bruce C, Dowall SD, et al. Development of a real-time RT-PCR assay for the detection of Crimean-Congo hemorrhagic fever virus. Vector Borne Zoonotic Dis. 2012;12:786–93. https://doi.org/10.1089/vbz.2011.0770
6. D'Addiego J, Wand N, Afrough B, Fletcher T, Kurosaki Y, Leblebicioglu H, et al. Recovery of complete genome sequences of Crimean-Congo haemorrhagic fever virus (CCHFV) directly from clinical samples: a comparative study between targeted enrichment and metagenomic approaches. J Virol Methods. 2024;323:114833. https://doi.org/10.1016/j.jviromet.2023.114833
7. Minh BQ, Schmidt HA, Chernomor O, Schrempf D, Woodhams MD, von Haeseler A, et al. IQ-TREE 2: new models and efficient methods for phylogenetic inference in the genomic era. Mol Biol Evol. 2020;37:1530–4. https://doi.org/10.1093/molbev/msaa015
8. Letunic I, Bork P. Interactive Tree Of Life (iTOL) v4: recent updates and new developments. Nucleic Acids Res. 2019;47(W1):W256–9. https://doi.org/10.1093/nar/gkz239

Address for correspondence: Dejan Jakimovski, University Clinic for Infectious Diseases and Febrile Conditions, Mother Teresa 17, Skopje 1000, North Macedonia; email: dejan.jakimovski@medf.ukim.edu.mk

Comparison of Contemporary and Historic Highly Pathogenic Avian Influenza A(H5N1) Virus Replication in Human Lung Organoids

Meaghan Flagg,[1] Brandi N. Williamson,[1] Johan A. Ortiz-Morales, Tessa R. Lutterman, Emmie de Wit

We compared virus replication and host responses in human alveolar epithelium infected with highly pathogenic avian influenza (HPAI) A(H5N1) viruses. A/Vietnam/1203/2004 replicated most efficiently, followed by A/Texas/37/2024, then A/bovine/Ohio/B24OSU-342/2024. Induction of interferon-stimulated genes was lower with A/Texas/37/2024 and A/bovine/Ohio/B24OSU-342/2024, which may indicate a reduced disease severity of those viruses.

Clade 2.3.4.4b highly pathogenic avian influenza (HPAI) A(H5N1) viruses have circulated in avian species in North America since 2021. Subsequently, those viruses have been detected in a wide range of mammal species (*1*). In 2024, clade 2.3.4.4b HPAI H5N1 virus was detected in dairy cattle, in both tissue samples and milk from infected animals (*2*), and then spread to multiple herds in 16 US states (https://www.aphis.usda.gov/livestock-poultry-disease/avian/avian-influenza/hpai-detections/hpai-confirmed-cases-livestock). The broadened host range of clade 2.3.4.4b H5N1 viruses and unprecedented levels of transmission to mammals has raised concerns about potential spillover into humans.

By January 6, 2025, the Centers for Disease Control and Prevention had confirmed 66 human cases of HPAI H5N1 virus infection in the United States (https://www.cdc.gov/bird-flu/situation-summary/index.html). Many of those cases were linked to exposure to infected cattle. However, recent outbreaks in Colorado have resulted in identification of additional human cases linked to infected poultry (*3*). Virus isolated from a worker at a dairy farm in Texas (A/Texas/37/2024) was shown to be closely related to viruses circulating in cattle, suggesting that this case was likely a result of direct cow-to-human transmission (*4*). Reported human symptoms included conjunctivitis, 1 person reported mild respiratory symptoms (*5*) , and 1 person died (https://ldh.la.gov/news/H5N1-death). Those symptoms starkly contrast prior HPAI H5N1 virus infections in humans, which resulted in severe respiratory disease and death in nearly 50% of cases (*6*). To assess the risk for developing severe disease after infection with contemporary HPAI H5N1 virus, we evaluated virus replication, host cell survival, and induction of innate immune responses in human alveolar epithelium infected with A/Texas/37/2024 or cattle isolate A/bovine/Ohio/B24OSU-342/2024, compared with a historic H5N1 isolate (A/Vietnam/1203/2004) derived from a fatal human case in 2004 (*7*).

The Study

Virus replication and host cell damage in the alveolar epithelium are key drivers of severe respiratory disease. Human lung organoids are a physiologically relevant state-of-the-art model of primary human alveolar epithelium. Lung organoids consisting of alveolar type 2 (AT2) epithelial cells can be cultured from adult stem cells isolated from lung tissue (*8*,*9*) or from induced pluripotent stem cells (iPSCs) differentiated into AT2 cells (*10*). Both model systems accurately recapitulate the fitness and pathogenicity of respiratory viruses as observed in humans (*8*,*9*,*11*,*12*). We infected AT2 cells from both iPSC-derived human

Authors affiliation: National Institute of Allergy and Infectious Diseases, National Institutes of Health, Hamilton, Montana, USA

DOI: https://doi.org/10.3201/eid3102.241147

[1]These authors contributed equally to this article.

lung organoids (ihLOs) and adult stem cell–derived human lung organoids (hLOs) (human donor lung tissue provided by Chuong D. Hoang and Nathanael Pruett, National Cancer Institute [NCI], National Institutes of Health [NIH], Bethesda, MD, USA). Deidentified human lung tissue samples were collected in accordance with institutional review board–approved protocols at the NIH Clinical Center. We infected ihLOs and hLOs with 3 HPAI H5N1 isolates and compared virus replication, host cell survival, and innate immune responses over time.

We found that the isolate A/Vietnam/1203/2004 replicated to higher titers in both ihLOs and hLOs (Figure 1, panels A, B) compared with cattle isolate A/bovine/Ohio/B24OSU-342/2024 (provided by Richard Webby, St. Jude Children's Research Hospital, Memphis, TN, USA, and Andrew Bowman, Ohio State University, Columbus, OH, USA). Of note, we detected a trend toward increased replication of A/Texas/37/2024 (provided by Todd Davis, CDC, Atlanta, GA, USA), compared with the bovine isolate, suggesting enhanced fitness of that virus in human cells compared with its predecessors circulating in cattle.

To evaluate potential pathogenicity of the contemporary HPAI H5N1 viruses, we quantified cell death over time in infected lung organoids. We observed cell death earlier in organoids infected with the A/Vietnam/1203/2004 isolate (Figure 1, panels C, D). Infection with the A/Texas/37/2024 and A/bovine/Ohio/B24OSU-342/2024 isolates also resulted in cell death, but at later timepoints (72–96 hours postinoculation). That finding is in accordance with the slower replication kinetics observed with those viruses compared with the A/Vietnam/1203/2004 isolate (Figure 1, panels A, B).

We quantified induction of interferon-stimulated genes (ISGs) ISG15, ISG20, interferon induced transmembrane 3, interferon-induced protein with tetratricopeptide 1, myxovirus resistance 1, 2′-5′-oligoadenylate synthetase 1, and retinoic acid-inducible 1 (Figure 2) and proinflammatory cytokines interferon

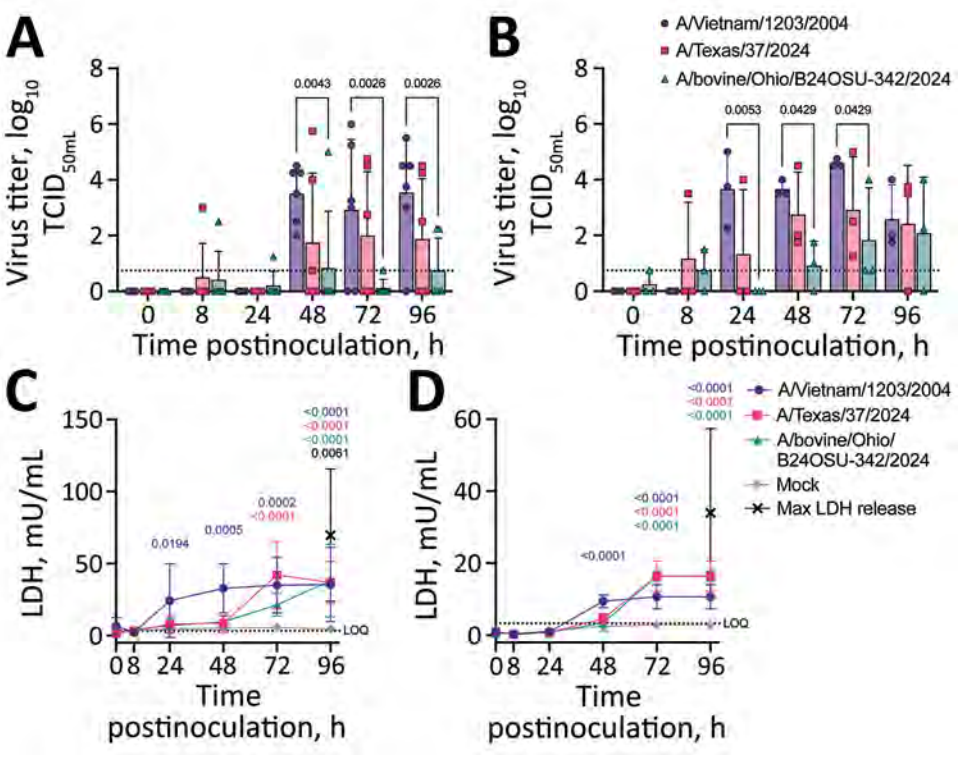

Figure 1. Virus replication and cytotoxicity in a comparison of contemporary and historic highly pathogenic avian influenza A(H5N1) virus replication in human lung organoids. A, B) Virus replication in ihLO (A) hLO (B). Cells were infected at a multiplicity of infection of 0.1 with 1 of the 3 indicated HPAI H5N1 virus isolates. Organoids were removed from Matrigel (Corning, https://www.corning.com) and incubated with virus for 1 hour at 37°C, after which virus was removed, organoids were washed, and replated in Matrigel. Culture supernatant samples were taken at 0, 8, 24, 48, 72, and 96 hours postinoculation and titered on Madin-Darby canine kidney cells. Titrations were read after 3 days by using a hemagglutination assay using turkey red blood cells. Dashed line indicates lower limit of detection; error bars denote means and SDs. p values <0.05 are indicated above bars. Of note, ihLOs and hLOs were derived from different donors. C, D) Cytotoxicity in ihLO (C) hLO (D). Culture supernatants from ihLOs (C) or hLOs (D) were collected and tested for release of lactate dehydrogenase into culture supernatant according to the LDH-Glo Cytotoxicity Assay protocol (Promega, https://www.promega.com) as an indicator of cell death. Results were converted to mU per mL LDH determined by the standard curve using a simple linear regression. Cells lysed with Triton X-100 (MilliporeSigma, https://www.sigmaaldrich.com) were included as maximum LDH release controls. Dashed line indicates lower limit of quantification. Error bars denote means and SDs of ihLO (n = 6) or hLO (n = 3) biologic replicates. Statistical analysis was conducted using 2-way analysis of variance followed by Tukey posttest. p values <0.05 are indicated and color coded by isolate. hLOs, adult stem cell–derived human lung organoids; HPAI, highly pathogenic avian influenza; ihLO, iPSC-derived human lung organoids; iPSCs, induced pluripotent stem cells; LDH, lactate dehydrogenase.

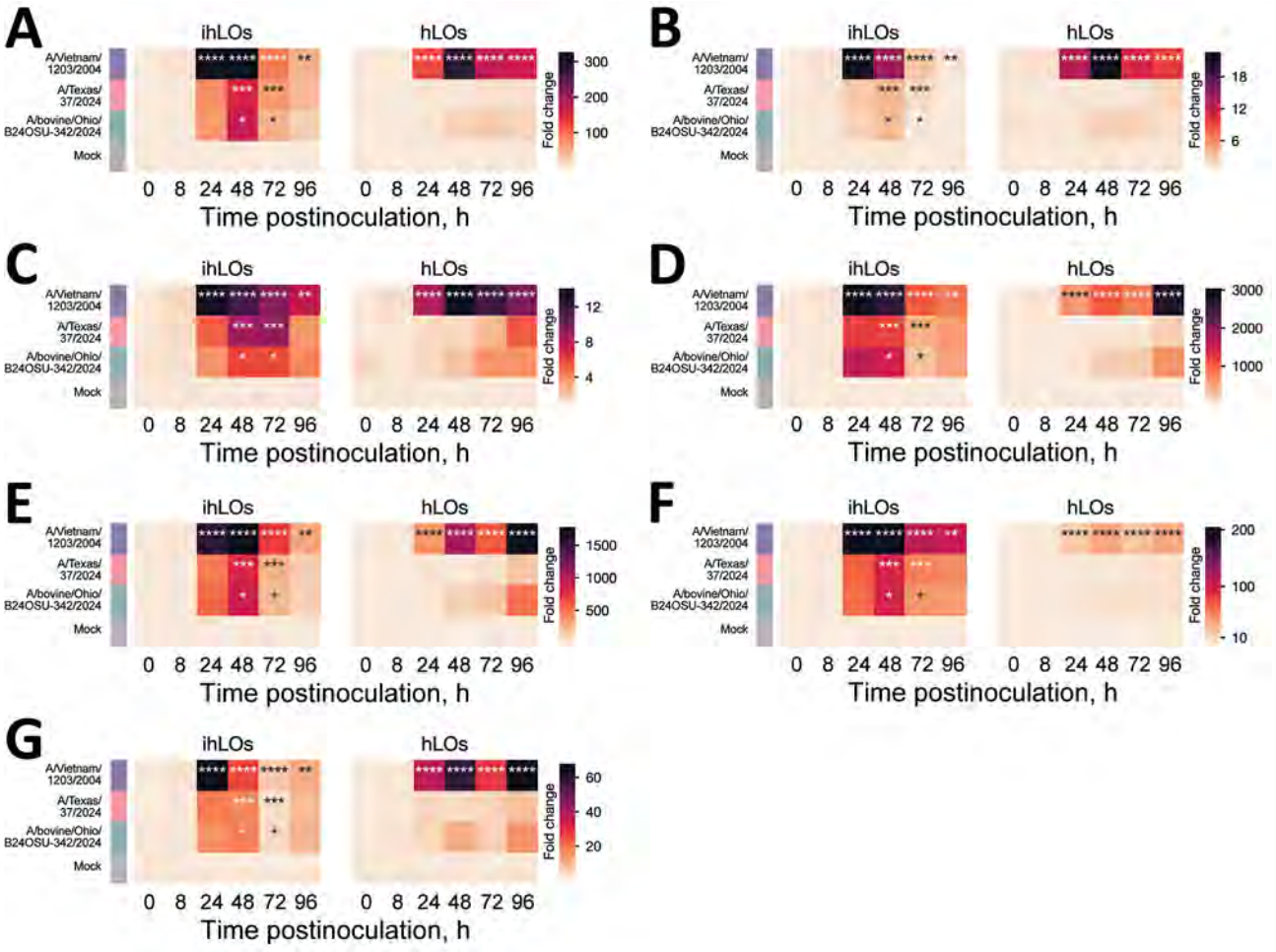

Figure 2. Induction of ISGs in a comparison of contemporary and historic highly pathogenic avian influenza A(H5N1) virus replication in human lung organoids. A) ISG15; B) ISG20; C) interferon-induced transmembrane 3; D) interferon-induced protein with tetratricopeptide 1; E) myxovirus resistance 1; F) 2′-5′-oligoadenylate synthetase 1; G) retinoic acid–inducible 1. We infected ihLO and hLO as described in Figure 1. We extracted RNA from 2.5 × 10^4 cells by using the QIAGEN RNeasy kit (QIAGEN, https://www.qiagen.com) following the tissue extraction instructions. We ran quantitative reverse transcription PCR by using primers (Integrated DNA Technologies, https://www.idtdna.com) to detect ISGs. Data were normalized to an internal control (ACTB), and fold change was calculated relative to timepoint-matched mock-infected controls. Mean fold change is reported for 6 ihLO and 3 hLO biologic replicates. Statistical analysis was performed using 2-way analysis of variance followed by Dunnett posttest; p values <0.05 for comparisons of infected versus mock samples are indicated. hLOs, adult stem cell–derived human lung organoids; HPAI, highly pathogenic avian influenza; ihLO, iPSC-derived human lung organoids; iPSCs, induced pluripotent stem cells; ISGs, interferon stimulated genes; LDH, lactate dehydrogenase.

β, tumor necrosis factor α, interleukin 6, and interleukin 1β (Figure 3) by quantitative reverse transcription PCR as a measure of the host innate immune response to infection. ISG induction was highest in organoids infected with the A/Vietnam/1203/2004 isolate. That result was most pronounced in the adult stem cell–derived hLOs, in which ISG induction was not detected in organoids infected with the A/Texas/37/2024 or A/bovine/Ohio/B24OSU-342/2024 isolates, despite the presence of replicating virus. We observed moderate ISG induction in ihLOs infected with the A/Texas/37/2024 and A/bovine/Ohio/B24OSU-342/2024 isolates. We observed a different pattern of induction for proinflammatory cytokines; detection was largely confined to A/Vietnam/1203/2004-infected ihLOs, and A/Vietnam/1203/2004-infected and A/bovine/Ohio/B24OSU-342/2024–infected hLOs (Figure 3).

The unusual transmission of clade 2.3.4.4b HPAI H5N1 viruses to mammals has raised concerns about the risk for spillover into the human population and the possibility of outbreaks leading to severe disease. We assessed virus replication and host responses in human alveolar epithelium because virus replication and host cell damage in that site is a key driver of severe respiratory disease. The reduced replication levels of the contemporary A/Texas/37/2024 and A/bovine/

Ohio/B24OSU-342/2024 isolates in lung organoids compared with the historic A/Vietnam/1203/2004 isolate could explain why recent human influenza cases involving the clade 2.3.4.4b viruses resulted in mild illness (*4*,*6*), as opposed to the severe respiratory disease associated with previous HPAI outbreaks in Vietnam (*13*,*14*). The presence of a lysine at position 627 in the polymerase basic (PB) 2 protein has been associated with adaption of avian influenza viruses to mammal hosts and is known to increase virus replication in the mammalian respiratory tract (*15*). That substitution (E627K) is in both the A/Vietnam/1203/2004 and A/Texas/37/2024 viruses but not the A/bovine/Ohio/B24OSU-342/2024 isolate (*4*), which could explain the increased replication observed for the A/Texas/37/2024 isolate compared with the bovine isolate.

Another factor contributing to the reduced disease severity in humans after infection with clade 2.3.4.4b viruses compared with previous HPAI H5N1 virus cases may be differential activation of the immune system. We observed substantially higher induction of ISGs in lung organoids infected with the A/Vietnam/1203/2004 isolate. An overly exuberant immune response, including cytokine storm, is known to play a role in the high mortality rates from HPAI H5N1 virus infections observed during the 2003 and 2004 outbreaks in Vietnam (*14*). Reduced ISG induction elicited by the A/Texas/37/2024 and A/bovine/Ohio/B24OSU-342/2024 isolates despite detection of virus replication might indicate that those viruses have further adapted to counteract the interferon system in humans, possibly due to their more extensive circulation in mammals. That limited innate immune activation may contribute to their reduced pathogenicity along with other factors, such as differences in prior immunity.

Despite differences in virus replication and ISG induction, we observed similar levels of cell death by 96 hours postinoculation for all 3 viruses. Previous work has shown that direct virus-induced cytotoxicity is not always indicative of pathogenicity in vivo because cytotoxicity was not observed in SARS-CoV-2–infected lung organoids (*11*), despite the ability of that virus to cause severe respiratory disease. Taken together, those data suggest that epithelial-extrinsic factors, possibly related to immune activation, govern pathogenicity in vivo.

Conclusions

In summary, this study provides a characterization of virus replication and host responses to infection in human alveolar epithelium between a contemporary clade 2.3.4.4b human HPAI H5N1 isolate and the highly virulent A/Vietnam/1203/2004 virus. Further studies are warranted to understand how these viruses interact with the innate immune system,

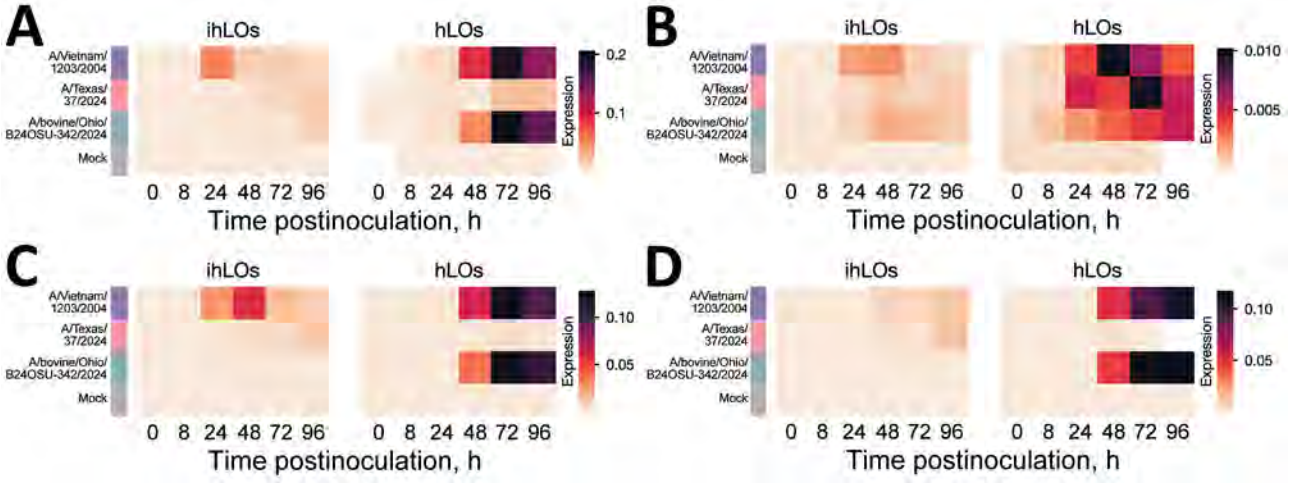

Figure 3. Induction of pro-inflammatory cytokines in a comparison of contemporary and historic highly pathogenic avian influenza A(H5N1) virus replication in human lung organoids. A) interferon β; B) tumor necrosis factor α; C) interleukin (IL) 6; D) IL-1β. iPSC-derived human lung organoids (ihLO) or adult-derived human lung organoids (hLO) were infected as described in Figure 1. We infected ihLO and hLO as described in Figure 1. We extracted RNA from 2.5 × 10^4 cells by using the QIAGEN RNeasy kit (QIAGEN, https://www.qiagen.com), following the tissue extraction instructions. We ran quantitative reverse transcription PCR by using primers (Integrated DNA Technologies, https://www.idtdna.com) to detect proinflammatory cytokines. Data were normalized to an internal control (ACTB), and expression was calculated using the $2^{-\Delta Ct}$ method, due to limited detection of proinflammatory cytokines in mock-infected samples. White cells indicate samples where PCR amplification was not detected. Mean expression for 6 ihLO and 3 hLO biologic replicates is shown. hLOs, adult stem cell–derived human lung organoids; ihLO, iPSC-derived human lung organoids; iPSCs, induced pluripotent stem cells.

particularly regarding differential ISG and proinflammatory cytokine induction, and how this affects pathogenesis in vivo. Nonetheless, our results indicate that the clade 2.3.4.4b HPAI viruses currently circulating in cattle will likely exhibit reduced human disease severity compared with historic HPAI viruses but should be closely monitored for changes that may influence pathogenicity or transmissibility.

This article was preprinted at https://doi.org/10.1101/2024.08.02.606417.

Data included in this manuscript have been deposited in Figshare (https://doi.org/10.6084/m9.figshare.26487574).

This work was supported by the Intramural Research Program of the National Institute of Allergy and Infectious Diseases, National Institutes of Health.

About the Author

Dr. Flagg is a postdoctoral fellow in the Molecular Pathogenesis Section of the Laboratory of Virology, Rocky Mountain Laboratories, National Institute of Allergy and Infectious Diseases, National Institutes of Health. Her primary interests are epithelial stem cell biology and repair during virus infection.

References

1. Elsmo EJ, Wünschmann A, Beckmen KB, Broughton-Neiswanger LE, Buckles EL, Ellis J, et al. Highly pathogenic avian influenza A(H5N1) virus clade 2.3.4.4b infections in wild terrestrial mammals, United States, 2022. Emerg Infect Dis. 2023;29:2451–60. https://doi.org/10.3201/eid2912.230464
2. Burrough ER, Magstadt DR, Petersen B, Timmermans SJ, Gauger PC, Zhang J, et al. Highly pathogenic avian influenza A(H5N1) clade 2.3.4.4b virus infection in domestic dairy cattle and cats, United States, 2024. Emerg Infect Dis. 2024;30:1335–43. https://doi.org/10.3201/eid3007.240508
3. Centers for Disease Control and Prevention. CDC confirms three human cases of H5 bird flu among Colorado poultry workers [cited 2024 Aug 2]. https://www.cdc.gov/media/releases/2024/s0725-three-human-cases-of-h5-bird-flu.html
4. Uyeki TM, Milton S, Abdul Hamid C, Reinoso Webb C, Presley SM, Shetty V, et al. Highly pathogenic avian influenza A(H5N1) virus infection in a dairy farm worker. N Engl J Med. 2024;390:2028–9. https://doi.org/10.1056/NEJMc2405371
5. Centers for Disease Control and Prevention Newsroom. CDC confirms second human H5 bird flu case in Michigan; third case tied to dairy outbreak [cited 2024 Aug 2]. https://www.cdc.gov/media/releases/2024/p0530-h5-human-case-michigan.html
6. Centers for Disease Control and Prevention. Technical report: June 2024 highly pathogenic avian influenza A(H5N1) viruses [cited 2024 Aug 2]. https://www.cdc.gov/bird-flu/php/technical-report/h5n1-06052024.html
7. Maines TR, Lu XH, Erb SM, Edwards L, Guarner J, Greer PW, et al. Avian influenza (H5N1) viruses isolated from humans in Asia in 2004 exhibit increased virulence in mammals. J Virol. 2005;79:11788–800. https://doi.org/10.1128/JVI.79.18.11788-11800.2005
8. Katsura H, Sontake V, Tata A, Kobayashi Y, Edwards CE, Heaton BE, et al. Human lung stem cell-based alveolospheres provide insights into SARS-CoV-2–mediated interferon pesponses and pneumocyte dysfunction. Cell Stem Cell. 2020;27:890–904.e8. https://doi.org/10.1016/j.stem.2020.10.005
9. Youk J, Kim T, Evans KV, Jeong YI, Hur Y, Hong SP, et al. Three-dimensional human alveolar stem cell culture models reveal infection response to SARS-CoV-2. Cell Stem Cell. 2020;27:905–919.e10. https://doi.org/10.1016/j.stem.2020.10.004
10. Jacob A, Vedaie M, Roberts DA, Thomas DC, Villacorta-Martin C, Alysandratos KD, et al. Derivation of self-renewing lung alveolar epithelial type II cells from human pluripotent stem cells. Nat Protoc. 2019;14:3303–32. https://doi.org/10.1038/s41596-019-0220-0
11. Flagg M, Goldin K, Pérez-Pérez L, Singh M, Williamson BN, Pruett N, et al. Low level of tonic interferon signalling is associated with enhanced susceptibility to SARS-CoV-2 variants of concern in human lung organoids. Emerg Microbes Infect. 2023;12:2276338. https://doi.org/10.1080/22221751.2023.2276338
12. Dobrindt K, Hoagland DA, Seah C, Kassim B, O'Shea CP, Murphy A, et al. Common genetic variation in humans impacts in vitro susceptibility to SARS-CoV-2 infection. Stem Cell Reports. 2021;16:505–18. https://doi.org/10.1016/j.stemcr.2021.02.010
13. Hien TT, Liem NT, Dung NT, San LT, Mai PP, Chau NV, et al.; World Health Organization International Avian Influenza Investigative Team. Avian influenza A (H5N1) in 10 patients in Vietnam. N Engl J Med. 2004;350:1179–88. https://doi.org/10.1056/NEJMoa040419
14. Peiris JS, Yu WC, Leung CW, Cheung CY, Ng WF, Nicholls JM, et al. Re-emergence of fatal human influenza A subtype H5N1 disease. Lancet. 2004;363:617–9. https://doi.org/10.1016/S0140-6736(04)15595-5
15. Hatta M, Hatta Y, Kim JH, Watanabe S, Shinya K, Nguyen T, et al. Growth of H5N1 influenza A viruses in the upper respiratory tracts of mice. PLoS Pathog. 2007;3:e133. https://doi.org/10.1371/journal.ppat.0030133

Address for correspondence: Emmie de Wit, National Institute of Allergy and Infectious Diseases, National Institutes of Health, 903 S 4th St, Hamilton, MT 59840, USA; email: emmie.dewit@nih.gov

Diphtheria Toxin–Producing *Corynebacterium ramonii* in Inner-City Population, Vancouver, British Columbia, Canada, 2019–2023

Christopher F. Lowe,[1] Gordon Ritchie,[1] Chiara Crestani, Miguel Imperial, Nancy Matic, Michael Payne, Aleksandra Stefanovic, Diana Whellams, Sylvain Brisse,[2] Marc G. Romney[2]

We conducted patient chart reviews and whole-genome sequencing of wound specimens containing presumptive *Corynebacterium ulcerans* from Vancouver, British Columbia, Canada, during July 2019–July 2023. Sequencing confirmed 8/14 isolates were *C. ramonii* and identified 2 distinct clusters. Molecular methods should be used to clinically differentiate potential toxin-producing *Corynebacterium* spp.

Corynebacterium ramonii, a member of the *C. diphtheriae* species complex, has recently been differentiated from *C. ulcerans* (*1*). *C. ulcerans* is associated with zoonotic transmission (predominantly from infected cats and dogs), whereas *C. ramonii* is suspected of potential human-to-human transmission; its zoonotic character has not been established (*1*). *C. ulcerans* can manifest as respiratory or cutaneous infection similar to *C. diphtheriae* (*2*,*3*). Fourteen isolates have been previously characterized as *C. ramonii* (*1*); some harbored the diphtheria toxin gene, underscoring the clinical and public health implications of correctly identifying this organism.

In Canada, where incidence of *C. ulcerans* infections is low, a 35% increase in toxin testing referrals to the National Microbiology Laboratory in Winnipeg, Manitoba, occurred during 2006–2019; twenty-two cases of *C. ulcerans* infection were identified (45% were diphtheria toxin positive) (*4*). Although multiple reports of nontoxigenic cutaneous diphtheria (caused by *C. diphtheriae*) have occurred in the inner city of Vancouver, British Columbia, only sporadic cases of toxigenic *C. ulcerans* have been reported (*5*,*6*). Because of the additional reported *C. ulcerans* cases, most of which were subsequently identified as *C. ramonii* infections, we conducted a clinical, epidemiologic, and genomic review of *C. ramonii* infections in Vancouver. The University of British Columbia/Providence Health Care Research Institute provided ethics approval for this study (approval no. H22-03695).

The Study

St. Paul's Hospital (SPH) microbiology laboratory and LifeLabs in Vancouver performed a retrospective review of all specimens collected during January 2019–July 2023 that had presumptive *C. ulcerans*, according to matrix-assisted laser desorption/ionization time-of-flight (MALDI-TOF) mass spectrometry analysis. We extracted clinical data from electronic medical records for patients seen at SPH (no clinical information was available for LifeLabs' cases), which included microbiology results, hospital course (inpatient/critical care admission), antimicrobial drugs, 30-day mortality, and risk factors for infection (housing status, substance use, and livestock/domestic animal exposure). We characterized bacterial cultures with *C. ulcerans* by using the MALDI Biotyper sirius System (Bruker,

Author affiliations: University of British Columbia, Vancouver, British Columbia, Canada (C.F. Lowe, G. Ritchie, M. Imperial, N. Matic, M. Payne, A. Stefanovic, D. Whellams, M.G. Romney); St. Paul's Hospital, Vancouver (C.F. Lowe, G. Ritchie, N. Matic, M. Payne, A. Stefanovic, M.G. Romney); Institut Pasteur–Université Paris Cité, Paris, France (C. Crestani, S. Brisse); LifeLabs, Vancouver (M. Imperial, D. Whellams); Institut Pasteur National Reference Center for Corynebacteria of the Diphtheriae Complex, Paris (S. Brisse)

DOI: https://doi.org/10.3201/eid3102.241472

[1]These first authors contributed equally to this article.

[2]These senior authors contributed equally to this article.

https://www.bruker.com) according to the manufacturer's recommendations without specific extraction. We analyzed the MALDI-TOF mass spectrometry data by using the Flex Analysis function on the MALDI Biotyper (BDAL version 12, MBT Compass Library version K). At SPH, we performed antimicrobial drug susceptibility testing by using ETEST penicillin, erythromycin, clindamycin, and vancomycin gradient strips (bioMérieux, https://www.biomerieux.com) (*7*). The National Microbiology Laboratory performed all toxin testing by using PCR and modified Elek tests. For whole-genome sequencing (WGS), we extracted DNA from isolated bacterial colonies obtained from our archives by using the MagNA Pure

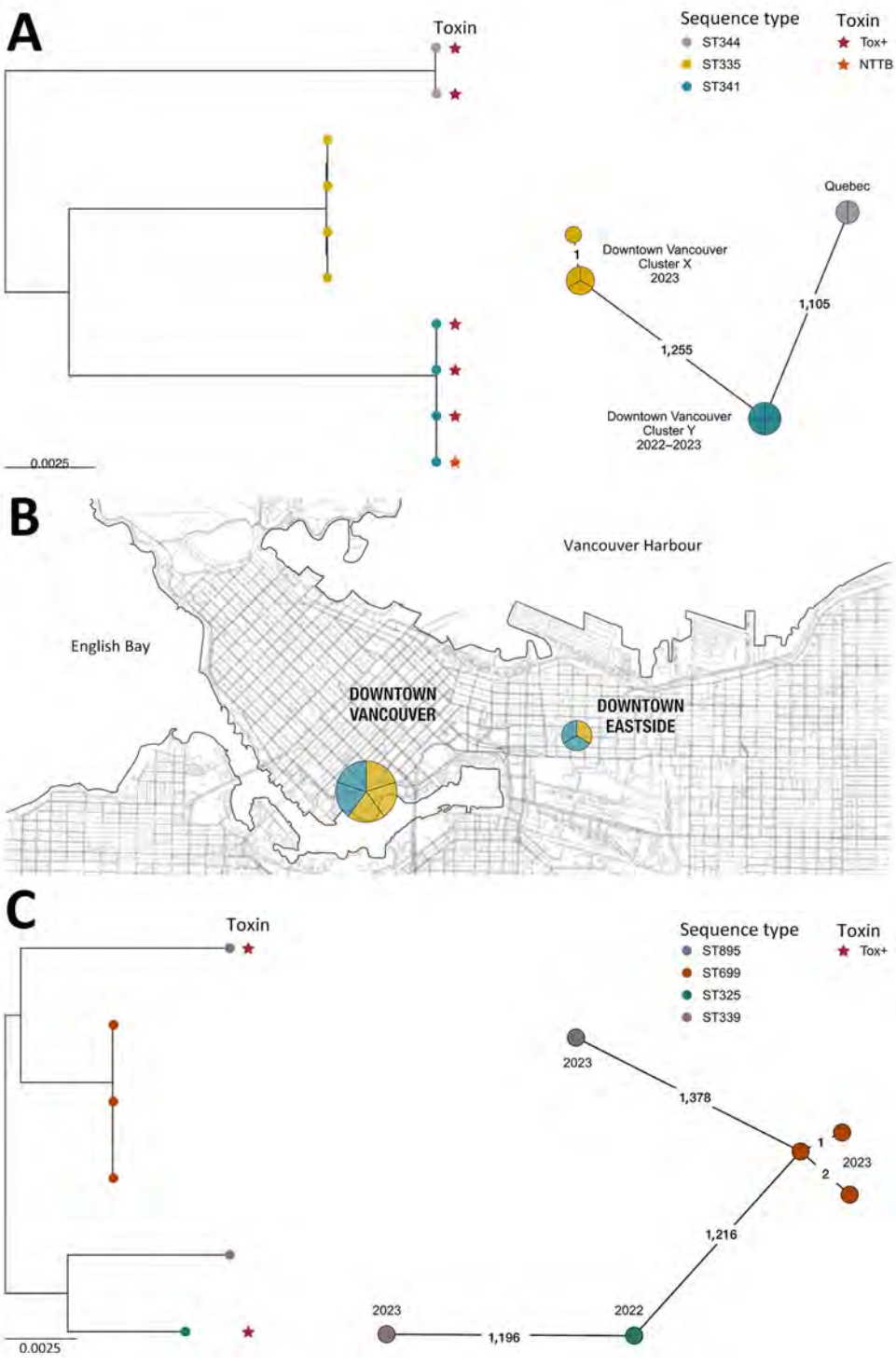

Figure. Phylogenetic analyses and location of *Corynebacterium ramonii* and *C. ulcerans* isolates in study of diphtheria toxin–producing *C. ramonii* in inner-city population, Vancouver, British Columbia, Canada, 2019–2023. Trees were rooted at midpoint. Colored circles indicate sequence type and colored stars indicate diphtheria toxin status. Numbers on lines in the spanning trees indicate number of allelic differences between sequence types; years the specimens were collected are indicated at spanning tree nodes. A) Maximum-likelihood phylogeny (left side) and minimum spanning tree (right side) of 8 *C. ramonii* isolates from this study (British Columbia) together with 2 isolates, LSPQ-04227 and LSPQ-04228, from Quebec, Canada (*1*); 2 clusters of infections can be observed, corresponding to ST335 and ST341 isolates. B) Spatial map of *C. ramonii* isolates from this study, all originating from downtown Vancouver. C) Maximum-likelihood phylogeny (left side) and minimum spanning tree (right side) of 6 *C. ulcerans* isolates from this study (British Columbia). Scale bars indicates nucleotide substitutions per site. NTTB, nontoxigenic *tox* gene–bearing; ST, sequence type; Tox+, *tox* gene and toxin both present.

Table. Antimicrobial drug susceptibility, co-isolated bacteria, and toxin test results for wound specimens containing *Corynebacterium ulcerans* and *C. ramonii* collected in Vancouver, British Columbia, Canada, 2019–2023*

Characteristics	*Corynebacterium ulcerans*, n = 6	*Corynebacterium ramonii*, n = 8
Antimicrobial drug susceptibility		
Penicillin	NA	Intermediate, n = 8
Erythromycin	NA	Susceptible, n = 8
Clindamycin	NA	Susceptible, n = 1; intermediate, n = 7
Vancomycin	NA	Susceptible, n = 8
Frequency of co-isolated bacteria from wound cultures	Enterobacterales, n = 4; MSSA, n = 3; coagulase-negative staphylococci,† n = 2; β-hemolytic *Streptococcus*,‡ n = 2; *Acinetobacter baumannii*, n = 1	β-hemolytic *Streptococcus*,§ n = 6; *Arcanobacterium hemolyticum*, n = 4; MSSA, n = 4; Enterobacterales, n = 3; yeast, n = 1; *Pasteurella multocida*, n = 1
Toxin testing, no. (%) isolates		
Nontoxigenic	4 (66.6)	4 (50.0)
Nontoxigenic, *tox* gene–bearing	0	1 (12.5)
Toxigenic	2 (33.3)	3 (37.5)

*Bacteria were isolated from wounds on lower extremities of patients. MSSA, methicillin-susceptible *Staphylococcus aureus*; NA, not applicable.
†*Staphylococcus pseudintermedius, S. lugdunensis*.
‡*Streptococcus dysgalactiae* and group G *Streptococcus*.
§*Streptococcus pyogenes, S. dysgalactiae* subspecies *equisimilis*.

24 System (Roche Diagnostics, https://diagnostics.roche.com) and sequenced those on a GridION instrument (Oxford Nanopore Technologies, https://www.nanoporetech.com) by using R10.4.1 flow cells. We performed data acquisition and base calling into fast5 files by using MinKNOW version 23.07.12 and Guppy version 6.4.6 (Oxford Nanopore Technologies) and assembled raw FASTQ files by using Flye version 2.9 (*8*). We checked genome assembly quality by using QUAST v5.2.0 and analyzed assemblies by using diphtOscan (*9*,*10*). We inferred maximum-likelihood phylogeny by using IQ-TREE version 2.3.4 and a general time reversible plus gamma model; we obtained a core gene alignment by using Panaroo version 1.5.0, visualized with Microreact (https://microreact.org/project/rgLWfs1derHFm4K5ShbxgJ-c-ramonii-and-c-ulcerans-vancouver-canada) (*11*–*13*). We obtained core genome multilocus sequence typing (cgMLST) profiles by tagging the genomes for known alleles within the BIGSdb-Pasteur database (https://bigsdb.pasteur.fr/diphtheria); we used the cgMLST_ulcerans scheme. We constructed minimum-spanning trees by using GrapeTree directly from the BIGSdb-Pasteur plug-in (*14*; C. Crestani et al., unpub. data, https://doi.org/10.1101/2024.08.22.609154).

C. ulcerans was initially identified in cultures from 14 patients (SPH, n = 9; LifeLabs, n = 5) by using MALDI-TOF mass spectrometry (scores ≥2.0). Eight of those samples had a spectral peak at 5405.40 (range 5404–5407) m/z, which is associated with *C. ramonii* (*1*). All 14 isolates underwent WGS and genotyping, confirming those 8 isolates were *C. ramonii* sequence type (ST) 335 (n = 4) and ST341 (n = 4) (Figure, panel A), originating from the inner-city Vancouver (Figure, panel B). The cgMLST results suggested 2 *C. ramonii* clusters existed; isolates in cluster X had 1 allelic mismatch, and cluster Y had no allelic mismatches (Figure, panel A). We confirmed the remaining 6/14 isolates were *C. ulcerans* (ST325, ST339, ST669 [3 isolates], and ST895) (Figure, panel C). Those 6 isolates did not originate from a specific neighborhood. All 14 cultures were polymicrobial and recovered from lower extremity wounds (Table).

Three of 8 patients with *C. ramonii* infection required admission to the hospital (average duration 6 days); critical care admissions were not required, and we observed no 30-day mortality. Toxigenic systemic signs were not observed in the 3 patients infected with diphtheria toxin-producing *C. ramonii*. Of the 6 patients who had electronic medical records, all were treated with antimicrobial drugs (piperacillin/tazobactam, amoxicillin/clavulanate, trimethoprim/sulfamethoxazole, cephalexin, cefazolin, or ceftriaxone). All 8 patients with *C. ramonii* infections were associated geographically within downtown Vancouver (Figure, panel B), including 5 persons experiencing homelessness. However, *C. ulcerans* cases were distributed throughout the city outside of downtown (according to postal codes). All patients with *C. ramonii* infections reported a history of substance use disorder, and none had documented livestock or domestic animal exposure.

Conclusions

C. ramonii cases clustered exclusively within downtown inner-city Vancouver, whereas *C. ulcerans* cases occurred outside of the city's downtown core. Human-to-human transmission of *C. ramonii* has been hypothesized (*1*), and our findings provide evidence for possible human-to-human transmission. WGS showed 2 distinct *C. ramonii* clusters (ST335 and ST341) within the same community. Vancouver's downtown core has high rates of poverty, persons experiencing homelessness, and substance abuse, and persons might transmit

bacteria via close contact, such as that observed for a previous cutaneous *C. diphtheriae* cluster (*5*). *C. ulcerans* infections are associated with zoonotic transmission; however, animal exposures were not observed for patients with *C. ramonii* infections. *C. ramonii* was identified in wounds along with other bacteria associated with human reservoirs, such as *Streptococcus pyogenes*, *S. dysgalactiae* subspecies *equisimilis*, and *Arcanobacterium hemolyticum*. The clinical manifestations of *C. ramonii* infections align more closely to those of cutaneous *C. diphtheriae* than to those of *C. ulcerans* infections (*5*).

Our study highlights the role for MALDI-TOF mass spectrometry identification of *C. ramonii*; the initial description of *C. ramonii* reported a unique peak at 5405.40 m/z (*1*). In this study, *C. ramonii* identification required WGS; however, a retrospective review of spectra confirmed the presence of the 5405.40 m/z peak, although the range was broader. MALDI-TOF mass spectrometry is used widely in clinical laboratories, and *C. ramonii* prevalence can be more accurately estimated when peak analysis of mass spectrograms is performed to avoid misidentification as *C. ulcerans*. Continual updating of MALDI-TOF mass spectrometry databases is also needed to enable accurate detection of emerging pathogens, such as *C. ramonii*. Although 16S rRNA gene sequence analysis has been increasingly used in clinical laboratories, it has not been as effective as *rpoB* gene sequence determinations for differentiating between *Corynebacterium* spp. (*1*).

The first limitation of our study is the relatively small number of cases available for analysis. Because wound cultures were polymicrobial, it is unclear to what degree *C. ramonii* contributed to wound infections. Second, we could not perform a formal case–control study; patients with *C. ulcerans* infection were primarily seen in outpatient clinics outside of our healthcare network, and complete medical records (including animal contact histories) were not accessible.

In conclusion, our findings correlate with the initial clinical description of *C. ramonii*, which appears to manifest symptoms similar to those of cutaneous *C. diphtheriae* infections. Using molecular methods, such as WGS or manual MALDI-TOF mass spectral analysis, will be needed to clinically differentiate between *C. ulcerans*, *C. ramonii*, and other members of the *C. diphtheriae* species complex.

Acknowledgments

We thank Jennifer Bilawka and Leah Gowland for their technical support and the British Columbia Centre for Disease Control Public Health Laboratory and National Microbiology Laboratory for coordinating and performing toxin tests.

Sequence data for this project are available at https://bigsdb.pasteur.fr/diphtheria, project number 30. Phylogenetic analyses of *C. ulcerans* and *C. ramonii*, together with all the relevant metadata, are available in Microreact (https://microreact.org/project/rgLWfs1derHFm4K5ShbxgJ-c-ramonii-and-c-ulcerans-vancouver-canada).

This research was funded, in part, by Institut Pasteur.

About the Author

Dr. Lowe is a medical microbiologist and infection prevention and control physician at St. Paul's Hospital in Vancouver and a clinical professor at the University of British Columbia, British Columbia, Canada. His research interests focus on molecular diagnostics, clinical virology, and the prevention of nosocomial infections.

References

1. Crestani C, Arcari G, Landier A, Passet V, Garnier D, Brémont S, et al. *Corynebacterium ramonii* sp. nov., a novel toxigenic member of the *Corynebacterium diphtheriae* species complex. Res Microbiol. 2023;174:104113. https://doi.org/10.1016/j.resmic.2023.104113
2. Otshudiema JO, Acosta AM, Cassiday PK, Hadler SC, Hariri S, Tiwari TSP. Respiratory illness caused by *Corynebacterium diphtheriae* and *C. ulcerans*, and use of diphtheria antitoxin in the United States, 1996–2018. Clin Infect Dis. 2021;73:e2799–806. https://doi.org/10.1093/cid/ciaa1218
3. Moore LSP, Leslie A, Meltzer M, Sandison A, Efstratiou A, Sriskandan S. *Corynebacterium ulcerans* cutaneous diphtheria. Lancet Infect Dis. 2015;15:1100–7. https://doi.org/10.1016/S1473-3099(15)00225-X
4. Bernard KA, Pacheco AL, Burdz T, Wiebe D. Increase in detection of *Corynebacterium diphtheriae* in Canada: 2006–2019. Can Commun Dis Rep. 2019;45:296–301. https://doi.org/10.14745/ccdr.v45i11a04
5. Chorlton SD, Ritchie G, Lawson T, Romney MG, Lowe CF. Whole-genome sequencing of *Corynebacterium diphtheriae* isolates recovered from an inner-city population demonstrates the predominance of a single molecular strain. J Clin Microbiol. 2020;58:e01651-19. https://doi.org/10.1128/JCM.01651-19
6. Dewinter LM, Bernard KA, Romney MG. Human clinical isolates of *Corynebacterium diphtheriae* and *Corynebacterium ulcerans* collected in Canada from 1999 to 2003 but not fitting reporting criteria for cases of diphtheria. J Clin Microbiol. 2005;43:3447–9. https://doi.org/10.1128/JCM.43.7.3447-3449.2005
7. Clinical and Laboratory Standards Institute. Methods for antimicrobial dilution and disk susceptibility testing of infrequently isolated or fastidious bacteria; third edition (M45). Wayne (PA): The Institute; 2015.
8. Kolmogorov M, Yuan J, Lin Y, Pevzner PA. Assembly of long, error-prone reads using repeat graphs. Nat Biotechnol. 2019;37:540–6. https://doi.org/10.1038/s41587-019-0072-8
9. Gurevich A, Saveliev V, Vyahhi N, Tesler G. QUAST: quality assessment tool for genome assemblies. Bioinformatics. 2013;29:1072–5. https://doi.org/10.1093/bioinformatics/btt086

10. Hennart M, Crestani C, Bridel S, Armatys N, Brémont S, Carmi-Leroy A, et al. A global *Corynebacterium diphtheriae* genomic framework sheds light on current diphtheria re-emergence. Peer Community J. 2023;3:e76. https://doi.org/10.24072/pcjournal.307
11. Nguyen L-T, Schmidt HA, von Haeseler A, Minh BQ. IQ-TREE: a fast and effective stochastic algorithm for estimating maximum-likelihood phylogenies. Mol Biol Evol. 2015;32:268–74. https://doi.org/10.1093/molbev/msu300
12. Tonkin-Hill G, MacAlasdair N, Ruis C, Weimann A, Horesh G, Lees JA, et al. Producing polished prokaryotic pangenomes with the Panaroo pipeline. Genome Biol. 2020;21:180. https://doi.org/10.1186/s13059-020-02090-4
13. Argimón S, Abudahab K, Goater RJE, Fedosejev A, Bhai J, Glasner C, et al. Microreact: visualizing and sharing data for genomic epidemiology and phylogeography. Microb Genomics. 2016;2:e000093. PubMed https://doi.org/10.1099/mgen.0.000093
14. Zhou Z, Alikhan N-F, Sergeant MJ, Luhmann N, Vaz C, Francisco AP, et al. GrapeTree: visualization of core genomic relationships among 100,000 bacterial pathogens. Genome Res. 2018;28:1395–404. https://doi.org/10.1101/gr.232397.117

Address for correspondence: Christopher F. Lowe, St. Paul's Hospital, 1081 Burrard St, Vancouver, BC V6Z 1Y6, Canada; email: christopher.lowe@ubc.ca

January 2024

Fastidious Bacteria

- Efficacy of Unregulated Minimum Risk Products to Kill and Repel Ticks
- *Auritidibacter ignavus*, an Emerging Pathogen Associated with Chronic Ear Infections
- Incidence of Legionnaires' Disease among Travelers Visiting Hotels in Germany, 2015–2019
- Early-Onset Infection Caused by *Escherichia coli* Sequence Type 1193 in Late Preterm and Full-Term Neonates
- Molecular Evolution and Increasing Macrolide Resistance of *Bordetella pertussis*, Shanghai, 2016–2022
- Disease-Associated *Streptococcus pneumoniae* Genetic Variation
- Effect of 2020–21 and 2021–22 Highly Pathogenic Avian Influenza H5 Epidemics on Wild Birds,the Netherlands
- COVID-19–Related School Closures, United States, July 27, 2020–June 30, 2022
- Effectiveness of Vaccines and Antiviral Drugs in Preventing Severe and Fatal COVID-19, Hong Kong
- Costs of Digital Adherence Technologies for Tuberculosis Treatment Support, 2018–2021
- Doxycycline Prophylaxis for Skin and Soft Tissue Infections in Naval Special Warfare Trainees, United States
- Emergence of Novel Norovirus GII.4 Strainson 3 Continents

- Predictive Mapping of Antimicrobial Resistance for *Escherichia coli*, *Salmonella*, and *Campylobacter* in Food-Producing Animals in Europe, 2000–2021
- Population-Based Study of Pertussis Incidence and Risk Factors among Persons >50 Years of Age, Australia
- Racial and Ethnic Disparities in Tuberculosis Incidence, Arkansas, USA, 2010–2021
- Reemergence of Human African Trypanosomiasis Caused by *Trypanosoma brucei* rhodesiense, Ethiopia
- *Helicobacter fennelliae* Localization to Diffuse Areas of Human Intestine, Japan
- Genomic Diversity and Zoonotic Potential of *Brucella neotomae*
- Tuberculosis Diagnostic Delays, Hospital Admissions, and Treatment Outcomes for Persons Also Diagnosed with COVID-19 within 120 Days in California, 2020
- Respiratory Viruses in Wastewater Compared with Clinical Samples, Leuven, Belgium
- Excess Deaths Associated with Rheumatic Heart Disease, Australia, 2013–2017
- Delayed *Plasmodium falciparum* Malaria in Pregnant Patient with Sickle Cell Trait 11 Years after Exposure, Oregon, United States
- Increased Peripheral Venous Catheter Bloodstream Infections during the COVID-19 Pandemic, Switzerland
- Avian Influenza A(H5N1) Neuraminidase Inhibition Antibodies in Healthy Adults after Exposure to Influenza A(H1N1)pdm09
- Clade I–Associated Mpox Cases Associated with Sexual Contact, the Democratic Republic of the Congo
- Macacine Alphaherpesvirus 1 (B Virus) Infection in Humans, Japan, 2019
- Estimation of Incubation Period of Mpox during 2022 Outbreak in Pereira, Colombia
- Autochthonous Dengue Fever in 2 Patients, Rome, Italy
- *Pseudomonas guariconensis* Necrotizing Fasciitis, United Kingdom

EMERGING INFECTIOUS DISEASES®

To revisit the January 2024 issue, go to:
https://wwwnc.cdc.gov/eid/articles/issue/30/1/table-of-contents

Bacteremia and Community-Acquired Pneumonia Caused by *Pantoea stewartii* Subspecies *indologenes*, Australia

Lawrence Huang, Erin P. Price, Derek S. Sarovich, Dean Johns, Shradha Subedi

We report infection with the phytopathogen *Pantoea stewartii* subspecies *indologenes* in a macadamia farmer from southeast Queensland, Australia. The patient had bloodstream infection and pneumonia develop after an unidentified inoculation event. Investigation determined that the most likely mode of transmission was inhalation from an environmental source on the farm.

Pantoea species are ubiquitous bacteria in both terrestrial and aquatic environments and have been isolated in animals, insects, and humans, although most of the 31 recognized species (*1*) are associated with plants (*2*). *Pantoea* species previously reported in human infections include *P. agglomerans*, *P. ananatis*, *P. brenneri*, *P. calida*, *P. conspicua*, *P. dispersa*, *P. eucrina*, and *P. septica*; *P. agglomerans* has been the most common (*2*).

P. stewartii, the cause of Stewart's wilt in sweet corn and maize, was first discovered in the late 1890s. Researchers proposed 2 subspecies in 1993 based on host range: *stewartii* and *indologenes* (*3*). Unlike subspecies *stewartii*, subspecies *indologenes* is nonpathogenic to corn, instead causing disease in other agronomically significant crops, such as foxtail millet, pearl millet, and onions. Because of the risk this organism (particularly subspecies *stewartii*) poses to economically critical crops, many countries classify *P. stewartii* as a quarantine organism (*4*,*5*).

Author affiliations: Sunshine Coast University Hospital, Birtinya, Queensland, Australia (L. Huang, D. Johns, S. Subedi); University of the Sunshine Coast Centre for Bioinnovation, Sippy Downs, Queensland, Australia (E.P. Price, D.S. Sarovich); Sunshine Cost Health Institute, Birtinya (E.P. Price, D.S. Saraovich, S. Subedi); The University of Queensland Centre for Clinical Research, Brisbane, Queensland, Australia (S. Subedi)

DOI: https://doi.org/10.3201/eid3102.240546

In 2022, researchers reported infection with *P. stewartii* in a human, initially identifying the species with moderate confidence as *P. septica* but then recategorizing the species designation based on 16S ribosomal RNA gene sequencing (*1*). We report phytopathogen *P. stewartii* subsp. *indologenes* infection in a macadamia farmer from southeast Queensland, Australia.

The Study

In summer 2021, an 82-year-old man sought care at the emergency department of Sunshine Coast University Hospital (Birtinya, QLD, Australia), for sudden onset of fever, myalgia, arthralgia, nonproductive cough, and shortness of breath. The patient had recently moved to a macadamia farm in the Sunshine Coast hinterland and had previously resided on a pineapple farm in the same region for several decades. He reported no overseas travel history, no preceding history of inoculating injury from plant material, no recent skin wounds or infections, and no direct zoonotic contacts. Chest radiograph (Figure 1, panel A) identified moderately severe community-acquired multilobar pneumonia, with dense consolidation in the left upper lobe. The patient deteriorated rapidly because of septic shock, necessitating intubation and ventilation, and was transferred to the intensive care unit on day 1 of admission.

We observed lactose-fermenting, nonmucoid, yellow-pigmented colonies cultivated on MacConkey and horse blood agars (Figure 2) from blood culture (isolate SCHI0154.S.1), tracheal aspirate, and bronchial washing specimens. We determined the colonies to be catalase positive, oxidase negative, and spot indole positive. VITEK MS matrix-assisted laser desorption/ionization time-of-flight mass spectrometry (bioMérieux, https://www.biomerieux.com) revealed *P. ananatis* with 99.9% probability. The VI-

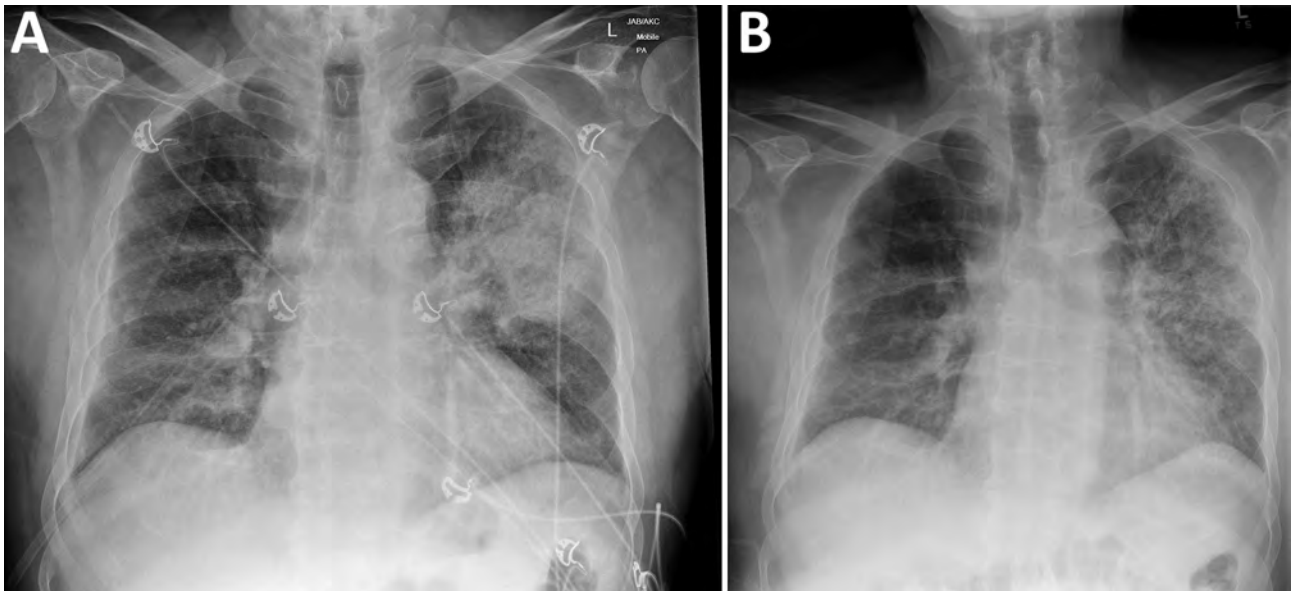

Figure 1. Chest radiographs of patient with *Pantoea stewartii* subspecies *indologenes* infection, Queensland, Australia. A) Radiograph at time of initial emergency department visit, showing dense left upper lobe consolidation consistent with pneumonia. B) Repeat radiograph on day 12 of hospital admission, showing resolving left upper and middle zone opacification.

TEK GN ID card identified the respiratory isolates as *Pantoea* sp. with 95% probability. SCHI0154.S.1 was resistant to ampicillin (MIC = 16 mg/L) and cephazolin (MIC ≥64 mg/L) but susceptible to amoxicillin/clavulanate (MIC ≤2 mg/L), ceftriaxone (MIC ≤1 mg/L), ciprofloxacin (MIC ≤0.25 mg/L), gentamicin (MIC ≤1 mg/L), meropenem (MIC ≤0.25 mg/L), piperacillin/tazobactam (MIC = 2 mg/L), and trimethoprim/sulfamethoxazole (MIC ≤20 mg/L).

We treated the patient with intravenous amoxicillin/clavulanate (2.2 g/8 h) for a total of 10 days and successfully extubated him on day 7. Chest radiograph opacification on day 12 showed improvements (Figure 1, panel B). At outpatient follow-up, the patient had reached full recovery.

To permit accurate speciation and genetic comparison with other *Pantoea* isolates, we compared Illumina NovaSeq 2 × 150-bp whole-genome sequencing reads generated for SCHI0154.S.1 (Australian Centre for Ecogenomics, St Lucia, Queensland, Australia) against 26 *Pantoea* spp. reference genomes (Appendix Table, https://wwwnc.cdc.gov/EID/article/31/2/24-0546-App1.pdf). We then analyzed those sequencing results against 48 publicly available *P. stewartii* genomes (Appendix Table). We carried out phylogenomic reconstruction of orthologous, biallelic single-nucleotide polymorphisms by using default SPANDx v4.0.3 (*6*) settings and PAUP* v4.0a.168 (*7*). We performed bootstrapping using 1,000 re-samples on the *P. stewartii* tree to assess clade confidence. We visualized trees in FigTree v1.4.0. We deposited the SCHI0154.S.1 assembly into GenBank (accession no. GCA_030144305.1).

Phylogenomic analysis revealed that SCHI0154.S.1 was most closely related to *P. stewartii* subsp. *indologenes* PANS 07–14 (Appendix Figure), which was isolated from a Verbena plant on an onion farm in Georgia, USA, in 2007 (*8*). SCHI0154.S.1 and PANS 07–14 differed by 1,015 single-nucleotide polymorphisms. In contrast, the only other genome-sequenced *P. stewartii* isolate from Australia, C10109_Jinnung (also subsp. *indologenes*), retrieved from a sick, captive western ground parrot (*Pezoporus flaviventris*), at Perth Zoo (Perth, WA, Australia) in 2021 (*9*), differed from SCHI0154.S.1 by 27,876 single-nucleotide polymorphisms.

One previous study reported *P. stewartii* associated with a human infection, with taxonomic assignment based on genetic similarity analysis of an unpublished 1,212-bp 16S ribosomal RNA amplicon reported to be 99.69% similar to *P. stewartii* strain 08BF11TN (GenBank accession KX146472.1) (*1*). To confirm this result, we repeated an 'All genomes' National Center for Biotechnology Information BLAST v2.15.0+ (https://blast.ncbi.nlm.nih.gov) analysis of the 1,451-bp KX146472.1 sequence on August 16, 2024, using both the 'Complete, Microbes' and 'Draft, Microbes' databases. We restricted search parameters to '*Pantoea* (taxid:53335)' and 'megablast'. Our BLAST analysis found a closer match to *P. agglomerans* 33.1 (accession no. NZ_CP083809.1; 99.45% identity and 100% query coverage) than to *P. stewartii* RON18713

Figure 2. Results of blood culture for patient with *Pantoea stewartii* subspecies *indologenes* infection, Queensland, Australia. Yellow pigmented colonies grew on horse blood agar on day 1 of subculture after incubation in 5% CO_2 at 35°C. VITEK MS matrix-assisted laser desorption/ionization time-of-flight mass spectrometry (bioMérieux, https://www.biomerieux.com) identified the pathogen as *Pantoea ananatis* with 99.9% probability, but comparitive gene analysis revealed that the pathogen was most closely related to *P. stewartii* subsp. *indologenes*.

(accession no. NZ_CP116285.1; 98.07% identity and 100% query coverage) using the 'Complete, Microbes' genome database. Similarly, the same BLAST search using the 'Draft, Microbes' genome database identified a closer match to *P. vagans* 848 (accession no. JUQR01000382.1; 99.79% identity and 100% query coverage) and *P. septica* FF5 (accession no. CCAQ010000001.1; 99.72% identity and 100% query coverage) than to *P. stewartii* (best hit was strain RSA36 [accession no. LDSK01000027.1]; 98.00% identity and 100% coverage).

Conclusions

This unusual case confirms that the phytopathogen *P. stewartii* can cause life-threatening infections in humans. Although 1 published study described *P. stewartii* bacteraemia after a poststroke stent implantation in a patient from Spain (*1*), our repeat analysis suggested that this previously reported case was more likely caused by *P. septica* or *P. agglomerans*.

Because almost nothing is known about *P. stewartii* disease in humans or potential virulence factors of *P. stewartii* and its subspecies, this organism might be clinically underdiagnosed by current diagnostic methods, being misidentified as other more familiar *Pantoea* species. In support of this hypothesis, previously described *P. agglomerans* clinical isolates deposited into type culture collections have been reclassified as *P. ananatis*, *Erwinia* spp., or *Enterobacter* spp. on the basis of housekeeping gene sequencing (*10*). Further complicating matters, many taxonomic reassignments have occurred within the Erwiniaceae family in recent decades, making it challenging to track potential historical reports of *P. stewartii* human infection.

In our study, once the farmer's infection was confirmed to be *P. stewartii*, we conducted a subsequent thorough clinical history to determine the likely source and mode of transmission. The patient reported no previous history of travel outside of Australia or recent injuries suggestive of dissemination from skin inoculation.

We noted just 1 previously report of *P. stewartii* in Australia, detected in a critically endangered native parrot that fell gravely ill in captivity (*9*), suggesting that birds may represent an underappreciated reservoir for *P. stewartii* subsp. *indologenes* global dissemination. However, in that case, the authors reported a link to parrot pellets commercially imported from the United States (*9*). It is therefore possible that *P. stewartii* was introduced into eastern Australia, and then to our patient's macadamia farm, through a commercially imported agricultural product originating from the United States. In our study, although we could not determine the precise source of infection from the research conducted, the farmer's clinical features (i.e., pneumonia with subsequent hematogenous dissemination), lack of clear inoculation source, and limited travel suggested the most likely mode of transmission to be inhalation from an environmental source on the farm.

Acknowledgments

We wish to thank Rhys White for helpful discussions on *Pantoea stewartii* genomics.

About the Author

Dr. Subedi is an infectious diseases physician, a clinical microbiologist, and a PhD candidate at the University of Queensland Centre for Clinical Research. Her main research interests include evaluation and implementation of new and innovative methods of diagnosis of infection.

References

1. Cobo F, González A, Pérez-Carrasco V, García-Salcedo JA. *Pantoea stewartii*: a new pathogen as a cause of bacteremia? Enferm Infecc Microbiol Clin (Engl Ed). 2022; 40:278–80. https://doi.org/10.1016/j.eimce.2021.03.005

2. Walterson AM, Stavrinides J. *Pantoea*: insights into a highly versatile and diverse genus within the Enterobacteriaceae. FEMS Microbiol Rev. 2015;39:968–84. https://doi.org/10.1093/femsre/fuv027
3. Mergaert J, Verdonck L, Kersters K. Transfer of *Erwinia ananas* (synonym, Erwinia uredovora) and *Erwinia stewartii* to the genus *Pantoea* emend. as *Pantoea ananas* (Serrano 1928) comb. nov. and *Pantoea stewartii* (Smith 1898) comb. nov., respectively, and description of *Pantoea stewartii* subsp. *indologenes* subsp. nov. Int J Syst Bacteriol. 1993;43:162–73. https://doi.org/10.1099/00207713-43-1-162
4. Pataky J. Pest risk analysis: the risk of introducing *Erwinia stewartii* in maize seed [cited 2025 Apr 15]. https://worldseed.org/wp-content/uploads/2015/10/Erwinia_stewartii.pdf
5. Bragard C, Dehnen-Schmutz K, Di Serio F, Gonthier P, Jacques MA, Jaques Miret JA, et al.; EFSA Panel on Plant Health (PLH). Risk assessment of the entry of *Pantoea stewartii* subsp. *stewartii* on maize seed imported by the EU from the USA. EFSA J. 2019;17:e05851.
6. Sarovich DS, Price EP. SPANDx: a genomics pipeline for comparative analysis of large haploid whole genome re-sequencing datasets. BMC Res Notes. 2014;7:618. https://doi.org/10.1186/1756-0500-7-618
7. Swofford DL. PAUP*. Phylogenetic Analysis Using Parsimony (*and Other Methods). Version 4.0. Sunderland (MA): Sinauer Associates; 2003.
8. Koirala S, Zhao M, Agarwal G, Gitaitis R, Stice S, Kvitko B, et al. Identification of two novel pathovars of *Pantoea stewartii* subsp. *indologenes* affecting *Allium* sp. and millets. Phytopathology. 2021;111:1509–19. https://doi.org/10.1094/PHYTO-11-20-0508-R
9. White RT, Taylor W, Klukowski N, Vaughan-Higgins R, Williams E, Petrovski S, et al. A discovery down under: decoding the draft genome sequence of *Pantoea stewartii* from Australia's critically endangered western ground parrot/kyloring (*Pezoporus flaviventris*). Microb Genom. 2023;9:001101. https://doi.org/10.1099/mgen.0.001101
10. Rezzonico F, Smits TH, Montesinos E, Frey JE, Duffy B. Genotypic comparison of *Pantoea agglomerans* plant and clinical strains. BMC Microbiol. 2009;9:204. https://doi.org/10.1186/1471-2180-9-204

Address for correspondence: Shradha Subedi, University of Queensland Centre for Clinical Research, Bld 71/918 Rbwh Herston, Brisbane, QLD 4029, Australia; email: s.subedi@uqconnect.edu.au

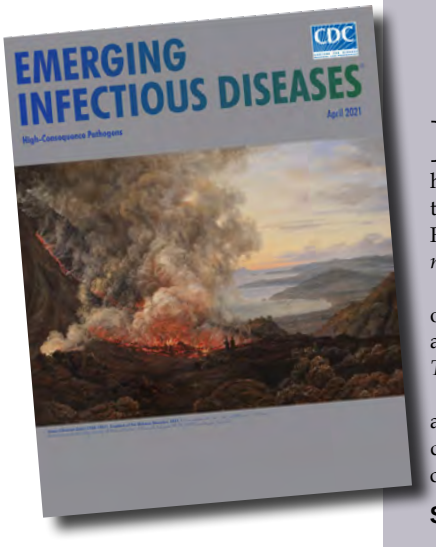

Originally published in April 2021

etymologia revisited

Treponema

[trep″o-ne′mə]

From the Greek *trepo* (rotate, turn) and *ne¯ma* (thread), *Treponema* is a genus of gram-negative, anaerobic or microaerophilic bacteria. They are spiral-shaped and have flagella, which extend from motors at the pole, producing undulating movement through fluids, enabling tissue invasion and dissemination. In 1905, microbiologist Fritz Richard Schaudinn and dermatologist Paul Erich Hoffmann described *Treponema pallidum* subsp. *pallidum* as *Spirochaeta pallida* from a fresh human vulvar lesion.

Treponema spp. can invade the epidermis and oral, intestinal, and genital mucosa of humans and animals. They cause human diseases, such as syphilis, yaws, pinta, and bejel, and animal diseases, such as digital dermatitis. *T. phagedenis*, *T. pedis*, and *T. medium* infect mainly cattle. *T. paraluiscuniculi* can cause syphilis in rabbits.

Most *Treponema* spp. are not cultivable, except for *T. palllidum* subsp. *pallidum* and *T. phagedenis*. *T. pallidum* subsp. *pallidum* causative syphilis is a reemerging disease in industrialized countries. Digital dermatitis, a polytreponemal disease, is considered to be the major infectious claw disease in cattle worldwide.

Sources

1. Dorland's illustrated medical dictionary. 32nd ed. Philadelphia: Elsevier Saunders; 2012.
2. Edmondson DG, Hu B, Norris SJ. Long-term in vitro culture of the syphilis spirochete *Treponema pallidum* subsp. *pallidum*. MBio. 2018;9:e01153. https://doi.org/10.1128/mBio.01153-18
3. Nally JE, Hornsby RL, Alt DP, Whitelegge JP. Phenotypic and proteomic characterization of treponemes associated with bovine digital dermatitis. Vet Microbiol. 2019;235:35–42. https://doi.org/10.1016/j.vetmic.2019.05.023
4. Oriel JD. The scars of Venus: a history of venereology. London: Springer-Verlag; 1994.
5. Šmajs D, Zobaníková M, Strouhal M, Čejková D, Dugan-Rocha S, Pospíšilová P, et al. Complete genome sequence of *Treponema paraluiscuniculi*, strain Cuniculi A: the loss of infectivity to humans is associated with genome decay. PLoS One. 2011;6:e20415. https://doi.org/10.1371/journal.pone.0020415

https://wwwnc.cdc.gov/eid/article/27/4/et-2704_article

Acute Q Fever Patients Requiring Intensive Care Unit Support in Tropical Australia, 2015–2023

Cody Price,[1] Simon Smith, Jim Stewart, Josh Hanson

Acute Q fever is classically described as a mild illness. We report 9 patients with acute Q fever in Queensland, Australia, who required intensive care unit support to survive. Clinicians should consider an acute Q fever diagnosis and its empirical treatment in critically ill persons in the appropriate clinical context.

Q fever, a zoonotic bacterial disease caused by *Coxiella burnetii*, has a global distribution (*1*). Most acute *C. burnetii* infections are asymptomatic or manifest as a self-limiting, nonspecific febrile illness. Respiratory and gastrointestinal symptoms can also occur, which might necessitate hospitalization, but severe, life-threatening acute disease is reported rarely (*1*,*2*). In 1 large study, only 3 (0.2%) of 1,806 patients with acute Q fever died; 2 of those deaths were because of underlying malignancy (*2*). We report the cases of 9 patients from Queensland in tropical Australia with laboratory-confirmed acute Q fever who required intensive care unit (ICU) support to survive their infection. The Far North Queensland Human Research Ethics Committee provided ethics approval for the study (approval no. EX/2023/QCH/95302–1707QA). Because the retrospective data were deidentified, the committee waived the requirement for informed consent.

The Study

Q fever is a notifiable disease in Australia. We used Queensland's notifiable conditions database and electronic laboratory reporting system to identify all cases of acute Q fever in the Far North Queensland (FNQ) region during January 1, 2015–December 31, 2023. We only included cases meeting definitive laboratory criteria for acute Q fever: positive PCR or seroconversion or ≥4-fold increase in antibody titer to phase II antigen in paired serum samples (*3*). We recorded the patients' demographic data and clinical, laboratory, and radiologic findings. We used the Charlson Comorbidity Index to quantify comorbidity; severe comorbidity was defined as a score of ≥5 (*4*). For patients with available data, we recorded the Queensland Adult Deterioration Detection System score, a vital signs–based early warning score, which was calculated when patients were first seen (*5*). We performed statistical analysis using Stata 18.0 (Stata, https://www.stata.com) and compared groups by using logistic regression and the Wilcoxon rank-sum, χ^2, and Fisher exact tests, as appropriate.

A total of 223 cases of Q fever in the FNQ region were reported to the notifiable diseases database during the study period; 127/223 (57%) patients sought care at a hospital in the region, 105/127 (83%) were admitted as inpatients, and 9/105 (9%) were admitted to the ICU (Table 1). Eight (89%) of the 9 patients requiring ICU admission lived in a rural location. None of the 9 patients had classical occupational exposure history, and none were known to be vaccinated against Q fever; 8/9 (89%) reported close contact with animals. Eight (89%) of 9 were >50 years of age, but only 1 (11%) had severe comorbidity. Only 1/9 (11%) was first seen within 7 days of symptom onset, but 7/9 (78%) had been prescribed antimicrobial drug therapy with activity against *C. burnetii* for ≥24 hours before their ICU admission. One otherwise healthy 55-year-old woman had received doxycycline for 4 days before her ICU admission (Appendix Table 1, https://wwwnc.cdc.gov/EID/article/31/2/24-0422-App1.pdf).

Author affiliations: Cairns Hospital, Cairns, Queensland, Australia (C. Price, S. Smith, J. Stewart, J. Hanson); University of New South Wales, Sydney, New South Wales, Australia (J. Hanson)

DOI: https://doi.org/10.3201/eid3102.240422

[1]Current affiliation: Royal Hobart Hospital, Hobart, Tasmania, Australia.

Table 1. Demographic and clinical characteristics of patients in study of acute Q fever infections requiring intensive care unit support in tropical Australia, 2015–2023*

Variable	Total no. patients with data†	All patients	Required ICU admission, n = 9	No ICU admission required, n = 118	p value
Median age, y (IQR)	127	54 (44–65)	60 (53–69)	54 (43–64)	0.14
Patient sex					
M	127	96 (76)	6 (67)	90 (76)	0.69
F	127	31 (24)	3 (33)	28 (24)	0.69
First Nations Australian‡	127	12 (9)	3 (33)	9 (8)	0.04
Rural residence	127	106 (84)	8 (89)	99 (84)	1.0
Vaccinated against *Coxiella burnetii*	58	0	0	0	NA
Immunocompromised	127	5 (4)	0	5 (4)	1.0
Pregnant female patients	31	0	0	0	NA
Median initial symptom duration, d (IQR)	124	5 (3–7)	7 (7–8)	5 (3–7)	0.055
Supplemental oxygen required§	57	6 (11)	2 (22)	4/48 (8)	0.24
Median systolic blood pressure,§ mm Hg (IQR)	57	130 (120–141)	122 (100–136)	131 (123–141)	0.051
Median heart rate,§ beats/min (IQR)	57	94 (77–104)	100 (90–115)	93 (74–104)	0.14
Median body temperature,§ °C (IQR)	57	37.4 (36.8–38.4)	37.2 (36.8–37.8)	37.9 (36.7–38.6)	0.71
Impaired consciousness§	56	0	0	0/47	NA
Early warning score (Q-ADDS)¶	57	2 (1–4)	4 (2–8)	2 (1–3)	0.01
Hepatitis#	127	79 (62)	2 (22)	77 (65)	0.03
Both hepatitis and pneumonia#**	127	33 (26)	6 (67)	28 (24)	0.01
Elevated cardiac biomarkers	21	6 (29)	2/6 (33)	4/15 (27)	1.0
Abnormal chest radiograph§	104	27 (26)	5 (56)	22/95 (23)	0.049
Died	127	0	0	0	NA

*Values are no. (%) except as indicated. p values compare the number of patients requiring ICU admission with the number of patients not requiring ICU admission for each variable. IQR, interquartile range; NA, not applicable; Q-ADDS, Queensland Adult Deterioration Detection System.
†Retrospective nature of this study precluded collection of complete data for each variable, especially for vital signs reported when the patient was first seen.
‡All patients seeking care in the Australia public health system are asked whether they identify as a First Nations Australian (Aboriginal or Torres Strait Islander).
§When patients were first seen.
¶Early warning score using vital signs, calculated on initial review.
#Hepatitis defined as a peak of elevated transaminase enzymes >2 times the upper limit of reference range during the patient's illness.
**Pneumonia defined as dyspnea, cough, or hemoptysis or radiographic abnormalities.

The small sample size and retrospective nature of the study precluded detailed statistical analysis; however, patients requiring ICU care were more likely to have multiorgan involvement (odds ratio [OR] 5.42 [95% CI 1.21–24.31]; p = 0.03), an abnormal chest radiograph (OR 4.15 [95% CI 1.02–16.80]; p = 0.046), and an elevated early warning score (OR 5.42 [95% CI 1.21–24.31]; p = 0.03) when they were first seen (Tables 1, 2). Testing for serum antiphospholipid antibodies was performed for only 1 ICU patient (case no. 5) (Appendix); the result was positive. Three patients not requiring ICU care had serum samples tested for antiphospholipid antibodies; 1 result was negative, and 2 results were borderline positive.

The actual diagnosis of Q fever in the 9 patients requiring ICU admission was often delayed or even retrospective. Initial serologic results suggested acute Q fever in only 3/9 (33%) patients; those results were negative for 5/9 (55%) and suggested previous *C. burnetii* infection in 1/9 (11%) (Appendix Table 2). Serum PCR was positive in every case that was tested with this method; however, access to those PCR results was often delayed because testing was performed by the statewide reference laboratory, which was 1,390 km away. Indeed, 2 ICU patients were discharged from the hospital before their Q fever diagnosis was confirmed, and both patients received less than the recommended 14 days of antimicrobial drug therapy (7 and 10 days) (*6*).

The 9 patients were in the ICU for a median of 3 (interquartile range 2–5) days; 6/9 (67%) required vasopressor support for hypotension and 1/9 (11%) required mechanical ventilation (Figure), whereas 2/9 (22%) needed no organ support but required monitoring of multiorgan dysfunction (Appendix, Table 1). No patient admitted to ICU required renal replacement therapy. Indeed, for a critically ill population, the patients' renal function was remarkably preserved; the highest recorded serum creatinine in any of the 9 patients during their hospitalization was 123 μmol/L (Appendix Table 3).

Patients requiring ICU admission spent a median of 11 (interquartile range 8–18) days in the hospital. All 9 ICU patients survived to hospital discharge, and none have subsequently received a diagnosis of chronic Q fever, although follow-up serologic testing has been performed for only 4/9 (44%) (Appendix). One patient required the insertion of a permanent

Table 2. Laboratory findings when patients were first seen in study of acute Q fever infections requiring intensive care unit support in tropical Australia, 2015–2023*

Variable	No. patients with data†	All patients, n = 127	Required ICU admission, n = 9	ICU admission not required, n = 118	p value
Hemoglobin, g/dL	127	144 (133–155)	157 (133–163)	144 (133–154)	0.21
Leukocyte count, × 10^9 cells/L	127	5.4 (4.0–6.9)	6.1 (5.4–7.7)	5.3 (4.0–6.8)	0.08
Neutrophil count, × 10^9 cells/L	127	3.9 (2.7–5.2)	4.8 (4.1–5.9)	3.7 (2.5–5.0)	0.04
Platelet count, × 10^9/L	137	120 (83–165)	93 (46–148)	121 (85–166)	0.14
Sodium, mmol/L	127	132 (130–135)	125 (125–133)	132 (130–135)	0.02
Potassium, mmol/L	127	3.9 (3.6–4.1)	4.0 (3.6–4.1)	3.9 (3.6–4.2)	0.74
Creatinine, μmol/L	127	84 (71–98)	86 (75–103)	84 (71–97)	0.51
Alanine aminotransferase, IU/L	127	103 (64–175)	125 (53–162)	102 (64–177)	0.97
Aspartate aminotransferase, IU/L	127	102 (71–167)	164 (56–251)	101 (72–165)	0.31
Total bilirubin, μmol/L	127	16 (10–22)	20 (16–58)	16 (10–22)	0.07
Serum alkaline phosphatase, IU/L	127	91 (70–149)	124 (93–172)	88 (68–148)	0.06
Gamma-glutamyl transferase, IU/L	127	78 (36–164)	107 (48–272)	75 (36–152)	0.33
Lactate dehydrogenase, IU/L	124	456 (364–604)	394 (356–673)	456 (362–593)	0.94
Prothrombin time, s	47	14 (12–15)	15 (13–17)	13 (12–15)	0.17
Activated partial thromboplastin time, s	46	32 (29–36)	35 (29–40)	31 (29–36)	0.30
Fibrinogen, g/L	46	4.1 (3.2–4.8)	3.6 (2.6–4.6)	4.2 (3.4–4.8)	0.13
Ferritin, μg/L	19	1,160 (835–2,065)	5,340 (2,260–8,420)	1,035 (752–1,678)	0.07
C-reactive protein, mg/L	115	133 (84–180)	158 (61–236)	132 (85–179)	0.64

*Values are median (interquartile range) except as indicated. p values compare the number of patients requiring ICU admission with the number of patients not requiring ICU admission for each variable. IU, international units.
†The retrospective nature of the study precluded the collection of complete data for all cases.

pacemaker for atrioventricular block 8 months after his hospital admission, although this need was considered to be unrelated to his *C. burnetii* infection.

Conclusions

Acute Q fever is classically thought to be a mild illness; however, 9/223 (4%) patients with a confirmed acute infection in the FNQ region of Australia required ICU care to survive their infection. Severe disease in those 9 patients might be explained by a delay in seeking medical care and in appropriate antimicrobial drug therapy; only 1 patient sought care within 7 days of symptom onset, and only 4 received antimicrobial drugs with activity against *C. burnetii* when they were first seen. The delay in effective therapy was partly explained by a lack of timely access to PCR results, which might have expedited initiation of targeted antimicrobial drug therapy and prevented some of the patients' subsequent deteriorations.

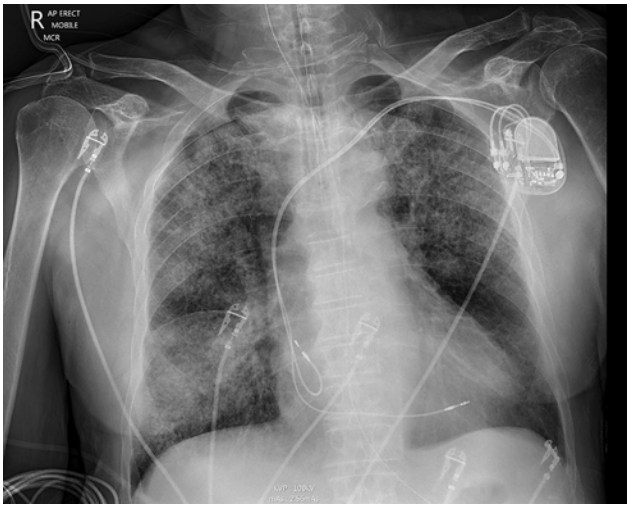

Figure. Chest radiograph of a patient (patient 7) showing right upper lobe opacification in study of acute Q fever infections in the intensive care unit in tropical Australia, 2015–2023. The patient required mechanical ventilation for 72 hours.

Acute Q fever can be life-threatening. Its complications include severe pneumonia, hepatitis, meningoencephalitis, and myocarditis (*1*); however, hypotension is rarely reported. It is, therefore, notable that 6 patients in this series required vasopressor support. We hypothesize that this hypotension was distributive and caused by sepsis because it responded relatively promptly to fluid resuscitation and antimicrobial drug therapy; vasopressor support was usually required for <72 hours (*7*). Severe disease and hypotension have not been a feature of large case series in Australia, although the clinical descriptions in those studies were frequently not detailed (*8*–*10*).

There is growing recognition of a marked geographic variation in the clinical phenotype of acute Q fever has increased, which might be explained by variation in lipopolysaccharide expression in different *C. burnetii* strains (*1*,*11*). Strain variation might, at least partly, explain the findings in our cohort. The presence of antiphospholipid antibodies during acute Q fever has also been associated with a complicated disease course (*2*) and were identified in the only patient admitted to ICU who had serum tested for antiphospholipid antibodies; this testing will now be performed routinely at our hospital. Expanded use

of PCR to test for *C. burnetii* during the study period (available since 2016) might also have contributed to greater recognition of the severe clinical phenotype described in this cohort (Appendix Figures 1, 2).

In conclusion, acute Q fever can cause life-threatening disease in otherwise healthy persons, and the clinical phenotype can evolve even after effective antimicrobial drug therapy begins. PCR is a far more sensitive diagnostic test than serology during early *C. burnetii* infection, and a positive result enables prompt, potentially lifesaving therapy and enhanced follow-up to identify chronic disease.

About the Author

Dr. Price is an infectious diseases registrar at the Royal Hobart Hospital in Hobart, Tasmania, Australia. His research interests include Q fever and infections in immunocompromised patients.

References

1. Eldin C, Mélenotte C, Mediannikov O, Ghigo E, Million M, Edouard S, et al. From Q fever to *Coxiella burnetii* infection: a paradigm change. Clin Microbiol Rev. 2017;30:115–90. https://doi.org/10.1128/CMR.00045-16
2. Melenotte C, Protopopescu C, Million M, Edouard S, Carrieri MP, Eldin C, et al. Clinical features and complications of *Coxiella burnetii* infections from the French National Reference Center for Q fever. JAMA Netw Open. 2018;1:e181580. https://doi.org/10.1001/jamanetworkopen.2018.1580
3. Australian Government, Department of Health and Aged Care. Q fever—laboratory case definition. 2017 [cited 2024 Feb 20]. https://www.health.gov.au/resources/publications/q-fever-laboratory-case-definition
4. Charlson ME, Pompei P, Ales KL, MacKenzie CR. A new method of classifying prognostic comorbidity in longitudinal studies: development and validation. J Chronic Dis. 1987;40:373–83. https://doi.org/10.1016/0021-9681(87)90171-8
5. Campbell V, Conway R, Carey K, Tran K, Visser A, Gifford S, et al. Predicting clinical deterioration with Q-ADDS compared to NEWS, Between the Flags, and eCART track and trigger tools. Resuscitation. 2020;153:28–34. https://doi.org/10.1016/j.resuscitation.2020.05.027
6. Koshy M, Jagannati M, Ralph R, Victor P, David T, Sathyendra S, et al. Clinical manifestations, antimicrobial drug susceptibility patterns, and outcomes in melioidosis cases, India. Emerg Infect Dis. 2019;25:316–20. https://doi.org/10.3201/eid2502.170745
7. Gyawali B, Ramakrishna K, Dhamoon AS. Sepsis: the evolution in definition, pathophysiology, and management. SAGE Open Med. 2019;7:2050312119835043. https://doi.org/10.1177/2050312119835043
8. Derrick EH. The course of infection with *Coxiella burneti*. Med J Aust. 1973;1:1051–7. https://doi.org/10.5694/j.1326-5377.1973.tb110910.x
9. Spelman DW. Q fever: a study of 111 consecutive cases. Med J Aust. 1982;1:547–53. https://doi.org/10.5694/j.1326-5377.1982.tb124169.x
10. Graves SR, Islam A. Endemic Q fever in New South Wales, Australia: a case series (2005–2013). Am J Trop Med Hyg. 2016;95:55–9. https://doi.org/10.4269/ajtmh.15-0828
11. Eldin C, Mahamat A, Demar M, Abboud P, Djossou F, Raoult D. Q fever in French Guiana. Am J Trop Med Hyg. 2014;91:771–6. https://doi.org/10.4269/ajtmh.14-0282

Address for correspondence: Josh Hanson, The Kirby Institute, Wallace Wurth Building, University of New South Wales, Kensington, NSW 2052, Australia; email: jhanson@kirby.unsw.edu.au

Dengue and Other Arbovirus Infections among Schoolchildren, Haiti, 2021

Rigan Louis, Tracey L. Moquin, Carla Mavian, Assonic Barthelemy, Ruiyu Pu, Benjamin Anderson, V. Madsen Beau De Rochars, Maureen T. Long, Marco Salemi, John A. Lednicky, J. Glenn Morris, Jr.

In 2021, we screened 91 children in Haiti with acute undifferentiated febrile illness for arbovirus infections. We identified a major outbreak of dengue virus type 2, with 67% of the children testing positive. Two others were positive for chikungunya East/Central/South African IIa subclade, and 2 were positive for Zika virus.

Since 2010, dengue (DENV), chikungunya (CHIKV), and Zika (ZIKV) viruses have been responsible for major outbreaks in the Caribbean region (*1*,*2*). In Haiti, reported DENV cases have tended to assume an endemic/sporadic pattern; cases surged in 2020–2022. CHIKV was responsible for epidemic disease in Haiti in 2014; ZIKV was associated with outbreaks in 2014–2016. Haiti has reported no CHIKV or ZIKV infections since 2019 (*3*,*4*). CHIKV and ZIKV are known to circulate intermittently in Brazil and other parts of South America and Central America since 2019 (*3*,*4*). Given the limitations of formal surveillance systems and arbovirus diagnostic capabilities in Haiti, we assessed the status of those viruses in Haiti to determine possible origins or evidence of persistence of viruses that might be present. We established surveillance during February–December 2021 for arboviral diseases among children attending schools operated by the Love a Child (LAC) Foundation (Fond Parisien, Haiti).

LAC schoolchildren who were brought to the LAC medical clinic for care for subjective fever without an obvious source of infection were invited to participate in the study; 91 children with febrile illness were enrolled. We collected clinical and epidemiologic data from participants and their parents and serum, nasal swab, and urine samples from case-patients, in accordance with standard protocols (*5*–*8*) (Appendix 1 Tables 1, 2, https://wwwnc.cdc.gov/EID/article/31/02/24-0791-App1.pdf. We screened serum samples by reverse transcription PCR (RT-PCR) for DENV, CHIKV, ZIKV, and Mayaro virus (MAYV) (*5*–*8*). Because COVID-19 was circulating in the community at the time of the study (*9*), we screened nasal swab samples from patients by RT-PCR for SARS-CoV-2. We further sequenced a random subset of 6 DENV-2–positive samples and 2 DENV-2–positive samples from patients positive for SARS-CoV-2, together with all samples positive for CHIKV, ZIKV, and SARS-CoV-2, and submitted sequences to GenBank/GISAID (Appendix 1 Table 1).

During the surveillance period, we identified a major DENV-2 outbreak (Figure 1); a total of 61 (67%) of the 91 participants had a positive serum RT-PCR result for DENV-2 virus RNA. Clinical findings were not significantly different among children who were DENV-2–positive than among those who were febrile but DENV-2-negative (Appendix 1 Table 2), underscoring the difficulties inherent in making a diagnosis of dengue fever based solely on clinical presentation. Among DENV-2–positive participants, 31% reported using mosquito nets, compared with 13% of DENV-2–negative participants ($p = 0.07$ by 2-tailed Fisher exact test); although not statistically significant, the trend is the opposite of what we would expect if mosquito nets were an effective tool for prevention of dengue.

Author affiliations: University of Florida College of Nursing, Gainesville, Florida, USA (R. Louis); University of Florida Emerging Pathogens Institute, Gainesville (R. Louis, T.L. Moquin, C. Mavian, R. Pu, B. Anderson, V.M.B. De Rochars, M.T. Long, M. Salemi, J.A. Lednicky, J.G. Morris, Jr.); University of Florida College of Public Health and Health Professions, Gainesville (T.L. Moquin, B. Anderson, V.M.B. De Rochars, J A. Lednicky); Smithsonian's National Zoo and Conservation Biology Institute, Washington, DC, USA (C. Mavian); University of Florida College of Medicine, Gainesville (C. Mavian, M. Salemi); Love A Child Foundation Medical Clinic, Fond Parisien, Haiti (A. Barthelemy)

DOI: https://doi.org/10.3201/eid3102.240791

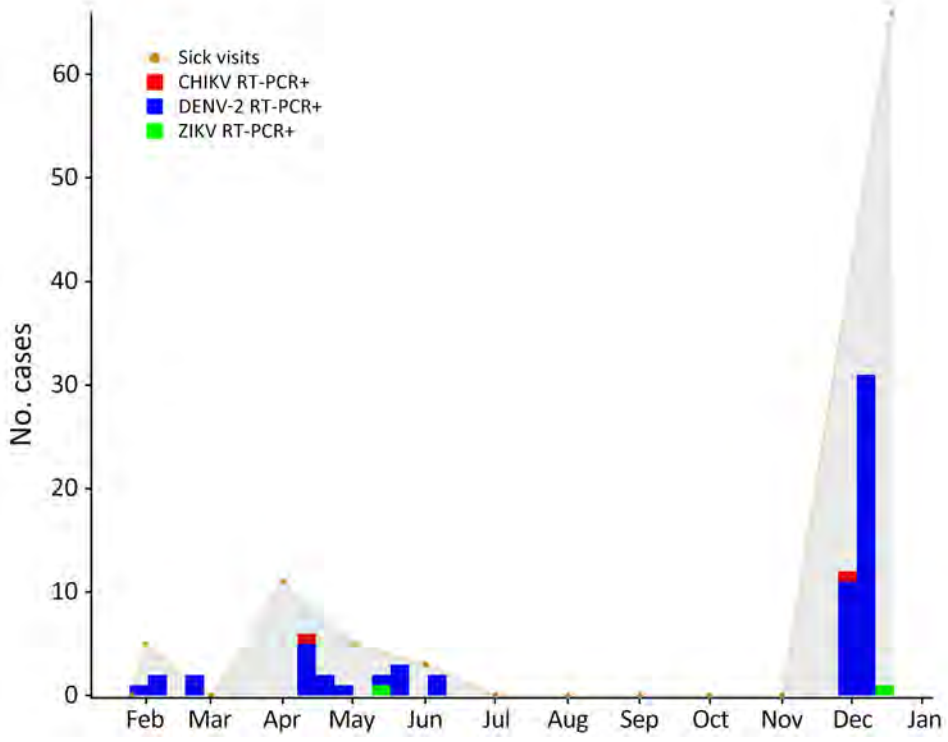

Figure 1. Numbers of children who had acute undifferentiated febrile illness and tested positive by RT- PCR for CHIKV, DENV-2, and ZIKV virus, by month, Haiti, 2021. Gray shading indicates the number of children seen in the clinic with symptoms of fever of undetermined etiology. CHIKV, chikungunya virus; DENV, dengue virus; RT-PCR, reverse transcription PCR; ZIKV, Zika virus; +, positive.

We detected CHIKV vRNA by RT-PCR in serum samples from 2 children (Appendix 1 Table 1). In contrast to the 2014 CHIKV epidemic in Haiti, infections were caused by a strain within the East/Central/South African (ECSA) IIa American subclade (*7*,*10*) (Appendix 1 Figure 2). Given that we were finding active ECSA CHIKV cases by RT-PCR, we were interested in assessing the frequency with which CHIKV antibodies were present among children in our cohort. IgG seropositivity was highly associated with age (Figure 2): of the 45 children ≤7 years of age, 2% were seropositive for CHIKV IgG, versus 78% of children >7 years of age ($p<0.001$ by 2-tailed Fisher exact test). Ten children were CHIKV IgM positive but CHIKV negative on RT-PCR. Eight of those 10 children, all >7 years of age, were also IgG positive; 7/8 were positive by RT-PCR for DENV-2.

We detected ZIKV vRNA in serum samples from 2 children, 16 and 7 years of age (Appendix 1 Table 1). Both had subjective fever; the 16-year-old reported headache, arthralgias, and upper respiratory symptoms, whereas the 7-year-old noted some abdominal pain but had no other complaints. Neither had a rash. Two children (both 3 years of age) were positive for SARS-CoV-2 by nasal swab; both also were serum RT-PCR positive for DENV-2 (Appendix 1 Table 1). All RT-PCR test results for MAYV were negative.

Phylogenetic analysis revealed 2 DENV-2 clades identified in Haiti and designated as American/Asian genotype—Haiti clade 1 and 2 (Figure 3; Appendix 1; Appendix 2 Table, https://wwwnc.cdc.gov/EID/article/31/2/24-0791-App2.xlsx). The DENV-2 strains from our study were clade 2, a Dominican Republic strain that initially seeded Haiti and returned in March 2020 (95% highest posterior density [HPD] June 2019–December 2020) (Figure 4). Although we could not infer directionality of spread, our analyses indicate continuous flow of DENV-2 between the 2 countries, leading to independent introductions into both.

CHIKV-positive samples from this study, together with previously reported 2016 CHIKV mosquito

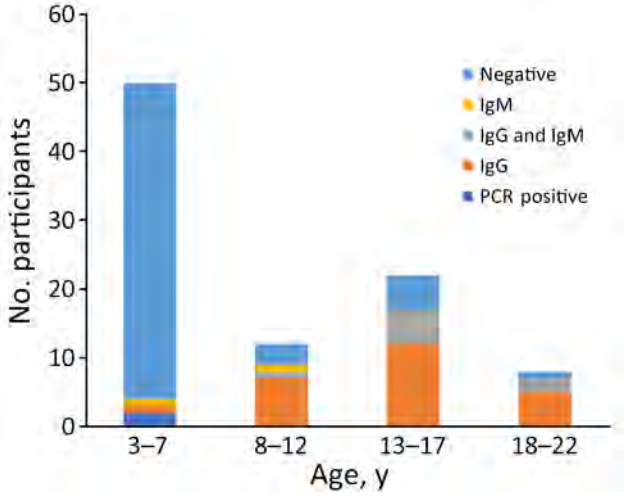

Figure 2. Results of chikungunya serologic testing by age group in study of arboviruses in children, Haiti.

isolates (*7*), cluster with strains belonging to the ECSA IIa Brazil-Haiti subclade, isolated in Brazil in 2014 (Appendix 1 Figure 2) (*2*,*10*,*11*). Including the 2016 mosquito isolates, the estimated time to the most recent common ancestor was November 2015 (95% HPD October 2014–April 2016) (Appendix 1 Figure 3). Sequences of both ZIKV strains were in what was previously designated as Zika Haiti clade 1, a Haiti-Brazil lineage found in Haiti in 2014 (Appendix 1 Figure 4). Time to most recent common ancestor for the emergence of the new strains is estimated at December 2020 (95% HPD August 2018–January 2021), suggesting that ZIKV has continued to circulate in Haiti since 2014 (95% HPD October 2013–August 2014) (Appendix 1 Figure 5) (*6*,*12*).

The generalizability of our study is limited by the small sample size and the collection of all samples from a single geographic location; nonetheless, it provides a snapshot of arboviruses circulating in Haiti in 2021. We unexpectedly identified a previously unrecognized dengue type 2 outbreak among children at the LAC school, in keeping with reports from the Ministere de la Sante Publique et de la Population of a surge of DENV infections nationally (*13*). Work by our group and others supports the concept that DENV is endemic in Haiti. At various times, Ministere de la Sante Publique et de la Population has reported occurrence of all 4 dengue serotypes (*13*). Given that occurrence of severe dengue has been associated with serial infection with different DENV serotypes, one might have expected an increased likelihood of severe dengue cases in Haiti (*14*). However, severe dengue has been rarely reported from Haiti (*13*,*14*), and,

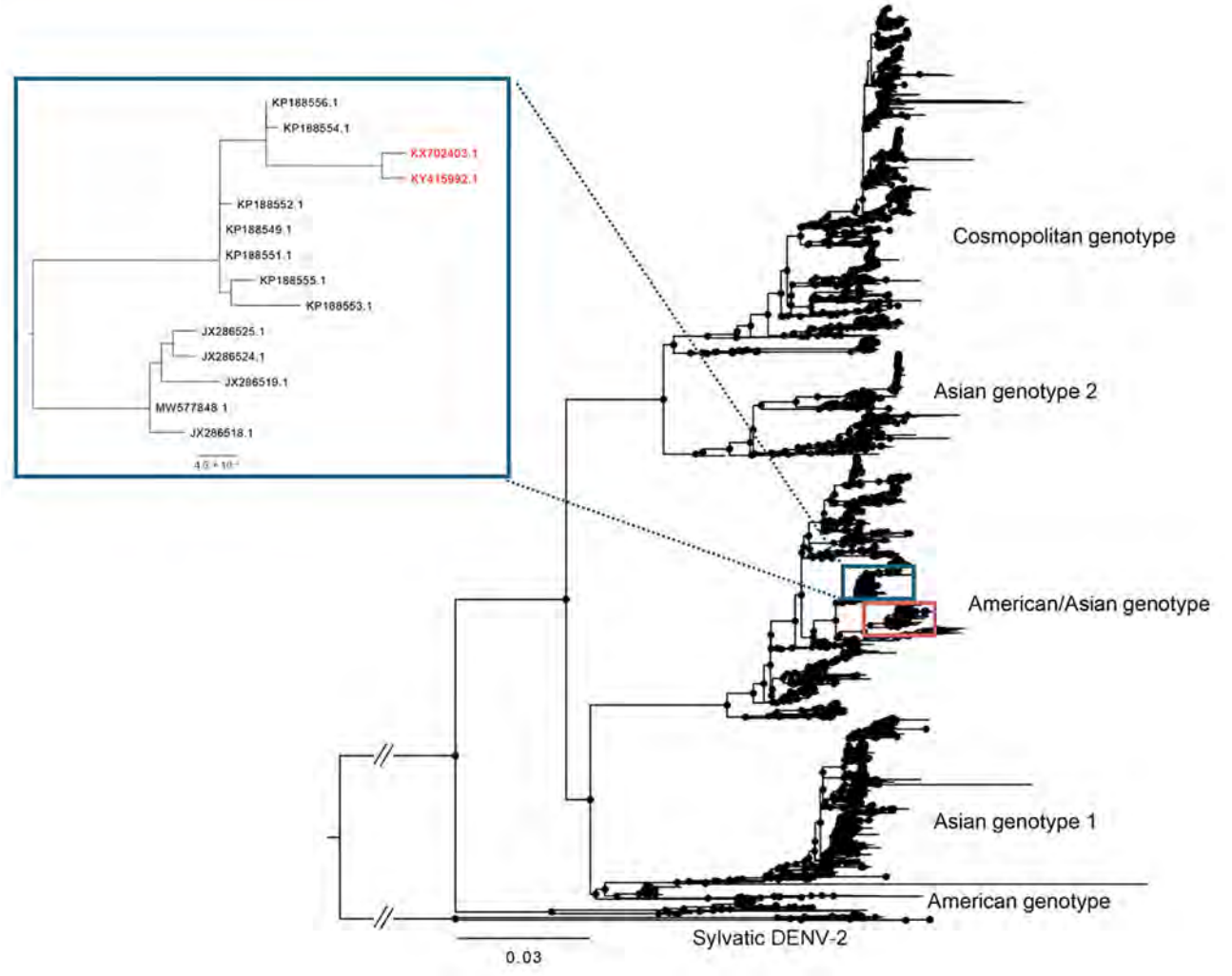

Figure 3. Global maximum-likelihood phylogeny of DENV-2 genotypes for all DENV-2 isolates available in GenBank inferred using IQ-TREE version 2.3.2 (http://www.iqtree.org). Haiti sequences cluster in 2 distinct clades (in boxes). Inset shows location of Haiti clade 1 strains KY415992, isolated in 2014, and Haiti strain KX702403, collected in 2016 (red text). Branch lengths reflect genetic distances. Black circles at each node shows strong statistical support based on ultrafast posterior probability bootstrap support (>90%). Scale bar represents nucleotide substitutions per site. DENV, dengue virus.

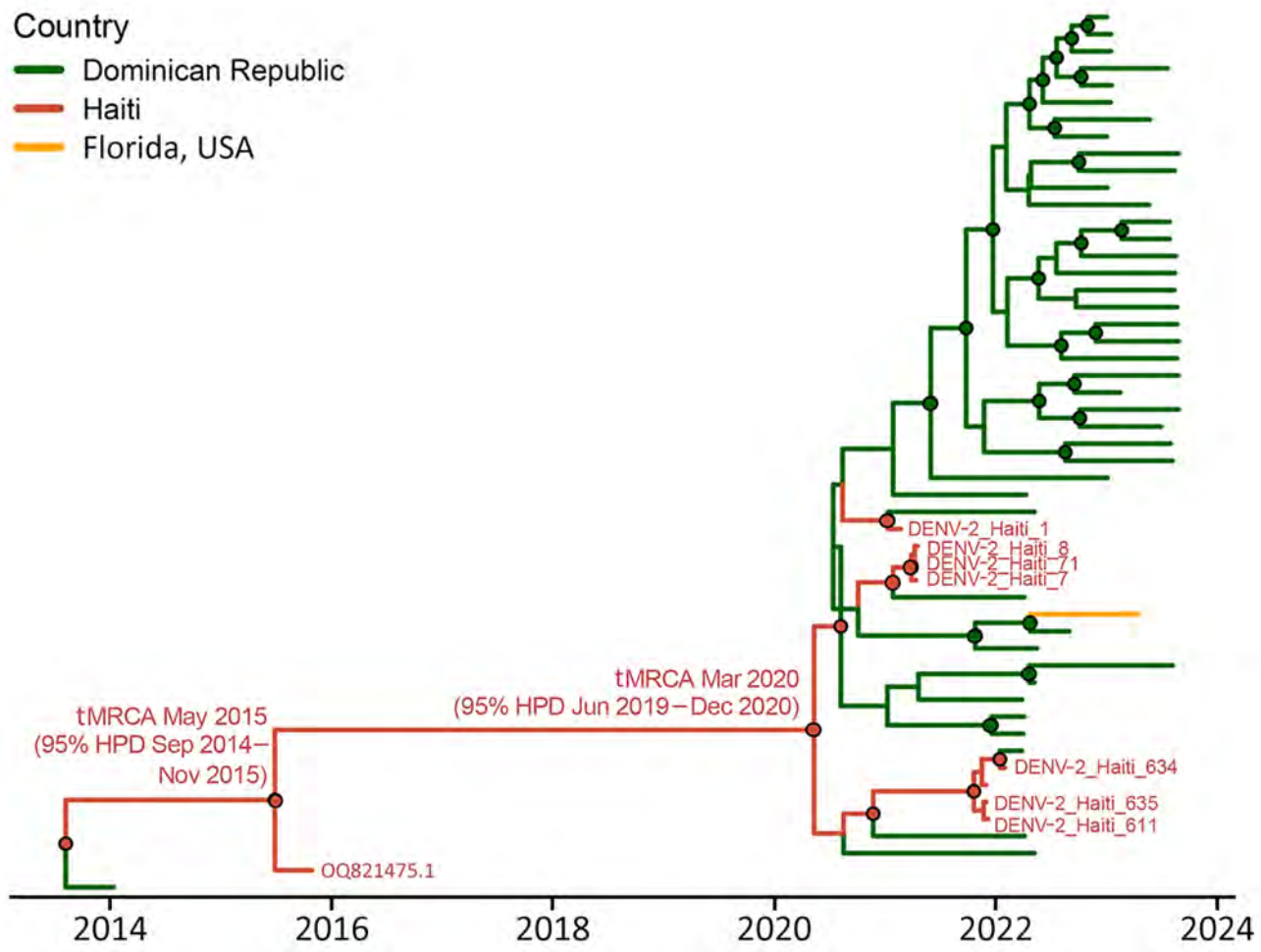

Figure 4. Phylogeography for the American/Asian genotype of DENV containing new Haiti isolates. Time-scaled phylogenetic maximum clade creditability tree for Haiti clade 2 (including GenBank accession no. OQ821475.1, isolated in 2015, and new 2021 strains, shown in red) was inferred using the phylogeographic frameworks in BEAST version 1.10.4 (https://beast.community) and enforcing the Bayesian Skyline demographic prior with an uncorrelated lognormal relaxed clock. Branch colors represent country of origin of the genome, and posterior probability bootstrap support >0.90 at each node is shown with a circle colored by the ancestral country of origin. DENV, dengue virus; HPD, highest posterior density; tMRCA, time to most recent common ancestor.

in our experience, is uncommon among children (A. Barthelemy, unpub. data).

The sharp increase in CHIKV IgG seropositivity after age 7 we observed is consistent with infection of virtually the entire population during the initial 2014 Asian clade epidemic; children born after the 2014 epidemic appear to have had minimal exposure to the virus, as reflected in the negative IgG results. Our phylodynamic studies are consistent with introduction of the Brazil-Haiti CSA IIa CHIKV strain into Haiti around 2015, shortly after its identification in Brazil (*2*). What is somewhat unexpected is that this same ECSA CHIKV strain has persisted in Haiti since 2015 or earlier. The 2016 ECSA IIa strain was isolated from *Aedes albopictus* mosquitoes; we isolated the Asia clade from *Ae. aegypti* mosquitoes (*7*), highlighting the potential for ECSA CHIKV transmission in areas in which *Ae. albopictus* mosquitoes are present, but not *Ae. aegypti* mosquitoes. The apparently low-level persistence of ZIKV in Haiti is also of interest; the strain we initially isolated in 2014 was still present in 2021 in this study (*6*,*12*).

Warming temperatures through the Caribbean and other parts of the Americas could cause further spread of arbovirus species and increased arbovirus transmission (*15*); rapid spread of DENV has been documented (*13*). Our findings that both CHIKV and ZIKV were present but unrecognized in Haiti, coupled with limited availability of specific diagnostics, raise concern that arboviruses may spread unrecognized into other areas in the region.

Acknowledgments

We thank the staff at the Love a Child Jesus Clinic for their work in providing medical care for patients included in this study.

The University of Florida institutional review board and the Comite National de Bioethique, Haiti, approved this study. We obtained signed parental informed consent and patient assent for all participants.

Studies were supported in part by National Institute of Allergy and Infectious Diseases (grant no. R21AI164007 for J.G.M. and R01AI155735 for J.G.M. and Hugh Fan, principal investigator).

About the Author

Mr. Louis is an assistant researcher at the University of Florida, Emerging Pathogens Institute, where he is currently completing his PhD. His research interests focus on *Vibrio cholerae*, SARS-CoV-2, and arboviruses.

References

1. Pan American Health Organization. Arbovirus bulletin. Epidemiological update for dengue, chikungunya, and Zika in 2022. 2022 [cited 2024 Oct 14]. https://www3.paho.org/data/index.php/en/mnu-topics/indicadores-dengue-en/annual-arbovirus-bulletin-2022.html
2. de Souza WM, Ribeiro GS, de Lima STS, de Jesus R, Moreira FRR, Whittaker C, et al. Chikungunya: a decade of burden in the Americas. Lancet Reg Health Am. 2024;30:100673. https://doi.org/10.1016/j.lana.2023.100673
3. Pan American Health Organization. PLISA Health Information Platform for the Americas—chikungunya cases. [cited 2024 Apr 17]. https://www3.paho.org/data/index.php/en/mnu-topics/chikv-en/550-chikv-weekly-en.html
4. Pan American Health Organization. PLISA Health Information Platform for the Americas—cases of Zika virus disease. [cited 2024 Oct 14]. https://www3.paho.org/data/index.php/en/mnu-topics/zika-weekly-en
5. Ball JD, Elbadry MA, Telisma T, White SK, Chavannes S, Anilis MG, et al. Clinical and epidemiologic patterns of chikungunya virus infection and coincident arboviral disease in a school cohort in Haiti, 2014–2015. Clin Infect Dis. 2019;68:919–26. https://doi.org/10.1093/cid/ciy582
6. Lednicky J, Beau De Rochars VM, El Badry M, Loeb J, Telisma T, Chavannes S, et al. Zika virus outbreak in Haiti in 2014: molecular and clinical data. PLoS Negl Trop Dis. 2016;10:e0004687. https://doi.org/10.1371/journal.pntd.0004687
7. White SK, Mavian C, Salemi M, Morris JG Jr, Elbadry MA, Okech BA, et al. A new "American" subgroup of African-lineage chikungunya virus detected in and isolated from mosquitoes collected in Haiti, 2016. PLoS One. 2018;13:e0196857. https://doi.org/10.1371/journal.pone.0196857
8. Blohm G, Elbadry MA, Mavian C, Stephenson C, Loeb J, White S, et al. Mayaro as a Caribbean traveler: evidence for multiple introductions and transmission of the virus into Haiti. Int J Infect Dis. 2019;87:151–3. https://doi.org/10.1016/j.ijid.2019.07.031
9. Tagliamonte MS, Mavian C, Zainabadi K, Cash MN, Lednicky JA, Magalis BR, et al. Rapid emergence and spread of severe acute respiratory syndrome coronavirus 2 gamma (P.1) variant in Haiti. Clin Infect Dis. https://doi.org/10.1093/cid/ciab736
10. Cunha MS, Cruz NVG, Schnellrath LC, Medaglia MLG, Casotto ME, Albano RM, et al. Autochthonous transmission of East/Central/South African genotype Chikungunya virus, Brazil. Emerg Infect Dis. 2017;23:1737–9. https://doi.org/10.3201/eid2310.161855
11. Giovanetti M, Vazquez C, Lima M, Castro E, Rojas A, Gomez de la Fuente A, et al. Rapid epidemic expansión of chikungunya virus East/Central/South African lineage, Paraguay. Emerg Infect Dis. 2023;29:1859–63. https://doi.org/10.3201/eid2909.230523
12. Alam MM, Mavian C, Okech BA, White SK, Stephenson CJ, Elbadry MA, et al. Analysis of Zika virus sequence data associated with a school cohort in Haiti. Am J Trop Med Hyg. 2022;107:873–80. https://doi.org/10.4269/ajtmh.22-0204
13. Pan American Health Organization. PLISA Health Information Platform for the Americas—reported cases of dengue fever in the Americas [cited 2024 Apr 17]. https://www3.paho.org/data/index.php/en/mnu-topics/indicadores-dengue-en/dengue-nacional-en/252-dengue-pais-ano-en.html
14. Pan American Health Organization. PLISA Health Information Platform for the Americas—dengue and severe dengue cases and deaths [cited 2024 May 10]. https://www3.paho.org/data/index.php/en/mnu-topics/indicadores-dengue-en/dengue-nacional-en/257-dengue-casos-muertes-pais-ano-en.html
15. Ryan SJ, Carlson CJ, Tesla B, Bonds MH, Ngonghala CN, Mordecai EA, et al. Warming temperatures could expose more than 1.3 billion new people to Zika virus risk by 2050. Glob Change Biol. 2021;27:84–93. https://doi.org/10.1111/gcb.15384

Address for correspondence: J. Glenn Morris, Jr., Emerging Pathogens Institute, University of Florida, PO Box 100009, Gainesville, FL 32610-0009, USA; email: jgmorris@epi.ufl.edu

Borrelia spielmanii–Associated Neuroborreliosis in Patient Receiving Rituximab, Belgium

Timothée Carette,[1] Louisien Lebrun,[1] Benoît Kabamba-Mukadi, Jean-Marc Raymackers, Jean-Louis Bayart

A 58-year-old woman in Belgium with a history of follicular lymphoma treated with rituximab sought care for a rapid sensory-motor deficit. Seronegative neuroborreliosis caused by *Borrelia spielmanii* was diagnosed, likely related to humoral deficiency. High CXC motif chemokine ligand 13 levels and PCR confirmed the diagnosis. Ceftriaxone treatment led to full recovery.

Neuroborreliosis is an infectious disease of the nervous system caused by tickborne *Borrelia* species, primarily *Borrelia burgdorferi* sensu lato. Common species pathogenic to humans include *B. burgdorferi* sensu stricto, *B. afzelii*, and *B. garinii*. *Borrelia spielmanii*, identified as a distinct species in 2006, has been associated with Lyme disease but not with neuroborreliosis (*1*,*2*).

The Study

A 58-year-old White woman in Belgium who had a history of follicular lymphoma treated with R-CHOP (rituximab monoclonal antibody, cyclophosphamide, hydroxydaunorubicin, vincristine, and prednisolone) and rituximab maintenance sought care for a 2-month history of worsening sensory-motor deficit in the distal right lower limb, accompanied by intense neuropathic pain and hyperesthesia. Electromyography of the right lower limb showed the absence of sural responses, severe axonal loss in both peroneal and tibial nerves, and absent F-waves, suggesting lumbar plexus involvement. Serum studies revealed an immunoglobulin profile altered by rituximab treatment (IgG 2.57 g/L [reference range (RR) 6.5–16 g/L], IgM 0.25 g/L [RR 0.50–3.00 g/L], IgA 0.51 g/L [RR 0.40–3.50 g/L]). We noted GM1 antibodies at low titers (IgG 1:80, IgM 1:32), whereas tests for other autoimmune and infectious markers (including for *Treponema pallidum* and herpes simplex virus 1 and 2) were negative. Results of serologic tests of cerebrospinal fluid (CSF) and serum samples for *Borrelia* were also negative (LIAISON *Borrelia* IgG and LIAISON *Borrelia* IgM II; DiaSorin, https://www.diasorin.com).

Analysis of CSF revealed 33 leukocytes/mm^3 (RR <5/mm^3) with 30% neutrophils, 45% lymphocytes, and 25% macrophages and an elevated protein concentration of 84 mg/dL (RR 15–45 mg/dL). Isoelectric-focusing electrophoresis showed no specific CSF oligoclonal bands. Results of a multiplex PCR targeting 15 microorganisms (QIAGEN, https://www.qiagen.com) was negative, and no lymphomatous CSF infiltration was found by flow cytometry analysis. Results of brain magnetic resonance imaging (MRI) were unremarkable, whereas MRI of the spine showed subtle intradural contrast enhancement without hypertrophy of the cauda equina roots or enhancement of the lumbosacral plexus (Figure 1). MRI of the lumbar plexus showed hyperintense infiltration of the right adductor muscle compartment and partial infiltration of the hamstrings on short tau inversion recovery sequences, without gadolinium enhancement (Figure 2). Whole-body ^{18}F-fluorodeoxyglucose positron emission tomography/computed tomography scans yielded negative results.

Given the patient's rituximab-related hypogammaglobulinemia, we hypothesized that she did not develop antibodies to the causative infectious agent. Elevated CXC motif chemokine ligand (CXCL) 13 levels were found in CSF (>350 pg/mL). Considering the clinical manifestation and the high sensitivity and

Author affiliations: Clinique Saint-Pierre Ottignies, Ottignies, Belgium (T. Carette, L. Lebrun, J.-M. Raymackers, J.L. Bayart); UCLouvain Institute of NeuroScience, Brussels, Belgium (L. Lebrun); UCLouvain Institut de Recherche Expérimentale et Clinique, Brussels (B. Kabamba-Mukadi); Cliniques Universitaires Saint-Luc, Brussels (B. Kabamba-Mukadi, J.-L. Bayart)

DOI: https://doi.org/10.3201/eid3102.240777

[1]These first authors contributed equally to this article.

specificity of CXCL13 in acute neuroborreliosis (*3*), we initiated a 21-day course of ceftriaxone (2 g/d).

After antibiotic therapy, the patient showed near-complete recovery from paresis and substantial improvement in neuropathic pain. This response supported the diagnosis of *Borrelia*-induced radiculoplexitis. Subsequent results of PCR testing of CSF were positive for the *Borrelia* OspA gene; sequencing confirmed *B. spielmanii*. The patient then recalled a possible arthropod bite 3 months earlier and transient erythema in the right popliteal fossa weeks before onset of these symptoms. Further serologic testing at 8 weeks after symptom onset (4 weeks after treatment completion) remained negative. For this later sample, measurements with an alternative method (VIDAS Lyme IgG II and IgM II; bioMérieux, https://www.biomerieux.com) were also negative. As a complement, we performed Western blot testing for *Borrelia* (RecomLine *Borrelia* IgM and RecomLine *Borrelia* IgG; Mikrogen Diagnostik, https://www.mikrogen.de); results were negative.

Figure 1. Contrast-enhanced T1-weighted magnetic resonance imaging scans of spine and cauda equina in study of *Borrelia spielmanii*–associated neuroborreliosis in patient receiving rituximab, Belgium. Subtle intradural contrast enhancement was noted after gadolinium injection. No hypertrophy of the cauda equina was found.

Conclusions

B. spielmanii is found mainly in central and western Europe and is relatively uncommon. In 2010, a study performed in Belgium identified *B. spielmanii* in only 1 of 524 *Ixodes* ticks analyzed (*4*). Radiculoneuritis is a frequent manifestation of neuroborreliosis. In this case, the patient's history of transient erythema, rapid symptom evolution, and pleocytosis suggested an infectious etiology, after recurrent lymphomatous disease was ruled out. High intrathecal CXCL13 levels strongly indicated neuroborreliosis (*3*), a hypothesis confirmed by CSF PCR positivity for *B. spielmanii* despite negative results of serologic testing for *Borrelia*.

Current diagnostic criteria for definite neuroborreliosis by the European Federation of Neurologic Societies include neurologic symptoms suggestive of Lyme neuroborreliosis, CSF pleocytosis, and intrathecal *B. burgdorferi* antibody production (*5*). Our patient did not meet those criteria because of the absence of *B. burgdorferi*–specific antibodies, raising the question of a possible need to consider alternative or supportive criteria, such as *Borrelia burgdorferi* s.l. PCR positivity or high CSF CXCL13 levels.

Borrelia burgdorferi s.l. serology tests have imperfect sensitivity and specificity for Lyme disease; reports indicate 70%–97% sensitivity and 98%–99% specificity for neuroborreliosis (*6*). Given the rarity of *B. spielmanii*, the sensitivity and specificity of serologic testing for this species are unclear, requiring direct analysis methods such as PCR or CXCL13 measurement. The negative results obtained using different serologic methods and immunoblots highlight this report. Previous diagnosis of borreliosis might have been infructuous if the species involved was *B. spielmanii* missed with common serologic tests. In our evaluation, the LIAISON *Borrelia* IgG assay uses a recombinant VlsE antigen, which is an outer surface lipoprotein, whereas the LIAISON IgM II assay uses the outer surface protein OspC and VlsE antigen. Whether the antibodies used in these assays have different immunoreactivity between the various *B. burgdorferi* s.l. species needs further investigation. Indeed, Mechai et al. (*7*) recently highlighted that genetic diversity of *B. burgdorferi* and genetic distance from the antigen used in diagnostic kits can affect the serodiagnosis of Lyme disease when the test is based on the OspC antigen. Moreover, diagnostic performance varies greatly among the numerous assays on the market.

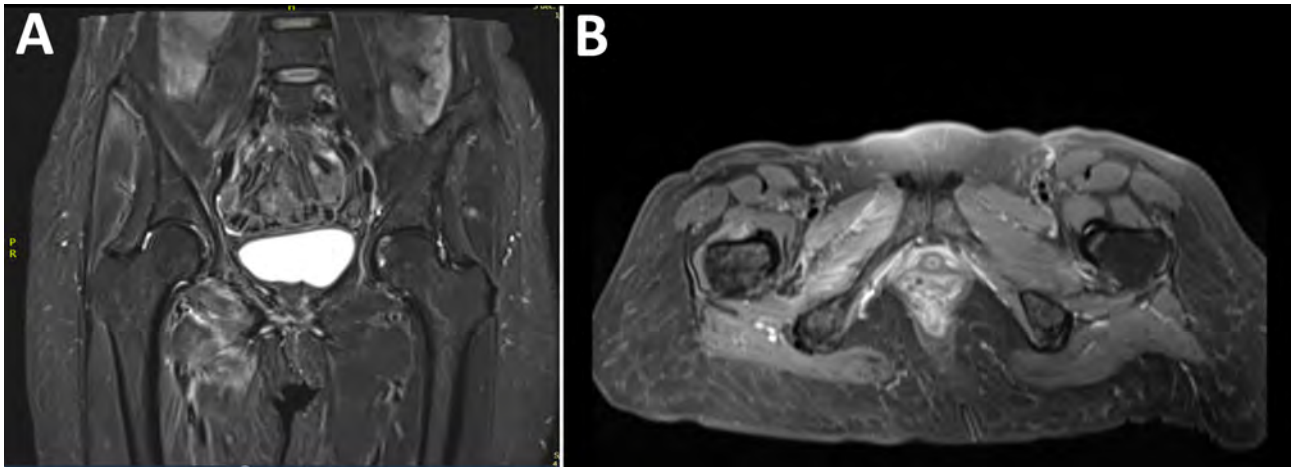

Figure 2. Coronal (A) and axial (B) T1 short-tau inversion recovery magnetic resonance imaging sequences of the hip in study of *Borrelia spielmanii*–associated neuroborreliosis in patient receiving rituximab, Belgium. Hyperintense infiltration of the right adductor muscle compartment (and partially of the hamstrings) was noted. No enhancement was seen after gadolinium injection.

Assays using recombinant antigens are generally considered to have higher specificity but lower sensitivity than assays using whole-cell antigens (*8*). Of note, results for our patient using 2 distinct methods were negative, and the patient had completely negative immunoblots.

Rituximab, an anti-CD20 molecule, depletes B cells and impairs antibody production, possibly explaining the absence of seroconversion in our patient. In 2011, a study showed that rituximab prevented antibody production against *B. hermsii* in humanized mice (*9*). Four other cases of seronegative neuroborreliosis in rituximab-treated patients have been reported, diagnosed through CSF PCR or antibody positivity (*10*–*13*) (Appendix Table, https://wwwnc.cdc.gov/EID/article/31/2/24-0777-App1.pdf).

In patients with humoral immunity deficiency and symptoms suggestive of neuroborreliosis, tests for CXCL13 should be performed on CSF samples because high specificity and sensitivity, compared with PCR, makes this test a valuable diagnostic tool (*3*). CXCL13 levels decrease rapidly with treatment, serving as a marker of therapeutic response (*14*).

This report raises questions about the pathogenic potential of *B. spielmanii* in immunocompetent hosts. In 2019, a study compared patients with erythema migrans, including those on rituximab, and found higher signs of dissemination and *Borrelia* PCR positivity than in immunocompromised hosts (*15*).

In conclusion, this case of neuroborreliosis caused by *B. spielmanii* highlights the need for vigilance in rituximab-treated patients because their impaired antibody production can affect results of serologic testing. Further studies are needed to determine whether *B. spielmanii* can cause neuroborreliosis in immunocompetent patients. Alternative diagnostic methods, such as CXCL13 assays and *Borrelia*-specific PCR testing of CSF samples, should be considered, along with empirical therapy if clinical suspicion is high.

Acknowledgments

We thank the infectious disease department and the hematology department of Clinique Saint-Pierre Ottignies for their support during management of this case.

About the Author

Dr. Carette is a neurologist at Clinique Saint-Pierre Ottignies, Belgium. His primary interest is the field of peripheral nervous diseases.

References

1. Richter D, Postic D, Sertour N, Livey I, Matuschka FR, Baranton G. Delineation of *Borrelia burgdorferi sensu lato* species by multilocus sequence analysis and confirmation of the delineation of *Borrelia spielmanii sp. nov*. Int J Syst Evol Microbiol. 2006;56:873–81. https://doi.org/10.1099/ijs.0.64050-0
2. del Giudice P, Freychet F, Kopec L, Fenollar F, Eldin C, Velin M, et al. Erythema migrans caused by *Borrelia spielmanii*, France. Emerg Infect Dis. 2023;29:2366–9. https://doi.org/10.3201/eid2911.230149
3. Senel M, Rupprecht TA, Tumani H, Pfister HW, Ludolph AC, Brettschneider J. The chemokine CXCL13 in acute neuroborreliosis. J Neurol Neurosurg Psychiatry. 2010;81:929–33. https://doi.org/10.1136/jnnp.2009.195438
4. Kesteman T, Rossi C, Bastien P, Brouillard J, Avesani V, Olive N, et al. Prevalence and genetic heterogeneity of *Borrelia burgdorferi sensu lato* in Ixodes ticks in Belgium. Acta Clin Belg. 2010;65:319–22. https://doi.org/10.1179/acb.2010.069
5. Mygland A, Ljøstad U, Fingerle V, et al. EFNS guidelines on the diagnosis and management of European Lyme neuroborreliosis. Eur J Neurol. 2010;17:8–16, e1–4.

6. Branda JA, Strle F, Strle K, Sikand N, Ferraro MJ, Steere AC. Performance of United States serologic assays in the diagnosis of Lyme borreliosis acquired in Europe. Clin Infect Dis. 2013;57:333–40. https://doi.org/10.1093/cid/cit235
7. Mechai S, Coatsworth H, Ogden NH. Possible effect of mutations on serological detection of *Borrelia burgdorferi sensu stricto* ospC major groups: An in-silico study. PLoS One. 2023;18:e0292741. https://doi.org/10.1371/journal.pone.0292741
8. Kodym P, Kurzová Z, Berenová D, Pícha D, Smíšková D, Moravcová L, et al. Serological diagnostics of Lyme borreliosis: comparison of universal and *Borrelia* species-specific tests based on whole-cell and recombinant antigens. J Clin Microbiol. 2018;56:e00601-18. https://doi.org/10.1128/JCM.00601-18
9. Vuyyuru R, Liu H, Manser T, Alugupalli KR. Characteristics of *Borrelia hermsii* infection in human hematopoietic stem cell-engrafted mice mirror those of human relapsing fever. Proc Natl Acad Sci U S A. 2011;108:20707–12. https://doi.org/10.1073/pnas.1108776109
10. Harrer T, Geissdörfer W, Schoerner C, Lang E, Helm G. Seronegative Lyme neuroborreliosis in a patient on treatment for chronic lymphatic leukemia. Infection. 2007;35:110–3. https://doi.org/10.1007/s15010-007-6121-0
11. van Dop WA, Kersten MJ, de Wever B, Hovius JW. Seronegative Lyme neuroborreliosis in a patient using rituximab. BMJ Case Rep. 2013;2013:bcr2012007627. https://doi.org/10.1136/bcr-2012-007627
12. Gampourou F, Taithe F, Moisset X, Clavelou P. Seronegative Lyme neuroborreliosis in a patient treated by rituximab. Rev Neurol (Paris). 2016;172:166–7. https://doi.org/10.1016/j.neurol.2015.06.009
13. Wagemakers A, Visser MC, de Wever B, Hovius JW, van de Donk NWCJ, Hendriks EJ, et al. Case report: persistently seronegative neuroborreliosis in an immunocompromised patient. BMC Infect Dis. 2018;18:362. https://doi.org/10.1186/s12879-018-3273-8
14. Erhart DK, Klose V, Schäper T, Tumani H, Senel M. CXCL13 in cerebrospinal fluid: clinical value in a large cross-sectional study. Int J Mol Sci. 2023;25:425. https://doi.org/10.3390/ijms25010425
15. Maraspin V, Bogovič P, Rojko T, Ružić-Sabljić E, Strle F. Erythema migrans: course and outcome in patients treated with rituximab. Open Forum Infect Dis. 2019;6:ofz292. https://doi.org/10.1093/ofid/ofz292

Address for correspondence: Louisien Lebrun, Institute of NeuroScience, Université Catholique de Louvain, Avenue Mounier 53 B1.53.04, 1200 Woluwe-Saint-Lambert, Brussels, Belgium; email: louisien.lebrun@uclouvain.be

etymologia revisited

Picobirnavirus [pi-ko-burʹnə-viʺrəs]

Picobirnavirus, the recently recognized sole genus in the family *Picobirnaviridae*, is a small (*Pico*, Spanish for small), bisegmented (*bi*, Latin for two), double-stranded RNA virus. Picobirnaviruses were initially considered to be birna-like viruses, and the name was derived from birnavirus (bisegmented RNA), but the virions are much smaller (diameter 35 nm vs. 65 nm).

Picobirnaviruses are reported in gastroenteric and respiratory infections. These infections were first described in humans and black-footed pigmy rice rats in 1988. Thereafter, these infections have been reported in feces and intestinal contents from a wide variety of mammals with or without diarrhea, and in birds and reptiles worldwide.

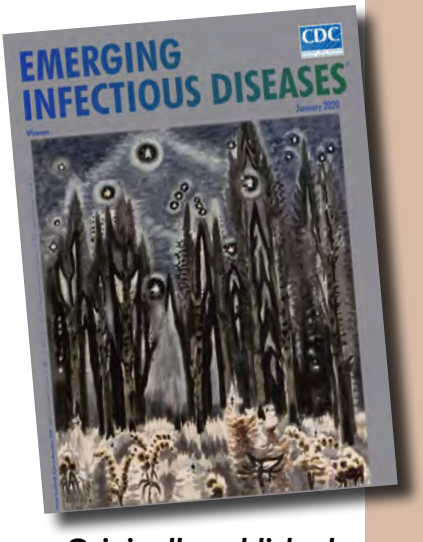

Originally published in January 2020

Sources

1. Delmas B, Attoui H, Ghosh S, Malik YS, Mundt E, Vakharia VN; ICTV Report Consortium. ICTV virus taxonomy profile: Picobirnaviridae. J Gen Virol. 2019;100:133–4. https://doi.org/10.1099/jgv.0.001186
2. Malik YS, Kumar N, Sharma K, Dhama K, Shabbir MZ, Ganesh B, et al. Epidemiology, phylogeny, and evolution of emerging enteric Picobirnaviruses of animal origin and their relationship to human strains. BioMed Res Int. 2014;2014:780752. https://doi.org/10.1155/2014/780752
3. Pereira HG, Flewett TH, Candeias JA, Barth OM. A virus with a bisegmented double-stranded RNA genome in rat (*Oryzomys nigripes*) intestines. J Gen Virol. 1988;69:2749–54. https://doi.org/10.1099/0022-1317-69-11-2749
4. Smits SL, van Leeuwen M, Schapendonk CM, Schürch AC, Bodewes R, Haagmans BL, et al. Picobirnaviruses in the human respiratory tract. Emerg Infect Dis. 2012;18:1539–40. https://doi.org/10.3201/eid1809.120507

https://wwwnc.cdc.gov/eid/article/26/1/et-2601_article

Outbreak of Serotype 1 Invasive Pneumococcal Disease, Kibera Urban Informal Settlement, Nairobi, Kenya, 2023

Terry Komo, Patrick K. Munywoki, Maria da Gloria Carvalho, Joshua Auko, Alice Ouma, Allan Audi, George O. Agogo, Daniel Omondi, Arthur Odoyo, Herine Odiembo, Newton Wamola, Mike Osita, Clayton Onyango, Naomi Lucchi, Peninah Munyua, Amy Herman-Roloff, Shanda Larson, Sopio Chochua, Fabiana C. Pimenta, Godfrey Bigogo, Jennifer R. Verani

Use of 10-valent pneumococcal conjugate vaccine in Kenya has led to substantial reductions in vaccine-type pneumococcal carriage and invasive pneumococcal disease. However, analysis of recent surveillance data indicates an outbreak of vaccine-type serotype 1 in 2023 in Kibera, Kenya. Continued monitoring of invasive pneumococcal disease in Kenya is warranted.

Streptococcus pneumoniae (pneumococcus) is a leading cause of pneumonia, sepsis, and meningitis and is most prevalent in resource-poor settings (*1*). Pneumococcal serotype 1 (ST1) is an important cause of disease, particularly in sub-Saharan Africa; it is highly invasive and infrequently detected in carriage (*2*). Pneumococcal conjugate vaccines (PCVs) protect against vaccine-type disease and carriage among vaccinated persons (direct effects), leading to decreased transmission of vaccine serotypes and reduced disease among unvaccinated persons (indirect effects) (*3*). All currently available PCVs protect against ST1.

In 2011, Kenya introduced 10-valent PCV (Synflorix; GlaxoSmithKline, https://www.gsk.com) (PCV10-GSK), which is administered in 3 doses, at 6, 10, and 14 weeks of age. Vaccine-type invasive pneumococcal disease (IPD) subsequently declined by ≈70%–90%, and vaccine-type carriage declined by ≈50%–60% (*3*). In 2022, Kenya switched to a newer 10-valent PCV (Pneumosil; Serum Institute of India, https://www.seruminstitute.com) (PCV10-SII).

Author affiliations: Kenya Medical Research Institute, Kisumu, Kenya (T. Komo, J. Auko, A. Ouma, A. Audi, D. Omondi, A. Odoyo, H. Odiembo, N. Wamola, M. Osita, G. Bigogo); US Centers for Disease Control and Prevention, Nairobi (P.K. Munywoki, G.O. Agogo, C. Onyango, N. Lucchi, P. Munyua, A. Herman-Roloff); US Centers for Disease Control and Prevention, Atlanta, Georgia, USA (M.D.G.Carvalho, S. Larson, “S. Chochua, F.C. Pimenta, J.R. Verani)

DOI: https://doi.org/10.3201/eid3102.241652

The Study

The Population-Based Infectious Disease Surveillance (PBIDS) platform is implemented in defined catchment populations in Kibera, an urban informal settlement in Nairobi County, and Asembo, a rural area in Siaya County (*4*); the Kibera site includes ≈25,000 persons in an area ≈1 km^2. Through household visits, we collected data on demographics, healthcare use, and vaccination. In both sites, PCV coverage among children ≤5 years of age has been stably >90%. At centrally located surveillance health facilities (an outpatient clinic in Kibera and an outpatient clinic with small inpatient ward in Asembo), PBIDS participants off all-ages meeting standardized criteria for acute febrile illness or severe acute respiratory illnesses (SARI) undergo blood culture; SARI case-patients additionally have a nasopharyngeal swab collected for culture to monitor pneumococcal carriage. The PBIDS protocol was approved by the Kenya Medical Research Institute and the US Centers for Disease Control and Prevention. We obtained written informed consent from participants before sample collection.

We used standard culture procedures to identify pneumococcus. We performed serotyping by real-time PCR, Quellung reaction, or both. At the US Centers for Disease Control and Prevention, we conducted antibiotic susceptibility testing (AST) through broth microdilution (*5*) for ST1 IPD and carriage isolates from 2023 and short-read whole-genome Illumina sequencing (*6*). We identified single-nucleotide

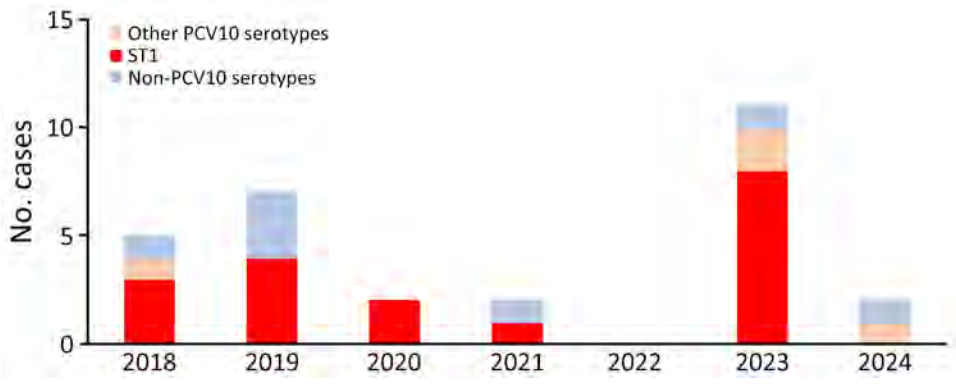

Figure 1. Serotype distribution among invasive pneumococcal disease cases, Kibera Urban Informal Settlement, Nairobi, Kenya, January 1, 2018–August 20, 2024. Other PCV10 serotypes are those common to Synflorix 10-valent PCV (GlaxoSmithKline, https://www.gsk.com) and Pneumosil 10-valent PCV (Serum Institute of India, https://www.seruminstitute.com) (5, 6B, 7F, 9V, 15, 19F, and 23F), Synflorix unique (4 and 18C), and Pneumosil unique (6A and 19A). PCV10, 10-valent pneumococcal conjugate vaccine; ST1, serotype 1.

polymorphisms (SNPs) for core genomes by using kSNP3.0 with k-Mer size of 19 (*7*) and generated pairwise comparisons by using MEGA version 7 (*6*,*8*).

We calculated crude incidence rates and 95% CIs by dividing the number of ST1 bacteremia cases by person-years of observation (PYO). We adjusted incidence rates to account for missed blood samples and healthcare seeking (i.e., cases of medically attended acute febrile illness or SARI reported during household visits for which care was sought at a nonsurveillance facility). We calculated 95% CIs for adjusted incidence rate estimates by using Monte Carlo simulations (0.025 and 0.975 quantiles of 10,000 simulations), sampling from Poisson distribution for crude incidence, and binomial distribution for adjustment factors (*9*).

We expressed overall and serotype-specific pneumococcal carriage among SARI cases as a percentage, excluding those with limited growth of any organisms, which we deemed poor-quality specimens. We examined ST1 IPD and carriage occurring during January 1, 2018–August 20, 2024. For ST1 isolates from 2023 in Kibera, we described sequence types and AST.

Among 4,913 blood samples collected in Kibera, 149 (3.0%) had bacteria isolated, of which 30 (20.1%) were *S. pneumoniae*. ST1 isolates accounted for 18/30 (60.1%) isolates; 8/18 (44.4%) ST1 isolates were collected in 2023 (Figure 1; Appendix, https://wwwnc.cdc.gov/EID/article/31/2/24-1652-App1.pdf). The crude ST1 IPD incidence rate during 2018–2022 was 8.7 cases/100,000 PYO (95% CI 4.7–16.2 cases/100,000 PYO) versus 35.5 cases/100,000 PYO (95% CI 17.7–71.0 cases/100,000 PYO) in 2023 (Appendix). The adjusted ST1 IPD incidence rate during 2018–2022 was 17.9 cases/100,000 PYO (95% CI 7.3–30.1 cases/100,000 PYO) versus 66.8 cases/100,000 PYO (95% CI 24.8–118.7 cases/100,000 PYO) in 2023 (Appendix). All ST1 IPD case-patients in 2023 were children 2–10 years of age (median 4.5 years of age), and all of them were age-eligible for PCV10-GSK; 5/8 (62.5%) were fully immunized (Table 1). No hospitalizations or fatalities occurred among ST1 case-patients.

Among serotyped carriage isolates from SARI cases during 2018–2022, 1.5% (7/464) were ST1, and frequency by year ranged from 0 to 3.1% (Table 2; Figure 2). In 2023, 17.9% (10/56) of serotyped carriage isolates from SARI cases in Kibera were ST1.

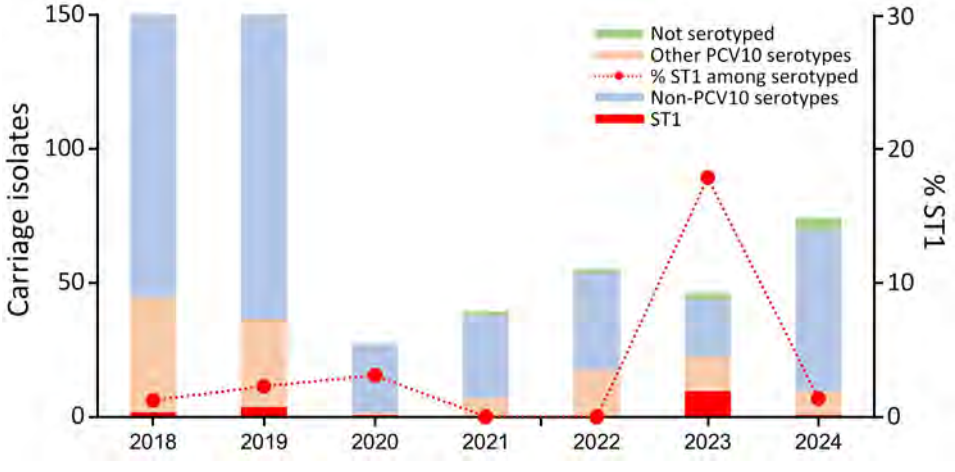

Figure 2. Serotype distribution among invasive pneumococcal disease carriage isolates, Kibera Urban Informal Settlement, Nairobi, Kenya, January 1, 2018–August 20, 2024. Other PCV10 serotypes are those common to Synflorix 10-valent PCV (GlaxoSmithKline, https://www.gsk.com) and Pneumosil 10-valent PCV (Serum Institute of India, https://www.seruminstitute.com) (5, 6B, 7F, 9V, 15, 19F, and 23F), Synflorix unique (4 and 18C), and Pneumosil unique (6A and 19A). PCV10, 10-valent pneumococcal conjugate vaccine; ST1, serotype 1.

Table 1. Characteristics of IPD cases, Kibera Urban Informal Settlement, Nairobi, Kenya, January 1, 2018–August 20, 2024*

Characteristic	Serotype and surveillance period		
	ST1, 2023	ST1, 2018–2022	Non-ST1, 2018–2024
No. cases	8	10	12
Median age of patient, y (range)	4.5 (2.5–9.7)	12 (0.79–36.6)	10.6 (0.44–45.5)
Sex of patient			
M	6 (75.0)	5 (50.0)	8 (66.7)
F	2 (25.0)	5 (50.0)	4 (33.3)
Age eligibility for PCV			
Age-eligible for PCV10-GSK	8 (100)	5 (50.0)	7 (58.3)
Age-eligible for PCV10-SII	0	0	2 (16.7)
Not age-eligible for PCV	0	5 (50.0)	3 (25.0)
Vaccination status known	8 (100)	2 (40.0)	7 (77.8)
0 PCV doses	1 (12.5)	0	3 (42.9)
1 PCV dose	1 (12.5)	1 (50.0)	0
2 PCV doses	1 (12.5)	0	1 (14.2)
3 PCV doses	5 (62.5)	1 (50.0)	3 (42.9)
Month of detection			
January	0	1 (10.0)	0
February	0	3 (30.0)	2 (16.7)
March	2 (25.0)	2 (20.0)	0
April	3 (37.5)	1 (10.0)	2 (16.7)
May	0	0	2 (16.7)
June	1 (12.5)	1 (10.0)	1 (8.3)
July	0	0	0
August	0	0	2 (16.7)
September	0	1 (10.0)	0
October	1 (12.5)	1 (10.0)	0
November	1 (12.5)	0	1 (8.3)
December	0	0	2 (16.7)
Disposition			
Discharged home from clinic	8 (100)	10 (100)	12 (100)
Alive at 1 month after IPD†	8 (100)	10 (100)	12 (100)

*Values are no. (%) except as indicated. IPD, invasive pneumococcal disease; PCV, pneumococcal conjugate vaccine; PCV10-GSK, Synflorix 10-valent PCV (GlaxoSmithKline, https://www.gsk.com); PCV10-SII, Pneumosil 10-valent PCV (Serum Institute of India, https://www.seruminstitute.com); ST1, serotype 1.
†Vital status at 1 month after date of blood culture was verified from household demographic data.

As of August 20, 2024, we had detected no ST1 IPD cases in 2024, and only 1.3% (1/74) of serotyped carriage isolates were ST1 (Tables 1, 2; Figures 1, 2). We observed no clear increase of ST1 in carriage or IPD in Asembo during the study period (data not shown).

We performed sequencing and AST for 13 ST1 isolates from 2023 (5 IPD and 8 carriage); 9 (69.2%) were sequence type 217, and 4 (30.8%) were sequence type 6056. Genomic analysis demonstrated a 4–15 SNP difference among sequence type 217 isolates and a 6–8 SNP difference among sequence type 6056 isolates, indicating close genomic relatedness. All isolates tested were susceptible to amoxicillin, cefuroxime, and erythromycin; had intermediate susceptibility to penicillin (nonmeningitis oral breakpoint); and were resistant to cotrimoxazole.

Table 2. Enrollment of SARI cases, pneumococcal carriage testing, and serotyping, Kibera Urban Informal Settlement, Nairobi, Kenya, January 1, 2018–August 20, 2024*

Year	SARI cases	NPs collected and tested	Poor growth†	Pneumococcus isolated‡	Serotyped	ST1	Other PCV10 types§	Non-PCV10 types	Serotype pending
2018	264	233 (88.3)	4 (1.7)	161/229 (70.3)	161 (100)	2 (1.2)	43 (26.7)	115 (71.4)	0
2019	318	312 (98.1)	0	174/312 (55.8)	174 (100)	4 (2.3)	33 (19.0)	137 (78.7)	0
2020	78	73 (93.6)	1 (1.4)	32/72 (44.4)	32 (100)	1 (3.1)	1 (3.1)	25 (78.1)	0
2021	133	110 (82.7)	11 (10.0)	40/99 (40.4)	39 (97.5)	0	7 (18.0)	31 (79.5)	1 (2.5)
2022	113	106 (93.8)	4 (3.8)	59/102 (57.8)	58 (98.3)	0	18 (31.0)	36 (62.1)	1 (1.7)
2023	125	120 (96.0)	11 (9.2)	58/109 (53.2)	56 (96.6)	10 (17.9)	13 (23.2)	21 (37.5)	2 (3.4)
2024	222	190 (85.6)	14 (7.4)	78/176 (44.3)	74 (94.9)	1 (1.4)	9 (12.2)	60 (81.1)	4 (5.1)

*Values are no. (row %) except as indicated. NP, nasopharyngeal swab sample; PCV10, 10-valent pneumococcal conjugate vaccine; PCV10-GSK, Synflorix 10-valent PCV (GlaxoSmithKline, https://www.gsk.com); PCV10-SII, (Pneumosil 10-valent PCV (Serum Institute of India, https://www.seruminstitute.com); SARI, severe acute respiratory illness; ST1, serotype 1.
†Poor growth defined as <10 colonies of any bacteria.
‡Excludes samples with poor growth.
§Includes serotypes common to PCV10-GSK and PCV10-SII (5, 6B, 7F, 9V, 15, 19F, and 23F), PCV10-GSK unique (4 and18C), and PCV10-SII unique (6A and 19A).

Conclusions

Although PCV10-GSK in the Kenya routine infant immunization program has led to substantial reductions in vaccine-type pneumococcal carriage and disease, the surveillance data indicate an outbreak of vaccine-type ST1 in 2023 in Kibera. The IPD case counts from the surveillance area are small, which limits statistical power. However, the ≈4-fold increase in crude and adjusted ST1 IPD incidence rates in 2023 compared with the preceding 5 years, the >10-fold increase in ST1 carriage prevalence (reflecting increased transmission in the community), and the close genetic relatedness of sequenced ST1 isolates from 2023 are consistent with an outbreak. Furthermore, the predominant sequence type detected has been associated with pneumococcal meningitis outbreaks in Malawi (*2*) and Ghana (*10*). Pneumococcal disease outbreaks often occur in crowded, closed environments (*11*); Kibera is densely populated, and the data highlight the risk for IPD outbreaks in urban informal settlements.

ST1 is an important cause of pneumococcal disease outbreaks in sub-Saharan Africa (*2*). Although PCV implementation has reduced ST1 disease globally (*12*), several countries, particularly in the meningitis belt have experienced ST1 IPD outbreaks even in the context of mature PCV programs with high coverage (*2*). The World Health Organization recommends 3-dose PCV schedules: either 3 primary doses and no booster or 2 primary doses and 1 booster. Booster doses can extend the duration of protection among vaccinated persons. The longer period of direct protection against vaccine serotypes might result in less circulation and more robust indirect protection, particularly against ST1, which frequently affects age groups beyond infancy (*13*,*14*). Kenya uses 3 primary doses and no booster schedule; however, if ST1 continues to pose a threat despite high PCV coverage, consideration of switching to 2 primary doses and 1 booster might be merited (*14*,*15*). Our data also highlight the importance of optimizing PCV coverage, given that ≈40% of the ST1 case-patients in 2023 had not completed PCV vaccination.

Of note, although this outbreak was detected after Kenya switched PCV product from PCV10-GSK to PCV10-SII, all children with ST1 IPD in 2023 were born before 2022 and therefore eligible for PCV10-GSK. Thus, despite the temporal association, the observed increase in ST1 cases in Kibera in 2023 should not be considered a reflection of PCV10-SII performance in Kenya.

All ST1 IPD patients were managed as outpatients, and none died. All ST1 isolates with available AST data were susceptible to first-line treatment for nonsevere pneumonia in Kenya (https://www.researchgate.net/figure/Kenyan-Ministry-of-Health-MoH-guidelines-for-management-of-children-aged-2-59-months_tbl1_264744317).

Preliminary data from 2024 suggest that the ST1 outbreak in Kenya might have resolved. However, continued monitoring of IPD in Kibera and other parts of the country is warranted.

Acknowledgments

We thank the funders, participants, and field and laboratory teams for their contributions to the study. We also thank Stacy Cobb for her guidance on the analysis.

Funding was provided to Washington State University Global Health Kenya by the US Centers for Disease Control and Prevention (cooperative agreement no. 5U01GH002346) and the Gates Foundation (grant no. INV-009150).

About the Author

Dr. Komo is an early career researcher at the Kenya Medical Research Institute. Her primary research interest is the epidemiology of infectious diseases with a current focus on pneumococcal diseases.

References

1. Wahl B, O'Brien KL, Greenbaum A, Majumder A, Liu L, Chu Y, et al. Burden of *Streptococcus pneumoniae* and *Haemophilus influenzae* type b disease in children in the era of conjugate vaccines: global, regional, and national estimates for 2000–15. Lancet Glob Health. 2018;6:e744–57. https://doi.org/10.1016/S2214-109X(18)30247-X
2. Chaguza C, Yang M, Jacques LC, Bentley SD, Kadioglu A. Serotype 1 pneumococcus: epidemiology, genomics, and disease mechanisms. Trends Microbiol. 2022;30:581–92. https://doi.org/10.1016/j.tim.2021.11.007
3. Hammitt LL, Etyang AO, Morpeth SC, Ojal J, Mutuku A, Mturi N, et al. Effect of ten-valent pneumococcal conjugate vaccine on invasive pneumococcal disease and nasopharyngeal carriage in Kenya: a longitudinal surveillance study. Lancet. 2019;393:2146–54. https://doi.org/10.1016/S0140-6736(18)33005-8
4. Feikin DR, Olack B, Bigogo GM, Audi A, Cosmas L, Aura B, et al. The burden of common infectious disease syndromes at the clinic and household level from population-based surveillance in rural and urban Kenya. PLoS One. 2011;6:e16085. https://doi.org/10.1371/journal.pone.0016085
5. Clinical and Laboratory Standards Institute. Performance standards for antimicrobial susceptibility testing (M100). 33rd edition. Wayne (PA): The Institute; 2023. p. 48–9.
6. Metcalf BJ, Chochua S, Gertz RE Jr, Li Z, Walker H, Tran T, et al.; Active Bacterial Core surveillance team. Using whole genome sequencing to identify resistance determinants and predict antimicrobial resistance phenotypes for year 2015

invasive pneumococcal disease isolates recovered in the United States. Clin Microbiol Infect. 2016;22:1002.e1–8. https://doi.org/10.1016/j.cmi.2016.08.001
7. Gardner SN, Slezak T, Hall BG. kSNP3.0: SNP detection and phylogenetic analysis of genomes without genome alignment or reference genome. Bioinformatics. 2015; 31:2877–8. https://doi.org/10.1093/bioinformatics/btv271
8. Kumar S, Stecher G, Tamura K. MEGA7: Molecular Evolutionary Genetics Analysis version 7.0 for bigger datasets. Mol Biol Evol. 2016;33:1870–4. https://doi.org/10.1093/molbev/msw054
9. Hall G, Yohannes K, Raupach J, Becker N, Kirk M. Estimating community incidence of *Salmonella, Campylobacter*, and Shiga toxin–producing *Escherichia coli* infections, Australia. Emerg Infect Dis. 2008;14:1601–9. https://doi.org/10.3201/eid1410.071042
10. Kwambana-Adams BA, Asiedu-Bekoe F, Sarkodie B, Afreh OK, Kuma GK, Owusu-Okyere G, et al. An outbreak of pneumococcal meningitis among older children (≥5 years) and adults after the implementation of an infant vaccination programme with the 13-valent pneumococcal conjugate vaccine in Ghana. BMC Infect Dis. 2016;16:575. https://doi.org/10.1186/s12879-016-1914-3
11. Zivich PN, Grabenstein JD, Becker-Dreps SI, Weber DJ. *Streptococcus pneumoniae* outbreaks and implications for transmission and control: a systematic review. Pneumonia. 2018;10:11. https://doi.org/10.1186/s41479-018-0055-4
12. Bennett JC, Hetrich MK, Garcia Quesada M, Sinkevitch JN, Deloria Knoll M, Feikin DR, et al.; The Pserenade Team. Changes in invasive pneumococcal disease caused by streptococcus pneumoniae serotype 1 following introduction of pcv10 and pcv13: findings from the PSERENADE Project. Microorganisms. 2021;9:696. https://doi.org/10.3390/microorganisms9040696
13. Hausdorff WP, Feikin DR, Klugman KP. Epidemiological differences among pneumococcal serotypes. Lancet Infect Dis. 2005;5:83–93. https://doi.org/10.1016/S1473-3099(05)70083-9
14. Klugman KP, Madhi SA, Adegbola RA, Cutts F, Greenwood B, Hausdorff WP. Timing of serotype 1 pneumococcal disease suggests the need for evaluation of a booster dose. Vaccine. 2011;29:3372–3. https://doi.org/10.1016/j.vaccine.2011.02.089
15. Rodgers GL, Whitney CG, Klugman KP. Triumph of pneumococcal conjugate vaccines: overcoming a common foe. J Infect Dis. 2021;224(Suppl 2):S352–9. https://doi.org/10.1093/infdis/jiaa535

Address for correspondence: Terry Komo, Kenya Medical Research Institute, PO Box 1578-40100, Kisumu, Kenya; email: tkomo@kemri.go.ke

etymologia revisited

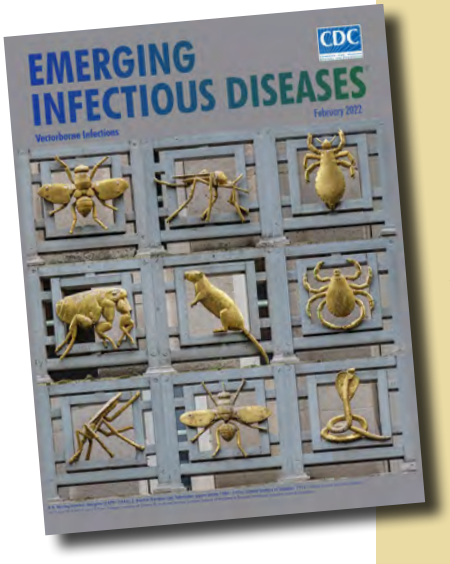

Originally published in February 2022

The Color Puce

For those with synesthesia, in whom stimulating 1 sensory pathway gives rise to a subjective sensation of a different character, the word plague may chromatically resonate with puce. In pre-revolutionary France, an era of "evocative color nomenclature," Marie Antoinette's reign was precipitating intense criticism. Her countrymen were experiencing severe socioeconomic stress, thus her sartorial self-indulgence was much resented.

After discovering the Queen wearing a new gown, her husband, Louis XVI, the King of France, chided her, describing the dress's unflattering purple–brown hue as "*couleur de puce*" (color of fleas). This admonishment had the unintended consequence of promoting puce as the exclusive color worn by the French court. Puce, the French word for flea, descends from *pulex* (Latin). Flea droppings leave puce colored "bloodstains" on bedsheets. The role of fleas, however, as a vector for bubonic plague was not proven until about 1895.

References:

1. Stedman's Medical Dictionary. 23rd ed. Baltimore: The Williams & Wilkins Company; 1976. p. 1392.
2. St. Clair K. The secret lives of color. New York: Penguin Books; 2017. p. 122–3.
3. Zietz BP, Dunkelberg H. The history of the plague and the research on the causative agent *Yersinia pestis*. Int J Hyg Environ Health. 2004;207:165–78. https://doi.org/10.1078/1438-4639-00259
4. Plague bacteria found in Arizona fleas, by Rachael Rettner, August 14, 2017 [cited 2021 Nov 4]. https://www.livescience.com/60130-plague-fleas-arizona.html.)

https://wwwnc.cdc.gov/eid/article/28/2/et-2802_article

Infection by Tickborne Bacterium *Candidatus* Midichloria Associated with First Trimester Pregnancy Loss, Tennessee, USA

John Newman, Caitlin Hughes, Karen C. Bloch, Khalil J. Deveaux, Scott Allen, Thao T. Truong, Behzad Najafian, Abelardo C. Moncayo, Lili Tao, Joshua Lieberman, Hernán Correa

A previously healthy 26-year-old woman in middle Tennessee, USA, experienced a first trimester pregnancy loss after multiple tick bites. Histopathology, 16S rRNA sequencing, and electron microscopy examination of the products of conception revealed an infection by a bacterium within the *Candidatus* Midichloria genus.

Chromosomal aneuploidy accounts for most first trimester pregnancy losses, but infections are estimated to cause ≈15% of early miscarriages (*1*). Evidence supporting an association of tickborne bacterial infections with early pregnancy loss is scarce and largely limited to case reports and small case series. Tickborne diseases with anecdotal associations to early pregnancy loss include Lyme disease, babesiosis, rickettsial diseases, and ehrlichiosis (*2*,*3*).

Candidatus Midichloriaceae represents a family of intracellular bacterial organisms first identified in the ovaries of the *Ixodes ricinus* tick, the primary vector of Lyme disease in Europe. Phylogenetic analysis led to the proposal for *Candidatus* Midichloriaceae to be separated into a third family under the order Rickettsiales, distinct from Rickettsiaceae and Anaplasmataceae, but likely more akin to Anaplasmataceae (*4*). Some members of the family boast a unique intramitochondrial life cycle, demonstrating tropism for a growing number of nonhuman hosts, such as aquatic invertebrates, protists, and various farm animals with unknown pathogenic potential (*5*). Further, the presence of *Candidatus* Midichloria genus mitochondrii DNA in human serum has rarely been documented without evidence of pathogenic effects (*6*). In this study, we describe a case of early pregnancy loss after tick exposure and the subsequent detection of *Candidatus* Midichloria sp. within the products of conception.

Figure 1. Left lateral torso rash with onset 2 weeks after tick removal in study of infection by tickborne bacterium *Candidatus* Midichloria associated with first trimester pregnancy loss, Tennessee, USA.

Author affiliations: Vanderbilt University Medical Center, Nashville, Tennessee, USA (J. Newman, C. Hughes, K.C. Bloch, L. Tao, H. Correa); University of Washington School of Medicine, Seattle, Washington, USA (K.J. Deveaux, S. Allen, T.T. Truong, B. Najafian, J. Lieberman); Tennessee Department of Health, Nashville (A.C. Moncayo)

DOI: https://doi.org/10.3201/eid3102.240870

Table. Laboratory testing at initial and follow-up evaluations in study of Infection by tickborne bacterium *Candidatus* Midichloria associated with first trimester pregnancy loss, Tennessee, USA*

Laboratory study	Acute testing, 2023 Apr 30, 2 weeks after tick bite	Convalescent testing, 2023 Jun 19, 11 weeks after tick bite
Complete blood count		
Leukocyte count, × 10^3 cells/μL	7.4	7.8
Platelets, × 10^3/μL	227	221
Liver function tests		
Alanine transaminase, U/L	Not evaluated	23
Aspartate transaminase, U/L	Not evaluated	24
Total bilirubin, mg/dL	Not evaluated	0.5
Alkaline phosphatase, U/L	Not evaluated	54
Serologic testing		
Borrelia burgdorferi Western blot		
IgM	0/3 bands	0/3 bands
IgG	2/10 bands	2/10 bands
Ehrlichia chaffensis EIA		
IgM	<1:16	<1:16
IgG	<1:64	<1:64
Spotted fever group *Rickettsia* EIA		
IgM	<1:16	<1:16
IgG	<1:64	<1:64
Routine prenatal infectious disease panel		
Chlamydia trachomatis, Neisseria gonorrhoeae, Treponema pallidum, HIV, hepatitis B virus, and hepatitis C virus	Negative	Not evaluated
Autoimmune panel		
Antinuclear antibody survey	Not evaluated	Positive 1:320, smooth pattern
SSA (Ro) IgG Qual	Not evaluated	Negative
SSA (La) IgG Qual	Not evaluated	Negative
Scl-70 IgG Qual	Not evaluated	Negative
Smith (Sm) IgG Qual	Not evaluated	Negative
RNP Ab Calc	Not evaluated	Negative
Anti-dsDNA	Not evaluated	Negative

*Anti-dsDNA, anti–double stranded DNA; EIA, enzyme immunoassay; RNP Ab Calc, anti–ribonucleoprotein antibody calculation; Scl-70 IgG Qual, scleroderma antibody qualitative.

The Study

A 26-year-old woman in her first pregnancy sought care at 8 weeks' gestation at an urgent care center in middle Tennessee, USA, with a 1-day history of a painful and pruritic rash on her torso at the site of a previous tick attachment (Figure 1). The rash consisted of a faint circular area of erythema surrounding a central shallow eschar. Two weeks before the rash developed, the patient removed 4 embedded ticks after walking her dogs in a field. The patient was unable to provide additional information regarding the physical characteristics of the ticks. The patient reported no systemic symptoms or recent domestic or international travel.

The patient was prescribed a 14-day course of cefuroxime axetil. Results of acute and convalescent serologic testing for *Ehrlichia chaffeensis*, *Borrelia burgdorferi*, and *Rickettsia rickettsii* infections were negative (Table). Results of complete blood count were unremarkable. After negative results of serologic testing were received, the patient was instructed to stop the prescribed antibiotic medications after ≈4 days of treatment.

The patient noted vaginal bleeding 2 weeks and 5 days after the urgent care visit; a subsequent prenatal ultrasound confirmed intrauterine fetal demise. The products of conception were routinely submitted for pathologic examination.

Hematoxylin and eosin–stained sections showed marked acute villitis involving most of the trophoblastic villi. Large intravillous abscesses involved many villi. In addition, the acute inflammatory reaction appeared to originate at the villous tip and spread proximally to involve nearly the entire villous in a confluent fashion (Figure 2, panels A, B). Gram staining for bacteria and immunohistochemistry for cytomegalovirus were both negative. Giemsa special staining (Appendix Figure, https://wwwnc.cdc.gov/EID/article/31/2/24-0870-App1.pdf) showed darkly stained intracellular rods.

Electron microscopy examination of the trophoblastic villi demonstrated intracellular bacterial organisms within cytoplasmic vacuoles (Figure 2, panel C) and freely within the cytosol (Figure 2, panel D). The morphology of the organisms closely resembled that of the species *Candidatus* Midichloria mitochondrii, although definitive speciation cannot be rendered (*7*). Specifically, the organisms were round in cross-sectional profiles and appeared as short rods in

longitudinal sections, measuring ≈0.25–0.34 μm in diameter and 0.40–0.53 μm in length. The bacteria exhibited an electron dense cytoplasm with vague granular content and an electron lucent outer membrane. Of note, the mitochondria were not involved in the sections examined.

After light microscopy examination, we submitted a formalin-fixed paraffin-embedded tissue block for a clinically available 16S rRNA broad range PCR, followed by Sanger sequencing (*8*). After primer and quality trimming, the resulting 297-bp product (Genbank accession no. PP102451) shared 95.9% nucleotide identity to *Candidatus* Midichloria mitochondrii strain IricVA (GenBank accession no. NC_015722) and 95.2% identity to another *I. ricinus*–associated 16S sequence (GenBank accession no. DQ788562). The identical sequence was subsequently detected in 2 replicate extractions from a second tissue block from the case. To assess for preanalytical contamination, we also tested 2 formalin-fixed paraffin-embedded blocks from different patients processed in the same batch as this case by broad-range bacterial PCR. Both blocks were negative for bacterial DNA, ruling out contamination during tissue processing.

We analyzed the patient-derived 16S sequence in the context of representative Rickettsiales sequences (Figure 3). In the resulting tree, the detected bacterial sequence had the highest homology with a sequence from Thailand (accession no. KY910125) and was in a clade with *Candidatus* Midichloria spp. (80%–90% bootstrap support). The detected sequence was distinct from *Candidatus* M. mitochondrii, as well as other endosymbionts within the genus including *Candidatus* Lariskella sp. (AB624350).

Conclusions

Candidatus Midichloriaceae are proposed as a separate family under the Rickettsiales order, but few studies have attempted to describe the biology of this relatively unexplored region of the bacterial taxonomy. Bacteria of this family have been isolated in numerous tick vectors known to transmit pathogenic bacteria, including members of the *Ixodes*, *Rhipicephalus*, *Amblyomma*, *Hyalomma*, and *Dermacentor* genera, and have the capacity for mammalian inoculation (*9*). *Candidatus* Midichloriaceae organisms have a predilection for female ticks and demonstrate tropism for the salivary glands and ovaries, enabling vertical transmission to tick progeny (*10*). Evidence suggests at least facultative mutualism between the tick host and some *Candidatus* Midichloriaceae organisms; *Candidatus* M. mitochondrii has been shown to increase the tick's feeding ability during blood meals, as well as aid in the production of superior larvae (*11*,*12*).

The pathogenic potential of *Candidatus* Midichloriaceae in intermediate hosts is incompletely

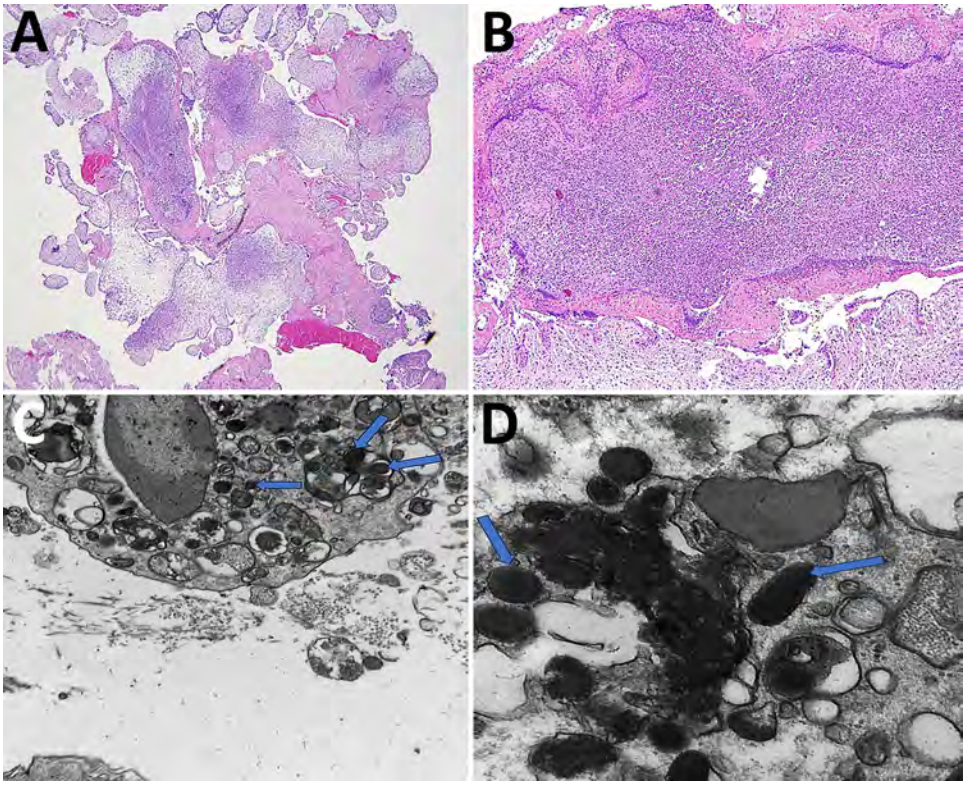

Figure 2. Imaging of samples from patient in study of infection by tickborne bacterium *Candidatus* Midichloria associated with first trimester pregnancy loss, Tennessee, USA. A, B) Formalin-fixed paraffin-embedded sections showing acute suppurative villitis and large intravillous abscesses. Original magnification ×40 for panel A and ×200 for panel B. C, D) Electron microscopy analysis was performed on tissue that was previously formalin-fixed but not paraffin-embedded. The formalin-fixed tissue was placed in a 2.5% glutaraldehyde solution before electron microscopy analysis. C) Intracellular bacterial forms in the cytosol (indicated by arrows) at ×20,000 magnification; D) cytoplasmic vacuoles (indicated by arrows) at ×60,000 magnification, measuring ≈0.25–0.34 μm × 0.40–0.53 μm.

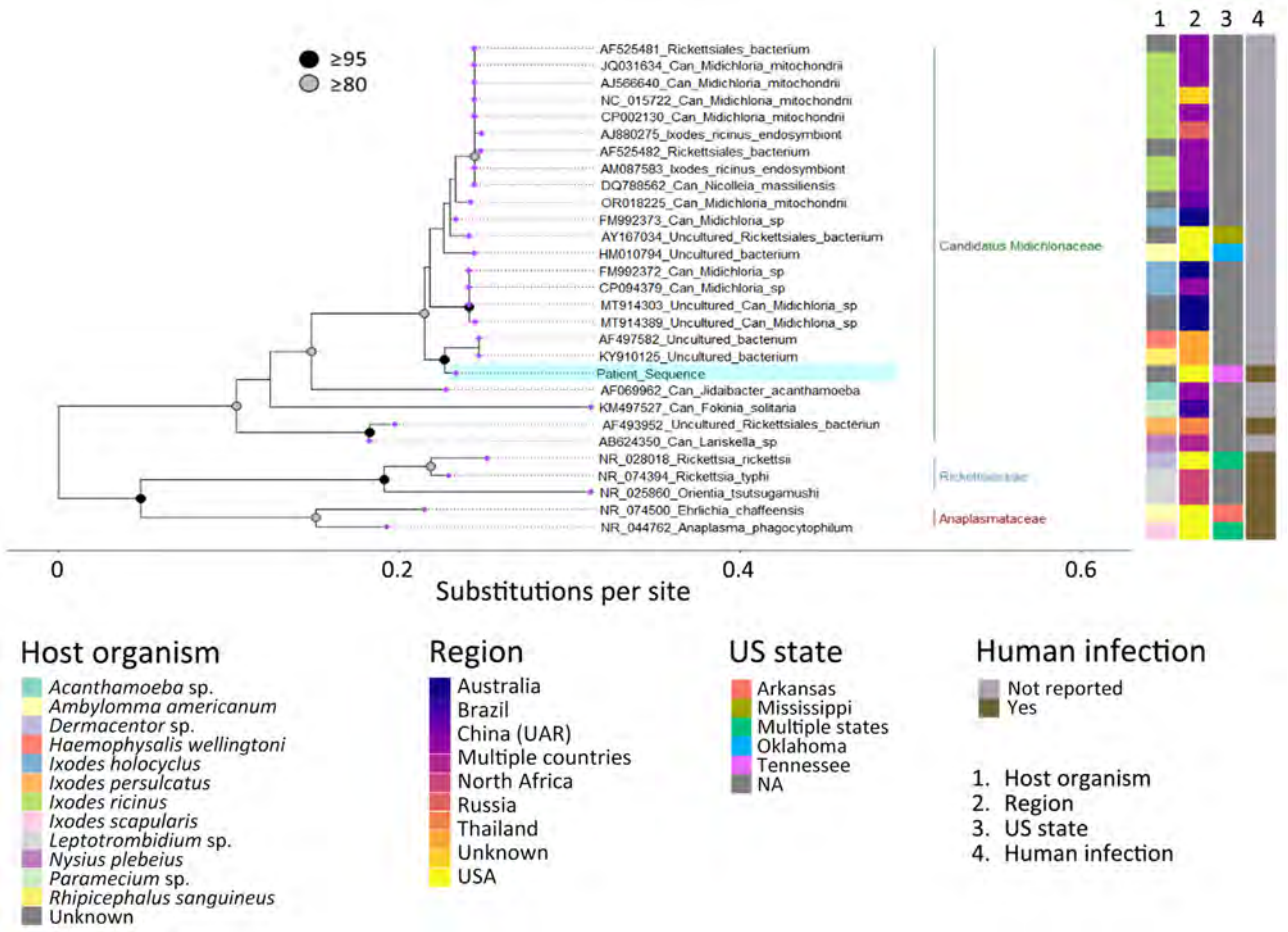

Figure 3. Phylogenetic analysis of a patient-derived sequence (highlighted in blue) in study of infection by tickborne bacterium *Candidatus* Midichloria associated with first trimester pregnancy loss, Tennessee, USA. Phylogenetic tree was generated using IQ-TREE (https://www.iqtree.org) with MAFFT-aligned (https://www.mafft.cbrc.jp/alignment/software) representative V1/V2 regions of 16S rRNA gene sequences from organisms within Rickettsiales and visualized with ggtree in R version 4.2.2 (The R Project for Statistical Computing, https://www.r-project.org). Sequences represented families Can. Midichloriaceae (green bar), Anaplasmataceae (red bar), and Rickettsiaceae (blue bar); most proximal sequences by BLAST analysis (https://blast.ncbi.nlm.nih.gov), including those used during clinical identification; and sequences previously associated with human specimens. GenBank accession numbers are indicated before the species name. Associated metadata indicate host tick, country reported, US state if applicable, and whether previously associated with a human infection. UAR, Uighur Autonomous Region. Nodes with >95% bootstrap support are in black, those with 80%–94.9% support are in gray. Tip labels are purple.

understood. Three studies have reported isolating antibodies to *Ca.* Midichloriaceae or microbial DNA from the blood of human hosts exposed to tick bites, with similar detection rates as a unique organism or in combination with another tickborne pathogen (*6*,*13*,*14*). Those results suggest that *Candidatus* Midichloriaceae antigens or nucleic acids can be transmitted to humans and used as a marker for tick bites but do not demonstrate independent pathogenicity or replicative ability. One of the 3 studies potentially identified a bacterium from the *Candidatus* Midichloriaceae family causing a mild febrile illness in east Russia in 2004 (*14*). Our results suggest a strong association between infection by *Candidatus* Midichloria sp. and the pregnancy loss in this patient.

Although electron microscopy images showed intracellular bacteria that could be compatible with *Candidatus* Midichloria sp., this study is limited by the lack of clear internal structures, although vague granular content suggestive of organelles was present. Therefore, definitive identification cannot be rendered. The only other known pathogen on the histologic differential diagnosis is *Listeria monocytogenes*, which classically displays villous microabscesses. However, the abscesses caused by *L. monocytogenes* are smaller, and the acute inflammation does not tend to be confluent or span the entire length of the villous

(*15*). Further, 16S rRNA sequencing did not detect *L. monocytogenes* in 2 replicate extractions, and *L. monocytogenes* organisms are typically situated in phagolysosomes and measure 500–2,000 nm in length.

This case describes an early pregnancy loss associated with an organism within the *Candidatus* Midichloriaceae family. This finding suggests tropism for human trophoblastic tissue and potentially deleterious effects for the fetus. Although further studies are needed to elucidate the taxonomy, hosts, life cycle, and pathogenesis of *Candidatus* Midichloria sp. and related endosymbionts, clinicians and patients should be aware of this emerging pathogen. Further, for pregnant patients with tick bites, treatment with doxycycline should be considered because the benefits could outweigh the risks. Pregnant patients, especially those in the southeastern United States, should be counseled on the risk for tick exposure during early pregnancy, as well as on proper tick removal technique.

About the Author

Dr. Newman is the neuropathology fellow at Stanford University Hospital, California, USA. His primary research interests include neurodegenerative disease, central nervous system neoplasia, and infectious diseases.

References

1. Giakoumelou S, Wheelhouse N, Cuschieri K, Entrican G, Howie SE, Horne AW. The role of infection in miscarriage. Hum Reprod Update. 2016;22:116–33. https://doi.org/10.1093/humupd/dmv041
2. Lambert JS. An overview of tickborne infections in pregnancy and outcomes in the newborn: the need for prospective studies. Front Med (Lausanne). 2020;7:72. https://doi.org/10.3389/fmed.2020.00072
3. Weber K, Bratzke HJ, Neubert U, Wilske B, Duray PH. *Borrelia burgdorferi* in a newborn despite oral penicillin for *Lyme borreliosis* during pregnancy. Pediatr Infect Dis J. 1988;7:286–9. https://doi.org/10.1097/00006454-198804000-00010
4. Sassera D, Beninati T, Bandi C, Bouman EAP, Sacchi L, Fabbi M, et al. '*Candidatus* Midichloria mitochondrii,' an endosymbiont of the tick *Ixodes ricinus* with a unique intramitochondrial lifestyle. Int J Syst Evol Microbiol. 2006;56:2535–40. https://doi.org/10.1099/ijs.0.64386-0
5. Giannotti D, Boscaro V, Husnik F, Vannini C, Keeling PJ. The "Other" Rickettsiales: an overview of the family "Candidatus Midichloriaceae." Appl Environ Microbiol. 2022;88:e0243221. https://doi.org/10.1128/aem.02432-21
6. Sgroi G, Iatta R, Lovreglio P, Stufano A, Laidoudi Y, Mendoza-Roldan JA, et al. Detection of endosymbiont *Candidatus* Midichloria mitochondrii and tickborne pathogens in humans exposed to tick bites, Italy. Emerg Infect Dis. 2022;28:1824–32. https://doi.org/10.3201/eid2809.220329
7. Comandatore F, Radaelli G, Montante S, Sacchi L, Clementi E, Epis S, et al. Modeling the life cycle of the intramitochondrial bacterium "*Candidatus* Midichloria mitochondrii" using electron microscopy data. MBio. 2021;12:e0057421. https://doi.org/10.1128/mBio.00574-21
8. McCormick DW, Rassoulian-Barrett SL, Hoogestraat DR, Salipante SJ, SenGupta D, Dietrich EA, et al. *Bartonella* spp. infections identified by molecular methods, United States. Emerg Infect Dis. 2023;29:467–76. https://doi.org/10.3201/eid2903.221223
9. Bazzocchi C, Mariconti M, Sassera D, Rinaldi L, Martin E, Cringoli G, et al. Molecular and serological evidence for the circulation of the tick symbiont *Midichloria* (Rickettsiales: Midichloriaceae) in different mammalian species. Parasit Vectors. 2013;6:350. https://doi.org/10.1186/1756-3305-6-350
10. Mukhacheva TA, Kovalev SY. Bacteria of the family 'Candidatus Midichloriaceae' in sympatric zones of *Ixodes* ticks: genetic evidence for vertical transmission. Microb Ecol. 2017;74:185–93. https://doi.org/10.1007/s00248-017-0932-z
11. Stavru F, Riemer J, Jex A, Sassera D. When bacteria meet mitochondria: the strange case of the tick symbiont *Midichloria mitochondrii*. Cell Microbiol. 2020;22:e13189. https://doi.org/10.1111/cmi.13189
12. Guizzo MG, Hatalová T, Frantová H, Zurek L, Kopáček P, Perner J. *Ixodes ricinus* ticks have a functional association with *Midichloria mitochondrii*. Front Cell Infect Microbiol. 2023;12:1081666. https://doi.org/10.3389/fcimb.2022.1081666
13. Mariconti M, Epis S, Gaibani P, Dalla Valle C, Sassera D, Tomao P, et al. Humans parasitized by the hard tick *Ixodes ricinus* are seropositive to *Midichloria mitochondrii*: is *Midichloria* a novel pathogen, or just a marker of tick bite? Pathog Glob Health. 2012;106:391–6. https://doi.org/10.1179/2047773212Y.0000000050
14. Mediannikov OI, Ivanov LI, Nishikawa M, Saito R, Sidel'nikov IN, Zdanovskaia NI, et al. Microorganism "Montezuma" of the order Rickettsiales: the potential causative agent of tick-borne disease in the far east of Russia [in Russian]. Zh Mikrobiol Epidemiol Immunobiol. 2004; (1):7–13.
15. Sepp AH, Roy TE. *Listeria monocytogenes* infections in metropolitan Toronto. A clinicopathological study. Can Med Assoc J. 1963;88:549–61.

Address for correspondence: Hernán Correa, 11219 Doctor's Office Tower, Vanderbilt Children's Hospital, 2200 Children's Way, Nashville, TN 37232-9065, USA; email: hernan.correa@vumc.org

Bjerkandera adusta Fungi as Causative Agent of Invasive Chronic Rhinosinusitis

Yuhei Kurata, Yoshifumi Kimizuka, Takashi Yaguchi, Kanshu Ito, Tetsuya Yamamoto, Yusuke Serizawa, Akira Kamiya, Takaaki Hamamoto, Taishi Sakima, Tomomi Tanigaki, Hiromi Edo, Yu Hongo, Akira Watanabe, Kazushi Suzuki, Terushige Toyooka, Akihiko Kawana

We report an invasive mycosis case in Japan caused by *Bjerkandera adusta*, a fungal species not previously reported as a causative pathogen of invasive mycosis. *B. adusta* was identified by using phylogenetic analysis. Voriconazole was used successfully for treatment. Immunodeficient patients may be susceptible to infection by rare causative fungi.

Sinonasal mycosis is a concerning deep-seated fungal disease. Invasive sinonasal mycosis is known for its poor prognosis and propensity for intracranial and intraorbital complications that are characterized by bone-destructive progression in immunodeficient conditions, including poorly managed diabetes, malignancies, long-term use of glucocorticoids and immunosuppressive drugs, and AIDS (*1*,*2*). The most common causative fungi are *Aspergillus* and *Mucor* spp.; however, other fungi, such as *Alternaria*, *Scedosporium*, *Candida*, and *Fusarium* spp. have been reported (*3*). In this article, we report the clinical course of an invasive mycosis case in Japan in which *Bjerkandera adusta*, a white-rot fungus that typically occurs on dead trees and stumps in forests, was identified in a patient biopsy specimen of a lesion. The patient provided written consent for the publication of this case report.

The Case

In November 2021, a 57-year-old woman with a history of type 2 diabetes and diabetic retinopathy experienced a headache that radiated throughout her head (numeric rating scale [NRS] 10) and a painful sensation in the right side of her face, radiating from under the jaw to the cheek. She was a housewife without any specific hobbies outside the home. We conducted magnetic resonance imaging (MRI) in February 2022 to investigate the cause of the symptoms. The MRI revealed a mild subacute cerebral infarction in the right parietal lobe but no other obvious abnormalities. The symptoms persisted despite cilostazol treatment. We conducted a repeat MRI in August 2022 that revealed a mass-like lesion near the right cavernous sinus. Extensive infiltrative growth patterns were found in the right sphenoid sinus, right orbital apex, right cavernous sinus, dura mater inside the right middle cranial fossa, right side of the clivus, right skull base, right temporalis muscle, right levator palatopharyngeus muscle, and soft tissue around the right eustachian tube (Figure 1, panel A).

Laboratory testing revealed an elevated erythrocyte sedimentation rate and unremarkable β-D-glucan levels, except for a slight elevation near the upper reference limit (Table 1). Cerebrospinal fluid analysis revealed elevated protein levels but unremarkable culture and cell count (Table 2). We conducted a transnasal biopsy of deep tissue from the right skull base with aseptic exposure of the orbital floor on August 26, 2022. Hematoxylin and eosin staining and Grocott methenamine silver staining of the tissue revealed branched, funguslike structures (Figure 2, panels A, B). However, cultures on bromothymol blue agar, sheep blood agar, and chocolate agar were negative, and the fungal species could not be identified. On October 13, we conducted an additional biopsy and curettage of the lesion. Cultures on potato dextrose agar grew filamentous fungi (Figure 2, panel C), and the samples

Author affiliations: National Defense Medical College, Saitama, Japan (Y. Kurata, Y. Kimizuka, K. Ito, T. Yamamoto, Y. Serizawa, T. Sakima, T. Tanigaki, H. Edo, Y. Hongo, K. Suzuki, T. Toyooka, A. Kawana); Chiba University, Chiba, Japan (T. Yaguchi, A. Watanabe); National Defense Medical College Hospital, Saitama (A. Kamiya, T. Hamamoto)

DOI: https://doi.org/10.3201/eid3102.241275

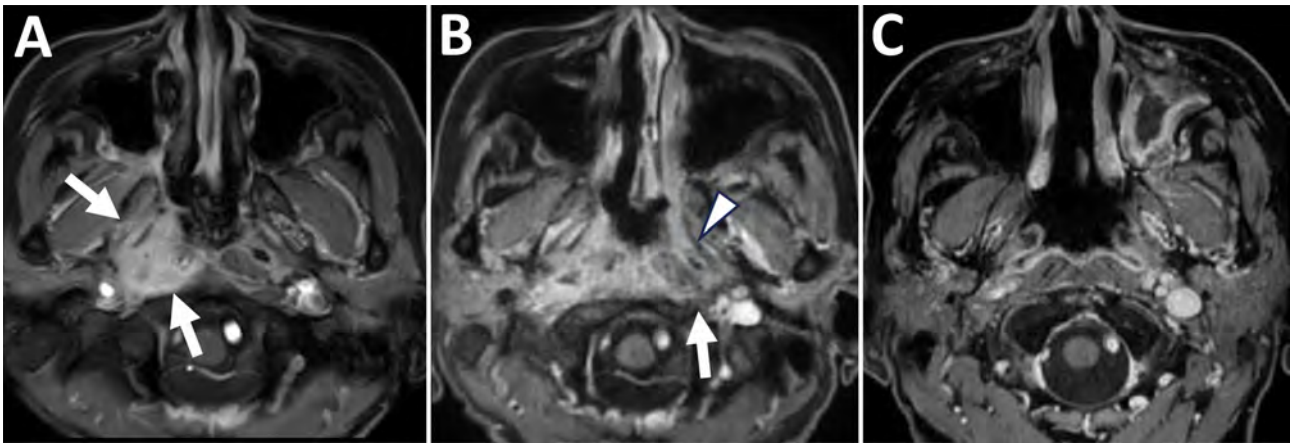

Figure 1. Chronological changes in lesions observed on contrast-enhanced fat-suppressed T1-weighted magnetic resonance imaging at the nasopharyngeal level in a patient in Japan with invasive chronic rhinosinusitis caused by *Bjerkandera adusta* fungi. A) Initial visit. Enhancement effects observed in the right nasopharynx, including the right torus tubarius and right prevertebral space (white arrows). B) Three months after the initial visit. Expansion of the enhancing lesion is seen, with enhancement extending to the left peritubal region (white arrowhead) and prevertebral space (white arrow). C) One year after the initial visit. The abnormal enhancement previously observed around both the torus tubarius and prevertebral space has regressed.

were sent to the Chiba University Mycology Center (Chiba, Japan) for species identification. The fungus was identified as *B. adusta* by using phylogenetic analysis (Appendix, https://wwwnc.cdc.gov/EID/article/31/2/24-1275-App1.pdf).

While waiting for the species to be identified, we initiated liposomal amphotericin B (L-AMB; 5 mg/kg/d) treatment on October 19, 2022, for invasive sinonasal fungal disease. However, on November 1, an MRI revealed that the contrast-enhanced lesion had spread to the left peritubal region and prevertebral space (Figure 1, panel B). Because of drug-induced renal damage, we added posaconazole (50 mg 3×/d) to the treatment regimen and performed a local nasal lavage on November 8. On the same day, the patient was reported to have a fever. We suspected a central venous catheter–related bloodstream infection and fever caused by posaconazole. Therefore, we discontinued posaconazole, initiated meropenem and vancomycin, and continued nasal lavage with the antifungal drug. On November 14, the fungal species was reported as *B. adusta*. On the basis of previously reported in vitro drug susceptibility data (*4*), we initiated voriconazole on December 7. The headache, initially rated at NRS 7–10, showed improvement beginning December 18, with a notable reduction to NRS 1. On December 26, an MRI revealed that the lesion expansion had stopped, with progression suppressed. We administered voriconazole intravenously for 3 weeks and then switched to oral administration on January 1, 2023, for a total treatment duration of 6 months. Blood β-D-glucan levels peaked at 52 pg/mL 4 months after the initial examination and decreased over time, returning to unremarkable levels by March 2023. We observed a gradual decrease in the abnormal contrast enhancement on MRI in March and July (Figure 1, panel C).

B. adusta is a white-rot fungus belonging to the phylum *Basidiomycota*, which forms mushrooms ≈4 inches in diameter (Figure 2, panel D). The mushrooms are widely distributed in temperate and subtropical zones worldwide and grow on dead or stunted broad-leaved trees. In humans, spores of this fungus act as allergens in the respiratory system,

Table 1. Blood test results obtained from a patient with *Bjerkandera adusta*–caused invasive chronic rhinosinusitis, August 2022

Test	Value
Total bilirubin, mg/dL	0.53
Aspartate aminotransferase, U/L	10
Alanine aminotransferase, U/L	7
Lactate dehydrogenase, U/L	202
Blood urea nitrogen, mg/dL	19
Creatinine, mg/dL	0.97
Sodium, mmol/L	137
Potassium, mmol/L	4.5
Chloride, mmol/L	99
C-reactive protein, mg/dL	0.8
Erythrocyte sedimentation rate, mm/h	105
β-D glucan, pg/mL	19
Candida antigen, U/mL	≤0.05
Aspergillus antigen cutoff index	0.3
Cryptococcus antigen	Negative
Leukocyte, 10^3 cells/μL	9.4
Neutrophils, %	55.6
Lymphocytes, %	39
Monocytes, %	3.8
Eosinophils, %	1.4
Basophils, %	0.2
Hemoglobin, g/dL	10.2
Platelet, 10^3/μL	480

causing chronic cough and throat discomfort (*5*). Together with other basidiomycetes, this condition is known as fungus-associated chronic cough (*6*). We were unable to find other reported cases of invasive sinusitis caused by *B. adusta*. The patient lives in a commuter town adjacent to Tokyo, which is relatively warm and humid throughout the year and is surrounded by woods, a habitat for *B. adusta* that might have led to this infection.

Conclusions

In invasive fungal sinusitis, such as mucormycosis and aspergillosis, the fungus invades the blood vessels and causes necrotizing infection of the surrounding organs due to vascular invasion with thrombosis, subsequently spreading from the sinuses to the orbit and sphenoid sinus and eventually intracranially, causing fatality. Symptoms include more severe headaches than those associated with sinusitis and neurologic symptoms such as rapidly progressing visual impairment, depending on the site of fungal invasion (*7*). Invasive sinonasal fungal disease was once considered a rare disease; however, the number of reported cases has increased. This change could be because of an increased number of patients with conditions that decrease immunity, such as diabetes, long-term steroid administration, and anticancer drug treatment (*2*,*8*). In this case, the underlying disease was poorly controlled; therefore, the infection spread from the sphenoid sinus into the cranium, causing headaches and visual and hearing impairments.

Table 2. Cerebrospinal fluid test results obtained from a patient with *Bjerkandera adusta*–caused invasive chronic rhinosinusitis, August 2022

Test	Value
Cell count/μL*	4
Specific gravity	1.006
pH	8.2
Protein, mg/dL	147
Glucose, mg/dL	92
Sodium, mmol/L	148
Potassium, mmol/L	3
Chloride, mmol/L	127
Albumin, g/dL	708.9
IgG, mg/dL	19.5
IgA, mg/dL	6.46
IgM, mg/dL	0.58

*Cell fractionation not detected.

A combination of surgery, systemic antifungal medications, and immunodeficient state improvement is recommended for treating invasive sinusitis (*9*). However, thorough removal is difficult if the infection has spread to the intracranial area, internal carotid artery, or cavernous sinus. Voriconazole is recommended as an antifungal drug for aspergillosis. In contrast, L-AMB is typically used for treating mucormycosis. Although the effective antifungal drug for *B. adusta* remains unclear, in this case, L-AMB treatment was ineffective; therefore, voriconazole was administered, and the patient recovered. After 6 months of treatment, no MRI findings suggested relapse.

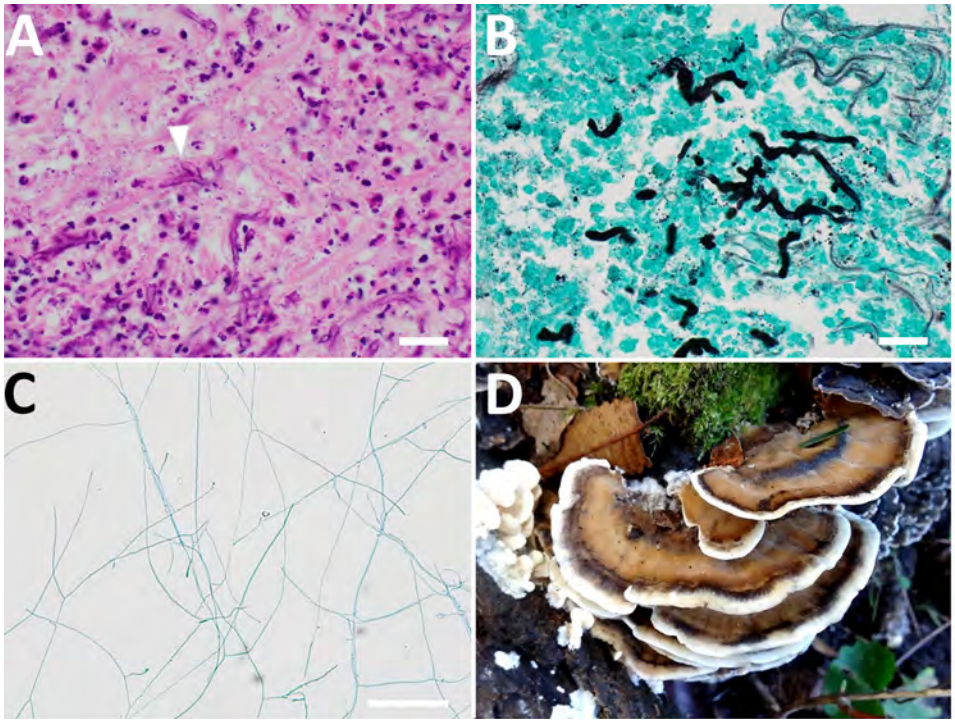

Figure 2. Imaging from a biopsy specimen from a sinus lesion in a patient in Japan with invasive chronic rhinosinusitis caused by *Bjerkandera adusta* fungi and a *Bjerkandera* spp. mushroom found in nature. A) Mycelium of filamentous fungi (arrowhead) shown by hematoxylin-eosin staining. Scale bar indicates 20 μm. B) Filamentus fungi shown by Grocott staining. Scale bar indicates 20 μm. C) Mycelium of fungi grown on potato dextrose agar. Scale bar indicates 100 μm. D) *Bjerkandera* spp., a burnt-looking stemless mushroom that grows in forests. Photograph courtesy of the Tokyo Mushroom Club.

β-D-glucan levels also decreased, which may reflect the disease course.

The first limitation of this study is that, although *B. adusta* was detected in the nasal biopsy specimen, mixed infections with other causative organisms of invasive sinusitis could not be ruled out. However, no other fungi were detected in the 2 tissue cultures, and we believe that *B. adusta* most likely led to invasive sinusitis. Second, *B. adusta* cannot be tested for drug susceptibility. Although we observed an improvement in the symptoms and laboratory findings after changing the treatment regimen from L-AMB to voriconazole, we cannot confirm that voriconazole is an effective antifungal drug against *B. adusta*.

In summary, we report a case of chronic invasive sinusitis caused by *B. adusta* in an immunocompromised patient with uncontrolled type 2 diabetes. The patient appeared to recover with a treatment regimen consisting of voriconazole. Clinicians should be aware that immunodeficient patients may experience invasive infections because of rare causative fungi.

About the Author

Dr. Kurata is a resident in the department of internal medicine at the National Defense Medical College. He is also a military physician specializing in infectious diseases and respiratory medicine.

References

1. Silveira MLC, Anselmo-Lima WT, Faria FM, Queiroz DLC, Nogueira RL, Leite MGJ, et al. Impact of early detection of acute invasive fungal rhinosinusitis in immunocompromised patients. BMC Infect Dis. 2019;19:310. https://doi.org/10.1186/s12879-019-3938-y
2. Chakrabarti A, Denning DW, Ferguson BJ, Ponikau J, Buzina W, Kita H, et al. Fungal rhinosinusitis: a categorization and definitional schema addressing current controversies. Laryngoscope. 2009;119:1809–18. https://doi.org/10.1002/lary.20520
3. Luo YT, Zhu CR, He B, Yan AH, Wei HQ. Diagnostic and therapeutic strategies of acute invasive fungal rhinosinusitis. Asian J Surg. 2023;46:58–65. https://doi.org/10.1016/j.asjsur.2022.05.006
4. González GM, Sutton DA, Thompson E, Tijerina R, Rinaldi MG. In vitro activities of approved and investigational antifungal agents against 44 clinical isolates of basidiomycetous fungi. Antimicrob Agents Chemother. 2001;45:633–5. https://doi.org/10.1128/AAC.45.2.633-635.2001
5. Ogawa H, Fujimura M, Takeuchi Y, Makimura K, Satoh K. Sensitization to *Bjerkandera adusta* enhances severity of cough symptom in patients with fungus-associated chronic cough (FACC). Med Mycol J. 2011;52:205–12. https://doi.org/10.3314/mmj.52.205
6. Ogawa H, Fujimura M, Takeuchi Y, Makimura K. Efficacy of itraconazole in the treatment of patients with chronic cough whose sputa yield basidiomycetous fungi-fungus-associated chronic cough (FACC). J Asthma. 2009;46:407–12. https://doi.org/10.1080/02770900902846331
7. Walsh TJ, Anaissie EJ, Denning DW, Herbrecht R, Kontoyiannis DP, Marr KA, et al.; Infectious Diseases Society of America. Treatment of aspergillosis: clinical practice guidelines of the Infectious Diseases Society of America. Clin Infect Dis. 2008;46:327–60. https://doi.org/10.1086/525258
8. Durand ML, Kitt TM, Song Y, Marty FM. Isavuconazole treatment of invasive fungal sinusitis: a post hoc analysis of the SECURE and VITAL trials. Clin Infect Dis. 2021;73:e1380–3. https://doi.org/10.1093/cid/ciab386
9. Kasapoglu F, Coskun H, Ozmen OA, Akalin H, Ener B. Acute invasive fungal rhinosinusitis: evaluation of 26 patients treated with endonasal or open surgical procedures. Otolaryngol Head Neck Surg. 2010;143:614–20. https://doi.org/10.1016/j.otohns.2010.08.017

Address for correspondence: Yoshifumi Kimizuka, National Defense Medical College, 3-2 Namiki, Tokorozawa, Saitama 359-8513, Japan; email: ykimizuka@ndmc.ac.jp

Amebiasis in Mexico, 2014–2023

Alberto Antonio-Campos, Keity J. Farfán-Pira, Alfonso D. Díaz-Fonseca, Carlos Ochoa-Velasco, Paola Hernández-Carranza, Diana M. Torres-Cifuentes

Amebiasis remains a public health challenge in Mexico, especially in areas with poor sanitation. Despite declining prevalence (2014–2023), hotspots persist because of socioeconomic factors such as poverty. Addressing regional disparities through targeted interventions, improved infrastructure, and education is crucial to further reduce the disease burden and prevent future outbreaks.

Amebiasis, caused by *Entamoeba histolytica* protozoan parasites, leads to ≈100 million annual cases worldwide, particularly in developing regions (*1*). About 90% of infections are asymptomatic, creating reservoirs that perpetuate community transmission. The 10% of symptomatic infections cause dysentery, diarrhea, abdominal pain, and fever, often progressing to invasive intestinal amebiasis (IIA), which invades the intestinal mucosa and damages intestinal walls (*2*). Some cases advance to extraintestinal forms, such as amebic liver abscess (ALA) (*3*). We studied the epidemiology of amebiasis in Mexico, where the disease remains a public health challenge, emphasizing the need for monitoring programs in high-risk regions to promptly manage cases and complications.

The Study

To analyze amebiasis trends in Mexico during 2014–2023, we examined IIA cases reported by healthcare providers to the Mexican Ministry of Health through the national epidemiologic surveillance system. We calculated prevalence per 100,000 inhabitants by using population data estimated from polynomial equations based on demographic data provided by the Instituto Nacional de Estadística y Geografía (Aguascalientes, Mexico). Reports were based on annual total confirmed cases recorded during the final week of each year (week 52 or 53); totals were summed for patients of both sexes. We evaluated the influence of socioeconomic factors and regional disparities on amebiasis by using 2015 IIA data, focusing on key population characteristics such as poverty and access to piped water and drainage (Appendix, https://wwwnc.cdc.gov/EID/article/31/2/24-1507-App1.pdf).

In 2014, the state of Hidalgo reported the highest number of IIA cases (2,535), 3.8 times that of Yucatan, the state reporting the second highest number of cases (Appendix Figure 1). Nationally, prevalence declined from 14.1% in 2014 to 5.86% in 2019 (Figure 1, panel A), potentially influenced by public health measures during the COVID-19 pandemic, as reported for other infectious diseases (*4*). Despite the decline, states such as Campeche, Chiapas, Guerrero, Hidalgo, Nayarit, Oaxaca, and Yucatan remain hot spots (Appendix Figure 1). During 2014–2023, a steady decrease in IIA cases indicated a reduction in illness (Appendix Table). Annual IIA case reports were as follows: 292,811 cases in 2014 (week 53), 251,416 in 2015 (week 52), 216,103 in 2016 (week 52), 222,813 in 2017 (week 52), 199,482 in 2018 (week 52), and 187,785 in 2019 (week 52). Declines in subsequent years were 111,054 cases in 2020, 111,284 in 2021, 116,012 in 2022, and 117,274 in 2023 (Figure 1, panel A).

ALA trends during 2014–2022 showed variability; prevalence peaked in Colima (7.79) and remained consistently high in Chihuahua and Sonora (Appendix Figure 2). National ALA cases increased until 2019, followed by a decline through 2023. Reported cases were as follows: 490 cases in 2014 (week 53), 609 in 2015 (week 52), 610 in 2016 (week 52), 524 in 2017 (week 52), 532 in 2018 (week 52), and a peak of 802 cases in 2019 (week 52). Subsequently, cases decreased to 540 in 2020 (week 53), 435 in 2021 (week 52), 528 in 2022, and 481 in 2023 (week 52) (Figure 1, panel B; Appendix Table). High-prevalence states such as Colima, Nayarit, Sinaloa, Sonora, and Oaxaca face persistent challenges, underscoring the need for improved hygiene and food safety.

Author affiliations: Instituto Politécnico Nacional, Mexico City, Mexico (A. Antonio-Campos); University of Arkansas, Fayetteville, Arkansas, USA (K.J. Farfán-Pira); Benemérita Universidad Autónoma de Puebla, Puebla, Mexico (A.D. Díaz-Fonseca, C. Ochoa-Velasco, P. Hernández-Carranza, D.M. Torres-Cifuentes)

DOI: https://doi.org/10.3201/eid3102.241507

Amebiasis exhibits demographic patterns in Mexico. Women are more frequently affected by IIA (Appendix Figure 3, panel A), whereas ALA is 10 times more prevalent among men (Appendix Figure 3, panel B).

During 2014–2023, southern states such as Nayarit, Tabasco, Chiapas, Oaxaca, Campeche, Guerrero, and Yucatan consistently reported high IIA prevalence (Figure 2, panels A, B). Conversely, ALA cases predominated in northern states, including Sinaloa, Sonora, Chihuahua, and Baja California, and in the central regions such as Nayarit and Aguascalientes; prevalence ranged from 0.96 to 1.70 (Figure 2, panels C, D). Of note, Nayarit and Sinaloa reported high prevalence for both IIA and ALA, highlighting substantial public health burdens.

Amebiasis disproportionately affects low-income areas (*5*). Analysis of 2015 IIA data revealed high prevalence, especially in rural regions with poor sanitation (e.g., Nayarit, Chihuahua, Yucatan, Guerrero, and Chiapas) (Appendix Figure 4, panel A). Piped water and drainage were low in states such as Chiapas, Guerrero, Oaxaca, San Luis Potosi, and Veracruz (Appendix Figure 4, panel B), and poverty exceeded 60% in regions such as Ciudad de Mexico, Guerrero, Oaxaca, and Puebla (Appendix Figure 4, panel C). The association between poverty and IIA prevalence was statistically significant ($r = 0.46$, $p<0.01$) (Appendix Figure 4, panel D).

Conclusions

Amebiasis remains a substantial health issue in Mexico, primarily because of its ease of transmission and associated illness and death rates. The US National Institute of Allergy and Infectious Diseases (Bethesda, MD, USA) classifies *E. histolytica* as a category B agent, underscoring the urgent need for enhanced diagnostic tools and surveillance systems (*6*,*7*). The consistently high prevalence of IIA in southern Mexico aligns with previous reports of elevated *E. histolytica* antibody levels compared with northern Mexico (*8*).

Of note, women are more frequently affected by IIA and men are more frequently affected by ALA. That difference may be attributed to factors such as hormonal effects, including the protective effect of iron-deficiency anemia or other hormonal factors in women of childbearing age (*9*) and potential increased susceptibility in men because of alcohol-associated liver damage (*10*).

Addressing the variable prevalence of ALA across Mexico is crucial. The complication is endemic to tropical regions but is increasingly reported globally, probably because of factors such as international travel and transmission through oral–anal contact (*1*). Although amebiasis primarily affects children in developing countries, the absence of detailed age-specific data from the Mexican Ministry of Health limits development of targeted interventions.

Our findings indicate an inverse relationship between IIA and ALA cases in Mexico, particularly in the southern regions. Previous studies suggest that 2%–5% of IIA cases progress to ALA and that genetic factors, such as specific alleles in the major histocompatibility complex (HLA-DRB1 and HLA-DQB1), play a critical role in resistance or susceptibility to ALA (*11*). That relationship is further complicated by regional differences in healthcare access, diagnostic practices, and reporting standards. ALA cases may be more readily identified in areas with advanced medical facilities, and IIA may be underreported in regions with limited infrastructure.

Although we found no direct link between sanitation and IIA prevalence, our analysis revealed a moderate correlation with socioeconomic conditions, which underscores the role of factors such as poverty, access to clean water, and sanitation

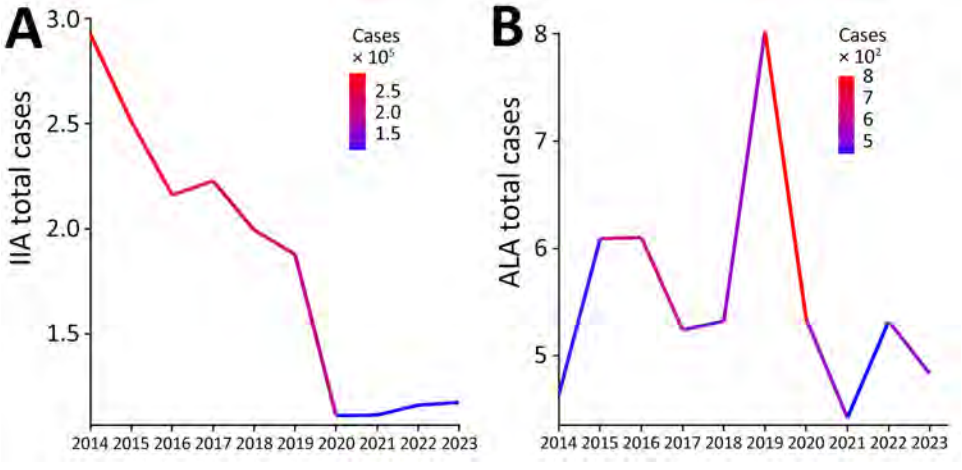

Figure 1. Annual prevalence (cases/100,000 inhabitants) of IIA (A) and ALA (B) in Mexico, by state, 2014–2023. ALA, amebic liver abscess; IIA, intestinal invasive amebiasis.

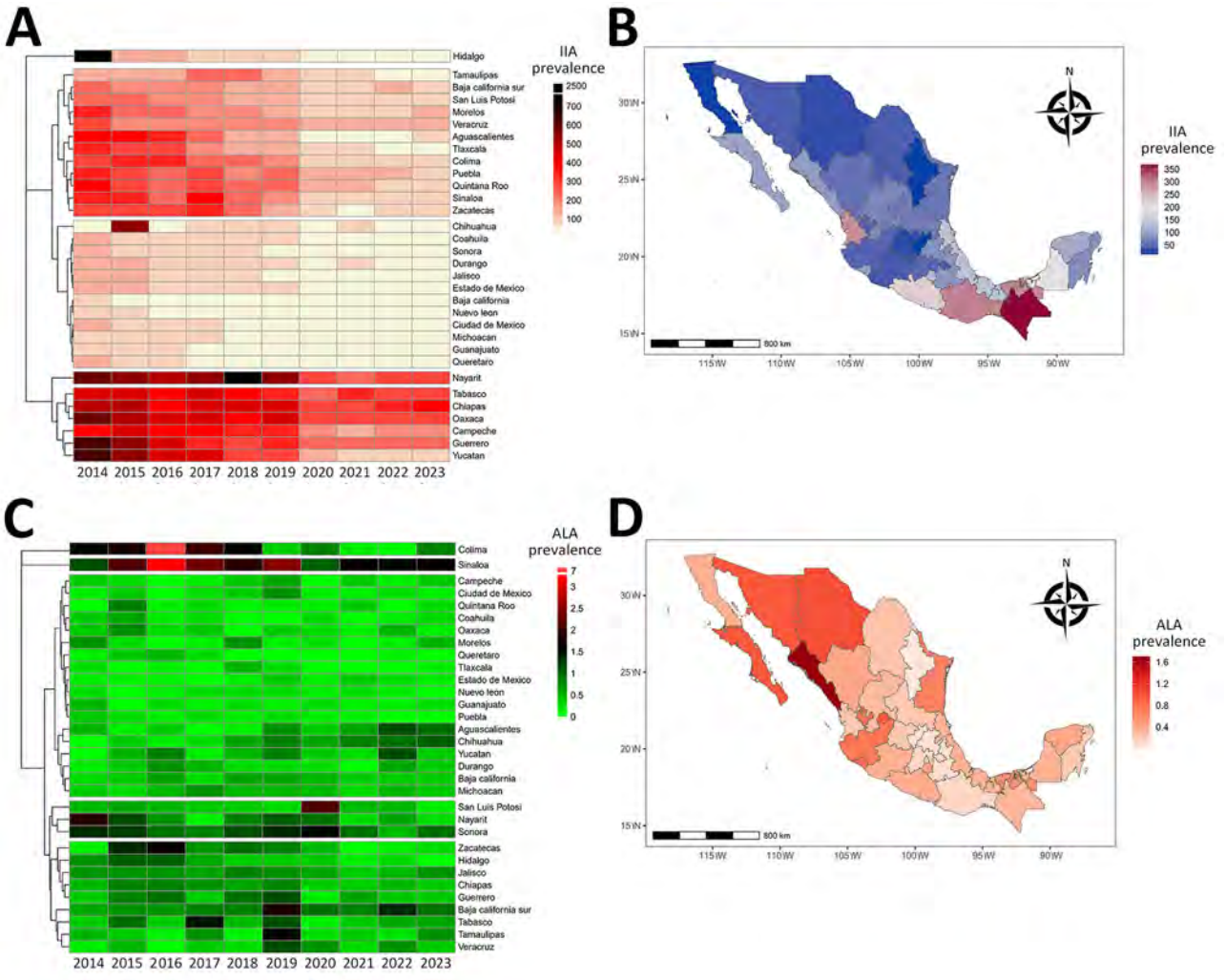

Figure 2. Distribution of IIA and ALA in Mexico by state, 2014–2023. A) Heatmap showing IIA prevalence across states, 2014–2023. B) Geographic distribution of IIA prevalence by state in 2023. C) Heatmap showing ALA prevalence across states, 2014–2023. D) Geographic distribution of ALA prevalence by state in 2023. ALA, amebic liver abscess; IIA, intestinal invasive amebiasis.

infrastructure in the burden of intestinal parasitic infections (*12*). Similar trends have been observed in other countries, including Malaysia (*13*), Iraq (*14*), and Ethiopia (*15*). Sociodemographic factors such as low income, inadequate sewage systems, and domestic animal waste contribute substantially to the prevalence of enteric infections. Enhanced hygiene practices and educational initiatives can play a crucial role in reducing prevalence.

In conclusion, amebiasis continues to pose a substantial health challenge in Mexico. Strengthening sanitation, health education, and surveillance efforts is essential. Ongoing research into virulence mechanisms and socioeconomic effects of the disease will support development of better treatment and prevention strategies and ultimately address the complex public health issues more effectively.

About the Author

Dr. Antonio-Campos is a professor of medical and veterinary protozoology in the Department of Parasitology at the National School of Biological Sciences, National Polytechnic Institute, Mexico City. His research focuses on the study of protozoan parasites responsible for diseases, such as *E. histolytica* and *Trypanosoma cruzi*.

References

1. Begum S, Gorman H, Chadha A, Chadee K. *Entamoeba histolytica*. Trends Parasitol. 2021;37:676–7. https://doi.org/10.1016/j.pt.2021.01.001
2. Nasrallah J, Akhoundi M, Haouchine D, Marteau A, Mantelet S, Wind P, et al. Updates on the worldwide burden of amoebiasis: a case series and literature review. J Infect Public Health. 2022;15:1134–41. https://doi.org/10.1016/j.jiph.2022.08.013

3. Usuda D, Tsuge S, Sakurai R, Kawai K, Matsubara S, Tanaka R, et al. Amebic liver abscess by *Entamoeba histolytica*. World J Clin Cases. 2022;10:13157–66. https://doi.org/10.12998/wjcc.v10.i36.13157
4. Crane MA, Popovic A, Panaparambil R, Stolbach AI, Romley JA, Ghanem KG. Reporting of infectious diseases in the United States during the coronavirus disease 2019 (COVID-19) Pandemic. Clin Infect Dis. 2022;74:901–4. https://doi.org/10.1093/cid/ciab529
5. Shirley DT, Farr L, Watanabe K, Moonah S. A review of the global burden, new diagnostics, and current therapeutics for amebiasis. Open Forum Infect Dis. 2018;5:ofy161. https://doi.org/10.1093/ofid/ofy161
6. Labruyère E, Thibeaux R, Olivo-Marin JC, Guillén N. Crosstalk between *Entamoeba histolytica* and the human intestinal tract during amoebiasis. Parasitology. 2019; 146:1140–9. https://doi.org/10.1017/S0031182017002190
7. Murphy BM, Chen JZ, Rolo M, Eldam M, Jordan L, Sivananthan SJ, et al. Intranasal delivery of a synthetic *Entamoeba histolytica* vaccine containing adjuvant (LecA + GLA-3 M-052 liposomes): in vitro characterization. Int J Pharm. 2022;626:122141. https://doi.org/10.1016/j.ijpharm.2022.122141
8. Caballero-Salcedo A, Viveros-Rogel M, Salvatierra B, Tapia-Conyer R, Sepulveda-Amor J, Gutierrez G, et al. Seroepidemiology of amebiasis in Mexico. Am J Trop Med Hyg. 1994;50:412–9. https://doi.org/10.4269/ajtmh.1994.50.412
9. Kantor M, Abrantes A, Estevez A, Schiller A, Torrent J, Gascon J, et al. *Entamoeba histolytica*: updates in clinical manifestation, pathogenesis, and vaccine development. Can J Gastroenterol Hepatol. 2018;2018:4601420. https://doi.org/10.1155/2018/4601420
10. Kumar R, Patel R, Priyadarshi RN, Narayan R, Maji T, Anand U, et al. Amebic liver abscess: an update. World J Hepatol. 2024; 16:316–30. https://doi.org/10.4254/wjh.v16.i3.316
11. Hernández EG, Granados J, Partida-Rodríguez O, Valenzuela O, Rascón E, Magaña U, et al. Prevalent HLA class II alleles in Mexico City appear to confer resistance to the development of amebic liver abscess. PLoS ONE. 2015; 10:e0126195. https://doi.org/10.1371/journal.pone.0126195
12. Forson AO, Arthur I, Ayeh-Kumi PF. The role of family size, employment and education of parents in the prevalence of intestinal parasitic infections in school children in Accra. PLoS ONE. 2018;13:e0192303. https://doi.org/10.1371/journal.pone.0192303
13. Chin YT, Lim YAL, Chong CW, Teh CSJ, Yap IKS, Lee SC, et al. Prevalence and risk factors of intestinal parasitism among two indigenous sub-ethnic groups in Peninsular Malaysia. Infect Dis Poverty. 2016;5:77. https://doi.org/10.1186/s40249-016-0168-z
14. Hasan HK, Mero WMS, Mohammed AB. Prevalence of amoebiasis and associated risk factors among population in Duhok city, Kurdistan Region, Iraq. J Infect Dev Ctries. 2023;17:542–9. https://doi.org/10.3855/jidc.17478
15. Gizaw Z, Yalew AW, Bitew BD, Lee J, Bisesi M. Development and validation of questionnaire to assess exposure of children to enteric infections in the rural northwest Ethiopia. Sci Rep. 2022;12:6740. https://doi.org/10.1038/s41598-022-10811-x

Address for correspondence: Diana Milena Torres-Cifuentes, Senda Quimica, Cd Universitaria, Jardines de San Manuel, 72570 Heroica Puebla de Zaragoza, Pue., CP 72590, Mexico; email: diana.torresc@correo.buap.mx

EID Podcast

Telework during Epidemic Respiratory Illness

The COVID-19 pandemic has caused us to reevaluate what "work" should look like. Across the world, people have converted closets to offices, kitchen tables to desks, and curtains to videoconference backgrounds. Many employees cannot help but wonder if these changes will become a new normal.

During outbreaks of influenza, coronaviruses, and other respiratory diseases, telework is a tool to promote social distancing and prevent the spread of disease. As more people telework than ever before, employers are considering the ramifications of remote work on employees' use of sick days, paid leave, and attendance.

In this EID podcast, Dr. Faruque Ahmed, an epidemiologist at CDC, discusses the economic impact of telework.

Visit our website to listen:
https://go.usa.gov/xfcmN

EMERGING INFECTIOUS DISEASES®

Detection of Chronic Wasting Disease Prions in Raw, Processed, and Cooked Elk Meat, Texas, USA

Rebeca Benavente, Fraser Brydon, Francisca Bravo-Risi, Paulina Soto, J. Hunter Reed, Mitch Lockwood, Glenn Telling, Marcelo A. Barria, Rodrigo Morales

We describe chronic wasting disease (CWD) prion detection in raw and cooked meat from a CWD-positive elk. We found limited zoonotic potential in CWD prions from those meat products. Nonetheless, risk for transmission to humans is still unclear, and monitoring of circulating and emerging CWD prion strains for zoonotic potential is warranted.

Prion diseases cause various diseases that affect several animal species, including scrapie in sheep and goats (*1*), Creutzfeldt-Jakob disease (CJD) in humans (*2*,*3*), bovine spongiform encephalopathy (BSE) in cattle (*4*), and chronic wasting disease (CWD) in cervids (*5*). In the 1990s, several atypical CJD cases occurred among persons who ingested cattle-derived products infected with BSE. Those cases later were attributed to the emergence of a new human prion strain templated by BSE prions (*6*). Subsequent studies have been conducted to investigate the zoonotic potential of other prionopathies, including CWD (*7*,*8*). Although no cases of CWD transmission to humans have been reported, the potential for human infection is still unclear because contradictory results have been reported from studies in animal models, in vitro systems, and nonhuman primates (*8*,*9*).

CWD prions have been detected in the muscle of both farmed and wild deer (*10*), and at concentrations relevant to sustain disease transmission (*11*). CWD prions have also been identified across several cervid species and in multiple tissues, including lymph nodes, spleen, tongue, intestines, adrenal gland, eyes, reproductive tissues, ears, lungs, and liver, among others (*12*–*14*). Those findings raise concerns about the safety of ingesting processed meats that contain tissues other than skeletal muscle (*15*) (Appendix, https://wwwnc.cdc.gov/EID/article/31/2/24-0906-App1.pdf). In addition, those findings highlight the need for continued vigilance and research on the transmission risks of prion diseases and for development of new preventative and detection measures to ensure the safety of the human food supply. Considering that humans consume products from ≈7,000–15,000 CWD-infected cervids each year (Appendix), the need for clarification of transmission risk for prion diseases is imperative. We investigated detection of CWD prions in seasoned and unseasoned raw and cooked meats prepared from a hunter-harvested elk. We also assessed the potential for CWD prions within meat products to template the misfolding of human cellular prion protein (PrP^{C}).

The Study

We obtained different unprocessed and processed meats from a hunter-harvested, CWD-infected elk that encoded both methionine and leucine polymorphic variations at prion protein (PrP) position 132. We used meat and meat-derived products, including filets, jerky steak cuts, hamburger meat, chili meat, sausage, ham, cutlets, and boneless steaks (Appendix Figure 1). The meat was prepared from a 5-year-old bull elk (*Cervus elaphus nelsoni*) that was positive for PrP^{Sc} (scrapie isoform of the prion protein) in the obex region of the brain; lymph node was not tested. The elk was harvested on December 10, 2020, and the sample was confirmed as CWD-positive January 8, 2021. The animal was collected in Medina County, Texas, on a private high-fenced hunting ranch.

Author affiliations: The University of Texas Health Science Center at Houston, Houston, Texas, USA (R. Benavente, F. Bravo-Risi, P. Soto, R. Morales); University of Edinburgh, Scotland, UK (F. Brydon, M.A. Baria); Universidad Bernardo O'Higgins, Santiago, Chile (F. Bravo-Risi, P. Soto, R. Morales); Texas Park and Wildlife Department, Kerrville, Texas, USA (J.H. Reed, M. Lockwood); Colorado State University, Fort Collins, Colorado, USA (G. Telling)

DOI: https://doi.org/10.3201/eid3102.240906

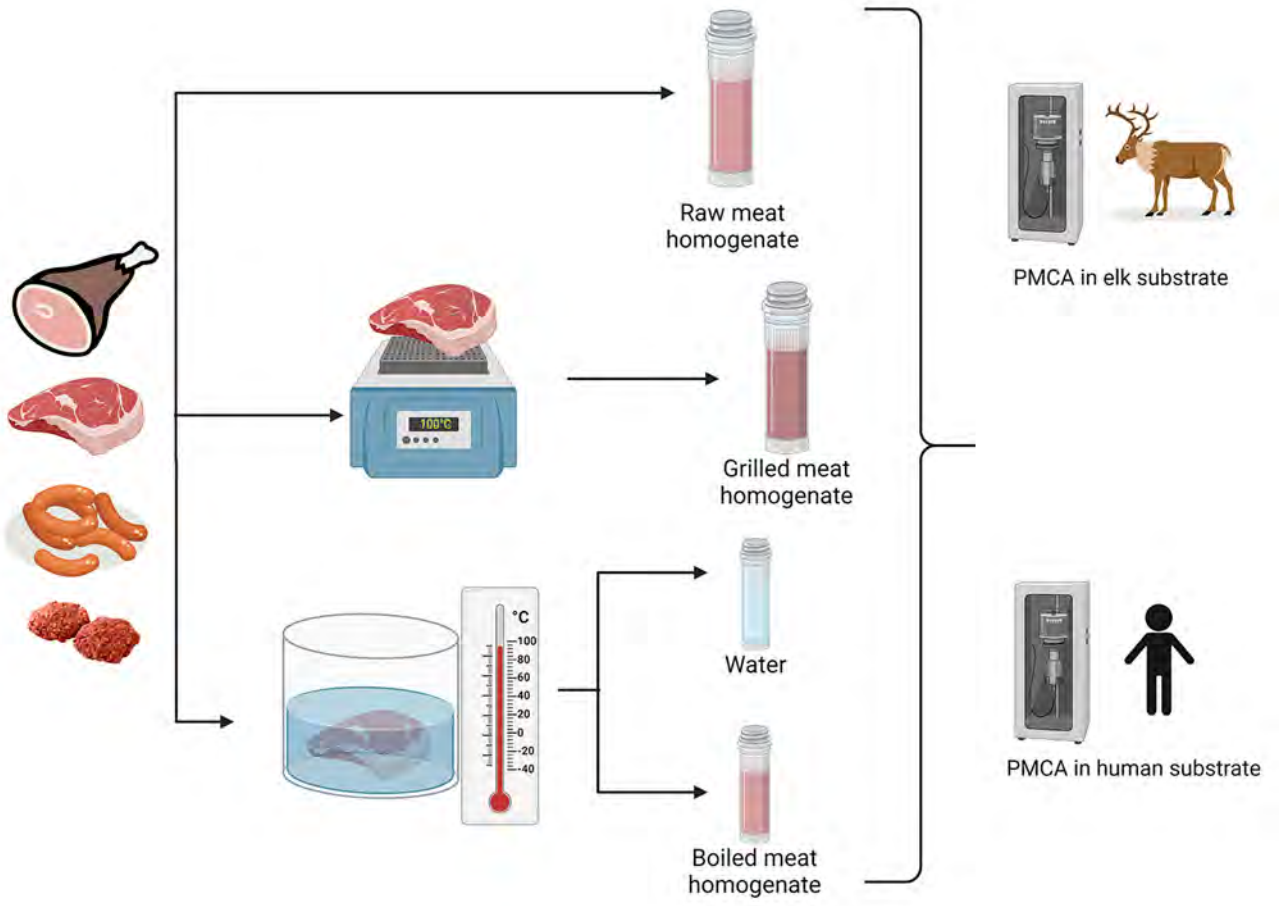

Figure 1. Flowchart of experimental strategy to detect chronic wasting disease prions in raw, processed, and cooked elk meat. We sampled ham, boneless steak, sausage, and hamburger meat from an elk that tested positive for chronic wasting disease. We homogenized raw meat samples and samples of meat cooking by grilling or boiling. We then tested homogenates of raw and cooked meat and the remnant water used in the boiling procedure by PMCA using elk and human substrates. PMCA, protein misfolding cyclic amplification.

We tested raw meat samples for CWD prions by using the protein misfolding cyclic amplification (PMCA) technique in an elk substrate (Figure 1). We selected the elk PMCA substrate to maintain the prion protein sequence homology between PrP^{C} and the suspected PrP^{Sc} in meats. In a first PMCA round, prion detection was negative for most of the raw meat samples, except the boneless steak, which had a positive PMCA signal in 1 of the replicates (Figure 2). To increase the sensitivity of prion detection, we performed 2 additional PMCA rounds (Appendix Figure 2). In a second PMCA round, we observed positive signals for additional specimens, including sausages and cutlets (Figure 2). The jerky sample also provided CWD prion signals in a third PMCA round (Figure 2). No other samples tested PMCA-positive in that analysis.

To test persistence of CWD prions in cooked meat products, we grilled and boiled different pieces of the meat types, mimicking a medium-well cooking status by considering the external and internal appearance and internal temperatures (Appendix Table). Of note, grilling substantially increased prion detection by PMCA, and 5 sample meat types, hamburger, chili meat, ham, cutlets, and boneless steak, were positive in a first PMCA round (Figure 2). We observed a positive PMCA signal for jerky meat in a second PMCA round and an increased number of positive replicates for the samples detected in the first round. At the third PMCA round, all grilled and boiled meats were positive for CWD prion in ≥1 replicate, strongly suggesting that grilling increased the availability of CWD prions for in vitro prion amplification (Figure 2). We observed similar results when we boiled different cuts of the same specimens. Of note, the water used to boil some of the meat samples was also positive by PMCA analyses (Figure 2; Appendix).

Considering the presence of CWD prions in the previously tested edible products, and their persistence after processing and cooking, we evaluated

the zoonotic properties of CWD prions by using the PMCA technique. PMCA previously has been reported to be useful in estimating zoonotic potential for multiple animal (i.e., nonhuman) prion isolates (Appendix). Here, we evaluated raw and cooked meats for their potential to template the misfolding of the human PrP^{C} in a single PMCA round to avoid further adaptation of the agent; hence, the goal of our experiment was to mimic initial interspecies transmission events. We specifically used a PMCA protocol optimized for human PrP encoding methionine at position 129. We used that specific human PrP version as PMCA substrate because of its increased susceptibility for misfolding in the presence of BSE prions (Appendix). The results demonstrated that none of the meat samples tested were able to induce conversion of human PrP^{C} to PrP^{Sc}, suggesting a limited zoonotic potential for such edible products (Figure 3). Of note, the results were the same regardless of the cooking status of the meat (Figure 3).

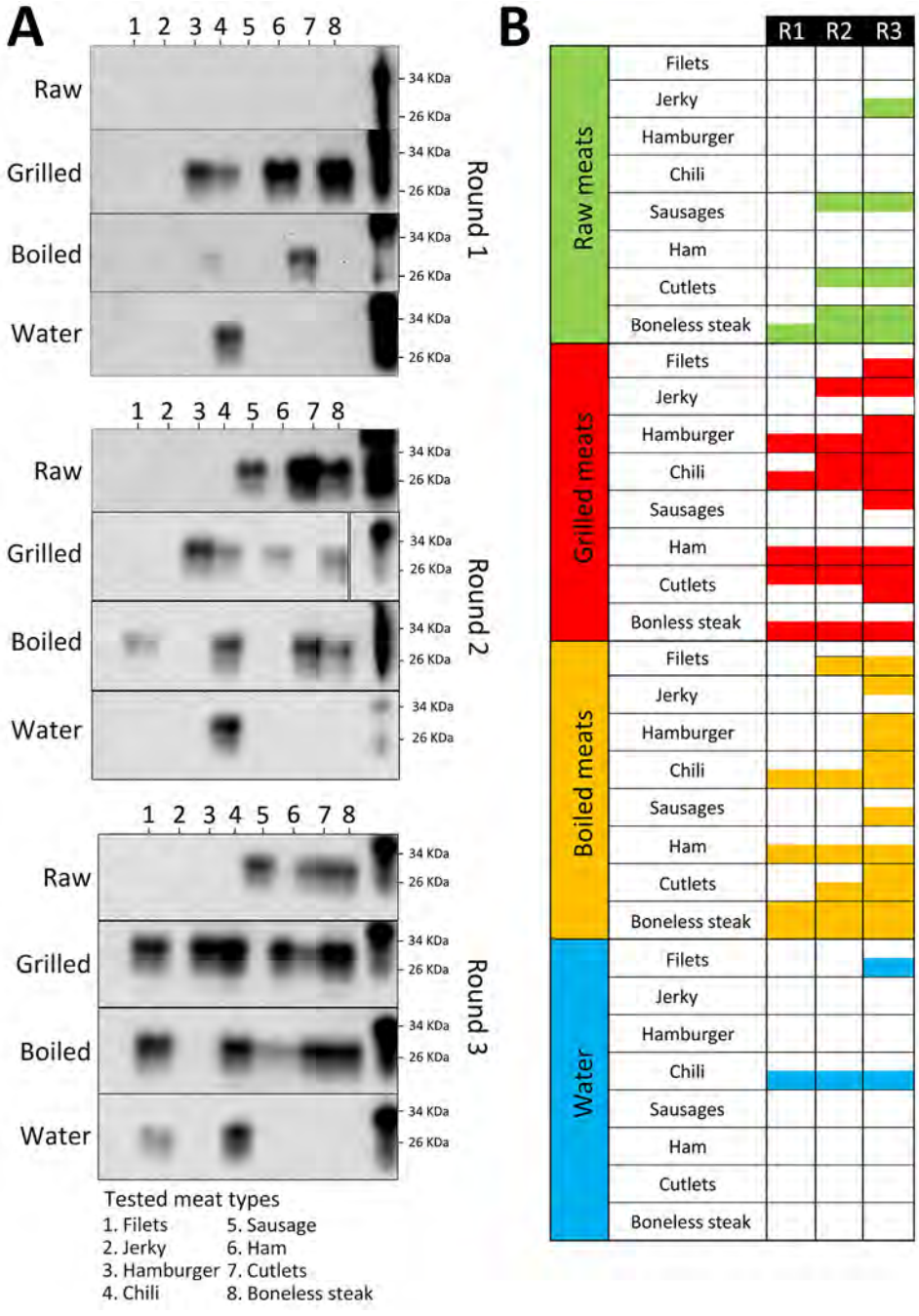

Figure 2. Western blot of PMCA used for detection of chronic wasting disease prions in raw, processed, and cooked elk meat. A) Representative PMCA data of the different samples tested. The panels depict the results obtained in 3 PMCA rounds of 1 of the replicates conducted in this analysis. All samples were treated with proteinase K, except for PrP^{C} that was used as a control for antibody activity and electrophoretic mobility. Numbers at the right depict molecular weight markers. B) Summary of the PMCA detection data in both replicates for raw, grilled, and boiled meats and for the water used in the boiling process. PMCA, protein misfolding cyclic amplification; PrP^{C}, cellular prion protein; R, round.

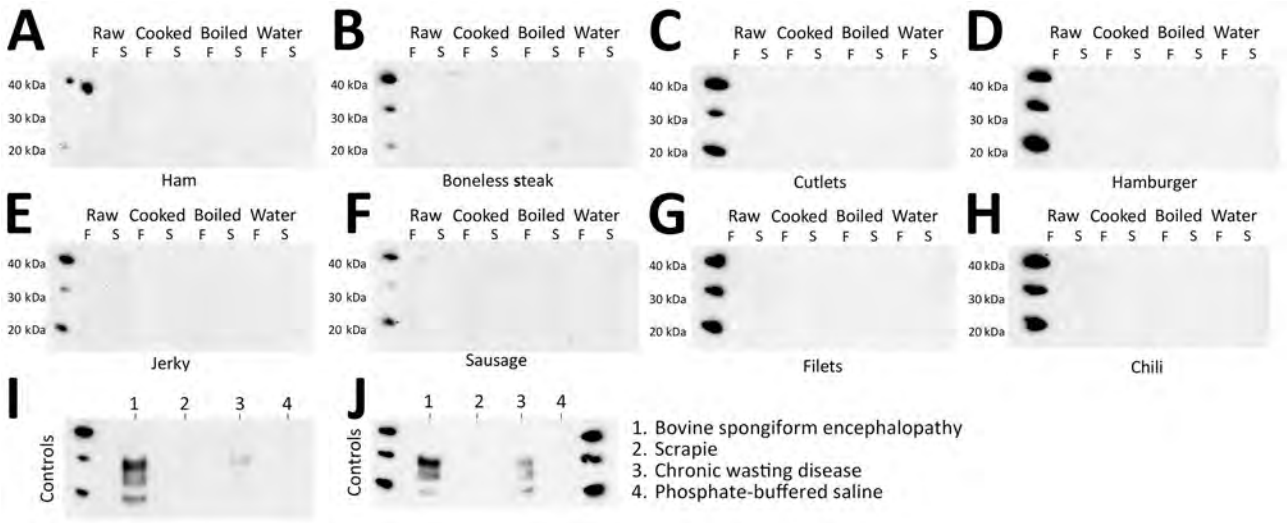

Figure 3. Western blot of PMCA to evaluate zoonotic potential of CWD-containing meats in a study of chronic wasting disease prions in raw, processed, and cooked elk meat. A) Ham; B) boneless steak; C) cutlets; D) hamburger; E) jerky; F) sausage; G) filets; H) chili meat; I) positive control; J) negative control. We evaluated raw, processed, and cooked meat from a CWD-positive elk for the ability to misfold the human prion protein in a single PMCA round. All samples were treated with proteinase K. The analysis depicts samples frozen before PMCA, or sonicated and submitted to PMCA. PBS and scrapie prions were used as negative controls for human PMCA reactions, and BSE and an elk CWD isolates were used as positive controls. Numbers at the left depict molecular weight markers. BSE, bovine spongiform encephalopathy; CWD, chronic wasting disease; F, frozen; PBS, phosphate-buffered saline; PMCA, protein misfolding cyclic amplification; S, sonicated.

To validate the PMCA method we used for modeling cross-species prion transmission, we incorporated classic BSE and sheep scrapie samples into the experimental protocol. We found PMCA reactions seeded by BSE prions and a CWD isolate were able to induce the misfolding of human PrP^C, as previously reported (Appendix), but that sheep scrapie was unable to do so.

Conclusions

Overall, our study results confirm previous reports describing the presence of CWD prions in elk muscles (*13*). The data also demonstrated CWD prion persistence in food products even after processing through different procedures, including the addition of salts, spices, and other edible elements. Of note, our data show that exposure to high temperatures used to cook the meat increased the availability of prions for in vitro amplification. Considering the potential implications in food safety and public health, we believe that the findings described in this study warrant further research. Our results suggest that although the elk meat used in this study resisted different manipulations involved in subsequent consumption by humans, their zoonotic potential was limited. Nevertheless, even though no cases of CWD transmission to human have been reported, the potential for human infection is still unclear and continued monitoring for zoonotic potential is warranted.

This work was supported by USDA/APHIS grant no. APP-35358 and NIH/NIAID grant no. 1R01AI132695 to R.M.

R.M. is listed as an inventor in one patent describing the PMCA technique. All other authors have no conflicts to disclose.

Author contributions: R.B. performed a single replicate elk-PMCA assay for all the samples tested in this study, prepared the final version of the figures, and wrote part of the original manuscript draft. F.B. executed the human-PMCA experiments. F.B.R. and P.S. performed replicates on the elk PMCA assay. J.H.R. and M.L. provided the meat samples. G.T. provided brains from Tg5037 mice to prepare the elk PMCA substrate. M.B. supervised the human PMCA experiments. R.M. supervised the whole execution of the project, wrote the first draft of the manuscript, and was responsible for funding. All the authors approved the final version of this article.

About the Author

Ms. Benavente is a master's student and graduate research assistant at the Department of Neurology, McGovern Medical School, The University of Texas Health Science Center in Houston, Texas, USA. Her research focuses on developing methods for prion detection and drug discovery, as well as risk factors contributing to the spread of CWD.

References

1. Mould DL, Smith W. The causal agent of scrapie. II. Extraction of the agent from infected goat tissue. J Comp Pathol. 1962;72:106–12. https://doi.org/10.1016/S0368-1742(62)80012-5
2. Gambetti P, Kong Q, Zou W, Parchi P, Chen SG. Sporadic and familial CJD: classification and characterisation. Br Med Bull. 2003;66:213–39. https://doi.org/10.1093/bmb/66.1.213
3. Bruce ME, Will RG, Ironside JW, McConnell I, Drummond D, Suttie A, et al. Transmissions to mice indicate that 'new variant' CJD is caused by the BSE agent. Nature. 1997;389:498–501. https://doi.org/10.1038/39057
4. Holt TA, Phillips J. Bovine spongiform encephalopathy. Br Med J (Clin Res Ed). 1988;296:1581–2. https://doi.org/10.1136/bmj.296.6636.1581
5. Miller MW, Williams ES. Chronic wasting disease of cervids. In: Compens RW, Cooper MD, Honjo T, Melchers F, Olsnes S, Vogt PK, editors. Current topics in microbiology and immunology, volume 284. Berlin: Springer-Verlag; 2004. p. 193–214.
6. Will RG, Ironside JW, Zeidler M, Estibeiro K, Cousens SN, Alperovitch A, et al. A new variant of Creutzfeldt-Jakob disease in the UK. Lancet. 1996;347:921–5. https://doi.org/10.1016/S0140-6736(96)91412-9
7. Cassard H, Torres J-M, Lacroux C, Douet J-Y, Benestad SL, Lantier F, et al. Evidence for zoonotic potential of ovine scrapie prions. Nat Commun. 2014;5:5821. https://doi.org/10.1038/ncomms6821
8. Hannaoui S, Zemlyankina I, Chang SC, Arifin MI, Béringue V, McKenzie D, et al. Transmission of cervid prions to humanized mice demonstrates the zoonotic potential of CWD. Acta Neuropathol. 2022;144:767–84. https://doi.org/10.1007/s00401-022-02482-9
9. Race B, Williams K, Chesebro B. Transmission studies of chronic wasting disease to transgenic mice overexpressing human prion protein using the RT-QuIC assay. Vet Res. 2019;50:6. https://doi.org/10.1186/s13567-019-0626-2
10. Li M, Schwabenlander MD, Rowden GR, Schefers JM, Jennelle CS, Carstensen M, et al. RT-QuIC detection of CWD prion seeding activity in white-tailed deer muscle tissues. Sci Rep. 2021;11:16759. https://doi.org/10.1038/s41598-021-96127-8
11. Angers RC, Browning SR, Seward TS, Sigurdson CJ, Miller MW, Hoover EA, et al. Prions in skeletal muscles of deer with chronic wasting disease. Science. 2006;311:1117. https://doi.org/10.1126/science.1122864
12. Bravo-Risi F, Soto P, Eckland T, Dittmar R, Ramírez S, Catumbela CSG, et al. Detection of CWD prions in naturally infected white-tailed deer fetuses and gestational tissues by PMCA. Sci Rep. 2021;11:18385. https://doi.org/10.1038/s41598-021-97737-y
13. Spraker TR, Gidlewski T, Powers JG, Nichols TA, Wild MA. Distribution of the misfolded isoform of the prion protein in peripheral tissues and spinal cord of Rocky Mountain elk (*Cervus elaphus nelsoni*) with naturally occurring chronic wasting disease. Vet Pathol. 2023;60:420–33. https://doi.org/10.1177/03009858231173467
14. Escobar LE, Pritzkow S, Winter SN, Grear DA, Kirchgessner MS, Dominguez-Villegas E, et al. The ecology of chronic wasting disease in wildlife. Biol Rev Camb Philos Soc. 2020;95:393–408. https://doi.org/10.1111/brv.12568
15. Lonergan SM, Topel DG, Marple DN. Sausage processing and production. In: Lonergan SM, Topel DG, Marple DN, editors. The science of animal growth and meat technology. Cambridge (MA): Elsevier; 2019. p. 229–53.

Address for correspondence: Rodrigo Morales, The University of Texas Health Science Center at Houston Ringgold standard institution–Neurology, 6431 Fannin St, Houston, TX 77030, USA; email: Rodrigo.MoralesLoyola@uth.tmc.edu

Eastern Africa Origin of SAT2 Topotype XIV Foot-and-Mouth Disease Virus Outbreaks, Western Asia, 2023

Antonello Di Nardo, Andrew E. Shaw, Mathilde Gondard, Jemma Wadsworth, Guillaume Girault, Krupali Parekh, Anna Ludi, Valerie Mioulet, Cindy Bernelin-Cottet, Hayley M. Hicks, Noemi Polo, Abdulnaci Bulut, Unal Parlak, Daniel Gizaw, Mustafa Ababneh, Maisa Al Ameer, Layth M.S. Abdulrasool, Fajur S. Al Saloom, Wafa A. Al-Rawahi, Nick J. Knowles, Labib Bakkali-Kassimi, Donald P. King

We describe detection of SAT2 topotype XIV foot-and-mouth disease viruses in western Asia during 2022–2023. Sequences show the viruses originated in eastern Africa and were introduced into western Asia on >1 occasion. The rapid spread in naive animals highlights risks for onward transmission and potential endemicity in Asia.

Cases of foot-and-mouth disease (FMD) were reported in buffalo in Baghdad, Iraq, during December 2022 (https://wahis.woah.org/#/in-review/4856). Genotyping of FMD virus (FMDV) variable protein (VP) 1 coding sequences generated by the SAP Institute in Turkey identified the causative FMDV as the SAT2/XIV topotype that is present in eastern Africa but is exotic to western Asia (*1*). Increased surveillance monitored the further spread of this topotype among naive livestock that had not been vaccinated or previously infected with this serotype. By January 2023, fresh outbreaks caused by SAT2/XIV were detected in Bahrain, Jordan, and Oman. In March 2023, outbreaks caused by this topotype were also reported in eastern Anatolia in Turkey and later in central Anatolia and the Adana Provinces. We used whole-genome sequences to investigate the likely timing and route of SAT2/XIV incursion and spread in western Asia.

The Study

We performed whole-genome sequencing of 49 SAT2/XIV FMDV isolates from clinical samples submitted to the World Reference Laboratory for FMD (WRLFMD; Pirbright, UK) or the French Agency for Food, Environmental and Occupational Health and Safety (ANSES; Paris, France). Specifically, sequences consisted of 12 samples from Ethiopia collected during May 2022–January 2023, six samples from Iraq collected during December 2022–February 2023, six samples from Jordan collected during January–February 2023, three samples collected in Bahrain in November 2021, seventeen samples from Turkey collected during March–June 2023 (all submitted to WRLFMD), and 5 samples from Oman collected during January–February 2023 (submitted to ANSES) (Appendix Table 1, https://wwwnc.cdc.gov/EID/article/31/2/24-0395-App1.pdf). Sequences were determined at WRLFMD using Illumina MiSeq technology (https://www.illumina.com) as previously described (*2*) and at ANSES using the Oxford Nanopore MinION platform (https://www.nanoporetech.com) (in-house protocol).

Bayesian phylogenetic reconstruction (*3*) (Figure 1) demonstrated that the SAT2/XIV FMDV sequences were assigned into distinct sister clades, providing

Author affiliations: The Pirbright Institute, Pirbright, UK (A. Di Nardo, A.E. Shaw, J. Wadsworth, K. Parekh, A. Ludi, V. Mioulet, H.M. Hicks, N. Polo, N.J. Knowles, D.P. King); ANSES Laboratory for Animal Health, Maisons-Alfort, France (M. Gondard, G. Girault, C. Bernelin-Cottet, L. Bakkali-Kassimi); Foot and Mouth Disease Institute, Ankara, Turkey (A. Bulut, U. Parlak); Animal Health Institute, Sebeta, Ethiopia (D. Gizaw); Jordan University of Science and Technology, Irbid, Jordan (M. Ababneh); Animal Health Laboratory Directorate, Amman, Jordan (M. Al Ameer); Central Veterinary Laboratories, Baghdad, Iraq (L.M.S. Abdulrasool); Ministry of Municipalities Affairs and Agriculture, Hawrat A'ali, Bahrain (F.S. Al Saloom); Sultan Qaboos University, Muscat, Oman (W.A. Al-Rawahi); Central Laboratory of Animal Health, Muscat (W.A. Al-Rawahi)

DOI: https://doi.org/10.3201/eid3102.240395

evidence for ancestors circulating in eastern Africa that moved into western Asia causing outbreaks in Iraq, Jordan, and Turkey (most recent common ancestor [MRCA] dated to March 2022 [95% Bayesian credible interval (BCrI) February–May 2022]); and independent introductions into Bahrain (MRCA dated May 2022, 95% BCrI April–June 2022) and Oman (MRCA dated July 2021, 95% BCrI June–September 2021). Those viruses are distantly related (98.70% ±13.01 nt identity) to a virus collected during March 2022 from the Wolayita Zone in southwestern Ethiopia. The MRCA of the SAT2/XIV topotype was estimated to be April 1991 (95% BCrI March–May 1991) with an evolutionary rate of 5.46×10^{-3} nt/site/year (95% BCrI $4.686.16 \times 10^{-3}$ nt/site/year). To our knowledge, SAT2/XIV was detected on only 1 other occasion, in 1991 on a dairy cattle farm located southwest of Addis Ababa, Ethiopia. However, infrequent sampling makes pinpointing the precise source of these viruses within eastern Africa difficult. Statistical parsimony network analysis (*4*) produced a similar topological representation of the SAT2/XIV FMDV sequences (Figure 2). However, this analysis highlighted several key additional points: infections in Oman were caused by 2 divergent viruses, providing evidence for 2 independent introductions; cases in Bahrain originated from a single virus ancestor, which evolved from viruses circulating in Ethiopia; viruses from Iraq evolved from an eastern Africa ancestor, which also provided the source for onward transmission to Turkey; and the SAT2/XIV outbreaks in Jordan were likely derived from a single independent virus introduction with a different genetic origin than cases reported in Iraq and Turkey.

We observed a single-point mutation at site 8080 (C>T) on the SAT2/TUR/16/2023 genome, shifting the termination to 21 nt downstream of the stop codon at a TGA leading to an extra 7 amino acids (QSLRCHN) on the end of the 3Dpol. A GenBank search of closely related genomes found that this mutation was also present on a SAT2/XIV genome reported separately from Jordan (GenBank accession no. PP112252).

We designed an FMDV lineage–specific real-time reverse transcription PCR (RT-PCR) assay within the 1D region to detect viruses from the SAT2/XIV topotype (Table). We assessed specificity in silico by using alignments of sequences from other viral lineages circulating in the region (A/ASIA/Iran-05, O/ME-SA/

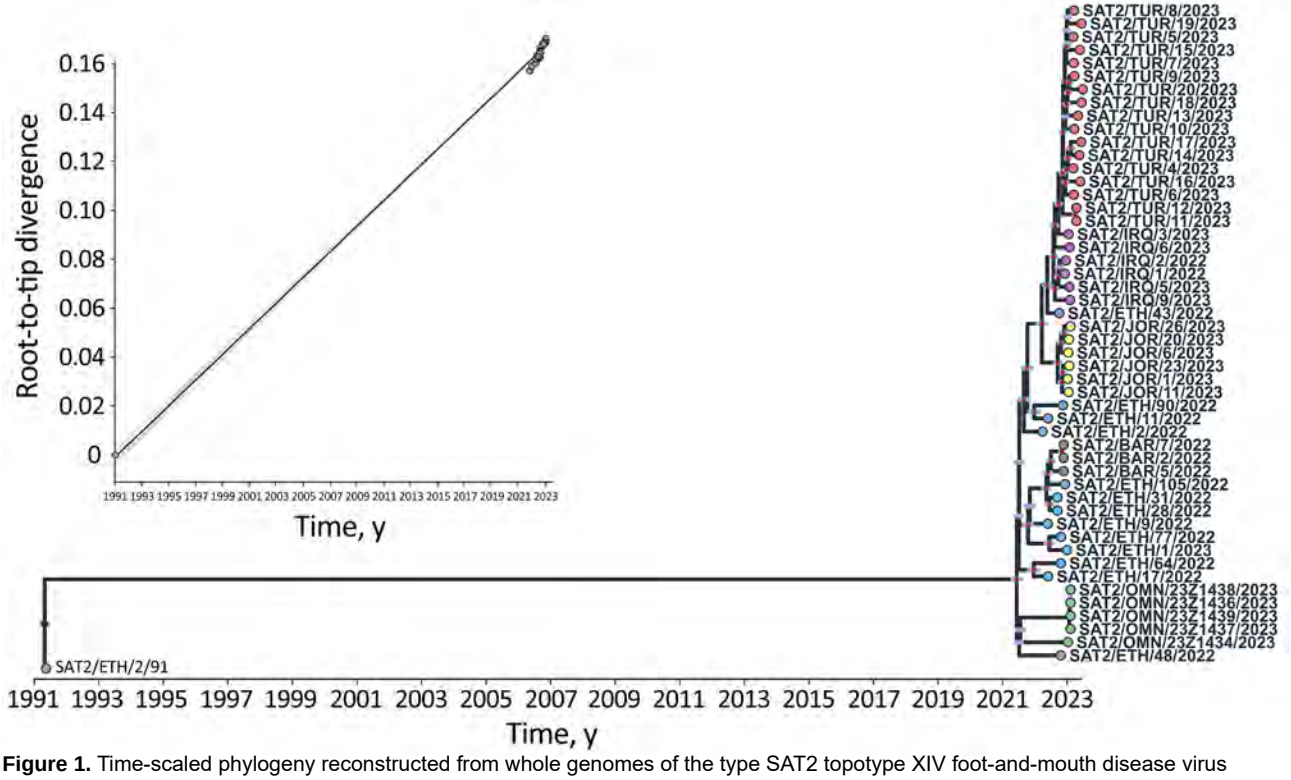

Figure 1. Time-scaled phylogeny reconstructed from whole genomes of the type SAT2 topotype XIV foot-and-mouth disease virus in study of eastern Africa origin of SAT2 topotype XIV foot-and-mouth disease virus outbreaks, western Asia, 2023. Tips are colored according to the country of isolation. Internal nodes colored in red identify those clades resulting with a posterior probability of >0.75. The 95% Bayesian credible interval reporting uncertainty region in the timing of each ancestral node is represented by the light blue horizontal bars. The inset shows the correlation of the SAT2 topotype XIV root-to-tip divergence with the time of sample collection. BAR, Bahrain; ETH, Ethiopia; IRQ, Iraq; JOR, Jordan; OMN, Oman; TUR, Turkey.

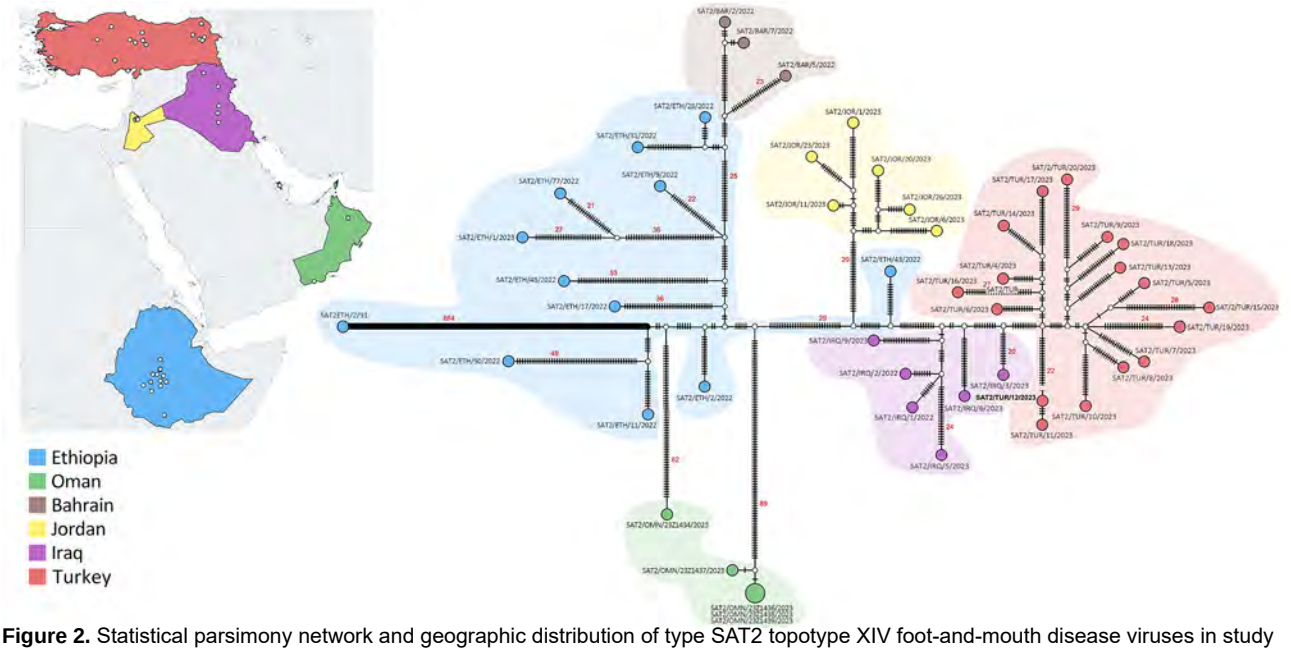

Figure 2. Statistical parsimony network and geographic distribution of type SAT2 topotype XIV foot-and-mouth disease viruses in study of eastern Africa origin of SAT2 topotype XIV foot-and-mouth disease virus outbreaks, western Asia, 2023. Nodes are colored according to the country of isolation; white nodes represent missing unsampled haplotypes. Hatch marks represent single nucleotide substitutions estimated between the connected nodes. Differences in nucleotide substitutions of ≥20 are reported in red numbers. BAR, Bahrain; ETH, Ethiopia; IRQ, Iraq; JOR, Jordan; OMN, Oman; TUR, Turkey.

PanAsia-2, Asia1/ASIA/Sindh-08, SAT2/VII) and then through experimental testing using representative samples. The real-time RT-PCR correctly categorized 56 samples as SAT2/XIV with no cross-reactivity observed with isolates of serotypes O, A, Asia1, or the SAT1/I and SAT2/VII topotypes (Figure 3).

We obtained evidence of antigen match of SAT2 vaccine strains against SAT2/XIV field viruses using 2D-VN testing (*6*); all (11/11) isolates were matched to the SAT2 Eritrea 98 vaccine, whereas 8 of the isolates were matched to the SAT2 ZIM 83 vaccine. Although no vaccine-protection data are available for SAT2/XIV viruses, the mean heterologous $\log_{10}$ titers (1.65 ± 0.12 for the SAT2 Eritrea 98 vaccine and 1.97 ± 0.17 for the SAT2 ZIM 83 vaccine) for bovine serum samples exceeded the cutoff of $\log_{10}$ 1.5 previously defined in a SAT 2 potency study for a SAT2/VII isolate (*7*) (Appendix Table 2).

Conclusions

We report the incursion of the FMDV SAT2/XIV topotype into western Asia and used whole-genome sequencing to reconstruct virus movements from eastern Africa. The emergence of exotic serotype SAT2, and the rapidity with which this virus lineage spread among a naive population, poses threats to the region, as well as to countries in Europe protected by the vaccination buffer zone in Turkish Thrace (*8*).

FMDV epidemiology is documented by dynamic cross-exchange and long-distance movements of viruses between the 7 endemic pools (*9*,*10*). Escapes of FMDV lineages endemic in Africa have been recorded for types A, O, SAT1, and SAT2 viruses; documented examples include SAT1 topotype VI in Bahrain (1962), Greece (1962), Iran (1962–1964), Iraq (1962), Israel (1962), Jordan (1962), Lebanon (1962), Syria (1962), and Turkey (1962–1965) (*11*). SAT1 was detected on 2 further occasions: an unknown genotype in Kuwait (1969–1970) and Saudi Arabia (1970) (12) and topotype VI in Yemen (1984) (N.J. Knowles, unpub. data). Serotype O, topotype EA-3, was recorded in Yemen during 1971–2009 and more recently in Israel (2017) and Palestine (2017–2018) (*13*). Serotype A topotype AFRICA lineages have

Table. Primers and probes designed for SAT2/XIV topotype-specific real-time reverse transcription PCR in study of east Africa origin of SAT2 topotype XIV foot-and-mouth disease virus outbreaks, western Asia, 2023*

Oligo name	Nucleotide sequence, 5′→ 3′	Genome location	Use
SAT2_XIV_AS_P	CCTCCACTGCCATCCGCGGTGAYAGG	3663–3688	Probe
SAT_XIV_AS_F	ACCGTGTACAACGGTGAGTG	3629–3648	Forward primer
SAT2_XIV_AS_R	TCAGCGTACTTGGCCRCAAG	3714–3695	Reverse primer

*FMDV genome locations are based on the ETH/2/2002 full genome sequence (GenBank accession no. OQ557397).

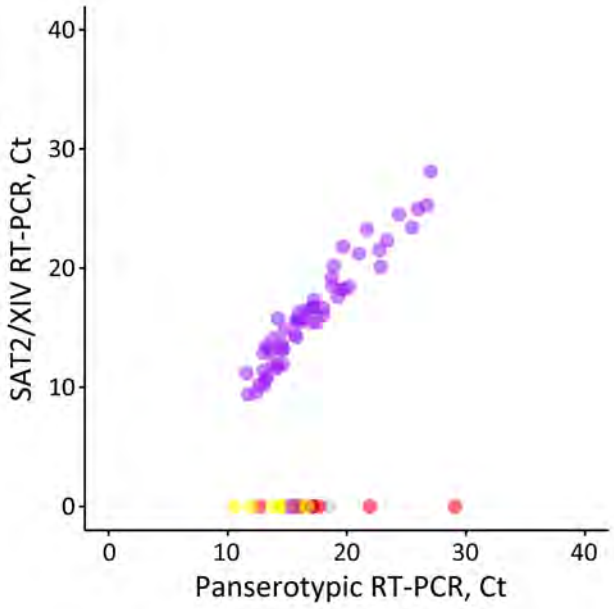

Figure 3. Performance of the SAT2/XIV-specific real-time RT-PCR for foot-and-mouth disease virus–positive samples representing different viral lineages and topotypes that are circulating or threaten countries in western Asia in study of eastern Africa origin of SAT2 topotype XIV foot-and-mouth disease virus outbreaks, western Asia, 2023. Plotted data shows real-time RT-PCR results for the SAT2/XIV specific test compared with results for the pan-serotype (3D) assay performed in parallel (*5*). Samples tested included clinical samples collected from confirmed SAT2/XIV cases (purple, n = 55) and characterized isolates from the O/ME-SA/PanAsia-2, O/ME-SA/Ind-2201 and O/EA-3 lineages (red, n = 8), the A/ASIA/Iran-05 lineage (blue, n = 1), the SAT1/I topotype (yellow, n = 7), the SAT2/VII topotype (purple, n = 8), and serotype Asia 1 (gray, n = 1). Ct, cycle threshold; RT-PCR, reverse transcription PCR.

been detected: G-II in Yemen (1985), G-VII in Yemen (1989 and 1998), and G-I in Oman (2018–2021) and Bahrain (2021) (*14*). Serotype SAT2 lineages have been reported on 6 occasions: topotype IV in Yemen (1990) and Bahrain (2012) and topotype VII in Kuwait (2000), Saudi Arabia (2000), Palestine (2012), and Oman (2015) (*15*). Those events highlight epidemiologic connections between eastern Africa and western Asia.

Incursions of exotic FMDVs into new areas, and especially from eastern Africa, have been associated with trade in livestock or products of animal origins (*10*). A recent risk assessment identifies likely pathways of SAT2/XIV diffusion within western Asia, which points to the risk posed by informal livestock trade routes and common grazing (*8*). Islamic festivals, such as Eid al-Adha, increase demand for meat across the region driving differential pricing, which could also potentially affect the epidemiology of FMD (https://cadmus.eui.eu/handle/1814/75333).

Although data are derived from opportunistic sampling, our findings support 2 hypotheses. First, recent introductions of SAT2/XIV into western Asia are defined by multiple independent incursions; furthermore, the outbreaks detected in Oman and Bahrain appear not to be directly linked, suggesting independent introductions of the virus could have occurred during 2022–2023. Second, cases in Iraq were caused by viruses derived from a single ancestor introduced during late 2022, and the cases subsequently detected in Turkey likely originated from Iraq; however, cases reported in Jordan are likely caused by a virus of a different origin. Uncertainties remain surrounding the origin of SAT2/XIV and how this topotype has been maintained during the 10 years before its reappearance in 2022 in eastern Africa, although a wildlife reservoir, likely within Cape buffalo populations, might represent its ecologic niche.

Acknowledgments

We thank the livestock keepers and colleagues in the different laboratories who contributed to the analyses of these samples.

Work conducted at the FAO World Reference Laboratory for Foot-and-Mouth Disease (Pirbright, UK) was supported by the Department of Environment, Food and Rural Affairs, UK (research grant no. SE2945) and funding provided to the European Commission for the Control of Foot-and-Mouth Disease (EuFMD) from the European Union. Nanopore MinION sequencing work at ANSES was funded by PREPMEDVET (research grant no. ANR-20-SEBM-0004). The Pirbright Institute receives grant-aided support from the Biotechnology and Biological Sciences Research Council of the United Kingdom (research grant nos. BB/X011038/1, BB/X011046/1, BBS/E/PI/230002C). The views expressed herein can in no way be taken to reflect the official opinion of the European Union.

About the Author

Dr. Di Nardo is a senior molecular epidemiologist at The Pirbright Institute. His research interests focus on the understanding of processes that drive transmission dynamics of infectious diseases at a multi-scale perspective, integrating analytical methods adopted from molecular evolution, epidemiology, population, and ecosystem ecology.

References

1. The Pirbright Institute. FAO World Reference Laboratory for foot-and-mouth disease genotyping report, Iraq (WRLMEG-2023-0004) [cited 2024 Feb 26]. https://www.wrlfmd.org/sites/world/files/quick_media/WRLMEG-2023-00004-IRQ-GTR-O-SAT2_001.pdf

2. Logan G, Freimanis GL, King DJ, Valdazo-González B, Bachanek-Bankowska K, Sanderson ND, et al. A universal protocol to generate consensus level genome sequences for foot-and-mouth disease virus and other positive-sense polyadenylated RNA viruses using the Illumina MiSeq. BMC Genomics. 2014;15:828. https://doi.org/10.1186/1471-2164-15-828
3. Suchard MA, Lemey P, Baele G, Ayres DL, Drummond AJ, Rambaut A. Bayesian phylogenetic and phylodynamic data integration using BEAST 1.10. Virus Evol. 2018;4:vey016. https://doi.org/10.1093/ve/vey016
4. Templeton AR, Crandall KA, Sing CF. A cladistic analysis of phenotypic associations with haplotypes inferred from restriction endonuclease mapping and DNA sequence data. III. Cladogram estimation. Genetics. 1992;132:619–33. https://doi.org/10.1093/genetics/132.2.619
5. Callahan JD, Brown F, Osorio FA, Sur JH, Kramer E, Long GW, et al. Use of a portable real-time reverse transcriptase-polymerase chain reaction assay for rapid detection of foot-and-mouth disease virus. J Am Vet Med Assoc. 2002;220:1636–42. https://doi.org/10.2460/javma.2002.220.1636
6. World Organisation for Animal Health. Foot and mouth disease (infection with foot and mouth disease virus). In: World Organisation for Animal Health, editor. Manual of diagnostic tests and vaccines for terrestrial animals. 2022 [cited 2024 Jan 10]. https://www.woah.org/fileadmin/Home/eng/Health_standards/tahm/3.01.08_FMD.pdf
7. Gubbins S, Paton DJ, Dekker A, Ludi AB, Wilsden G, Browning CFJ, et al. Predicting cross-protection against foot-and-mouth disease virus strains by serology after vaccination. Front Vet Sci. 2022;9:1027006. https://doi.org/10.3389/fvets.2022.1027006
8. McLaws M, Ahmadi BV, Condoleo R, Limon G, Kamata A, Arshed M, et al. Risk of foot-and-mouth disease SAT2 introduction and spread in countries in the Near East and West Eurasia–FAO qualitative risk assessment, October 2023. Rome: Food and Agriculture Organization of the United Nations; 2023. https://doi.org/10.4060/cc8173en
9. Paton DJ, Sumption KJ, Charleston B. Options for control of foot-and-mouth disease: knowledge, capability and policy. Philos Trans R Soc Lond B Biol Sci. 2009;364:2657–67. https://doi.org/10.1098/rstb.2009.0100
10. Di Nardo A, Knowles NJ, Paton DJ. Combining livestock trade patterns with phylogenetics to help understand the spread of foot and mouth disease in sub-Saharan Africa, the Middle East and Southeast Asia. Rev Sci Tech. 2011;30:63–85. https://doi.org/10.20506/rst.30.1.2022
11. Food and Agriculture Organization of the United Nations. Report of the Seminar on the Control of Foot-and-Mouth Disease in the Near East. Ankara, Turkey; October 18–21, 1982 [cited 2024 Feb 26]. https://openknowledge.fao.org/items/4cbf774f-0782-4cd4-95b6-d86c10bf0f9e
12. Ferris NP, Donaldson AI. The World Reference Laboratory for Foot and Mouth Disease: a review of thirty-three years of activity (1958-1991). Rev Sci Tech. 1992;11:657–84. https://doi.org/10.20506/rst.11.3.626
13. Canini L, Blaise-Boisseau S, Nardo AD, Shaw AE, Romey A, Relmy A, et al. Identification of diffusion routes of O/EA-3 topotype of foot-and-mouth disease virus in Africa and Western Asia between 1974 and 2019 - a phylogeographic analysis. Transbound Emerg Dis. 2022;69:e2230–9. https://doi.org/10.1111/tbed.14562
14. Al-Rawahi WA, Elshafie EI, Baqir S, Al-Ansari A, Wadsworth J, Hicks HM, et al. Detection of foot-and-mouth disease viruses from the A/AFRICA/G-I genotype in the Sultanate of Oman. Prev Vet Med. 2024;223:106113. https://doi.org/10.1016/j.prevetmed.2023.106113
15. The Pirbright Institute. FAO World Reference Laboratory for Foot-and-Mouth Disease Genotyping Report, Oman (WRLFMD). 2015 Jun 8 [cited 2024 Feb 26]. https://www.wrlfmd.org/sites/world/files/quick_media/WRLFMD-2015-00007-OMN-GTR-O-SAT2_001.pdf

Address for correspondence: Antonello Di Nardo, The Pirbright Institute, Ash Road, Pirbright, Woking GU24 0NF, UK; email: antonello.di-nardo@pirbright.ac.uk

Reemergence of *Echinococcus granulosus* Infections after 2004 Termination of Control Program in Magallanes Region, Chile

Cristian A. Alvarez Rojas, Juan Francisco Alvarez

After termination of a control program in 2004, *Echinococcus granulosus* infections have reemerged in Magallanes Region, Chile. Prevalence in sheep >2 years of age in 2023 resembled levels observed at the start of the program. Resurgence underscores the need for continued surveillance, particularly in younger sheep, to monitor recent transmission trends.

Cystic echinococcosis (CE) is a zoonotic disease caused by the taeniid tapeworm *Echinococcus granulosus* sensu lato (*1*). This neglected disease occurs worldwide in humans and animals. Several control programs for CE have been implemented worldwide; eradication by those programs has been achieved in insular settings, such as Iceland (*2*), New Zealand (*3*), and Tasmania (*4*), only after ≥40 years of intervention (*5*). Although Tasmania was declared provisionally hydatid disease-free in 1996, cases in nonimported dogs, sheep, and young cattle persist in northern Tasmania (*6*,*7*).

In March 2004, rural dogs from the Magallanes Region in southern Chile were the last animals to be treated with praziquantel under the Magallanes hydatid disease control project, which began in 1979 and lasted 25 years. This program substantially reduced CE prevalence in dogs, sheep, and humans. Before 1979, the Magallanes Region had an alarming percentage of dogs (60%) and sheep (82%) infected with *E. granulosus*, and human incidence risk reached 46.8 cases/100,000 persons annually. The control program reversed those figures considerably, reducing them to 0.5% in dogs and 0.7% in sheep by 2004; human incidence dropped to 10.4 cases/100,000 persons (Figure 1). The program is considered one of the most successful interventions for controlling this parasite in continental settings (*5*,*8*). However, the project did not advance to the consolidation phase, which aimed to target farms having persistent dog infections; funding was redirected to address other diseases. We report a reemergence of *E. granulosus* in the Magallanes Region.

The Study

We analyzed data from official reports on viscera condemnation at abattoirs and arecoline purgation tests for dog infections collected by the Servicio Agrícola y Ganadero (SAG) in Chile and obtained human incidence data from hospital records during 1979–2023 (Figure). In 1996, no data were collected because of a severe snowfall, which caused a high number of sheep deaths. In 1998 and 1999, a major scabies outbreak in sheep required the full attention of SAG staff, and, thus, no arecoline purgation tests of dogs were conducted during those years.

After 2004, a steady increase in sheep infections was observed, reaching 6% in 2023. Prevalence of *E. granulosus* infections in sheep >2 years of age increased to 32.5% in 2023, comparable to rates observed in 1983. Linear regression analysis confirmed significant changes in prevalence before and after 2004, indicating the effectiveness of the control program and infection reemergence after its termination (Appendix Figure, https://wwwnc.cdc.gov/EID/article/31/2/24-0980-App1.pdf). Infection data during 1999–2023 might reflect the productive life of sheep, highlighting the need for targeted surveillance and interventions in young sheep that indicate recent infections (Appendix Table).

Author affiliations: Pontificia Universidad Católica de Chile, Santiago, Chile (C.A. Alvarez Rojas); Servicio Agrícola y Ganadero, Magallanes Region, Punta Arenas, Chile (J.F. Alvarez)

DOI: https://doi.org/10.3201/eid3102.240980

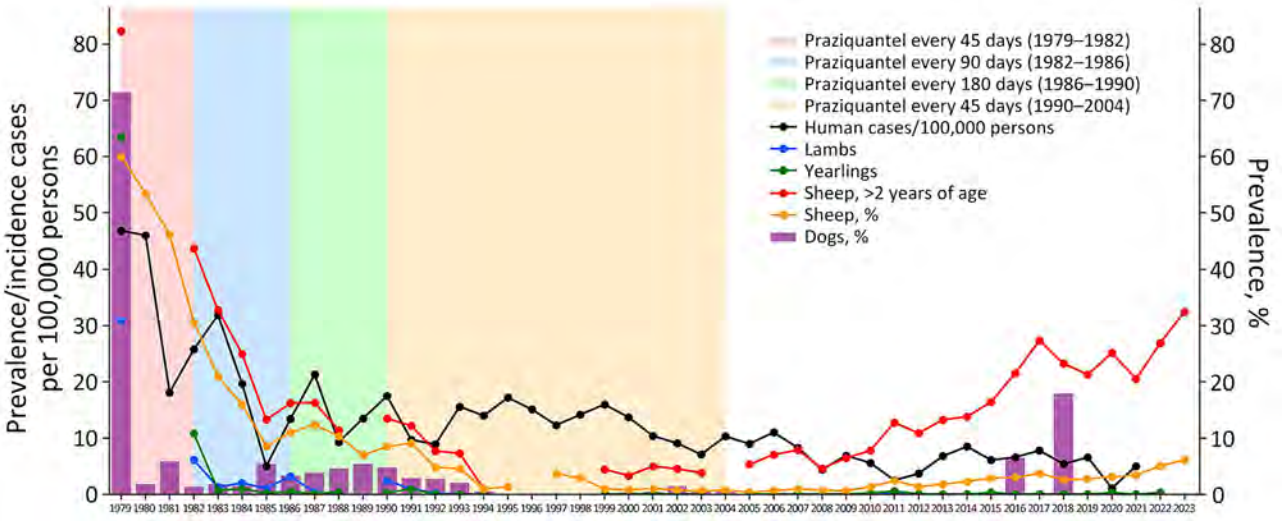

Figure. Prevalence of *Echinococcus granulosus* infections after 2004 termination of control program in Magallanes Region, Chile. Prevalence is indicated for humans, sheep, and dogs during 1979–2023. Prevalence of cystic echinococcosis in sheep was calculated according to official condemnation data of viscera in abattoirs; *E. granulosus* infections in dogs was according to arecoline purgation tests until 2004 and human incidence of cystic echinococcosis for the period 1979–2021. Shading indicates praziquantel dosage intervals for treatment of dogs. No data for sheep are presented for 1996 because of the high death rates caused by a large snowfall. Also, in 1998 and 1999, all staff from Servicio Agrícola y Ganadero, Chile, were dedicated to fighting an outbreak of scabies in sheep, and no arecoline purgation tests in dogs were performed.

Human CE incidence in Magallanes Region has fluctuated from 2.5 to 8.5 cases/100,000 inhabitants during 2010–2017. Although some variability is expected at low incidence, the concerning trend is the overall increase in cases during this period, emphasizing the need for continuous monitoring and intervention to address the growing public health threat posed by CE.

We did not explore transmission dynamics; however, sheep and dogs appear to play a central role in domestic transmission. The consistent observation that older sheep represent most infected cases underscores the need for targeted control measures, including vaccination of younger sheep to prevent infection buildup over time. To reinforce the importance of sustained control measures, Chile has piloted vaccination strategies for disease control in sheep (*9*,*10*). Ongoing efforts by SAG in collaboration with regional veterinary authorities aim to reduce the burden of parasitic infections through targeted vaccination campaigns, which could also be a complementary strategy to dog deworming to control CE.

The high proportion of *E. granulosus*–infected older sheep (84%–98%) suggests cumulative exposure over time, and transmission surveillance should also focus on younger animals. A similar trend has been observed in Wales, where older sheep harbored infectious stages of the tapeworm after a control program (*11*). Furthermore, 1 study reported sheep >4 years of age harbored 80% of the protoscolices despite those sheep constituting only 28% of the population at slaughter (*12*). Older sheep play a critical role in CE epidemiology; longer life spans create more opportunities for *E. granulosus* egg exposures in pastures. Targeting older sheep for surveillance can help identify infection hotspots and reduce the costs associated with random selection in slaughterhouses.

Increases in the dog population (>8 million owned dogs) in Chile, particularly in urban and periurban areas, present a considerable challenge for CE control (*13*). Dogs are the definitive hosts for *E. granulosus*, and their feces can contaminate the environment with parasite eggs, promoting transmission to intermediate hosts, such as sheep and humans. The rise in dog populations in Punta Arenas and other parts of Magallanes Region exacerbates this issue, making it imperative to implement effective dog population management strategies, including deworming, vaccination, and public education campaigns. Canine infection data after 2004, although limited, show increased prevalence; 1 study showed spatial clusters in rural areas by using ClusterSeer (BioMedware, https://www.biomedware.com) (*14*). That study analyzed 1,069 environmental dog fecal samples across Magallanes Region by using PCR, revealing substantial *E. granulosus* prevalence, particularly clustered in rural areas (*14*). Another study found a 6.9% prevalence of *E. granulosus* DNA in dog fecal samples from

Tierra del Fuego, Chile, indicating continued risk for transmission (*15*).

Fluctuations in human CE incidence indicate a need for improved diagnostic and reporting systems. Enhanced surveillance and reporting mechanisms are essential for accurately assessing the burden of CE and implementing timely and effective control measures. Collaboration among public health authorities, veterinary services, and local communities is crucial for the success of those efforts. Existing technologies have already been integrated into control programs to improve epidemiologic surveillance and population screening. Diagnostic tools, such as coprologic PCR and ELISA, are being used for the detection of *E. granulosus* infections in dogs, offering higher sensitivity and specificity compared with traditional methods. In addition, environmental monitoring of dog fecal samples can identify areas with high levels of contamination. Ultrasound has been applied as a noninvasive method to detect hydatid cysts in older sheep and monitor infection status. Those technologies, combined with regular deworming campaigns, play a crucial role in maintaining effective *E. granulosus* surveillance and ensuring timely interventions.

Conclusions

The historical context of the Magallanes Region hydatid disease control program provides valuable lessons for current and future control initiatives. The program's success in reducing *E. granulosus* prevalence underscores the effectiveness of sustained, coordinated efforts in controlling zoonotic diseases. However, the reemergence of infections after ending the program emphasizes the need for sustained funding and political support for such initiatives. Whereas Tierra del Fuego is an island, ongoing control across Magallanes Region and mainland Chile remains crucial to prevent reinfection and manage cross-border transmission risks.

CE remains a considerable public health threat in the Magallanes Region, which has Chile's largest sheep population, accounting for 57% of the national total. The elevated prevalence of *E. granulosus* in mature sheep reflects their role in sustaining the parasite's life cycle. Furthermore, increasing dog populations, particularly in urban and periurban areas, raise the risk for environmental contamination with *E. granulosus* eggs and CE transmission within the community. The reemergence of *E. granulosus* after ending the Magallanes Region control program illustrates the critical need for sustained control measures and long-term postelimination surveillance to prevent resurgence. Continued intervention and monitoring of *E. granulosus* infections will be needed to secure lasting public health benefits and similar efforts should be implemented worldwide.

About the Authors

Dr. Alvarez Rojas is a veterinarian and parasitologist working as an assistant professor at the School of Veterinary Medicine, Pontificia Universidad Católica de Chile. His primary research interests include parasitic diseases of veterinary and zoonotic importance with a focus on their diagnosis, control, and prevention.

Dr. Alvarez is a veterinarian and epidemiologist and head of the laboratory at the Servicio Agrícola y Ganadero, Magallanes Region. He has a special interest investigating control tools for *Echinococcus granulosus*.

References

1. Eckert J, Deplazes P. Biological, epidemiological, and clinical aspects of echinococcosis, a zoonosis of increasing concern. Clin Microbiol Rev. 2004;17:107–35. https://doi.org/10.1128/CMR.17.1.107-135.2004
2. Beard TC. The elimination of echinococcosis from Iceland. Bull World Health Organ. 1973;48:653–60.
3. Burridge MJ, Schwabe CW, Fraser J. Hydatid disease in New Zealand: changing patterns in human infection, 1878–1972. N Z Med J. 1977;85:173–7.
4. Beard TC, Bramble AJ, Middleton MJ. Eradication in our lifetime: a log book of the Tasmanian hydatid control programs, 1962–1996. Hobart, Tasmania: Department of Primary Industry, Water, and Environment; 2001.
5. Craig PS, Hegglin D, Lightowlers MW, Torgerson PR, Wang Q. Echinococcosis: control and prevention. Adv Parasitol. 2017;96:55–158. PubMed https://doi.org/10.1016/bs.apar.2016.09.002
6. Jenkins DJ, Lievaart JJ, Boufana B, Lett WS, Bradshaw H, Armua-Fernandez MT. *Echinococcus granulosus* and other intestinal helminths: current status of prevalence and management in rural dogs of eastern Australia. Aust Vet J. 2014;92:292–8. https://doi.org/10.1111/avj.12218
7. Phythian CJ, Jackson B, Bell R, Citer L, Barwell R, Windsor PA. Abattoir surveillance of *Sarcocystis* spp., *Cysticercosis o*vis and *Echinococcus granulosus* in Tasmanian slaughter sheep, 2007–2013. Aust Vet J. 2018;96:62–8. https://doi.org/10.1111/avj.12670
8. Craig PS, Larrieu E. Control of cystic echinococcosis/hydatidosis: 1863–2002. Adv Parasitol. 2006;61:443–508. https://doi.org/10.1016/S0065-308X(05)61011-1
9. Poggio TV, Chacon T, Larrieu E. Successful control of echinococcosis in Argentina and Chile through a One Health approach, including vaccination of the sheep intermediate host. Parasitology. 2024 May 3 [Epub ahead of print]. https://doi.org/10.1017/S0031182024000519
10. Gädicke P, Heath D, Medina-Brunet A, Siva-de la Fuente MC, Espinoza-Rojas H, Villaguala-Pacheco C, et al. Assessment of the vaccination program against cystic echinococcosis in sheep in the Pehuenche community of Central Chile. Animals (Basel). 2022;12:679. https://doi.org/10.3390/ani12060679

11. Palmer SR, Biffin AH, Craig PS, Walters TM. Control of hydatid disease in Wales. BMJ. 1996;312:674–5. https://doi.org/10.1136/bmj.312.7032.674
12. Torgerson PR, Ziadinov I, Aknazarov D, Nurgaziev R, Deplazes P. Modelling the age variation of larval protoscoleces of *Echinococcus granulosus* in sheep. Int J Parasitol. 2009;39:1031–5. PubMed https://doi.org/10.1016/j.ijpara.2009.01.004
13. Seremi de Salud de Coquimbo. Programa de prevencion y control de la hidatidosis. 2015 [cited 2024 May 1]. https://hidatidosischile.wordpress.com
14. Alvarez JF, Ruiz R, Ríos J, Alvarez Rojas CA. Molecular detection of *Echinococcus granulosus* sensu stricto in environmental dog faecal samples from the Magallanes Region, Patagonia, Chile. Parasitologia. 2021;1:238–46. https://doi.org/10.3390/parasitologia1040025
15. Eisenman EJL, Uhart MM, Kusch A, Vila AR, Vanstreels RET, Mazet JAK, et al. Increased prevalence of canine echinococcosis a decade after the discontinuation of a governmental deworming program in Tierra del Fuego, Southern Chile. Zoonoses Public Health. 2023;70:213–22. https://doi.org/10.1111/zph.13017

Address for correspondence: Cristian A. Alvarez Rojas, Pontificia Universidad Católica de Chile, Av Vicuña Mackenna 4860, 7820436 Macul, Región Metropolitana, Santiago, Chile; email: c.alvarezrojas@uc.cl

etymologia revisited

Haematospirillum jordaniae

[Hae.ma.to.spi.ril'lum jor.da'ni.ae]e

For the sesquipedalian term *Haematospirillum*, *Haema* is derived from the Greek haima, meaning blood. *Spirillum* is derived from Medieval Latin in the mid-13th century Latin (*spiralis*), French in the 1550s (*spiral*), and Greek (*speira*). All suggest a winding or coil. A New Latin reference book entry in 1875 implied a little coil (Figure 1).

Isolated from human blood, *Haematospirillum jordaniae* was reported as a novel genus and species in 2016 by Centers for Disease Control and Prevention (CDC) scientist Ben W. Humrighouse and his laboratory team, which included Jean G. Jordan, a microbiologist (Figure 2). This gram-negative bacterium was isolated 14 times in 10 states during 2003–2012 before its identification in 2016.

H. jordaniae was previously considered an environmental bacterium with limited pathogenicity, but increasing numbers of isolates indicated a possible emerging pathogen. All cases occurred in male patients, and the pathogen showed a predilection for infecting lower leg injuries. In 2018, Hovan and Hollinger reported a case of infection in a Delaware man who, in 2016, had sepsis from a lower leg wound. The organism isolated was identified at the CDC Special Bacteriology Reference Laboratory (SBRL) in the Division of High-Consequence Pathogens and Pathology, National Center for Emerging and Zoonotic Infectious Diseases.

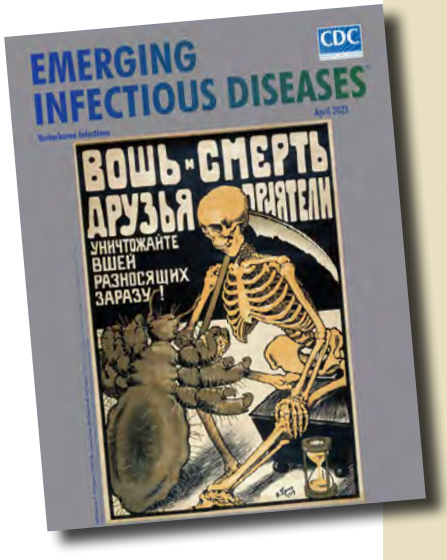

Originally published in April 2023

References:

1. Hovan G, Hollinger A. Clinical isolation and identification of *Haematospirillum jordaniae*. Emerg Infect Dis. 2018;24:1955–6.
2. Humrighouse BW, Emery BD, Kelly AJ, Metcalfe MG, Mbizo J, McQuiston JR. *Haematospirillum jordaniae* gen. nov., sp. nov., isolated from human blood samples. Antonie van Leeuwenhoek. 2016;109:493–500.
3. LPSN List of prokaryotic names with standing in nomenclature. Species *Haematospirillum jordaniae* [cited 2022 May 21]. https://lpsn.dsmz.de/species/haematospirillum-jordaniae
4. Jean Jordan obituary. Published by the Atlanta Journal-Constitution on May 28, 2014. [cited 2022 Oct 17]. https://www.legacy.com/us/obituaries/atlanta/name/jean-jordan94
5. Pal E, Štrumbelj I, Kišek TC, Kolenc M, Pirš M, Rus KR, et al. *Haematospirillum jordaniae* cellulitis and bacteremia. Emerg Infect Dis. 2022;28:2116–9.
6. Persiana (1875) (Latin Edition): Heckmanns, Alexius. *Spirillum* (n.) [cited 2022 May 21]. https://www.etymoline.com/word/spirillum
7. Weyant RS, Moss CW, Weaver RE. Hollis, Jordan JG, Cook E, et al.; Centers for Disease Control and Prevention. Identification of unusual pathogenic gram-negative aerobic and facultatively anaerobic bacteria. The Orange Book, 2nd ed. Philadelphia: Lippincott Williams and Wilkins; 1996

https://wwwnc.cdc.gov/eid/article/29/4/et-2904_article

Acute Encephalopathy Associated with Human Adenovirus Type 14 Infection in 7-Year-Old Girl, Japan

Shinsuke Mizuno, Yoshihiko Tanimoto, Ai Mori, Tomoaki Fuseya, Yusuke Ishida, Masahiro Nishiyama, Azusa Maruyama, Masashi Kasai

Author affiliations: Hyogo Prefectural Kobe Children's Hospital, Kobe, Japan (S. Mizuno, Y. Ishida, M. Nishiyama, A. Maruyama, M. Kasai); Kobe Institute of Health, Kobe (Y. Tanimoto, A. Mori, T. Fuseya)

DOI: https://doi.org/10.3201/eid3102.241168

Only 2 cases of human adenovirus type 14 (HAdV-14) have been reported in Japan since 1980. We report a 7-year-old girl with acute encephalopathy associated with HAdV-14 infection genetically similar to strains from the United States. The patient had not had contact with international travelers. HAdV-14 surveillance should be strengthened in Japan.

Human adenoviruses (HAdVs) are nonenveloped double-stranded DNA viruses that are relatively physicochemically stable (*1*). To date, >111 HAdV types have been recognized. Their clinical manifestations differ according to type and can result in respiratory, ocular, gastrointestinal, and urogenital diseases (*1*). Respiratory infections are often caused by HAdV types 3, 7, and 55 in East Asia, and most resolve spontaneously (*2*). Pneumonia caused by HAdV types 7, 8, and 55 is more severe (*2*,*3*). HAdV-14 was first identified as an acute respiratory pathogen in the Netherlands in 1955 but is rarely reported (*4*), although outbreaks have been reported in the United States and Europe (*5*–*7*). In Japan, the National Epidemiologic Surveillance of Infectious Diseases system conducts sentinel surveillance nationwide, but only 2 cases of HAdV-14 have been reported since 1980 (*8*). We report the case of a 7-year-old girl with influenza-like symptoms and acute encephalopathy associated with HAdV-14 infection that was genetically identical to strains isolated in the United States in 2019, despite the patient having no contact with international travelers.

A 7-year-old girl sought care at the Hyogo Prefectural Kobe Children's Hospital (Kobe, Japan) for fever, cough, and seizures. She had a history of febrile seizures. No abnormalities were detected on electroencephalography. After her arrival at the emergency department, the generalized seizures continued and stopped ≈2 hours after onset after administration of multiple anticonvulsants. The patient was febrile (39.5°C) with a pulse rate of 160–170 beats/min, respiratory rate of 28 breaths/min, oxygen saturation of 94% breathing room air, and a pediatric Glasgow coma scale of 9 (E4V1M4). The physical examination was otherwise unremarkable. Routine laboratory tests and a cerebrospinal fluid analysis revealed no abnormalities. Chest radiography revealed no evidence of pneumonia. Computed tomography of the head plane revealed no abnormalities, and electroencephalography showed slow wave activity. Multiplex PCR testing of a nasopharyngeal swab specimen was positive for HAdV. We diagnosed acute encephalopathy because the patient remained unconscious 6 hours after seizure onset. We initiated targeted temperature management for 48 hours, along with coma therapy using barbiturates. On day 9, magnetic resonance imaging of the brain revealed high intensity in the subcortical white matter and caudate nuclei bilaterally (Figure 1). On day 11, the patient was discharged with upper limb weakness. Outpatient follow-up at 1 month after diagnosis revealed no neurologic problems.

Viral cultures of nasopharyngeal swab and stool samples in A549 cells were positive for HAdV. Whole-genome sequencing showed that the isolated strain was the same clade as the first reported strain, de Wit

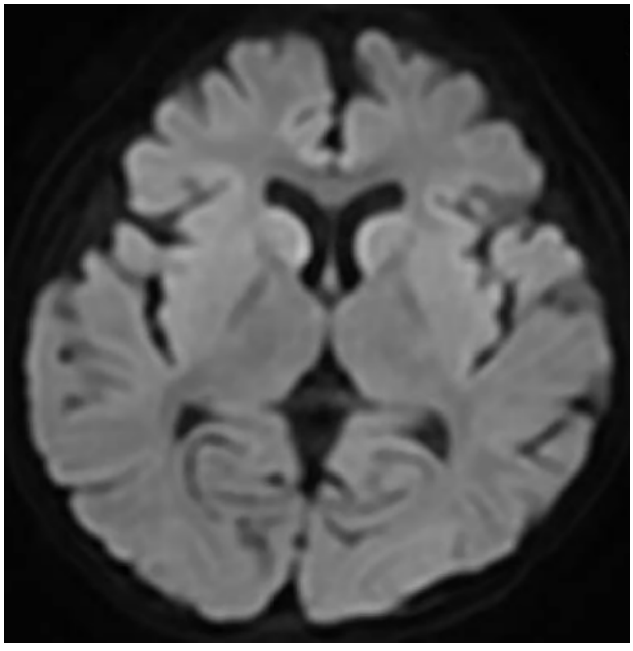

Figure 1. Diffusion weighted magnetic resonance imaging scan of brain in study of acute encephalopathy associated with human adenovirus type 14 infection in 7-year-old girl, Japan. Image shows high intensity in the subcortical white matter and bilateral caudate nuclei.

Figure 2. Phylogenetic analysis of HAdV complete sequences from patient isolates in study of acute encephalopathy associated with human adenovirus type 14 infection in 7-year-old girl, Japan, and reference sequences. The most recent reference strain was from the United States in 2019. The tree was created by IQ-TREE (*9*) using the maximum composite-likelihood methods with 1,000 bootstrap replicates. GenBank accession numbers are provided for reference sequences. Scale bar indicates number of substitutions per site.

strain, and highly similar to the strains reported during 2003–2019, differing from the most recent reported strains (identified in the United States in 2019) by only a single nucleotide variant (noncoding region) and a 2-nucleotide insertion (open reading frame 3 protein) (Figure 2). Results of PCR testing and viral culture of cerebrospinal fluid and blood samples were negative. Further questioning of the patient's parents revealed no contact with international travelers.

The patient had influenza-like illness and acute encephalopathy and tested positive for HAdV-14. Although uncommon, HAdVs can cause central nervous system dysfunction. The most common clinical manifestations are febrile seizures and encephalitis (*1*,*10*). Few cases of HAdV-14–associated acute encephalopathy have been reported. We diagnosed our patient with acute encephalopathy associated with HAdV-14 infection on the basis of clinicoradiological correlation and viral detection in nasopharyngeal and fecal samples. The diagnosis of acute encephalopathy is usually made on the basis of neurologic manufestations and abnormal brain imaging findings, combined with HAdV detection in the cerebrospinal fluid or other sites (*10*). Although the definite mechanism of acute encephalopathy remains unknown, inflammatory cytokines produced in response to HAdV infection might induce excitotoxicity in the brain, resulting in neuronal damage (*10*).

According to the national surveillance system in Japan, only 2 cases of HAdV-14 have been reported in the past 40 years (*8*). The source of this patient's HAdV-14 exposure is unknown. The isolate showed a high similarity to strains isolated in the United States in 2019, despite the patient having no history of contact with international travelers from countries with HAdV-14 outbreaks. Because HAdV is excreted in feces over a long period and is resistant to dessication and alcohol, community outbreaks are difficult to control (*1*). Because HAdV-14 is highly contagious and has high mortality rates, understanding its molecular evolution and clinical manifestations are key to prepare for future outbreaks. This case suggests that HAdV surveillance in Japan, including HAdV-14 surveillance, should be strengthened.

The nucleotide data are available in the DDBJ/EMBL/GeneBank databases (accession nos. LC830687 and LC830688).

About the Author

Dr. Shinsuke is an pediatric infectious diseases physician working at the Hyogo Prefectural Kobe Children's Hospital in Japan. His primary research interests are viral infection and travel medicine.

References

1. Lion T, Wold WSM. Adenoviruses. In: Howley PM, Knipe DM, Cohen JL, Damania BA, editors. Field's virology. 7th ed. Vol 2. Philadelphia: Lippincott Williams & Wilkins; 2021. p. 129–171.
2. Liu MC, Xu Q, Li TT, Wang T, Jiang BG, Lv CL, et al. Prevalence of human infection with respiratory adenovirus in China: a systematic review and meta-analysis. PLoS Negl Trop Dis. 2023;17:e0011151. https://doi.org/10.1371/journal.pntd.0011151
3. Lee J, Choi EH, Lee HJ. Clinical severity of respiratory adenoviral infection by serotypes in Korean children over 17 consecutive years (1991–2007). J Clin Virol. 2010;49:115–20. https://doi.org/10.1016/j.jcv.2010.07.007
4. Van Der Veen J, Kok G. Isolation and typing of adenoviruses recovered from military recruits with acute respiratory disease in the Netherlands. Am J Hyg. 1957;65:119–29.
5. Kajon AE, Lu X, Erdman DD, Louie J, Schnurr D, George KS, et al. Molecular epidemiology and brief history of emerging adenovirus 14-associated respiratory disease in the United States. J Infect Dis. 2010;202:93–103. https://doi.org/10.1086/653083
6. Carr MJ, Kajon AE, Lu X, Dunford L, O'Reilly P, Holder P, et al. Deaths associated with human adenovirus-14p1 infections, Europe, 2009–2010. Emerg Infect Dis. 2011;17:1402–8. https://doi.org/10.3201/1708.101760
7. O'Flanagan D, O'Donnell J, Domegan L, Fitzpatric F, Counnell J, et al. First reported cases of human adenovirus serotype 14p1 infection, Ireland, October 2009 to July 2010. Euro Surveill. 2011;16:19801.
8. National Institute of Infectious Diseases. Infectious agents surveillance report. Adenovirus [cited 2024 Jun 20]. https://www.niid.go.jp/niid/ja/iasr/510-surveillance/iasr/graphs/1535-iasrgv-adeno.html
9. Minh BQ, Schmidt HA, Chernomor O, Schrempf D, Woodhams MD, von Haeseler A, et al. IQ-TREE 2: new models and efficient methods for phylogenetic inference in the genomic era. Mol Biol Evol. 2020;37:1530–4. https://doi.org/10.1093/molbev/msaa015
10. Huang YC, Huang SL, Chen SP, Huang YL, Huang CG, Tsao KC, et al. Adenovirus infection associated with central nervous system dysfunction in children. J Clin Virol. 2013;57:300–4. https://doi.org/10.1016/j.jcv.2013.03.017

Address for correspondence: Shinsuke Mizuno, Department of Pediatrics Infectious Diseases, Hyogo Prefectural Kobe Children's Hospital, 1-6-7 Minamimachi Minatojima, Cho-ku, Kobe City, Hyogo, 6500047, Japan; email: 4t0121@gmail.com

Mycoplasma phocimorsus in Woman with Tendinous Panaritium after Cat Scratch, Denmark

Axel Skafte-Holm, Thomas Roland Pedersen, Maria Frølund, Marc Stegger, Søren Hallstrøm, Astrid Rasmussen, Jørgen Skov Jensen

Author affiliations: Statens Serum Institut, Copenhagen, Denmark (A. Skafte-Holm, T.R. Pedersen, M. Frølund, M. Stegger, S. Hallstrøm, A. Rasmussen, J.S. Jensen); Harry Butler Institute, Murdoch University, Perth, Western Australia, Australia (M. Stegger)

DOI: https://doi.org/10.3201/eid3102.241219

A panaritium developed in a woman in Demark after her cat scratched her. Analysis of tissue by 16S rRNA gene sequencing revealed *Mycoplasma phocimorsus*, known to cause seal finger. The source of the bacterium likely transmitted by the cat is unknown, but awareness of potential zoonotic transmission from cats should be raised.

A 54-year-old woman who had a medical history of hypertension, hypercholesterolemia, and right-sided carpal tunnel syndrome sought treatment for panaritium-like symptoms in the right hand. One month before hospital admission in July 2013, the patient was scratched by her domestic cat on the right wrist and subsequently showed signs of infection. Fourteen days postscratch, the woman was treated with phenoxymethylpenicillin. Because of worsening symptoms, 1 g flucloxacillin 4 times daily was initiated on day 26 postscratch. On day 30 postscratch, the woman was hospitalized for signs of carpal tunnel infection and suspicion of underlying abscess formation.

The patient was afebrile, and laboratory tests were marginally affected (Table). Clinicians suspected acute pyogenic tenosynovitis and performed surgical intervention for decompression, revealing severe edema and synovitis in the underlying tissue. Intravenous cefuroxime (1,500 mg) was given during surgery, and amoxicillin/clavulanic acid (500 mg/125 mg 3×/d) was initiated. The next day, a clinical assessment of the soft tissue and secondary suturing was performed, and the patient was discharged. Because of severe pain radiating toward the elbow and clawhand formation, the patient was readmitted 4 days after hospital discharge (day 35 postscratch). An acute surgical intervention involving fasciotomy of the distal forearm was performed because of suspected compartment syndrome, during which massive synovitis and serous fluid were observed. The serous fluid was collected for microbiological examination, a local gentamicin implant was applied, and intravenous cefuroxime was initiated.

On day 38 postscratch, antibiotic drugs were broadened to piperacillin/tazobactam (4 g/4 g 4×/d). However, laboratory results from a blood culture showed increased levels of infection markers, and the patient experienced increasing pain at day 40 postscratch, leading to surgery and application of another gentamicin implant. Tissue from the lesion was sent to Statens Serum Institut (SSI) in Copenhagen, Denmark, for additional analysis. On day 43 postscratch, the existing treatment regimen was supplemented with intravenous gentamicin (5 mg/kg), after which C-reactive protein levels decreased and the patient's clinical condition improved by day 46 postscratch. All antibiotic drugs were discontinued on day 49 postscratch, and the patient was discharged with scheduled outpatient visits, which were unremarkable.

In August (day 59 postscratch), analysis from SSI showed bacteria from the Mycoplasmataceae family associated with seal finger, which is a painful subacute infection typically afflicting persons' fingers after contact with seals (*1*). Despite normal laboratory test results but increasing patient-reported pain and wound secretion, the patient was given doxycycline for 3 weeks and moxifloxacin (400 mg 1×/d) for 14 days. After completing that drug regimen, the patient continued to experience burning pain, restricted movement, and swelling of her right hand. In October, after completion of therapy, she had persistent symptoms, limiting her work as a service assistant at the local hospital to only 2 hours per day.

After *M. phocimorsus* was identified at SSI, whole-genome metagenomics sequencing was unsuccessfully attempted from the original specimen.

Table. Laboratory results detected in a case of *Mycoplasma phocimorsus* infection in woman with tendinous panaritium after cat scratch, Denmark*

Laboratory tests	Reference range	Day 30	Day 35	Day 38	Day 40	Day 46	Day 59
C-reactive protein, mg/L	≤8.0	21	26	36	83	24	9
Leukocytes	3.50–10.00	7.10	8.9	13.8	13.0	5.30	6.10
Neutrophils	2.00–7.00	4.68	5.67	10.58	8.62	2.82	3.13
Lymphocytes	1.30–3.50	1.91	2.65	2.58	3.52	2.00	2.40
Monocytes	0.20–0.70	0.30	0.40	0.60	0.67	0.36	0.36
Eosinophils	≤0.50	0.15	0.20	0.01	0.14	0.13	0.17
Basophils	≤0.10	0.04	0.02	0.02	0.08	0.03	0.05

*Values are 1 × 10^9 cells/L except as indicated.

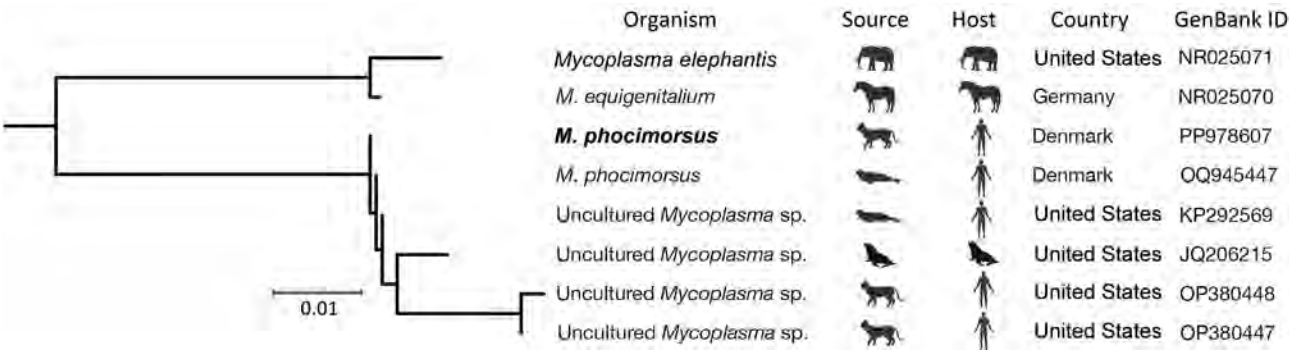

Figure. Phylogram of *Mycoplasma* species described in a case of *Mycoplasma phocimorsus* in woman with tendinous panaritium after cat scratch, Denmark. Bold text indicates species from this study. GenBank accession numbers are provided. Scale bar indicates number of nucleotide substitutions per site. ID, identification number.

However, using PCR primers covering the complete 16S rRNA sequence, a near-complete sequence was obtained. At the time of diagnosis, tissue from the lesion was examined for *Mollicutes* DNA by conventional PCR using primers targeting the 16S rRNA gene (*1*) (Appendix, https://wwwnc.cdc.gov/EID/article/31/2/24-1219-App1.pdf). Analysis of the V1–V9 sequence (1,415 bp) showed the sequence from this study had the best homology (100% coverage and 99.72% identification) with *M. phocimorsus* (GenBank accession no. OQ945447), a species identified in 2023 in patients from Scandinavia who had seal finger infection after contact with seals (*1*) (Figure; Appendix).

In 1983, a painful swollen finger developed in a veterinary surgeon after a cat scratch. After 10 days, the infection developed into septic tenosynovitis, despite treatment with oral erythromycin. The patient was hospitalized, treated with different antibiotic drugs, and underwent multiple surgeries; however, the symptoms persisted. After 3 months, mycoplasma from the wound discharge was isolated on horse serum agar; the patient was treated with tetracycline, and symptoms ceased (*2*). A 2024 case report found 16S rRNA gene sequences of *Mycoplasma* spp. in specimens taken from a patient's septic hand and knee after a cat bite (*3*). Alignment against the sequence reported in this study does not suggest similar species (Figure; Appendix).

Future research should investigate whether cats are natural carriers of *M. phocimorsus* because they are carriers of *Bartonella henselae*, which is frequently found in blood and claw samples and is known to cause cat-scratch disease (*4*). Whether *M. phocimorsus* is part of the normal bacterial flora in cats or was a transient colonizer before zoonotic transmission is still uncertain. An explanation could involve wet food containing fish remnants as the source, or the cat may have been in contact with a stranded marine mammal, in which mycoplasmas are known to colonize mycoplasma mucosal surfaces (*5*).

In summary, this patient had prolonged hospitalization and multiple surgeries as the result of her infection. Empirically, infections are often treated with β-lactam antibiotic drugs, but they are ineffective against *Mycoplasma* spp. because these bacteria lack a cell wall (*1*). Moreover, conventional bacteriologic cultures usually yield negative results for *Mycoplasma* spp., which generally do not grow on media used for standard bacteriologic cultures because they require specialized media for growth (*1*). Consequently, healthcare providers should recognize the significance of integrating diagnostic techniques such as 16S rRNA gene analysis for bacterial identification.

Acknowledgments

We thank all staff in the involved departments. In particular, we thank our colleague Lena Ingrid G. von Varfalva Palffy for her contributions to sampling and data management. Moreover, we thank colleagues at Statens Serum Institut, Ida Stenroos-Dam, Christina Nørgaard, Mette Holm, Suhella Tulsiani Drud, Berit Larsen, Gitte H. Riisgaard Christensen, Benjamin Andersen, and Elvira Chapka for excellent technical laboratory assistance.

The GenBank accession number for the 16S rRNA gene sequencing of the specimen is PP978607.

The patient has provided verbal and written consent for disclosing and publishing content related to medical findings, patient records, and laboratory investigations.

J.S.J. reports grants, personal fees, and nonfinancial support from Hologic (https://www.hologic.com), grants from Nabriva (https://www.nabriva.com), and personal fees from LeoPharma (https://www.leo-pharma.com), Abbott (https://www.abbott.com), and bioMérieux

(https://www.biomerieux.com) all outside the submitted work. The remaining authors declare that the research was conducted in the absence of any commercial or financial relationships that could be construed as a potential conflict of interest.

A.S.H. wrote the first draft of the manuscript, participated in sample and data management and sample analysis. T.R.P. and M.F. participated in sample management and analysis. M.S., S.H., and A.R. contributed to the sample analysis. J.S.J. conceptualized and designed the study, organized sample analysis, developed laboratory methods, supervised the manuscript, and participated in the writing. All authors contributed to the article and reviewed and approved the submitted manuscript.

About the Author

Dr. Skafte-Holm is a researcher at the Department for Bacteria, Parasites, and Fungi at Statens Serum Institut, Copenhagen, Denmark. His research interests include sexually transmitted infections, reproductive microbiology, and infectious diseases.

References

1. Skafte-Holm A, Pedersen TR, Frølund M, Stegger M, Qvortrup K, Michaels DL, et al. *Mycoplasma phocimorsus* sp. nov., isolated from Scandinavian patients with seal finger or septic arthritis after contact with seals. Int J Syst Evol Microbiol. 2023;73:1–10. https://doi.org/10.1099/ijsem.0.006163
2. McCabe SJ, Murray JF, Ruhnke HL, Rachlis A. Mycoplasma infection of the hand acquired from a cat. J Hand Surg Am. 1987;12:1085–8. https://doi.org/10.1016/S0363-5023(87)80119-3
3. Khan F, Engers D, Lieberman JA, Moudgal V. Disseminated infection with a previously undescribed mycoplasma species from a cat bite. Infect Dis Clin Pract. 2024;32:1–4. https://doi.org/10.1097/IPC.0000000000001314
4. Chomel BB, Boulouis HJ, Breitschwerdt EB. Cat scratch disease and other zoonotic *Bartonella* infections. J Am Vet Med Assoc. 2004;224:1270–9. https://doi.org/10.2460/javma.2004.224.1270
5. Pitcher DG, Nicholas RA. Mycoplasma host specificity: fact or fiction? Vet J. 2005;170:300–6. https://doi.org/10.1016/j.tvjl.2004.08.011

Address for correspondence: Jørgen Skov Jensen, Statens Serum Institute, Artillerivej 5, DK-2300 Copenhagen S, Denmark; email: jsj@ssi.dk

Zika Virus Infection in Pregnant Traveler Returning to Denmark from Phuket, Thailand, 2024

Ingrid Maria Cecilia Rubin, Puk Sandager, Lone Laursen, Shila Mortensen, Vithiagaran Gunalan, Raluca Datcu, Peter H.S. Andersen, Morten Rasmussen, Lasse S. Vestergaard, Uffe Vest Schneider

Author affiliations: Copenhagen University Hospital, Copenhagen, Denmark (I.M.C. Rubin); Statens Serum Institut, Copenhagen, (I.M.C. Rubin, S. Mortensen, V. Gunalan, R. Datcu, P.H.S. Andersen, M. Rasmussen, L.S. Vestergaard, U.V. Schneider); Aarhus University Hospital, Aarhus, Denmark (P. Sandager, L. Laursen); University of Copenhagen, Copenhagen (U.V. Schneider)

DOI: https://doi.org/10.3201/eid3102.241510

We report a case of Zika virus (ZIKV) infection in a pregnant woman from Denmark who traveled to Thailand during her first trimester. Late in the second trimester, severe microcephaly was diagnosed in the fetus, and ZIKV infection was confirmed. Travelers and clinicians should be aware of ongoing ZIKV risk in Thailand.

Zika virus (ZIKV) is an RNA virus spread by *Aedes* spp. mosquitoes, and symptoms of ZIKV infection are similar to those of other flaviviruses, such as dengue virus (DENV). A 2015–2016 outbreak in Brazil linked maternal ZIKV infection to serious pregnancy complications, called congenital Zika syndrome (CZS), including miscarriage and birth defects, particularly if the mother is infected during the first trimester (*1*,*2*). Although most ZIKV infections in pregnancy are asymptomatic, the virus can transfer vertically from mother to child, and the estimated risk for transfer is 10%–30% (*3*). Identified in Malaysia in 1966, ZIKV was initially reported in Thailand in 2006, and surveillance that commenced in 2016 confirmed that the virus had been circulating since at least 2002 (*4*).

During March–April 2024, a pregnant woman from Denmark and her partner traveled to Phuket, Thailand, for a 3-week vacation during her first trimester (gestational weeks 8–10) (Figure 1). The couple traveled around Phuket Province and visited the town of Phuket and several popular tourist sites and beaches in the Mueang and Kathu districts. The woman used mosquito repellents but noted a few mosquito bites during her travel. She was not aware of ZIKV

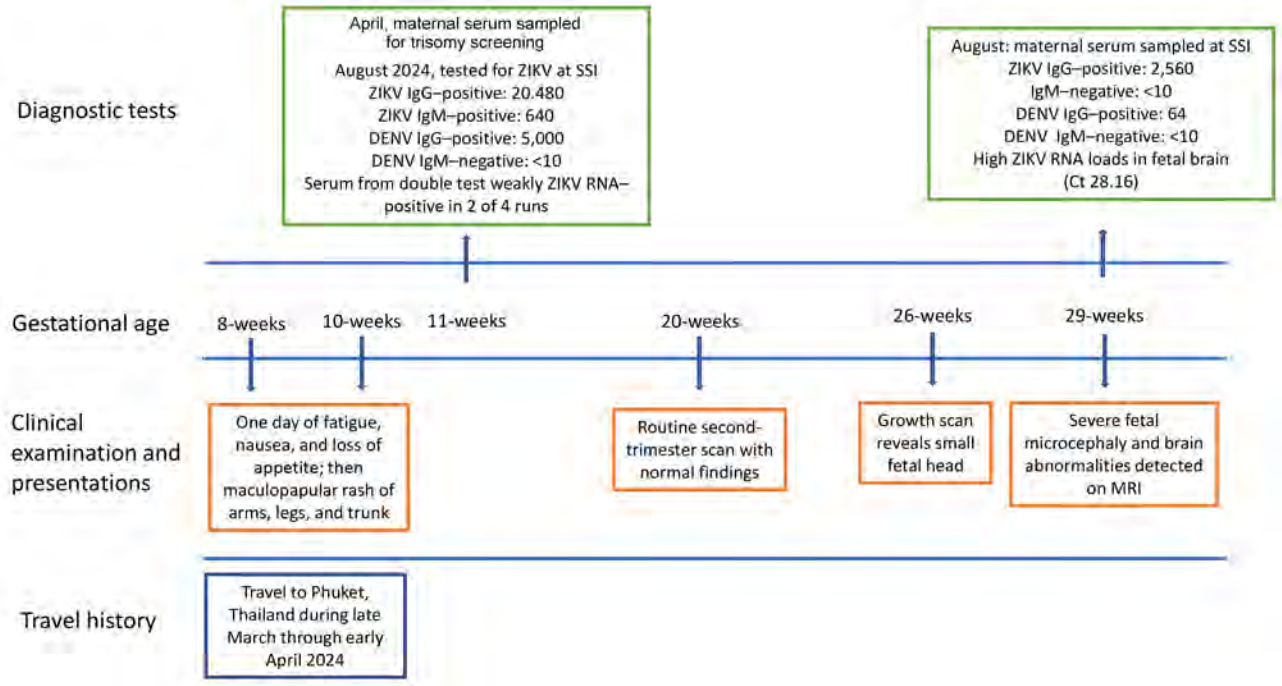

Figure 1. Timeline of patient's travel history, clinical examinations, and diagnostic tests in case of Zika virus infection in pregnant traveler returning to Denmark from Phuket, Thailand, 2024. Testing was performed the national Virology Reference Laboratory at SSI. Ct, cycle threshold; DENV, dengue virus; MRI, magnetic resonance imaging; SSI, Statens Serum Institut; ZIKV, Zika virus.

risk. On day 12 after her arrival in Phuket, she had mild illness with nausea, loss of appetite, and fatigue for 1 day. Two days later, a maculopapular rash developed on her trunk, arms, and legs.

Upon her return to Denmark, then in gestational week 11, she had a routine prenatal examination, including collection of a blood sample for trisomy screening, first trimester ultrasound, and combined risk assessment for fetal chromosomal abnormalities. In addition, a chorion villus sample was performed because of fetal chromosomal abnormality in a previous pregnancy. All routine tests showed unremarkable results. The subsequent routine second trimester ultrasound examination also was unremarkable, including appropriate fetal biometrics, and no signs of any anomalies. However, in gestational week 26, an extra growth scan was performed in relation to newly diagnosed gestational diabetes. That scan showed a fetal head circumference substantially below reference size for age (−3.4 SD).

The patient was referred for further examination. Fetal magnetic resonance imaging revealed severe microcephaly with mild unilateral ventriculomegaly, increased subarachnoid space, and decreased cerebral mantle. Results of serologic testing for toxoplasmosis, cytomegalovirus, and parvovirus were all negative. The pregnancy was terminated because of severe microcephaly.

Serum samples from the woman and fetal tissue biopsy samples were sent to the national Virology Reference Laboratory at Statens Serum Institut (SSI) for ZIKV testing. Reverse transcription PCR (RT-PCR) analysis for ZIKV RNA from the fetal brain showed intermediate positive results, a cycle threshold (Ct) value of 28.16 (Appendix, https://wwwnc.cdc.gov/EID/article/31/2/24-1510.pdf). Formalin fixed samples from the placenta and fetal meninges and liver yielded negative for ZIKV by RT-PCR. Maternal serologic test results from August 2024 showed a high level of ZIKV IgG (titer 2,560) but were IgM-negative for ZIKV. Previous blood samples from gestational week 10 (taken for trisomy screening) showed extremely high ZIKV IgG (20,480) and IgM (640) titers. Furthermore, the sample was positive for DENV IgG with a titer of 5,000 but was DENV IgM-negative. The serum test from the gestational week 10 testing was weakly positive in 2 of 4 replicates, consistent with a weakly RT-PCR positive sample.

Phylogenetic analysis of the consensus genome, designated hZikaV//Denmark/VFU-1/2024 (GISAID accession no. EPI_ISL_19550928; https://www.gisaid.org), showed that the genome clustered with the Asian ZIKV lineage and was closely related to a sequence from a previous case of travel-associated fetal microcephaly from a visitor to Thailand (Figure

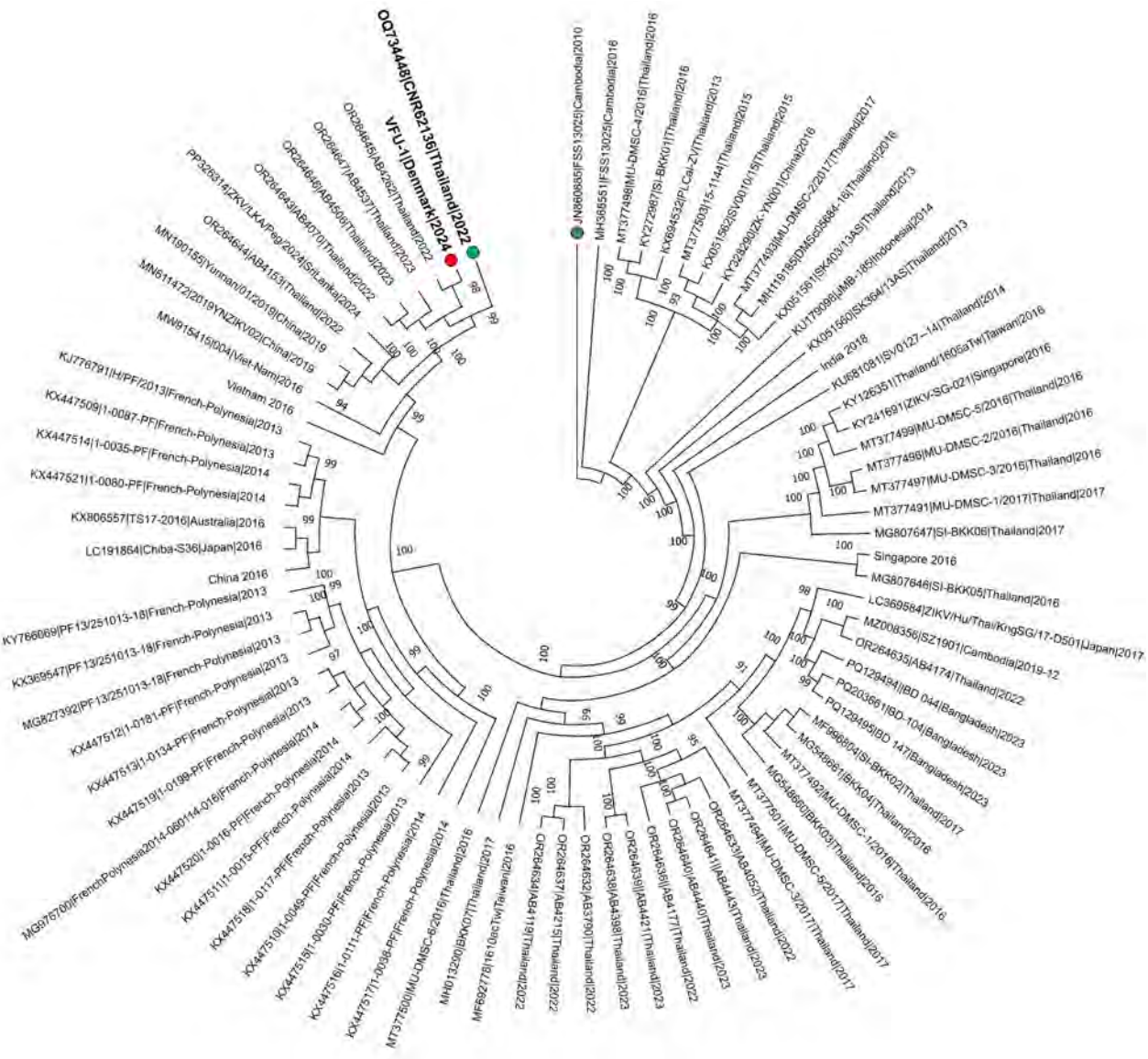

Figure 2. Phylogenetic tree of Zika virus infection in pregnant traveler returning to Denmark from Phuket, Thailand, 2024. Tree was rooted using the oldest genome available in the curated dataset (blue dot); red dot indicates the sequence from this study, VFU-1|Denmark|2024. Green dot indicates a previously sequenced Zika virus genome from a case of travel-associated microcephaly is indicated.

2) (*5*). Other genomes observed within this cluster were all sampled from Thailand and Sri Lanka within the previous 8 years. None of the mutations associated with neurovirulence in the other studies were detected (*5*,*6*).

ZIKV is linked to CZS, including microcephaly, especially in symptomatic pregnant women (*3*). However, ZIKV infection often is asymptomatic or causes mild symptoms, as seen in this case. A similar case involved a woman from France who had an asymptomatic travel-related ZIKV infection from Thailand, leading to abortion because of microcephaly detected at 24 weeks' gestation (*5*).

ZIKV is endemic in 87 countries, and Thailand is a notable source of travel-related infections and CZS cases (*7*,*8*). Diagnosing ZIKV is challenging because of short detection windows and serologic cross-reactivity with other flaviviruses, like DENV (*9*). Furthermore, prenatal microcephaly usually cannot be diagnosed until late in pregnancy.

In this case, ZIKV RNA was strongly detected in the fetal brain and weakly detected in maternal serum. Phylogenetic analysis showed the virus clustered with the Asian lineage circulating in Southeast Asia, which is 1 of the 2 major ZIKV lineages (Figure 2) (*10*).

In conclusion, this case illustrates the ongoing risk for ZIKV infection in Thailand. Obstetricians, travel medicine experts, and other clinicians should recognize the risk for acquired ZIKV infections during travel, and all travelers, especially those who are planning to conceive or are already pregnant, should be aware of the Zika risk and take necessary precautions, such as avoiding travel to ZIKV-endemic countries.

Acknowledgments

We are grateful for the patient's willingness to participate in this case report. We also thank Ellinor Lindberg Marving for her help with the technical proofreading.

About the Author

Dr. Rubin is a clinical microbiologist at the National One-Health Virus Reference Laboratory at Statens Serum Institut, Denmark. Her research interests include multiresistant organisms, the gut microbiome, and more recently emerging viral infections.

References

1. Rasmussen SA, Jamieson DJ, Honein MA, Petersen LR. Zika virus and birth defects—reviewing the evidence for causality. N Engl J Med. 2016;374:1981–7. https://doi.org/10.1056/NEJMsr1604338
2. de Araújo TVB, Ximenes RAA, Miranda-Filho DB, Souza WV, Montarroyos UR, de Melo APL, et al.; investigators from the Microcephaly Epidemic Research Group; Brazilian Ministry of Health; Pan American Health Organization; Instituto de Medicina Integral Professor Fernando Figueira; State Health Department of Pernambuco. Association between microcephaly, Zika virus infection, and other risk factors in Brazil: final report of a case-control study. Lancet Infect Dis. 2018;18:328–36. https://doi.org/10.1016/S1473-3099(17)30727-2
3. Pomar L, Musso D, Malinger G, Vouga M, Panchaud A, Baud D. Zika virus during pregnancy: from maternal exposure to congenital Zika virus syndrome. Prenat Diagn. 2019;39:420–30. https://doi.org/10.1002/pd.5446
4. Ruchusatsawat K, Wongjaroen P, Posanacharoen A, Rodriguez-Barraquer I, Sangkitporn S, Cummings DAT, et al. Long-term circulation of Zika virus in Thailand: an observational study. Lancet Infect Dis. 2019;19:439–46. https://doi.org/10.1016/S1473-3099(18)30718-7
5. Marquine S, Durand GA, Modenesi G, Khouadhria S, Piorkowski G, Badaut C, et al. Sequence data from a travel-associated case of microcephaly highlight a persisting risk due to Zika virus circulation in Thailand. J Infect Dis. 2024;229:443–7. https://doi.org/10.1093/infdis/jiad322
6. Khongwichit S, Chuchaona W, Vongpunsawad S, Poovorawan Y. Molecular epidemiology, clinical analysis, and genetic characterization of Zika virus infections in Thailand (2020–2023). Sci Rep. 2023;13:21030. https://doi.org/10.1038/s41598-023-48508-4
7. European Centre for Disease Control. Travel-associated Zika virus disease cases: place of infection of cases imported to the EU/EEA [cited 2024 Oct 2]. https://www.ecdc.europa.eu/en/zika-virus-infection/surveillance-and-disease-data/travel-associated-cases.
8. Kitro A, Imad HA, Pisutsan P, Matsee W, Sirikul W, Sapbamrer R, et al. Seroprevalence of dengue, Japanese encephalitis and Zika among long-term expatriates in Thailand. J Travel Med. 2024;31:taae022. https://doi.org/10.1093/jtm/taae022
9. Tappe D, Rissland J, Gabriel M, Emmerich P, Günther S, Held G, et al. First case of laboratory-confirmed Zika virus infection imported into Europe, November 2013. Euro Surveill. 2014;19:4. https://doi.org/10.2807/1560-7917.ES2014.19.4.20685
10. Cao-Lormeau VM, Roche C, Teissier A, Robin E, Berry AL, Mallet HP, et al. Zika virus, French Polynesia, South Pacific, 2013. Emerg Infect Dis. 2014;20:1084–6. https://doi.org/10.3201/eid2006.140138

Address for correspondence: Maria Ingrid Cecilia Rubin, Statens Serum Institut, Virus and Microbiological Special Diagnostics Ringgold Standard Institution, Artillerivej 5, Kobenhavn 2300, Denmark; email: imcr@ssi.dk or irub0009@regionh.dk

Sin Nombre Virus as Unlikely Reverse Zoonotic Threat

Jérémie Prévost, Nikesh Tailor, Anders Leung, Bryce Warner,[1] David Safronetz

Author affiliations: Public Health Agency of Canada, Winnipeg, Manitoba, Canada (J. Prévost, N. Tailor, A. Leung, B. Warner, D. Safronetz); University of Manitoba, Winnipeg (D. Safronetz)

DOI: https://doi.org/10.3201/eid3102.241532

We inoculated clinical materials into deer mice to attempt isolation of Sin Nombre virus. We did not observe productive infection in the natural rodent reservoir. Genomic comparisons between rodent reservoirs and human disease may provide insight into hantavirus evolution and genetic determinants, but reverse zoonosis of Sin Nombre virus appears unlikely.

Sin Nombre virus (SNV) is the primary cause of human hantavirus cardiopulmonary syndrome (HCPS) in North America. In nature, *Peromyscus maniculatus* deer mice are the reservoir host for SNV, although other rodents may also serve as competent

[1]Current affiliation: Vaccine and Infectious Disease Organization, Saskatoon, Saskatchewan, Canada.

reservoir hosts (*1*). Human HCPS is characterized by a sudden onset of respiratory distress that rapidly progresses and requires urgent medical attention.

As for many hantaviruses, SNV isolation has proven challenging. The extended prodromal phase, often ≥14 days, precludes collection of optimal samples with peak viral titers and minimal host immune responses for virus isolation. In previous studies, Andes virus (ANDV) was isolated from serum samples fortuitously collected immediately before HCPS disease onset, as well as from oral, nasal, or urine specimens (*2*,*3*). Those detections were likely achievable because of ANDV's ability to transmit from human to human, an attribute not known in SNV, and higher viral burdens in mucosal specimens of patients infected with ANDV (*4*).

Samples submitted for diagnostic confirmation of HCPS are collected after symptom onset and commonly include only serum or whole blood. In Canada, hantavirus diagnostic testing is done through a combination of serologic and molecular testing at the National Microbiology Laboratory of the Public Health Agency of Canada (*5*). By 2024, >150 cases of HCPS in Canada had been confirmed. Despite efforts to propagate SNV from acute samples, isolation attempts on standard Vero cell culture have been unsuccessful. We previously showed that Vero cell propagation alters the virulence of SNV in nonhuman primates (NHPs) and infectivity in deer mice (*6*,*7*). We sought to assess whether direct inoculation of deer mice with clinical material would enable isolation of virus without prior Vero propagation.

We inoculated laboratory-reared deer mice (*Peromyscus maniculatus rufinus*, both sexes, >4 weeks of age, 3–6 per group) via intraperitoneal injection with acute serum from laboratory-confirmed symptomatic HCPS (n = 10) case-patients, SNV-infected NHPs with HCPS (n = 5), or cell culture supernatant containing Vero-propagated SNV (n = 2) (Table; Appendix, https://wwwnc.cdc.gov/EID/article/31/2/24-1532-App1.pdf). Acute specimens from HCPS case-patients were positive for SNV by reverse transcription PCR (RT-PCR), were IgM positive, and had low or no detectable IgG against hantaviruses in serum. NHP samples infected with the deer mice–only passaged SNV (*6*) were collected immediately before or shortly after apparent signs of disease. Those samples were positive by reverse transcription PCR (RT-PCR) and IgM-positive by serology but also had detectable IgG. When possible, serum from HCPS case-patients was inoculated into deer mice without a freeze-thaw cycle. Serum from NHPs and the SNV cell culture supernatant were previously cryopreserved.

At 14 days after infection, when SNV in experimentally inoculated deer mice is readily detectable in multiple organs (*7*,*8*), we euthanized the mice and collected

Table. Results of experimental inoculation using deer mice in a study of SNV as an unlikely reverse zoonotic threat*

		Original infected sample				Experimental infection of deer mice					
		qRT-PCR, relative Ct value†		Serology, endpoint titer‡		qRT-PCR, positive/total samples†					Serology,
Sample ID	Origin	Blood	BAL, others	IgM	IgG	Lung	Liver	Spleen	Kidney	Blood	endpoint IgG titer§
HAN67/23	Human	22.9	SNS	≥6,400	–	0/3	NA	NA	NA	0/3	3/3 (100)
HAN79/23	Human	25.0	29.2	1,600	–	0/3	NA	NA	NA	0/3	2/3 (100–1,600)
HAN124/23	Human	31.5	28.4	≥6,400	–	0/4	0/4	0/4	0/4	0/4	4/4 (400–1,600)
HAN126/23	Human	+	SNS	1,600	–	0/4	0/4	0/4	0/4	0/4	4/4 (100–400)
HAN238/23	Human	+	SNS	1,600	400	0/3	0/3	0/3	0/3	0/3	N/A
HAN018/21	Human	28.0	SNS	400	–	0/4	0/4	0/4	0/4	0/4	4/4 (100–400)
HAN176/22	Human	25.0	SNS	1,600	–	0/4	0/4	0/4	0/4	0/4	4/4 (400–1,600)
HAN173/23	Human	+	29.5	≥6,400	–	0/4	0/4	0/4	0/4	0/4	4/4 (100–1,600)
HAN194/23	Human	27.7	SNS	1,600	400	0/4	0/4	0/4	0/4	0/4	4/4 (400–1,600)
HAN266/23	Human	28.1	SNS	≥6,400	100	1/4	1/4	0/4	0/4	0/4	4/4 (100–400)
Total human samples						1/37	1/31	0/31	0/31	0/37	33/34
EC983	NHP	24.3	27.1	1,600	1,600	0/6	0/6	0/6	0/6	0/6	6/6 (100–1,600)
MB1599	NHP	23.4	27.2	400	800	0/4	0/4	0/4	0/4	0/4	4/4 (400)
EC1545	NHP	24.1	28.5	3,200	1,600	0/4	0/4	0/4	0/4	0/4	3/4 (100–400)
MB1291	NHP	25.6	>35	400	400	0/4	0/4	0/4	0/4	0/4	4/4 (100–400)
NV1021	NHP	24.0	30.5	800	800	0/4	0/4	0/4	0/4	0/4	4/4 (100–400)
Total NHP samples						0/22	0/22	0/22	0/22	0/22	21/22
Vero-adapted SNV 77734	VCL prep 1	NA	22.0	NA	NA	3/3	2/3	3/3	3/3	2/3	NA
	VCL prep 2	NA	17.5	NA	NA	4/4	3/4	4/4	4/4	0/4	4/4 (≥6,400)
Total Vero samples						7/7	5/7	7/7	7/7	2/7	4/4

*Deer mice (*Peromyscus maniculatus*) were inoculated with specimens from SNV-infected humans, cynomolgus macaques (*Macaca fascicularis*), and Vero cells. Endpoint titers are measured in reciprocal serum dilution. BAL, bronchoalveolar lavage; Ct, cycle threshold; NA, not available; NHP, nonhuman primate; OD, optical density; qRT-PCR, qualitative reverse transcription PCR; SNS, sample not submitted; SNV, Sin Nombre virus; VCL, Vero cell line; +, RT-PCR–positive sample but Ct value not available; –, not detected.
†qRT-PCR threshold: Ct <35.
‡Seropositivity threshold: >0.6 net OD_{405}.
§Seropositivity threshold: mean OD_{650} from negative control + 3 SD (Appendix, https://wwwnc.cdc.gov/EID/article/31/2/24-1532-App1.pdf).

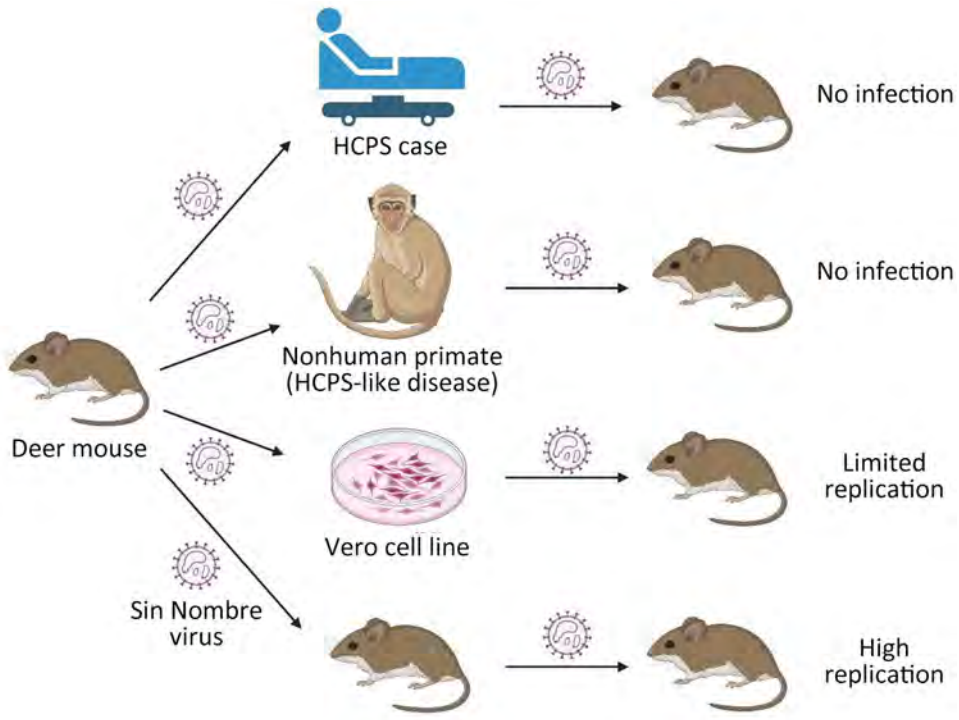

Figure. Experimental infection of North American deer mice (*Peromyscus maniculatus*) with Sin Nombre virus (SNV) to determine whether direct inoculation with clinical material would enable isolation of virus without prior Vero propagation. Infection of humans or nonhuman primates with deer mouse–derived SNV causes HCPS. This study shows that SNV retrieved from HCPS cases in infected nonhuman primates does not generate a productive infection in deer mice. SNV can also infect the Vero cell line upon passaging and adaption, but it reduces its infectivity in deer mice compared with deer mouse–only passaged SNV. The figure was prepared using images from BioRender.com (https://www.biorender.com). HCPS, hantavirus cardiopulmonary syndrome.

samples (blood, serum, lung, liver, spleen, kidney) for analyses. Deer mice inoculated with serum from HCPS case-patients or experimentally infected NHPs tested negative for SNV RNA. All but 1 animal had detectable IgG against the nucleocapsid protein and showed exposure to SNV (Table). Another animal inoculated with human serum had low levels of SNV detected in lung and liver specimens, although strand-specific RT-PCR could not detect antigenome RNA, suggesting inoculum-derived infection. All 7 deer mice injected with Vero-propagated SNV had multiple SNV-positive tissues, which is contradictory to our previous findings (*7*). Strand-specific quantitative RT-PCR confirmed the presence of replicating SNV; however, the presence of replicating SNV was 2–4 logs less than comparable tissues from mice inoculated with deer mice–only passaged SNV (Appendix Table).

The original aim of this study was to create a reliable method to isolate hantaviruses from clinical materials from confirmed HCPS cases by using natural reservoirs. However, after attempting that approach with samples from 10 unique HCPS case-patients and material from 5 NHPs experimentally infected with an SNV strain originally isolated from the deer mice colony founders, developing that method does not seem possible, at least not as outlined here (Figure). Although we did not determine SNV-neutralizing titers, the lack of IgG response indicates that all clinical samples were likely not completely neutralized before inoculation of deer mice. Nevertheless, this work addresses an overlooked aspect of hantaviruses: the potential ability to spillback and create reverse zoonotic events. Our work suggests that spillback is unlikely, at least for SNV, which implies that humans are truly dead-end hosts of SNV. Thus, virus evolution is primarily, if not exclusively, occurring in the natural rodent reservoirs.

In conclusion, genetically, hantaviruses have proven difficult to adapt in disease modeling efforts, and only rodent-derived isolates or inocula have recapitulated human disease in hamsters and NHPs (*6*,*9*,*10*). The molecular determinants of virulence are largely unknown, and without a reverse genetics system will be difficult to elucidate. Thus, to clarify hantavirus evolution and genetic factors associated with human disease, SNV genomic surveillance is needed, especially to elucidate hantavirus evolution and genetic factors associated with human disease.

Acknowledgments

We thank Kevin Tierney and Kimberly Azaransky for animal husbandry and procedures and Chris Taylor for overseeing the breeding colony.

This work was reviewed and approved by the animal care and use committee of the Canadian Science Centre for Human and Animal Health and conducted by trained staff in a Canadian Council for Animal Care certified facility. All work with infectious SNV was conducted in a Biosafety Level 4 facility.

This work was funded by the Public Health Agency of Canada.

About the Author

Dr. Prévost is a postdoctoral research scientist within the Special Pathogens program at the Public Health Agency of Canada. His primary research interests include emerging viral pathogens and the evaluation of medical countermeasures to treat and prevent them.

References

1. Goodfellow SM, Nofchissey RA, Schwalm KC, Cook JA, Dunnum JL, Guo Y, et al. Tracing transmission of Sin Nombre virus and discovery of infection in multiple rodent species. J Virol. 2021;95:e0153421. https://doi.org/10.1128/JVI.01534-21
2. Ferrés M, Martínez-Valdebenito C, Henriquez C, Marco C, Angulo J, Barrera A, et al. Viral shedding and viraemia of Andes virus during acute hantavirus infection: a prospective study. Lancet Infect Dis. 2024;24:775–82. https://doi.org/10.1016/S1473-3099(24)00142-7
3. Galeno H, Mora J, Villagra E, Fernandez J, Hernandez J, Mertz GJ, et al. First human isolate of hantavirus (Andes virus) in the Americas. Emerg Infect Dis. 2002;8:657–61. https://doi.org/10.3201/eid0807.010277
4. Wells RM, Young J, Williams RJ, Armstrong LR, Busico K, Khan AS, et al. Hantavirus transmission in the United States. Emerg Infect Dis. 1997;3:361–5. https://doi.org/10.3201/eid0303.970314
5. Warner BM, Dowhanik S, Audet J, Grolla A, Dick D, Strong JE, et al. Hantavirus cardiopulmonary syndrome in Canada. Emerg Infect Dis. 2020;26:3020–4. https://doi.org/10.3201/eid2612.202808
6. Safronetz D, Prescott J, Feldmann F, Haddock E, Rosenke R, Okumura A, et al. Pathophysiology of hantavirus pulmonary syndrome in rhesus macaques. Proc Natl Acad Sci U S A. 2014;111:7114–9. https://doi.org/10.1073/pnas.1401998111
7. Warner BM, Stein DR, Griffin BD, Tierney K, Leung A, Sloan A, et al. Development and characterization of a Sin Nombre virus transmission model in *Peromyscus maniculatus*. Viruses. 2019;11:183. https://doi.org/10.3390/v11020183
8. Botten J, Mirowsky K, Kusewitt D, Bharadwaj M, Yee J, Ricci R, et al. Experimental infection model for Sin Nombre hantavirus in the deer mouse (*Peromyscus maniculatus*). Proc Natl Acad Sci U S A. 2000;97:10578–83. https://doi.org/10.1073/pnas.180197197
9. Safronetz D, Prescott J, Haddock E, Scott DP, Feldmann H, Ebihara H. Hamster-adapted Sin Nombre virus causes disseminated infection and efficiently replicates in pulmonary endothelial cells without signs of disease. J Virol. 2013;87:4778–82. https://doi.org/10.1128/JVI.03291-12
10. Safronetz D, Ebihara H, Feldmann H, Hooper JW. The Syrian hamster model of hantavirus pulmonary syndrome. Antiviral Res. 2012;95:282–92. https://doi.org/10.1016/j.antiviral.2012.06.002

Address for correspondence: David Safronetz, National Microbiology Laboratory, Public Health Agency of Canada, 1015 Arlington St, Winnipeg, MB R3E 3R2, Canada; email: david.safronetz@phac-aspc.gc.ca

Human Infection with Avian Influenza A(H9N2) Virus, Vietnam, April 2024

Minh Hang Duong, Thi Ngoc Uyen Phan, Trung Hieu Nguyen, Ngoc Hien Nhon Ho, Thu Ngoc Nguyen, Viet Thinh Nguyen, Minh Thang Cao, Chan Quang Luong, Vu Thuong Nguyen, Vu Trung Nguyen

Author affiliation: Pasteur Institute in Ho Chi Minh City, Ho Chi Minh City, Vietnam

DOI: https://doi.org/10.3201/eid3102.241146

In April 2024, Vietnam confirmed its first human case of influenza A(H9N2) in a 37-year-old man, marking a critical point in regional infectious disease monitoring and response. This case underscores the importance of robust surveillance systems and One Health collaboration in managing emerging zoonotic threats.

Influenza A(H9N2) virus is a low-pathogenicity avian influenza virus endemic in poultry across the world. The virus presents ongoing zoonotic risk; according to the GISAID database (https://www.gisaid.org), ≈100 human cases were detected since 2010, and the virus's unique evolutionary trajectory shows it could cause pandemics (*1*). The risk for transmission and genetic mixing of avian influenza viruses, including H9N2, among wild birds, swine, and humans highlights the necessity for robust surveillance systems to manage the potential threat of these influenza viruses (*2*–*4*). In Vietnam, H9N2 accounts for 36% of detected avian influenza viruses (*5*) and shares genetic similarities with strains from neighboring countries, particularly China (3,6). Although human H9N2 cases have been reported in Asia *(7,8*), Vietnam had not previously reported a human case until 2024. The first human case of H9N2 influenza in Vietnam was officially confirmed in April 2024, marking a significant event in regional surveillance and response efforts.

A 37-year-old man with a known history of alcohol abuse from Tien Giang Province, Vietnam, experienced fever and cough on March 9, 2024. He sought medical care on March 16 at a provincial hospital, where he received a diagnosis of cirrhosis and was transferred to the Hospital for Tropical Diseases in Ho Chi Minh City, Vietnam, the same day. Initially, his chest radiograph results were unremarkable. However, on March 19, he had pneumonia with

dyspnea, fatigue, and extensive alveolar and interstitial damage evident on chest radiograph. He was intubated on March 21; osletamivir treatment was initiated, which improved his condition and enabled him to be weaned from the ventilator. He continued treatment in a negative-pressure intensive care unit;

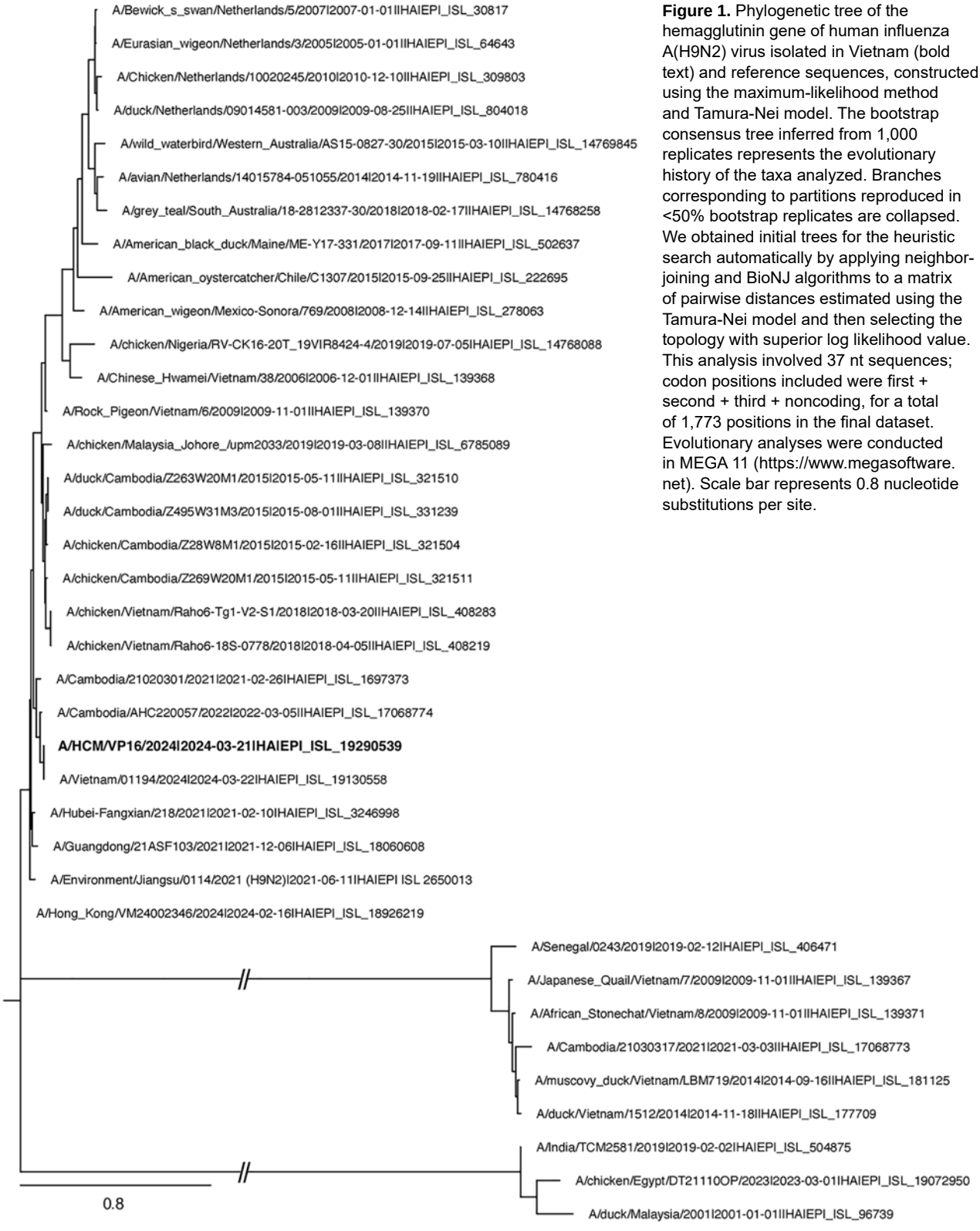

Figure 1. Phylogenetic tree of the hemagglutinin gene of human influenza A(H9N2) virus isolated in Vietnam (bold text) and reference sequences, constructed using the maximum-likelihood method and Tamura-Nei model. The bootstrap consensus tree inferred from 1,000 replicates represents the evolutionary history of the taxa analyzed. Branches corresponding to partitions reproduced in <50% bootstrap replicates are collapsed. We obtained initial trees for the heuristic search automatically by applying neighbor-joining and BioNJ algorithms to a matrix of pairwise distances estimated using the Tamura-Nei model and then selecting the topology with superior log likelihood value. This analysis involved 37 nt sequences; codon positions included were first + second + third + noncoding, for a total of 1,773 positions in the final dataset. Evolutionary analyses were conducted in MEGA 11 (https://www.megasoftware.net). Scale bar represents 0.8 nucleotide substitutions per site.

diagnoses were sepsis, influenza A, invasive fungal infection, respiratory failure, pulmonary hemorrhage, gastrointestinal bleeding, acute kidney injury, alcohol-related cirrhosis, and a suspected liver tumor. On May 5, 2024, he was discharged from the hospital to receive palliative care; he died on May 6, 2024.

The patient had not received influenza or COVID-19 vaccinations and had no known exposure to sick or dead poultry. All 15 close contacts, including family, neighbors, a driver, and healthcare workers, remained asymptomatic during 24 days of monitoring; we did not collect samples from them. His neighborhood had informal markets for poultry and other animals, but no avian influenza outbreaks were reported in the preceding 3 months. Testing geese from his home 27 days after symptom onset found no influenza H5 or H9 viruses, whereas 1 sample from nearby poultry markets tested positive for H5N1 virus but none for H9 viruses.

At the time of this case, southern Vietnam lacked surveillance for severe acute respiratory infection, and influenza-like illness surveillance was limited to 6 sentinel sites, excluding the hospitals involved in this study. The patient was enrolled in Pasteur Institute in Ho Chi Minh City (PIHCM) severe viral pneumonia (SVP) surveillance system, active since 2020, after developing pneumonia with significant respiratory symptoms and chest radiograph findings. On April 1, 2024, PIHCM received the patient's sample, which had been collected by Hospital for Tropical Diseases on March 21, 2024. On April 8, we performed real-time reverse transcription PCR in accordance with the H9N2 protocol of the Regional Animal Health Office No. 6 Vietnam (RAHO6). The Ct value for H9 was 28.81 and for N2, 29.6, indicating significant viral presence. The sample, cultured on MDCK cells from April 5, underwent whole-genome sequencing from culture passage 2 using MiSeq (https://www.illumina.com) after the US Centers for Disease Control and Prevention pipeline with bioinformatics analysis using the MIRA tool (https://cdcgov.github.io/MIRA) and MEGA version 11 (https://www.megasoftware.net).

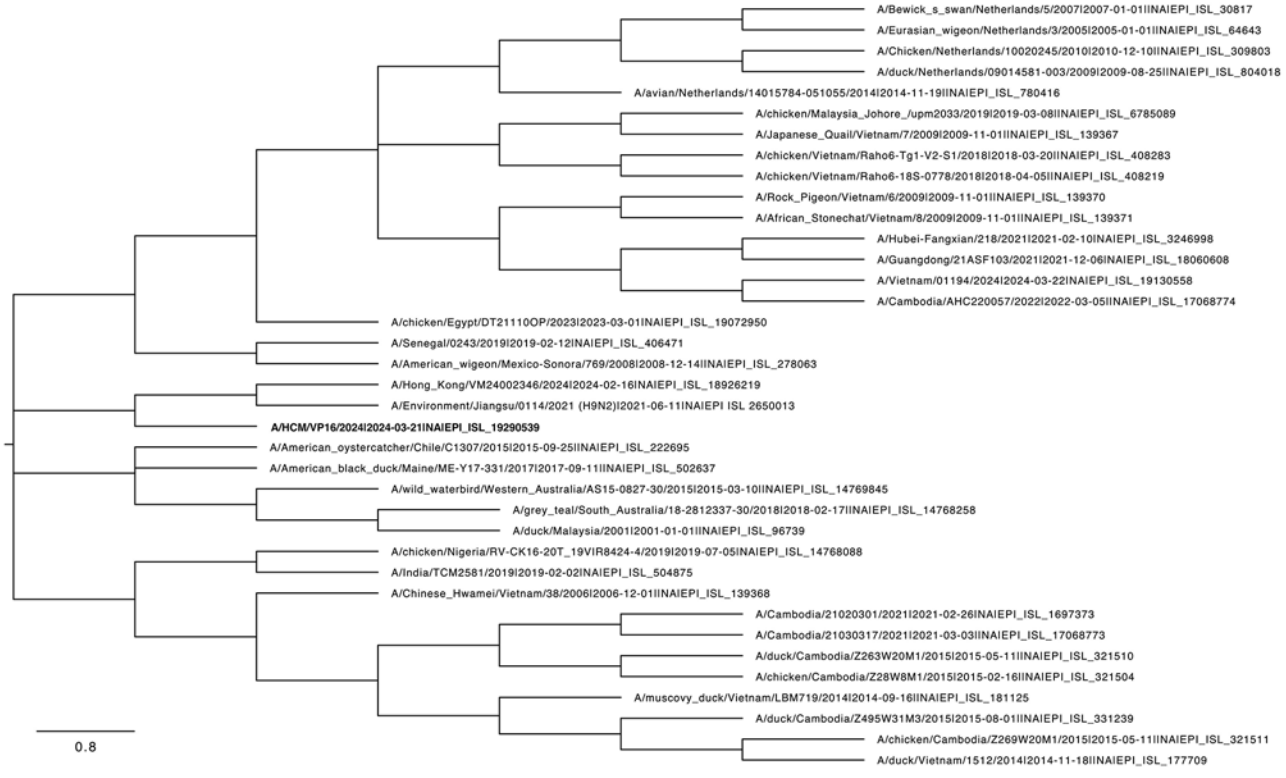

Figure 2. Phylogenetic tree of the neuraminidase gene of human influenza A(H9N2) virus isolated in Vietnam (bold text) and reference sequences, constructed using the maximum-likelihood method and Tamura-Nei model. The bootstrap consensus tree inferred from 1,000 replicates represents the evolutionary history of the taxa analyzed. Branches corresponding to partitions reproduced in <50% bootstrap replicates are collapsed. We obtained initial trees for the heuristic search automatically by applying neighbor-joining and BioNJ algorithms to a matrix of pairwise distances estimated using the Tamura-Nei model and then selecting the topology with superior log likelihood value. This analysis involved 37 nt sequences; codon positions included were first + second + third + noncoding, for a total of 1,524 positions in the final dataset. Evolutionary analyses were conducted in MEGA 11 (https://www.megasoftware.net). Scale bar represents 0.8 nucleotide substitutions per site.

We conducted phylogenetic analyses of the viral genes from the sequence we obtained, A/Vietnam/01194/2024 (GISAID accession no. EPI_ISL_19290539), using 37 sequences of H9N2 viruses from the GISAID database that were isolated from humans and avians in Vietnam and Cambodia, as well as from other continents. We assessed the reliability of the phylogenetic trees using 1,000 bootstrap replications. The hemagglutinin gene (accession no. EPI3464272) clustered with lineage viruses from H9N2 human cases A/Cambodia/AHC220057/2022 (accession no. EPI_ISL_17068774) and A/Cambodia/21020301/2021 (accession no. EPI_ISL_1697373) (8) (Figure 1). The neuraminidase gene (accession no. EPI3464270) clustered with human viruses A/Hong Kong/VM24002346/2024 (accession no. EPI_ISL_18926219) and A/Environment/Jiangsu/0114/2021 (accession no. EPI_ISL_2650013), chicken viruses from RAHO6 A/chicken/Vietnam/Raho6-18S-0778/2018 (accession no. EPI_ISL_408219) and A/chicken/Vietnam/Raho6-Tg1-V2-S1/2018 (accession no. EPI_ISL_408283) (Figure 2). The genetic distances between our sequence and other human and poultry viruses in Asia and America (Figure 2) suggest household poultry as the likely source of exposure. In addition, our findings highlight the geographic spread of H9N2 virus.

Moving forward, several key research questions arise from this case. First, it is crucial to understand the progression of the disease, particularly the mechanism by which H9N2 influenza contributed to the worsening of the patient's condition, ultimately leading to multiorgan failure. Second, analyzing samples from close contacts to determine H9N2 positivity is important to identify potential human-to-human transmission, understand transmission dynamics, and guide public health interventions. Although Vietnam lacks a formal One Health rapid response team, this case highlighted the value of cross-sector collaboration. Contributions from public health and animal health sectors, including sequencing expertise and environmental testing, underscore the need to strengthen One Health partnerships for effective surveillance and outbreak response.

This case has also been posted at https://www.cdc.gov/bird-flu/spotlights/vietnam-human-infection.html and at https://www.who.int/emergencies/disease-outbreak-news/item/2024-DON514.

Acknowledgments

We thank the Influenza and Animal-Human Interface Program at the US Centers for Disease Control and Prevention (CDC) in Vietnam for generously supporting us with sequencing reagents and training, especially Philip Gould, Nguyen Thi Phong Lan, Nguyen Thi Minh Thoa, and Siripaporn Phuygun from National Institute of Health in Thailand. We also thank the Regional Animal Health Office No. 6 (RAHO6) and the National Centre for Veterinary Diagnosis Vietnam for providing positive controls and a reverse transcription PCR protocol for H9N2 influenza. Our appreciation goes to everyone involved in the investigation and contributed to this report, including teams at the Epidemiology Department and National Influenza Center (especially Nguyen Thi Ngoc Thao, Nguyen Thi Nhung) under the Microbiology and Immunology Department of Pasteur Institute in Ho Chi Minh City. We also acknowledge all those involved in the Influenza Surveillance System in Southern Vietnam, particularly CDC Tien Giang province (especially Vo Thanh Nhon, Huynh Tuyet Trang, Nguyen Thi Thao) and the Hospital for Tropical Diseases in Ho Chi Minh City (especially Nguyen Thanh Dung, Vo Thanh Lam, Truong Ngoc Trung, and Nghiem My Ngoc). We further thank all researchers who have submitted sequences to GISAID database.

The findings and conclusions in this publication are those of the authors and do not necessarily represent the official position of the Vietnamese Ministry of Health and the Pasteur Institute in Ho Chi Minh City.

About the Author

Dr. Duong is a medical doctor at the National Influenza Center Respiratory Viruses Laboratory of the microbiology and immunology department of Pasteur Institute in Ho Chi Minh City, Vietnam. Her research focuses on influenza viruses, SARS-CoV-2, and other viruses such as RSV and measles.

References

1. Carnaccini S, Perez DR. H9 influenza viruses: an emerging challenge. Cold Spring Harb Perspect Med. 2020;10:a038588. https://doi.org/10.1101/cshperspect.a038588
2. Takakuwa H, Yamashiro T, Le MQ, Phuong LS, Ozaki H, Tsunekuni R, et al. The characterization of low pathogenic avian influenza viruses isolated from wild birds in northern Vietnam from 2006 to 2009. Comp Immunol Microbiol Infect Dis. 2013;36:581–90. https://doi.org/10.1016/j.cimid.2013.06.004
3. RahimiRad S, Alizadeh A, Alizadeh E, Hosseini SM. The avian influenza H9N2 at avian-human interface: a possible risk for the future pandemics. J Res Med Sci. 2016;21:51. https://doi.org/10.4103/1735-1995.187253
4. Baudon E, Chu DKW, Tung DD, Thi Nga P, Vu Mai Phuong H, Le Khanh Hang N, et al. Swine influenza viruses in Northern Vietnam in 2013–2014. Emerg Microbes Infect. 2018;7:1–16. https://doi.org/10.1038/s41426-018-0109-y
5. Belser JA, Sun X, Brock N, Pappas C, Pulit-Penaloza JA, Zeng H, et al. Genetically and antigenically divergent

influenza A(H9N2) viruses exhibit differential replication and transmission phenotypes in mammalian models. J Virol. 2020;94:e00451-20. https://doi.org/10.1128/jvi.00451-20
6. Le KT, Nguyen LT, Huynh LT, Chu DH, Nguyen LV, Nguyen TN, et al. Genetic, antigenic, and pathobiological characterization of H9 and H6 low pathogenicity avian influenza viruses isolated in Vietnam from 2014 to 2018. Microorganisms. 2023;11:244. https://doi.org/10.3390/microorganisms11020244
7. Tan M, Zeng X, Xie Y, Li X, Liu J, Yang J, et al. Reported human infections of H9N2 avian influenza virus in China in 2021. Front Public Health. 2023;11:1255969 https://doi.org/10.3389/fpubh.2023.1255969
8. Um S, Siegers JY, Sar B, Chin S, Patel S, Bunnary S, et al. Human infection with avian influenza A(H9N2) virus, Cambodia, February 2021. Emerg Infect Dis. 2021;27:2742–5. https://doi.org/10.3201/eid2710.211039

Address for correspondence: Minh Hang Duong, Microbiology and Immunology Department, Pasteur Institute in Ho Chi Minh City, 167 Pasteur St, Ward Vo Thi Sau, District 3, Ho Chi Minh City, Vietnam; email: hangdm@pasteurhcm.edu.vn

Henipavirus in Northern Short-Tailed Shrew, Alabama, USA

Rhys H. Parry, KayLene Y.H. Yamada, Wendy R. Hood, Yang Zhao, Jinlong Y. Lu, Andrei Seluanov, Vera Gorbunova, Naphak Modhiran, Daniel Watterson, Ariel Isaacs

Author affiliations: University of Queensland School of Chemistry and Molecular Biosciences, Brisbane, Queensland, Australia (R.H. Parry, N. Modhiran, D. Watterson, A. Isaacs); Auburn University, Auburn, Alabama, USA (K.Y.H. Yamada, W.R. Hood); University of Rochester, Rochester, New York, USA (Y. Zhao, J.Y. Lu, A. Seluanov, V. Gorbunova)

DOI: http://doi.org/10.3201/eid3102.241155

RNA metagenomic analysis of tissues from 4 wild-caught northern short-tailed shrews in Alabama, USA, revealed a novel henipavirus (family Paramyxoviridae). Phylogenetic analysis supported the placement of the virus within the shrew henipavirus clade, related to human-infecting shrewborne henipaviruses. Our study results highlight the presence of henipavirus infections in North America.

Henipaviruses (family Paramyxoviridae) are zoonotic, negative-sense RNA viruses harbored primarily by bats. Henipaviruses can cross species barriers, infecting various mammals, including humans; they often cause severe respiratory illness and encephalitis and are associated with high case fatality rates (*1*). The 2 most notable henipaviruses are Hendra virus and Nipah virus. Hendra virus, first identified in Australia, has caused outbreaks with mortality rates up to 70% (*1*). Nipah virus has been linked with numerous outbreaks in Southeast Asia, particularly in Malaysia and Bangladesh, with case-fatality rates estimated at 40%–75% (*1*), depending on surveillance and clinical management.

In 2018, researchers identified a novel henipavirus, Langya virus (LayV), in patients from China's Shandong and Henan Provinces (*2*). A total of 35 persons were infected with LayV, displaying such symptoms as fever, fatigue, and cough and, in some cases, impaired liver or kidney function. No fatalities have been reported thus far. Most investigators believe the primary reservoir host for LayV to be shrews, but the virus has also been detected in goats and dogs, indicating a wide potential host range.

In 2021, researchers conducting a mammalian longevity study captured 4 northern short-tailed shrews (*Blarina brevicauda*; order: Eulipotyphla, family: Soricidae) in the wild at Camp Hill, Auburn, Alabama, USA (latitude 32.82, longitude −85.65) (*3*). The collection process adhered to protocols approved by the Institutional Animal Care and Use Committee at Auburn University (PRN 2021-3848). Technicians dissected and froze skin, heart, kidney, liver, and brain samples for subsequent analysis. We pulverized the frozen tissues under liquid nitrogen and subjected them to RNA extraction using TRIzol Reagent (Thermo Fisher Scientific, https://www.thermofisher.com). We then treated the RNA with deoxyribonuclease, purified the treated sample, and sequenced the RNA by using the TruSeq Stranded Total RNA RiboZero Gold kit (Illumina, https://www.illumina.com) on an Illumina HiSeq 4000 platform at the New York University Genome Technology Center (New York, NY, USA). We assembled the generated sequence data by using MEGAHIT v1.2.9 software (https://github.com/voutcn/megahit) and subjected the data to virus discovery analysis with BLASTx (https://blast.ncbi.nlm.nih.gov/Blast.cgi?LINK_LOC=blasthome&PAGE_TYPE=BlastSearch&PROGRAM=blastx).

We assembled a single 16,681–16697nt contig from all virus genomes (220, 221, 217, 218; Genbank accesson nos. PQ140948–51) containing conserved *Henipavirus* genome order N-C/P-M-F-G-L, along

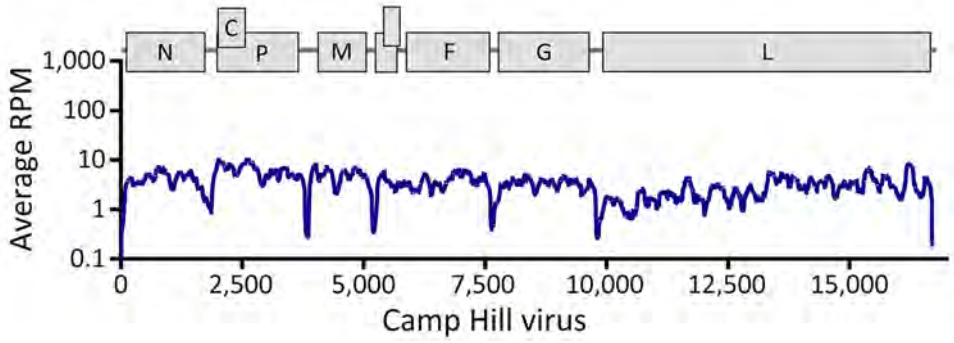

Figure 1. Genome organization and coverage of Camp Hill virus identified in *Blarina brevicauda* shrews from Alabama, USA. Coverage shows subgenomic expression (in RPM) of henipavirus genes (shown across top). RPM, reads per million.

with a novel open reading frame between M-F, which had been predicted in LayV and other shrew henipaviruses (Figure 1). We noted the largest predicted protein sequence from this contig to be most closely related to the RNA-dependent RNA polymerase of Ninorex virus (Genbank accesson nos. WJL29506.1; identity 74.58%, E-value 0), identified from Eurasian pygmy shrew (*Sorex minutus*) kidney samples in Belgium (*4*) and *Chodsigoa hypsibia* henipavirus from the De Winton's shrew in China (*5*). Given the divergence from the closest relative, host species, and geographic location, we named the putative virus Camp Hill virus (CHV). CHV reads across all shrews were positive only in kidney tissues, suggesting renal tropism (Appendix Figure 1, https://wwwnc.cdc.gov/EID/article/31/2/24-1155-App1.pdf).

For the phylogenetic analysis of CHV, we aligned the deduced CHV-221 RNA-dependent RNA polymerase protein with 19 other henipaviruses using the MAFFT-G-INS-1 multiple sequence alignment program (https://github.com/GSLBiotech/mafft). We trimmed ambiguous alignments with Gblocks 0.91b (http://phylogeny.lirmm.fr/phylo_cgi/one_task.cgi?task_type=gblocks). A maximum-likelihood phylogeny generated using IQ-TREE v2.1.3 (http://www.iqtree.org) on the final alignment indicated that CHV grouped within a well-supported shrew clade with other shrew henipaviruses from Eurasia (Figure 2) and supported the delineation of CHV as a separate henipavirus on the basis of the species demarcation for the *Henipavirus* genus (International Committee on Taxonomy of Viruses, https://ictv.global/report/chapter/paramyxoviridae/paramyxoviridae/henipavirus).

The discovery of a novel henipavirus in *B. brevicauda* shrews highlights the potential of this shrew species as a zoonotic reservoir, capable of harboring multiple viruses that pose a risk to humans. Of note, the *B. brevicauda* shrew is a known host of Camp Ripley virus

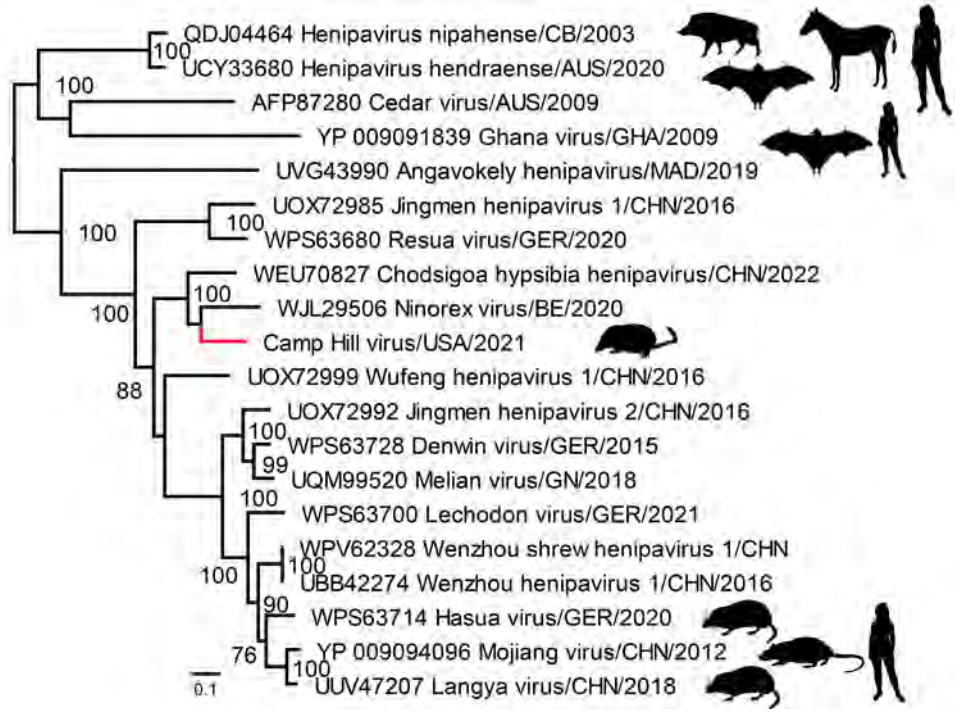

Figure 2. Phylogenetic placement of Camp Hill virus (red) within the *Henipavirus* genus identified in *Blarina brevicauda* shrews from Alabama, USA. GenBank accession numbers are provided for reference sequences. Maximum-likelihood phylogeny is midpoint rooted. Scale bar indicates amino acid substitutions per position.

(genus *Orthohantavirus*) (*6*,*7*), a viral genus associated with severe human disease. Camp Ripley virus was abundant in tissues from all the individual shrews analyzed, suggesting mixed co-infections of hantaviruses and henipaviruses in the shrews we studied. In addition, a prior report has implicated *B. brevicauda* shrews as reservoir for Powassan virus (genus *Orthoflavivirus*) (*8*), capable of causing life-threatening encephalitis.

The northern short-tailed shrew is widely distributed across central and eastern North America, from southern Saskatchewan to the Atlantic provinces of Canada and south to northern Arkansas and Georgia in the United States (Appendix Figure 2). Despite their solitary nature, short-tailed shrews are territorial and highly active, commonly found in rural and urban areas near livestock, agricultural settings, and human populations. Although the shrews have large home ranges that sometimes overlap with human activity, they typically inhabit woodland areas with ≥50% herbaceous cover (*9*), making direct encounters with humans uncommon.

Given the high case-fatality rates associated with henipaviruses, detection of CHV in North America raises concerns about past and potential future spillover events. Further investigation is needed into the potential for human infection and strategies for mitigating transmission. Our findings help elucidate the prevalence and geographic distribution of CHV in *B. brevicauda* shrews. The exact transmission mechanisms of shrew henipaviruses remain unclear, but direct contact with infected animals or their excreta poses a risk to humans.

About the Author

Dr. Parry is a postdoctoral researcher at the School of Chemistry and Molecular Biosciences, University of Queensland, Australia. His research topics cover virus bioinformatics and molecular characterization of metagenomics-identified viruses.

References

1. Eaton BT, Broder CC, Middleton D, Wang LF. Hendra and Nipah viruses: different and dangerous. Nat Rev Microbiol. 2006;4:23–35. https://doi.org/10.1038/nrmicro1323
2. Zhang XA, Li H, Jiang FC, Zhu F, Zhang YF, Chen JJ, et al. A zoonotic henipavirus in febrile patients in China. N Engl J Med. 2022;387:470–2. https://doi.org/10.1056/NEJMc2202705
3. Lu JY, Simon M, Zhao Y, Ablaeva J, Corson N, Choi Y, et al. Comparative transcriptomics reveals circadian and pluripotency networks as two pillars of longevity regulation. Cell Metab. 2022;34:836–856.e5. https://doi.org/10.1016/j.cmet.2022.04.011
4. Horemans M, Van Bets J, Joly Maes T, Maes P, Vanmechelen B. Discovery and genome characterization of six new orthoparamyxoviruses in small Belgian mammals. Virus Evol. 2023;9:vead065. https://doi.org/10.1093/ve/vead065
5. Cui X, Fan K, Liang X, Gong W, Chen W, He B, et al. Virus diversity, wildlife-domestic animal circulation and potential zoonotic viruses of small mammals, pangolins and zoo animals. Nat Commun. 2023;14:2488. https://doi.org/10.1038/s41467-023-38202-4
6. Arai S, Song JW, Sumibcay L, Bennett SN, Nerurkar VR, Parmenter C, et al. Hantavirus in northern short-tailed shrew, United States. Emerg Infect Dis. 2007;13:1420–3. https://doi.org/10.3201/eid1309.070484
7. Liphardt SW, Kang HJ, Arai S, Gu SH, Cook JA, Yanagihara R. Reassortment between divergent strains of Camp Ripley virus (Hantaviridae) in the northern short-tailed shrew (*Blarina brevicauda*). Front Cell Infect Microbiol. 2020;10:460. https://doi.org/10.3389/fcimb.2020.00460
8. Goethert HK, Mather TN, Johnson RW, Telford SR III. Incrimination of shrews as a reservoir for Powassan virus. Commun Biol. 2021;4:1319. https://doi.org/10.1038/s42003-021-02828-1
9. George SB, Choate JR, Genoways HH. *Blarina brevicauda*. Mammalian Species. 1986;261:1–9. https://doi.org/10.1093/mspecies/261.1

Address for correspondence: Rhys Parry, School of Chemistry and Molecular Biosciences, University of Queensland, Brisbane, QLD, 4072 Australia; email: r.parry@uq.edu.au

Burkholderia pseudomallei Sequence Type 46 Transmission from Asia to Australia

Ella M. Meumann, Mirjam Kaestli, Jessica R. Webb, Vanessa Rigas, Celeste Woerle, Mark Mayo, Bart J. Currie

Author affiliations: Territory Pathology, Darwin, Northern Territory, Australia (E.M. Meumann); Menzies School of Health Research and Charles Darwin University, Darwin (E.M. Meumann, M. Kaestli, J.R. Webb, V. Rigas, C. Woerle, M. Mayo, B.J. Currie); Royal Darwin Hospital, Darwin (E.M. Meumann, B.J. Currie); University of Melbourne at The Peter Doherty Institute for Infection and Immunity, Melbourne, Victoria, Australia (J.R. Webb)

DOI: https://doi.org/10.3201/eid3102.241385

Melioidosis is caused by the environmental pathogen *Burkholderia pseudomallei*. Among 1,331 patients with melioidosis during 1989–2023 in the Darwin Prospective Melioidosis Study in Australia, we identified 6 locally acquired cases caused by *B. pseudomallei* sequence type 46. Because of global transmission and expansion of endemicity, clinicians should increase awareness of melioidosis.

The environmental bacterium *Burkholderia pseudomallei* causes melioidosis and is globally endemic in tropical and subtropical regions. At the continental level, *B. pseudomallei* populations remain distinct, and phylogeographic analyses suggest an origin in Australia and subsequent dispersal to Asia, Africa, and the Americas (*1*). Intercontinental transmission events are rare but have occurred in association with contaminated products (*2*) and imported animals (*3*).

The Darwin Prospective Melioidosis Study (DPMS) has documented all culture-confirmed melioidosis cases in the Top End of Australia's Northern Territory since October 1989 (Appendix 1, https://wwwnc.cdc.gov/EID/article/31/2/24-1385-App1.pdf). We previously described emergence of *B. pseudomallei* sequence type (ST) 562 in the Top End; ST562 from Asia is now the most common cause of melioidosis in the Darwin region (*4*–*6*). Another *B. pseudomallei* strain, ST46, likely of origin from Asia, was identified in the DPMS and had caused 6 cases in the region.

Of the 1,374 DPMS melioidosis cases during October 1, 1989–September 30, 2023, multilocus sequence typing was available for 1,331 *B. pseudomallei* isolates, 6 of which were ST46 (Table). The ST46 occurrences were during the wet season (November–April) during 2013–2023. Of the 6 case-patients, 5 resided in the rural area (30–35 km south of Darwin) and 1 in the urban area; none reported recent overseas travel. Of the 5 persons from the rural area, 4 reported recent gardening activities. The person from the urban area visited the rural area but did not report any specific environmental exposure. All 6 persons sought treatment for community-acquired pneumonia, 4 had *B. pseudomallei* isolated from blood cultures, and 2 had septic shock. All 6 patients survived.

Isolation from the environment is crucial for confirming local establishment of *B. pseudomallei* ST46. Despite extensive sampling in the Darwin region as part of previous studies (*7*,*8*), we did not find *B. pseudomallei* ST46 in the environment. Six *B. pseudomallei* ST46 genomes in the context of 41 publicly available global ST46 genomes, 128 genomes from other Australia cases in the DPMS, and 149 publicly availably international genomes underwent phylogenetic analysis (Appendix 2 Table, https://wwwnc.cdc.gov/EID/article/31/2/24-1385-App2.xlsx). The 6 ST46 genomes from our study were closely related to ST46 genomes from Asia and, along with ST562, were within the Asian clade of the global phylogeny (Figure, panel A). The 6 ST46 genomes from Australia were closely related, separated by only 3–9 single-nucleotide polymorphisms (SNPs). Among all 47 ST46 genomes, median pairwise distance was 100 SNPs (maximum 176 SNPs).

We generated an ST46-only time-calibrated tree (Figure, panel B; Appendix 1). The 6 ST46 genomes from Australia formed a single clade, and the most recent common ancestor was predicted to have occurred in 2004 (95% highest posterior density 1994–2012). Genomes from across Asia, including southern China, countries surrounding the Mekong, the Malay peninsula, and Indonesia, were interspersed within the tree, and the most recent common ancestor for the whole phylogeny was predicted to have occurred in 1775 (95% highest posterior density 1598–1897). In PubMLST (https://pubmlst.org/organisms/burkholderia-pseudomallei), ST46 is the most common ST found in Asia.

Table. Epidemiology and clinical features of *Burkholderia pseudomallei* cases identified in Australia as part of a study of intercontinental transmission of *B. pseudomallei* sequence type 46*

DPMS ID	Age, y/sex	Exposure risk	Underlying conditions	Location, year	Clinical manifestations
861	57/M	Landscape grading	Hazardous alcohol consumption, COPD	Rural area of Darwin, 2013	Acute pneumonia
1100	62/M	Lawn mowing	Diabetes, hazardous alcohol consumption	Rural area of Darwin, 2013	Acute pneumonia with septic shock
1102	43/F	Lawn mowing	Diabetes, previous lymphoma	Rural area of Darwin, 2018	Acute pneumonia with septic shock
1266	78/M	Repotting plants	Myelofibrosis, prostate cancer	Rural area of Darwin, 2018	Acute pneumonia
1329	41/M	Camping	Diabetes, hazardous alcohol consumption	Rural area of Darwin, 2022	Chronic pneumonia
1401	31/M	No identified exposure	No underlying conditions	Urban area of Darwin, 2022	Acute pneumonia with secondary soft tissue abscess left leg

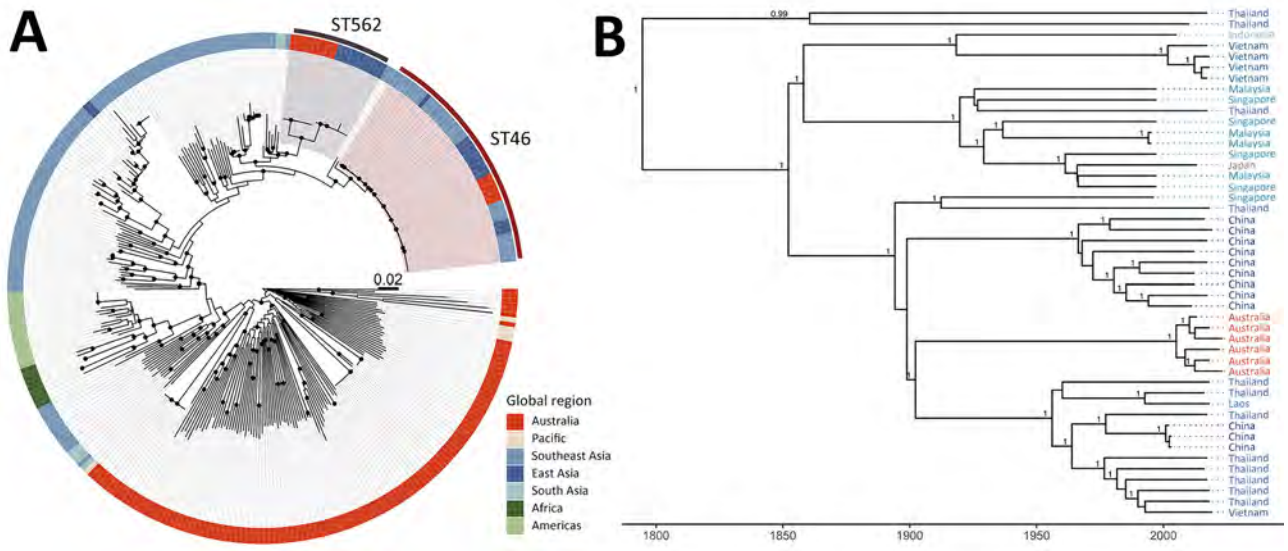

Figure. Phylogenies of *Burkholderia pseudomallei* ST46 shown in an investigation of *B. pseudomallei* ST46 transmission from Asia to Australia. A) Midpoint-rooted maximum-likelihood global phylogeny; B) maximum clade credibility tree. Trees include genomes collected as part of the Darwin Prospective Melioidosis Study in Darwin, Northern Territory, Australia, and others available in public sources (Appendix 1 Table, https://wwwnc.cdc.gov/EID/article/31/2/24-1385-App1.xlsx). Black circles indicate nodes with an approximate likelihood ratio >95 and ultrafast bootstrap >95. Labels indicate nodes with posterior support >0.8. ST, sequence type.

The source of *B. pseudomallei* ST46 introduction to northern Australia is unclear. Within the ST46 phylogeny, the 6 genomes from Australia sit within a clade comprising genomes from Hainan and Guangdong Provinces in China (*9*) (Appendixes 1, 2) and several provinces in northeast Thailand (Appendixes 1, 2). Of note, ST562 is also reported from Hainan (*6*–*8*) and Guangdong (*9*) Provinces.

Although previous studies in northern Australia showed that most STs are highly geographically restricted (*7*,*8*), phylogeographic analyses of *B. pseudomallei* in Asia showed those STs are more geographically dispersed, and STs often span multiple countries (*1*) (Appendix 1). That dispersal may occur through large river systems such as the Mekong River, airborne transmission in association with strong winds, transport through historic and current trade routes, extensive agriculture (e.g., rice paddies), and high population density (*1*) (Appendixes 1, 2). Although *B. pseudomallei* genomes from Thailand are distributed throughout most clades in the ST46 phylogeny, suggesting Thailand (or the Mekong region) as a possible ST46 transmission source, because of sampling limitations, determination of the origin of ST46 is not possible.

Arrival mode of ST46 in northern Australia remains uncertain and is difficult to ascertain but might relate to imported animals, plants, other products, or migratory birds. The Darwin rural area is experiencing strong growth and is an agricultural hub comprising fruit farms and residential rural blocks with animals. The area has several lagoons and wetlands nearby with abundant birdlife. Importation through 1 of those routes is more likely than a severe weather event because the Darwin rural area has an inland location, and *B. pseudomallei* is likely to be inactivated by ultraviolet light on such a long journey (*10*).

In summary, global epidemiology of melioidosis is changing with increasing globalization, environmental disturbance associated with construction and urbanization, and severe weather events associated with climate change. Genomics is crucial for understanding that dynamic situation, including identifying long-range transmission events and differentiating those from previously unrecognized endemicity. Because of the global spread and potential for transmission, clinicians should increase their awareness of melioidosis and its manifestations.

Acknowledgments

We thank the microbiology staff at Territory Pathology, Darwin, for *B. pseudomallei* isolates and the infectious diseases staff at Royal Darwin Hospital, Darwin, for their care of the patients.

About the Author

Dr. Meumann is an infectious diseases physician and medical microbiologist at Royal Darwin Hospital and senior research fellow at Menzies School of Health

Research, Darwin, Northern Territory, Australia. Her research interests include implementing genomics for infectious disease surveillance and response.

References

1. Chewapreecha C, Holden MT, Vehkala M, Välimäki N, Yang Z, Harris SR, et al. Global and regional dissemination and evolution of *Burkholderia pseudomallei*. Nat Microbiol. 2017;2:16263. https://doi.org/10.1038/nmicrobiol.2016.263
2. Gee JE, Bower WA, Kunkel A, Petras J, Gettings J, Bye M, et al. Multistate outbreak of melioidosis associated with imported aromatherapy spray. N Engl J Med. 2022;386:861–8. https://doi.org/10.1056/NEJMoa2116130
3. Mollaret HH. The botanical garden affair and how melioidosis appeared in France [in French]. Med Mal Infect. 1988;18:643–54. https://doi.org/10.1016/S0399-077X(88)80175-6
4. Chen H, Xia L, Zhu X, Li W, Du X, Wu D, et al. *Burkholderia pseudomallei* sequence type 562 in China and Australia. Emerg Infect Dis. 2015;21:166–8. https://doi.org/10.3201/eid2101.140156
5. Price EP, Sarovich DS, Smith EJ, MacHunter B, Harrington G, Theobald V, et al. Unprecedented melioidosis cases in Northern Australia caused by an Asian *Burkholderia pseudomallei* strain identified by using large-scale comparative genomics. Appl Environ Microbiol. 2015;82:954–63. https://doi.org/10.1128/AEM.03013-15
6. Meumann EM, Kaestli M, Mayo M, Ward L, Rachlin A, Webb JR, et al. Emergence of *Burkholderia pseudomallei* sequence type 562, northern Australia. Emerg Infect Dis. 2021;27:1057–67. https://doi.org/10.3201/eid2704.202716
7. Chapple SN, Price EP, Sarovich DS, McRobb E, Mayo M, Kaestli M, et al. *Burkholderia pseudomallei* genotype distribution in the Northern Territory, Australia. Am J Trop Med Hyg. 2016;94:68–72. https://doi.org/10.4269/ajtmh.15-0627
8. Rachlin A, Mayo M, Webb JR, Kleinecke M, Rigas V, Harrington G, et al. Whole-genome sequencing of *Burkholderia pseudomallei* from an urban melioidosis hot spot reveals a fine-scale population structure and localised spatial clustering in the environment. Sci Rep. 2020;10:5443. https://doi.org/10.1038/s41598-020-62300-8
9. Shafiq M, Ke B, Li X, Zeng M, Yuan Y, He D, et al. Genomic diversity of resistant and virulent factors of *Burkholderia pseudomallei* clinical strains recovered from Guangdong using whole genome sequencing. Front Microbiol. 2022;13:980525. https://doi.org/10.3389/fmicb.2022.980525
10 Sagripanti JL, Levy A, Robertson J, Merritt A, Inglis TJJ. Inactivation of virulent *Burkholderia pseudomallei* by sunlight. Photochem Photobiol. 2009;85:978–86. https://doi.org/10.1111/j.1751-1097.2008.00518.x

Address for correspondence: Ella M. Meumann, Menzies School of Health Research, PO Box 41096, Casuarina, NT 0811, Australia; email: ella.meumann@menzies.edu.au

Venezuelan Equine Encephalitis Virus Infection in Nonhuman Primate, Guatemala, 2023

Wendy K. Jo, Marta Piche-Ovares, Lincoln Carranza, Carlo Fischer, Sebastian Brünink, Laura Paul, Alejandro Morales, Fernando Martinez, Jan Felix Drexler

Author affiliations: Charité–Universitätsmedizin Berlin, corporate member of Freie Universität Berlin and Humboldt-Universität zu Berlin, Institute of Virology, Berlin, Germany (W.K. Jo, M. Piche-Ovares, C. Fischer, S. Brünink, L. Paul, J.F. Drexler); Wildlife Rescue and Conservation Association, Flores, Guatemala (L. Carranza, A. Morales, F. Martinez); German Centre for Infection Research, associated partner site Charité, Berlin (W.K. Jo, J.F. Drexler)

DOI: https://doi.org/10.3201/eid3102.241484

We isolated Venezuelan equine encephalitis virus (VEEV) subtype IE phylogenetically related to Gulf Coast strains in a spider monkey (*Ateles geoffroyi*) released from a rescue center in Guatemala. Serologic testing of 118 monkeys indicated no additional VEEV infections. Infection of a primate warrants intensified surveillance of VEEV transmission cycles in North America.

Venezuelan equine encephalitis virus (VEEV) is an alphavirus in the Americas that can cause febrile illness and severe disease, including encephalitis. In humans, overall case-fatality rates are <1% but higher in children; in horses, case-fatality rates are 50%–70% (https://www.woah.org/en/disease/venezuelan-equine-encephalitis). In the United States, VEEV is classified as a select agent because of its pathogenicity and aerosolization capacity (https://www.selectagents.gov/sat/list.htm). The transmission of the arthropodborne VEEV involves an epizootic cycle (antigenic subtypes IAB and IC), entailing higher numbers of human infections, and an enzootic cycle (the common transmission cycle for antigenic subtypes ID and IE), entailing sporadic human infections (*1*,*2*). The emergence of VEEV epizootics is poorly understood but might involve genetic exchanges from enzootic subtypes (*1*). VEEV subtype IE has been reported in Central America and Mexico since the 1960s (*3*). Subtype IE has been detected almost exclusively in mosquitoes and sentinel hamsters (*3*,*4*) but sporadically in horses and humans (*2*,*3*,*5*); the subtype has been associated with 2 epizootics in horses in Mexico in the 1990s (*6*). We report the detection and isolation

Figure 1. Geographic origins of reported Venezuelan equine encephalitis virus subtype IE sequences identified in Central America. Circles indicate geolocation of subtype IE sequences. Enlarged map shows the geolocation of the strains grouping with the virus from this study (Petén Department, Guatemala, 2023).

of a VEEV IE strain in a healthy nonhuman primate (NHP) in Guatemala in 2023.

We investigated 211 animals from 22 species (orders Artiodactyla, Carnivora, Didelphimorphia, Pilosa, Primates, and Rodentia) (Appendix Figure 1, https://wwwnc.cdc.gov/EID/article/31/2/24-1484-App1.pdf). We collected plasma samples from animals living in the Wildlife Rescue and Conservation Association (ARCAS) (https://arcasguatemala.org), a nongovernment organization in Petén Department in northern Guatemala. Animals are brought to ARCAS after being seized by police or customs officials at roadblocks or local markets. All animals are tested against selected pathogens and quarantined for 2–3 months upon arrival to the center and usually stay for another few months before being released into the wild (Appendix). We extracted RNA from plasma samples and screened it for alphaviruses and flaviviruses by using broadly reactive reverse transcription PCR (RT-PCR) assays (Appendix). By using an alphavirus RT-PCR, we identified VEEV in 1 adult male spider monkey (*Ateles geoffroyi*), an endangered species occurring from southern Mexico to Panama. No sample was positive for flavivirus RNA. Viral load in plasma was 1.8×10^5 VEEV RNA copies/mL, determined through real-time RT-PCR (Appendix). At 2 days postinfection, Vero E6 cells displayed a cytopathic effect and reached high concentrations of 1.4×10^{10} VEEV RNA copies/mL of supernatant. We applied deep sequencing (Appendix) to the virus isolate and obtained a near-complete genome (4.7 million reads, >50,000× mean depth of coverage), encompassing 11,477 nt and lacking only 12 nt in the 5′ untranslated region (GenBank accession no. PQ406672). The VEEV genome showed typical organization; the predicted regions encoded nonstructural protein genes (*nsP1*–*nsP4*) and structural protein genes (*capsid*, *E1*–*E3*, and *6K*). The VEEV from Guatemala had pairwise nucleotide sequence distances of 1.4%–7.4% with VEEV subtype IE sequences available in GenBank that mostly originated from Central America (Figure 1). We identified no amino acid exchange at position 117 of the E2 glycoprotein, which previously had been associated with a VEEV subtype IE infection outbreak in horses (*1*). Pressure analyses that identify pervasive and episodic selection showed no sign of adaptive mutation in the E2 glycoprotein (Appendix Figure 2), suggesting strong purifying selection that might limit adaptation to new hosts (*3*). Bayesian phylogenetic analysis showed that the NHP-associated virus grouped with viruses obtained from the 1960s circulating in the Gulf Coast across a ≈200–700 km distance (most recent common ancestor 1954) (Figure 2), suggesting a lack of surveillance and continued circulation of genetically closely related strains in North America.

Natural VEEV infection in an NHP might be indicative of an outbreak. Therefore, we tested all plasma samples from primates residing in ARCAS (n = 118), including 80 spider monkeys and 38 howler monkeys (*Alouatta pigra* and *A. palliata*), for VEEV-specific IgM by using a modified commercial immunofluorescence assay (IFA) (Appendix). IFA detected no positive samples, including in the PCR-positive animal (Appendix Figure 3). The NHP infected with VEEV showed no clinical symptoms and

was released into the wild on the day of blood sampling, suggesting that the animal was viremic upon release. In humans, severe disease characterized by neurologic complications occurs more frequently in children; therefore, future investigations might consider VEEV as a differential diagnosis, particularly in young NHP with acute neurologic disease in VEEV-endemic areas.

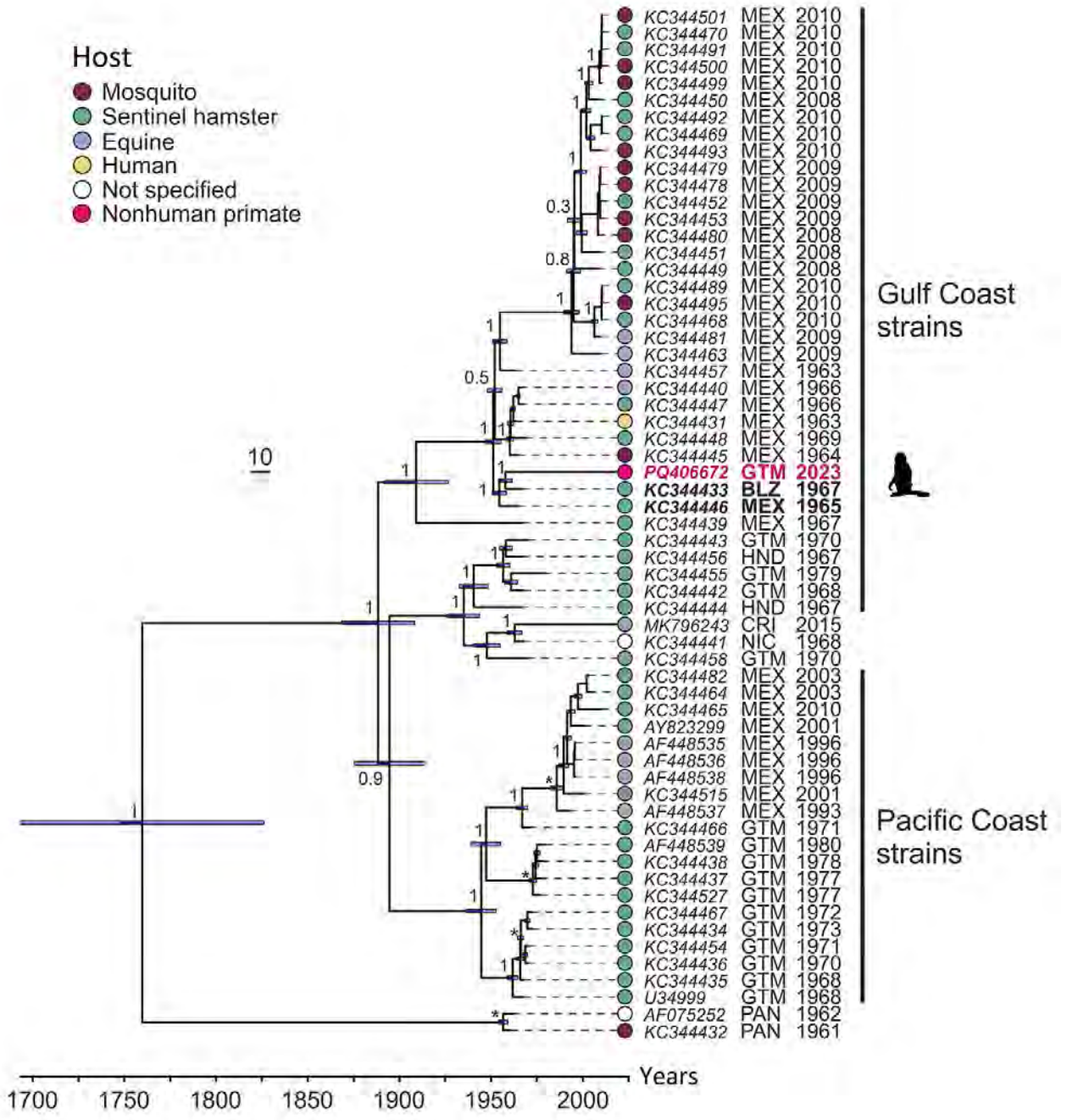

Figure 2. Time-scaled Bayesian maximum-clade credibility tree of Venezuelan equine encephalitis virus subtype IE identified in Central America. Bayesian phylogeny of the concatenated nonstructural and structural open reading frames with removal of the coding regions for the C-terminus of nonstructural protein 3 and N terminus of the capsid protein. Taxa indicate GenBank accession number, country abbreviation, and year of collection. Branch tips indicate host by color coding, including a sequence (strain no. 63Z1) isolated from blood of a sick human infected in the rainforest near Sontecamapan, Veracruz, Mexico, in August 1963 (*2*). Numbers at nodes indicate posterior probabilities of all major branches. Asterisks indicate clades previously used for dating according to a previous publication (*3*). Bars in node branches represent the 95% height posterior density intervals of the node ages. Scale bar represents time in years. BLZ, Belize; CRI, Costa Rica; GTM, Guatemala; HND, Honduras; MEX, Mexico; NIC, Nicaragua; PAN, Panama; SLV, El Salvador.

Although the neotropics are a probable hot spot for primate-associated emerging infections, neotropical NHPs are understudied for emerging pathogens (*7*). NHPs are among the most relevant sources of zoonotic viruses (in >20% of primate species zoonotic pathogens have been found) (*7*). Infection with other human pathogenic arthropodborne viruses, such as chikungunya and yellow fever viruses, has been reported in NHPs (*8*,*9*). Movement of NHPs by wildlife trafficking might contribute to the geographic expansion of VEEV and other pathogens. Although we identified no adaptive mutation in our study, the determinants of epizootics are not well understood, and new hosts might entail viral adaptation, potentially altering the viral phenotype. Seroepidemiologic and experimental infection studies, such as those conducted in rodents (*10*), are needed to clarify the role of NHPs in VEEV transmission cycles.

Acknowledgments

We thank Melanie Roggow, Sabrina Figueroa, Kim Grützmacher, and Michael Nagel.

Export permits were approved by the local authority Consejo Nacional de Areas Protegidas (National Council for Protected Areas), including Convention on International Trade in Endangered Species of Wild Fauna and Flora (CITES) permit nos. 493-494/2023, 496-497/2023, and 1363-64/2023, and non-CITES permit nos. 276/2023 and 398/2023. The export sanitary certificate (DPSP-E-15598) was approved by the Ministerio de Agricultura, Ganaderia, y Alimentacion (Minister of Agriculture and Food Supply) in Guatemala. Import permits were obtained from the Bundesamt für Naturschutz (Federal Agency for Nature Conservation), including CITES permit nos. DE-E-02185-86/23, DE-E-02188-86/23, DE-E05070/23, and DE-E05072/23, and import notification no. 223. Veterinary health permit nos. EG I-2023/60 and EG I-2024/08 were approved by the Senatsverwaltung für Justiz und Verbraucherschutz (Senate Department for Justice and Consumer Protection), in Berlin, Germany.

This work was supported by the German Federal Ministry of Economic Cooperation and Development through the Deutsche Gesellschaft für Internationale Zusammenarbeit GmbH (project no. 81284476), the European Union through the project Zoonosis Emergence across Degraded and Restored Forest Ecosystems (project no. 101135094), the Global Centers for Health and Pandemic Prevention (project no. 57592642), and a doctoral program scholarship from the German Academic Exchange Service (grant no. 91609043).

About the Author

Dr. Jo is a virologist working as a postdoctoral researcher at the Institute of Virology at the Charité–Universitätsmedizin Berlin. Her research interests focus on the evolutionary origins of emerging viruses and the factors that drive their emergence.

References

1. Brault AC, Powers AM, Holmes EC, Woelk CH, Weaver SC. Positively charged amino acid substitutions in the E2 envelope glycoprotein are associated with the emergence of Venezuelan equine encephalitis virus. J Virol. 2002;76:1718–30. https://doi.org/10.1128/JVI.76.4.1718-1730.2002
2. Scherer WF, Campillo-Sainz C, de Mucha-Macías J, Dickerman RW, Chia CW, Zarate ML. Ecologic studies of Venezuelan encephalitis virus in southeastern Mexico. VII. Infection of man. Am J Trop Med Hyg. 1972;21:79–85. https://doi.org/10.4269/ajtmh.1972.21.79
3. Forrester NL, Wertheim JO, Dugan VG, Auguste AJ, Lin D, Adams AP, et al. Evolution and spread of Venezuelan equine encephalitis complex alphavirus in the Americas. PLoS Negl Trop Dis. 2017;11:e0005693. https://doi.org/10.1371/journal.pntd.0005693
4. Adams AP, Navarro-Lopez R, Ramirez-Aguilar FJ, Lopez-Gonzalez I, Leal G, Flores-Mayorga JM, et al. Venezuelan equine encephalitis virus activity in the Gulf Coast region of Mexico, 2003–2010. PLoS Negl Trop Dis. 2012;6:e1875. https://doi.org/10.1371/journal.pntd.0001875
5. Aguilar PV, Estrada-Franco JG, Navarro-Lopez R, Ferro C, Haddow AD, Weaver SC. Endemic Venezuelan equine encephalitis in the Americas: hidden under the dengue umbrella. Future Virol. 2011;6:721–40. https://doi.org/10.2217/fvl.11.50
6. Oberste MS, Fraire M, Navarro R, Zepeda C, Zarate ML, Ludwig GV, et al. Association of Venezuelan equine encephalitis virus subtype IE with two equine epizootics in Mexico. Am J Trop Med Hyg. 1998;59:100–7. https://doi.org/10.4269/ajtmh.1998.59.100
7. Han BA, Kramer AM, Drake JM. Global patterns of zoonotic disease in mammals. Trends Parasitol. 2016;32:565–77. https://doi.org/10.1016/j.pt.2016.04.007
8. Althouse BM, Guerbois M, Cummings DAT, Diop OM, Faye O, Faye A, et al. Role of monkeys in the sylvatic cycle of chikungunya virus in Senegal. Nat Commun. 2018;9:1046. https:// doi.org/10.1038/s41467-018-03332-7
9. Moreira-Soto A, Torres MC, Lima de Mendonca MC, Mares-Guia MA, Dos Santos Rodrigues CD, Fabri AA, et al. Evidence for multiple sylvatic transmission cycles during the 2016–2017 yellow fever virus outbreak, Brazil. Clin Microbiol Infect. 2018;24:1019.e1–e4.
10. Deardorff ER, Forrester NL, Travassos-da-Rosa AP, Estrada-Franco JG, Navarro-Lopez R, Tesh RB, et al. Experimental infection of potential reservoir hosts with Venezuelan equine encephalitis virus, Mexico. Emerg Infect Dis. 2009;15:519–25. https://doi.org/10.3201/eid1504.081008

Address for correspondence: Jan Felix Drexler, Institute of Virology, Charitéplatz 1, 10117 Berlin, Germany; email: felix.drexler@charite.de

Bayou Hantavirus Cardiopulmonary Syndrome, Louisiana, USA, 2022–2023

Emma Ortega, Sean Simonson, Elizabeth Shedroff, Shannon Whitmer, Amy Whitesell, Mary J. Choi, Trevor Shoemaker, Joel M. Montgomery, John D. Klena, Joseph Hennig, Theresa Sokol

Author affiliations: Louisiana Department of Health, New Orleans, Louisiana, USA (E. Ortega, S. Simonson, T. Sokol); Centers for Disease Control and Prevention, Atlanta, Georgia, USA (E. Shedroff, S. Whitmer, A. Whitesell, M.J. Choi, T. Shoemaker, J.M. Montgomery, J.D. Klena); Louisiana State University, Lafayette, Louisiana, USA (J. Hennig)

DOI: https://doi.org/10.3201/eid3102.241069

During 2020–2023, we sequenced Bayou virus from 2 patients in Louisiana, USA, with hantavirus cardiopulmonary syndrome. Direct virus sequencing demonstrated an inferred evolutionary relationship to previous cases. Our findings demonstrate that separate virus spillovers cause isolated cases and probable wide distribution of Bayou hantavirus in rodents across Louisiana.

Hantavirus cardiopulmonary syndrome (HCPS) is a rodentborne zoonotic disease caused by infection with New World hantaviruses located predominantly in the Americas (*1*). HCPS is an acute febrile illness that can rapidly progress to acute respiratory distress syndrome and death; cases with fever but no respiratory involvement have also been identified (*2*). During 1993–2021, the hantavirus mortality rate in the United States was 35% (*3*). Disease is acquired after exposure to rodents, through inhalation of aerosolized virus from rodent urine and feces and, less frequently, from rodent bites (*4*). In the United States, 5 New World hantaviruses cause human disease (Table) (*5*,*6*).

Oryzomys palustris marsh rice rats are native to the southeastern United States, and Bayou virus–infected rodents have been identified in Texas, Louisiana, Georgia, and South Carolina (*7*,*8*). Only 7 human cases of Bayou virus infection have been reported, 5 in Texas and 2 in Louisiana, 1 of which was fatal (*2*,*4*,*5*). During 1993–2021, Louisiana reported 7 hantavirus cases; however, virus sequence information is available for only 1993 and 2013 cases (*4*,*6*). We describe 2 unrelated cases of Bayou HCPS from Louisiana reported in 2022–2023.

Patient 1 was a 66-year-old man with a medical history of tobacco use disorder who sought care at an emergency department after 4 days of chest pain, weakness, nausea, cough, and shortness of breath (*9*). Laboratory values indicated hemoconcentration, mildly elevated creatinine level, elevated lactate dehydrogenase level, and thrombocytopenia. Chest radiographs were concerning for bilateral infiltrates, and chest computed tomography (CT) showed small pleural effusions with patchy ground-glass opacities. At the time of arrival, the patient's oxygen saturation was 91% with bilevel positive airway pressure and his oxygen requirements quickly escalated. His blood oxygen level decreased, and he was intubated. Laboratory analyses were notable for leukocytosis, worsening thrombocytopenia, and a granulocytic left shift; chest radiography showed worsening opacities. The patient had bilateral femoral artery clots and widespread petechiae, and he died 4 days after admission. Hantavirus serologic testing of samples collected before death were posthumously positive for IgM and negative for IgG. We could not obtain exposure information.

Patient 2 was a 56-year-old man with no relevant medical history. He experienced a syncopal episode preceded by a 1-week history of fever, cough, shortness of breath, malaise, diarrhea, and vomiting. At the time of arrival at the emergency department, he experienced a second syncopal episode. He had visited the emergency department once for this illness, which was diagnosed as a stomach virus. At admission, he was hypotensive with thrombocytopenia, leukocytosis, mildly elevated liver enzymes, elevated creatinine, and elevated lactate dehydrogenase level. Chest radiography was suggestive of bronchitis with pulmonary edema, and CT showed moderate interstitial pulmonary edema. Patient 2 was transferred to the intensive care unit for septic shock, complicated by thrombocytopenia, acute renal failure, and metabolic acidosis. Because his respiratory status

Table. Most common New World hantaviruses known to cause hantavirus cardiopulmonary syndrome and the associated rodent reservoir, United States

Virus	Rodent reservoir
Bayou	Rice rat (*Oryzomys palustris*)
Black Creek Canal	Cotton rat (*Sigmodon hispidus*)
Monongahela	Deer mouse (*Peromyscus maniculatus*)
New York	White-footed mouse (*P. leucopus*)
Sin Nombre	Deer mouse (*P. maniculatus*)

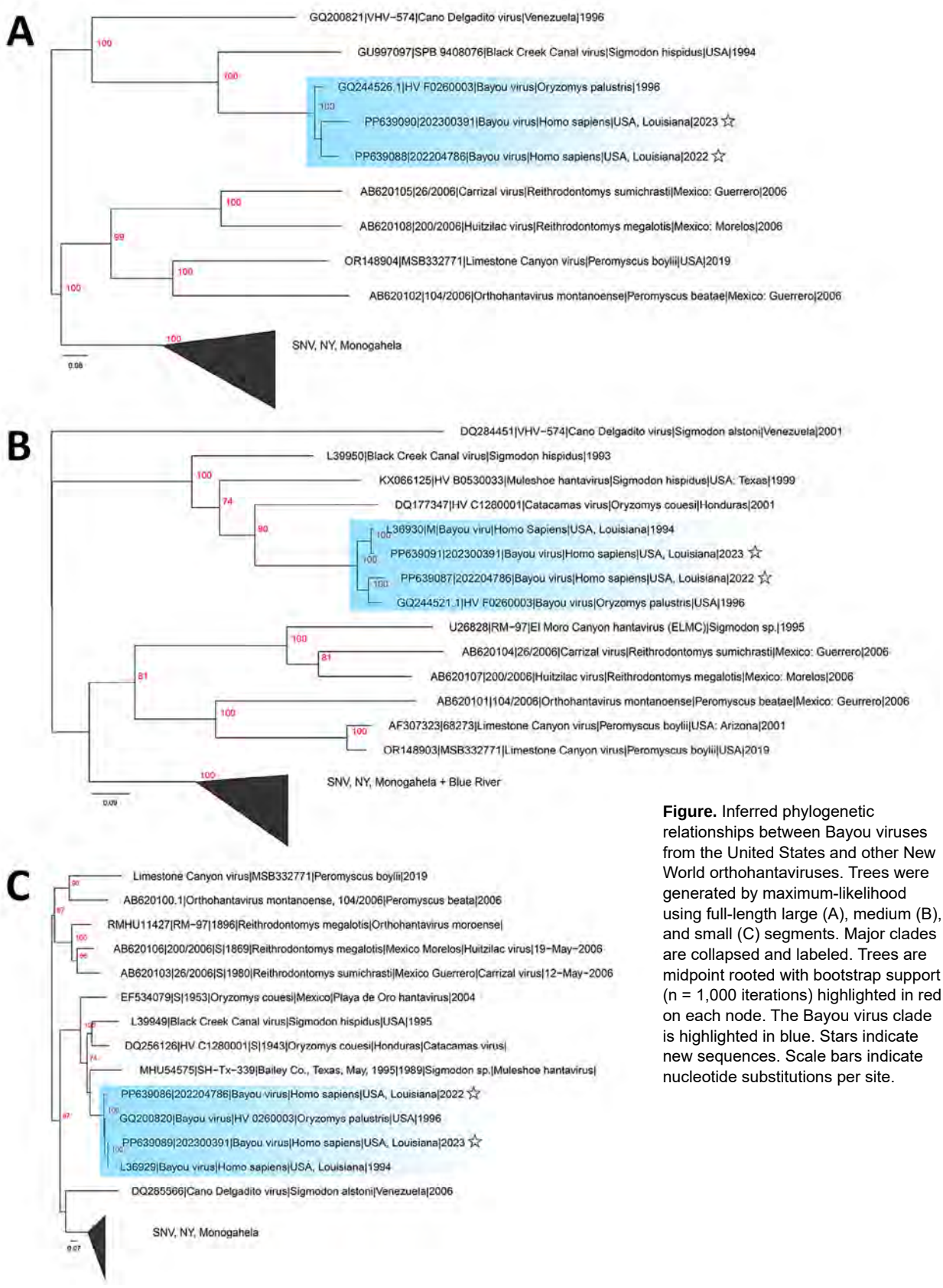

Figure. Inferred phylogenetic relationships between Bayou viruses from the United States and other New World orthohantaviruses. Trees were generated by maximum-likelihood using full-length large (A), medium (B), and small (C) segments. Major clades are collapsed and labeled. Trees are midpoint rooted with bootstrap support (n = 1,000 iterations) highlighted in red on each node. The Bayou virus clade is highlighted in blue. Stars indicate new sequences. Scale bars indicate nucleotide substitutions per site.

deteriorated, bilevel positive airway pressure was administered, and metabolic encephalopathy developed. Subsequent CT showed bilateral pleural effusions and partial encapsulation of the left lower lung with left-sided pleural effusion. Thrombocytopenia worsened, and leukocytosis and creatinine level increased. Hemodialysis was started, and steroids and antimicrobial drugs were administered. The patient's signs/symptoms gradually resolved, and he was discharged 15 days after admission. Hantavirus infection was confirmed by the presence of hantavirus-reactive IgM (IgG-negative) in a specimen collected 7 days after symptom onset; no subsequent specimens were collected. During a follow-up interview, the patient reported having cleaned out an uninhabited trailer during the 2–3 weeks before symptom onset, including tearing up carpets and insulation and working under the trailer without proper personal protective equipment.

Using the Altona hantavirus quantitative reverse transcription PCR (https://altona-diagnostics.com), we determined that virus cycle thresholds were 28.4 for patient 1 and 28.8 for patient 2. We generated complete Bayou virus large (L), medium (M), and small (S) segments directly from patient serum by using the RNA Exome Library Preparation unbiased sequencing method (Illumina, https://www.illumina.com) with pan-hantavirus enrichment oligonucleotides, followed by de novo assembly and reference mapping. L segment sequences from patients 1 (GenBank accession no. PP639088) and 2 (GenBank accession no. PP639090) were closely related to a rodentborne Bayou virus collected in 1996 (Figure 1, panel A). The M and S segments from both patients also clustered on Bayou virus-specific clades (Figure 1, panels B, C). M and S segments from both patients were more closely related to historic Bayou sequences than to each other; demonstrating that separate zoonotic spillovers probably caused disease (Figure 1, panels B, C). Patient 1 M and S segments (GenBank accession nos. PP639086 and PP639087) were related to Bayou sequences from *O. palustris* rats collected in 1996 from Galveston, Texas, whereas patient 2 M and S segments (GenBank accession nos. PP639091 and PP639089) were associated with a fatal Bayou virus case from northeastern Louisiana in 1993.

For both patients, hantavirus infection was initially exhibited by nonspecific signs/symptoms and quickly progressed to severe disease. Increasing surveillance efforts and clinician education, along with implementing the hantavirus 5-point screening tool, could improve rapid diagnostics during indistinguishable disease manifestation (*10*).

Acknowledgments

We thank Angie Orellana, Leslie Arceneaux, and the Louisiana Department of Health Infectious Disease Epidemiology regional surveillance teams for their work in these investigations.

All authors declare no competing interests.

About the Author

Ms. Ortega is an epidemiologist at the Louisiana Department of Health. Her research interests include vectorborne diseases and zoonotic infections.

References

1. Jonsson CB, Figueiredo LT, Vapalahti O. A global perspective on hantavirus ecology, epidemiology, and disease. Clin Microbiol Rev. 2010;23:412–41. https://doi.org/10.1128/CMR.00062-09
2. National Notifiable Diseases Surveillance System. Hantavirus pulmonary syndrome (HPS) 2015 case definition [cited 2024 Jul 3]. https://ndc.services.cdc.gov/case-definitions/hantavirus-pulmonary-syndrome-2015
3. Centers for Disease Control and Prevention. Reported cases of hantavirus disease [cited 2024 Jul 3]. https://www.cdc.gov/hantavirus/data-research/cases/index.html
4. Knust B, Rollin PE. Twenty-year summary of surveillance for human hantavirus infections, United States. Emerg Infect Dis. 2013;19:1934–7. https://doi.org/10.3201/eid1912.131217
5. Whitmer SLM, Whitesell A, Mobley M, Talundzic E, Shedroff E, Cossaboom CM, et al. Human Orthohantavirus disease prevalence and genotype distribution in the U.S., 2008–2020: a retrospective observational study. Lancet Reg Health Am. 2024;37:100836.https://doi.org/10.1016/j.lana.2024.100836
6. Louisiana Office of Public Health, Infectious Disease Epidemiology Section. Hantavirus infection (including pulmonary syndrome) [cited 2025 Jan 16]. https://ldh.la.gov/assets/oph/Center-PHCH/Center-CH/infectious-epi/Annuals/2021/Hantavirus_LaIDAnnual.pdf
7. Ksiazek TG, Nichol ST, Mills JN, Groves MG, Wozniak A, McAdams S, et al. Isolation, genetic diversity, and geographic distribution of Bayou virus (Bunyaviridae: hantavirus). Am J Trop Med Hyg. 1997;57:445–8. https://doi.org/10.4269/ajtmh.1997.57.445
8. Torrez-Martinez N, Bharadwaj M, Goade D, Delury J, Moran P, Hicks B, et al. Bayou virus–associated hantavirus pulmonary syndrome in eastern Texas: identification of the rice rat, Oryzomys palustris, as reservoir host. Emerg Infect Dis. 1998;4:105–11. https://doi.org/10.3201/eid0401.980115
9. Hennig J, Rosson J, Curry K. 551: A complex case of hantavirus pulmonary syndrome and hemorrhagic fever with renal syndrome. Crit Care Med. 2023;52:S249. https://doi.org/10.1097/01.ccm.0001000380.16526.9a
10. Koster F, Foucar K, Hjelle B, Scott A, Chong YY, Larson R, et al. Rapid presumptive diagnosis of hantavirus cardiopulmonary syndrome by peripheral blood smear review. Am J Clin Pathol. 2001;116:665–72. https://doi.org/10.1309/CNWF-DC72-QYMR-M8DA

Address for correspondence: Shannon Whitmer, Centers for Disease Control and Prevention, 1600 Clifton Rd NE, Mailstop H18-SSB, Atlanta, GA 30329-4018, USA; email: evk3@cdc.gov

Ixodes scapularis Tick Parasitizing Dog in Dawson County, Montana, USA, 2023

Philip E. Stewart, Justin B. Lack, Marni Rolston, Kimmo Virtaneva, Paul A. Beare, Craig M. Martens, Marshall E. Bloom, Tom G. Schwan

Author affiliations: National Institutes of Health Rocky Mountain Laboratories, Hamilton, Montana, USA (P.E. Stewart, K. Virtaneva, P.A. Beare, C.M. Martens, M.E. Bloom, T.G. Schwan); National Institutes of Health, Rockville, Maryland, USA (J.B. Lack); Montana State University, Bozeman, Montana, USA (M. Rolston)

DOI: https://doi.org/10.3201/eid3102.241308

In October 2023, a partially engorged female *Ixodes* tick was removed from a dog in Bozeman, Montana, USA, that had recently spent time in eastern Montana. The tick was identified as *I. scapularis* according to morphologic characteristics and genomic sequencing, suggesting an expanded geographic distribution requiring continued public health surveillance.

The blacklegged tick, *Ixodes scapularis*, is the vector of several human pathogens and the primary vector of the Lyme disease spirochete *Borrelia burgdorferi* in the eastern half of the continental United States (*1*). During the past 40 years, intensive investigations of this tick's geographic distribution have documented its spread north and west, with new populations established in eastern North and South Dakota (*2*,*3*). Montana has remained free of *I. scapularis* ticks and their western counterparts, *I. pacificus* ticks (*2*). As part of a citizen science investigation during 2016–2017, a specimen of *I. scapularis* tick was submitted from Liberty County, Montana; however, the tick stage and host were not given, and the authors concluded that either the tick had been recently imported to the area or had been misidentified (*4*).

On October 12, 2023, a partially engorged female *Ixodes* tick was removed from the lower neck of a 7.5-year-old female French Brittany hunting dog in Bozeman, Montana, USA; the dog had recently returned with its owners from a pheasant hunting trip north of Ritchey, Dawson County, in eastern Montana. The specimen was submitted to the Schutter Diagnostic Laboratory at Montana State University in Bozeman for identification, and subsequently stored in alcohol and forwarded to the Rocky Mountain Laboratories, National Institutes of Health (Hamilton, MT, USA) for further examination. The specimen lacked the hypostome and 1 palp but, when examined microscopically, the characteristics were consistent with an *I. scapularis* tick (Figure 1, panels A–D). The specimen and 3 other museum specimens of unengorged female *I. scapularis* ticks matched *I. scapularis* (*5*,*6*) but not any of the 9 *Ixodes* spp. previously recorded in Montana (Appendix Table, https://wwwnc.cdc.gov/EID/article/31/2/24-1308-App1.pdf). The dog had not traveled outside the state before acquiring the tick, and the presumed time of attachment correlated with the trip to Dawson County (Appendix Figure 1).

Because of the condition of the specimen and potential significance of its identity, we processed the tick for genomic sequencing. We removed the tick from alcohol, froze it in liquid nitrogen, then pulverized it and extracted genomic DNA by using the MagAttract HMW DNA Kit (QIAGEN, https://www.qiagen.com) according to the manufacturer's protocol. DNA isolated from this tick was partially degraded and produced a low yield, likely because of the long-term storage in alcohol; however, we performed whole-genome sequencing.

Sequencing coverage was ≈1× for the nuclear genome; the median mitochondrial genome coverage mapped to the published *I. scapularis* mitochondrial DNA sequence (GenBank accession no. MZ645749.1) (*7*). We extracted the *cox1* gene consensus sequence from the data and generated a maximum-likelihood phylogeny that had 100% bootstrap support for identity between *I. scapularis* and this specimen. The uncorrected pairwise identity between *I. scapularis* and this specimen was 99.49%, whereas pairwise identity with several other *Ixodes* spp. established in Montana was <89% (Figure 2). We deposited the *cox1* sequence into GenBank (accession no. PQ284574).

As an independent approach separate from mapping to the *I. scapularis* reference genome, we mapped the Illumina sequencing reads from this specimen to a database of >5 million *cox1* sequences (*8*). The highest count (6,174,692 reads) mapped to *I. scapularis*, far more than the next highest count, which was *I. ricinus* (718,590 reads). In addition, we analyzed the microbial sequences from this tick specimen and identified 340,000 reads mapping to the *I. scapularis*–specific endosymbiont bacterium *Rickettsia buchneri* (Appendix Figure 2) (*9*), further supporting the identification of this tick. A relatively low number (1,509) of reads mapped to the family Borreliaceae, which includes the causative agents of Lyme disease and relapsing fever. Although this low number of reads requires independent verification, it suggests the tick specimen might have been infected with a member of the genus *Borrelia*.

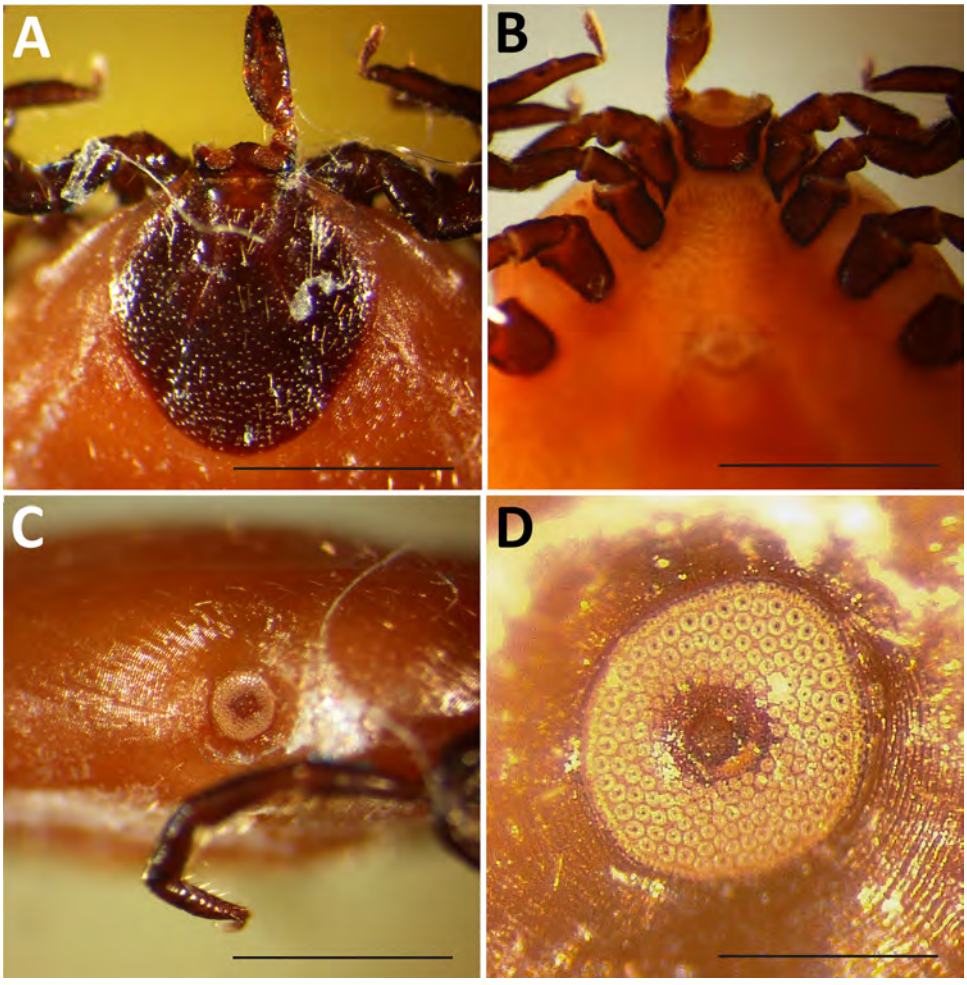

Figure 1. Partially engorged female *Ixodes scapularis* tick from Dawson County, Montana, USA, 2023. Tick was found on a dog, and key characteristics were used for identification. A) Dorsal view of capitulum showing shape of scutum and palp, basis capituli, and porose areas. Scale bar = 1 mm. B) Ventral view of capitulum showing shape and length of internal spurs on coxae I. Scale bar = 1 mm. C) Right lateral view of idiosoma showing spiracular plate. Scale bar = 1 mm. D) Enlargement of spiracular plate showing number and size of the goblet cells. Scale bar = 0.25 mm.

In conclusion, the continued range expansion of *I. scapularis* ticks is thought to be complex and multifactorial (*10*). Here, we confirmed that a tick acquired in eastern Montana was *I. scapularis* by using 2 independent methods: morphologic characterization and genomic DNA sequence alignments. Identification is further supported by the presence of *R. buchneri* in the tick's microbiome. In 2023, the Centers for Disease Control and Prevention predicted the western boundary of the *I. scapularis* tick range terminated

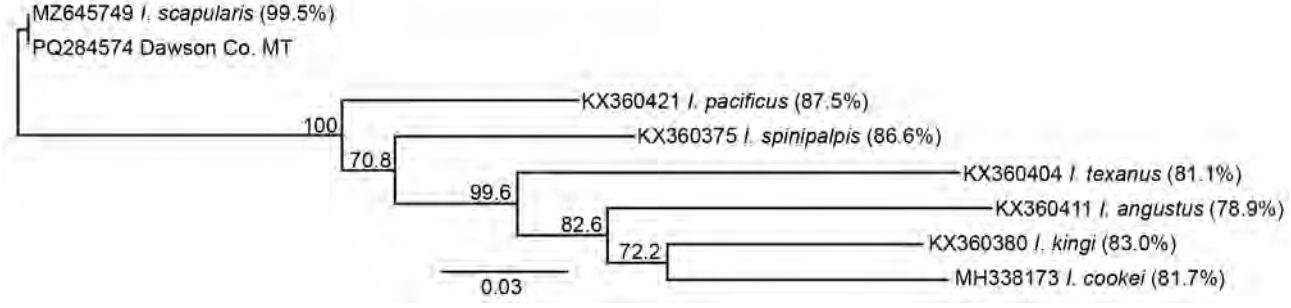

Figure 2. Phylogenetic analysis of *Ixodes scapularis* tick parasitizing dog in Dawson County, Montana, USA, 2023. Phylogram of cytochrome oxidase C subunit I (*coxI*) sequences showing near identity of the Dawson County tick with *I. scapularis*. We used RAxML (https://github.com/amkozlov/raxml-ng) to generate an unrooted maximum-likelihood phylogeny of 583-bp *coxI* sequences with 500 bootstrap replicates. Genbank accession numbers for each sequence precede the species name. Branch labels indicate the percentage of bootstrap replicates supporting a given branch. Percentages of uncorrected pairwise identity to the Dawson County, Montana, specimen are indicated in parentheses. With the exceptions of *I. cookei* and *I. pacificus*, the other *Ixodes* spp. ticks in this tree are indigenous to Montana. Scale bar indicates nucleotide substitutions per site.

in the middle of North Dakota (Appendix Figure 1). The collection of a single specimen does not signify an established population in Montana, but the public health concern regarding this tick species warrants further investigation into the potential range expansion of the *I. scapularis* tick. If an established *I. scapularis* tick population is confirmed, continued surveillance and characterization of any corresponding human pathogens will be required.

Acknowledgments

We thank Kimberly Ellingson Kotur for collecting and submitting the tick for identification and S.J. Tudor and Anita Mora for graphics expertise.

This work was supported, in part, by the Division of Intramural Research, National Institute of Allergy and Infectious Diseases, National Institutes of Health, USA.

About the Author

Dr. Stewart is a staff scientist at the Rocky Mountain Laboratories campus of the National Institutes of Health. His research focuses on ticks and tick-transmitted pathogens.

References

1. Eisen RJ, Eisen L. The blacklegged tick, Ixodes scapularis: an increasing public health concern. Trends Parasitol. 2018;34:295–309. https://doi.org/10.1016/j.pt.2017.12.006
2. Eisen RJ, Eisen L, Beard CB. County-scale distribution of Ixodes scapularis and Ixodes pacificus (Acari: Ixodidae) in the continental United States. J Med Entomol. 2016;53:349–86. https://doi.org/10.1093/jme/tjv237
3. Maestas LP, Adams SL, Britten HB. First evidence of an established population of Ixodes scapularis (Acari: Ixodidae) in South Dakota. J Med Entomol. 2016;53:965–6. https://doi.org/10.1093/jme/tjw038
4. Nieto NC, Porter WT, Wachara JC, Lowrey TJ, Martin L, Motyka PJ, et al. Using citizen science to describe the prevalence and distribution of tick bite and exposure to tick-borne diseases in the United States. PLoS One. 2018;13:e0199644. https://doi.org/10.1371/journal.pone.0199644
5. Cooley RA, Kohls GM. The genus *Ixodes* in North America. Natl Inst Health Bull No. 184. Washington: US Government Printing Office; 1945
6. Keirans JE, Clifford CM. The genus Ixodes in the United States: a scanning electron microscope study and key to the adults. J Med Entomol. Suppl. 1978;2:1–149. https://doi.org/10.1093/jmedent/15.suppl2.1
7. Price DC, Brennan JR, Wagner NE, Egizi AM. Comparative hologenomics of two *Ixodes scapularis* tick populations in New Jersey. PeerJ. 2021;9:e12313. https://doi.org/10.7717/peerj.12313
8. Balech B, Sandioniggi A, Marzano M, Pesole G, Santamaria M. MetaCOXI: an integrated collection of metazoan mitochondrial cytochrome oxidase subunit-I DNA sequences. Database (Oxford). 2022;2022:baab084. https://doi.org/10.1093/database/baab084
9. Kurtti TJ, Felsheim RF, Burkhardt NY, Oliver JD, Heu CC, Munderloh UG. Rickettsia buchneri sp. nov., a rickettsial endosymbiont of the blacklegged tick Ixodes scapularis. Int J Syst Evol Microbiol. 2015;65:965–70. https://doi.org/10.1099/ijs.0.000047
10. Telford SR 3rd, Stewart PE, Bloom ME. Increasing risk of tick-borne disease: what should clinicians know? JAMA Intern Med. 2024;184:973–4. https://doi.org/10.1001/jamainternmed.2024.1754

Address for correspondence: Philip Stewart, Rocky Mountain Laboratories, NIAID, NIH, 903 South 4th St, Hamilton, MT 59840, USA; email: pestewart@niaid.nih.gov

etymologia

Mycoplasma phocimorsus (mī-kō-ˈplaz-mə fō-ki-ˈmȯr-səs), panaritium (pan-ə-ˈrish-ē-əm)

Clyde Partin

This issue of EID incudes a report of patient with a cat scratch–induced panaritium caused by infection with the bacterium *Mycoplasma phocimorsus* (see page 380). In 2023, researchers at Statens Serum Institut in Denmark reported a novel species of the bacterial class Mollicutes (from the Latin *mollis* for soft and *cutis* for skin). The new species was named *Mycoplasma phocimorsus* (*phoca* for seal, *morsus* for bite); 6 strains were found in samples from Denmark, Norway, and Sweden.

The associated infection, first described in 1907, was called seal, blubber, or spekk (Norwegian for blubber) finger because infected persons had been exposed to seals in marine environments. The superficial lesions around the fingernail are called whitlows, but deeper penetration involves the tendon sheath, a painful condition deemed panaritium tendineum. (Panaritium, used interchangeably with whitlow or paronychia, more correctly implies purulent inflammation and infection of digital tendons.)

The etymology for *Mycoplasma* (*mykes* for fungus, *plasma* for formed) is complicated. The word was introduced by A.B. Frank in 1889 to denote an intimate relationship between plant-invading fungi or other microorganisms and their host cells, whose cytoplasm is altered by the infection. Frank described mycoplasma as a "mixture of fungal and plant protoplasm…that it gave rise to bacteroid tissue."

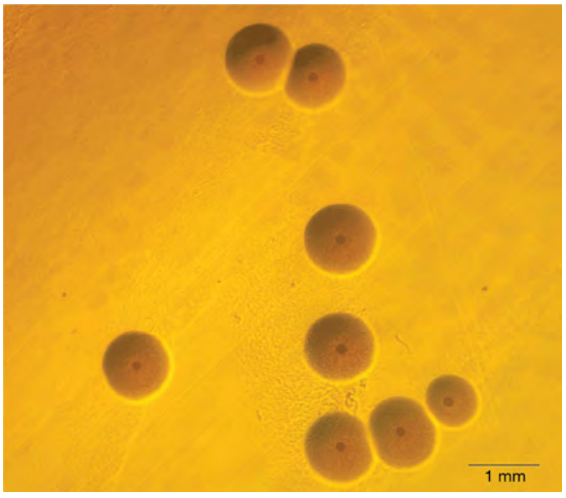

Figure. *Mycoplasma phocimorsus*. Copyright ©2023 International Journal of Systematic and Evolutionary Microbiology. Used with permission.

Sources

1. Bidenknap JH. Spackflegmonen. Norsh Magazin for Legevidenskaben. 1907;68:515–23.
2. Krass CJ, Gardner MW. Etymology of the term Mycoplasma. Int J Syst Evol Microbiol. 1973;23:62–64.
3. Lewin MR, Knott P, Lo M. Seal finger. Lancet. 2004;364:448.
4. Newman Dorland WA. The American illustrated medical dictionary. 22nd edition. Philadelphia: W.B. Saunders Company; 1951. p. 1084.
5. Panaritium. Wiktionary [cited 2024 Nov 11]. https://en.wiktionary.org/wiki/panaritium
6. Skafte-Holm A, Pedersen TR, Frølund M, Stegger M, Qvortrup K, Michaels DL, et al. *Mycoplasma phocimorsus* sp. nov., isolated from Scandinavian patients with seal finger or septic arthritis after contact with seals. Int J Syst Evol Microbiol. 2023;73. https://doi.org/10.1099/ijsem.0.006163
7. Skafte-Holm A, Pedersen TR, Frølund M, Stegger M, Hallstrøm S, Rasmussen A, et al. *Mycoplasma phocimorsus* in woman with tendinous panaritium after cat scratch, Denmark. Emerg Infect Dis. 2025;31:380–385.
8. Species Mycoplasma phocimorsus. LPSN—List of Prokaryotic names with Standing in Nomenclature [cited 2024 Nov 11]. https://lpsn.dsmz.de/species/*mycoplasma-phocimorsus*
9. White CP, Jewer DD. Seal finger: a case report and review of the literature. Can J Plast Surg. 2009;17:133–5. https://doi.org/10.1177/229255030901700415

Author affiliation: Emory University School of Medicine, Atlanta, Georgia, USA

Address for correspondence: Clyde Partin, Emory Clinic, 1365 Clifton Rd NE, Bldg A, 1st Fl, Atlanta, GA 30322, USA; email: wpart01@emory.edu

DOI: https://doi.org/10.3201/eid3102.241778

Ending Epidemics: A History of Escape from Contagion

Richard Conniff; The MIT Press, Cambridge, MA, USA, 2023; ISBN-13: 978-0262047968; Pages: 376; Price: $24.98 (hardcover); $27.95 (paperback)

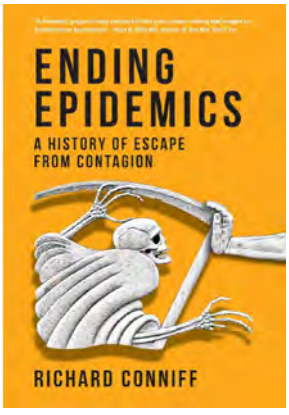

In 310 pages, the author tells the "story of humanity's long and, until now, extraordinarily successful struggle against infectious diseases" and weaves together 3 centuries of progress in managing infectious disease. The 31 chapters are presented chronologically, each typically recounting 1 or 2 diseases, key scientists or physicians involved in conquering the contagion, and their methods. Chapter 9 reminds us that the foundation of public health is not necessarily the image of the physician-scientist triumphantly standing with each pathogen discovery. Real progress had more to do with confronting mundane forces of hygiene, primarily disposal of human waste and the advent of the sanitation revolution.

The author ends the book with the last known case of smallpox, in Janet Parker, who died in 1978. Inevitably, he confronts COVID-19 in the epilogue, juxtaposing pessimistic caution, "the reality is that victory over infectious diseases was never a done deal," with an idealistic goal, "the job now is to protect not just the human species but the world itself. It will take 'delusional optimism' on a global scale."

The Yale-educated author is a decorated journalist, with a record of publishing science articles about human and animal behavior and nature. The writing style is lively, convincing, and spiced with literary references. Fascinating trivia is plentiful. For example, Russian zoologist Metchnikoff was so enamored of his time at Institut Pasteur that he asked to be cremated with the research animals. The personal life of these researchers is also explored.

Chapters 12 and 13 are particularly well done, introducing nuanced background information. Italian physician/microscopist Filippo Pacini did much to elucidate the pathologic nature and cause of cholera. He named the organism *Vibrio cholerae* in an 1854 article, as John Snow was gaining notoriety. Reverend Henry Whitehead was a keen observer and "unexpectedly proved to be a better epidemiological detective," having recognized the ground zero cholera case in a 5-month-old girl. Whitehead, a man of the cloth more than science, was an underappreciated sleuth whose astute observations were essential in understanding a cholera outbreak.

Several underheralded figures introduced by the author include Reverend Cotton Mather and Isabel Morgan. Mather, a controversial clerical figure in Boston, was interested in medicine and science. When smallpox landed in Boston, Mather was aware of the practice of variolation, which he learned from his servant, Onesimus, who was a native of Ghana. Identifying Bostonians born in Africa with variolation scars helped Mather overcome initial resistance from the Boston medical community to the technique. Morgan, a brilliant researcher, left the Rockefeller Institute because advancement for a woman was not likely there. In a polio group at Johns Hopkins University, she pioneered an inactivated poliovirus, refuting the dogma that only a live vaccine would work.

Topics such as contagionism, germ theory, antivivisection, and spontaneous generation are expertly woven into the narrative. References to misogynist statements will make the reader pause.

This author condensed >3 millennia of human misery related to infections, plagues, and poor sanitation, followed by a cogent narrative chronicling the ingenuity of physician-scientists and others who solved those problems. More depth and greater insight are provided than typical with the historical scenarios the author has presented.

Clyde Partin

Author affiliation: Emory University Orthopaedics & Spine Hospital, Tucker, Georgia, USA

DOI: https://doi.org/10.3201/eid3102.241462

Address for correspondence: Clyde Partin, Emory Clinic, 1365 Clifton Rd NE, Bldg A, 1st Fl, Atlanta, GA 30322, USA; email: wpart01@emory.edu

2000 Years of Pandemics: Past, Present, and Future

Claudia Ferreira, Marie-Françoise J. Doursout, Joselito S. Balingit; Springer International Publishing AG, Cham, Switzerland, 2023; ISBN-10: 3031100344; ISBN-13: 978-3031100345; Pages: 810; Price: US $179.99 (hardcover), US $129.99 (paperback), US $119.00 (ebook)

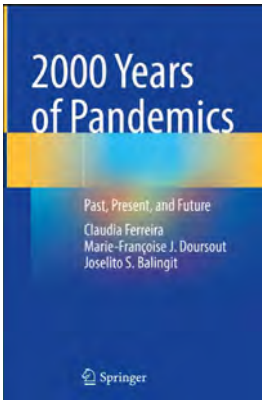

In *2000 Years of Pandemics: Past, Present, and Future*, the authors expertly describe the microbiologic origins and dire consequences of contagions when they spread through global populations. The authors bring diverse experiences to their work. Dr. Ferreira, a physician-scientist in France, is engaged in responses to emerging pathogens, whereas Drs. Doursout and Balingit are both medical educators in the United States. They argue that pandemics are not random events but are the direct result of imbalances created by humanity's interactions with the environment. As mobility has evolved from the Silk Road to air travel, dangerous microbes have found new, increasingly efficient ways to spread globally. The book includes a timely discussion of how climate change might exacerbate pandemic emergence.

Ferreira and others catalog pandemics starting in 165 CE, thoroughly describing most likely etiologies, effects on contemporary societies, and human responses. The accounts provide vivid and engaging descriptions of what it must have been like to go through those times. The book suggests parallels among pandemics over millennia. Even the vignettes in the pre–germ theory era offer valuable takeaways. During the bubonic plague in Italy, Venetians implemented quarantine and isolation measures, which lowered incidence rates in the city. Those practices remain crucial in infection prevention and control today. Plague doctors donned one of the first and most elaborate forms of personal protective equipment, complete with masks with glass red eyes and birdlike beaks packed with aromatic herbs and spices thought to filter and purify the air they inhaled. Their bodies were almost completely sealed off from environmental contact. The eerie ensemble resembles modern air-purifying respirators and layered protective gear worn by healthcare workers treating Ebola patients. This work draws parallels between the stigmatization of the homosexual community during the HIV/AIDS pandemic and the misdirected xenophobia and discrimination witnessed in the past. The book also illuminates the horrific history of using disease as a weapon, referencing the gruesome tactic of the Mongol army hurling plague victims' remains into Caffa, Italy, and the intentional spread of smallpox to Native Americans.

Consistency and organization are the main shortcomings of the book. Some sections read like a compelling history text and others a medical textbook with extensive treatment tables listing antibiotic choice, dose, and duration, specific guidelines for vaccination, and detailed options for diagnostic tests. This level of detail is inconsistent and unnecessary, leading to outdated treatment tables. The authors try to cover too many issues, thus, providing superficial reviews of some topics. In our view, a clearly defined philosophy and a consistent analytical framework would have enhanced this work. Such a framework would have resulted in deeper explorations of each pandemic, drawing out valuable insights from societal responses and their implications for future pandemics.

This engaging book offers instructive insights for a wide range of audiences, including biomedical trainees and practitioners and policymakers actively involved in pandemic responses. Published in 2023, this book uniquely connects the responses to and effects of pandemics, drawing parallels and extracting valuable lessons. It provides crucial observations into how pandemics have shaped surveillance, preparedness, and treatment of infectious diseases, and how they will continue to influence human history.

Nkuchia M. M'ikanatha, Keith Hamilton

Author affiliations: Pennsylvania Department of Health, Harrisburg, Pennsylvania, USA (N.M. M'ikanatha); University of Pennsylvania, Philadelphia, Pennsylvania, USA (K. Hamilton)

DOI: https://doi.org/10.3201/eid3102.240798

Address for correspondence: Nkuchia M. M'ikanatha, Pennsylvania Department of Health, Division of Infectious Disease Epidemiology, Health and Welfare Bldg, 7th and Forster St, Rm 933, Harrisburg, PA 17120, USA; email: nmikanatha@pa.gov

Franz (Ferenc) Paczka (1856–1925), *Un Cas Grave ou La Leçon de Médecine* (*A Serious Case or The Medical Lesson)* (ca. 1875–1880). Oil on canvas, 39.5 in × 53.3 in/100.3 cm × 135.5 cm. Image courtesy of Musée de Fécamp, Fécamp, France.

A Pictorial Human Case of "Furious Rabies"

Antonio Perciaccante, Marina De Luca, Corinne Déchelette, Nadège Sébille, Philippe Charlier

Franz (Ferenc) Paczka was a Hungarian genre painter and portraitist who studied in Paris and Rome and exhibited a few paintings at the 1878 Paris Universal Exhibition, in the Austria-Hungary section. When Paczka left France to serve in the military in his native country, he had to sell his Parisian studio collection (*1*). On April 21, 1880, an anonymous donor offered one of his paintings, considered unfinished, "*Un Cas Grave ou La Leçon de Médecine*" ("A Serious Case or The Medical Lesson)," to the fledgling Musée de Fécamp, barely 2 weeks before its official inauguration. The painting is unusual, given that Paczka usually painted portraits or small groups in calm everyday settings. Instead, it represents 2 doctors examining an unclear skin lesion on the side of a young girl who has a towel in her mouth and seems to be suffering and agitated so that she has to be held still.

Author affiliations: Azienda Sanitaria Universitaria Giuliano Isontina, "San Giovanni di Dio" Hospital, Gorizia, Italy (A. Perciaccante, M. De Luca); International Society of Iconodiagnosis, Paris, France (A. Perciaccante, C. Déchelette, P. Charlier); UVSQ/Paris-Saclay, Montigny-le-Bretonneux, France (A. Perciaccante, C. Déchelette, P. Charlier); La Peau Autrement, Toulouse, France (C. Déchelette); Les Pêcheries, Musée de Fécamp, Fécamp, France (N. Sébille)

DOI: https://doi.org/10.3201/eid3102.AC3102

There was no record as to the medical condition affecting the girl depicted in the painting. One nefarious conjecture might be that this picture may have demoniac overtones, a hypothesis that may be supported by several elements and symbols, such as the girl's red hair, the possible presence of a priest (with his skullcap and his black clothes) behind the doctors and the way he is pointing to the "mark," and the wound that may represent "the devil's mark." Moreover, in 1850–1900, France experienced a revival of occultism, spiritualism, magic, astrology, and mysticism.

However, a recently found newspaper article describing the painting and published on February 6, 1954, in Le Progrès de Fécamp by its director Jules Rolland (under the pseudonym Gihères), reveals that the lesion the doctors are examining is a dog bite wound: "'Un cas grave': a large canvas by Paczka. Two doctors examine suspicious spots on the body of a girl bitten by a dog. The grandfather's and grandmother's attitudes are fairly conventional" (*2*). This useful indication, which at that time probably appeared on the work's label, reveals an element for an interesting retrospective diagnosis and an alternative hypothesis on this painting's meaning.

The bite mark in a rabies victim usually heals before the onset of symptoms. However, the presence of the bite mark/scar months later might depend on the severity of the bite, whether it was subsequently infected, or the bite's location on the body. On the basis of that information and on the evident agitation of the young girl, we speculate that this painting represents a case of the encephalic form of rabies, known as furious rabies. The painting, preserved in Musée de Fécamp, predates Émile Roux's first inoculation of a human with rabies vaccine in July 1885; it reveals the powerlessness of families and doctors in the face of such violent symptoms and, in case of rabies, the fatal diagnosis for the victim. Cases of the disease now called rabies were recorded during the classical antiquity period (*3*). In the 4th Century BCE, Aristotle described the disease in his History of Animals*:* "Dogs suffer from three diseases … of these, rabies produces madness, and when rabies develops in all animals that the dog has bitten… it kills them; and this disease kills the dogs too" (*4*).

Rabies is a zoonotic disease caused by viruses of the genus *Lyssavirus*, family Rhabdoviridae, order Mononegavirales. Viruses are transmitted by the saliva of the infected animal. Similar to the situation in France in the 1800s, dogs today remain the biggest concern for human rabies exposures globally, and in certain parts of the world, wildlife such as bats, foxes, jackals, mongooses, racoons, skunks, and others also transmit rabies (*5*). Rabies virus first enters in peripheral motor neurons and then passes to the central nervous system, causing signs and symptoms (*5*). Rabies can be exhibited in 2 forms—encephalitic (or furious) and paralytic—but the determining factors are not well known. Signs and symptoms depend on the form. The incubation period is 20–90 days after exposure. A short prodromal phase while the virus replicates in the dorsal root ganglia includes fever, pain, paraesthesia, pruritus, or a combination of those symptoms. In cases of furious rabies, a next acute neurologic phase is characterized by hyperactivity, confusion and agitation, hypersalivation, piloerection, hydrophobia, aerophobia resulting from electrolyte imbalance, dysphagia, hyperventilation, coordination disorders, hallucinations, and, finally, coma and death (*5*,*6*).

Primary prevention is based on animals' vaccination to reduce the virus reservoirs. Because in most areas the primary reservoir is dogs, vaccination and elimination of stray dogs reduce virus circulation, as does dissemination of vaccine-containing bait for wild animals in rural areas. Progression to clinical disease can be prevented if wound care and postexposure prophylaxis by immunoglobulin and vaccination are administered rapidly after animal bite, thus sparing many people around the world from suffering the same fate as the young girl depicted by Paczka in his painting. Unfortunately, the therapeutic is not available everywhere.

Although Louis Pasteur developed the first effective rabies vaccines for humans in the 19th Century, today, the virus is still endemic among animals in some regions of the world (i.e., throughout Asia and Africa), and human rabies remains a serious public health challenge (*6*,*7*). *Un Cas Grave ou La Leçon de Médecine* is an example of how art can tell the history of medicine and focus on a health issue that is perhaps underestimated today.

Acknowledgments

We thank the team of Les Pêcheries, Musée de Fécamp: Aurélien Arnaud, Céline Magnan, Benjamin Loesel, and Quentin Panel.

References

1. Hue C. Historique du musée de peinture et d'objets d'art de Fécamp. Fécamp, France; Memorial du Cauchois; 1880.
2. Rolland J. "Le musée municipal: l'Histoire et l'Art y ont accumulé de véritables trésors, enviés des grands musées nationaux." Le Progrès de Fécamp, 6 février 1954.
3. Tarantola A. Four thousand years of concepts relating to rabies in animals and humans, its prevention and its cure.

Trop Med Infect Dis. 2017;2:5. https://doi.org/10.3390/tropicalmed2020005
4. Aristotle. History of animals [translated by Peck AL, Balme DM, Gotthelf A]. London (UK), Cambridge (MA): Harvard University Press; 1965. p: 182–3.
5. Fooks AR, Cliquet F, Finke S, Freuling C, Hemachudha T, Mani RS, et al. Rabies. Nat Rev Dis Primers. 2017;3:17091. https://doi.org/10.1038/nrdp.2017.91
6. Fooks AR, Banyard AC, Horton DL, Johnson N, McElhinney LM, Jackson AC. Current status of rabies and prospects for elimination. Lancet. 2014;384:1389–99. https://doi.org/10.1016/S0140-6736(13)62707-5
7. Pattnaik P, Mahal A, Mishra S, Alkhouri A, Mohapatra RK, Kandi V. Alarming rise in global rabies cases calls for urgent attention: current vaccination status and suggested key countermeasures. Cureus. 2023;15:e50424. https://doi.org/10.7759/cureus.50424

Address for correspondence: Antonio Perciaccante, Department of Medicine, Azienda Sanitaria Universitaria Giuliano Isontina, "San Giovanni di Dio" Hospital, via Fatebenefratelli, 34 Goriza 34170, Italy; email: antonioperciaccante1976@gmail.com

The Public Health Image Library

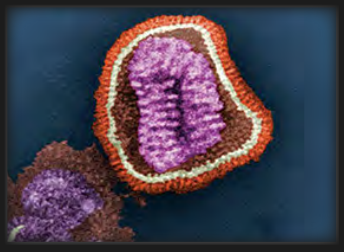
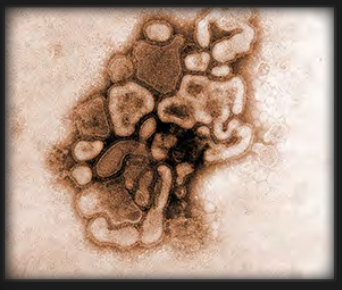
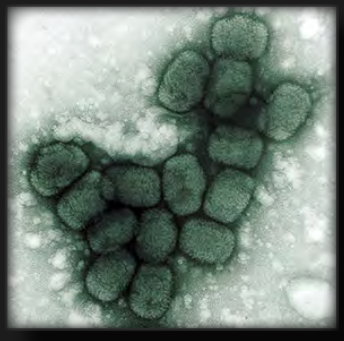



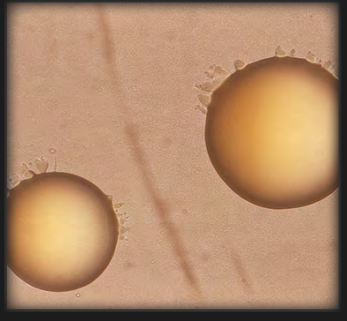
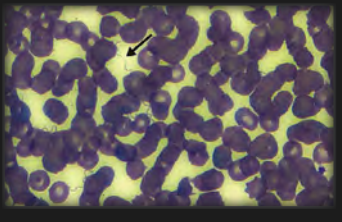

The Public Health Image Library (PHIL), Centers for Disease Control and Prevention, contains thousands of public health–related images, including high-resolution (print quality) photographs, illustrations, and videos.

PHIL collections illustrate current events and articles, supply visual content for health promotion brochures, document the effects of disease, and enhance instructional media.

PHIL images, accessible to PC and Macintosh users, are in the public domain and available without charge.

Visit PHIL at:
https://phil.cdc.gov/

EMERGING INFECTIOUS DISEASES®

Upcoming Issue
Tuberculosis

- *Corynebacterium diphtheriae* Infections, South Africa, 2015–2023
- *Mycobacterium nebraskense* Isolated from Patients in Connecticut and Oregon, USA
- Genomic Characterization of Circulating Dengue Virus, Ethiopia, 2022–2023
- High Prevalence of AtpE Mutations in Bedaquiline-Resistant *Mycobacterium tuberculosis* Isolates, Russia
- Effect of Prior Influenza A(H1N1)pdm09 Virus Infection on Pathogenesis of Human Influenza A(H5N1) Clade 2.3.4.4b Virus Isolate in Ferret Model
- Efficacy and Safety of 4-Month Rifapentine-Based Tuberculosis Treatments in Persons with Diabetes
- Impact, Costs, and Cost-Effectiveness of Tuberculosis Outbreak Investigations, United States
- Reemergence of *Brucella abortus*, Israel, 2021
- Influenza A(H5N1) Immune Response among Ferrets with Preexisting Influenza A(H1N1)pdm09 Immunity
- Macrolide-Resistant Mycoplasma pneumoniae Infections among Children after COVID-19 Pandemic, Ohio, USA
- Cefotaxime-Resistant *Neisseria meningitidis* ST-4821 Causing Fulminant Meningitis
- Neurosarcocystosis in Patient with HIV-Induced Immunodeficiency
- Fluoroquinolone Resistance in Drug-Resistant Tuberculosis, Kharkiv, Ukraine, 2019–2023
- Community-Acquired Pneumonia Caused by Avian *Chlamydia abortus*, the Netherlands
- Evaluation of High-Dose Isoniazid Use in Multidrug-Resistant Tuberculosis Treatment
- Lack of Competence of US Mosquito Species in Circulating Oropouche Virus

Complete list of articles in the March issue at https://wwwnc.cdc.gov/eid/#issue-319

Earning CME Credit

To obtain credit, you should first read the journal article. After reading the article, you should be able to answer the following, related, multiple-choice questions. To complete the questions (with a minimum 75% passing score) and earn continuing medical education (CME) credit, please go to http://www.medscape.org/journal/eid. Credit cannot be obtained for tests completed on paper, although you may use the worksheet below to keep a record of your answers.

You must be a registered user on http://www.medscape.org. If you are not registered on http://www.medscape.org, please click on the "Register" link on the right hand side of the website.

Only one answer is correct for each question. Once you successfully answer all post-test questions, you will be able to view and/or print your certificate. For questions regarding this activity, contact the accredited provider, CME@medscape.net. For technical assistance, contact CME@medscape.net. American Medical Association's Physician's Recognition Award (AMA PRA) credits are accepted in the US as evidence of participation in CME activities. For further information on this award, please go to https://www.ama-assn.org. The AMA has determined that physicians not licensed in the US who participate in this CME activity are eligible for *AMA PRA Category 1 Credits*™. Through agreements that the AMA has made with agencies in some countries, AMA PRA credit may be acceptable as evidence of participation in CME activities. If you are not licensed in the US, please complete the questions online, print the AMA PRA CME credit certificate, and present it to your national medical association for review.

Article Title

National Surveillance of Human Ehrlichiosis Caused by *Ehrlichia ewingii*, United States, 2013–2021

CME Questions

1. Which of the following species is responsible for most cases of ehrlichiosis in the United States?

A. *Ehrlichia ewingii*
B. *E. chaffeensis*
C. *E. muris eauclairensis*
D. *E. canis*

2. Which of the following statements regarding ehrlichiosis is most accurate?

A. Infection associated with *E. ewingii* is generally milder than infection with *E. chaffeensis*
B. The severity of infection does generally not vary by *Ehrlichia* species
C. The mortality rate of ehrlichiosis caused by *E. ewingii* approaches 30%
D. Serologic testing remains dependable in discriminating between different species of *Ehrlichia* species

3. Which of the following statements regarding the epidemiology of *E. ewingii* ehrlichiosis in the current study is most accurate?

A. The annual incidence was 14 cases per 1 million population
B. The annual case count increased gradually from 2013 to 2019, at which point it increased dramatically through 2021
C. Nearly half of the cases during the study period occurred in Missouri
D. Case rates dropped in states like Kansas and Virginia during the study period

4. Which of the following statements regarding the demographics of *E. ewingii* ehrlichiosis in the current study is most accurate?

A. Most cases occurred among female persons
B. 70% of cases occurred among persons who identified as White
C. Cases were most common among persons aged 10 to 19 years
D. Cases were most common among persons aged 20 to 29 years

Earning CME Credit

To obtain credit, you should first read the journal article. After reading the article, you should be able to answer the following, related, multiple-choice questions. To complete the questions (with a minimum 75% passing score) and earn continuing medical education (CME) credit, please go to http://www.medscape.org/journal/eid. Credit cannot be obtained for tests completed on paper, although you may use the worksheet below to keep a record of your answers.

You must be a registered user on http://www.medscape.org. If you are not registered on http://www.medscape.org, please click on the "Register" link on the right hand side of the website.

Only one answer is correct for each question. Once you successfully answer all post-test questions, you will be able to view and/or print your certificate. For questions regarding this activity, contact the accredited provider, CME@medscape.net. For technical assistance, contact CME@medscape.net. American Medical Association's Physician's Recognition Award (AMA PRA) credits are accepted in the US as evidence of participation in CME activities. For further information on this award, please go to https://www.ama-assn.org. The AMA has determined that physicians not licensed in the US who participate in this CME activity are eligible for *AMA PRA Category 1 Credits*™. Through agreements that the AMA has made with agencies in some countries, AMA PRA credit may be acceptable as evidence of participation in CME activities. If you are not licensed in the US, please complete the questions online, print the AMA PRA CME credit certificate, and present it to your national medical association for review.

Article Title

Streptococcus pyogenes emm Type 3.93 Emergence, the Netherlands and England

CME Questions

1. According to the current study, which of the following statements regarding invasive group A *Streptococcus* (iGAS) infections in the Netherlands and England in 2023 to 2024 is most accurate?

A. iGAS infections did not follow any seasonal pattern after the height of the COVID-19 pandemic
B. The rates of *emm* type 3.93 (*emm*.393) iGAS infections increased in the Netherlands from November 2023 to March 2024 but decreased in England during this same period
C. The rates of *emm*.3.93 iGAS infections decreased in both the Netherlands and England from November 2023 to March 2024
D. Rates of antimicrobial resistance of iGAS caused by *emm*.393 were low in England

2. Which age group suffered the highest risk for iGAS infection caused by *emm*.3.93 in the current study?

A. 6 months to 3 years
B. 6 to 17 years
C. 35 to 44 years
D. 65 to 76 years

3. In the current study, *emm*.3.93 was particularly associated with a higher rate of iGAS of what anatomical site in both the Netherlands and England?

A. Abdominal cavity
B. Central nervous system
C. Skin and soft tissue
D. Lung

4. Which of the following statements regarding the genomic analysis of *emm*.3.93 iGAS infections in the current study is most accurate?

A. *emm*.3.93 was clustered into 2 distinct clades
B. *emm*.3.93 was clustered into 7 distinct clades
C. All clades were separated by country of testing
D. There was evidence of genomic changes associated with increased survival and virulence

Emerging Infectious Diseases
Photo Quiz Articles

Volume 14, Number 9
September 2008

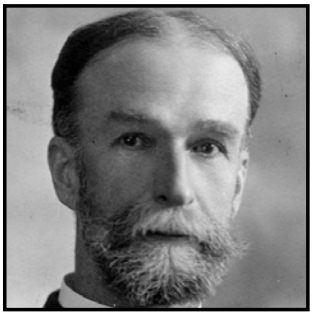

Volume 14, Number 12
December 2008

Volume 15, Number 9
September 2009

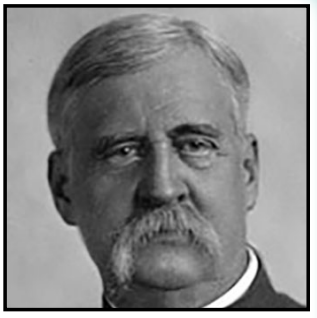

Volume 15, Number 10
October 2009

Volume 16, Number 6
June 2010

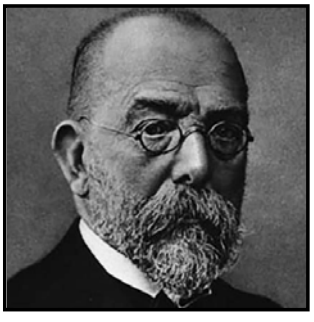

Volume 17, Number 3
March 2011

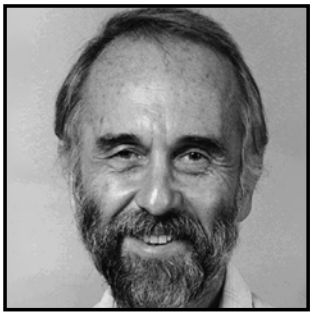

Volume 17, Number 12
December 2011

Volume 19, Number 4
April 2013

Volume 20, Number 5
May 2014

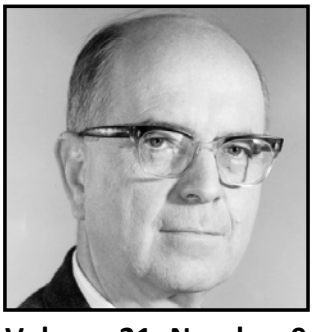

Volume 21, Number 9
September 2015

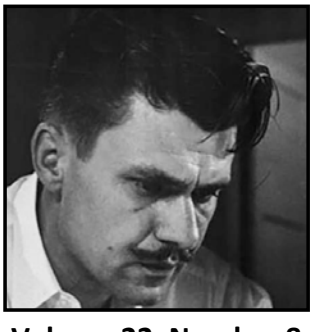

Volume 22, Number 8
August 2016

Volume 28, Number 3
March 2022

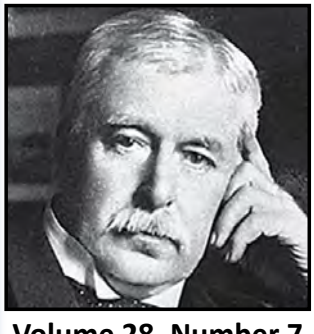

Volume 28, Number 7
July 2022

Click on the link below to read about the people behind the science.

https://bit.ly/3LN02tr

See requirements for submitting a photo quiz to EID.

https://bit.ly/3VUPqfj

EID Journal